Safety in Mines Research Advisory Committee

DRAFT FINAL REPORT

Improvement of worker safety through the investigation of the site response to rockbursts

R J Durrheim, A M Milev, S M Spottiswoode, and B Vakalisa

Research agency : CSIR: Division of Mining Technology
Project number : GAP201
Date : December 1997

Table of contents

	Page
Executive summary	8
Preface	10
Acknowledgements	13
List of figures	14
List of tables	41
1. Introduction	43
1.1 The rockburst problem	43
1.2 The site response	43
1.3 Project outputs	44
1.4 Methodology	45
1.5 Structure of report	46
2. Quantitative measurements of the site response	46
2.1 Review of related work	46
2.2 Research methodology	50
2.2.1 Instrumentation	50
2.2.2. List of Analysis techniques used	54
2.3 Site response measurements and analysis	55
2.3.1 Peak velocity and acceleration parameters, frequency spectra in tunnels, cross-cut and stopes	55
2.3.2 Time domain analysis of tunnel sidewall motion	63
2.3.3 Spectral analysis to quantify the influence of fracturing and support on the dynamic behaviour of the hangingwall	70
2.3.4 Measurements of site response during actual rockbursts	111
2.3.5 Transfer function for a seismic signal recorded in solid rock and on the skin of an excavation	115
2.3.6 Velocity amplification considered as a phenomenon of elastic energy release due to softening	122
3 Rockburst investigations	132
3.1 Review of previous work	132
3.2 Methodology	136
3.3 Scope of investigations	137

3.4 Factors affecting the severity of rockburst damage..... 147
3.4.1 Layout and mining sequence..... 147
3.4.2 Numerical modelling..... 153
3.4.3 Tunnels and service excavations..... 154
3.4.4 Gullies..... 156
3.4.5 Stopes..... 158
3.4.6 Seismicity..... 161
3.4.7 Strong ground motion..... 161
3.4.8 Preconditioning..... 162
3.4.8 Conclusions..... 162
4 Conclusions..... 163
5 References..... 166
6 The following materials have been published..... 174
Appendix A Transfer function for a seismic signal recorded in solid rock and on the skin of an excavation..... A-1
1 Introduction..... A-2
2 Dynamic structural systems..... A-2
3 Recursive prediction error methods..... A-5
4 Data, results and discussions..... A-6
4.1 Experiment 1 (Blyvooruitzicht Gold Mine)..... A-6
4.2 Is site response non-linear?..... A-8
4.3 Model of output: Mode presentation..... A-9
4.4 Experiment 2 (Vaal Reefs No.5 Shaft)..... A-20
4.5 Experiment 3 (Vaal Reefs No.5 Shaft)..... A-42
5 Conclusions..... A-55
Appendix B Rockburst case study..... B-1
1 Leeudoorn, 10/1/94, M_L=2,6 and M_L=1,9..... B-2
1.1 Introduction..... B-2
1.2 Mining environment..... B-2
1.3 Observations at the rockburst site..... B-4
1.4 Assessment of support performance..... B-8
1.5 Assessment of layout..... B-8

1.6 Rockburst mechanism..... B-9
1.7 Conclusions..... B-11
1.8 Recommendations..... B-11
2 Deelkraal, 4/5/94, M_L=2,1..... B-12
2.1 Introduction..... B-12
2.2 Mining environment..... B-12
2.3 Observations at the rockburst site..... B-14
2.4 Assessment of support performance..... B-20
2.5 Assessment of layout..... B-21
2.6 Seismic history..... B-22
2.7 Rockburst mechanism..... B-23
2.8 Conclusions..... B-27
2.9 Recommendations..... B-28
3 Western Deep Levels (West), 3/11/94, M_L=2,5..... B-29
3.1 Introduction..... B-29
3.2 Mining environment..... B-29
3.3 Observations at the rockburst site..... B-34
3.4 Assessment of support performance..... B-37
3.5 Assessment of the layout..... B-38
3.6 Seismic history..... B-42
3.7 Rockburst mechanism..... B-42
3.8 Conclusions..... B-47
3.9 Recommendations..... B-48
4 Buffelsfontein, 4/7/95, M_L=3,4..... B-49
4.1 Introduction..... B-49
4.2 Mining environment..... B-49
4.3 Observations at the rockburst site..... B-50
4.4 Assessment of support performance..... B-56
4.5 Rockburst mechanism..... B-58
4.6 Conclusions..... B-59
4.7 Recommendations..... B-60
5 ERPM, 24/7/95, M_L<0,5 and 15/8/95, M_L=0,9..... B-61
5.1 Introduction..... B-61
5.2 Mining environment..... B-61

5.3 Observations at the rockburst site..... B-63
5.4 Seismic history..... B-65
5.5 Rockburst mechanism..... B-65
5.6 Conclusions..... B-67
5.7 Recommendations..... B-69
6 East Driefontein, 14/9/95, M_L=3,6..... B-69
6.1 Introduction..... B-70
6.2 Mining environment..... B-70
6.3 Observations at the rockburst site..... B-75
6.4 Assessment of support performance..... B-78
6.5 Assessment of layout..... B-80
6.6 Rockburst mechanism..... B-82
6.7 Conclusions..... B-83
6.8 Recommendations..... B-84
7 Western Deep Levels (South), 18/9/95, M_L=2,2..... B-85
7.1 Introduction..... B-85
7.2 Mining environment..... B-85
7.3 Observations at the rockburst site..... B-91
7.4 Assessment of support..... B-92
7.5 Assessment of layout..... B-93
7.7 Rockburst mechanism..... B-93
7.8 Conclusions..... B-97
7.9 Recommendations..... B-98
8 Blyvooruitzicht, 30/1/96, M_L=2,2..... B-99
8.1 Introduction..... B-99
8.2 Mining environment..... B-99
8.3 Observations at the rockburst site..... B-107
8.4 Assessment of support performance..... B-114
8.5 Assessment of layout..... B-115
8.6 Seismic history..... B-115
8.7 Rockburst mechanism..... B-116
8.8 Seismic hazard..... B-119
8.9 Conclusions..... B-120
8.10 Recommendations..... B-122

9 Western Deep Levels (South), 15/2/96, M_L=1,8..... B-122
9.1 Introduction..... B-122
9.2 Mining environment..... B-123
9.3 Observations at the rockburst site..... B-124
9.4 Rockburst mechanism..... B-127
9.5 Conclusions..... B-132
9.6 Recommendations..... B-134
10 East Driefontein # 1, 5/6/96, M_L=2,7..... B-134
10.1 Introduction..... B-134
10.2 Mining environment..... B-135
10.3 Observations at the rockburst site..... B-135
10.4 Assessment of support performance..... B-139
10.5 Assessment of layout..... B-141
10.6 Seismic history..... B-142
10.7 Rockburst mechanism..... B-143
10.8 Conclusions..... B-144
10.9 Recommendations..... B-144
11 Western Deep Levels (East), 18/11/96, M_L=3..... B-146
11.1 Introduction..... B-146
11.2 Mining environment..... B-147
11.3 Observations at the rockburst site..... B-149
11.4 Assessment of support performance..... B-150
11.5 Assessment of layout..... B-152
11.6 Seismic history..... B-152
11.7 Rockburst mechanism..... B-153
11.8 Conclusions..... B-153
11.9 Recommendations..... B-154
12 Vaal Reefs # 5, 10/2/97, M_L=4,0..... B-155
12.1 Introduction..... B-155
12.2 Mining environment..... B-156
12.3 Observations at the rockburst site..... B-159
12.4 Assessment of support performance..... B-164
12.5 Assessment of layout..... B-166
12.6 Seismic history..... B-169

12.7 Rockburst mechanism..... B-173
12.8 Conclusions..... B-174
12.9 Recommendations..... B-175
13 Leeudoorn, 10/4/97, M_L=1,7 and 16/4/97, M_L=2,3..... B-176
13.1 Introduction..... B-176
13.2 Mining environment..... B-177
13.3 Observations at the rockburst site..... B-180
13.4 Rockburst mechanism..... B-181
13.5 Conclusions..... B-185
13.6 Recommendations..... B-185
14 Western Deep Levels (East), 17/4/97, M_L=2,7..... B-186
14.1 Introduction..... B-186
14.2 Mining environment..... B-186
14.3 Rockburst mechanism..... B-189
14.4 Assessment of support performance..... B-190
14.5 Conclusions..... B-191
14.6 Recommendations..... B-191
15 West Driefontein # 6, 23/5/97, M_L=2,7..... B-191
15.1 Introduction..... B-192
15.2 Mining environment..... B-192
15.3 Observations at the rockburst site..... B-196
15.4 Assessment of support performance..... B-197
15.5 Rockburst mechanism..... B-200
15.6 Conclusions..... B-201
15.7 Recommendations..... B-202
16 East Driefontein # 4, 25/9/97, M_L=4,4..... B-203
16.1 Introduction..... B-203
16.2 Mining environment..... B-204
16.3 Observations at the rockburst site..... B-204
16.4 Assessment of support performance..... B-216
16.5 Rockburst mechanism..... B-217
16.6 Conclusions..... B-219
16.7 Recommendations..... B-220

Executive summary

Rockbursts are a major hazard in South African deep-level gold mines. The severity of damage due to a seismic event often varies greatly over small distances. The goal of this project is to discover the reasons for this variation in the severity of damage. It is believed that a detailed understanding of the damage mechanisms, and the application of this knowledge to the design and support of excavations, will lead to a reduction in the hazard posed by rockbursts.

Ground motion monitors were installed in tunnels and stopes in several deep gold mines. Peak velocity measurements made on the skin of an excavation were found to be four to ten times greater than those within the solid rock at similar distances from the source. Techniques to analyse the measurements were developed. It was found that the amplitude and phase of ground motion at points about 1 m apart may vary considerably for small amplitude events, indicating strain across intervening fractures. This phenomenon could have a pronounced influence on the stability of the hangingwall during larger, potentially damaging events. The damped harmonic oscillator model, widely used in earthquake engineering, was found to be useful for analysing the ground motion. Four hypotheses to explain the amplification of ground motion were investigated: resonance, energy trapping in a channel, energy release due to slab buckling, and energy release due to softening.

Detailed investigations of twenty-eight rockbursts were conducted. A team of specialists inspected damage to the excavations and support elements, mapped mining-induced fractures and other geological features, and interviewed witnesses. Seismograms were analysed to determine the source parameters, and the seismic history was reviewed in each case. Numerical modelling was used to evaluate the mining layouts. Finally, recommendations were formulated and presented to the mines concerned. It was found that the severity of damage is strongly influenced by local rock conditions and support systems. Certain shortcomings in the application of current technology, such as numerical modelling for mine design, were also identified. It was also found that published guidelines, e.g. for pillar design, have limitations which are not explicitly stated. The performance of new technologies such as preconditioning and pre-stressed yielding elongates was assessed under rockburst conditions and it was found that effective

implementation depends to a large extend on training and discipline, and there were certain deficiencies in some of these support types.

In the short term, the most important means of reducing the severity of rockburst damage is to ensure that: support is always up to standard, stope support is as close to the face as possible, frequent inspections are conducted by personnel able to identify changes in the rock mass condition and with the authority to recommend and implement appropriate changes to layout and support systems, and sound layouts are adhered to regardless of the demands of production. Further gains may be achieved, in the medium term, through the improvement of areal coverage in gullies and stopes. In the long term, the effectiveness of support systems may be improved by applying earthquake engineering principles which take factors such as the duration of shaking, repeated seismic loading and the structural response into account.

Preface

The dissemination of knowledge and the transfer of technology is a key element of SIMRAC research. The knowledge gained during the course of this project has been disseminated by means of workshops, conferences, symposia and seminars, which are listed below. In addition, reports on the findings of rockburst investigations have been presented to mine management. Key findings will be included in the revision of the Industry Guide to the Amelioration of the Hazards of Rockfalls and Rockbursts (COMRO, 1988), scheduled for publication in 1998.

26th International Conference of Safety in Mines Research Institutes,
8 September 1995, Katowice, Poland.
Durrheim, R. J., Jager, A.J., Klokow, J.W., & Booyens, D. (paper read by A. T. Haile), Back analysis to determine the mechanism and risk of rockbursts - 3 case histories from South African gold mines.

8th International Conference on Rock Mechanics,
25-30 September 1995, Tokyo, Japan.
Gay, N. C., Durrheim, R. J., Spottiswoode, S.M. & van der Merwe, A. J. Effect of geology, in-situ stress, and mining methods on seismicity in Southern African gold and platinum mines.

2nd North American Rock Mechanics Symposium,
19-21 June 1996, Montreal, Canada.
Durrheim, R. J., Kullmann, D. H. Stewart, R. D. & Cichowicz, A. Seismic excitation of the rock mass surrounding an excavation in highly stressed ground.

SIMRAC Seminar,
13-14 May, 1997, Freegold Club, Welkom, South Africa.
Durrheim, R. J. Site response to rockbursts.

4th International Symposium on Rockbursts & Seismicity in Mines,

11-14 August 1997, Krakow, Poland.

Durrheim, R. J., Handley, M. F., Haile, A. T., Roberts, M. K. C. & Ortlepp, W. D. Rockburst damage to tunnels in a deep South African gold mine caused by a M=3,6 seismic event.

Rockburst Workshop,

18 July 1997, Mining Technology, Johannesburg.

Review of rockburst investigations, presented by members of the rockburst team (R. J. Durrheim, M. K. C. Roberts, W. D. Ortlepp, M. F. Handley, T. O. Hagan, A. T. Haile, R. Johnson, A. J. Jager). Attended by 40 representatives from the mining industry and Department of Minerals and Energy.

Rockburst Workshop,

29 August 1997, Mining Technology, Johannesburg.

Review of rockburst investigations, presented by members of the rockburst team (R. J. Durrheim, M. K. C. Roberts, A. T. Haile, T. O. Hagan, A. J. Jager). Attended by 6 representatives from NUM.

SAIMM Colloquium, Rockbursts - what are they?,

4 September 1997, Gold Fields Training Centre, Kloof Gold Mine.

R. J. Durrheim presented a talk entitled *Systematic recording of rockburst damage* and was a member of the panel which addressed issues of rockburst prediction, control and containment. Over 100 delegates attended the colloquium.

1st Southern African Rock Engineering Symposium,

15-17 September 1997, Johannesburg, South Africa.

Cichowicz, A. & Durrheim, R. J. The site response of the tunnel sidewall in a deep gold mine, analysis in the time domain.

Durrheim, R J., Roberts, M. C. K., Haile, A. T., Hagan, T. O., Jagar, A. J., Handley, M. F., Spottiswoode, S.M. & Ortleep, W. D. Factors influencing the severity of rockburst damage in South African gold mines.

Spottiswoode, S. M., Durrheim, R. J., Vakalisa, B. & Milev, A. M. Influence of fracturing and support on the site response in deep tabular stopes.

SIMRAC Symposium,

19 November, 1997, Village Club, Western Deep Levels, South Africa.

Durrheim, R.J., Spottiswoode, S. M., Vakalisa, B., & Milev, A. M. Rockburst site response: criteria for support design.

SAIMM School, Shotcrete and its application,

25-26 February 1998.

R. J. Durrheim invited to present a talk entitled *Observations of shotcrete behaviour.*

3rd International Conference on the Mechanics of Jointed and Faulted Rock, 6-9 April 1998, Vienna, Austria.

Linkov, A. M. & Durrheim, R. J. Velocity amplification considered as a phenomenon of elastic energy relese due to softening.

Acknowledgements

The authors of the report would like to express their thanks to SIMRAC for financial support for project GAP201, and to the management of Blyvooruitzicht, Vaal Reefs and Western Deep Levels, South and East Mines for permission to make measurements of the site response. The rockburst investigations depended on the support of many people on many mines. We are grateful for the willing assistance we received.

List of figures

		Page
Figure 2.2.1.	CSIR Ground Motion Monitor with accelerometers (indicated by arrows) attached to the stope face, and the hanging- and footwall.....	50
Figure 2.2.2.	High frequency acceleration seismogram recorded by the CSIR Ground Motion Monitor. Peak acceleration is equal to 5,07 m/s^2.....	52
Figure 2.2.3.	Velocity seismogram resulting from integration of the accelerograms in Figure 2.2.1. Data were high-pass filtered to remove low frequency effect caused by integration.....	52
Figure 2.2.4.	Typical velocity spectra of three seismograms recorded on the hanging wall. Seismograms 1 and 2 are horizontal components while 3 is the vertical component.....	53
Figure 2.3.1	Deployment of PSS geophones (P1-P6) and CSIR Ground Motion Monitors (A, B and C) at the 17-24W Preconditioning Site, Blyvooruitzicht Gold Mine.....	56
Figure 2.3.2.	Measurement of the peak velocity parameter Rv_{max} at the 17-24W Preconditioning Site, Blyvooruitzicht Gold Mine. PSS measurements made in the solid rock are indicated by open circles. CSIR Ground Motion Monitor measurements made on the wall of the excavation are indicated by solid diamonds. R is the hypocentral distance. (a) Footwall Drive (b) Stope (c) Cross-cut.....	58

Figure 2.3.3. Typical spectra of accelerograms recorded by the CSIR Ground Motion Monitor on the wall of the excavation at the 17-24 W Preconditioning Site, Blyvooruitzicht Gold Mine. The seismic event had a local magnitude of -1,8. The spectra of the face-parallel and face-perpendicular components are numbered 1 and 2, respectively. Theoretical spectra for the Brune model are shown (seismic moment $M_o=10^8$ Nm, corner frequency f_o = 200 Hz and 900 Hz)..... 60

Figure 2.3.4. Velocity spectra of the ground motion recorded in the solid rock by a geophone grouted in a 10 metre long borehole (solid line), and by a geophone attached to the sidewall of the footwall drive near the collar of the borehole (dashed line). The seismograms were recorded by the PSS at a sampling rate of 10 kHz. The seismic event had a local magnitude of -0,7. Note the enhancement of the higher frequencies and the presence of resonant peaks..... 61

Figure 2.3.5. Seismic shaking caused by a M_L= -0,7 event located in the B17 stabilizing pillar at Blyvooruitzicht Gold Mine. Seismogram s_1 (t) was recorded by a vertical component geophone in solid rock and s_2(t) by a horizontal component geophone attached to the sidewall of a footwall drive. The sampling rate was 10 kHz. In this example the peak velocity (V_{max}) on the tunnel sidewall is more than twice that recorded in the solid rock, even though it is further from the source. The duration of shaking also increased substantially on the tunnel sidewall..... 64

Figure 2.3.6. System identification. The solid rock seismogram s_1 (t) is represented by a fine solid line and the seismogram recorded on the sidewall of the tunnel, which has a strong site effect, s_2 (t) is represented by a dashed line. The bold solid line denotes the error signal e(t) obtained by subtracting the output of the adaptive system from s_2 (t). Note the relatively small amplitude of the error signal, indicating that the data adaptive filter has succeeded in identifying the transfer characteristic of the system..... 66

Figure 2.3.7. Damped oscillator model. Three seismograms are superimposed. The solid rock seismogram (s_1(t), fine solid line), the seismogram recorded on the sidewall of the tunnel which has a strong site effect (s_2(t), dashed line), and the theoretical output obtained by convolving s_1(t) with the damped oscillator with natural frequency 440 Hz and damping coefficient D=0,03 (bold solid line). Note the good match with s_2(t)..... 69

Figure 2.3.8. A plot of spectral amplitude ratios of one event and the median value at each frequency for a group of events. The median values, in bold, are clearly more stable..... 72

Figure 2.3.9. Median value of amplitude ratio, channels 2 to 3, site 84/49/W1. Three overlapping windows of 128 samples were taken, starting just before the P wave arrival..... 72

Figure 2.3.10. A picture illustrating the relationship between phase difference, $\delta(f)$, and phase velocity..... 73

Figure 2.3.11. Median value of the absolute phase difference, the same windows as for Figure 2.3.9. 74

Figure 2.3.12. A sketch showing two black boxes (sites 1 and 2) at Panel P14, Vaal Reefs Mine..... 78

Figure 2.3.13 (a). Log_{10} median spectral ratio as a function of frequency. Ratios are taken between G2 and G3 for site VLR/P14/S1..... 79

Figure 2.3.13 (b). P spectra for geophones G2 and G3..... 79

Figure 2.3.14 (a). Log_{10} median spectral ratio between G1 and G2, plotted as a function of frequency. This is site VLR/P14/S2..... 80

Figure 2.3.14 (b). Log_{10} median spectral ratio G2/G3 plotted as a function of frequency. This is site VLR/P14/S2..... 81

Figure 2.3.14 (c). Log_{10} median spectral ratio as a function of frequency between G1 and G3 at site VLR/P14/S2..... 81

Figure 2.3.14 (d). Absolute median phase diagram of relative motion between G1 and G3..... 82

Figure 2.3.15. Maximum velocities recorded at G2 and G3 at VLR/P14/S1..... 82

Figure 2.3.16. The ratios of G3/G2 as a function of time at site VLR/P14/S1..... 83

Figure 2.3.17. Maximum velocities recorded at G1, G2, G3 in VLR/P14/S2..... 84

Figure 2.3.18. The ratio G2/G1 and G3/G1 as a function of time at VLR/P14/S2..... 85

Figure 2.3.19. A sketch showing the position of two black boxes at sites VLR/P11/S3 and VLR/P11/S4..... 86

Figure 2.3.20 (a). Log_{10} amplitude ratio as a function of frequency at VLR/P11/S3..... 87

Figure 2.3.20 (b). Median phase difference as a function of frequency at VLR/P11/S3..... 87

Figure 2.3.21 (a). Log_{10} amplitude ratio as a function of frequency at VLR/P11/S4..... 88

Figure 2.3.21 (b). Median phase difference as function of frequency at VLR/P11/S4..... 89

Figure 2.3.22. Maximum velocities recorded at VLR/P11/S3 on the FW, HW1 and HW2..... 90

Figure 2.3.23. Maximum velocities recorded at VLR/P11/S4 on the FW, HW1 and HW2..... 90

Figure 2.3.24. Diagram showing a layout of geophones (G1, G2, G2*, G3) at two sites in a backfilled stope, WDL-E/94E1/S1 and .WDL-E/94E1/S2 geophones G1 are embedded in backfill and G2, G2* and G3 are attached to the hangingwall..... 92

Figure 2.3.25 (a). A plot of Log_{10} median spectral ratio against frequency. Spectral ratios were calculated for geophones G1 and G2 of WDL-E/94E1/S1 shown in Figure 2.3.24..... 93

Figure 2.3.25 (b). A plot of Log_{10} median spectral ratio against frequency. Spectral ratios were calculated for geophones G1 and G2* of WDL-E/94E1/S1 shown in Figure 2.3.24..... 94

Figure 2.3.26 (a). Log_{10} median spectral ratio between G1 and G2 plotted as a function of frequency. At WDL-E/94E1/S2..... 95

Figure 2.3.26 (b). Median absolute phase difference between geophones G1 and G2 from WDL-E/94E1/S2..... 95

Figure 2.3.27 (a). A plot of Log_{10} median spectral ratio against frequency. Spectral ratios were calculated for 20 events taken in the earliest stage, 30 April and 1 May '97, after the backfill was placed for geophones G1 and G2 of WDL-E/94E1/S2 shown in Figure 2.3.24..... 96

Figure 2.3.27 (b). A plot of Log_{10} median spectral ratio against frequency. Spectral ratios were calculated for 20 events taken 20 days later, 19 May '97 when the backfill was more consolidated. The same set of geophones, WDL-E/94E1/S2, was used as in the Figure 2.3.27 (a)..... 97

Figure 2.3.28. Maximum velocities at WDL-E/94E1/S1, geophones G1 and G2..... 98

Figure 2.3.29. Maximum velocities at WDL-E/94E1/S1, geophones G1 and G2*..... 98

Figure 2.3.30. Maximum velocities at WDL-E/94E1/S2 geophones G1, G2 and G3..... 99

Figure 2.3.31. The geophones and black boxes location at Western Deep Levels - East Mine (WDL-E/93/E4)..... 100

Figure 2.3.32. The spectral ratios between Eben Haeser prop, the footwall and hangingwall for box 1 at WDL-E/93/E4..... 101

Figure 2.3.33. The spectral ratios between Eben Haeser prop, the footwall and hangingwall for box 2 at WDL-E/93/E4... 102

Figure 2.3.34. Absolute phase differences between Eben Haeser prop, the footwall and hangingwall at WDL-E/93/E4..... 102

Figure 2.3.35. The maximum velocities in [mm/s] at G1, G2 and G3 as a function of time at WDL-E/93/E4 box no.1..... 103

Figure 2.3.36. Layouts of the vertical accelerometers on the hangingwall at WDL-S/91/W5..... 105

Figure 2.3.37. A plot of median phase difference as a function of frequency for a layout shown in Figure 2.3.36 (site WDL-S/91/ W5)..... 105

Figure 2.3.38. Log_{10} amplitude ratio as a function of frequency for a layout shown in Figure 2.3.36 (site WDL-S/91/ W5)..... 106

Figure 2.3.39. Phase diagram showing limits to elastic behaviour..... 107

Figure 2.3.40. Log of ratio of motion due to deviation from elasticity to motion in perfectly elastic medium plotted against frequency..... 108

Figure 2.3.41. Cumulative number of events as a function of peak velocity for 71 panel-days..... 109

Figure 2.3.42. Accelerogram recorded at the time of the (rockfall) rockburst on 15 August 1995 at ERPM. Peak acceleration is equal to 184,8 m/s^2. The ground motion monitor was installed in the 32-level cross-cut..... 112

Figure 2.3.43. Plot illustrating measurements of acceleration before and after a peak in the velocity seismogram..... 113

Figure 2.3.44. A plot of V_0' as a function of V_0 for data from the Vaal Reefs. The identity line Y=X is shown for comparison..... 114

Figure 2.3.45. An example of ground motion recorded in solid rock (solid line) and recorded in footwall drive (dashed line)..... 120

Figure 2.3.46. Velocity spectrum recorded in solid rock (solid lines), and velocity spectrum recorded in footwall drive (dashed line)... 120

Figure 2.3.47. The transfer function defined by coefficients of A (q) and B (q) polynomials..... 121

Figure 2.3.48. Shear wave impinging on a softening contact: (a) contact between soft and very stiff media; (b) contact between two similar half-planes..... 125

Figure 2.3.49. Curve showing the contact interaction with softening modulus..... 127

Figure 3.3.1. Analysis of rockburst and rockfall fatalities in South African gold mines for the three year period 1994 to 1996 according to reef..... 139

Figure 3.3.2. Analysis of rockburst and rockfall fatalities in South African gold mines for the three year period 1994 to 1996 according to location..... 140

Figure 3.4.1. Increased effective unconfined height of remnant or pillar owing to a change in reef elevation..... 149

Figure 3.4.2. The possibility of shear slip between footwall strata with low cohesion may be increased by an unfavourable stress trajectory..... 152

Figure 3.4.3. Diagram showing conceptual mechanisms of excavation deformation as a function of support interaction with the rock mass. Within the South African gold mining environment the vertical virgin stress level is approximately twice that of the horizontal, and induced stresses are generally sub-vertical. Consequently the depth of failure within the sidewalls of the excavations is substantially greater than in the hangingwall or footwall. The tendons on the left hand side of the tunnel are anchored within the zone of instability, hence the entire sidewall is displaced inwards due to bulking of the unstable rock mass. A similar effect will be observed if the tendons snap or debond. In contrast, the tendons on the right hand side of the tunnel remain anchored in solid rock, hence the sidewall bulks between the tendons..... 155

Figure A.1. An example of real seismograms (event A7915), recorded in solid rock - solid line, and in a footwall drive - dashed line..... A-7

Figure A.2. Velocity spectrum of the seismograms from Figure A.1.7 A-7

Figure A.3. The coefficients of the polynomials A (q) and B (q) versus time..... A-9

Figure A.4 (a). The system response dominated by mode one..... A-10

Figure A.4 (b). The system response dominated by mode three..... A-10

Figure A.4 (c). The system response dominated by mode four..... A-11

Figure A.4 (d). The system response dominated by mode five..... A-11

Figure A.4 (e). The system response dominated by mode six..... A-12

Figure A.4 (f).	The system response dominated by mode seven.....	A-12
Figure A.4 (g).	The system response dominated by mode eight.....	A-13
Figure A.4 (h).	The system response dominated by mode fifteen.....	A-13
Figure A.5.	Sum of fifteen modal responses calculated at time of 0,0980 s.....	A-14
Figure A.6.	The spectrum of the seismograms from Figure A.5 and their transfer function.....	A-15
Figure A.7.	An example of real seismograms (event A7640), recorded in solid rock - solid line, and in a footwall drive - dashed line.....	A-16
Figure A.8.	Velocity spectrum of the seismograms from Figure A.7...	A-16
Figure A.9.	Sum of 15 modal responses calculated at time 0,098 s...	A-17
Figure A.10.	The spectrum of the seismograms from Figure A.9 and their transfer function.....	A-17
Figure A.11.	Sum of thirteen modal responses calculated at time 0,098 s.....	A-18
Figure A.12.	The spectrum of the seismograms from Figure A.11 and their transfer function.....	A-18
Figure A.13.	An example of real seismograms (event FG02), recorded in solid rock - solid line, and in a fractured rock - dashed line.....	A-20
Figure A.14.	Velocity spectrum of the seismograms from Figure A.13...	A-21

Figure A.15.	Sum of five modal responses calculated at time 0,153 s	A-21
Figure A.16.	The spectrum of the seismograms from Figure A.15 and their transfer function.....	A-22
Figure A.17.	An example of real seismograms (event FG04), recorded in solid rock - solid line, and in a fractured rock - dashed line.....	A-22
Figure A.18.	Velocity spectrum of the seismograms from Figure A.17...	A-23
Figure A.19 (a).	The system response dominated by mode one.....	A-23
Figure A.19 (b).	The system response dominated by mode two.....	A-24
Figure A.19 (c).	The system response dominated by mode three.....	A-24
Figure A. 19 (d).	The system response dominated by mode four.....	A-25
Figure A.19 (e).	The system response dominated by mode five.....	A-25
Figure A.20.	Sum of five modal responses calculated at time 0,153 s	A-26
Figure A.21.	The spectrum of the seismograms from Figure A.20 and their transfer function.....	A-26
Figure A.22.	An example of real seismograms (event FG07), recorded in solid rock - solid line, and in a fractured rock - dashed line.....	A-27
Figure A.23.	Velocity spectrum of the seismograms from Figure A.22	A-27
Figure A.24.	Sum of five modal responses calculated at time 0,153 s	A-28

Figure A.25. The spectrum of the seismograms from Figure A.24 and their transfer function..... A-28

Figure A.26. An example of real seismograms (event FG100), recorded in solid rock - solid line, and in a fractured rock - dashed line..... A-29

Figure A.27. Velocity spectrum of the seismograms from Figure A.26 A-29

Figure A.28. The coefficients of the polynomials A (q) and B (q) versus time..... A-30

Figure A.29 (a). The system response dominated by mode two..... A-30

Figure A.29 (b). The system response dominated by mode four..... A-31

Figure A.30. Sum of five modal responses calculated at time 0,153 s... A-31

Figure A.31. The spectrum of the seismograms from Figure A.30 and their transfer function..... A-32

Figure A.32. An example of real seismograms (event FG101), recorded in solid rock - solid line, and in a fractured rock - dashed line..... A-32

Figure A.33. Velocity spectrum of the seismograms from Figure A.32... A-33

Figure A.34. The coefficients of the polynomials A (q) and B (q) versus time..... A-33

Figure A.35. The sum of four modal responses calculated at time 0,153 s..... A-34

Figure A.36. The spectrum of the seismograms from Figure A.35 and their transfer function..... A-34

Figure A.37. The sum of four modal responses calculated at time 0,153 s..... A-35

Figure A.38. The spectrum of the seismograms from Figure A.37 and their transfer function..... A-35

Figure A.39. The sum of four modal responses calculated at time 0,153 s..... A-36

Figure A.40. The spectrum of the seismograms from Figure A.39 and their transfer function..... A-36

Figure A.41 (a). The system response dominated by mode one..... A-37

Figure A.41 (b). The system response dominated by mode two..... A-37

Figure A.41 (c). The system response dominated by mode three..... A-38

Figure A.42. The sum of three modal responses calculated at time 0,153 s..... A-38

Figure A.43. The spectrum of the seismograms from Figure A.32 and their transfer function..... A-39

Figure A.44. The sum of three modal responses calculated at time 0,153 s..... A-39

Figure A.45. The spectrum of the seismograms from Figure A.44 and their transfer function..... A-40

Figure A.46. The sum of four modal responses calculated at time 0,153 s..... A-43

Figure A.47. The spectrum of the seismograms from Figure A.46 and their transfer function..... A-44

Figure A.48. Sum of five modal responses calculated at time 0,153 s... A-44

Figure A.49. The spectrum of the seismograms from Figure A.48 and their transfer function..... A-45

Figure A.50. The coefficients of the polynomials A (q) and B (q) versus time..... A-45

Figure A.51 (a). The system response dominated by mode one..... A-46

Figure A.51 (b). The system response dominated by mode three..... A-46

Figure A.51 (c). The system response dominated by mode four..... A-47

Figure A.52. Sum of five modal responses calculated at time 0,153 s. A-47

Figure A.53. The spectrum of the seismograms from Figure A.52 and their transfer function..... A-48

Figure A.54. An example of real seismograms (event FG05), recorded in solid rock - solid line, and in a fractured rock - dashed line..... A-48

Figure A.55. Velocity spectrum of the seismograms from Figure A.54. A-49

Figure A.56. The coefficients of the polynomials A (q) and B (q) versus time..... A-49

Figure A.57 (a). The system response dominated by mode one..... A-50

Figure A.57 (b). The system response dominated by mode two..... A-50

Figure A.57 (c).	The system response dominated by mode three.....	A-51
Figure A.57 (d).	The system response dominated by mode four.....	A-51
Figure A.58.	Sum of four modal responses calculated at time 0,153 s.	A-52
Figure A.59.	The spectrum of the seismograms from Figure A.58 and their transfer function.....	A-52
Figure A.60.	An example of real seismograms (event FG100), recorded in solid rock - solid line, and in a fractured rock - dashed line.....	A-53
Figure A.61.	Velocity spectrum of the seismograms from Figure A.60...	A-53
Figure A.62.	Sum of five modal responses calculated at time 0,153 s....	A-54
Figure A.63.	The spectrum of the seismograms from Figure A.62 and their transfer function.....	A-54
Figure B.1 (a).	Map of Leeudoorn Gold Mine showing the sub-outcrop of the Booysens Shale Formations and the locations of the cross-sections used to construct the composite cross-section shown in Figure B.1 (b).....	B-3
Figure B.1 (b).	Composite geological cross-section of Leeudoorn Gold Mine. The VCR stope in which the accident occurred is situated about 80 m above the quartzite/shale contact.....	B-3
Figure B.2.	Map showing the site of the rockburst on 10 January 1994 damaging the 24-74 stope, Leeudoorn Gold Mine. Mined out areas are indicated by diagonal lines. Areas of active mining are cross-hatched.....	B-5

Figure B.3. Plan of the panels damaged by the rockburst, indicating rockburst damage and estimates of co-seismic closure..... B-6

Figure B.4. Plan showing stope support. Solid circles indicate the positions of the fatalities..... B-7

Figure B.5. Map of a portion of Deelkraal Gold Mine showing the site of the rockburst of 4 May 1994 and major geological features. Stoping in the 3 months preceding the accident is indicated by diagonal hatching. The 1 W up-dip working place where the fatalities occurred is 2294 m below the surface..... B-13

Figure B.6. Plan showing the support installed in the 21-3E VCR 1W up-dip working place at the time of the rockburst, and the extent of the fall of ground..... B-16

Figure B.7. Cross-section through the 21-3 E VCR 1 W Up-dip working place..... B-17

Figure B.8. Plan of the 21-3 E VCR stope showing the positions of observations made during the inspection of the rockburst site..... B-18

Figure B.9. Photo-mosaic showing the up-dip face where the fatalities occurred, viewed from position H (Figure B.8) and looking up-dip. The timber packs on the right are situated to the east of the roll. The corresponding section is shown in Figure B.7. The hangingwall fragmented during the rockburst. Most of the fallen rock was subsequently removed. Note the numerous fractures and joints in the face, and the smooth surface marking the parting above the collapsed brow..... B-19

Figure B.10. Rock ejected from the footwall and face between F and G (see Figure B.8) into the space between the original face position and the first dip line of packs. The photograph is taken looking up-dip with the face to the left. Note the intact hangingwall..... B-20

Figure B.11. Spatial distribution of all seismic events with ML=1 recorded at Deelkraal Gold Mine during the period 1984 to 1994. The size of the symbols is proportional to magnitude, the largest event in the area displayed having M_L=3,9..... B-22

Figure B.12 (a). Location of events with M_L=2 in relation to face positions in the areas of 29-21 and 33-21 longwalls. The horizontal error bars indicate location error. Negative distances indicate the back area..... B-24

Figure B.12 (b). Location of events with M_L=2 in relation to face positions in the areas of 25-15, 29-15 and 33-15 longwalls. Location error is indicated by the horizontal error bars. Negative distances indicate the back area..... B-25

Figure B.13. Plan showing the location of the rockburst at Western Deep Levels (Ltd) West Mine on 3 November 1994 damaging the 113-36 West 3 Carbon Leader panel..... B-31

Figure B.14. Stratigraphy of the Carbon Leader Reef (CLR) zone. The CLR forms part of the Main Conglomerate Formation close to the base of the Central Rand Group..... B-32

Figure B.15. Plan showing the support installed November in the 113 - 36 West 3 Carbon Leader panel and the extent of the fall of ground during the rockburst of 3 November 1994..... B-39

Figure B.16. Plan showing major fractures and joints in the 113-36 West 3 Carbon Leader panel (mapped by S. Reddy, Senior Geologist, Western Deep Levels (Ltd) West Mine) B-40

Figure B.17 (a). Plan and section showing seismicity for the period 1/1/94 to 3/11/94 in the vicinity of the 113-36 Carbon Leader longwall. Face positions as at June 1994. Data provided by A. G. Butler (Senior Seismologist, Western Deep Levels, West mine). Note the M_L=2,3 and M_L=2,6 events close to the position of the W3 panel, and the M_L=3,2 event close to the Tarentaal dyke..... B-44

Figure B.17 (b). Section from Figure B.17 (a) showing seismicity in the vicinity of the 113-36 Crbon Leader longwall..... B-45

Figure B.18. Schematic plan of 24 level tunnels, Orangia Shaft, Buffelsfontein Gold Mine, damaged by the M_L=3,4 rockburst on 4 July 1995..... B-50

Figure B.19. View north along 24-26 haulages east showing severe damage and deformation of the eastern sidewall of the tunnel. Note displacement of tracks (bottom right) and material rail car..... B-51

Figure B.20. Shear deformation of smooth bar rock bolt in upper east sidewall of 24-26 haulages east..... B-52

Figure B.21. Tensile failure of a smooth bar rock bolt in the immediate hangingwall of the 24-26 haulage east..... B-53

Figure B.22. View south along 24-26 haulages east showing collapse of hangingwall over an estimated height of 1,5 m to 2,0 m B-54

Figure B.23. View south along 24-26 haulage east at end of area of hangingwall collapse showing the highly fractured nature of the immediate hangingwall rock mass, and remaining rock bolt reinforcement..... B-55

Figure B.24. View north-west along 24-27 cross-cut showing large deformation of the south-west sidewall of the tunnel..... B-55

Figure B.25. Diagram showing conceptual mechanisms of excavation deformation as a function of support interaction with the rock mass. Within the South African gold mining environment the vertical virgin stress level is approximately twice that of the horizontal, and induced stresses are generally sub-vertical, the depth of failure within the sidewalls of the excavations is substantially greater than in the hangingwall or footwall. The tendons on the left hand side of the tunnel are anchored within the zone of instability, hence the entire sidewall is displaced inwards due to bulking of the unstable rock mass. A similar effect will be observed if the tendons snap or debond. In contrast, the tendons on the right hand side of the tunnel remain anchored in solid rock, hence the sidewall bulks between the tendons..... B-57

Figure B.26. Plan showing the location of the rockfalls at ERPM on 24 July and 15 August 1995 damaging the Hercules secondary incline shaft between 32- and 33-level..... B-62

Figure B.27. Diagram showing the interpreted mechanism of the rockbursts on 24 July and 15 August 1995 damaging the Hercules secondary incline shaft between 32- and 33-level..... B-68

Figure B.28. Plan showing damage to tunnels serving No. 4 Shaft, East Driefontein Gold Mine, by a M_L=3,6 seismic event on 14 September 1995. The locations of all seismic events with M_L>2 which occurred in the preceding two year period are shown. Falls of ground (FOG) and damaged sections of tunnels are indicated by shading..... B-71

Figure B.29. Damage to 34K footwall drive at Site A showing falls of ground between grouted shepherd's crook rebars. Mesh and lacing had not yet been installed in this section of the tunnel. In this area the south-western (right hand) side of the drive was most severely damaged. The view is taken looking to the south-east, away from the shaft..... B-77

Figure B.30. Damage to 34 K footwall drive at Site B showing complete closure of the tunnel..... B-78

Figure B.31. A haulage on 34 level showing the effect of the support system on damage. The section of the tunnel in the foreground was supported only by grouted rebars, and significant damage was sustained. The support system in the section of the tunnel beyond the miner consisted of grouted rebars, mesh, lacing and shotcrete. Damage was negligible..... B-79

Figure B.32. Kinked shepherd's crook rebar observed in the hangingwall of the 34K footwall drive between Sites B and C. Some bars had been sheared by the movement along bedding planes..... B-80

Figure B.33. Plan showing the location of the rockburst at Western Deep Levels South Mine on 18 September 1995 damaging the 84-61 West 4 VCR panel..... B-87

Figure B.34. Plan showing the extent of the damage to the 84-61 West 4 VCR panel caused by the rockburst of 18 September 1995. Open squares show the approximate position of packs. AB is the section line along which Figure B.36 is drawn. Scale 1:500..... B-88

Figure B.35. Plan showing the seismicity (events with M>1) in the vicinity of the 84-61 West longwall for the period 1 August - 18 September 1995. The approximate face position on 18 September is indicated with a dashed line. Data provided by F. Naude (Senior Seismologist, Western Deep Levels, South Mine)..... B-96

Figure B.36. Diagram showing the interpreted mechanism of the rockburst at Western Deep Levels South Mine on 18 September 1995 damaging the 84-61 West longwall. The position of the section line AB is shown on Figure B.34... B-97

Figure B.37. Plan of the 17-24W stope, Blyvooruitzicht Gold Mine, showing the layout of the panels being mined at the time of the M_L=2,2 rockburst on 30 January 1996. The position of the research seismic network monitoring the preconditioning experiment at the site is also shown (black squares indicate the geophone positions: triaxial sites are labelled e.g. P2ijk; uniaxial sites are labelled e.g. P1+). Face position as at 31 December 1995..... B-100

Figure B.38 (a, b). Orientations of the six major fracture sets (Groups I to VI) identified at the 17-24 W site. (a) Plan showing the orientations with respect to the pillar geometry. (b) Contoured Schmidt Net (lower hemisphere projection) of poles to all mapped fractures..... B-102

Figure B.39. Schematic vertical section through a deep-level stope illustrating the fractured nature of the rock mass surrounding the opening..... B-103

Figure B.40. Preconditioning layout in an overhand mining sequence. Panel 2 has been mined to limit and the next hole is drilled up to 5,5 m from the current face..... B-105

Figure B.41. Conceptual diagram showing the effects of positioning an 89 mm diameter preconditioning hole within the fractured rock mass ahead of the stope face..... B-106

Figure B.42. Sketch plan of the lower portion of the pillar showing the orientation and position of the two major fracture sets that controlled size of the fall of ground. Note that the lower gulley is positioned within the zone of intense pillar parallel fractures..... B-108

Figure B.43. Plan and sections showing the damage caused by the rockburst on 30 January 1996 to the Panel 2 strike gully in the 17-24 W stabilizing pillar, Blyvooruitzicht Gold Mine: Prepared by L. Schultz and H. Redelinghuys, Blyvooruitzicht Gold Mine..... B-111

Figure B.44 (a). Photograph showing a rockburst damage in a Carbon Leader Reef gully..... B-112

Figure B.44 (b). Sketch diagram showing the possible mechanism of rockburst damage to a Carbon Leader Reef gully: 1) Situation prior to damage, note the region of intense pillar parallel fractures (dark shading); 2) Slip on the Green Bar (direction is shown by arrows) causes buckling and underthrusting of the Green Bar. The underthrusting causes fallout of the hangingwall quartzite below the Green Bar; 3) Continued thrusting and buckling causes extensive falls of both hangingwall quartzite and Green Bar..... B-113

Figure B.45. Plan showing the locations, as determined from the research seismic network records, of the M_L=2,2 and M_L=2,3 seismic events which occurred on 30 January 1996 damaging the 17-24 W stope, Blyvooruitzicht Gold Mine..... B-120

Figure B.46. Schematic plan of West 2 (Diagonal) Panel (Not to scale). B-123

Figure B.47 (a). Convergence-ride measurements at West 2 (Diagonal) Panel at station 2WE00K..... B-128

Figure B.47 (b). Convergence-ride measurements at West 2 (Diagonal) Panel at station 3WW00J..... B-128

Figure B.48 (a). Convergence-ride measurements at West 3 (Diagonal) Panel at station 2WE00K..... B-129

Figure B.48 (b). Convergence-ride measurements at West 3 (Diagonal) Panel at station 3WW00J..... B-129

Figure B.49. Plan of WDLS 87-49 stope, showing the location of the rockburst seismic event (star) as determined from the PSS recording. The ellipse around the star indicates the possible source region as given by the Brune model of the seismic source, assuming slip on a steeply dipping plane oriented parallel to the large seismically induced shear zones observed underground. The positions of the PSS recording sites are shown by the labelled squares..... B-131

Figure B.50. Plan showing the 34-19 Carbon Leader stope, No. 1 Shaft, East Driefontein Gold Mine, damaged by a M_L=2,7 rockburst on 5 June 1996..... B-137

Figure B.51. A Rocprop observed in the 2 W panel of the 34-19 Carbon Leader stope showing a barrel that had split as a result of closure..... B-139

Figure B.52. A Rocprop showing a headboard that had failed so that the prop was exerting a point load on the hangingwall..... B-140

Figure B.53. Plan showing the stoping layout and epicentre of the M_L=3,0 seismic event which occurred on 18 November 1996 damaging the 115 W1 lower strike gully, Western Deep Levels East Mine. Areas which sustained rockburst damage are shaded..... B-148

Figure B.54. Tilting of the headboard and cap of a Madoda prop..... B-152

Figure B.55. Plan showing the epicentre of the M_L=4,0 seismic event which occurred on 10 February 1996, damaging the haulages on 50-50 and 62 levels, No. 5 Shaft, Vaal Reefs Gold Mine. Major geological structures and the location of 19 other events with $M_L \geq 3,9$ occurring since 1972 are also shown..... B-158

Figure B.56. Plan showing tunnels damaged by the M_L=4,0 seismic event which occurred on 10 February 1996, No. 5 Shaft, Vaal Reefs Gold Mine..... B-160

Figure B.57. Cross-section of seismic event area where mining is approaching the fault from both sides..... B-168

Figure B.58. Slip profile on the fault..... B-169

Figure B.59. Regional mining plan showing the stoping layout in the vicinity of the 35 Level 78 Line, Leeudoorn Division of Kloof Gold Mine, which experienced damage due to a M_L=1,7 seismic event on 10 April 1997 and a M_L=2,3 seismic event on 16 April 1997..... B-178

Figure B.60. Local mining plan showing the locations of the M_L=1,7 seismic event on 10 April 1997 and a M_L=2,3 seismic event on 16 April 1997 and the distribution of damage in the 35/78 VCR stope, Leeudoorn Division of Kloof Gold Mine. The stoped out area of the VCR and the sub-cropping Kloof reef are shown by vertical and horizontal hatching, respectively..... B-179

Figure B.61. Possible source mechanism of face burst due to lava in face, and high face dimension..... B-182

Figure B.62. Possible seismic mechanism due to relative position of Kloof reef under-mining..... B-183

Figure B.63. Proposed mechanism of footwall shear due to unconformable footwall stratigraphy (north-south section, up dip view)..... B-184

Figure B.64. Plan showing the location of the M_L=2,7 seismic event which occurred at 22h32 on 17 April 1997, Section 336 Western Deep Levels East Mine..... B-187

Figure B.65. Plan showing the location of the M_L=2,7 seismic event which caused damage to the 106/E1 gully along a stabilising pillar, Section 336 Western Deep Levels East Mine..... B-188

Figure B.66. Section of a stope and stabilising pillar that has failed. Horizontal dilation of the rock in the vicinity of the shear plane causes buckling and collapse of hangingwall above the gully..... B-190

Figure B.67. Plan showing the stoping layout and epicentre of the M_L=2,7 seismic events which occurred on 23 May 1997 damaging the 36-35 C/L West mini-longwall, West Driefontein Gold Mine..... B-193

Figure B.68. Stope and gully support standard for West Driefontein No. 6 Shaft..... B-195

Figure B.69. View towards the west of the fall of ground in the 3 W strike gully, 36-35 C/L west mini-longwall, West Driefontein No. 6 shaft..... B-199

Figure B.70. Schematic plan of tunnel and stoping layout, East Driefontein No. 4 Sub-vertical Shaft, and the distribution of damage caused by the M_L=4,4 event on 25 September 1997 and inspected during the investigation..... B-205

Figure B.71. Schematic section of shaft layout and major fault planes with distribution of damage..... B-206

Figure B.72. View of south sidewall of 38 level pump chamber showing distribution of fracturing within the sidewall rock mass at the junction of the pump chamber and dam access excavations..... B-207

Figure B.73. View west along 38 level deep footwall drive showing large scale bulking of the rock mass, particularly of the lower north sidewall..... B-210

Figure B.74. View east along 38 level deep footwall drive of south sidewall showing more uniform containment and deformation of the sidewall rock mass with isolated areas of mesh failure..... B-211

Figure B.75. View south-west along 42 level haulage showing highly fractured nature of the rock mass, footwall heave of approximately 1,5 m, bulk sidewall deformation (bottom right) and failure of mesh and lacing in upper portions of excavation..... B-214

Figure B.76. View north east along 42 level haulage showing failure of rock bolt reinforcement (left) and thus loss of fabric anchorage (right) and collapse of approximately 1,5 m of fractured sidewall rock mass..... B-215

Figure B.77. Bulking of fractured sidewall rock mass between rock bolt reinforcement and lacing within 42 level haulage..... B-216

List of tables

		Page
Table 2.1.1.	Suggested relationship between peak ground velocity and seismic moment.....	48
Table 2.2.1.	Specifications of the CSIR Ground Motion Monitor.....	51
Table 2.3.1.	Spatial configurations of the recorded geophones and number of events.....	76
Table 3.3.1.	Rockburst and Rockfall investigations conducted during the period 1 January 1994 to 30 September 1997.....	141
Table A.1.	Modal frequencies and damping ratios obtained at the end of the seismogram for all five pairs of seismograms.....	A-19
Table A.2.	The data recorded in May 1997.....	A-41
Table A.3.	The data recorded in June 1997.....	A-42
Table A.4.	Modal frequencies for five pairs of seismograms.....	A-43
Table B.1.	Dyke mineralogy determined by thin section petrography	B-32
Table B.2.	Uniaxial compressive strength determined by point load tests.....	B-33
Table B.3.	Source Parameters.....	B-46
Table B.4.	Results of in situ Stress Measurements.....	B-73
Table B.5.	Summary of ESS Results (MPa) for Three Benchmark Sheets.....	B-81

Table B.6. Source parameters of the seismic event, which damaged the 84-61 West longwall..... B-96

Table B.7. Source parameters of the seismic event which damaged the 34-19 Carbon Leader stope..... B-147

Table B.8. Source parameters..... B-177

Table B.9. Source parameters..... B-205

1. Introduction

1.1 The rockburst problem

Rockbursts are a major hazard in South African deep-level gold mines. For example, an average of 64 workers per annum were fatally injured by rockbursts between 1994 and 1996, and many more sustained serious injuries.

The severity of damage owing to a seismic event often varies greatly over small distances. One panel in a longwall may be severely damaged, while an adjacent panel (perhaps even closer to the focus of the seismic event) is unscathed. The vast majority of casualties are owing to the ejection or fall of slabs less than 1,6 m in thickness (Roberts, 1995). While it is the failure of this skin, usually a few tens of centimetres to two metres in thickness, that damages the excavation and causes injury to workers, the dynamic behaviour of the fractured skin of an excavation (such as a stope or tunnel) when subjected to a seismic wave is poorly understood. Support systems are intended to prevent the disintegration and collapse of the fractured rock mass surrounding excavations following a seismic event, but sometimes fail to do so with tragic consequences.

The chief objective of this SIMRAC project (GAP201: Improvement of worker safety through the investigation of the site response to rockbursts) is to discover the reasons for this variation in the severity of damage. It is believed that a detailed understanding of both the source and damage mechanisms, and the application of this knowledge to the design and support of excavations, will lead to a reduction in the hazard posed by rockbursts.

1.2 The site response

It is important to distinguish between the terms rockburst source mechanism, rockburst damage mechanism, and site response. The source mechanism refers to phenomena associated with the failure of the rocks, often at a pre-existing weakness such as a fault or

dyke, which releases seismic energy. When the seismic waves radiated by the source interact with an excavation, the motion of the skin may vary greatly due to numerous factors such as the geometry of the cavity, effect of support systems, and the degree of fracturing. This variability is termed the *site response*. In situations where the hanging or sidewall collapses or the face bursts, the term rockburst *damage mechanism* is used to refer to these phenomena. It is believed that an understanding of site response will enable areas, which have a high potential for sustaining rockburst damage to be identified, and provide design criteria for support systems. In some cases part of the excavations lies within the near filed of seismic source and so the source and the damage mechanism can not be really separated.

The current level of understanding of seismic site effects was summarized by several speakers at the *Third International Symposium on Rockbursts and Seismicity in Mines*, held in Kingston, Canada. McGarr (1993) reiterated a statement made a decade earlier by Ortlepp (1984): "The design and selection of materials for various support components, such as rockbolts and grouted steel tendons, and for hydraulic props in stopes, would be improved if quantitative measurements were made of the velocity and acceleration of the damaged rock surfaces, particularly in the vicinity of large seismic sources. Unfortunately, even today, almost no strong ground motion data exists from the immediate vicinity of a large source". Jesenak et al. (1993) commented: "Many investigators have developed direct relationships between damage levels and ground motion parameters. However, difficulties resulting from highly subjective assessment criteria and incomplete or questionable peak ground motion data severely limit the applicability of these relationships. This limitation will only be overcome when high quality strong ground motion data has been collected and properly analysed".

1.3 Project outputs

The primary output of the project is a set of observations and measurements of the site response to rockbursts which will ultimately be used to reduce the rockburst hazard through the improved design of support systems and excavations.

Other outputs include:

- Measurements of the dynamic behaviour (acceleration, velocity, displacement, duration of shaking, dominant frequency) of the fractured rock surrounding an excavation. These measurements will provide design criteria for support elements such as props and tendons. They may also be used to validate and calibrate computer programs developed to model the dynamic response of the rock mass.
- Observations and analysis of rockfalls and rockbursts to determine the influence of geotechnical characteristics (e.g. composition of hanging- and footwall, faults, dykes, joints, fractures etc.), mining method (layout, sequencing etc.), and support systems (pillars, packs, props, bolts, backfill, etc.) on the damage that is sustained.
- A methodology for assessing the damage caused by rockbursts.
- The findings of this project will contribute to a revision of *An Industry Guide to Methods of Amelioration of the Hazards of Rockfalls and Rockbursts* (COMRO, 1988), to be published in 1998.

1.4 Methodology

The project had two main components:

1. The first, involved quantitative measurements and analysis of the site response at a variety of sites including both tunnels and stopes, and different reefs, rock mass conditions, and support systems. The fractured skin is that part of the rock which props, packs and bolts seek to support. Prior to this project, few reliable measurements of the motions and forces that should be resisted by support elements existed, and models of the mechanisms of rockburst damage were largely conjectural. This lack of information is primarily owing to the difficulties of operating seismographs in an environment where drilling, blasting and cleaning of the face is taking place. In all existing mine seismic networks the transducers are installed in boreholes drilled deeply

into the rocks in order to eliminate the influence of the excavation and the fractured skin on the measurements. To overcome this problem a robust, inexpensive and compact seismograph was designed and built by engineers at CSIR: Mining Technology. This device is known informally as the black box, it is designed to survive a catastrophic failure of an excavation and provide a record of events.

2. The second component involved detailed and comprehensive investigations of rockbursts when and wherever opportunities arose. The investigation by a team of specialists typically encompassed an assessment of the source and damage mechanisms, layout, and support performance. The service was advertised to mine management. It was envisaged that three investigations would be conducted in 1995, and five each in succeeding years. It transpired that 23 investigations (including a few carried out under contract to mines) were conducted during the period 1996-1997. Several investigations carried out in 1994 prior to the SIMRAC project, and sponsored by the CSIR, have been included in the body of work.

1.5 Structure of report

The quantitative measurement and analysis of the site response is described in Section 2 and Appendix A of this report. The rockburst investigations are described in Section 3 and Appendix B. General conclusions and recommendations are contained in Section 4.

2. Quantitative measurements of the site response

2.1. Review of related work

Rockbursts are a serious hazard in the deep gold mines of South Africa. The vast majority of rockburst casualties are owing to the ejection or fall of slabs less than 1,6 metres in thickness (Roberts, 1995). Support systems are intended to prevent the disintegration and collapse of the fractured rock mass surrounding excavations when shaken by a seismic event, but sometimes fail to do so with tragic consequences. Quantitative measurements

of the velocity and acceleration of the rock surfaces and the frequency and duration of the shaking, particularly in the proximity of large seismic sources, are required for the design of support systems. In this report measurements of the motion of the hangingwall of stopes caused by nearby seismic events are discussed. In particular variations in ground motion at points about 1 m apart are considered in order to study local site effects, and the phase velocity is estimated. It is proposed that the phase velocity could be used as an indicator of hangingwall quality.

A simple model of support requirements under rockburst conditions was developed by Wagner (1984) using the following relationship from McGarr et al. (1981), which describes the peak ground velocity caused by mine tremors :

$$\log RV_{max} = 0{,}57\ M_L - 0{,}05 \qquad (2.1)$$

where M_L is the local magnitude of the event; R is the hypocentral distance and the scaled peak velocity; RV_{max} , is in m^2/s.

Wagner (1984) compared the distribution of damage caused by several rockbursts with the peak ground velocity predicted by the formula. Very little damage was reported where the peak ground velocity was predicted to be less than 1 m/s, while damage was severe where velocities greater than 2 m/s were predicted. Wagner (1984) concluded that support systems should have the following characteristics to provide adequate protection under rockburst conditions:

1. The support elements must be capable of yielding at closure rates in excess of 2 m/s.
2. The support system must be capable of accommodating rock wall displacements of not less than 400 mm in stopes and 60 mm in tunnels.
3. The support system must have a minimum support resistance of 200 kN/m^2 in stopes and 100 kN/m^2 in tunnels.
4. The ability of the support system to do work against the dynamic rock movement during a rockburst is as important as its load-bearing capacity.
5. The support system must be able to maintain the integrity of the surrounding rock mass during the entire yield process.

Following this study, two new support elements for rockburst conditions were developed by the Research Organisation of the Chamber of Mines of South Africa (COMRO): a light-weight hydraulic prop with load spreader capable of yielding at 3 m/s, and a yielding tendon called a cone bolt (Jager, 1992).

Table 2.1.1

Suggested relationship between peak ground velocity and seismic moment.

Confidence limit	Stress drop	Recommended relationship : log Rv_{max} =
50 %	≤ 5 MPa	0.5 log M_0 -1.0
90-95 %	< 2.5 MPa	0.5 log M_0 -0.6

Table 2.1.1. Represents suggested relationships between peak ground velocity and seismic moment, from Kaiser and Maloney (1996), where M_0 has the units of GN-m and the peak velocity parameter RV_{max} has the units of m^2/s.

Kaiser and Maloney (1996) pointed out that a magnitude-ground velocity relationship providing only an average fit to the data is not suitable for the design of support, as there will be many cases where the ground velocity predicted by the relationship is exceeded. Following a world-wide review of data from rockburst prone mines, Kaiser and Maloney (1996) recommended that the relationships in Table 2.1.1 should be used to estimate the maximum ground velocity. These relationships were chosen at the 90-95-percentile level: 5-10 percent of all their events exceeded this relationship.

This is a more conservative, or higher, value than the conventional least squares or median (50 percentile) fit. It is important to note that the relationships derived by McGarr et al. (1981) and Kaiser and Maloney (1996) are based on measurements made by transducers embedded in solid rock. The effects of the excavation and the fractured rock around it are not taken into account, as well as the relative motion of the hangingwall and footwall.

Measurements of the ground velocity produced by four seismic events on the sidewall of a tunnel in a South African gold mine were compared with the velocities predicted by the empirical relationships (Gibbon et al., 1987). The local magnitudes of the events ranged from 1,9 to 2,5, and the hypocentral distances ranged from 70 to 204 metres. The ratios of the measured velocity to the predicted velocity were 6,9, 1,8, 4,7 and 1,9.

As part of a study of the effect of backfill on the transmission of seismic energy, Spottiswoode and Churcher (1988) placed geophones 10 m from the face on the hangingwall and footwall of a longwall stope in which packs were used as support. The peak velocity of 350 well-located events recorded in the stope exceeded the predicted peak velocity (for a sensor in solid rock) by a factor of about 2,5. Adams et al. (1990) report similar amplifications. In another study of the effect of backfill on ground motion in a stope, Hemp and Goldbach (1993) found that the ground motion recorded in the stope is considerably higher than that recorded off-reef (in the solid rock). The median value of amplification of in-stope to off-reef ground velocities (corrected for distance) for the filled areas was 5,3, while the value for the unfilled areas was 9,9.

The main reason for the lack of data describing the dynamic response of the skin of an excavation to a seismic event is probably the difficulty of operating seismographs in environments where drilling, blasting and removal of the ore is taking place and conditions of high humidity and temperature prevail. Experience has shown that external cables (for power or data transmission) are prone to damage. Consequently, an ideal monitor should be self-contained and battery powered with low power consumption in order to minimize the frequency of visits to change batteries. It is also desirable that the instrument be relatively cheap, as it is likely that some instruments will be damaged or destroyed during rockbursts.

As no suitable seismograph was commercially available, the CSIR developed a robust ground motion monitor for use in stopes. The first results obtained using the CSIR Ground Motion Monitor (black box) were described by Durrheim et al. (1996). Recordings of 146 seismic events by monitors installed in a stope, tunnel and cross-cut at a pillar extraction site at Blyvooruitzicht Gold Mine indicate a 4 - 10 fold magnification of the maximum ground velocities.

2.2 Research methodology

2.2.1 Instrumentation

At the beginning of 1995 a new design of black box using externally mounted transducers was introduced. A set of three mutually perpendicular piezoelectric transducers is mounted inside a cylindrical aluminium boat, whose dimensions are 70 mm long and 65 mm in diameter. A typical installation is shown in Figure 2.2.1.

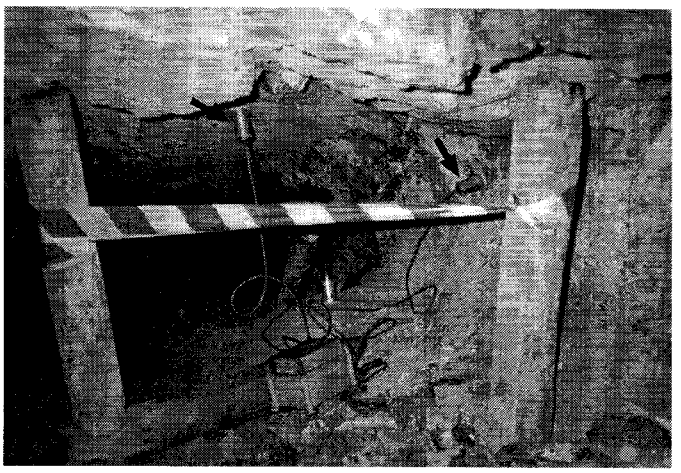

Figure 2.2.1 CSIR Ground Motion Monitor with accelerometers (indicated by arrows) attached to the stope face, and the hanging- and footwall.

The specifications of the CSIR Ground Motion Monitor are summarised in Table 2.2.1.

Table 2.2.1

Specifications of the CSIR Ground Motion Monitor

Dimensions:	140 mm x 185 mm x 155 mm
Transducers:	Atochem® piezo film accelerometers
Range:	0,2 g - 100 g
Sampling rate:	3 kHz - 5 kHz
Filter:	Anti-alias filter, 3 dB down at 1 kHz.
Record length:	User definable, typically 512 samples giving a 170 ms record at 3 kHz.
Trigger:	STA/LTA method.
Memory:	256 kb of waveform memory, typically holding 84 3-component accelerograms, each 512 samples in length.
Power:	4 D size alkaline cells provide power for about 21 days. The memory has its own battery backup.
Comms:	The Ground Motion Monitor is configured and data down-loaded using ProComm Plus® *via* a RS232 serial interface.

Typical acceleration seismograms recorded in the stopes are shown in Figure 2.2.2.

Figure 2.2.3 is velocity seismogram obtained by integrating Figure 2.2.2. It was found that integrating black box acceleration seismograms introduced an artificially low frequency signal. Therefore high-pass filtering was used to remove this artefact.

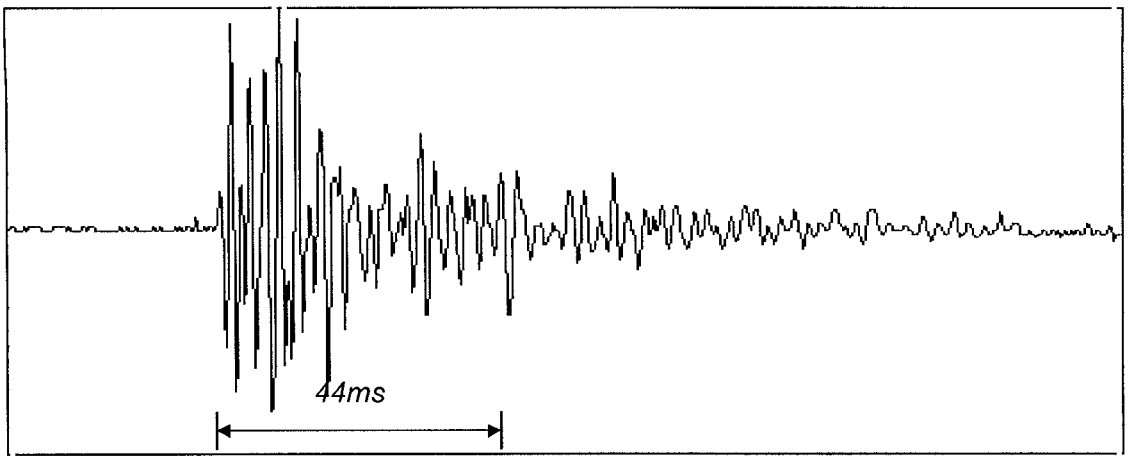

Figure 2.2.2 Acceleration seismogram recorded by the CSIR Ground Motion Monitor. Peak acceleration is equal to 5,07 m/s^2.

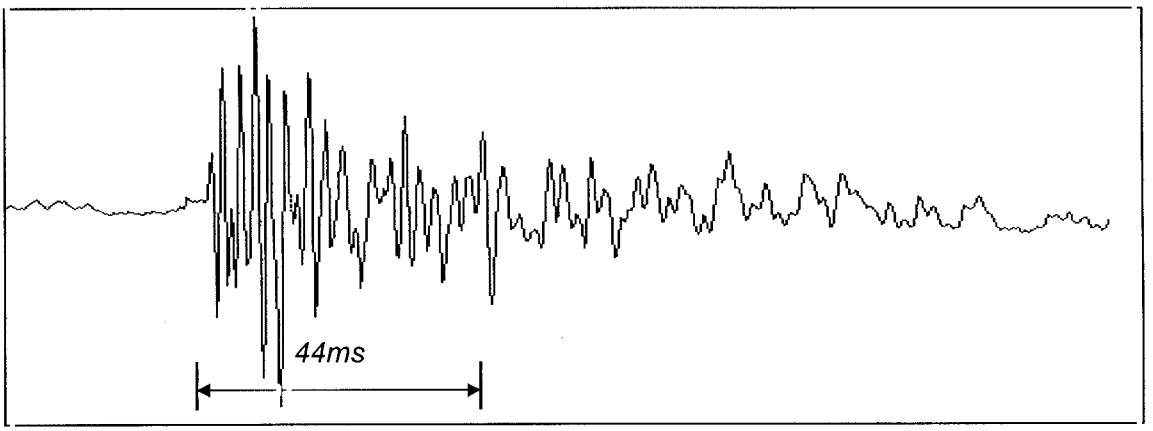

Figure 2.2.3 Velocity seismogram resulting from integration of the accelerograms in Figure 2.2.2. Data were high-pass filtered to remove low frequency effect caused by integration.

Typical velocity spectra for vertical and two horizontal components are shown in Figure 2.2.4. These are not spectra of seismograms shown in Figures 2.2.2 and 2.2.3, but they show general characteristics of many black box spectra studied here. An increase in energy at frequencies below 100 Hz can be seen. This is thought to be due to recording artefact instead of the true site response. A peak, believed to be resonance, is observed

around 500 Hz and this is followed by a sharp decay between 800 Hz and 1000 Hz. This decay is to a large extent owing to an anti-aliasing filter at 1000 Hz. The filter tapers off before 1000 Hz.

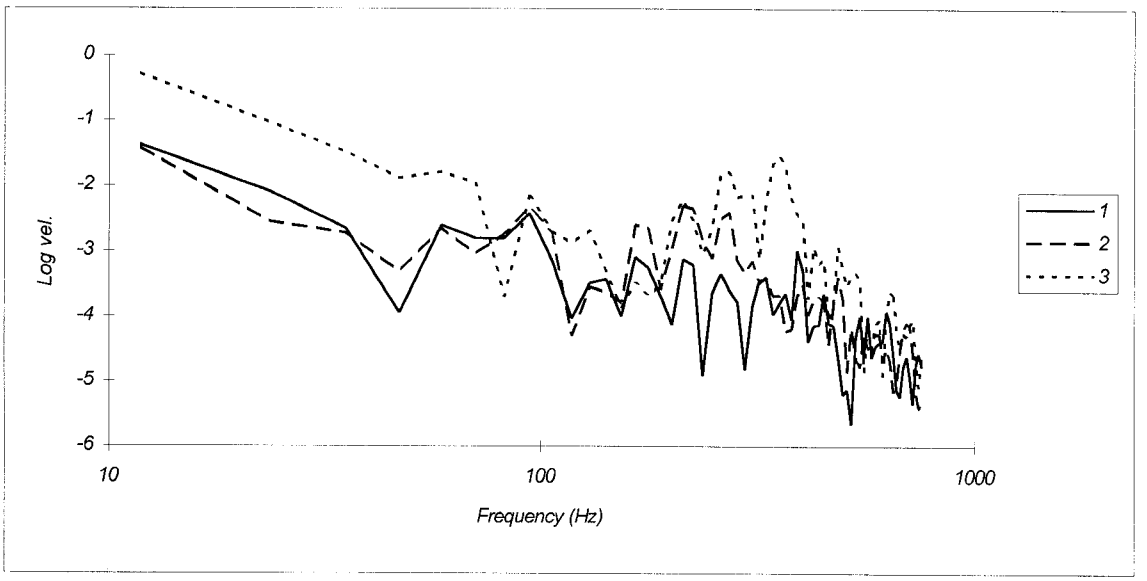

Figure 2.2.4 Typical velocity spectra of three seismograms recorded on the hanging wall. Seismograms 1 and 2 are horizontal components while 3 is the vertical component.

Around mid 1996 three uniaxial transducers recording vertical motion at three different points replaced triaxial transducers. This configuration was initially used with accelerometers, which were later replaced by geophones to give a direct measure of ground velocity. The use of three uniaxial transducers allowed for comparison of motion at any three points in the stope during the seismic impact. The length of the cables connecting the sensors limits distance between sensors and a box from several centimetres to several metres.

In 1997 a new generation of back box, with eight channels, the "Octobox", was developed. This box combines all the useful features of the existing models e.g. portability, independent power supply, external transducers, easy installation and operation, and the following improvements:

(i) eight recording channels, instead of three in the previous model

(ii) expanded memory; standard 2Mb (255 events x 8 ch.), upgraded 4Mb (510 events x 8 ch.) instead of 256 Kb (84 events x 3 ch.) in the previous model

(iii) a graceful decline, entitled a quality control in the overwriting mode

(iv) improved sensitivity

(v) over damped channel working in a low gain, reserved for very strong events only

At this stage the box has been developed and tested on surface. Underground testing and further exploration are ongoing process.

2.2.2. List of Analysis techniques used

The site response to rockburst is a complicated process taking place on the skin of the excavation. To study this phenomenon various techniques have to be considered. In this work the problem is approached in two ways. Firstly, by investigating the seismic waves recorded in solid and fractured rock in frequency and time domains. Secondly by investigating the dynamic behaviour of the hangingwall and the different support systems during the seismic event. During these investigations new theories were developed to explain the amplification of the seismic signal on the skin of the excavations, and to characterised the dynamic behaviour of the hangingwall and support interaction.

In this section each of these techniques is listed. The full description is provided in Section 2.3 followed by experimental analysis of real seismic data recorded at Blyvooruitzicht Gold Mine, Western Deep Levels East and South Mines, East Rand Proprietary Mine and Vaal Reefs.

1. Peak velocity and acceleration parameters, frequency spectra in tunnels, cross-cut and stopes.
2. Time domain analysis of tunnel sidewall motion.
3. Spectral analysis to quantify the influence of fracturing and support on the dynamic behaviour of the hangingwall.

4. Transfer function for seismic signals recorded in solid rock and on the skin of excavations.
5. Velocity amplification considered as a phenomenon of elastic energy release owing to softening.

2.3 Site response measurements and analysis

2.3.1 Peak velocity and acceleration parameters, frequency spectra in tunnels, cross-cut and stopes

Measurement of the strong ground motion produced by a rockburst is subject to two main difficulties. Firstly, it is necessary to predict when and where a seismic event is likely to happen in order to record the near-source ground motion within a reasonable time period. Secondly, special instruments are required to make measurements within a stope where mining is taking place. A robust ground motion monitor was developed by the CSIR to perform this function.

Research site

Measurements were made at a preconditioning research site on Blyvooruitzicht Gold Mine (Kullmann et al, 1996) where a stabilizing pillar is currently being mined 1900 metres below surface. The Carbon Leader Reef was largely mined out during the 1970's, except for 40 metre broad strike-parallel stabilizing pillars. Total closure of the old stope has since occurred, relieving the stress sufficiently for the stabilizing pillar to be extracted. Nevertheless, the rockburst hazard is considered to be high, and preconditioning is being implemented in order to reduce the hazard of face bursts. Accelerographs were installed in a footwall drive, cross-cut and stope (see Figure 2.3.1).

A Portable Seismic System or PSS (Pattrick et al, 1990) is used to monitor the seismicity associated with the preconditioning and mining of the pillar, and to determine the source parameters of the seismic events. A sampling rate of 10 kHz and record length of 2046

samples are used at this site. The geophones are grouted in boreholes drilled 10 metres or more into the solid rock. All seismic events which occur within the network and have local magnitudes greater than –1,8 are detected. An accuracy of ± 5 metres has been verified through the location of blasts.

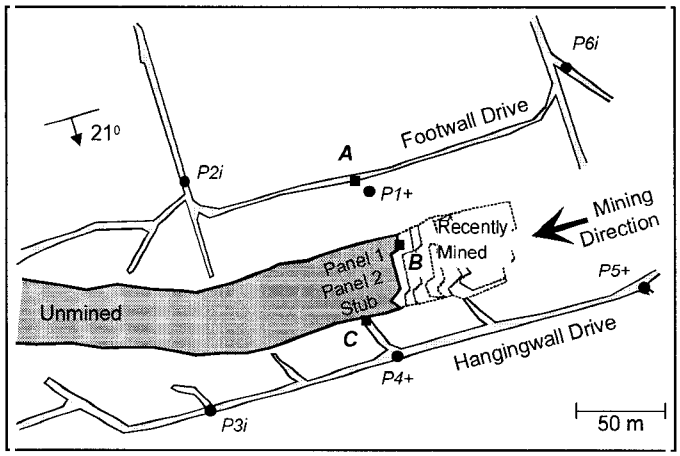

Figure 2.3.1 Deployment of PSS geophones (P1-P6) and CSIR Ground Motion Monitors (A, B and C) at the 17-24W Preconditioning Site, Blyvooruitzicht Gold Mine.

Results

The ground motions produced by preconditioning blasts and any subsequent seismic events were recorded by the PSS. The CSIR Ground Motion Monitors were configured to trigger at accelerations greater than 1 g. During a two month period (mid-November 1994 to mid-January 1995), 147 seismic events were recorded by both the PSS and at least one Ground Motion Monitor. The local magnitudes of these events ranged from –1,9 to 1,8.

Analysis

The accelerogram recorded by a Ground Motion Monitor attached to the wall of an excavation is the convolution of the source function, the effect of the ray path, the site effect and the instrument response. In order to determine the site effect from the recorded accelerogram, the other three factors must be estimated.

1. The source parameters (seismic moment, corner frequency) were obtained from the PSS recordings. A theoretical source spectrum was calculated using the Brune model (Spottiswoode, 1993).

2. The ray paths were less than 50 metres for all the events used in this analysis, and it was found that attenuation along the ray path was negligible for frequencies below 1 kHz.

3. The instrument response was determined by calibration on a shake table. Tests were carried out at frequencies ranging from 12 Hz to 1024 Hz. The amplitude response was found to be essentially flat.

Peak velocity and peak acceleration parameters

An initial estimate of the site effect was made by comparing measurements of the peak velocity parameter (Rv_{max} where R is the hypocentral distance) and peak acceleration parameter (ρRa_{max} where ρ is the density) made in the solid rock with measurements made on the wall of the excavation. The distance between the hypocentres and Ground Motion Monitors ranged from 20 to 50 metres.

The peak velocity parameter results for the footwall drive, stope and cross-cut are shown in Figures 2.3.3 (*a*), 2.3.3 (*b*) and 2.3.3 (*c*) respectively. When compared to the PSS recordings within the solid rock, an amplification of v_{max} on the wall of the excavation by 4 to 10-fold is indicated. Furthermore, each site appears to have a different site response.

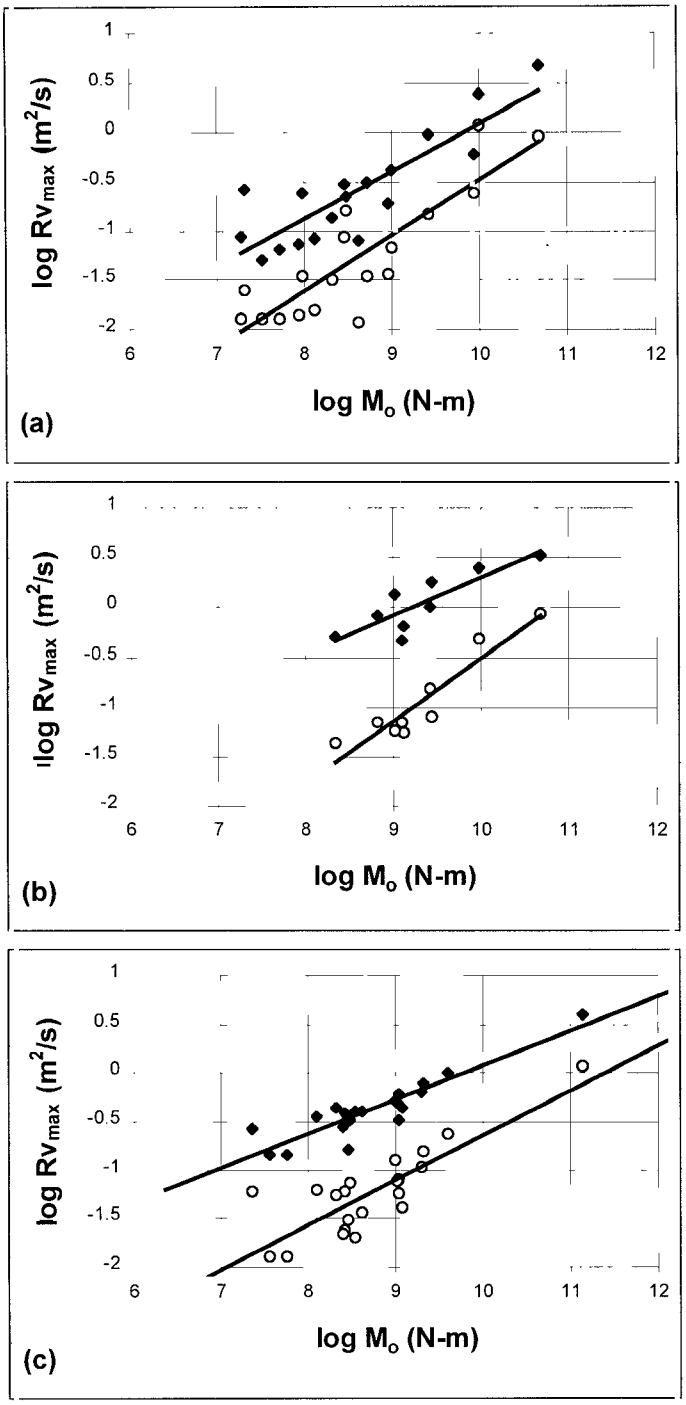

Figure 2.3.2 Measurement of the peak velocity parameter Rv_{max} at the 17-24W Preconditioning Site, Blyvooruitzicht Gold Mine. PSS measurements made in the solid rock are indicated by open circles. CSIR Ground Motion Monitor measurements made on the wall of the excavation are indicated by solid diamonds. R is the hypocentral distance. (a) Footwall Drive (b) Stope (c) Cross-cut.

Frequency spectra

The next step was the characterization of the site effect using the full seismogram. Comparison of the ground motions recorded in the solid rock and on the wall of the excavation showed that the latter has higher peak velocities, longer durations and higher dominant frequencies. Analysis was carried out in the frequency domain. Typical acceleration spectra are shown in Figure 2.3.3. The general form of the spectra can be described in terms of low-, mid- and high frequency trends.

1. Low-frequency trend: According to seismic source theory, at low frequencies the acceleration spectrum should increase as f^2. However, the observed spectra from 10-150 Hz do not follow this trend. This is owing to electronic distortion caused by switching on of the dormant processor when an acceleration exceeding the trigger level is detected. This effect is imperceptible on the accelerograms, but is sometimes prominent when integrating to velocity. Low-pass filtering removed this effect in the time domain. As some of the larger, potentially damaging events (M>1) are likely to have significant energy below 100 Hz, the electronic distortion of the spectrum will complicate the interpretation of these events. However, none of the events discussed in this report had significant energy in this range.

2. Mid-frequency trend: Seismic source theory predicts that this part of the acceleration spectrum should be flat (in the far field in a homogeneous medium). However, one or more strong peaks are observed in the range 400-1000 Hz. A PSS geophone was fixed to the sidewall of the footwall drive near the collar of a 10 metre long borehole containing an identical geophone grouted in the solid rock (A and P1 respectively, Figure 2.3.1). Comparison of the velocity spectra clearly shows the enhancement of the higher frequencies and the presence of resonant peaks (Figure 2.3.4).

3. High-frequency trend: All observed spectra show a sharp decay of amplitudes above 1000 Hz owing to the electronic anti-alias filter.

Energy of the seismic signal

The energy of the seismic signal was obtained by integration in the time domain of the P- and S-waves. Six events were considered. The amplification of the energy measured on the sidewall compared to the energy measured in the solid rock varied quite widely (2- to 39-fold, with an average of 18-fold).

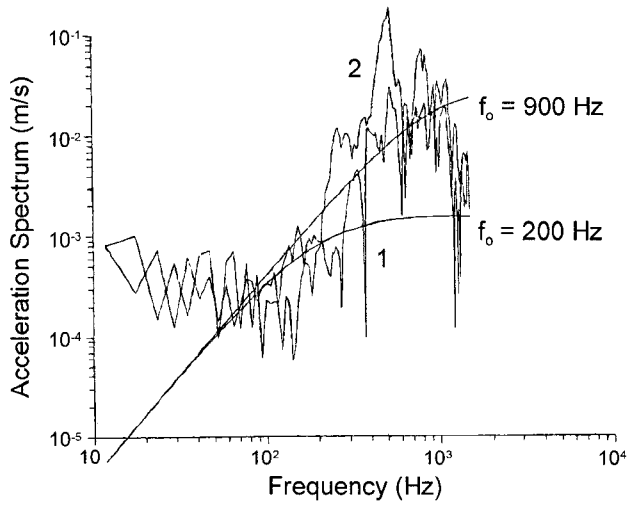

Figure 2.3.3 Typical spectra of accelerograms recorded by the CSIR Ground Motion Monitor on the wall of the excavation at the 17-24W Preconditioning Site, Blyvooruitzicht Gold Mine. The seismic event had a local magnitude of –1,8. The spectra of the face-parallel and face-perpendicular components are numbered 1 and 2, respectively. Theoretical spectra for the Brune model are shown (seismic moment $M_o=10^8$ Nm, corner frequency f_o = 200 Hz and 900 Hz).

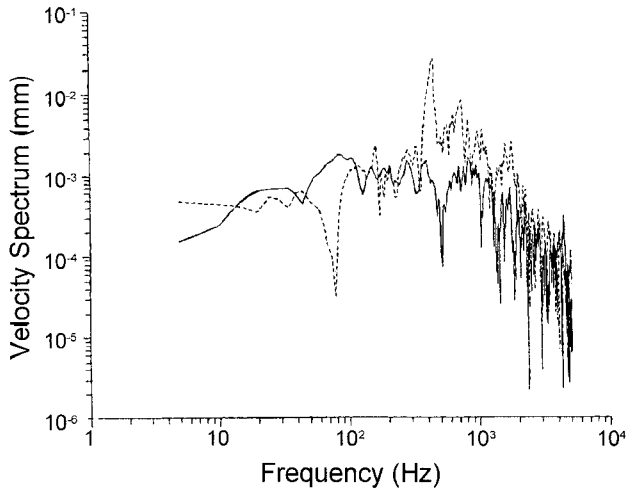

Figure 2.3.4 Velocity spectra of the ground motion recorded in the solid rock by a geophone grouted in a 10 metre long borehole (solid line), and by a geophone attached to the sidewall of the footwall drive near the collar of the borehole (dashed line). The seismograms were recorded by the PSS at a sampling rate of 10 kHz. The seismic event had a local magnitude of -0,7. Note the enhancement of the higher frequencies and the presence of resonant peaks.

Discussion

McGarr (1993) compiled measurements of Rv_{max} for seismic moments M_o in the range 10^9-10^{17} Nm. Our measurements in the solid rock for M_o in the range 10^7-10^{11} Nm are in reasonable accord with those data.

Reflection of the incident seismic wave from the surface of the excavation can account for a 2-fold amplification of the ground motion. However, an amplification of v_{max} of 4- to 10-fold is observed. This may be due to the trapping of energy in the fractured rock around the excavation by multiple reflection, and the generation of surface waves.

In a study investigating the effect of backfill on ground motion in a stope, Hemp and Goldbach (1993) found that the ground motion recorded on-reef is considerably higher

than that recorded off-reef. The median value of amplification of in-stope to off-reef ground velocities (corrected for distance) for the filled areas of mine A and mine B was 5,3, while the value for the unfilled area of mine B was 9,9. Spottiswoode and Churcher (1988) and Adams et al (1990) found that the peak ground velocity measured by stope geophones was 2 to 2,5 times greater than that measured in the solid rock.

The rock mass around deep-level stopes is highly fractured, facilitating a high rate of convergence in the stopes (Kullmann et al., 1996). Typically, under these conditions, the quasi-static convergence from day to day exceeds the convergence predicted by elastic theory by about a factor of 3, through a variety of mechanisms. We suggest that some of these mechanisms are active during seismic events, resulting in a site amplification effect in any stope with a high rate of inelastic convergence.

The observed spectra are quite different from the prediction of seismic source theory: considerable energy is present at frequencies above the corner frequency of the source determined by PSS measurements within the solid rock. It was first thought that this was due to resonance of the transducer mounting in the CSIR Ground Motion Monitor. However, several other observations have led us to believe that this is a genuine non-linear site effect. (i) A PSS geophone mounted on the sidewall close to a Ground Motion Monitor, and sampling at 10 kHz, recorded similar data. (ii) Measurements made within a borehole showed a similar enhancement of high frequencies within the fractured zone around the excavation (Goldbach, 1990). (iii) Recordings of the rock resonance made in stopes on several other deep gold mines (as part of a project investigating a laser rock-breaking technique) showed resonances in the frequency range 500-800 Hz (Stevenson, 1995). Similar results were obtained in the footwall drive at Blyvooruitzicht Gold Mine. However, it should be noted that these resonances at frequencies above the corner frequency are absent at some sites in other mines.

Conclusions

Measurements of the motion of the skin of tunnels and stopes excited by seismic events at Blyvooruitzicht Gold Mine reveal that energy is trapped in the fractured rock surrounding highly stressed excavations. When compared to the ground motion in solid rock, an increase in the duration of shaking and an amplification of v_{max} and a_{max} are observed. It is anticipated that this study will provide criteria for the design of support systems for excavations under rockburst conditions.

2.3.2 Time domain analysis of tunnel sidewall motion

The analysis of the site response of the sidewall of a tunnel at Blyvooruitzicht Gold Mine is described using time domain methods, complementing the frequency domain analysis of Durrheim et al. (1996). Time domain methods have the advantage that the time history of the vibrating structure may be analysed.

System identification

In general, seismograms are controlled by the parameters of the seismic source, the ray path, the site effect, and the instrument response. The site effect may be expressed using the convolution equation:

$$s_2(t)=s_1(t) * h(t) \qquad (2.2)$$

where $s_2(t)$ is the seismogram with the site effect, $s_1(t)$ is the seismogram recorded in the solid rock nearby, and $h(t)$ is the model of the site effect. System identification involves the calculation of $h(t)$ from measurements of $s_1(t)$ and $s_2(t)$.

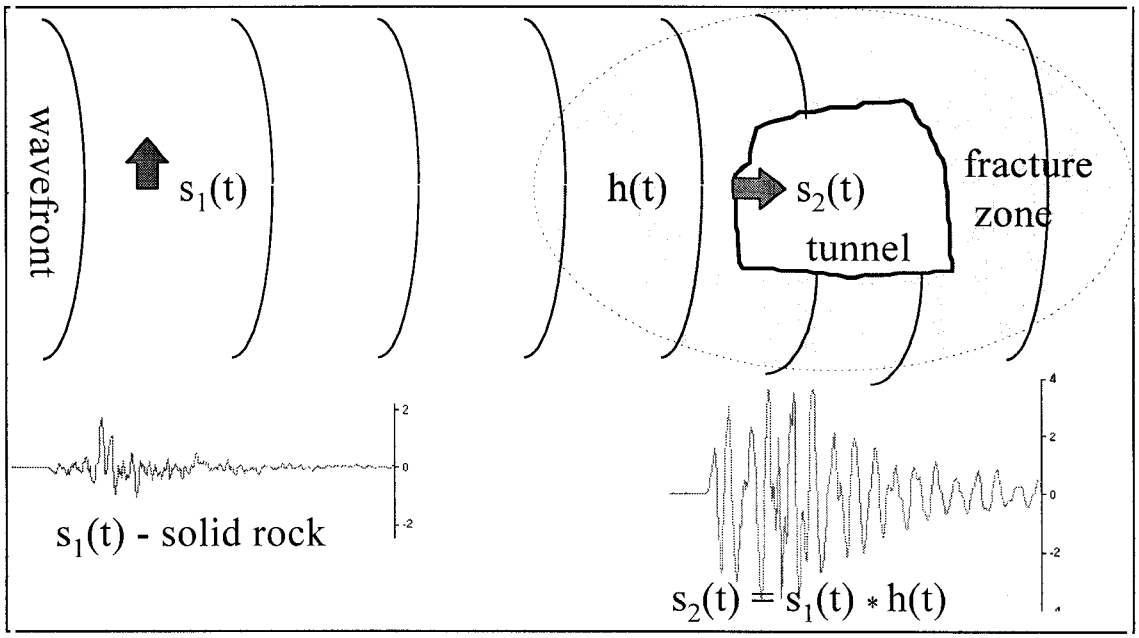

Figure 2.3.5 Seismic shaking caused by a M_L= -0,7 event located in the B17 stabilizing pillar at Blyvooruitzicht Gold Mine. Seismogram $s_1(t)$ was recorded by a vertical component geophone in solid rock and $s_2(t)$ by a horizontal component geophone attached to the the sidewall of a footwall drive. The sampling rate was 10 kHz. In this example the peak velocity (v_{max}) on the tunnel sidewall is more than twice that recorded in the solid rock, even though it is further from the source. The duration of shaking also increased substantially on the tunnel sidewall.

Adaptive filters are used extensively for system identification where the system is considered to have a time varying structure (Widrow and Glover, 1975). The adaptive filter changes with time to accommodate itself to changes in the time series being filtered. The application uses the signal $s_1(t)$ recorded in solid rock and the desired output signal $s_2(t)$, to determine the transfer function which minimizes the difference between the $s_2(t)$ and the output $z(t)$ of the adaptive system. The difference is known as the error signal $e(t)$.

$$e(t) = s_2(t) - z(t) \qquad (2.3)$$

where:

$$z(t) = \sum w_t(i)\, s_1(i) \quad i = 0,1,2 \ldots M \tag{2.4}$$

Seeking to minimize the error signal, an adaptive algorithm adjusts weights of the adaptive filter *w(t)* and tries to emulate or identify the transfer characteristic *h(t)* of the system. The least mean square (LMS) algorithm is the most widely used of the gradient based adaptation algorithms, and was used here. The algorithm iteratively calculates the set of filter coefficients that minimizes *e(t)*. The coefficient vector obtained at iteration t+1 is:

$$w_{t+1}(i) = \alpha\, w_t(i) + \mu\, s_1(i)\, e(i) \tag{2.5}$$

The filter has three adjustable parameters:

length *M* of the filter *w(i)*;

step length $\mu = k / \sum s_1^2(t)$ 0,1 < *k* < 2,0 ; and leakage coefficient α, which is slightly less than unity e.g. 0,98.

First attempts to apply the adaptive filter were unsuccessful as the filter was found to be oversensitive when raw data were used. A high cut filter was applied to both the input and desired signal and satisfactory results were obtained (Figure 2.3.6). The changes of $w_t(i)$ with time are significant. Therefore it is impossible to use one transfer function *h(t)* to describe the site effect occurring during ground motion vibration. It was found that the adaptive filter was not affected by the step length μ, and satisfactory results were obtained for *k* = 0,5; 1,0 and 1,5. The filter length *M* can range between 30 and 100 coefficients. A short filter (say 30 coefficients) gives an error signal with a white spectrum but the filter can sometimes be unstable. Long filters (say 100 coefficients) always give a small error signal *e(t)*, but the spectrum of *e(t)* is not white. Power spectra of the error signal often display peaks at about 440 Hz, suggesting that a parametric model of the transfer function could be more appropriate.

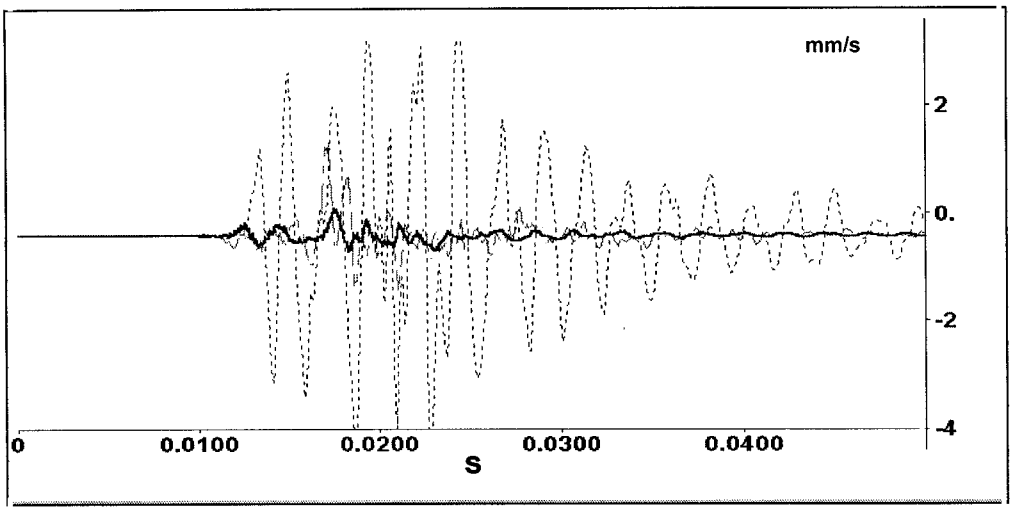

Figure 2.3.6 System identification. The solid rock seismogram $s_1(t)$ is represented by a fine solid line and the seismogram recorded on the sidewall of the tunnel, which has a strong site effect, $s_2(t)$ is represented by a dashed line. The bold solid line denotes the error signal e(t) obtained by subtracting the output of the adaptive system from $s_2(t)$. Note the relatively small amplitude of the error signal, indicating that the data adaptive filter has succeeded in identifying the transfer characteristic of the system.

Adaptive noise cancelation filter

The presence of a dominant frequency in the power spectrum of the error signal motivated a study of sinusoidal noise rejection. It is generally inadvisable to simply subtract an estimate of the noise from a signal as such an operation could produce an increase in the average power of the output noise. However, when the subtraction is controlled by an adaptive process it is possible to achieve good results (Widrow and Glover, 1975).

The contribution of the site is considered to be a sinusoidal noise signal superimposed on the solid rock signal $s_1(t)$. The problem is defined by Equations (2.3) and (2.4) where $z(t)$ is given by:

$$z(t) = \sum w_t(i) \sin(2\pi \tilde{f}_o \Delta t_i) \qquad (2.6)$$

where Δt_i is a descretization step, and

$\tilde{f}_o$ is the estimation of f_o

The filter output $z(t)$ is subtracted from the signal with the site effect $s_2(t)$. In this case $e(t)$ is an estimate of the signal in the solid rock. The effect of the sinusoidal interference is diminished while the signal power $s_1(t)$ is unaffected.

The geophone installed in the footwall drive showed clear resonance frequencies. The spectra of the seismograms were used to define the frequency of the sinusoidal noise. The sinusoidal disturbance is thus cancelled from the $s_2(t)$ seismogram.

The error signal $e(t)$ was found to have a similar envelope to the seismogram $s_1(t)$ recorded in solid rock. When power spectra were compared in detail it was found that the power spectrum of the error signal $e(t)$ had more in common with the spectrum of the seismogram with the site effect $s_2(t)$ than with the spectrum of the seismogram $s_1(t)$ recorded in solid rock. In some cases, however, the low frequency pulse $s_1(t)$ was remarkably restored from $s_2(t)$ after cancelling the f=440 Hz sinusoidal disturbance.

It was concluded that the site effect cannot be modelled simply as a sinusoidal interference. Sinusoidal interference does, however, describe a major part of the site effect. It was considered necessary to describe the site effect using a meaningful physical model.

Damped oscilator

The results achieved by using data adaptive filters suggest that a damped oscillator be considered as a candidate for modelling the rock mass surrounding an excavation. This approach is used by earthquake engineers to estimate the response of a structure to a given found motion (e.g. Clough and Penzien, 1975, p. 535; Dowrick, 1987, p. 15).

The equation of motion for an elastic, single degree of freedom, damped oscillator excited by seismically induced ground motion may be expressed as:

$$m\ddot{y}(t)+c\dot{y}(t)+ky(t)=-m\ddot{x}(t) \tag{2.7}$$

where $\ddot{x}(t)$ is the acceleration of the base of the system, *y(t)* is the displacement response of the oscillator, *m* is the mass of the oscillator (structure of rock mass surrounding an excavation), *c* is the viscous damping of the oscillator and *k* is the stiffness. This equation is normally written as:

$$\ddot{y}(t)+2D(2\pi f_O)\dot{y}(t)+(2\pi f_O)^2 y(t)=-\ddot{x}(t) \tag{2.8}$$

where

$f_O=\frac{\sqrt{k/m}}{2\pi}$ is the natural frequency, and $D=c/2\sqrt{km}$ is the critical damping.

It is assumed that the parameters *m, k* and *c* remain constant during the entire period of excitation. The displacement response for linear systems is given by:

$$y(t)=-\ddot{x}(t)*h(t) \tag{2.9}$$

where

$$h(t)=\frac{e^{-D\omega_o t}\sin[\omega_O t\sqrt{1-D^2}]}{\omega_O\sqrt{1-D^2}} \text{ for } t>0 \tag{2.10}$$

and $\omega_O=2\pi f_O$ (Solnes, 1974)

The impulse response function *h(t)* of the structure is a filter corresponding to the vibratory characteristic of the structure provided that the system is initially at rest.

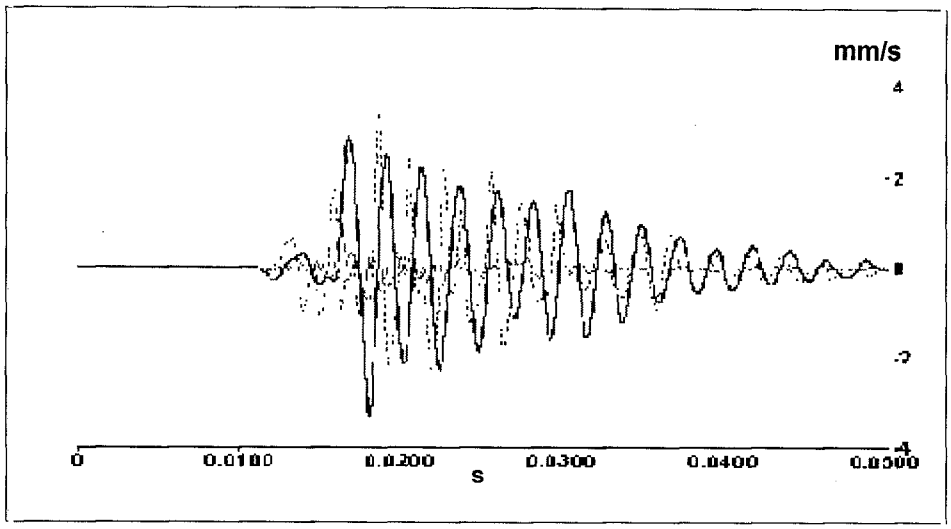

Figure 2.3.7 Damped oscillator model. Three seismograms are superimposed. The solid rock seismogram ($s_1(t)$, fine solid line), the seismogram recorded on the sidewall of the tunnel which has a strong site effect ($s_2(t)$, dashed line), and the theoretical output obtained by convolving $s_1(t)$ with the damped oscillator with natural frequency 440 Hz and damping coefficient D=0,03 (bold solid line). Note the good match with $s_2(t)$.

Figure 2.3.7 shows a seismogram $s_1(t)$ recorded in solid rock convolved with the impulse response of a damped oscillator whose natural frequency f_O was obtained from inspection of the frequency spectrum of the seismogram $s_2(t)$ with the site effect. The ratio of critical damping D was obtained by trial and error. The convolution of the seismogram fits the seismogram recorded on the tunnel sidewall very well, although the result is very sensitive to the oscillation parameters. At this site the parameters of the oscillator were as follows: natural frequency varies from 440 Hz to 480 Hz, and the ratio of critical damping varies from 0,03 to 0,06. It was found that the natural frequency shifts slightly during the period of ground motion.

Conclusions

Several time domain approaches for analysing the site response to seismic shaking of the walls of tunnels and stopes have been investigated. It proved possible to perform system identification using a data adaptive filter. The physical interpretation of the system identification function is uncertain. The single degree of freedom damped oscillator approach is particularly promising as it has a clear physical basis. This approach is also used in earthquake engineering, and can be extended to analyse the dissipation of energy by structures through damping and damage (e.g. Zarah and Hall, 1984; Lin et al., 1991; Zhang and Soong, 1992). This formalism has the potential to be used in the design of rockburst-resistant support systems. The strategy is to minimize the energy dissipated by damage, and maximize the energy that is dissipated by damping.

It has been found that structural damage in civil engineering systems is manifested by changes in modal parameters (natural frequencies, mode shapes and modal damping values). This effect offers the possibility of using data from dynamic testing to detect, locate and quantify damage (Salawu, 1997).

2.3.3. Spectral analysis to quantify the influence of fracturing and support on the dynamic behaviour of the hangingwall

Quantification of the ground motion in the stope

The most direct measure of strong ground motion for damage control is the peak ground velocity. Wagner (1984) considered the energy absorption requirements for support to arrest an intact beam of hangingwall ejected at a high velocity. One of the objectives of installing Ground Motion Monitors in the stope is therefore to record extreme values of strong ground motion. In principal, measured values larger than 3 m/s could lead to increasing the support design criteria. In practice, it is questionable whether the hangingwall would be able to maintain its integrity at values in excess of 3 m/s. Most deep-level stope hangingwall rocks are already intensely fractured and could fall out in between individual support elements under ground velocities well below 3 m/s. The major

purpose of this study is to present an analysis of differential movement between nearby points in the hangingwall of deep-level stopes to provide some insights into the problem of hangingwall instability.

Cichowicz and Green (1989) showed that scattering from the zone of fractured rock around the stope dominate the coda waves recorded at sites remote from the stopes. Coda waves are more strongly developed in stopes than out in the solid rock (Spottiswoode and Churcher, 1988). It is suggested that the strong motions and persistent coda waves could be caused by trapping of seismic energy within the 2-D region, about 10 m into the hangingwall and footwall, and 100's of metres along the reef when it has been extensively mined out.

As stope support elements are placed about 1 m to 2 m apart, sets of two or three accelerometers were attached to the hangingwall about 1 m apart. In some cases, the third accelerometer was attached to the footwall.

To compare the ground motion at different sites (A and B), the full waveforms were Fourier transformed:

$$V_A(t) \Leftrightarrow \tilde{V}_A(f) \quad \text{and} \quad V_B(t) \Leftrightarrow \tilde{V}_B(f) \tag{2.11}$$

and then the ratio of the complex spectrum at each frequency was expressed as amplitude ratio R(f) and phase difference δ(f).

$$\tilde{V}_B(f) / \tilde{V}_A(f) = A(f)\exp(2\pi \mathrm{i}\delta(f)) \tag{2.12}$$

Seismic spectra are typically noisy in that values at adjacent frequencies can vary strongly. Spectral ratios, such as A(f) in Equation (2.12), are more prone to noise. To obtain stable values, many events were recorded and the median values were obtained, R′(f) and δ' (f), of all spectral components for R(f) and δ(f) at each frequency. The benefit of this approach is evident in Figure 2.3.8 where no spectral smoothing was done to reduce noise.

Figure 2.3.8 shows, in addition, that these spectral ratios are stable even with time from the start of the seismogram the end.

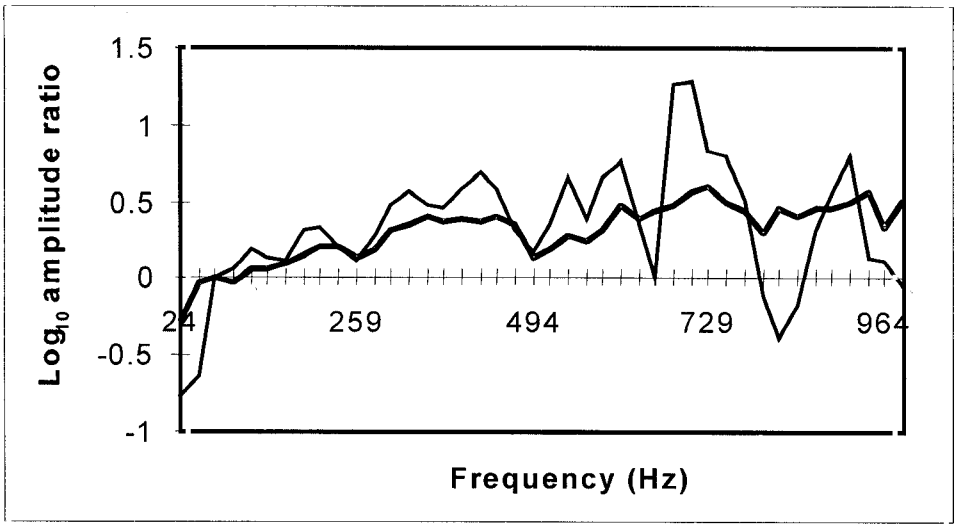

Figure 2.3.8 A plot of spectral amplitude ratios of one event and the median value at each frequency for a group of events. The median values, in bold, are clearly more stable.

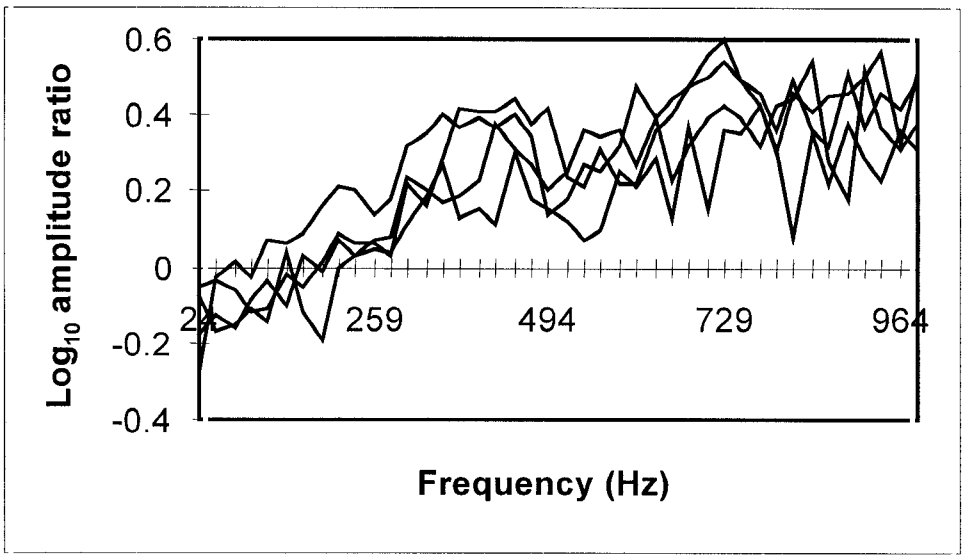

Figure 2.3.9 Median value of amplitude ratio, channels 2 to 3, site 84/49/W1. Three overlapping windows of 128 samples were taken, starting just before the P wave arrival.

Values of A (f) either bigger or smaller than 1,0 have direct engineering implications as they suggest that some parts of the hangingwall are less stable than others. Locally higher values of velocity not only require more support resistance, but large differential vertical movements could indicate inelastic deformations and cause damage to the hangingwall.

The absolute phase difference in radians ($|\delta(f)|$) in Equation (2.12) at any frequency can be interpreted in terms of wavelength (λ), phase velocity (V), frequency (f), distance between accelerometers (D), and angle (ϕ) between the direction of propagation of the wave and vector AB (see Figure 2.3.10).

$$\delta(f) = 2\pi\, D\cos(\phi) / \lambda = 2\pi\, Df\cos(\phi) / V$$
$$or \qquad (2.13)$$
$$V = 2\pi\, Df\cos(\phi) / \delta(f)$$

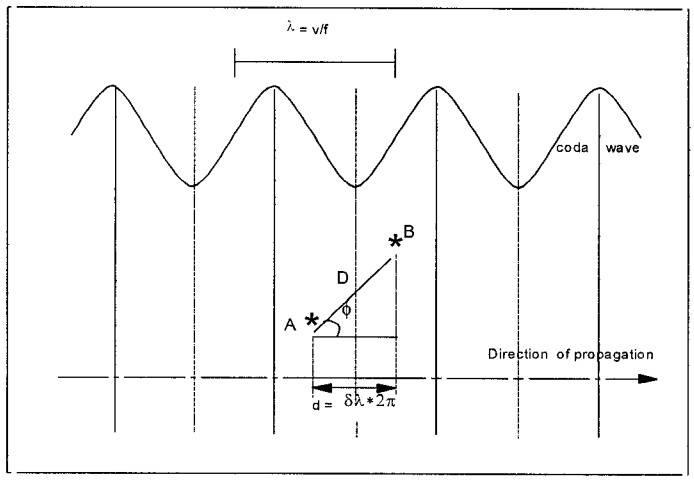

Figure 2.3.10 A diagram illustrating the relationship between phase difference, $\delta(f)$, and phase velocity.

If we assume that waves (P and SV) propagate in all horizontal directions at random, then 50 percent of all waves travel within the quadrants described by $|\phi| < 45^0$ and $|\phi| > 135^0$. Equation (2.13) can then be rewritten as:

$$V = 2\pi D\sqrt{2} / (|\delta(f)|/f) \qquad (2.14)$$

$|\delta(f)| / f$ can be derived from the slope of a plot of $|\delta(f)|$ as a function of f, as shown in Figure 2.3.11.

It can be seen in Figure 2.3.11 that the median absolute phase difference increases approximately in a linear fashion to 90°. Some pairs of transducers $|\delta(f)|$ increases to more than 90° before decreasing to 90°. This is in agreement with a simple numerical model with random values of ϕ. Note that $|\delta(f)| = 90°$ for random phase differences, such as should occur at very high frequencies.

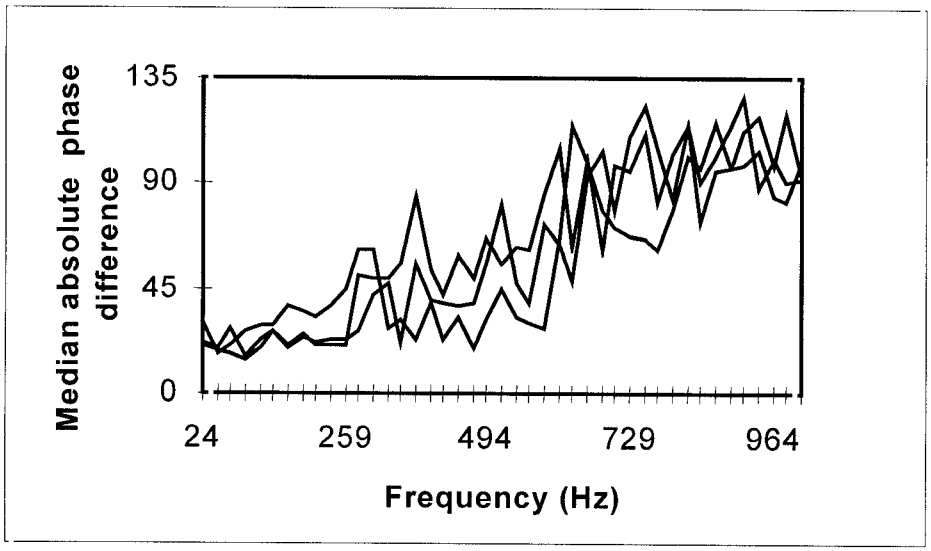

Figure 2.3.11 Median value of the absolute phase difference, the same windows as for Figure 2.3.9. The line is used by Equation (1.2.4) to estimate the phase velocity between the two transducers.

Field measurements and analysis

At the end of 1996 it was realised that the black boxes using accelerometers were unreliable. The inexpensive accelerometers were physically faulted and the integration to velocity was poor at low frequency. Thus, at the beginning of 1997, the transducers used in the black boxes were changed to geophones. These were found to be more stable.

Data have been recorded by black boxes installed in stopes in the following mines: Vaal Reefs, Western Deep Levels-East Mine, Western Deep Levels-South Mine.

The transducers were placed at the hangingwall, footwall, in the backfill or on the support unit with configurations especially designed for each individual case. More details are given in Table 2.3.1.

Table 2.3.1

Spatial configurations of the recorded geophones and number of events.

SITE	NUMBER OF EVENTS	DISTANCE TO THE SUPPORT D (s)	COMPONENT PAIRS	DISTANCE BETWEEN PAIRS D (m)
VLR Site 1	105	1.35 & 0.6	G3 & G2	0.75
VLR Site 2	290	0.6 & 1.0	G1 & G2	1.14
		9.0 & 1.0	G3 & G2	1.34
		0.9 & 0.6	G3 & G1	0.30
VLR Site 3	236	0.8 & 0.1	G1 & G2	N/A
		1.1 & 0.1	G3 & G2	1.03
		1.1 & 0.8	G3 & G1	N/A
VLR Site 4	240	0.7 & 0.1	G1 & G2	N/A
		1.3 & 0.1	G3 & G2	1.10
		1.3 & 0.7	G3 & G1	N/A
WDL_E Site 1	53	0.0 & 0.1	G1 & G2	1.21
	60	0.0 & 0.1	G1 & G2*	0.74
WDL_E Site 2	273	0.0 & 0.4	G1 & G2	0.74
		0.1 & 0.4	G3 & G2	0.27
		0.1 & 0.0	G3 & G1	0.66
WDL_E Site 3	243	0.1 & 0.0	G1 & G2	N/A
		0.1 & 0.0	G3 & G2	N/A
		0.1 & 0.1	G3 & G1	N/A
WDL_E Site 4	129	0.2 & 0.0	G1 & G2	N/A
		0.1 & 0.0	G3 & G2	N/A
		0.1 & 0.2	G3 & G1	N/A
WDL_S Site 1	22	0.99 & 0.22	G2 & G3	0.77
WDL_S Site 2	7	0.25 & 0.25	G2 & G3	0.87
WDL_S Site 3	56	0.93 & 0.11	G3 & G2	0.82
WDL_S Site 4	25	0.31 & 0.32	G2 & G3	0.66
WDL_S Site 5	56	0.30 & 0.15	G1 & G2	1.00
		1.00 & 0.30	G3 & G2	0.50
		1.00 & 0.15	G3 & G1	0.60
WDL_S Site 6	64	1.0 & 1.0	G1 & G2	1.00
		1.0 & 1.0	G3 & G2	0.50
		1.0 & 1.0	G3 & G1	0.50

Vaal Reefs

Geology

Black boxes were located in VLR / Panels 11 and 14/ in 68 L-57 stope. The actual sites were inaccessible for later mapping and the area close to the sites was examined.

The hangingwall is a very coarse grained and immature quartzite with argillaceous partings. The hangingwall was defined by a smooth, undulating surface developed on a persistent argillaceous parting plane. The next persistent parting planes were 33 cm and 58 cm above the roof of the stope. The footwall is a coarse grained, immature quartzite with, argillaceous parting planes.

Fracture density varied considerably from 20-45 fractures/m, with fracture strike along the dip direction. Persistent fractures dip at 75^{0} towards the back area while the second set of fractures dips at 60^{0} towards the face. The persistent fractures may be followed along the whole of the panel and are more recent as they bisect the face dipping fractures.

Spectral ratios and phase difference at the Vaal Reefs, Panel 14 (Sites VLR/P14/S1 and VLR/P14/S2)

Figure 2.3.12 shows the layout of geophones at two sites at Vaal Reefs mine. Geophones labelled G1, G2, and G3 were glued to the hangingwall and are separated by distances of less than 2 metres. For this experiment geophones were placed away from the packs. About 400 events were recorded by the two black boxes. One event with M=2,8 and whose damage coincided with the site, was recorded by the box site VLR/P14/S1. However, the records were saturated. A method for estimating V_{max} is presented below.

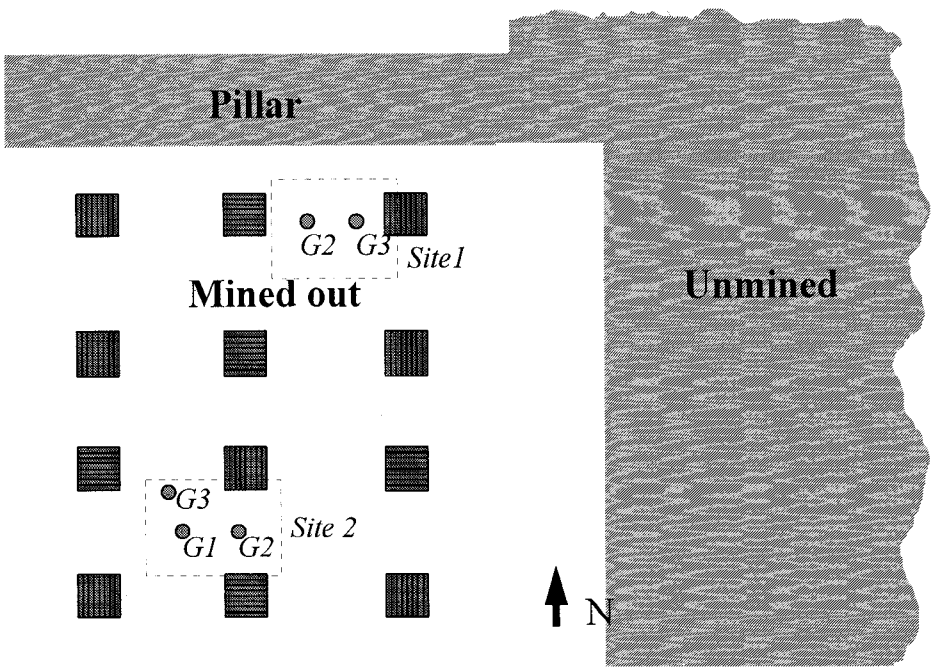

Figure 2.3.12 A sketch showing two black boxes (sites 1 and 2) at Panel P14, Vaal Reefs Mine.

The Vaal Reefs experiment investigates relative motion between two geophone stations. For VLR/P14/S1 median spectral ratios of geophone G2/G3 are plotted against frequency in Figure 2.3.13 *(a)* and *(b)*. Except in the frequency between 100 Hz and 300 Hz, where a significant deviation from zero occurs, $\log_{10}$ median spectral ratio values are, at 0,2, very close to zero. The deviation from zero can be interpreted as resonance occurring in that frequency band. This is further confirmed in the plot of spectra for the two geophones in Figure 2.3.13 *(b)* where, a resonance between 90 and 160 Hz. is obtained.

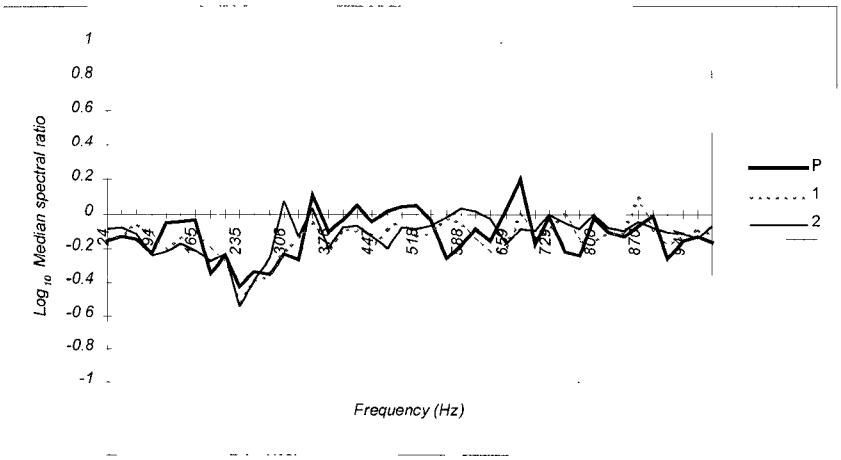

Figure 2.3.13 (a) Log_{10} median spectral ratio as a function of frequency. Ratios are taken between G2 and G3 for site VLR/P14/S1.

The "P" symbol denotes that the spectral window was taken from the P-wave onset of the seismogram, and "1" and "2" are two consecutive windows. The first window is 128 counts or 40 ms long and 1 and 2 are 64 and 128 counts onwards.

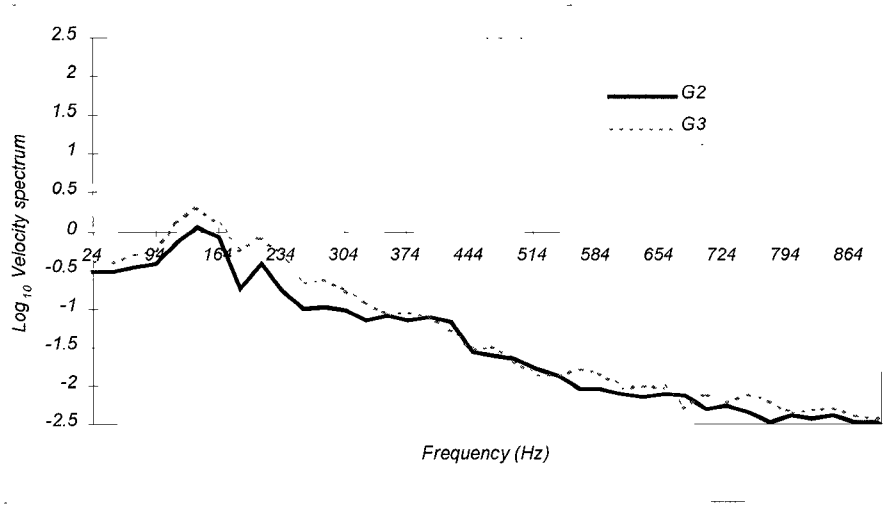

Figure 2.3.13 (b) P spectra for geophones G2 and G3.

At site VLR/P14/S2 median spectral ratios of G1 to G2 show resonance at high frequencies (above 600 Hz). The same situation exists for ratios between G2 and G3. Below 600 Hz the ratio is almost one. Figures 2.3.15 *(a)* and 2.3.15 (*b*) show the respective plots. At these frequencies, the area monitored by the geophones acts as a single block. Median spectral ratios between G1 and G3 are shown in Figure 2.3.14 *(c)*. The median spectral ratio is close to zero at all frequencies. This means that the motion is exactly the same at the positions of the two geophones, and therefore, the hangingwall behaves as a unit. The plot of the median absolute phase difference in Figure 2.3.14 *(d)* agrees with this assertion.

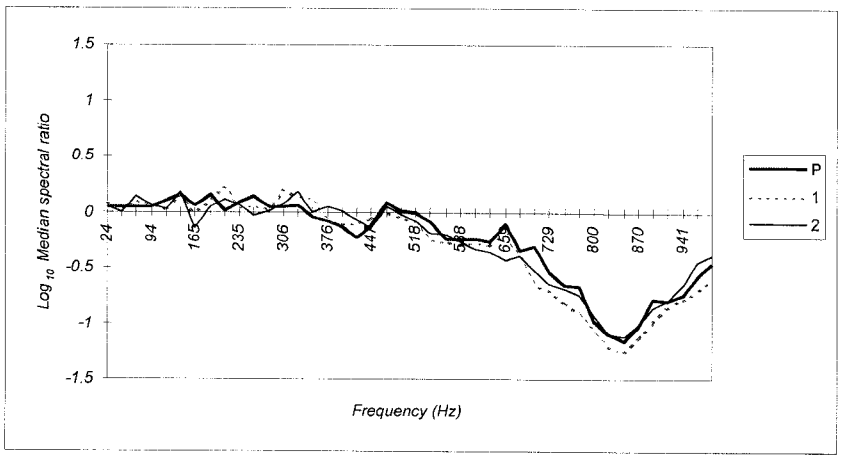

Figure 2.3.14 (a) Log_{10} median spectral ratio between G1 and G2, plotted as a function of frequency. This is site VLR/P14/S2.

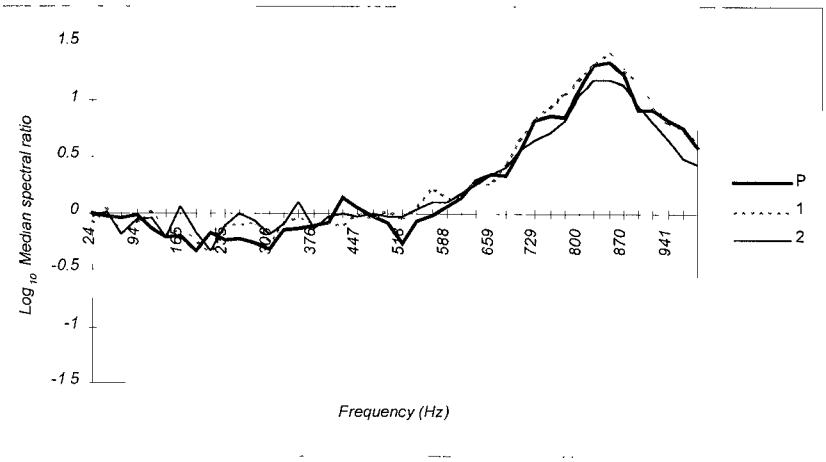

Figure 2.3.14 (b) Log_{10} median spectral ratio G2/G3 plotted as a function of frequency. This is site VLR/P14/S2.

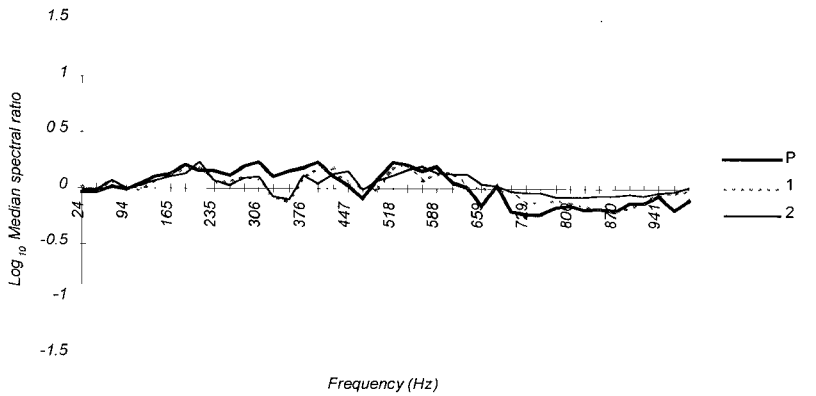

Figure 2.3.14 (c) Log_{10} median spectral ratio as a function of frequency between G1 and G3 at site VLR/P14/S2.

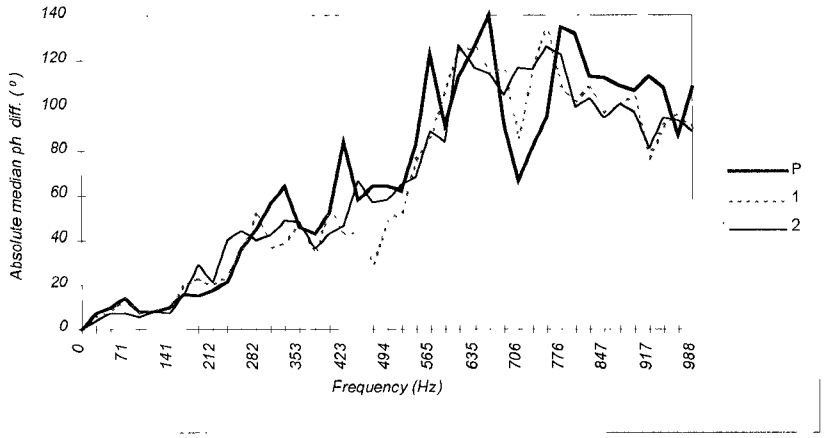

Figure 2.3.14 (d). Absolute median phase diagram of relative motion between G1 and G3.

The Vaal Reefs mine experiment indicates that the hangingwall between the support, at least over the area occupied by the geophones, is competent. It is not yet clear what the contribution of the support is to this behaviour. Previous experiments done at WDL South mine showed large differential movements between any two sensors (accelerometers) even when they were very close to each other.

Seismic evidence for stress redistribution before and after a strong (M = 2,8) seismic event.

Site One (VLR/P14/S1)

The maximum velocities recorded at site one (see Figure 2.3.12) are presented in Figure 2.3.15. It can be seen that the maximum velocities recorded by G2 are grouped into two clusters. These clusters correspond to the time period before and after the strong seismic event respectively. The maximum velocities recorded by G2 at about seven hours before the event differed substantially from those recorded by G3. However, immediately after the event and over the next two days the maximum velocities at both geophones

were similar. This effect is also illustrated on Figure 2.3.16 where the ratio of G2 and G3 was plotted as a function of time.

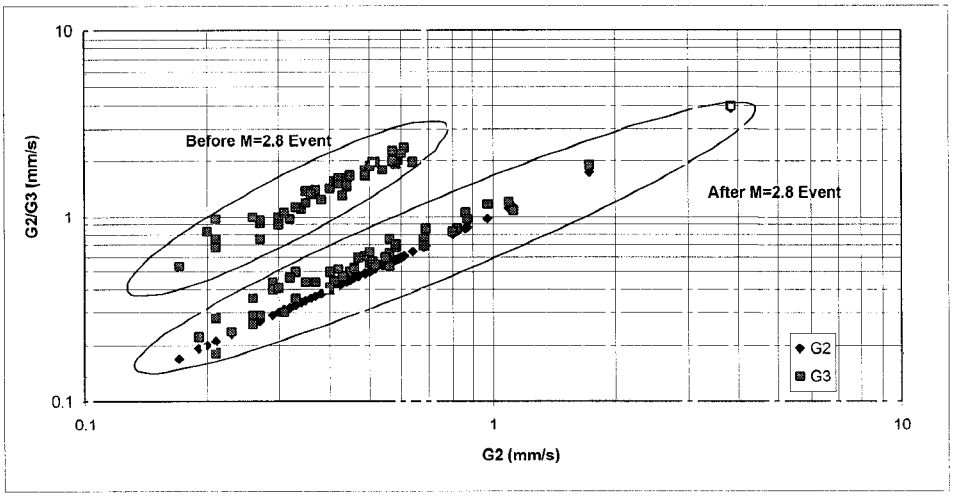

Figure 2.3.15 Maximum velocities recorded at G2 and G3 at VLR/P14/S1.

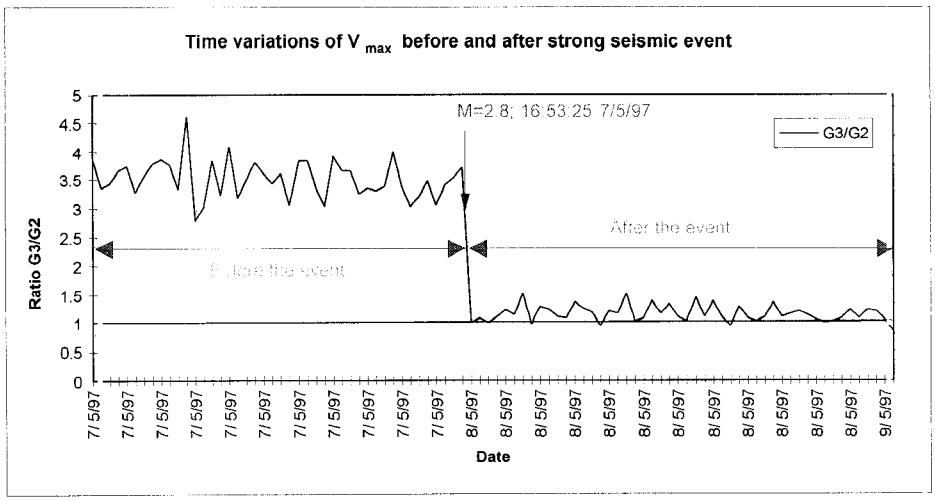

Figure 2.3.16 The ratios of G3/G2 as a function of time at site VLR/P14/S1.

Site Two (VLR/P14/S2)

A similar effect is recorded at site two (see Figure 2.3.12) located in the same panel 6-7 m down dip from the site. The data recorded at this site starts about five days before the event and ends at the moment of the event. The rockburst caused by this event destroyed the sensors. The effect of increasing the scattering in maximum velocities among geophones one, two and three before the same event is clearly obtained. Figure 2.3.18 shows the ratios between G2/G1 and G3/G1 as a function of time. It can be seen that at about hour before the event the maximum velocities at G2 and G3 increased significantly.

However, the data analysed for both sites were limited in time and it was not possible to trace the beginning and the end of this effect in real time.

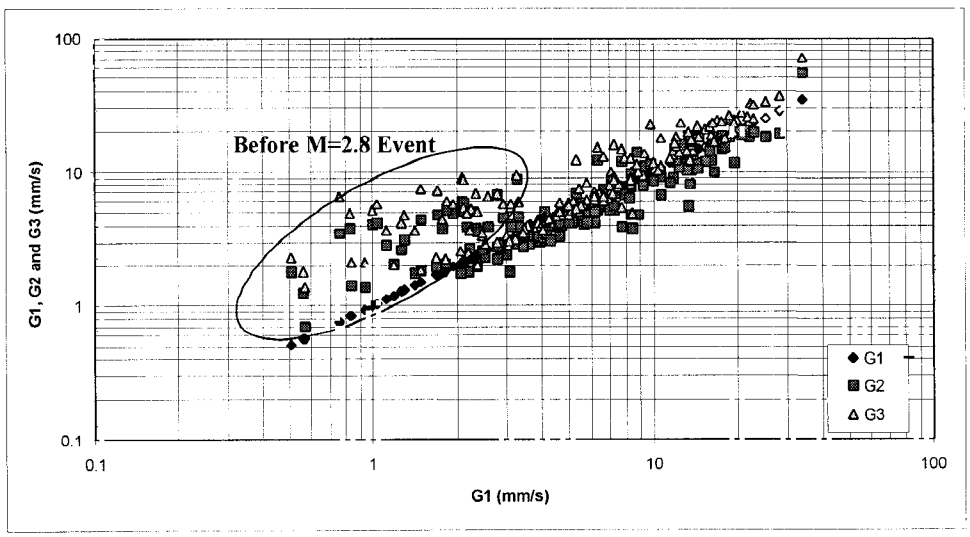

Figure 2.3.17 Maximum velocities recorded at G1, G2, G3 in VLR/P14/S2.

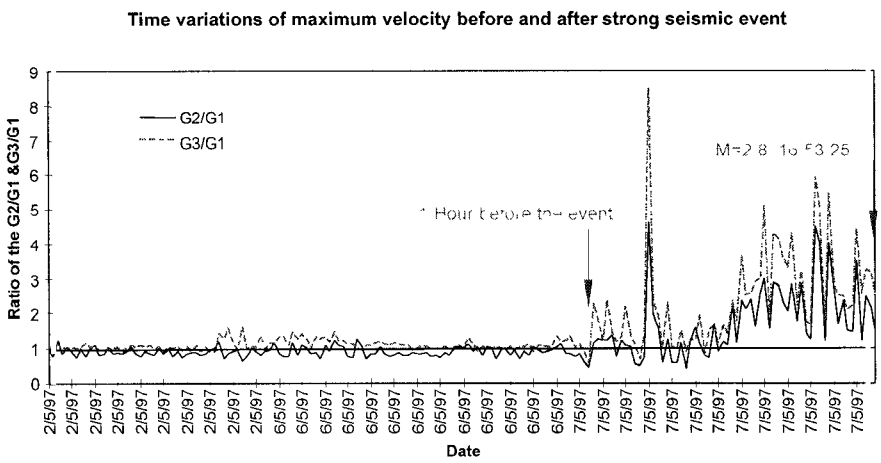

Figure 2.3.18 The ratio G2/G1 and G3/G1 as a function of time at VLR/P14/S2.

Mechanism

Two possible mechanisms are discussed here:

(i) The redistribution of the skin stresses before and after the event.

During the pre-event period or loading phase the stresses in the origin zone are increased, which often leads to relaxation of the pressure on the fractures in the back area. This effect is accompanied by more freedom of movement on each block, and, very often causes a rockburst deep in the back area. After the event there is a relaxation of the vertical stresses and the shear stresses are transferred further into the back area. This improves the stiffness of the hangingwall and decreases the scattering in the maximum velocities recorded by the different geophones.

(ii) Increasing the resistance of the support system after the event.

This effect normally takes place in the post event period, where the pressure of the support system increases. However, it is difficult to apply this mechanism for the pre-event period.

Spectral ratios and phase difference at the Vaal Reefs, Panel P11 (Sites VLR/P11/S3 and VLR/P11/S4)

Figure 2.3.19 shows the layout and the geophones positions at two sites (site 3 & 4) at panel P11 Vaal Reefs Mine. Geophones labelled as G1 at both sites were placed on the footwall, G2, and G3 are glued to the hangingwall. The geophones G2 were installed very close to the support and G3 were installed midway between two support units.

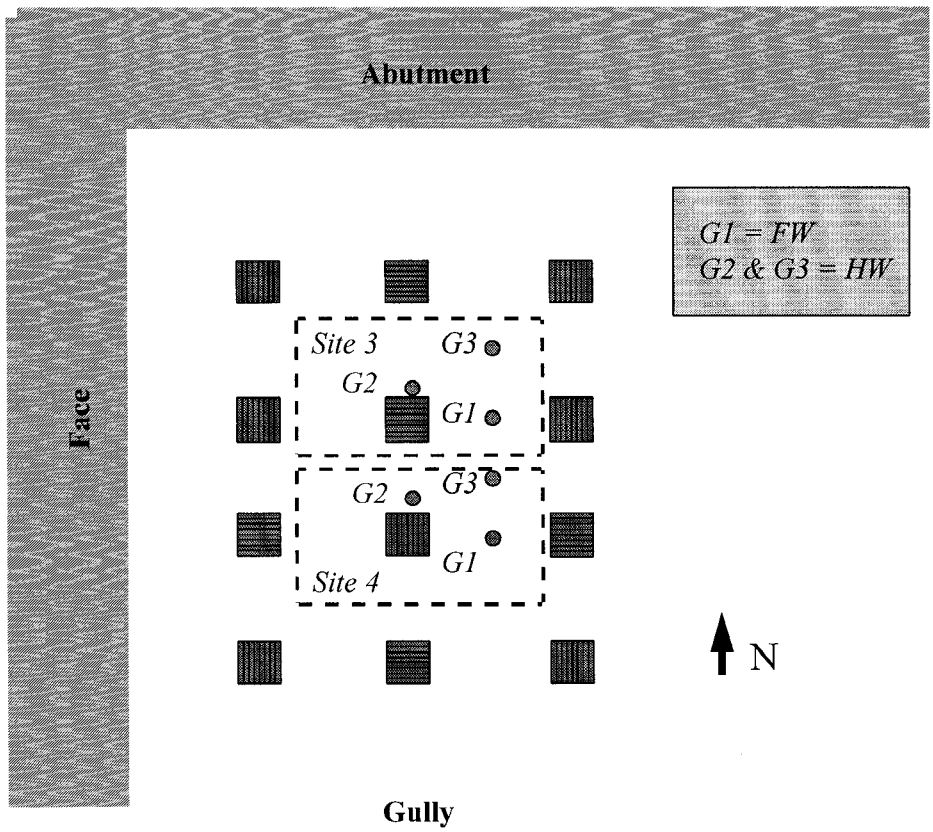

Figure 2.3.19 A sketch showing the position of two black boxes at sites VLR/P11/S3 and VLR/P11/S4.

Figure 2.3.20 *(a)* shows a plot of amplitude ratio as a function of frequency. At this site hangingwall sensors at G2 and G3 show a significant variation in their amplitude spectra above 600 Hz. At these frequencies motion at G2 is greater than at G3. Hangingwall motion at G2 is greater than footwall motion at G1 for frequencies, above 140 Hz.

Footwall motion at G1 is generally lower than hangingwall motion at G3, with $\log_{10}$ (G1/G3) remaining constant throughout the frequency range.

The phase differences plot in Figure 2.3.20 *(b)* shows that motions between all geophones (G1, G2, and G3) are not coherent throughout the frequency range.

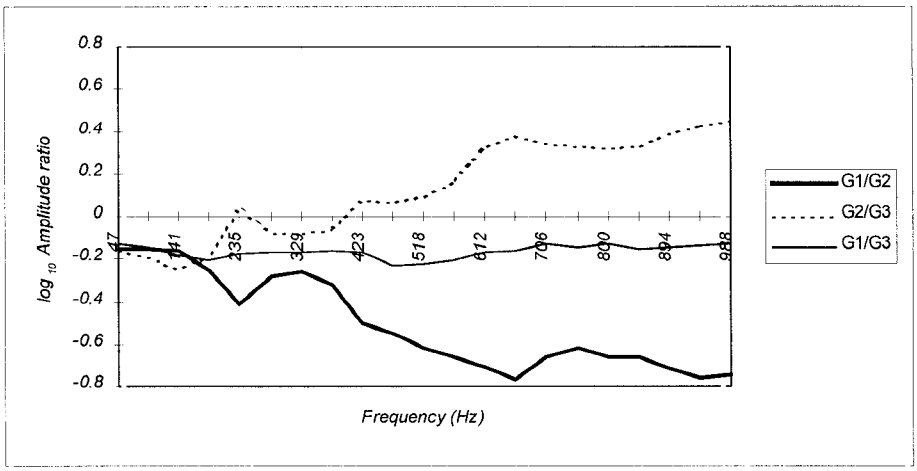

Figure 2.3.20 (a) Log_{10} amplitude ratio as a function of frequency at VLR/P11/S3.

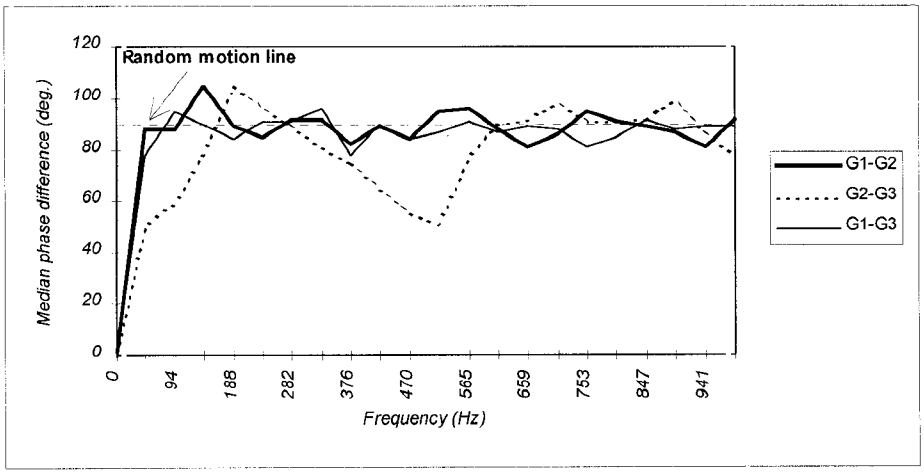

Figure 2.3.20 (b) Median phase difference as a function of frequency at VLR/P11/S3.

Data for Figure 2.3.21 (*a* and *b*) plots were recorded for sites G1 on the footwall, and G2 and G3 on the hangingwall. Amplitude ratio plot in Figure 2.3.21 *(a)* shows that the log (G2/G3) is nearly equal to zero throughout the frequency range. This means that site response to amplitude in the area encompassing G2 and G3 is the same. Footwall motion seems to have lower amplitudes than hangingwall motion between 50 Hz and 800Hz. This is more evident for amplitude ratios between sites G1 and G2. Sites G1 and G3 show a similar trend but deviations from the log (G1/G3) = 0 are smaller. This is believed to be due to noise in the data and possible recording errors.

Figure 2.3.23 *(b)* shows a plot of phase differences as a function of frequency. It can be seen that motion in the footwall (site G1) and the hangingwall (sites G2 and G3) is not coherent even at very low frequencies. Hangingwall motion at sites G2 and G3 becomes totally none coherent around 300 Hz.

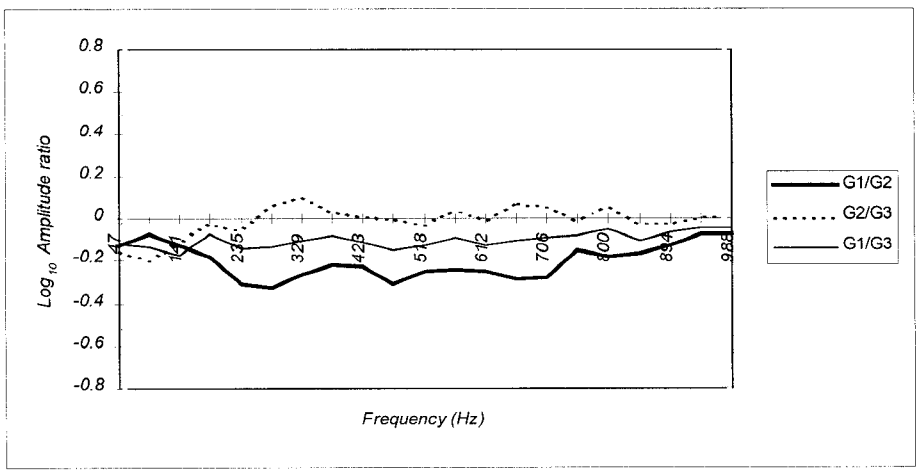

Figure 2.3.21 (a) Log_{10} amplitude ratio as a function of frequency at VLR/P11/S4.

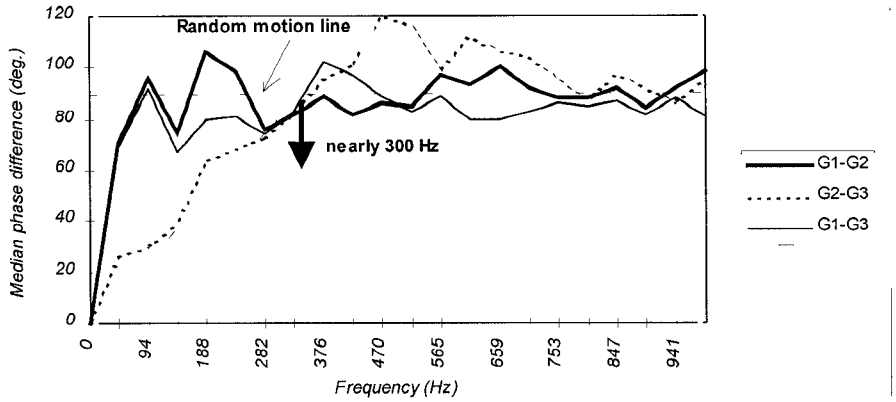

Figure 2.3.21 (b) Median phase difference as function of frequency at VLR/P11/S4.

Maximum velocities at sites VLR/P11/3 and VLR/P11/S4

The maximum velocities for site 3 are shown in Figure 2.3.22 and for site 4 are shown on Figure 2.3.23. In both figures the two hangingwall and the footwall components are plotted against the footwall component.

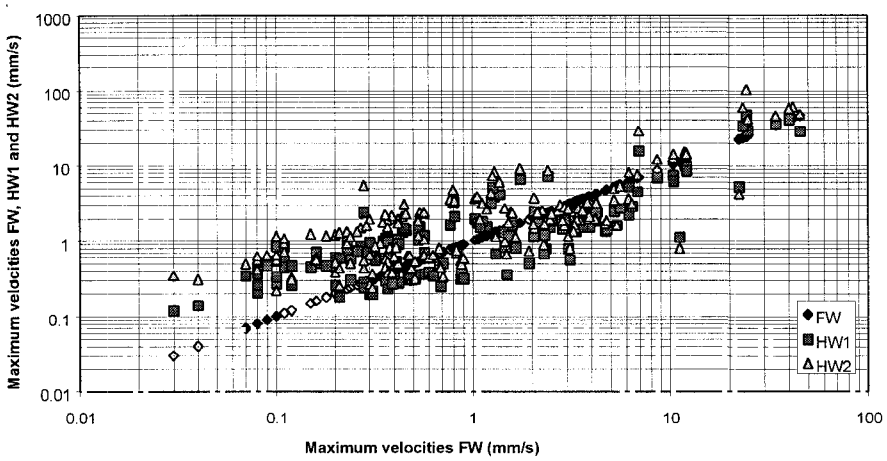

Figure 2.3.22 Maximum velocities recorded at VLR/P11/S3 on the FW, HW1 and HW2.

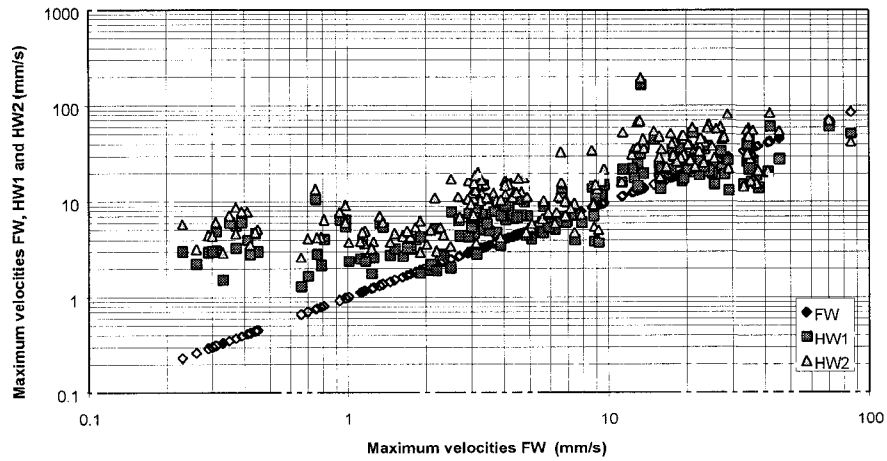

Figure 2.3.23 Maximum velocities recorded at VLR/P11/S4 on the FW, HW1 and HW2.

The maximum velocities at both sites range between 0,003 and 10 mm/s and are relatively consistent. In many cases the velocities recorded at the hangingwall are higher than the velocities recorded at the footwall. The exceptions in Figure 2.3.22 (VLR/P11/S3) are caused by the large number of footwall events recorded there (from the visual inspection of the seismograms).

The values of the maximum velocities recorded at the hangingwall, Figures 2.3.22 and 2.3.26, indicate that the maximum velocities recorded at the point (G3) midway between two support units are higher then the maximum velocities recorded next to the support unit. However, the difference is not great.

Western Deep Levels, East Mine

Geology

Black boxes were installed at the bottom of WDL-E/91/E1 panel near backfill and in WDL-E/93/E4 panel, about 10 m below the gully.

The first site was located down-dip and on the downthrow side of a NE-trending fault with 0,5 m throw. The base of the Green Bar is exposed and a well-laminated pyritic siltstone with a smooth, tectonized base. Fracturing dips steeply to the east and is oriented in the dip direction. Fracturing is rare in the Green Bar and fracture density is 5/m.

The second site is characterised by the typical siliceous hangingwall and argillaceous footwall quartzites. The Green Bar - hangingwall distance is about 1,5 m. The majority of fractures are steeply dipping to the east with strikes in the dip direction. Fracture density is 40/m. The hangingwall had been falling out, with blocks being defined by the steeply dipping fractures and parting planes. Parting planes were 20-30 cm above the stope. The footwall was smooth, being defined by a well-developed argillaceous parting plane. Separation along parting planes deeper in the footwall was evident where footwall blocks had been loosened but not removed.

Site description

A sketch showing the geophone layout for the WDL East Mine experiment is shown in Figure 2.3.24. At both sites geophones G1 were installed in 60 cm long pipes which were in-turn embedded in the backfill. The other two geophones (G2 and G3) were glued to the hangingwall. The experiment is aimed at comparing the backfill response to that of the hangingwall during the passage of the seismic wave. The same analysis as that done on non-damaging events for the Vaal Reefs experiment was done on this data set.

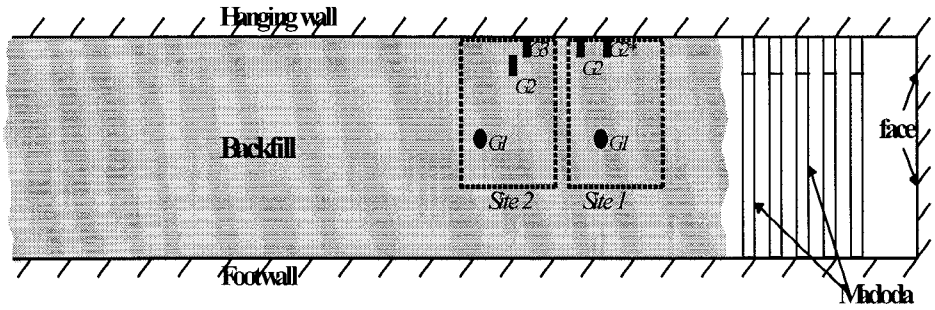

Figure 2.3.24 Diagram showing a layout of geophones (G1, G2, G2*, G3) at two sites in a backfilled stope, WDL-E/94E1/S1 and WDL-E/94E1/S2 geophones G1 are embedded in backfill and G2, G2* and G3 are attached to the hangingwall.

Spectral ratios and phase difference

A ratio between velocity spectra of an event recorded at two geophone stations was calculated for each event in the data set. From this a median spectral ratio was computed at each frequency value. Figure 2.3.25 *(a)* shows a $\log_{10}$ median spectral ratio plotted against frequency. This is data from WDL-E/94E1/S1 of Figure 2.3.24 and ratios were taken between geophones G1 and G2. The plot shows a downward deviation from zero (equal amplitude value) between 24 Hz and 212 Hz. This indicates that the backfill does not respond well in that frequency band, which is a low frequency band. A more

pronounced upward deviation from zero is experienced at high frequencies (more than 680 Hz). At intermediate frequencies the pattern is not well defined.

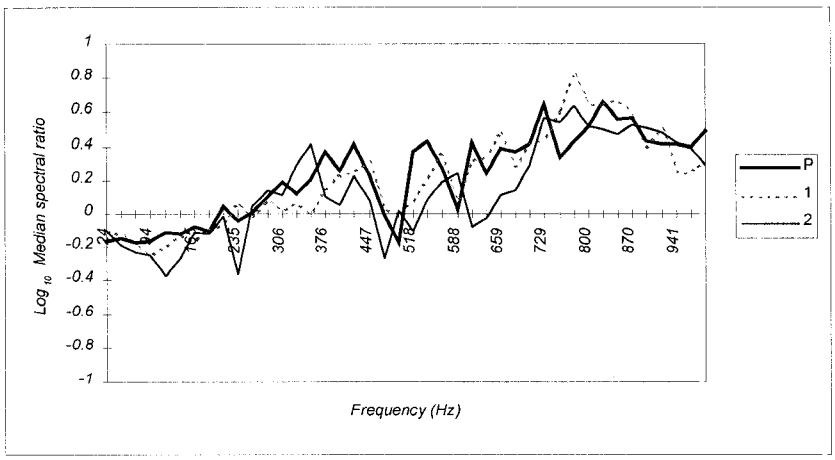

Figure 2.3.25 (a) A plot of Log_{10} median spectral ratio against frequency. Spectral ratios were calculated for geophones G1 and G2 of WDL-E/94E1/S1 shown in Figure 2.3.24.

Figure 2.3.25 *(b)* shows a similar plot for events recorded by geophones G1 and G2* at WDL-E/94E1/S1. In this configuration the geophone G2* is located near to the edge of the backfill and as a result is less influenced. The energy contributed into the low frequencies is more than the energy contributed into the high frequencies.

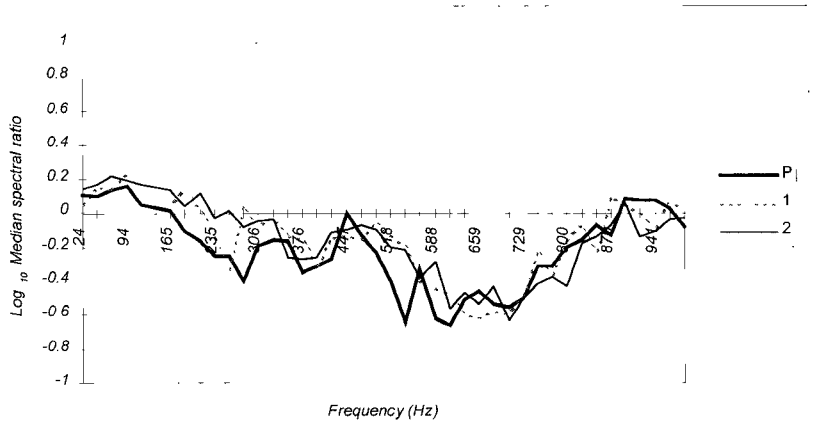

Figure 2.3.25 (b) A plot of Log_{10} median spectral ratio against frequency. Spectral ratios were calculated for geophones G1 and G2* of WDL-E/94E1/S1 shown in Figure 2. 3.24.

Figure 2.3.26 *(a)* is a plot of $\log_{10}$ median spectral ratio against frequency. All the events in the data set have been included. For frequencies between 165 Hz and 500 Hz the backfill has more energy than the hangingwall. Plotted in Figure 2.3.26 *(b)* is the absolute median phase difference between G1 and G2 against frequency. From this plot it is immediately clear that the phase difference is around 90^0 at all frequencies in the frequency range. This means that the motion of the backfill is not in phase with that of the hangingwall.

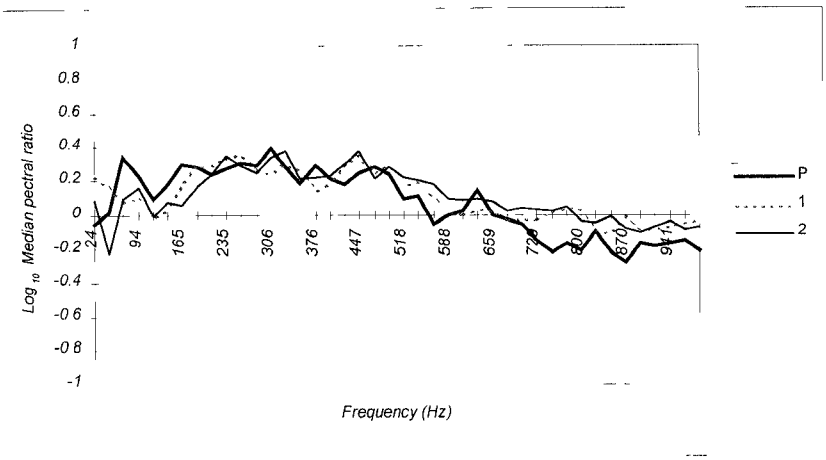

Figure 2.3.26 (a) Log_{10} median spectral ratio between G1 and G2 plotted as a function of frequency. At WDL-E/94E1/S2.

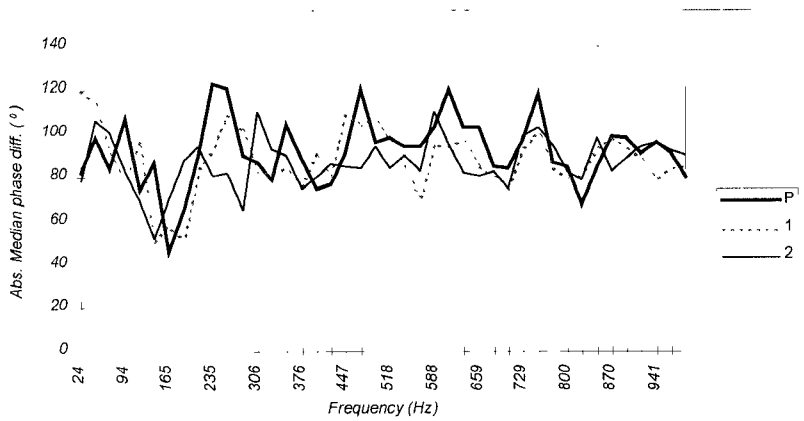

Figure 2.3.26 (b) Median absolute phase difference between geophones G1 and G2 from WDL-E/94E1/S2.

Variations in maximum velocities in respect of the backfill hardening (WDL-E/94E1/S2)

Figure 2.3.27 (*a* and *b*) Illustrates the behaviour of the backfill with time as a function of frequency. It is clear from the Figure 2.3.27 *(a)* that in the earliest stage (30 April and 1 May '97), when the backfill was still soft, less energy was transmitted in the frequency range above 600 Hz. In the next stage, 20 days later (19 May '97), when the backfill became compressed, the deviations in the spectral ratio became smaller and equal along the entire frequency range. It indicates that the interaction between the hangingwall and the backfill improves with time and the support provided by the backfill is more effective.

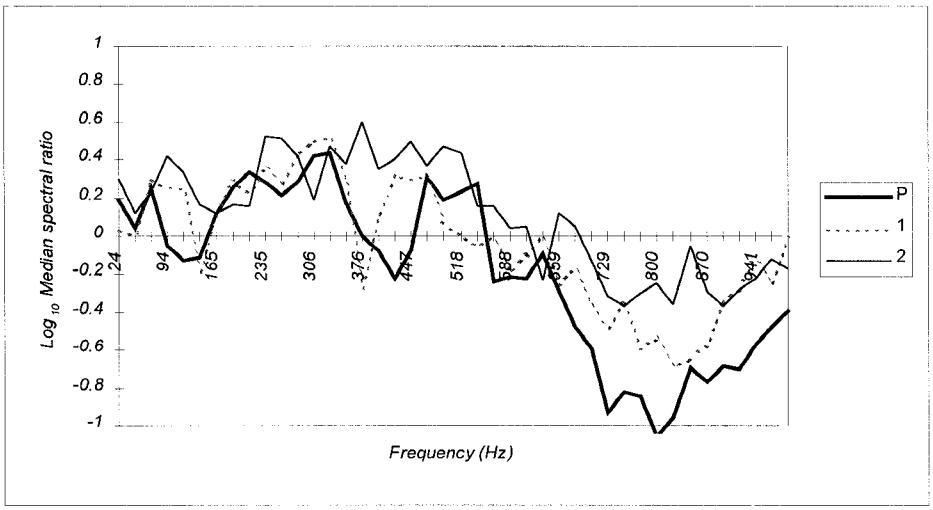

Figure 2.3.27 (a) A plot of Log_{10} median spectral ratio against frequency. Spectral ratios were calculated for 20 events taken in the earliest stage, 30 April and 1 May '97, after the backfill was placed for geophones G1 and G2 of WDL-E/94E1/S2 shown in Figure 2.3.24.

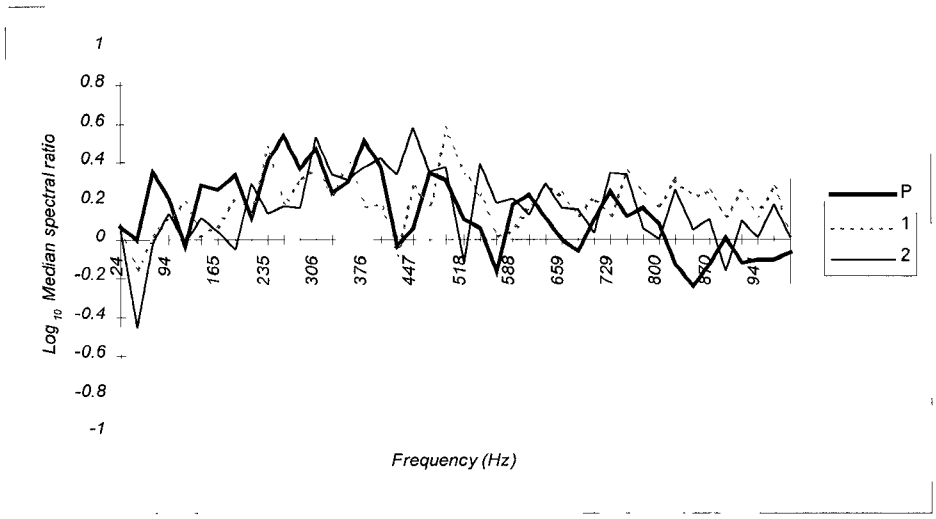

Figure 2.3.27 (b) A plot of Log_{10} median spectral ratio against frequency. Spectral ratios were calculated for 20 events taken 20 days later, 19 May '97 when the backfill was more consolidated. The same set of geophones, WDL-E/94E1/S2, was used as in the Figure 2.3.27 (a).

The WDL, East Mine experiment shows that the backfill responds independently of the hangingwall, hence the value of the median absolute phase difference of around 90^0 at all frequencies. This behaviour is expected to change with time. However, time dependent analysis does not show any obvious change with respect to phase difference. This may be due to the fact that the duration of the experiment was insufficient, or may point to the need for a careful selection of time windows.

Maximum velocities at sites WDL-E/94E1/S1 and WDL-E/94E1/S2

The maximum velocities recorded at WDL-E/94E1/S1 at G1& G2 and G1 & G2* are presented on Figures 2.3.31 and 2.3.32. The maximum velocities recorded at WDL-E/94E1/S2 at G1, G2 and G3 are presented in Figure 2.3.30. The hangingwall geophones were plotted against those geophones embedded in the backfill for all sites. The range of maximum velocities for site one (Figure 2.3.28) is between 0,08 and 35 mm/s, where the scattering of their values is comparatively low.

The maximum velocity shown in Figure 2.3.30 indicates a similar behaviour of the hangingwall components and the backfill component, with a tendency for velocity in the backfill to be slightly higher.

Site WDL-E/94E1/S1 G2 and G2* have the same backfill component but the position of the hangingwall component has been moved. The hangingwall component of the site G2* is closer to the face. The maximum velocities shown on Figure 2.3.28 indicate higher scattering for the hangingwall component than the maximum velocities shown in Figure 2.3.29.

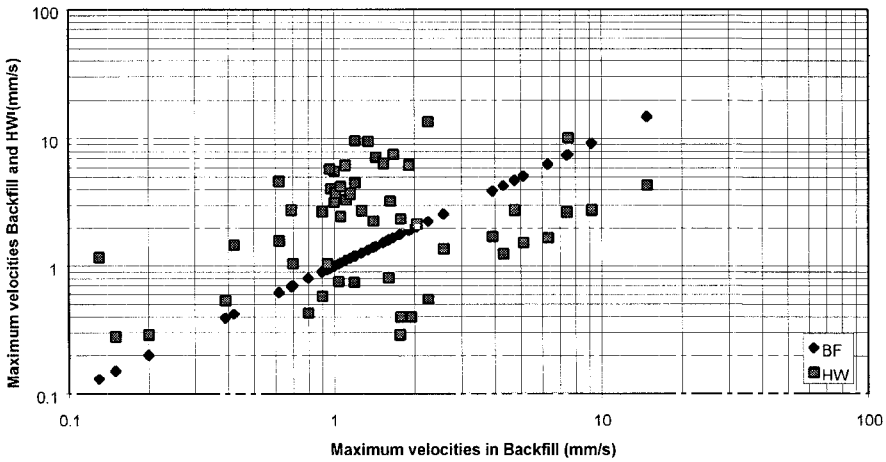

Figure 2.3.28 Maximum velocities at WDL-E/94E1/S1, geophones G1 and G2.

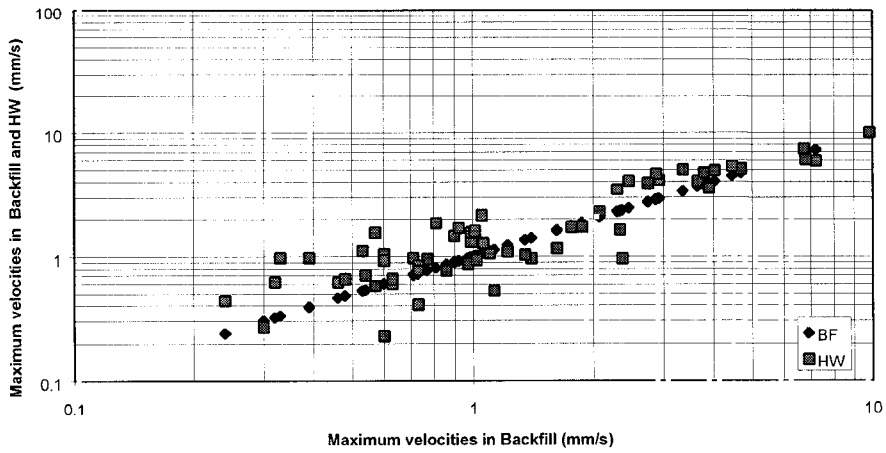

Figure 2.3.29 Maximum velocities at WDL-E/94E1/S1, geophones G1 and G2*.

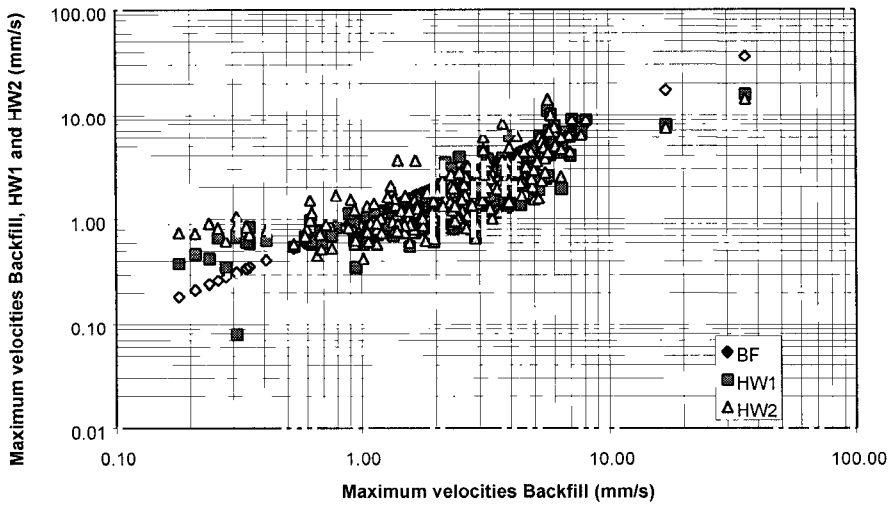

Figure 2.3.30 Maximum velocities at WDL-E/94E1/S2 geophones G1, G2 and G3.

Dynamic behaviour of the " hangingwall - Eben Haeser prop - footwall system " under seismic impact

The 93/E4 and its up dip neighbour 91/E1 stopes at WDL East Mine were chosen for the investigation into stope support. The support system consist of Eben Haeser (EH) elongates with rectangular gully packs and square timber pack. Both panels were blasted at the same time with face advance rate of 15 to 20 m per month.

Two black boxes, with three geophones each, were installed in WDL-E/93/E4. The geophones were in the hangingwall, footwall and on the middle of an EH prop (see Figure 2.3.31).

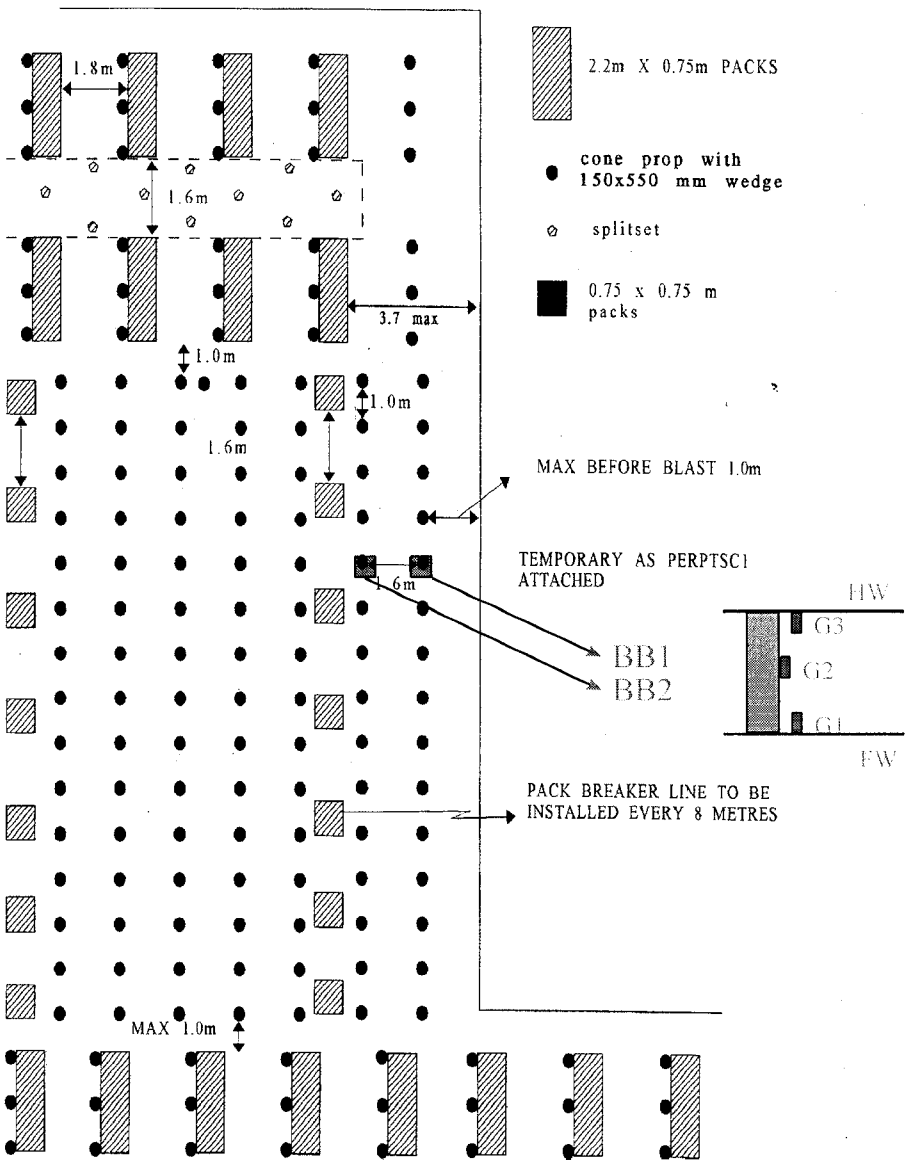

Figure 2.3.31 The geophones and black boxes location at Western Deep Levels - East Mine (WDL-E/93/E4).

Amplitude ratios and phase differences

The data recorded at these sites have been analysed in respect to the behaviour of EH props under dynamic conditions and their interactions with the hanging- and footwall.

The spectral ratio between the EH prop & footwall and EH prop & hangingwall for Black Box 1 is presented on Figure 2.3.32. It can be seen that the vibrations of "EH prop - footwall – hangingwall system" have a minimum in the lower frequency (below 250 Hz), a maximum between 300 and 650 Hz (possible resonance), and very similar behaviour for frequencies above 700 Hz.

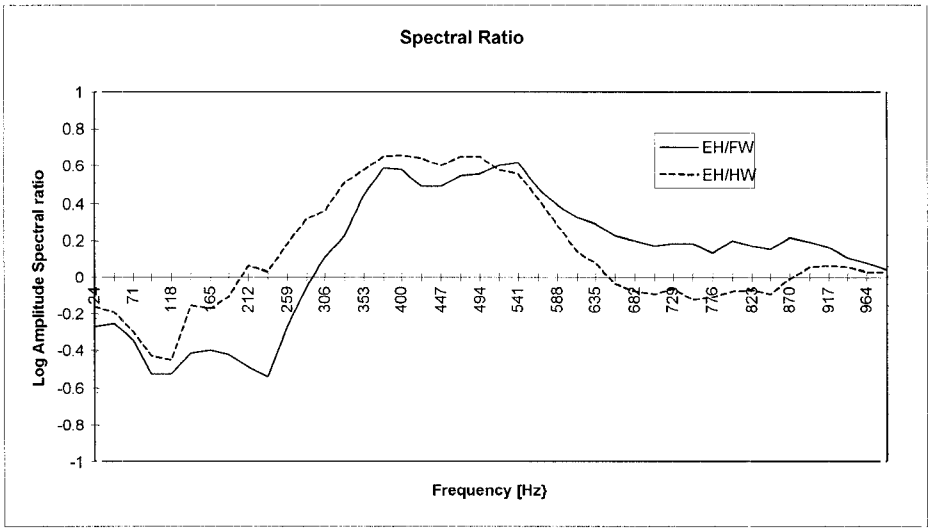

Figure 2.3.32 The spectral ratios between Eben Haeser prop, the footwall and hangingwall for box 1 at WDL-E/93/E4.

Similar behaviour in the spectral ratio is obtained for Black Box 2, Figure 2.3.33. However, the peak below 250 Hz is not so well developed, most probably because of the shorter interval of observations.

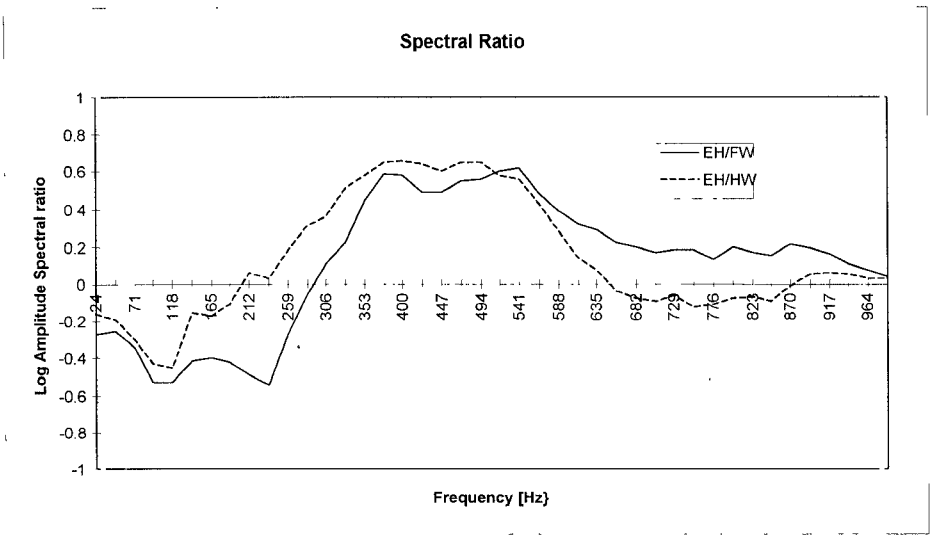

Figure 2.3.33 The spectral ratios between Eben Haeser prop, the footwall and hangingwall for box 2 at WDL-E/93/E4.

The absolute phase difference between EH and hanging- and footwall is presented in Figure 2.3.34. The straight line at 90^0 is the boundary of randomness or the other words the region where, the movement in the "hangingwall – EH prop – footwall" is not correlated. The phase difference reaches this line very quickly and stays there for the entire frequency band.

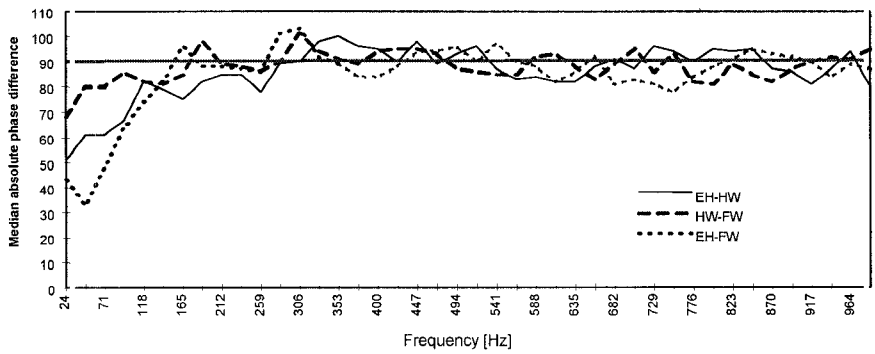

Figure 2.3.34 Absolute phase differences between Eben Haeser prop, the footwall and hangingwall at WDL-E/93/E4.

The maximum velocities recorded in the "Hangingwall – EH prop – Footwall system ", are shown on Figure 2.3.35. It can be seen that the maximum velocities have changed in time. During the earliest period after the installation the upper part of the prop is less stiffer, than the lower part because of the yielding element located in the upper part. The maximum velocities recorded on the EH prop are higher in range at this time and are more similar to those recorded on the footwall. During the later stage, when the closure starts to affect the element, the stiffness of the upper and the lower part become more similar and the scattering amongst the maximum velocities declines.

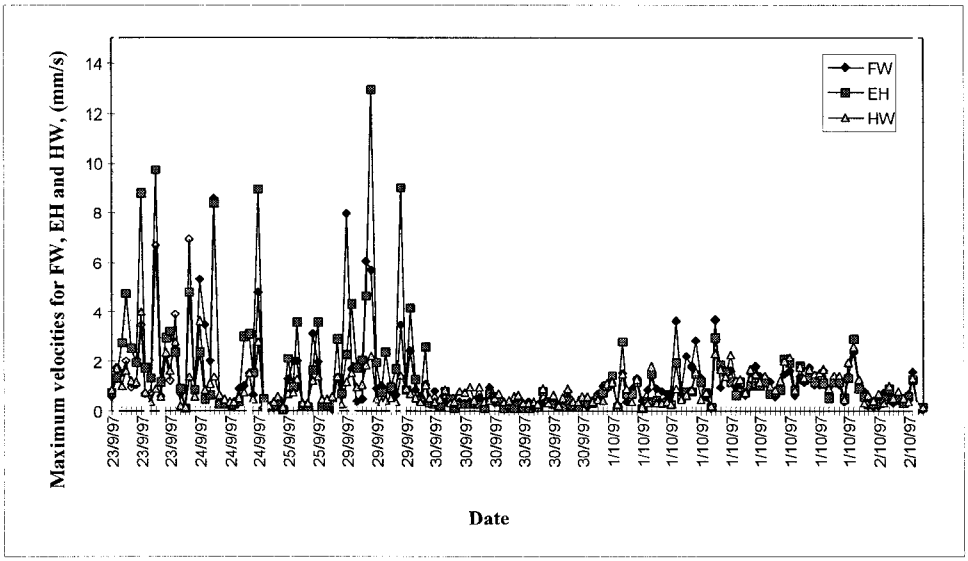

Figure 2.3.35 The maximum velocities in [mm/s] at G1, G2 and G3 as a function of time at WDL-E/93/E4 box no.1.

Western Deep Levels, South Mine

Geology

The VCR in this area has an average thickness of 1 m and dips at 21° in a southerly direction. The reef is polymictic and comprises two conglomeritic bands intercalated by an immature to sub-mature channel bar with no complex geomorphology. The reef lies unconformably on the coarse, gritty, light grey Elsburg Quartzites. The competent, andesitic type lava of the Alberton Porphry Formation forms the hangingwall.

Site description

A site at WDL South Mine at 91 level W5 panel was identified for this study. Accelerometers were attached to the hangingwall as shown in Figure 2.3.36. The distance between the adjacent accelerometers is nearly equal to 0,5 m. Twenty seismic events were recorded. For each event, phase differences and amplitude ratios between ground motions (x,y), (y,z), and (z,x), were calculated to study relative motion between the sites.

Figure 2.3.37 shows the plot of median phase difference as a function of frequency. The median is calculated for the 20 events. As can be seen from this plot that the (x,z) combination has a lower rate of increase of phase difference with frequency than the (y,z) and (z,x) combinations. Taking the (x,y) and (y,z) combinations, the phase difference rapidly goes to maximum (90^{0}) around 300 Hz , meaning that, even at low frequencies, relative ground motion at these sites is independent.

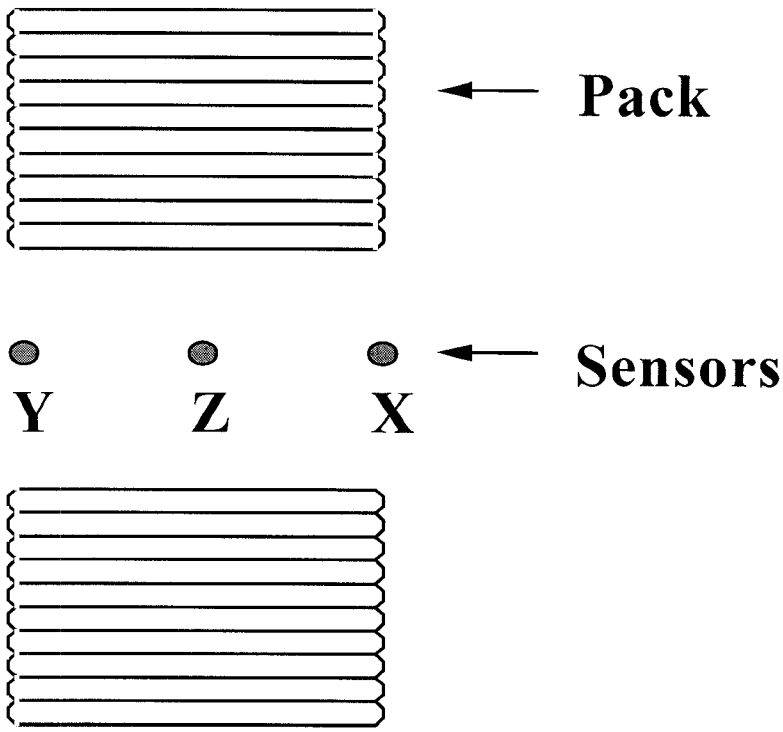

Figure 2.3.36 Layouts of the vertical accelerometers on the hangingwall at WDL-S/91/W5.

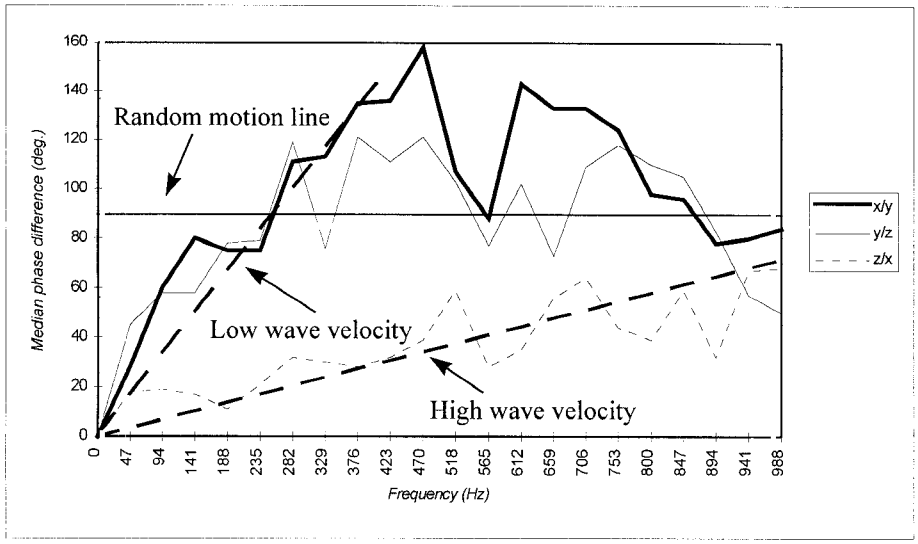

Figure 2.3.37 A plot of median phase difference as a function of frequency for a layout shown in Figure 2.3.36 (site WDL-S/91/ W5).

Amplitude ratios between sites are plotted in Figure 2.3.40. Ratios between sites x and z are in agreement with phase difference analysis, with log amplitude ratios close to zero (an amplitude ratio of one is for similar amplitudes) throughout the frequency range. Except for relative motion between x and y, which shows a decrease in the ratio above 330 Hz, amplitude ratios do not show a clear-cut difference between the sites for this data set.

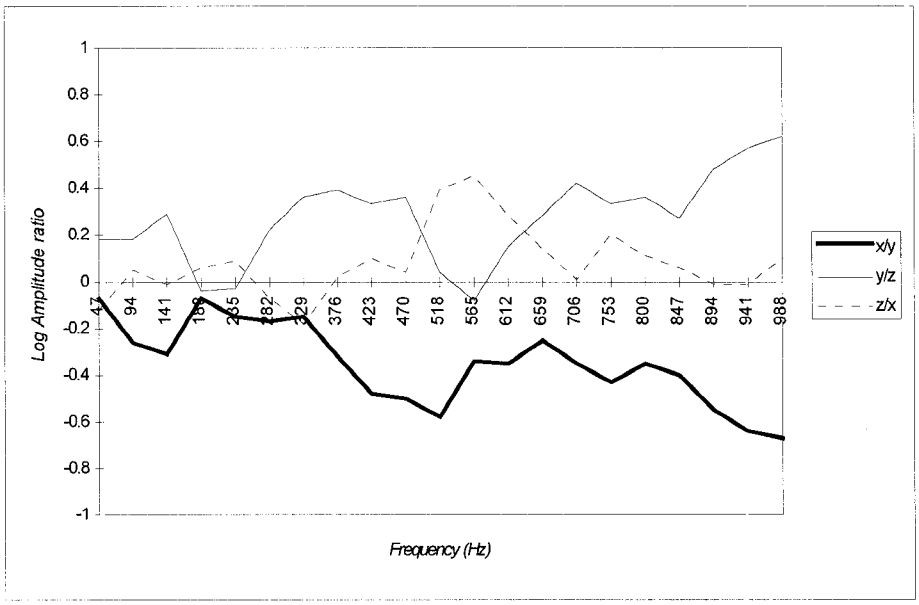

Figure 2.3.38 Log amplitude ratio as a function of frequency for a layout shown in Figure 2.3.36 (site WDL-S/91/ W5).

Analysis of elastic and inelastic components during the seismic motion

For two sensors (A and B) in a perfectly elastic medium, the maximum phase difference, $\delta(f)$ at any frequency (f) is limited by the distance between them (D) and the phase velocity (V) as follows:

$$|\delta(f)| \leq 2\pi fD/V \qquad (2.15)$$

The maximum phase difference will occur for the smallest phase velocity for waves travelling between A and B. In the stope footwall or hangingwall, the slowest phase is the Rayleigh wave, which is approximately equal to 0,9 times the S-wave velocity for a perfect half-space. In the earth, Rayleigh-wave phase velocities are a function of frequency due to lower P- and S-wave velocities near surface. In this study, we are assuming that the rock mass has a constant velocity and are attempting to analyse any variations. Similarly, the difference in amplitude at A and B will be very small for distant events, where the hypocentral distance, R >> D. The amplitude and a phase can then be illustrated as in Figure 2.3.39.

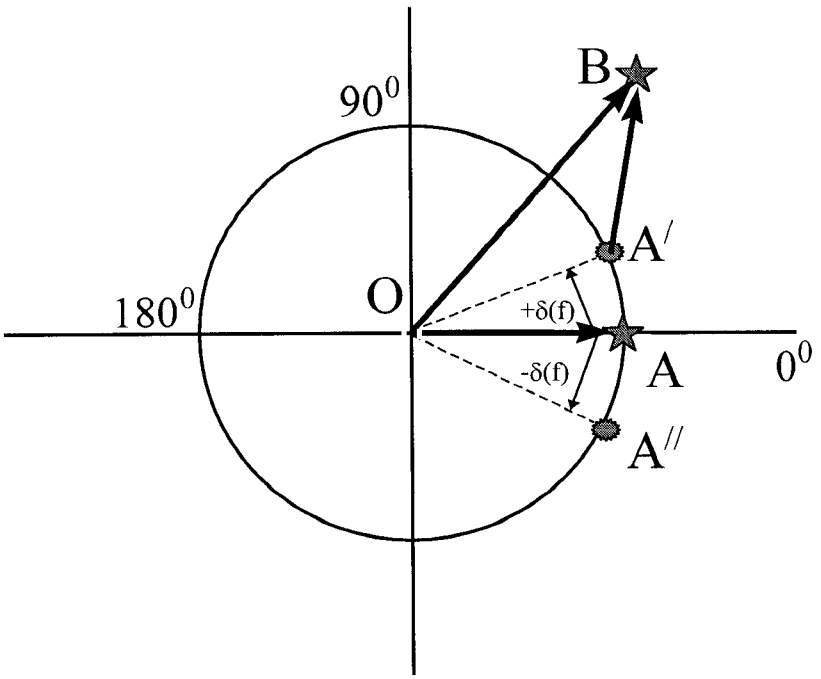

Figure 2.3.39 Phase diagram showing limits to elastic behaviour.

In this figure, the amplitude and phase at each frequency can be represented by points A and B. The arc $\overrightarrow{A'AA''}$ is then the allowable range of amplitude and phase at point B for elastic solid rock, where the phase difference is described by Equation (2.15).

In practice, we have found that point B does not fall on this arc: departing from the ideal both in amplitude and phase. Whereas ground motion at A and B can be properly

described by the vectors $\overrightarrow{0\mathrm{A}}$ and $\overrightarrow{0B}$, the difference in ground motion between points A and B is $\overrightarrow{\mathrm{A}B}$. As elastic behaviour in solid rock dictates that point B should plot along the arc $\overrightarrow{A'AA''}$, $\overrightarrow{A'B}$ is then a minimum estimate of the departure from ideal behaviour. This departure from ideal behaviour, expressed as a ratio of behaviour at one of the geophones, say at A, is then $\frac{\overrightarrow{A'B}}{\overrightarrow{0A}}$.

Data recorded in the Vaal Reefs Mine was used to calculate this factor (Figure 2.3.40) as a function of frequency. Ground quality decreases as we move from low to high frequencies. These are preliminary results and further application and interpretation of the method still needs to be done.

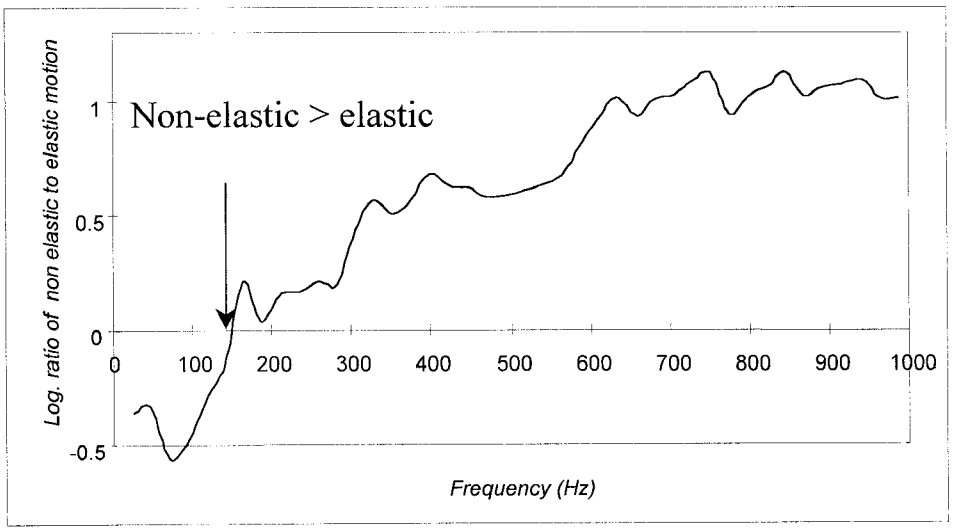

Figure 2.3.40 Log of ratio of motion due to deviation from elasticity to motion in perfectly elastic medium plotted against frequency.

Peak velocity frequency magnitude plot

This analysis evaluates the expected number of events with a particular peak velocity. Figure 3.2.44 shows a plot of a cumulative number of events as a function of peak velocity. A decrease in the cumulative number with the increase in velocity can be seen and the dotted line is an extrapolation that suggests that about one event with v_{max} = 0,4 m/s would occur per day. Also extrapolation to longer time periods is possible, although prone to errors.

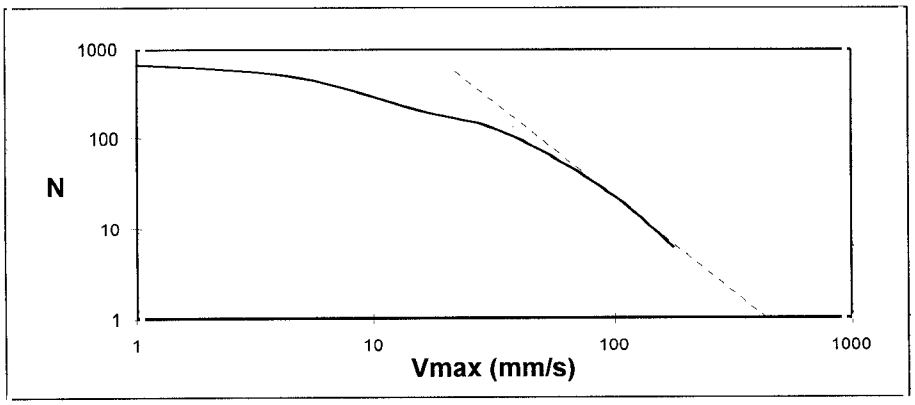

Figure 2.3.41 Cumulative number of events as a function of peak velocity for 71 panel-days.

Conclusions

Vaal Reefs Mine:

The surface of the rock to which the geophones G2 and G3, site VLR/P14/S1, 1m apart vibrate in phase over the entire frequency range 24 Hz - 965 Hz.

At a frequency greater than 600 Hz, the energy at the geophone G2 at site VLR/P14/S2 is nearly 400 times greater than at the nearby geophones G1 and G3.

Variations in the maximum velocities recorded before and after a strong seismic event have been obtained. This phenomenon has been recorded at two sites at Vaal Reefs (VLR/P14/S1 and VLR/P14/S1).

The mechanism of these variations is multi-purposed. Two possible interpretations have been proposed: (i) redistribution of the shear stresses before and after the event, and (ii) increasing effect of the support system after the event.

Western Deep Level East Mine:

Backfill site

Phase difference plots show no coherence between hangingwall and backfill motions at all frequencies.

In the frequency range 200 Hz - 520 Hz, backfill energy is nearly 2,5 times greater than that of the hangingwall.

Elongate site

The coherent vibrations of "Eben Haeser prop - footwall – hangingwall system" indicate: a minimum in the lower frequency (below 250 Hz), a maximum between 300 and 650 Hz (possible resonance), and very similar behaviour for frequency above 700 Hz.

The variations in the maximum velocities show dependence on time. While the stiffness of the "Eben Haeser prop - footwall – hangingwall system" increased, the maximum velocities decreased.

2.3.4. Measurements of site response during actual rockbursts

Initially the Ground motion monitor was designed to record very strong seismic events in extreme conditions of rockburst. A few cases are described in this section.

East Rand Proprietary Mines

On 24 July 1995 a rockfall occurred at East Rand Proprietary Mine (ERPM), damaging the secondary incline of the Hercules shaft between 32- and 33-level, about 1500 m below surface. The rockfall, which caused the death of four workers, took place at 01h45. The seismic network recorded no seismic event at this time. A few weeks later a ground motion monitor (black box) was installed near the site of the rockfall, to investigate any further seismic activities.

A second (rockfall) rockburst occurred on 15 August 1995 at 22h10, causing injuries to workers installing support in the incline shaft. A large seismic event of magnitude M=0,9 was detected by the mine seismic network at this time. The ground motion monitor also recorded the event. The seismogram is shown on Figure 2.3.42. A total number of 19 seismic events located in the vicinity of the black box were recorded during the period of observation in the range of maximum velocities from 2,8 to 184,8 mm/s.

The data recorded by this black box were visually inspected and compared with the data recorded by the conventional seismic network operating at the mine. It was found that the quality of the seismograms recorded by the CSIR Ground Motion Monitor is sufficient enough to study microseismicity on a local scale around active mining structure.

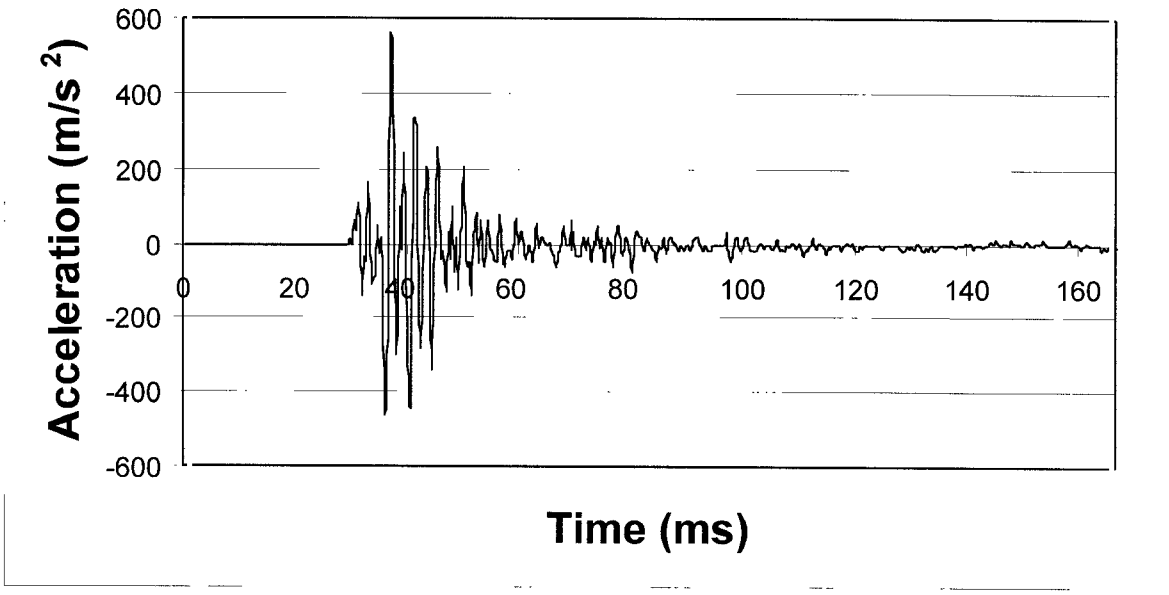

Figure 2.3.42 Accelerogram recorded at the time of the (rockfall) rockburst on 15 August 1995 at ERPM. Peak velocity is equal to 184,8 mm/s. The ground motion monitor was installed in the 32-level cross-cut.

Vaal Reefs

Estimation of peak velocity for saturated seismograms.

Both the PSS and the Black Box have limited dynamic range and the signals saturate, or clip, when the amplifier output stage reaches 10 V. In many cases, the geophone itself has not reached its limit and the signal resumes its "normal" behaviour when its level falls below the full-scale level, either negative or positive. It can therefore be assumed that the seismogram is simply clipped without any instrumental problems occurring during recovery from the clipped portion of the trace.

The purpose of this short code is to present and test a simple algorithm for estimating the peak value of any swing of a seismogram, using the half-period as measured on either side of this swing and the averaged first difference at the adjacent zero cross-over points.

Consider a sinusoidal velocity seismogram, with peak velocity V_0:

$$V = V_0 * \sin(\omega t) \tag{2.16}$$

The corresponding acceleration seismogram would be:

$$A = A_0 * \cos(\omega t) \tag{2.17}$$

where the peak acceleration $A_0 = \omega V_0$

The angular frequency, ω, is related to the period, T, by $\omega = 2\pi/T$. The values of A_0 and the half-period, T/2, can be measured even when the velocity signal is clipped and we can calculate the peak using:

$$V_0' = (T/2) * A_0 / \pi \tag{2.18}$$

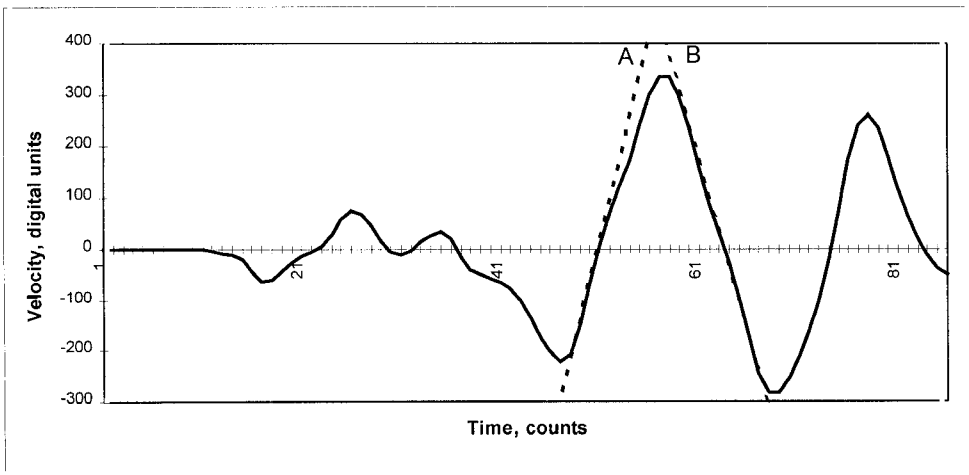

Figure 2.3.43 Plot illustrating measurements of acceleration before and after a peak in the velocity seismogram.

Of course, a seismogram is not a pure sinusoidal signal and has a rich spread of frequencies across the entire seismogram. Therefore the applicability of Equation (2.18)

was tested on some black box data, by adding an option in program BBOX, the program that is used to analyse the black box seismograms.

As A_0 can be measured at the zero cross-over positions either before or after the peak value of V, V_0' was firstly estimated using the smaller and larger of these values of A_0. Inspection of the plot of the inferred values of peak velocity, $V_{0\,max}'$ and $V_{0\,min}'$, as a function of V_0, led to the following best estimate of A_0 :

$$V_0' = 2 / (1/V_{0\,max}' + 1/V_{0\,min}') \qquad (2.19)$$

Application of this Equation for data recorded at Vaal Reefs in plotted in Figure 2.3.44.

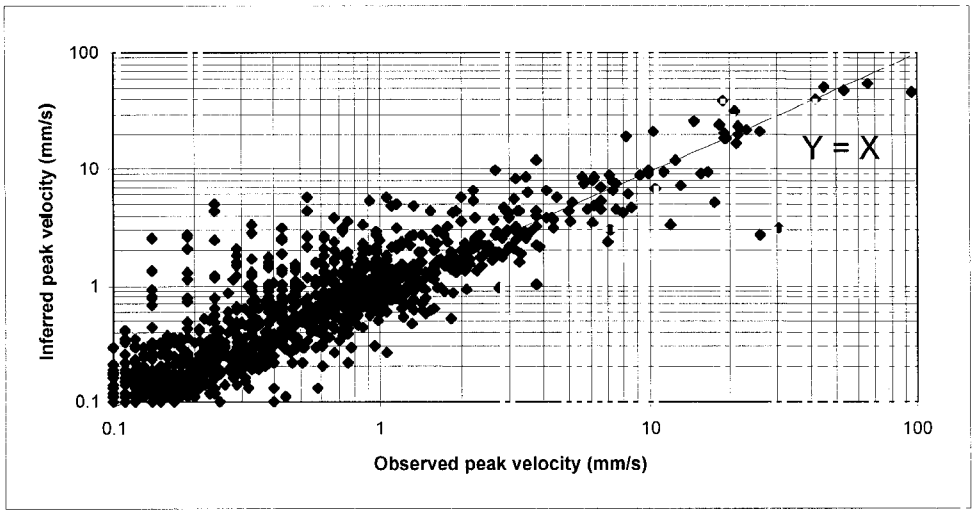

Figure 2.3.44 A plot of V_0' as a function of V_0 for data from the Vaal Reefs. The identity line Y=X is shown for comparison.

It can be seen in Figure 2.3.44 that the inferred peak velocity as obtained from Equations (2.18) and (2.19) above is approximately equal to the observed peak velocity.

This method can be used to estimates values of peak velocity for saturated traces, 269 of the 303 peak values for V_{max} > 1 mm/s (89%) were estimated within a factor of two (0,5 mm/s to 2,0 mm/s) by this method. Given the variations in ground motion for nearby sites, this estimate is considered to be fairly good.

2.3.5. Transfer function for a seismic signal recorded in solid rock and on the skin of an excavation

Introduction

The objective of this work is to quantify the effect of the rock mass surrounding a stope or tunnel on the seismic signal. Work done as part of this project in 1996 shows that the transfer function of rock mass surrounding an excavation can be modelled using a damped oscillator (Cichowicz, 1996).
In this report the method of estimation of transfer function is extended further. Parameters of a damped oscillator are estimates using inversion techniques. The transfer function is modelled as a time varying system. Application of the technique of time varying systems is essential to track the time variation of the natural frequency during ground motion caused by a seismic event.

Method

Ljung and Soderstrom (1983) and Ljung (1987) studied methods for the time-domain identification of linear structural dynamic systems wit multiple degree of freedom. The term identification refers to the determination of analytical models for structure, based on the observations of the system. Recordings of a single input and single output are sufficient to determine all the modal frequencies and damping ratios in a structure (Safak, 1989).

The equivalent discrete-time equation for a single input, single output dynamic system can be written in the following form:

$$y(t) + a_1 y(t-1) + \ldots + a_l y(t-l) = b_1 u(t-1) + \ldots + b_m u(t-m) \qquad (2.20)$$

where u(t) and y(t) are the input and output sequences, respectively; a_i and b_i are constants for time invariant systems and functions of time for time varying systems. Although the equation represents a linear system, it was suggested that any non-linear

system can also be represented by a similar equation with time varying parameters (a_i,b_i), by introducing the following polynomials in the back-ward-shift operator q^{-i} , where q^{-i} is defined as q^{-i} y(t)= y(t-i),

$$A(q) = 1 + a_1 q^{-1} + ... + a_l q^{-l} \tag{2.21}$$

$$B(q) = b_1 q^{-1} + ... + b_m q^{-m} \tag{2.22}$$

Equation (2.20) can be written in a more compact form as:

$$y(t) = \frac{B(q)}{A(q)} u(t) \tag{2.23}$$

The polynomial ratio B(q)/A(q) is called the system transfer operator, H(q). Discrete-time equations can also be expressed in the frequency domain by taking the Z-transform of time domain equations. By taking the Z-transform of both sides in Equation (2.23) we can write:

$$Z[y(t)] = \frac{B(z)}{A(z)} Z[u(t)] \tag{2.24}$$

where Z[y(t)] = the Z-transform and z is any complex number. The polynomials A(z) and B(z) are the same as defined by Equations (2.21) and (2.22) except all the qs are replaced by the zs. The transfer function can be represented in terms of harmonic functions by selecting $z = \exp(i2\pi f \Delta t)$, where f denotes the frequency and Δt is the sampling interval.

The stability conditions require that the roots of the denominator polynomial A(z) should all have a magnitude less than one. This means that the roots of A(z) are all in complex-conjugate pairs located inside the unit circle in the complex plane. The transfer function can be put into the following form:

$$H(z) = \sum_{j=1}^{n_a/2} H_j(z) \tag{2.25}$$

where:

$$H_j(z) = \frac{2R(q_j) - 2R(q_j \bar{p}_j)z^{-1}}{1 - 2R(p_j)z^{-1} + |p_j|^2 z^{-2}} \tag{2.26}$$

where $H_j(z)$ is the second order filter, R(q) is the real part of q, $\bar{p}$ is the complex conjugate, p_j is the complex root of the polynomial A(z) and q_j is the corresponding residue of H(z). The filter output y(t) is modelled as the linear combination of the outputs of second-order filter each subjected to input u(t). The form given by Equation (2.25) is known as the parallel form of realisation. Each second-order filter $H_j(z)$ corresponds to a simple, damped oscillator. The damping d_j and the frequency f_j of each oscillator are defined by the equations (Safak, 1989):

$$d_j = \frac{\ln(\frac{1}{r_j})}{[F_j^2 + \ln^2(\frac{1}{r_j})]^{1/2}} \tag{2.27}$$

$$f_j = \frac{\ln(\frac{1}{r_j})}{2\pi d_j \Delta t} \tag{2.28}$$

where: $r_j=|p_j|$, F_j are the modulus and the arguments of the jth pole (or of its complex-conjugate).

The recordings from dynamic systems are always contaminated by noise existing in the recording environment, as well as by the imperfections in the recording instrument. Hence the following equations for the signal:

$$A(q)y(t) = B(q)u(t) + C(q)e(t) \tag{2.29}$$

where:

$$C(q) = 1 + c_1 q^{-1} + ... + c_n q^{-n} \tag{2.30}$$

and e(t) is a white noise sequence. Equation (2.30) represents a family of model structures for noise systems. The A(q) corresponds to poles that are common between the dynamic model and the noise model. The motivation for introducing C(q) polynomial is to provide for flexibility in the noise descriptions.

Recursive prediction error methods

System identification constitutes determining the coefficients of the polynomials in A(z), B(z) and C(z) for a given pair of input and output sequences:

$$\Omega = (a_1,...,a_l,b_1,...,b_m,c_1,....,c_n) \tag{2.31}$$

The one step ahead prediction $y_{pred}(t, u(t),a_i,b_i,c_i)$ of y(t) at time t is based on the past values of input u(t), output y(t) and parameters a_i b_i c_i. The difference:

$$E(t,\Omega) = y(t) - y_{pred}(t,\Omega) \tag{2.32}$$

gives the error in the estimation at time t. System identification aims to determine the vector ,Ω, such that the total error $\sum E^2(t,\Omega)$ is minimum. The measure of the total estimation of error must be decided. The most convenient way is the least square method. The least-square method uses quadratic criteria for measuring errors. A weighting factor (forgetting factor) is also included in the criteria.

$$E = \sum_{k=1}^{t} L^{t-k} E^2(t,\Omega) \tag{2.33}$$

L is the forgetting factor. Measurements that are older carry less weight in (14) than the current values. For time invariant systems, weighting factors can all be taken as equal to one. For time varying systems, weighting factors are essential to track the time variation of system parameters. The forgetting factors localise the identification by giving more weight to the current values, and by gradually discounting the past values.

A recursive identification algorithm is:

$$\Omega(t) = \Omega(t-1) + K(t)[y(t) - y_{pred}(t)] \qquad (2.34)$$

where $\Omega(t)$ is the parameter estimate at time t, and y(t) is the observed output at time t. y_{pred} (t) is a prediction of the value y(t) based on observation up to time t-1. The gain K(t) determiners in what way the current prediction error y(t) – y_{pred}(t) affects the update of the parameter estimation. In this report the Matlab implementation of Equation (2.35) is used.

Data and results

Three tests have been conducted at:

1. Blyvooruitzicht Gold Mine, where two geophones were used to study the transfer function. The geophones were installed in close proximity to each other; the first in solid rock and the second in the footwall drive.

2. Vaal Reefs No.5 Shaft, two geophones were used installed in hangingwall of stope; one close to support and another 1,1 m away.

3. Vaal Reefs No.5 Shaft, where two geophones were used., one was installed on the footwall and the second one on hangingwall.

Examples of ground motion, sum of five modal response, velocity spectra and the transfer function is shown on Figures 2.3.45, 2.3.46 and 2.3.47.

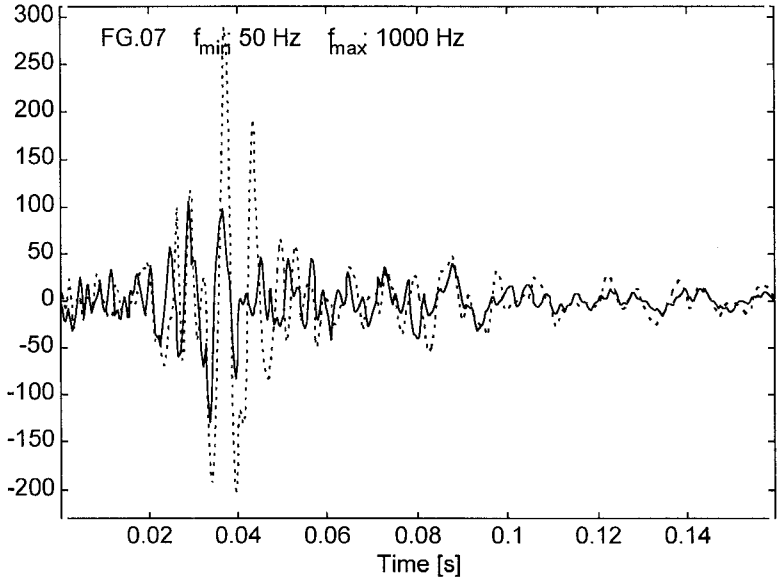

Figure 2.3.45 An example of real seismograms (event FG07), recorded in solid rock - solid line, and in a fractured rock - dashed line.

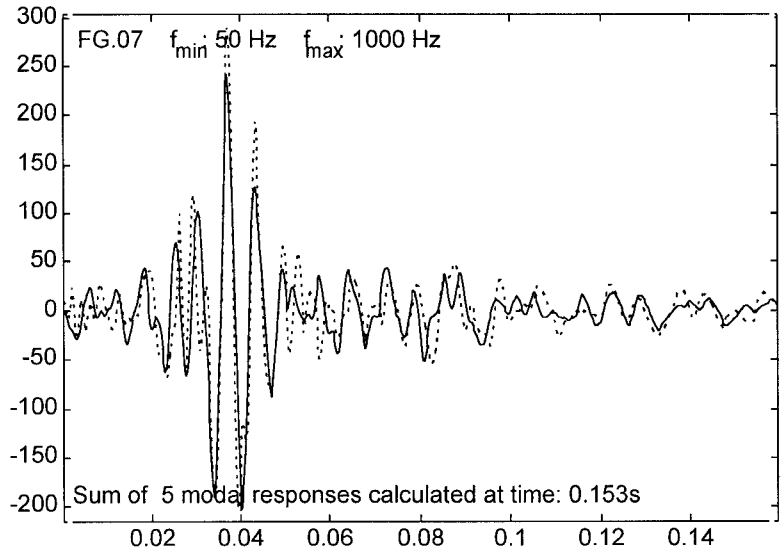

Figure 2.3.46 Sum of five modal responses calculated at time 0.153 s.

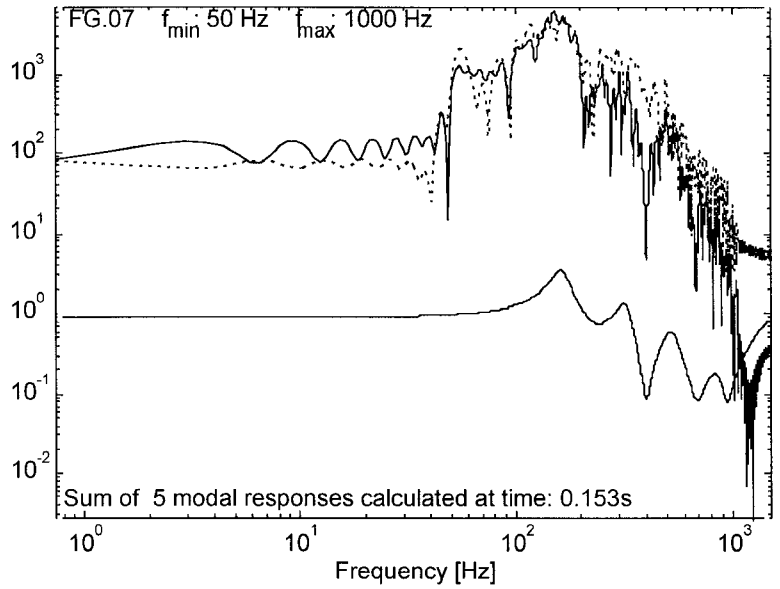

Figure 2.3.47 The spectrum of the seismograms from Figure A.2.3.46 and their transfer function.

The results obtained from all data and their detailed discussion are presented in Appendix 1.

Conclusions

Experiment 1:

The models of transfer function are reliable, as all models are similar.

The first pulse of the seismogram has a different transfer function from the rest of record. This could be an indication that the initial behaviour of the site is non-linear.

Experiment 2

The Influence of support on vibration in the hangingwall is measurable. The algorithm presented in this report estimated different vibrations at different sites in the hangingwall. The obtained model of transfer function is reasonable.

There is strong indication that properties of the site change with time (weeks).

Experiment 3

The difference between ground motion in the footwall and ground motion in the hangingwall cannot be properly modelled with modal transfer function.

2.3.6 Velocity amplification considered as a phenomenon of elastic energy release due to softening

Introduction

The amplification of wave motion on the walls of excavations in the deep, hard rock gold mines of South Africa has been observed and reported: peak velocity and acceleration parameters at the surface of an excavation indicate a 4 to 10 fold increase when compared to measurements within the solid rock (Durrheim et al. 1996). The observed amplification is considerably greater than the two-fold amplification expected at a free surface. The effect is, additionally, although indirectly, confirmed by observations of wall-rock velocities which sometimes reach 10 m/s (Ortlepp 1993). The author of the cited paper distinguishes between source mechanism and damage mechanism; he writes (p. 104): "This dichotomy will highlight paradoxes such as, importantly, how the relatively low PPV generated in the rock mass does not reconcile with the high velocity displacements of the wall rock." From this we may see a clear recognition of the differences between parameters of an incident wave and those appearing near the surface of an excavation. McGarr (1996) also states that the velocity of the wall rock is "substantially greater than ground velocities associated with the primary seismic events". Discussing a quantitative

relation between these velocities, he writes: "Whereas several types of evidence suggest that slip across a fault at the source of an event generates nearby particle velocities of at most, several m/s, numerous observations, in nearby damaged tunnels, for instance, imply wall-rock velocities of the order of 10 m/s and greater".

Three different mechanisms have been suggested to explain the source of energy for this phenomenon: (i) resonance, which is discussed, with reservations, by Durrheim et al. (1996); (ii) trapping of energy within a channel (Spottiswoode, pers. comm. 1997); and (iii) energy release due to slab buckling (McGarr, 1996). All three hypotheses invoke changes in the structure of rock near an excavation due to growth of cracks induced by rock pressure. The first and the second hypotheses consider purely geometrical changes; which implies that amplification may occur even in unloaded rock, given that the crack geometry exists. The third hypothesis, in contrast, requires the supply of elastic energy from highly stressed rock. Hence, it implies that the amplification will not appear in unloaded rock. Resonance is not considered to be a likely mechanism as there is no periodic excitation sufficiently long. (Spottiswoode, pers. comm. 1997). The "channel" hypothesis seems more plausible. While this hypothesis cannot explain the fact that the amplification occurs both at surfaces with nearby cracks parallel to them and at surfaces with nearby cracks perpendicular to them, channelling may provide its input into amplification. In the extreme case, where a small seismic event triggers a greater event (a rockburst in particular), the main source of energy supply for velocity amplification is the elastic energy stored in rock. Consequently, the third hypothesis appears the most attractive.

McGarr (1996) has explicitly expressed the energy hypothesis, attributing high wall-rock velocities to the buckling of rock slabs stressed near to their compressive strength. Note, however, that buckling is but one of a variety of possible mechanisms for instability with energy excess. The buckling mechanism places emphasis on the aspect of a geometrical non-linearity appearing in slab flexure. However, there exists another type of non-linearity *viz.* a physical non-linearity. The latter is of major importance for compressed rock (Linkov 1994 and 1995). Taking this as the point of departure, we suggest another mechanism of energy release, which places emphasis on the physical, rather than geometrical, non-linearity of highly compressed rock. This non-linearity is termed softening (or weakening) and has been shown to be responsible for dynamic phenomena in mines (Cook 1965; Salamon 1970; Linkov 1994 and 1995).

In conclusion of this brief review, note that the pioneering papers by Ortlepp (1993) and McGarr (1996), although concerned with wave amplification, do not address it in a direct way. They do not trace amplification of the same seismic wave coming from a remote source to an excavation. In this study, we attempt to treat the problem explicitly by directly studying the amplification of the same wave. Our aim is to consider wave amplification as a phenomenon of energy release due to softening.

Wave amplification at softening contacts

Amplification of a reflected wave

The essence of wave amplification due to softening can be explained by considering the simplest scheme of a plane shear incident wave. A displacement wave $w=f(x - ct)$ arrives at a moment $t=0$ at the plane boundary $x=0$ (Figure 2.3.48 (a)). The displacements generate shear stresses τ. These displacements and stresses are added to the displacement u_o and stresses σ_o of the initial state; the latter is supposed to be given. The total displacements u and shear stresses σ_τ are the sums:

$$u = u_o + w\,;\ \sigma_\tau = \sigma_o + \tau. \tag{2.35}$$

The contact interaction at the boundary $x=0$ occurs via specific "springs" which exhibit softening with the softening modulus M_c after reaching the limit shear strength τ_m corresponding to the shear displacement u_m in a reversible process with the contact modulus E_c (Figure 2.3.49). The analytical expression for the interaction if given by the formula:

$$-\sigma_\tau(0,t) = \begin{cases} E_c u(0,t) & u<u_m \\ \tau_m - M_c\,[u(0,t) - u_m] & u_m<u<u_* \\ \tau_* & u_*<u \end{cases} \tag{2.36}$$

The "minus" sign at $-\sigma_\tau(0,t)$ accounts for the fact that the normal to the surface $x=0$ is taken in the direction of the x axis; the value of the shear strength τ_m depends on the

normal stress in the medium; assuming the normal stress is fixed, the shear strength τ_m is also fixed.

Inside the medium *(x < 0)*, the total shear stress σ_τ is related to the total displacement, *u*, by Hooke's law $\sigma_\tau = G\partial u/\partial x$ where *G* is the shear modulus of the medium. Due to the linear elasticity of the medium the same law relates the values in the wave:

$$\tau(x,t) = G\,\partial w/\partial x \qquad (2.37)$$

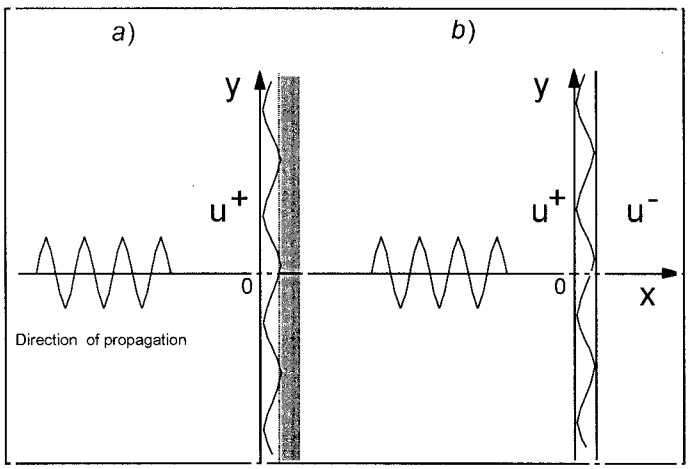

Figure 2.3.48 Shear wave impinging on a softening contact: (a) contact between soft and very stiff media: (b) contact between two similar half-planes.

The initial (static) displacement u_o at the boundary *x=0* may correspond to either the ascending (point A) or the descending (point B) portion of the curve of contact interaction shown in Figure 2.3.49. In the latter case the contact is in a limit state. Note that in this state there is an alternative: further contact deformation may proceed as either softening (path BC) or elastic unloading (path BD), depending on the direction of displacements in the incident wave. We shall first discuss the case where displacements, *u*, in the wave have the same direction as initial displacement u_o, i. e. the case where unloading does not occur. Then from (2.37) it follows for the displacement and shear stress in the wave at the contact:

$$\tau(0,t) = - k\, w(0,t) \tag{2.38}$$

$$\text{where} \quad k = \begin{cases} E_c & u<u_m \\ -M_c & u_m<u<u_* \end{cases} \tag{2.39}$$

The mathematical formulation of the problem is as follows. We need to solve the 1-D wave equation:

$$\partial^2 w/\partial t^2 - c\partial^2 w/\partial x^2 = 0 \tag{2.40}$$

under

(i) the initial condition $w=f(x,0)$ $(x<0)$,

(ii) the boundary condition (3) at $x=0$ $(t>0)$, and (iii) the dependence

$$\tau(0,t) = G\, \partial w/\partial x \qquad (t>0) \tag{2.41}$$

expressing Hooke's law (2.38) for points on the boundary $x=0$. The general solution of (2.41) is represented by the sum of the incident $f(x,t)$ and reflected $g(t)$ waves $w(x,t) = f(x-ct) + g(x+ct)$. Then (2.22) and (2.24) yield the ordinary differential equation for the reflected wave:

$$(1/c)dg(0+ct)/dt + (k/E)g(0+ct) = (1/c)df(0-ct)/dt - (k/E)f(0-ct) \tag{2.42}$$

Its solution is

$$g(0+ct) = f(0-ct) - 2\omega_o \int_0^t exp\,[-\omega_o(t-\tau)]\, f(0-c\tau)d\tau \tag{2.43}$$

$$\text{where} \quad \omega_o = ck/G \tag{2.44}$$

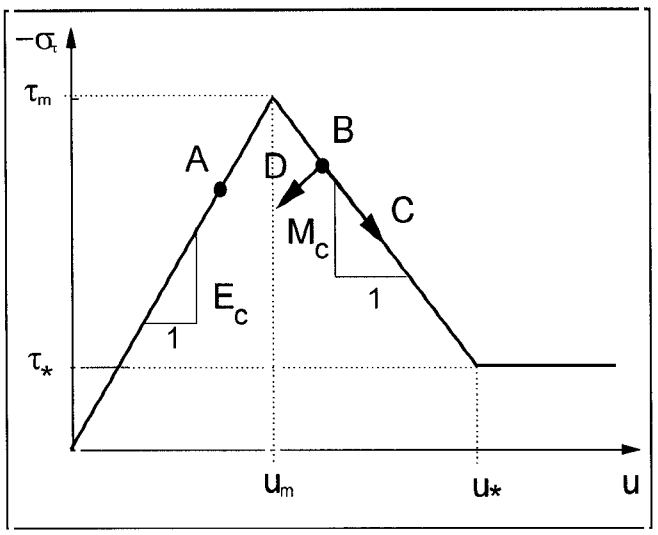

Figure 2.3.49 Curve showing the contact interaction with softening modulus.

The modulus of the inverse value of ω_o is the characteristic time of the contact interaction:

$$T_c = |G/(ck)| \tag{2.45}$$

The latter can also be written in terms of the attenuation $Z = G/c$ as:

$$T_c = |Z/k| \tag{2.46}$$

The modulus is used for softening, because the coefficient k is negative ($k = -M_c$). The solution (6) accounts for both the continuous increase of $f(0)$ from the zero value, and the case where it is presented by a step function at $t=0$. In the latter case (2.44) yields:

$$g(0+ct) = -1 + 2\exp(-\omega_o t) \tag{2.47}$$

From (10) we may see that for elastic interaction (k, $\omega_o > 0$) the reflected wave is equal to +1 at small times ($t << T_c$), which corresponds to the reflection from a free surface. Opposite to that, at large times ($t >> T_c$), $g(0+ct)$ tends to -1, which corresponds to the reflection from a rigid boundary. Both these conclusions are obvious from the physical point of view.

For softening interaction *(k, ω_0<0)* the picture changes dramatically because the exponent in (2.48) increases with time. The velocity and acceleration also grow with the same positive power. Their direction coincides with that of the incident wave. Thus we have exponential amplification of displacements, velocities and acceleration due to softening.

Observing the solution (2.44) for an arbitrary incident wave *f(x-ct)*, we conclude that this effect is general if the contact reaction is softening *(ω_0<0)*. In particular, for a harmonic wave with frequency ω, and incident wave function $f(\xi) = exp(i\omega\xi)$ we have from (2.25):

$$g(0+ct) = [2/(1+\omega/\omega_0)]\, exp(-\omega_0 t) - [(1-i\omega/\omega_0)/(1+i\omega/\omega_0)]\, exp(i\omega t) \qquad (2.48)$$

The first term in the r. h. s. grows infinitely and suppresses the second (harmonic) term in a case of softening *(ω_0<0)*. We see that stationary reflected harmonic waves are impossible for contact interaction in a regime of softening. Note also that the last formula is true only for active softening, i. e. for positive phase of velocity in the incident wave. Thereafter, we have unloading and the result of integration in (2.44) changes.

Amplification of reflected and transmitted waves

The scheme of Figure 2.3.48 (a) has served to reveal the effect in the simplest form. It corresponds to a wave coming from a compliant medium at the contact with a very stiff medium. Meanwhile, the observed amplifying influence of softening is quite general. It can also be easily revealed for the case where a contact generates both a reflected and transmitted wave. In particular, it appears when a plane incident shear wave arrives at a contact between two similar half-planes (Figure 2.3.48 (b)). This corresponds to the interaction of a wave with a crack or fault in a limit state. Shear traction τ stays continuous through the contact:

$$\tau^+(0,t) = \tau^-(0,t) = \tau(0,t) \qquad (2.49)$$

and the contact condition (3) now takes the form:

$$\tau(0,t) = - k\, \Delta w(0,t) \qquad (2.50)$$

Herein, $\Delta w(0,t) = w^{+}-w^{-}$ is the displacement discontinuity at the contact $x=0$; the superscript "plus" marks the value from the side of the incoming incident wave; the superscript "minus" refers to the opposite side of a crack or fault. The Equations (2.21), (2.23) and (2.24) and initial conditions are the same as in the previous case when applied to the left or to the right of the contact.

For the scheme Figure 2.3.48 (b) we have a transient wave $h(x-ct)$ in addition to the incident $f(x-ct)$ and reflected $g(x-ct)$ waves. Hence, the general solution of (2.41) is presented as:

$$w^{+}(x,t) = f(x-ct) + g(x+ct),\ w^{-}(x,t)= h(x-ct) \tag{2.51}$$

Substitution of (2.51) into (2.37), (2.49) and (2.50) gives a system of ordinary differential equations with respect to functions $g(0+ct)$ and $h(0-ct)$:

$$\begin{gathered} dg(0+ct)/dt + \omega_0 g(0+ct) - \omega_0 h(0-ct) = df(0-ct)/dt - \omega_0 f(0-ct) \\ dh(0-ct)/dt + \omega_0 h(0-ct) - \omega_0 g(0+ct) = \omega_0 f(0-ct) \end{gathered} \tag{2.52}$$

where ω_0 is given by (2.45). From (2.52) we find for the reflected wave:

$$g(0+ct)=f(0-ct)-2\omega_0 \int_0^t exp[-2\omega_0(t-\tau)]\, f(0-c\tau)d\tau \tag{2.53}$$

which differs from (2.44) only by the multiplier 2 in the exponent in the integrand. This multiplier accounts for the fact that the scheme of Figure 2.3.48 (b) includes two similar surfaces of contact interaction, whereas the scheme of Figure 2.3.48 (a) contains only one surface. For the transmitted wave, it follows from (2.52), (2.53):

$$h(0-ct) = 2\omega_0 \int_0^t exp[-2\omega_0(t-\tau)]\, f(0-c\tau)d\tau \tag{2.54}$$

If the incident wave is given by the step function, (2.53) and (2.54) yield:

$$g(0+ct)=exp(-2\omega_0 t);\quad h(0-ct)=1-exp(-2\omega_0 t) \tag{2.55}$$

From these expressions we see that for elastic interaction *(k, ω_0>0)*, the instant reaction *(t<<1/ω_0)* of a contact is that of a free surface, while the long-term reaction *(t>>1/ω_0)* is that of an ideal contact. In other words, high frequency incident waves are mostly reflected while low frequency waves do not feel the contact. The same is obvious from the solution for the harmonic incident wave function $f(\xi) = exp(i\omega\xi)$. In this case:

$$g(0+ct) = [1/(1+1/2i\omega/\omega_0)]exp(-2\omega_0 t) + [1/2i\omega/\omega_0 /(1+1/2i\omega/\omega_0) exp(i\omega t) \quad (2.56)$$

and

$$h(0-ct) = [1/(1+1/2i\omega/\omega_0)][exp(i\omega t) - exp(-2\omega_0 t)] \quad (2.57)$$

In the case of elastic contact *(k, w_0>0)* the terms containing $exp(-2\omega_0 t)$ decay and we have a well-studied stationary regime (e. g. Pyrak-Nolte 1996). In case of a softening contact *(k, ω_0<0)* all the expressions (2.53)-(2.57) contain a positive exponent and grow infinitely with time. We have amplification of the displacement, velocity and acceleration. Obviously, a stationary regime is impossible.

Discussion

In the previous section we have seen that amplification due to softening has a characteristic time $T_c = -1/\omega_0$, or substituting (2.45) and (2.46):

$$T_c = G/(cM_c) = Z/M_c \quad (2.58)$$

where G is the elastic shear modulus; M_c is the contact softening modulus; c is the velocity of shear wave propagation. For estimations of T_c in hard elastic rock, take $2G = 7{,}5\times10^4$ MPa, $c = 5\times10^3$ m/s, and $M_c = M/d$ where M is the shear softening modulus of the material interacting at the contact and d is the average contact thickness. Assume that M is of the order of $2G$. Then $T_c = 10^{-4} d$ where d is taken in metres, T_c is in seconds. For $d < 10^{-3}$ m, the characteristic time T_c is less then 10^{-7} s. This means that amplification may be pronounced even for very short impulses with a duration of microseconds. In numerical calculations it will appear as a new seismic event generated by the incident wave. Note

also the interesting fact that, as it follows from (2.57) and (2.58), displacements in the amplified transient wave have a direction opposite to that in the incident wave. This may serve to check the proposed mechanism of amplification.

So far we have considered the simplest case of a plane incident wave. Hence, our study was restricted to wavelengths less than the size of the surfaces in contact, and in particular, the size of cracks. For cracks with sizes of 0,2 to 1 m, this corresponds to rather high frequencies exceeding 5 kHz. Meanwhile, the effect of amplification, observed in mines, occurs at frequencies of about 0,5 kHz, which is an order less than, the given estimate.

The case of low frequencies is more difficult for analytical treatment. Nevertheless, from physical considerations, it may be seen that amplification will occur at these frequencies as well. Indeed, one may use a quasi-static approximation to reveal energy excess from instability due to contact softening (Linkov 1994 and 1995). This instability appears as exponential growth of the particle velocity (Linkov 1997). In other words, in a quasi-static approximation we again have exponential amplification caused by elastic energy release due to softening. Having a set of cracks with interacting surfaces at or near a limit state, one can expect their input into amplification. This action certainly produces changes in waveforms when compared with those in the incident wave far from the cracked, highly stressed zone. It should also be mentioned that amplification resulting from crack propagation, induced by the incident wave, is a particular case of the mechanism suggested.

Conclusions

The conclusions of this study can be summarised as follows.

1. Wave amplification may be attributed to energy release from rock under stresses high enough to generate cracks at a state close to instability; the amplification occurs due to physical non-linearity at interacting softening surfaces.

2. Wave amplification appears as an exponential growth of displacements, velocities and accelerations with a characteristic time of the order Z/M_c where Z is the rock attenuation; M_c is the contact modulus of softening.

3. Stationary waves do not exist for the regime of amplification.

4. The triggering of seismic events, rockbursts in particular, by an incident wave or in apparent "static" conditions, may be an extreme case of amplification.

Further investigation of the proposed mechanism is necessary. It may be carried out by means of numerical simulation of waves impinging on cracks close to an unstable state. This will provide synthetic data on the magnitude of amplification and changes in waveforms.

3. Rockburst investigations

3.1. Review of previous work

Efforts to solve the rockburst problem

Rockbursts have posed a major hazard to workers in the gold mines of South Africa for almost a century. As early as 1908, the problem was sufficiently serious for the Ophirton Earth Tremors Committee to be appointed, who concluded that tremors were due to the shattering of pillars. In 1915 the Witwatersrand Earth Tremors Committee recommended the elimination of pillars and the use of substantial artificial support. The Witwatersrand Rockburst Committee made comprehensive recommendations in a report in 1924, most of which were endorsed forty years later by a further state-appointed body, the 1964 Rockburst Committee.

Co-ordinated research into rockbursts commenced in 1952 when the Central Mining and Investment Corporation contracted the S. A. Council for Scientific and Industrial Research (CSIR) to undertake research into the problem. Later the Transvaal and Orange Free

State Chamber of Mines took over the sponsorship and co-ordination of several research agencies. Cook et al. (1966) synthesise the results of ten years of research effort up to 1965, and describe a four stage approach to the rockburst problem:

1. Observations.
2. Attach rational significance to the documented experience and thereby develop hypotheses concerning certain aspects of the rockburst problem.
3. Combine the hypotheses to postulate a rockburst mechanism consistent with the observations.
4. Design controlled experiments underground to test the proposed mechanism.

In terms of the rockburst mechanism, Cook et al. (1966) conclude that the "existence or otherwise of the rockburst hazard depends on whether the geometrical rate at which energy must be released, is greater or less than the rate at which energy can by dissipated non-violently as the excavation is enlarged".

Salamon (1983), in a summary of progress to date, suggested that the hazard of rockbursts could be alleviated through improvements in support systems, better layout design, and the reduction of convergence through backfilling or reduced stoping width. Many of these suggestions are incorporated in the *Industry Guide to the Amelioration of Rockburst and Rockfalls* (COMRO, 1988).

Systematic investigation of rockbursts

Several projects involving the systematic study of rockbursts have been conducted. Seventeen large seismic events in the Klerksdorp mining district were investigated by Hepworth (1983). The case studies involved a description of damage (supported by mine plans and photographs) and an assessment of support performance. The principal findings were:

- Stopes: To prevent excessive inelastic convergence in stopes, support should be as stiff as possible, but should also have sufficient yield to allow elastic convergence.
- Gullies: A great deal more attention should be given to gully support, for example by increasing tendon density and tendon yield, or event meshing and lacing the centre gully roof.

- Tunnels: A vast improvement in the performance of tendons during seismic events can be achieved by improving the yield characteristic. In highly stressed areas, where slabby and blocky conditions exist, mesh and lace should be used in conjunction with tendons.

The Rockburst Research Project at Western Deep Levels Gold Mine was another systematic effort to document the rockburst phenomenon. The project lasted from 1975 to 1987, inclusive. One component of the project was the detailed study of 30 rockbursts, ranging in magnitude from 0,4 to 3,5 during a one year period (October 1982 to October 1983) (Hagan et al., 1984). Only two rockbursts affected the VCR, the remainder causing damage to Carbon Leader stopes. Locations and magnitudes of the events were obtained from a seismic network. Other data recorded or calculated included the distance of the source from the face, length of the face or gully affected, stoping width, percent closure, ERR, local geology, nature of damage to rock and support. Sketch plans of the affected area; and photographs of damage were used to illustrate the studies. The principal findings of this report were:

- The formula

$$y = 59,6 + 63,6v \qquad (3.1)$$

(where v is derived from the relation $logRv = 3,95 + 0,57M_L$)

relates face/gully damage to event size and distance from the damaged face. It was suggested that this formula could be used by line management to decide how many panels to evacuate before an impending event.

- The rockburst site observations indicated the existence of at least two rockburst mechanisms associated with relatively homogeneous rock and geologically disturbed rock, respectively. The first mechanism is associated with events of less than magnitude 1,9 and do not generally result in serious damage to support. The second mechanism, on the other hand, is associated with a much larger range of magnitudes and can result in serious support damage and damage to the face.

Ortlepp (1984) presented seven particularly instructive case histories, out of more than one hundred rockbursts examined by him in a 16 year period. Principal findings were:

- Rockbursting is a complex phenomenon covering a wide range of magnitudes as well as modes of origin. There is no single model that can account for the diversity of the phenomenon.
- Events of intermediate magnitude, which occur within a few metres to tens of metres from the stope face, are most hazardous. Here the shape of the excavation plays a significant role in determining the magnitude and stress changes in the zone of potential instability. The instability can involve movement along an existing geological discontinuity or a fresh shear fracture through previously intact and massive rock.

Ortlepp's meticulous observations of rock fracture and rockbursts, compiled during a career spanning over forty years, were recently published (Ortlepp, 1997).

International efforts

While the rockburst problem is certainly most severe in South African mines, it exists in deep mines everywhere. The Rockburst Handbook for Ontario Hardrock Mines (Hedley, 1992) is an excellent review of the rockburst problem in Canada. This volume includes five case histories, which include discussions of the geology and mining methods, rockburst history, rockburst mechanisms, and computer modelling. While the approaches employed by the Canadians to alleviate rockbursts and control rockburst damage are interesting, the ore bodies and mining methods differ considerably from the South African case, and the findings are not directly applicable.

A series of international symposia has focused specifically on the problem of rockbursts and seismicity in mines (Gay and Wainwright 1984; Fairhurst, 1993; Young, 1993; Gibowicz and Lasocki, 1984). While many interesting and important papers have been presented at these meetings, they have tended to focus on particular aspects of the rockburst phenomenon, and there have been relatively few papers providing a comprehensive case histories of rockbursts in South African mines.

This study: new technologies and the human factor

Despite all these efforts to understand and combat rockbursts, the hazard has not been substantially reduced. This lack of progress may be partly explained by the fact that the depth and difficulty of mining has steadily increased as the ore bodies have been exploited, but the main reason is that mining-induced seismic events, like hurricanes and earthquakes, are not easily tamed. They are powerful, destructive and unpredictable phenomena. For real gains to be made in reducing the rockburst hazard, it was clear that the investigation of rockbursts should go beyond physical observations such as the local geology, assessment of support performance, and seismic source parametres. The human factor is probably as important as technology in solving the rockburst problem. Rockburst investigations must also include an understanding of the history which led to the layout existing at the time of the event, and "conventional wisdom" and mining practice must be critically reviewed. Specifically:

- Published guidelines and methodologies (e.g. COMRO, 1988) concerning face shape, face orientation, regional support strategies, pillar dimensions, support design etc.
- Mine design criteria such as ESS and ERR.
- The use of numerical modelling computer programs for mine design.
- Seismic forecasting and prediction methods.
- The effectiveness of technologies such as backfill, shotcrete, yielding tendons, prestressed elongates etc.
- Rock engineering practice on the mine, ranging from adherence to codes of practice, the quality of blasting and support installation, to the implementation of new technology.

3.2 Methodology

The execution of comprehensive rockburst investigations under the auspices of this SIMRAC project was widely advertised. Rockburst investigations are usually initiated by mine management, though in a few instances the Department of Mineral and Energy Affairs has provided the impetus. Several of the rockburst investigations have been carried out under contract to the mines. In these cases, the detailed findings are not

published, although the general findings inform other investigations and are included in the general conclusions.

The following procedure is generally adopted in the investigation of a rockburst:

- The team of specialists visits the site shortly after the event, in most cases prior to any rehabilitation so that the only disturbance is due to the rescue operation. The damage to the excavation and support elements is carefully studied, dynamic closure is estimated, and mining-induced fractures, joints and other geological features are recorded. Interviews are held with witnesses to the rockburst and rock engineering staff at the mine. Each member of the team has a good general knowledge of rock engineering and mining in addition to an area of specialist expertise (e.g. layouts, support, geology, seismology).
- Seismograms are used to determine the source parameters of the rockburst.
- The seismic history of the area in the vicinity of the rockburst and nearby structures (dykes and faults) is assessed.
- Numerical modelling is used to evaluate the mining layout and sequence at the time of the rockburst by calculating parameters such as Energy Release Rate and Excess Shear Stress.
- Support elements such as props and tendons may be recovered from the rockburst site and tested in the laboratory.
- Rock samples may be collected so that the properties of the strata can be determined.
- Future mining strategies are investigated and recommendations formulated.

3.3. Scope of investigations

Twenty-eight rockburst investigations were conducted in the period from January 1994 to December 1997 (Table 3.3.1). Fifteen investigations took place in the Far West Rand gold field (East and West Driefontein, Western Deep Levels, Deelkraal, and Blyvooruitzicht mines), five in the Klerksdorp gold field (Vaal Reefs, Hartebeestfontein and Buffelsfontein mines), five in the West Rand gold field (Durban Deep, Leeudoorn and Western Areas mines), two in the East Rand gold fields (ERPM), and one in Australia. No investigations were conducted in the Free State or Kinross gold fields. Some investigations were of rockbursts which did not cause injury to workers, either because the event occurred off-

shift, or because no workers were in the area at the time. However, many of the investigations were at sites of fatal accidents. In total, 79 workers were fatally injured in the rockbursts investigated by the CSIR team. In order to assess how representative these investigations are of the rockburst problem in South Africa, the rockburst statistics for the three year period 1994-1996 were reviewed.

Most rockburst fatalities occurred in the mining of the VCR (83 fatalities), followed by the Carbon Leader reef (51 fatalities), Vaal reef (25 fatalities), and the Basal reef (15 fatalities). The number of rockbursts investigated by the team is roughly in the same proportion: VCR (9 investigations), Carbon Leader reef (6 investigations), the Vaal reef (6 investigations), and the Main reef (3 investigations). With the exception of the Basal Reef, the rockburst investigations sampled areas of greatest rockburst hazard. (Figure 3.3.1)

The rockburst statistics were also analysed in terms of the location of the fatal accident (Figure 3.3.2). Most fatalities occurred in the stope (131 fatalities), followed by gullies (57 fatalities) and cross-cuts, haulages and developments (22 fatalities). While the damage due to a single rockburst may affect stopes, gullies and haulages, an attempt has been made to classify the investigations in terms of the area of most serious damage: stopes (11 investigations), gullies (7 investigations), cross-cuts and haulages (7 investigations), and shafts and service excavations (3 investigations). Again the investigations are fairly representative of the problem in the industry.

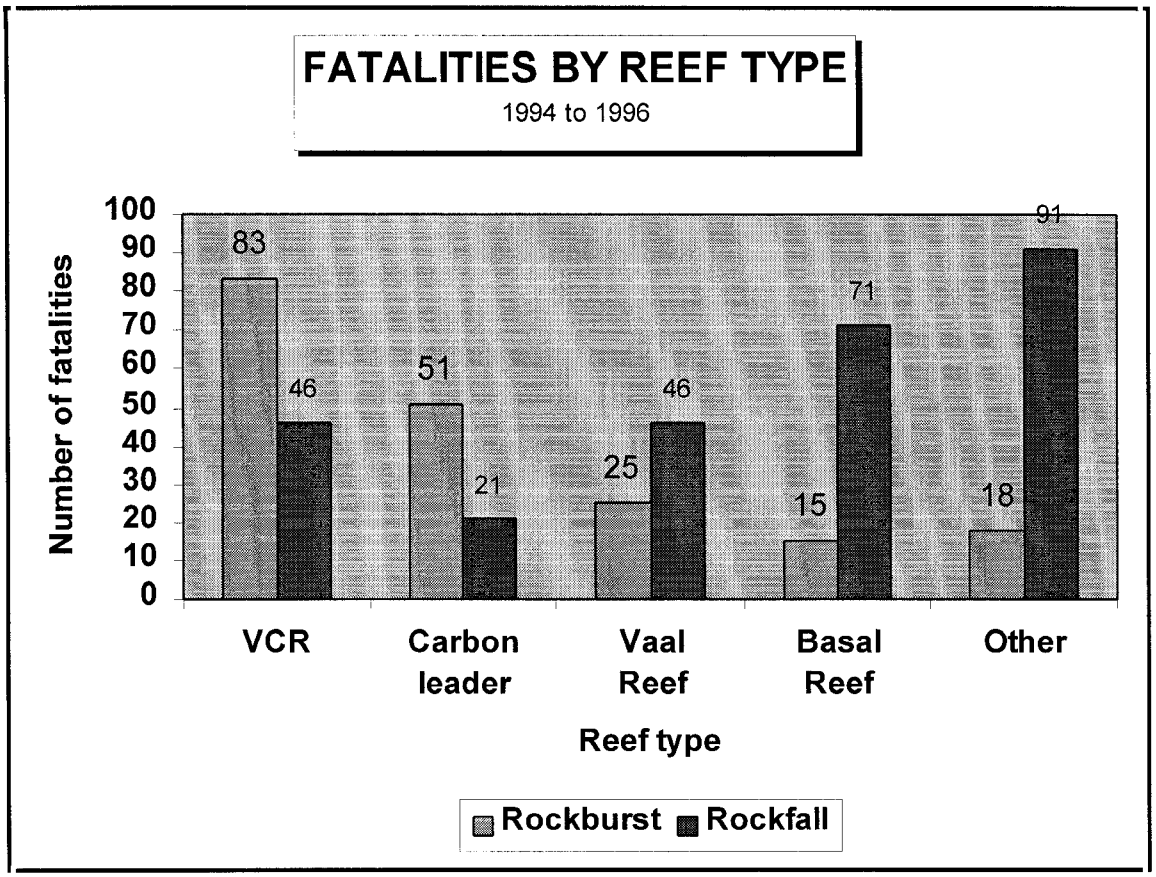

Figure 3.3.1 Analysis of rockburst and rockfall fatalities in South African gold mines for the three year period 1994 to 1996 according to reef.

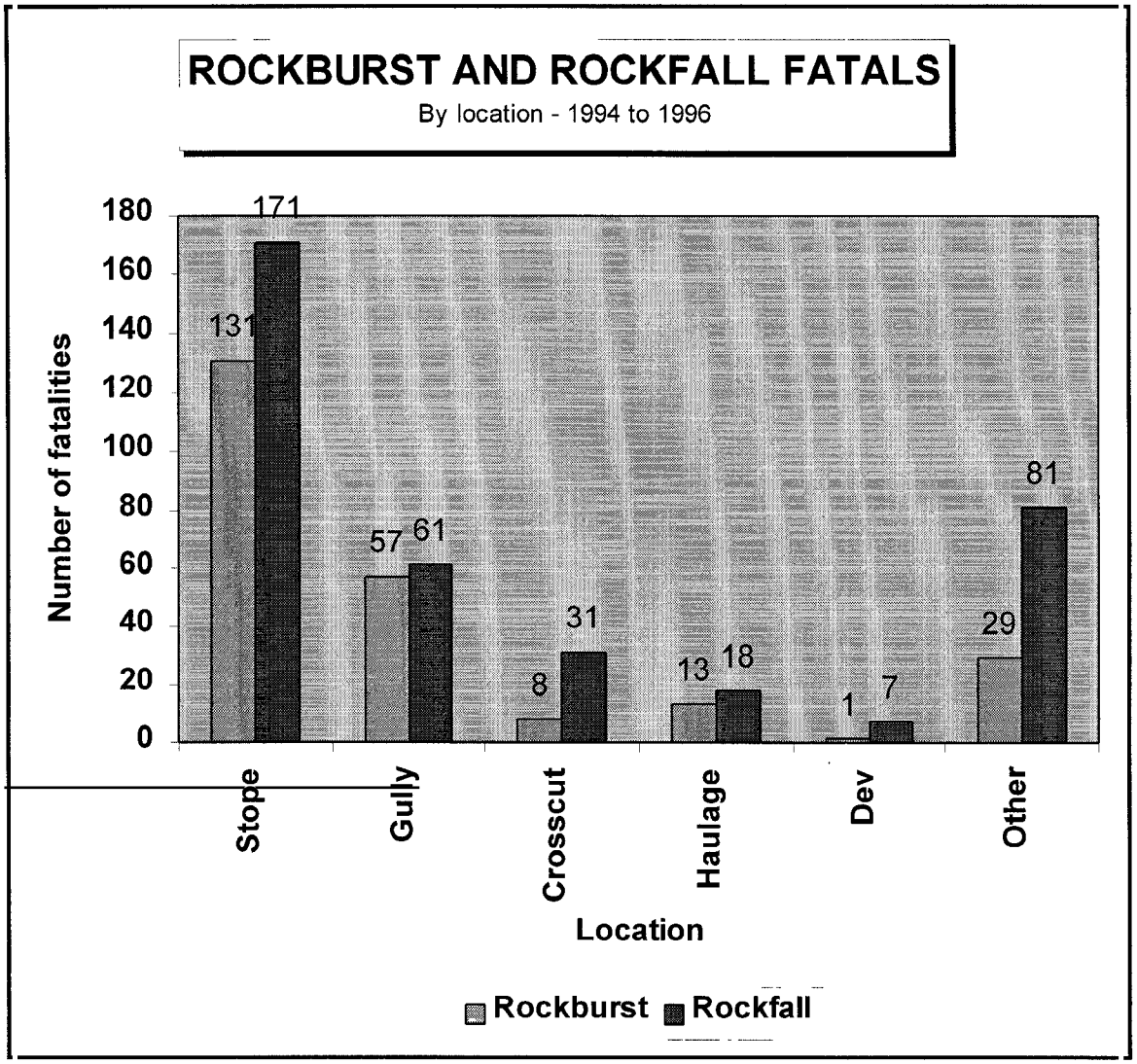

Figure 3.3.2 Analysis of rockburst and rockfall fatalities in South African gold mines for the three year period 1994 to 1996 according to location.

Table 3.3.1

Rockburst and Rockfall investigations conducted during the period 1 January 1994 to 30 September 1997.

Date & Time	Mine	Case History	M_L	Casualties	Mining Scenario	Depth (m)	Reef	Source Mechanism	Damage Mechanism
940110 12h15	Leeudoorn	1	2,6; 1,9	11 fatalities	Extraction of island remnant	1800	VCR	Remnant failure	Hangingwall shakedown Face burst
940504 9h49	Deelkraal	2	2,1	4 fatalities	Extraction of peninsular remnant	2300	VCR	Remnant failure	Hangingwall shakedown Face burst
940901	Vaal Reefs # 2		2,4	3 fatalities	Extraction of pillar		Vaal	Pillar failure	Bulking of cross-cut and haulage side- and footwall. Failure of rebar, mesh and lacing support.
941103 7h19	Western Deep Levels (West)	3	2,5	6 fatalities	Longwall negotiating dyke	3000	Carbon Leader	Slip on dyke	Hangingwall shakedown Face burst
950621 20h15	Durban Roodepoort Deep		2,3	0					Collapse of section of shaft
950704 11h42	Buffelsfontein, Orangia Shaft	4	3,4	1 fatality	Extraction of final remnants near shaft	2220	Vaal	Slip on fault	Bulking of haulage sidewall. Failure of rebar, mesh and lacing support.

Table 3.3.1

(continuation)

950724 01h45	ERPM Hercules Shaft	5	<0,5	4 fatalities	Rehabilitation of incline shaft	1500	Main Reef	Pillar failure	Shakedown of hangingwall of incline shaft
950815 22h10	ERPM Hercules Shaft		0,9	0	Rehabilitation of incline shaft	1500	Main Reef	Pillar failure	Shakedown of hangingwall of incline shaft. Damage to station.
950914 16h04	East Driefontein # 4	6	3,6	0	Support being installed in tunnels	2500	VCR & Carbon Leader	Slip on fault	Bulking and shearing of hanging- and sidewall of tunnels. Failure of rebar, mesh and lacing support.
950918 8h17	Western Deep Levels (South)	7	2,2	1 fatality	Mining of remnant between longwalls	2200	VCR	Slip on face parallel rupture	Shakedown of stope and advance gully hangingwall.
960130 8h52	Blyvooruitzicht	8	2,2; 2,3	6 fatalities	Extraction of stabilizing pillar	1900	Carbon Leader	Pillar failure	Shakedown of strike gully

Table 3.3.1

(continuation)

960202	Randfontein Estates, Cooke # 1		fog	7 fatalities	Rehabilitation of 95 W 10 cross-cut close to the shaft pillar	800		n/a	Stress from abutment causing fracturing & bulking of rock around excavation. Mesh & lace support system lost integrity.
960213	Vaal Reefs # 11		fog	5 fatalities	Excavation of pump chamber	2400			
960215 7h56	Western Deep Levels (South)	9	1,8	0	Stoping, up-dip panel	2500	VCR	Slip on face parallel rupture	Shakedown of stope and dip gully hangingwall
960219 18:30	East Driefontein # 1		3,2	0	Mining of longwall	22000	Main	Slip on face parallel rupture	Convergence of stope due to footwall heave. Face ejection.
960605 10h57	East Driefontein # 1	10	2,7	22 injuries	Mining of longwall	2300	Carbon Leader	Slip on face parallel rupture	Scattered falls of ground in stope. Bullking of cross-cut sidewall.

Table 3.3.1

(continuation)

961118 9h10	Western Deep Levels (East)	11	3,0	1 fatality 1 injury	Mining of longwall	3300	Carbon Leader	Slip on dyke	Collapse of strike gully hangingwall
970210 18h08	Vaal Reefs # 5	12	4,4	0	Mining of remnant	1900	Vaal	Slip on dyke	Bulking of tunnel and cross-cut hanging- and sidewalls. Failure of rebar, mesh and lacing support.
970410	Leeudoorn	13	1,7	1 fatality	Mining of longwall	2630	VCR	Face burst	Ejection of face. Collapse of hangingwall.
970416	Leeudoorn	13	2,3	0	Mining of longwall	2680	VCR	Slip on face parallel rupture	
970417 22h32	Western Deep Levels (East)	14	2,7	3 fatalities	Mining of longwall		Carbon Leader	Pillar foundation failure	Collapse of hangingwall of gully next to stabilising pillar.
970507 12h04	Deelkraal		3,4	9 fatalities 24 injuries	Mining of longwall	2700	VCR	Slip on fault	Shakedown of stope hangingwall & face ejection

Table 3.3.1

(continuation)

970516	Western Areas, North Shaft		fog	3 fatalities	Rehabilitation of 43 N f/w drive	1170	E9EC		
970523 12h58	West Driefontein # 6	15	2,7	several injuries	Mining of longwall	2300	Carbon Leader	Slip on face parallel rupture	Collapse of strike gully hangingwall
970701 20h20	Deelkraal		2,1	1 fatality	Mining of longwall, up-dip panel	2785	VCR	Slip on face parallel rupture	Collapse of dip gully hangingwall
970721 10:45	Hartebeestfontein		3,7	18 fatalities 32 injuries	Mining of remnants	2000	Vaal	Slip on fault	Shakedown of stope hangingwall. Faceburst Bulking of tunnel side-, hanging- and footwalls
970812 11:00	Western Areas Gold Mine		< 0	2 fatalities 4 injuries	Developing reef drive	1950	Elsburg EC	Strain burst	Ejection of sidewall, shakedown of hangingwall
970901	Victor Ore Body, Kambalda, W. Kosten, Australia		1,4	2 fatalities					

Table 3.3.1

(continuation)

970918 2:39	Western Deep Levels (East) 97E1		3,3	0 fatalities	Mining of longwall, breast panel	2900	Carbon Leader	Slip on fault	Shakedown of hangingwall in gully adjacent to stablising pillar
970925 2:02	East Driefontein # 4		4,3, 2,1, 3,1	1 fatality	Mining of longwalls	2300	VCR	Slip on fault	
971011 22:00	Hartebeestfontein		3,3	6 fatalities 41 injuries					Damage to stopes and tunnels

3.4 Factors affecting the severity of rockburst damage

The severity of rockburst damage often varies greatly. One panel in a longwall may be severely damaged, while an adjacent panel (perhaps even closer to the focus of the seismic event) is unscathed. The condition of a tunnel may change from being sound to one of total collapse over a distance of a few metres. Why is this so? The rockburst investigations were undertaken with the objective of determining the factors that control the distribution and severity of rockburst damage. It is believed that a detailed understanding of both the source and damage mechanisms, and the application of this knowledge to the design and support of excavations, will lead to a reduction in the hazard posed by rockbursts.

The findings of the twenty-eight rockburst investigations conducted from January 1994 to December 1997 are synthesized in this section , with the aim of highlighting common themes and key issues. Detailed descriptions of individual case histories are given in Appendix B.

3.4.1. Layout and mining sequence

Guidelines and empirical design criteria found in publications such as An Industry Guide to Methods of Ameliorating the Hazards of Rockfalls and Rockbursts (COMRO, 1988) are generally used for the design of excavations. During the course of the rockburst investigations it was found that some of these guidelines and criteria have limitations which are not always appreciated by the rock mechanics practitioner. In some instances, the limitations are not clearly expressed in the publications. The notes that follow for the most part endorse existing guidelines, but in some instances reflect a slowly evolving change in knowledge and approach.

Remnants

(see Case Histories 1,2 and 7)

The mining of remnants poses particular challenges as these parts of the ore body have usually been left because of geological complications such as faulting, or because of damage caused by a previous rockburst.

The formation of remnants should be avoided in a longwall situation. If possible, underhand mining from the raise should be carried out. The mining of the remnant between approaching longwall faces is inherently hazardous and must be carefully managed. If up-dip mining is being practised, the up-dip faces should be changed to a breast configuration sufficiently far away to prevent the development of a heading in a very high stress environment.

The formation of rectangular or L-shaped remnants should be avoided, as the whole structure may fail in a single event. Rather, a triangular remnant should be formed and mined in a direction such that the part to be mined last is closest to the nearest large solid area, allowing the apex of the triangle to crush continuously.

Pillar width:height ratios

(see Case Histories 2 and 13)

If trenching is carried out owing to a sudden change in reef elevation (e.g. faulting or "roll"), the effective unconfined height of the remnant or pillar is increased (Figure 3.4.1). Calculations of the pillar dimension using guidelines based on the width:height ratio should be treated with caution.

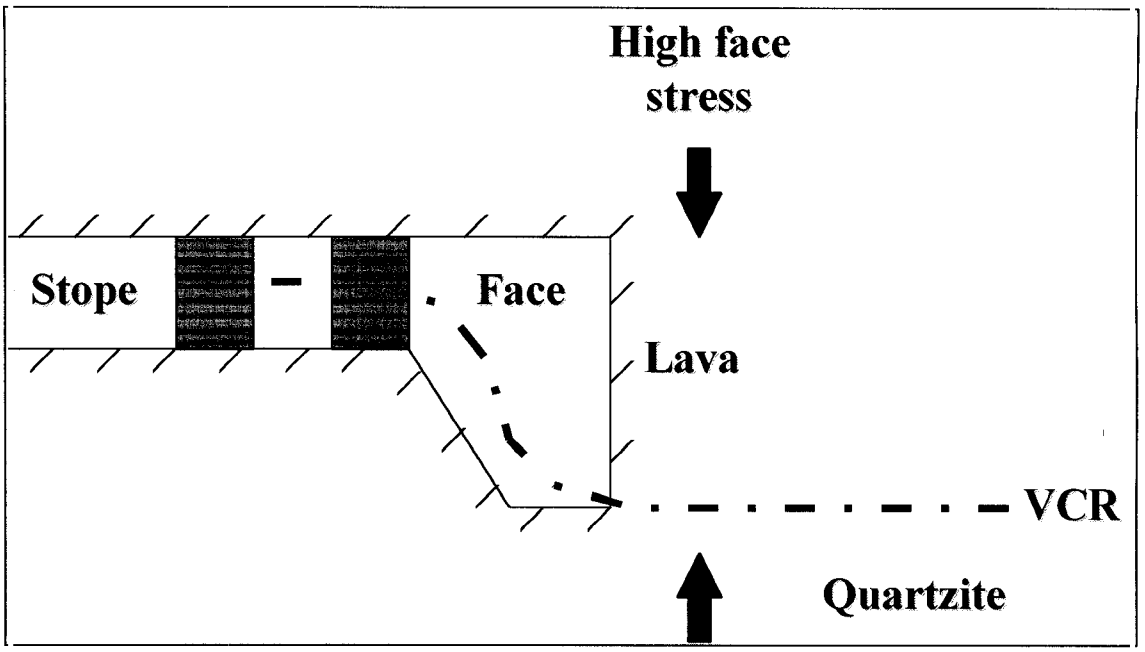

Figure 3.4.1 Increased effective unconfined height of remnant or pillar owing to a change in reef elevation.

Face orientation

(see Case History 3)

The angle between the longwall and geological features such as dykes, faults, or dominant joint sets must be carefully considered. Experience shows that an angle greater than 30° between the feature and the orientation of the longwall (not the individual panel) is desirable.

In situ stress

(see Case History 6)

The *in situ* stress is an important factor in designing underground excavations, and cannot simply be assumed to be the overburden load yielding a k-ratio of 0,5. Measurements should be made to determine whether any anomalous stress state exists.

In some areas significant residual stresses have been found to exist giving k-ratios as high as 1,8.

Shape of stope face

(see Case History 10)

Panel length and lead/lags require trade-offs between practical production constraints and the theoretical ideal. The use of shorter panels is recommended to limit the extent of ruptures along face-parallel shears and the consequent damage, and to facilitate escape from rockburst damaged panels. A long straight face should be avoided. Gully headings in advance of long straight faces are particularly prone to damage.

Panels lagging by large amounts are subjected to high ERR's and should be supported particularly well, with a strictly enforced "no blast if support not up to standard" regulation. The leading panels should be stopped or slowed down to remedy the situation.

Service excavations and facilities

(see Case History 10)

Facilities such as the stope entrance infrastructure (timber and material bay), refuge bay and waiting place should be located away from seismically hazardous areas such as faults.

Faults

(see Case History 12)

Mining in the vicinity of major faults may result in increased fault instability, and the use of bracket pillars parallel to the major faults should be considered.

Stope access

(see Case History 10)

The number of accessways to the face should be adequate for the rescue and rehabilitation work that may be required following a rockburst.

Multi-reef mining

(see Case History 13)

Relative face positions and the resultant stress fields should be carefully considered. One face should lag the other by an amount equal to the middling distance, until the reef separation is such that face stresses do not interact significantly.

Angular unconformities

(see Case History 13)

If strata are not parallel, the refraction of the stress field due to mining may increase the shear stress on a bedding plane with low cohesion (Figure3.4.2). This may contribute to a seismic event.

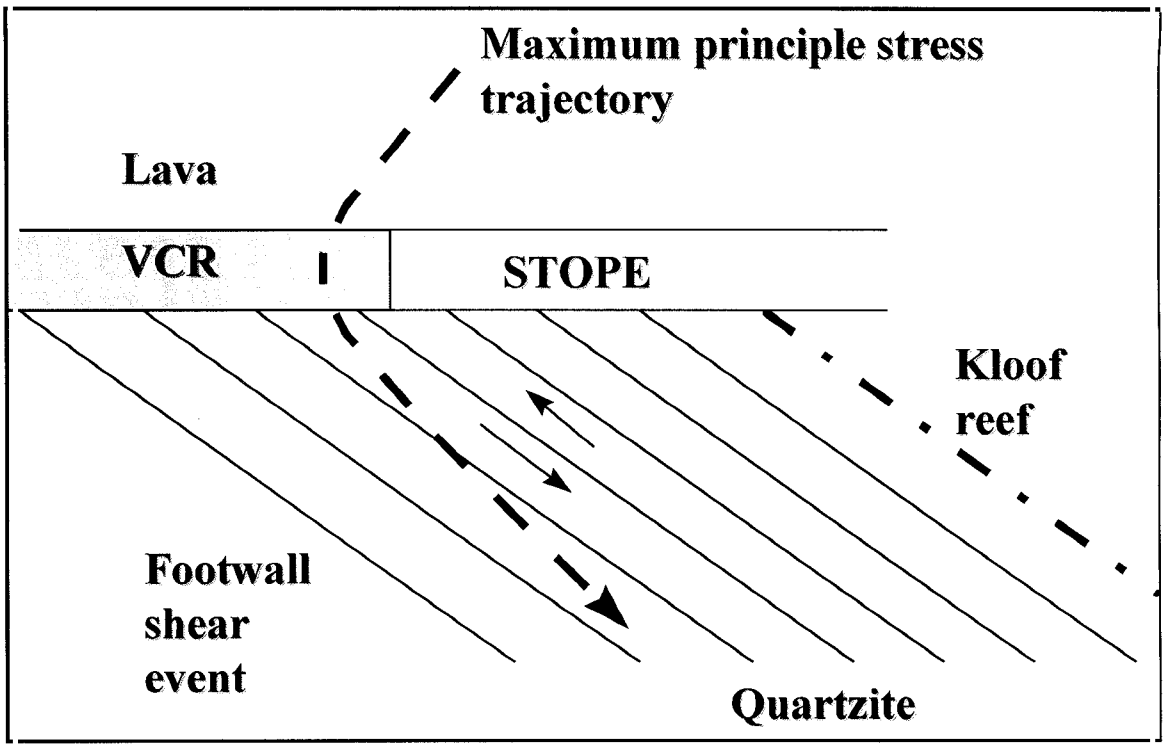

Figure 3.4.2 The possibility of shear slip between footwall strata with low cohesion may be increased by an unfavourable stress trajectory.

Stabilizing pillars and abutments

(see Case History 14)

Highly stressed stabilizing pillars and abutments may experience foundation failure. The situation may be alleviated by higher volumes of backfill and improved placement techniques, thereby reducing the likelihood of further foundation failures. For mines without backfill systems, consideration may need to be given to changes in layout including increasing pillar size and reducing the spacing between pillars.

3.4.2. Numerical modelling

(see Case Histories 1, 2, 3, 7, and 12)

When mining layouts are designed, the guidelines and empirical criteria are often supplemented by the calculation of Energy Release Rate (ERR) and Excess Shear Stress (ESS) using standard numerical modelling computer programs. During the rockburst investigations it was found that the fundamental assumptions of elastic modelling techniques, and the need to apply engineering judgement in the interpretation of the results, is not always appreciated by the rock engineers on the mines.

Mines should develop strategies to mine in the proximity of geological discontinuities such as dykes and faults using back analyses of past rockbursts. ESS and ERR should provide empirical design criteria.

Extreme care must be taken in the interpretation of calculated stresses, ERR and ESS. The ratio of the average pillar stress (APS) to the uniaxial compressive strength (UCS) of the rock comprising the pillar is commonly used as an emprical design criterion. Elastic modelling programs do not take the fracturing of the face into account, and produce unrealistically high values of stress at the edges of pillars and abutments. In reality these areas fracture and crush, are shifting the load away from the face. The core of the pillar is subjected to greater stress than is indicated by the numerical model, and the APS produced by the elastic model is not appropriate for calculating the APS/UCS ratio. This can become critical when the pillar dimensions are small.

The mining and seismic history should be considered when assigning strength to blocks of ground. Narrow pillars, small remnants and areas that have hosted large seismic events should not be modelled as solid, but rather as failed areas incapable of bearing significant load. Footwall punching and complete stope closure may relieve stresses within pillars and remnants.

Other important factors are the sizes of mesh and the window used for numerical modelling. The mesh size should be small enough to represent the local mining geometry in adequate detail, while the window size should be large enough to take into account all significant contributions to the stress in the area of interest.

3.4.3 Tunnels and service excavations

(see Case Histories 4, 5, 6, 12, and 16)

The quality of the support system is of key importance. With regard to the performance of tunnel support under rockburst conditions, there has been a great deal of synergy between this project and SIMRAC project GAP335 *Strata Control in tunnels and evaulation of support units and systems currently used with a view to improving the effectiveness of support, stability and safety of tunnels.* A method for analysing the deformation of tunnels caused by rockbursts, and diagnosing the modes of failure has been developed.

Long term excavations that are likely to be subjected to seismicity during their lifetimes should be supported with pre-stressed yielding units that can accommodate shear deformations (e.g. grouted rope anchors or cone bolts), integrated with mesh and lacing. In areas where severe shaking is expected, these supports should be supplemented with shotcrete.

The collapse of large sections of tunnel may be precipitated by the failure of a single weak link. Consequently it is important that the lacing be properly clamped so that the failure of a single cable does not cause the whole system to unravel.

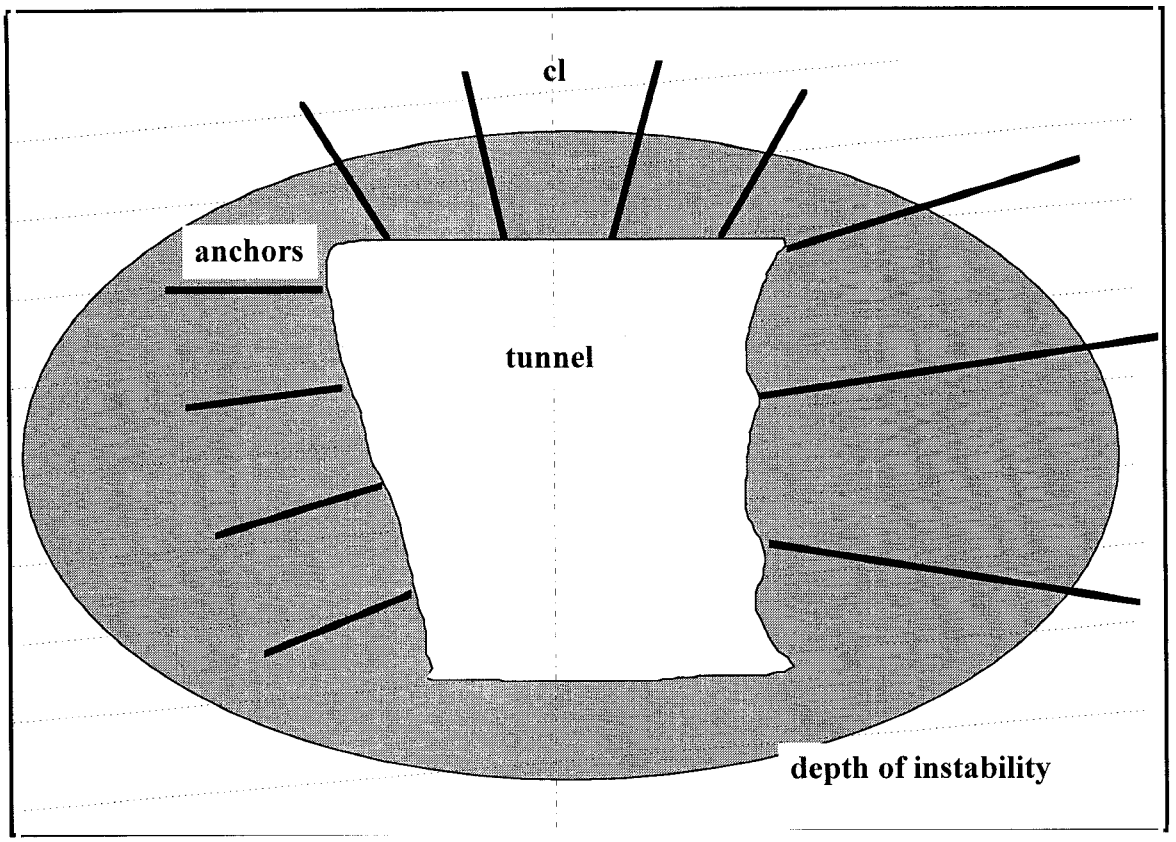

Figure 3.4.3 Diagram showing conceptual mechanisms of excavation deformation as a function of support interaction with the rock mass. Within the South African gold mining environment the vertical virgin stress level is approximately twice that of the horizontal, and induced stresses are generally sub-vertical. Consequently the depth of failure within the sidewalls of the excavations is substantially greater than in the hangingwall or footwall. The tendons on the left hand side of the tunnel are anchored within the zone of instability, hence the entire sidewall is displaced inwards due to bulking of the unstable rock mass. A similar effect will be observed if the tendons snap or debond. In contrast, the tendons on the right hand side of the tunnel remain anchored in solid rock, hence the sidewall bulks between the tendons.

Rehabilitation of tunnels and shafts by "bleeding-off" the fractured rock may have unforseen results. For example, the barring of unstable rock from the hangingwall of an incline shaft had the effect of increasing the height to width ratio of the pillar separating the shaft from an old stope, causing the previously stable pillar to fail. Furthermore, it is also crucial that adequate temporary support is in place while rehabilitation is being performed. Other vulnerable situations arise when tunnels traverse faults, approach the reef intersection, or the stress regime changes owing to over- or under-stoping.

3.4.4 Gullies

Gully support

(see Case Histories 8, 11, 13, 14 and 15)

Rockburst resistant support must be installed in gullies, especially when traversing faults and dykes. The use of softer support on gully edges (e.g. soft packs, or bringing backfill down to the gully edge with gaps left for storage) is encouraged. The integration of elongates with packs in gullies appears to show improved performance when compared to current standards. The idea of using elongates with special headboards to allow lagging across gullies also looks promising.

The gully heading should be supported with rockburst resistant support (such as rapid yielding hydraulic props with headboards) installed in the face area.

Gullies adjacent to pillars and abutments

(see Case Histories 13 and 14)

Gullies along pillars and abutments are particularly prone to damage, as these areas can host large seismic events and the gullies are exposed to high stresses over long distances. The support systems in these gullies should be especially robust. Continual recognition must be given to the fact that rockbursts are the destructive or damaging manifestations of seismic energy release. Innovative thinking is necessary. Some methods of reducing the rockburst hazard are suggested below.

- Use foam cement in the south siding alongside and behind the packs to absorb the impact of the dilating rock and to maintain the integrity of the hangingwall rocks.
- Use yield tendons together with some form of areal support to pin the gully hangingwall. This type of support is more capable of accommodating shear along weak planes parallel to the hangingwall. Angle this support to be at right angles to the dominant fracturing.
- Get backfill closer to the gully edge. Prevent backfill from dilating into the gully by using mesh between packs.
- Precondition the pillar edges by drilling and blasting from the heading. This will create a buffer zone and ensure that the shear zone, resulting from foundation failure, is that much more distant from the pillar edge.
- The gully siding should be deep enough so that the pillar edge and the packs on the down dip side are separated by at least a metre. This will reduce the likelihood of buckling due to violent dilation of rock from the pillar edge. Use foam cement to maintain the integrity of the hangingwall in this area.

Gully sidewalls

(see Case History 3)

Gully packs sometimes collapse or are ejected during rockbursts due to poor foundations. The sidewall may be damaged by scraping, poor blasting practice, or may have failed due to the gully packs bearing excessively high loads.

Gullies in Carbon Leader Reef stopes

(see Case Histories 8, 11, 14 and 15)

Carbon Leader Reef gullies appear to be prone to damage due to the geotechnical properties of the hangingwall strata. The Carbon Leader Reef is immediately overlain by a competent siliceous quartzite, 1,4 m to 4 m in thickness in the Carletonville area; which is in turn overlain by the Green Bar, a 1 m to 2,5 m thick argillaceous unit. Owing to the poor cohesion between the hangingwall quartzite and the Green Bar, the quartzite beam is susceptible to fracture and collapse. In some instances there has apparently been lateral

motion along the Green Bar. In one case the gully had been excavated along the lower edge of the stabilizing pillar where a prominent set of mining induced fractures orientated parallel to the edge of the pillar was present, giving rise to poor hangingwall conditions.

Strike gully sidings must be mined strictly on dip so that the Green Bar contact is kept a maximum distance above the stope. The final cleaning of the siding can take place from the following down-dip panel where applicable.

3.4.5 Stopes

With regard to the performance of stope support under rockburst conditions, there has been a great deal of synergy between this project and SIMRAC project GAP330 *Stope face support systems*.

Support

(see Case Histories 1, 2, 3, 7, 8, 9, 10, and 13)

Rockburst resistant support such as rapid yielding hydraulic props or yielding elongates must be installed in the face area. This is especially critical at the top and bottom of the panels where cross fracturing exists due to the adjacent leading or lagging panel. Non-yielding support elements such as mechanical props and mine poles have very low energy absorption capabilities under rockburst conditions. Headboards should be fitted to props and elongates to limit falls of ground, especially in areas where the hangingwall is friable and prone to fragmentation. Face area support should be in place 24 hours a day, and not removed for blasting or cleaning. Back areas should be barricaded to prevent casual access, as these areas are prone to shake out.

Brows

(see Case History 2)

It is imperative that horizontal confinement be applied to brows formed by falls of ground, negotiation of faults and rolls.

Rolls in the Ventersdorp Contact Reef

(see Case Histories 1, 2, and 13)

Special care should be taken to support the hangingwall when mining in the vicinity of rolls, especially when associated with bedding-parallel faulting, as the frequency of weak calcite-coated joints appears to increase in these areas. The rock hangingwall has a greater propensity to disintegrate when subjected to seismically induced shaking. An additional hazard is posed by the exposure of lava in the face. The lava has a higher uniaxial compressive strength (UCS) and Young's modulus than the VCR, and can therefore store more strain energy and appears to be prone to face bursting (see Figure 3.4.1).

Backfill

(see Case Histories 3, 10, 14 and 15)

It should be ensured that the backfill bags are large enough to tightly fill the stope. In areas where fall out of the hangingwall has occurred, larger backfill bags should be used. Backfill should be extended to the gully packs. This would increase the filling by about 5% and reduce the potential for falls of ground between the gully packs.

Stoping width

(see Case History 10)

Careful blasting should be practised and a conservative blast design implemented, as a reduction in stoping width will improve the effectiveness of both the face area support and the backfill.

Rapid yielding hydraulic props (RYHPs) and prestressed yielding elongates (PSYEs)

(see Case Histories 3, 10 and 14)

RYHPs were introduced almost 30 years ago, and were received with great acclaim once initial teething problems had been overcome. For more than two decades their performance was deemed satisfactory. In recent years, however, the mining industry has become reluctant to continue using RYHPs owing to operational difficulties. The real cause of the poor performance of RYHPs should be determined. Factors which could contribute to the high fall-out rate are:

- Failure to use loadspreaders. In the highly fractured ground the relatively small diameter of the end of the prop or extensions could punch a few millimetres and thus drop load. A similar effect is obtained from setting on a poorly cleaned footwall.
- Pump pressures are incorrect. This could be caused by low air or water supply to the pump or dirty filters.
- Not allowing the pump to stall properly when setting a prop.
- Extensions are not seated properly.
- Valves and seals are faulty.

PSYEs have been introduced only in the last few years. They have been enthusiastically received as a way of avoiding the problems encountered in managing hydraulic prop systems, while retaining the advantages of a prestressed and yielding face support system. Assessment of their performance under rockburst conditions has revealed a number of design weaknesses, particularly related to headboard design, which have been addressed by manufacturers. Some PSYEs show great variability in performance, particularly those where timber forms a large component of the unit. This variability must

be taken into account in the design of the face area support system, as failure of a single unit could lead to disintegration of the hangingwall or increase the load on the adjacent units and precipitate their failure. Once these initial problems are overcome, it is believed that PSYEs will be an effective components of a stope support system.

3.4.6 Seismicity

A mine-wide seismic network (yielding locations with an accuracy better than 20 m) should be installed on all mines which experience rockbursts, to facilitate the identification of hazardous areas and aid the back analysis of rockbursts. The seismicity data should be carefully analysed to identify which parameters are most useful as indicators of increased rockburst hazard.

Many of the rockbursts occurred on mines which had a good seismic system in place. Even when analysing the data in hindsight using the best methods available, not a single example of a significant precursor was found. It is concluded that the reliable and timeous prediction of rockbursts remains a remote possibility at this stage.

3.4.7 Strong ground motion

(see Case History 6)

Observations of co-seismic closure and ejection velocities provide useful parameters for the design of support. In one instance the mass of an ejected block and the evidence of a failed rebar enabled a minimum ejection velocity of 1,4 m/s to be estimated.

In most of the investigated rockbursts the dynamic closure was considerably less than the capacity of the support systems, and the bulk of the damage was due to disintegration of the rockwalls between support elements, rather than failure of the elements. This illustrates the importance of determining the stable dynamic span for the support system and geotechnical area. It is important to realise, however, that should the containment support such as mesh and lacing be improved, a much greater dynamic load would be imposed on the bolts or tendons and their inadequacies would become evident.

3.4.8 Preconditioning

(see Case Histories 7, 8, and 9)

Several of the rockburst investigations were conducted at sites where preconditioning was being implemented. These investigations supported the view that preconditioning reduces the hazard of face bursts. It is important, however, that production personnel adhere to the preconditioning guidelines. As the effectiveness of preconditioning is believed to diminish with time, intervals between face-parallel preconditioning blasts should be based on the elapsed time, not merely on the face advance.

3.4.8 Conclusions

Why does the severity of rockburst damage vary so much? There is no single, simple answer. Probably the most important factors are variations in the condition of the rock mass and the failure of inadequate support systems. Neither is there an easy, instant solution to the rockburst hazard. Given the current methods of mining, the most important steps to be taken to reduce the rockburst hazard would involve:

- discipline in ensuring that support is always up to standard, and that the stope support system is as close to the face as possible;
- frequent inspections of working places by personnel able to identify changes in the rock mass condition, and with the authority to recommend and implement appropriate changes to layout and support systems; and
- adherence to sound layouts, regardless of the demands of production.

Further gains will be achieved through the improvement of areal coverage in gullies and stopes.

4. Conclusions

The most important results emerging from this study can be summarised in following conclusions:

Influence of fracturing and support on the site response in deep tabular stopes

Dynamic behaviour of the hangingwall under seismic impact

- Ground motion at two points on the hangingwall, one close to the support unit and the other about 1 m apart, and the mind way between two support units vary considerably, where the maximum velocities recorded at the point apart from the support are higher.
- Amplitude spectral ratios and phase differences can be used as criteria of stability of the hangingwall at any frequency.
- Surface of the rock to which the geophones are attached (1m apart from each other) vibrates in phase in the whole frequency range (24 Hz - 965 Hz).
- At frequencies greater than 600 Hz, the energy at one of the geophones is nearly 400 times greater than the other nearby geophones. Therefore this geophone is freer to move at these frequencies.

Dynamic behaviour of the backfill site

- Phase difference plot shows no coherence between hangingwall and backfill motions at all frequencies.
- In the frequency range 200 Hz - 520 Hz, backfill energy is nearly 2,5 times greater than that of the hangingwall.
- In the earliest stage, when the backfill was still soft, less energy was transmitted in the frequency range above 600 Hz. In the next stage, 20 days later, when the backfill became compressed, the deviations in the spectral ratio became smaller and equal in the entire frequency range.
- The interaction between the hangingwall and the backfill improves with time and the support provided by the backfill is more effective.

Dynamic behaviour of "hangingwall - Eben Haeser prop - footwall system"

- The coherent vibrations of "hangingwall - Eben Haeser prop - footwall system" indicate: a minimum in the lower frequency (below 250 Hz), a maximum between 300 and 650 Hz (possible resonance), and very similar behaviour for frequency above 700 Hz.
- The variations in the maximum velocities show dependence on time. While the stiffness of the "hangingwall - Eben Haeser prop - footwall system" increased, the maximum velocities decreased.

Seismic evidence for stress redistribution before and after a strong seismic event

- Variations in the maximum velocities recorded before and after a strong seismic event were obtained. The scattering in maximum velocities recorded by five near by geophones installed on the hangingwall increases largely several hours before the event and than back to normal, after the event.
- Two possible hypothesis for interpretation of this phenomenon have been proposed:

  (i) redistribution of the stresses during the preparatory period of the strong event, and

  (ii) increasing the resistance of the support system in post event period.

Analyses of seismic signal recorded in tunnels, cross-cuts and stopes in frequency and time domain

Peak velocity and acceleration parameters, frequency spectra in tunnel, cross-cut and stope.

- Measurements of the motion of the skin of tunnels and stopes excited by seismic signal indicate an increase in duration of shaking and an amplification of v_{max} and a_{max}.

Time domain analysis of tunnel sidewall motion.

- A damped oscillator model with signal degree of freedom can be used to analyse the energy dissipated by the structures through the process of damping and damage. The strategy, in this process, is to minimise the energy dissipated by damage and maximise the energy dissipated by damping.
- The structural damage in oscillating systems can be characterised by the changes in modal parameters, such as natural frequencies, mode shapes and modal damping values.

Transfer function for a seismic signal recorded in solid rock and on the skin of an excavation

- The Influence of support on vibration in the hangingwall is measurable. The algorithm presented in this report estimated different vibrations in the different sites in the hangingwall. The obtained model of transfer function is reasonable.
- There is strong indication that properties of the site change with time (weeks).
- The difference between ground motion in the footwall and ground motion in the hangingwall cannot be properly modelled with modal transfer function.

New interpretation techniques and theoretical developments

Velocity amplification considered as a phenomenon of elastic energy release due to softening

- The wave amplification may be attributed to energy release from rock under stresses high enough to generate cracks at a state close to instability; the amplification occurs due to physical non-linearity at interacting softening surfaces.
- The wave amplification appears as an exponential growth of displacements, velocities and accelerations with a characteristic time proportional to the attenuation in the rocks and the contact modulus of softening.
- Stationary waves do not exist for a regime of amplification.
- Triggering of seismic events, rockbursts in particular, by an incident wave or in apparent "static" conditions are extreme cases of amplification.

Rockburst investigations

Why does the severity of rockburst damage vary so much? There is no single, simple answer. Probably the most important factors are variations in the condition of the rock mass and the failure of inadequate support systems. Neither is there an easy, instant solution to the rockburst hazard. Given the current methods of mining, the most important steps to be taken to reduce the rockburst hazard would involve:

- discipline in ensuring that support is always up to standard, and that the stope support system is as close to the face as possible;
- frequent inspections of working places by personnel able to identify changes in the rock mass condition, and with the authority to recommend and implement appropriate changes to layout and support systems; and
- adherence to sound layouts, regardless of the demands of production.

Further gains will be achieved through the improvement of areal coverage in gullies and stopes.

5. References

Adams, D. J., Hemp, D.A. and Spottiswoode, S. M. 1990. Ground motion in a backfilled stope during seismic events. In: Static and Dynamic Considerations in Rock Engineering, R. K. Brummer (ed.), Balkema, Rotterdam, pp. 13-22.

Adams, D.J., Brenchley, P.R., and Lightfoot, N., 1992. Assessment of a rockburst in a preconditioning stope at Blyvooruitzicht Gold Mine. *Chamber of Mines of South Africa Research Organisation (COMRO), Reference Report 6/92.*

Bolt, B. A., 1988. Earthquakes, W. H. Freeman, New York.

Cichowicz, A., and Green, R. W. E. 1989. Changes in the early part of the seismic coda due to localized scatterers: the estimation of Q in a stope environment, PAGEOPH, 129:497-511.

Cichowicz, A. 1996. Data adaptive filter and damped oscillator used to study surrounding of excavation, Report

Clough, R. W., and Penzien, J., 1975. *Dynamics of Structures.* McGraw-Hill, New York.

Cook N. G. W. 1965. A note on rockbursts considered as a problem of stability. J. South African Inst. Mining and Metallurgy, 65, 437-446.

COMRO 1988. *Industry Guide to Methods of Amelioration of Rockfalls and Rockbursts.* Research Organization of the Chamber of Mines of South Africa.

Coward M. P. 1987. *Geometry of Normal Faults*, Short Course offered by the Bernard Price Institute, University of the Witwatersrand, Johannesburg, 1987.

Dede, T. & Handley, M.F. 1997. Bracket pillar design charts. SIMRAC Interim project report, CSIR Division of Mining Technology.

Dowrick, D. J., 1987. *Earthquake resistant design.* 2nd ed., John Wiley & Sons, Cichester.

Durrheim, R. J., Jager, A. J., Klokow, J. W. & Booyens, D. 1995. Back analysis to determine the mechanism and risk of rockbursts - 3 case histories from South African gold mines. *Proc. 26th Int. Conf. of Safety in Mines Research Institutes*, Katowice, Poland, vol. 5, pp. 41-56.

Durrheim, R. J., Kullmann, D. H. Stewart, R. D. and Cichowicz, A. 1996. Seismic excitation of the rock mass surrounding an excavation in highly stressed ground. In: Proceedings of the 2nd North American Rock Mechanics Symposium, Montreal, 19-21 June 1996, M. Aubertin, F. Hassani and H. Mitri (Editors), Balkema, Rotterdam, pp. 389-394.

Durrheim, R.J., Kullmann, D. H., Stewart, R. D. and Grodner, M. 1996. Seismic excitation of the rock mass surrounding an excavation in highly stressed ground. In M. Aubertin, F. Hassani and H. Mitri (eds), *Proc. 2nd North American Rock Mechanics Symposium:* 389-394. Rotterdam: Balkema.

Durrheim, R. J., Haile, A. T., Roberts, M. K. C., Schweitzer, J. K., Spottiswoode, S. M. & Klokow, J. W. 1997a. Violent failure of a remnant in a deep South African gold mine. *Tectonophysics*, in press

Durrheim, R. J., Handley, M. F., Haile, A. T., Roberts, M. K. C. & Ortlepp, W. D. 1997b. Rockburst damage to tunnels in a deep South African gold mine caused by a M=3,6 seismic event. *Proc. 4th Int. Symp. on Rockbursts & Seismicity in Mines*, S. J. Gibowicz & S. Lasocki (Eds), Balkema: 223-226.

Durrheim, R. J., Roberts, M. K. C., Haile, A. T., Hagan, T. O., Jager, A. J., Handley, M. F. & Ortlepp, W. D. 1997c. Factors influencing the severity of rockburst damage in South African gold mines. Proc. 1st Southern African Rock Engineering Symposium, R. G. Gürtunca & T. O. Hagan (Eds), SANGORM: 17-24.

Ebrahim Trollope, R. and S. N. Glazer, S. N. 1997, Assessment of seismic monitoring in a deep level scattered gold mining environment. Proc. 5th Tech. Mtg. S. A. Geophys. Assn., pp. 66-70.

Fairhurst, C., (ed.), 1993. *Proc.2nd Int. Symp. Rockbursts and Seismicity in Mines.* Rotterdam: A. A. Balkema.

Gay, N. C., Spencer, D., Van Wyk, J. J. & Van der Heever, P. K., 1984. The control of geological and mining parameters in the Klerksdorp gold mining district, in N. C. Gay and E. H. Wainwright (eds), *Proc. 1st Int. Symp. Rockbursts and Seismicity in Mines*, Johannesburg: SAIMM, 107-122.

Gay, N. C. & Wainwright, E. H., (eds), 1984. *Proc. 1st Int. Symp. Rockbursts and Seismicity in Mines*, SAIMM.

Gibbon, G. J., de Kock, A. and Mokebe, J. 1987. Monitoring of peak ground velocity during rockbursts, IEEE Transaction on Industry Applications, 23: 1094-1098.

Gibowicz, S. J. & Losocki, S., (eds), 1984. *Proc. 4th Int. Symp.. Rockbursts and Seismicity in Mines.* Rotterdam: A. A. Balkema.

Glazer, S. N., 1997. Applied mine seismology: a Vaal Reefs perspective. In S. J. Gibowicz, pp. 227-231

Goldbach, O.D. 1990. The use of seismogram waveforms to characterize the fracture zone around a mine excavation. MSc thesis, University of the Witwatersrand.

Hagan, T. O., Grobbelaar D. M. & Holtzhausen, P. J., 1984. *Rockburst damage at Western Deep Levels, Limited.* Report No. RP. 111, Anglo American Corp. S. A. Ltd.

Handley M. F., Hildyard M. W., & Spottiswoode S. M., 1996. The influence of deep mine stopes on seismic waves. *Proceedings of the Second North American Rock Mechanics Symposium*, Montreal, Canada, June 1996. Rotterdam: A. A .Balkema.

Hanks T.C. & Kanamori H. 1979. A moment-magnitude scale. *J. Geophys. Res.,* 84: 2348-2350.

Hedley, D. G. F., 1992. *Rockburst handbook for Ontario hardrock mines.* Special Report SP92-1E, CANMET, Energy, Mines and Resources Canada.

Hemp, D.A. & O.D. Goldbach, 1993. The effect of backfill on ground motion in a stope during seismic events. In: Proc. 3rd Int. Symp. on Rockbursts and Seismicity in Mines:. Balkema, Rotterdam, pp. 75-80.

Hepworth, N. 1983. *Damage to underground excavations caused by seismic events in the Klerksdorp mining district.* Internal report, Research Organization of the Chamber of Mines of South Africa.

Jager, A. J., 1992. Two new support units for the control of rockburst damage. In: Proceedings of the International Symposium on Rock Support, Sudbury, 16-19 June 1992, P. K. Kaiser and D. R. McCreath (Editors), Balkema, Rotterdam, pp. 621-631.

Jesenak, P., Kaiser, P, K., and Brummer R. K., 1993. Rockburst damage potential assessment. *Proc. 3rd Int. Symp. on Rockbursts and Seismicity in Mines:* 81-86. Rotterdam, Balkema.

Kaiser, P. K., and S. M. Maloney, 1996. Ground motion determination for rock support design. In: Proceedings of the 2nd North American Rock Mechanics Symposium, Montreal, 19-21 June 1996, M. Aubertin, F. Hassani and H. Mitri (Editors), Balkema, Rotterdam, pp. 217-224.

Kullmann, D. H., Stewart, R. D., & Lightfoot, N. 1994. Verification of a discontinuum model used to investigate rock mass behaviour around a deep-level stope. *The Application of Numerical Modelling in Geotechnical Engineering,* SANGORM, Pretoria.

Kullmann, D. H., Stewart, R. D., Lightfoot, N. and Longmore, P. 1995. Interim report on the progress towards the implementation of preconditioning as a technique for controlling face bursting on deep-level mines. *SIMRAC Interim Report - Project GAP030*, June 1995.

Kullmann, D.H., Stewart, R. D. & Grodner, M. 1996. A pillar preconditioning experiment on a deep-level South African gold mine. *Proc. 2nd North American Rock Mechanics Symposium:* Balkema: 375-380.

Lightfoot, N., Kullmann, D. H. & Leach, A. R., 1994. A conceptual model of a hardrock, deep level, tabular ore body that incorporates the potential for face bursting as a natural product of mining. *Proc.1st N. Amer. Rock Mech. Symp.*, Rotterdam: A.. A. Balkema,.

Lightfoot, N. Kullmann, D. H., Toper, A. Z., Stewart, R. D., Grodner, M., Janse van Rensburg, A. L., & Longmore, P. L.. 1996. Preconditioning to reduce the incidence of face bursts in highly stressed faces. *SIMRAC Final Report - Project GAP030*, January 1996.

Lin, R., Liangz, C., and Soong, T. T., 1991. An experimental study on seismic behaviour of viscoelastic damped structure. *Engrg. Struct.*: 13, pp. 75-84.

Linkov A. M. 1994. Dynamic phenomena in mines and the problem of stability. Lisboa, Cedex: Int. Soc. for Rock Mech, P-1799.

Linkov A. M. 1995. Keynote address: Equilibrium and stability of rock masses. In T. Fujii (ed.), Proc. 8-th Int. Congress on Rock Mechanics. Rotterdam: Balkema.

Linkov A. M. 1997. Keynote address: New geomechanical approaches to develop quantitative seismicity. In S. J. Gibowicz and S. Lasocki (eds.), Proc. 4th Int. Symposium "Rockbursts and Seismicity in Mines". Rotterdam: Balkema.

Ljung., L., and Soderstrom, T. 1983. Theory and practice of recursive identification. MIT Press Cambridge, Mass

Ljung,. L. 1987. System Identification. Prentice-Hall Inc Englewood Cliffs, N. J.

McGarr, A. 1993. Keynote address: Factors influencing the strong ground motion from mining-induced tremors. *Proc. 3rd Int. Symp. on Rockbursts and Seismicity in Mines:* 3-12. Rotterdam, Balkema.

McGarr A. 1996. A mechanism for high wall-rock velocities in rockbursts, Workshop on Induced Seismicity, NARMS'96, Montreal, Canada.

McGarr, A, R., W. E. Green and S. M. Spottiswoode, 1981. Strong ground motion of mine tremors: some implications for near source ground motion parameters. Bull. Seism. Soc. Am., 71: 295-319.

Napier, J.A.L., 1990. Modelling of fracturing near deep level gold mine excavations using a displacement discontinuity approach. in *Mechanics of Jointed and Fractured Rock*, P. Rossmanith (ed.), Rotterdam: Balkema.

Napier, J. A. L. & Stephenson S. J. 1987. Analysis of deep-level mine design problems using the MINSIM-D boundary element program. *Proceedings of the 20th International Symposium on the Application of Computers and Mathematics in the Mineral Industries. Volume 1: Mining*: 3-19. Johannesburg, SAIMM.

Ortlepp W. D. 1993. High ground displacement velocities associated with rockburst damage. In P. Young (ed.), Proc. 3rd Int. Symp. "Rockbursts and Seismicity in Mines". Rotterdam: Balkema, p. 101-106.

Ortlepp, W.D. 1984. Rockbursts in South African gold mines: a phenomenological view. *Proc. 1st Int. Symp. on Rockbursts and Seismicity in Mines:* 165-178. Johannesburg, SAIMM.

Ortlepp W. D. 1997.. *Rock fracture and rockbursts,* Monograph Series M9, Johannesburg: S. Afr. Inst. Min. Met.

Roberts, M. K. C., 1995. Stope and Gully Support, Final Report Project GAP032, Safety in Mines Research Advisory Committee.

Pattrick, K.W., A.M. Kelly & S.M. Spottiswoode 1990. A Portable Seismic System for rockburst applications. *Technical Challenges in Deep Level Mining:* 1133-1146. Johannesburg, SAIMM.

Pyrak-Nolte L. J. 1996. The seismic response of fractures and the interrelations among fracture properties. Int. J. Rock. Mech. Min. Sci. & Geomech. Abstr., 33, 787-802.

Safak. E. 1989. Adaptive modelling, Identification, and Control of Dynamic Structure Systems. I Theory. Journal of Engineering Mechanics.

Salamon M. D. G. 1970. Stability, instability and design of pillar working. Int. J. Rock. Mech. Min. Sci., 7, 613-631.

Salawu, O. S., 1997. Detection of structural damage through changes in frequency: a review. *Engrg. Struct.*: 19, pp. 718-723.

Solnes, J., 1974. Engineering seismology and earthquake engineering. *NATO Advanced Study Institute Series.*

Spottiswoode, S. M., and J. M. Churcher, 1988. The effect of backfill on the transmission of seismic energy. Backfill in South African Mines, Johannesburg, SAIMM, pp: 203-217.

Spottiswoode, S.M. 1993. Seismic attenuation in deep-level mines. In R.P Young (ed.), *Proc. 3rd Int. Symp. on Rockbursts and Seismicity in Mines:* 409-414. Rotterdam, Balkema.

Stewart, R.D. & Spottiswoode, S.M. 1993. A technique for determining the seismic risk in deep-level mining. *Proc. 3rd. Int. Symp. on Rockbursts and Seismicity in Mines*, 123-128, AA Balkema, Rotterdam.

Spottiswoode S. M. 1997. Personal communication

Stevenson, W. 1995. *Personal communication,* CSIR Aerotek.

Vermaakt D. T., Lambert P. E. & Barnard H. C. 1989. *Evidence of Northwards Thrusting on East Driefontein Gold Mine,* Internal Geological Report, East Driefontein Gold Mine, August 1989.

Vlietstra D. & Smith G. L. 1995. *In Situ Stress Measurements at East Driefontein Gold Mine Using the Doorstopper Technique : 42 Level RAW South.* CSIR Mining Technology Consultancy Report No. RE 06/95, CSIR Mining Technology, 9 March 1995.

Wagner, H, 1984. Support requirements for rockburst conditions, in Proceedings of the 1st International Congress on Rockbursts and Seismicity in Mines, Johannesburg, 1982, N. C. Gay and E H Wainwright (Editors), SAIMM, Johannesburg

Widrow, B., and Glover, J., 1975. Adaptive noise cancelling: principle and application. *Proc. IEEE*: 63, pp. 1692-1715.

Wyss, M. (editor) 1991, Evaluation of proposed earthquake precursors. American Geophysical Union, Washington.

Young, R. P, (ed.), 1993. *Proc.3rd Int. Symp. Rockbursts and Seismicity in Mines.* Rotterdam: A. A. Balkema.

Zahrah, T. F., and Hall, W. J., 1984. Earthquake energy absorption in SDOF structures. *J. Struct. Eng.*: 110, pp. 1757-1772.

Zhang, R., and Soong, T. T., 1992. Seismic design of viscoelastic damper for structural application. *J. Struct. Eng.*: 118, pp. 1375-1392.

7. The following materials have been published

Cichowicz, A, 1995. Study of the influence of rock mass surrounding a stope or tunnel on the seismic signal, internal report.

Cichowicz, A. 1996. Data adaptive filter and damped oscillator used to study surrounding of excavation, internal report.

Durrheim, R J, Roberts, M. K. C., Gurtunca, R. G. and Spottiswoode, S. M. 1995. Rock engineering aspects of the rockburst at Western Deep Levels (Ltd.) Mine on 3 November 1994 damaging the 113-36 Carbon Leader Stope, internal report.

Durrheim, R J, Roberts, M. K. C. and Haile, A, T. 1995. Rock engineering aspects of the rockfalls at East Rand Proprietary Mine on 24 July and 15 August 1995, internal report.

Durrheim, R J, Haile, A. T., Handley, M. F., Ortlepp, W. D. and Roberts, M. K. C. 1995. Rock engineering aspects of the rockburst at East Driefontein Mine on 14 September 1995 damaging the No. 4 Shaft access development to the K and L longwalls, report.

Durrheim, R J, Handley, M. F., Roberts, M. K. C., Spottiswoode, S. M. and Ortlepp, W. D. 1996. Preliminary Report on Rock Engineering Aspects of the Rockburst at Blyvooruitzicht Gold Mine on 30 January 1996 damaging the 17-24W Stope, report.

Durrheim, R J, Eve, R., Haile A. T. and Jager, A. 1996. Rock Engineering aspect of the rockburst at 1 Shaft East Driefontein Gold Mine on 5 June 1996 damaging the 34-19 Carbon Leader East Stope, report.

Durrheim, R J, Haile, A. T., Roberts, M. K. C., Schweitzer, J. K., Spottiswoode, S.M. and Klokow, J. W. 1998. Violent failure of a remnant in a deep South African gold mine, Tectonophysics, in press.

Haile, A., Durrheim, R. J. and Eve, R. 1996. Observations and considerations for the mining of 34-19 Carbon Leader East stope, No. 1 shaft East Driefontein, report.

Linkov, A. M. and Durrheim, R. J. 1998. Velocity amplification considered as a phenomenon of elastic energy release due to softening, in press, MJFR-3, Vienna.

Pernegger, J. 1995. MINSIM modelling: rockburst Western Deep Levels, North Mine, 110-113/36 longwall, internal report.

Roberts, M K C, Wojno, L., Haile, A. T. and Durrheim, R. J. 1996. Preliminary Note. Rockfall Accident at 11 Shaft, Vaal Reefs Gold Mine on 13 February 1996, report.

Toper, A. Z., Grodner, M., Stewart, R. D., Durrheim, R. J., Janse van Rensburg, A., Kullmann, D. H. and N Lightfoot, N. 1996. Rock Engineering aspects of the rockburst at Western Deep Levels South Mine on 15 February 1996 which resulted in damage to the 87-49 longwalls, report.

APPENDIX A

Transfer function for a seismic signal recorded in solid rock and on the skin of an excavation

1 Introduction

The objective of this report is to quantify the effect of the rock mass surrounding a stope or tunnel on the seismic signal. Work done as part of this project in 1996 shows that the transfer function of rock mass surrounding an excavation can be modelled using a damped oscillator (Cichowicz, 1996).

In this report the method of estimation of transfer function is extended further. Parameters of a damped oscillator are estimated using inversion techniques. The transfer function is modelled as a time varying system. Application of this technique of time varying systems is essential to track the time variation of the natural frequency during ground motion caused by a seismic event.

2 Dynamic structural systems

Ljung and Soderstrom (1983) and Ljung (1987) studied methods for the time-domain identification of linear multidegree on freedom of structural dynamic systems. The term identification refers to the determination of analytical models for structure, based on the observations of the system. Recordings of a single input and single output are sufficient to determine all the modal frequencies and damping ratios in a structure (Safak, 1989).

The equivalent discrete-time equation for a single input, single output dynamic system can be written in the following form:

$$y(t) + a_1 y(t-1) + \ldots + a_l y(t-l) = b_1 u(t-1) + \ldots + b_m u(t-m) \qquad \text{(A.1)}$$

where: u(t) and y(t) are the input and output sequences, respectively; a_i and b_i are constants for time invariant systems and functions of time for time varying systems. Although the equation represents a linear system, it has been suggested that any non-linear system can also be represented by a similar equation with time varying parameters

(a_i,b_i), by introducing the following polynomials in the back-ward-shift operator q^{-i} , where q^{-i} is defined as q^{-i} y(t)= y(t-i),

$$A(q) = 1 + a_1 q^{-1} + ... + a_l q^{-l} \tag{A.2}$$

$$B(q) = b_1 q^{-1} + ... + b_m q^{-m} \tag{A.3}$$

Equation (A.1) can be written in a more compact form as:

$$y(t) = \frac{B(q)}{A(q)} u(t) \tag{A.4}$$

The polynomial ratio B (q)/A (q) is called the system transfer operator, H(q). Discrete-time equations can also be expressed in the frequency domain by taking the Z-transform of time domain equations. By taking the Z-transform of both sides in equation (A.4) we can write:

$$Z[y(t)] = \frac{B(z)}{A(z)} Z[u(t)] \tag{A.5}$$

where Z[y(t)] = the Z-transform and z is any complex number. The polynomials A(z) and B(z) are the same as defined by equations (A.2) and (A.3) except all the *qs* are replaced by *zs*. The transfer function can be represented in terms of harmonic functions by selecting $z = \exp(i2\pi f \Delta t)$, where f denotes the frequency and Δt is the sampling interval.

The stability conditions require that the roots of the denominator polynomial A(z) should all have a magnitude less than one. This means that the roots of A(z) are all in complex-conjugate pairs located inside the unit circle in the complex plane. The transfer function can be put into the following form:

$$H(z) = \sum_{j=1}^{n_a/2} H_j(z) \tag{A.6}$$

where:

$$H_j(z) = \frac{2R(q_j) - 2R(q_j \bar{p}_j)z^{-1}}{1 - 2R(\bar{p}_j)z^{-1} + |\bar{p}_j|^2 z^{-2}} \quad \text{(A.7)}$$

where $H_j(z)$ is the second order filter, R(q) is the real part of q, $\bar{p}$ is the complex conjugate, p_j is the complex root of the polynomial A(z) and q_j is the corresponding residue of H(z). The filter output y(t) is modelled as the linear combination of the outputs of second-order filter each subjected to input u(t). The form given by equation (A.6) is known as the parallel form of realisation. Each second-order filter $H_j(z)$ corresponds to a simple, damped oscillator. The damping d_j and the frequency f_j of each oscillator are defined by the following equations (Safak, 1989):

$$d_j = \frac{\ln(\frac{1}{r_j})}{[F_j^2 + \ln^2(\frac{1}{r_j})]^{1/2}} \quad \text{(A.8)}$$

$$f_j = \frac{\ln(\frac{1}{r_j})}{2\pi d_j \Delta t} \quad \text{(A.9)}$$

where: $r_j=|p_j|$, F_j is the modulus and the arguments of the jth pole (or of its complex-conjugate).

The recordings from dynamic systems are always contaminated by noise existing in the recording environment, as well as by the imperfections in the recording instrument. Hence the following equations for the signal:

$$A(q)y(t) = B(q)u(t) + C(q)e(t) \quad \text{(A.10)}$$

where:

$$C(q) = 1 + c_1 q^{-1} + ... + c_n q^{-n} \quad \text{(A.11)}$$

and e(t) is a white noise sequence. Equation (A.10) represents a family of model structures for noise systems. The A(q) corresponds to poles that are common between the dynamic model and the noise model. The motivation for introducing C(q) polynomial is to provide for flexibility in the noise descriptions.

3 Recursive prediction error methods

System identification constitutes determining the coefficients of the polynomials in A(z), B(z) and C(z) for a given pair of input and output sequences:

$$\Omega = (a_1,..., a_l, b_1,..., b_m, c_1,...., c_n) \quad \text{(A.12)}$$

The one step ahead prediction $y_{pred}(t, u(t),a_i,b_i,c_i)$ of y(t) at time t is based on the past values of input u(t), output, y(t) and parameters a_i b_i c_i. The difference:

$$E(t,\Omega) = y(t) - y_{pred}(t,\Omega) \quad \text{(A.13)}$$

gives the error in the estimation at time t. System identification aims to determine the vector $,\Omega$, such that the total error $\sum E^2(t,\Omega)$ is minimum. For identification, how to measure the total estimation error must be decided. The most convenient way is the least squares method. The least squares method uses quadratic criteria for measuring errors. A weighting factor (forgetting factor) is also included in the criteria, to the flexibility of manipulating the effect of data on total error.

$$E = \sum_{k=1}^{t} L^{t-k} E^2(t,\Omega) \quad \text{(A.14)}$$

where: L is the forgetting factor.

Measurements that are older carry less weight in (A.14) than the current values. For time invariant systems, weighting factors can all be taken as equal to one. For time varying systems, weighting factors are essential to track the time variation of system parameters. The forgetting factors localise the identification by giving more weight to the current values, and by gradually discounting the past values.

A recursive identification algorithm is:

$$\Omega(t) = \Omega(t-1) + K(t)[y(t) - y_{pred}(t)] \qquad \text{(A.15)}$$

where: $\Omega(t)$ is the parameter estimate at time t, and y(t) is the observed output at time t. $y_{pred}(t)$ is a prediction of the value y(t) based on observation up to time t-1. The gain K(t) determiners in what way the current prediction error $y(t) - y_{pred}(t)$ affects the update of the parameter estimation. In this report the Matlab implementation of equation (A.15) is used.

4 Data, results and discussions

4.1 Experiment 1 (Blyvooruitzicht Gold Mine)

Data from the experiment with two geophones were used to study the transfer function of the rock mass surrounding an excavation. The geophones were installed in close proximity to each other; the first in solid rock and the second in a footwall drive. Figure A.1 shows an example of ground motion recorded in solid rock (solid line) and recorded in a footwall drive (dashed line). The velocity spectrum of the geophone in solid rock is exactly as the theory predicts (see Figure A.2 bold lines). The geophone installed in the footwall drive shows very clear resonance frequencies (see Figure A.2 dashed lines).

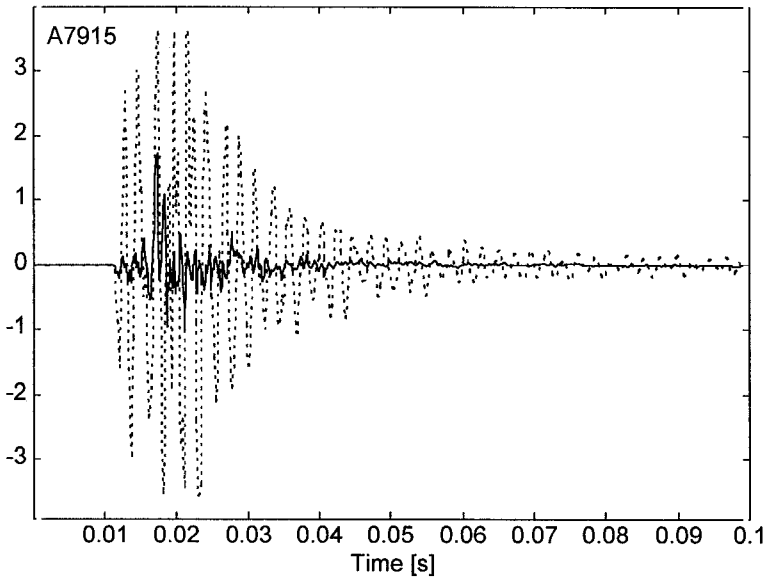

Figure A.1 An example of real seismograms (event A7915), recorded in solid rock - solid line, and in a footwall drive - dashed line

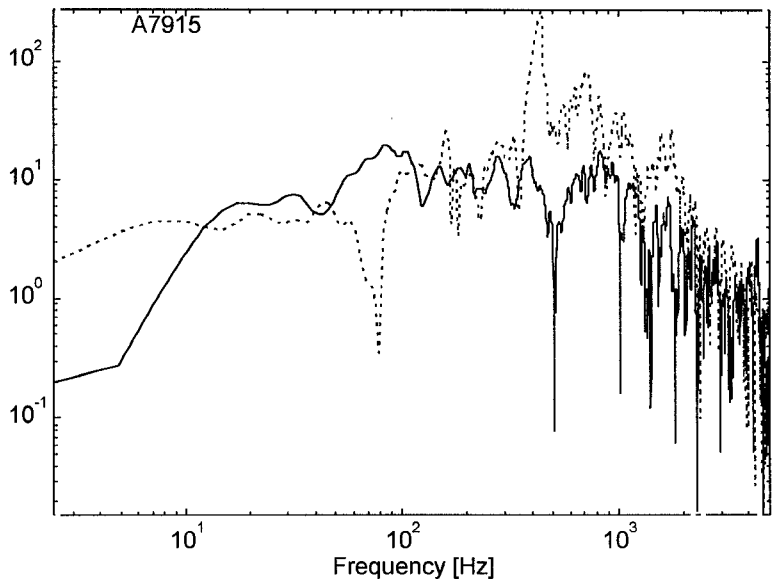

Figure A.2 Velocity spectrum of the seismograms from Figure A.1.

The transfer function of the site effect is calculated using the method described in the previous section of the report. To improve modelling precision it is good practice to remove very high frequency contents from a signal using the low pass Butterworth filter. To preserve the shape of the signal a zero-phase filter is applied by processing in both the forward and reverse directions. Parameters of transfer function were calculated for several orders of A (q), B (q) and C (q) polynomials.

4.2 Is site response non-linear?

The transfer function is defined by coefficients of A (q) and B (q) polynomials, therefore Figure A.3 reflects the changes of transfer function. As a consequence there is not only one transfer function, which can be applied to the entire seismogram.

Figure A.3 shows the coefficient of polynomial A (q) and B (q) versus time. The forgetting parameter is equal to 1,0. The initial part of the time series should be ignored, as the learning time for the filter (from 0 s to 0,01 s). The next part shows some significant changes in all coefficient values. This suggests that the P wave caused the non-linear response of the system. During the vibration caused by the P wave there is no interval of time with fixed values of coefficient. The arrival of the P wave shows initial abrupt changes (0,015 s) and then the coefficient stabilises at time 0,035 s.

It is difficult to separate the effect of the adapting coefficient due to the adaptive algorithm from a non-linear response of the system.

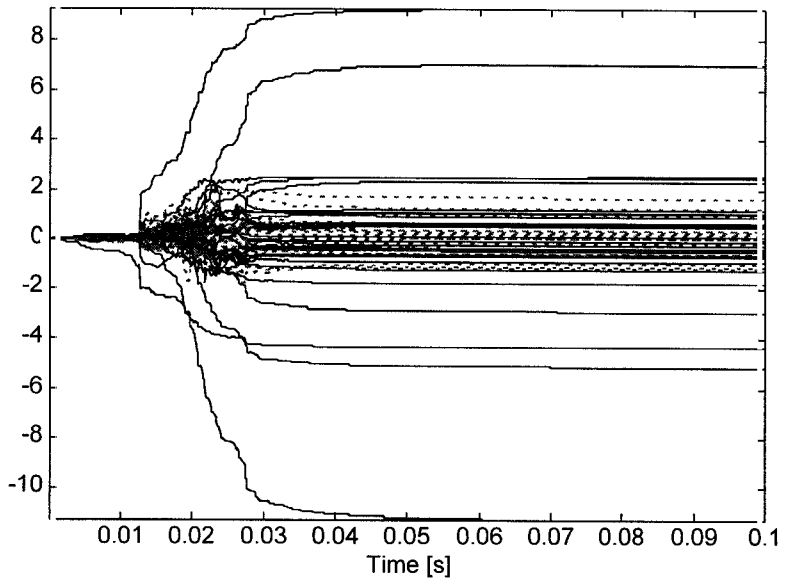

Figure A.3 The coefficients of the polynomials A (q) and B (q) versus time.

4.3 Model of output: Mode presentation

The mode contribution to ground motion can be obtained by combining equations (A.4) and (A.6). Figure A.4 (*a*) (solid line) shows ground motion caused by Mode 1, calculated at time 0,0980 s. For comparison, the output of the system (seismogram installed in the wall of the tunnel) is shown on Figure A.4 (*a*) by dashed line. The system response is dominated by Modes 1, 3, 4, 5, 6, 7, 8 and 15 (see Figures A.4 a, b, c, d, e, f, g, h). The sum of the contribution from each of the modes to the response is plotted in Figure A.5 along with the recorded response. However, some modes are fairly close and have different phases. Therefore, when they are added together, most of the amplitudes cancel each other and do not appear in the final response.

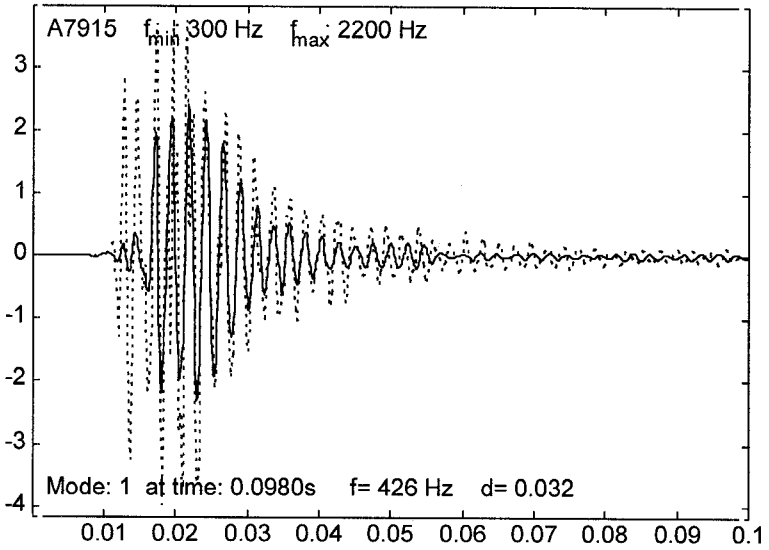

Figure A.4 (a) The system response dominated by mode one.

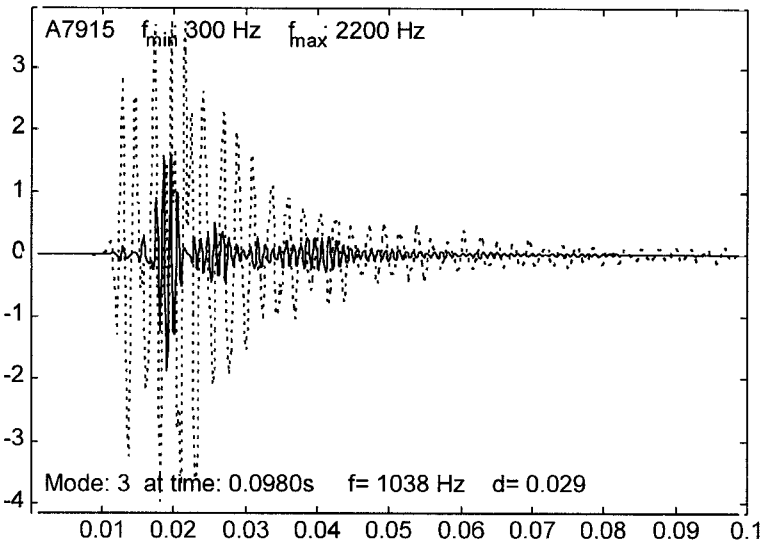

Figure A.4 (b) The system response dominated by mode three.

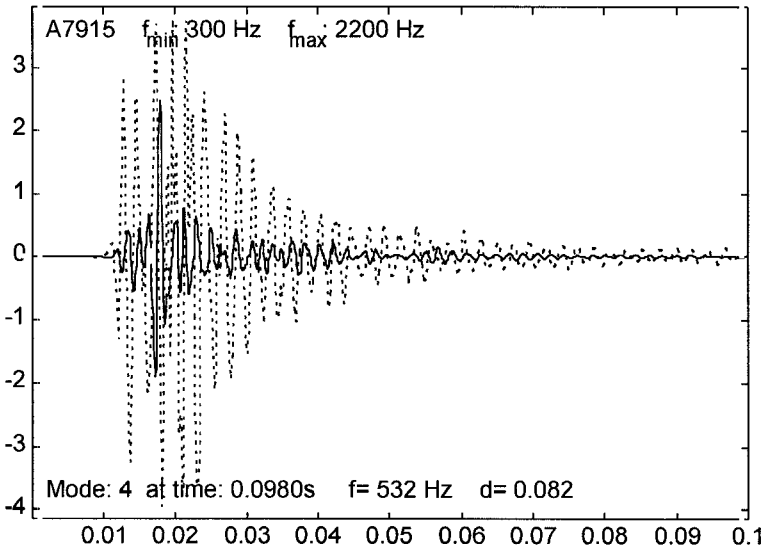

Figure A.4 (c) The system response dominated by mode four.

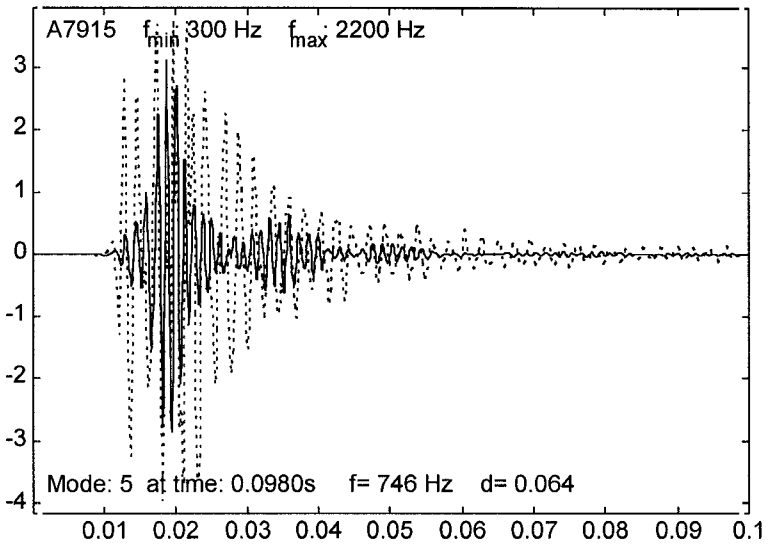

Figure A.4 (d) The system response dominated by mode five.

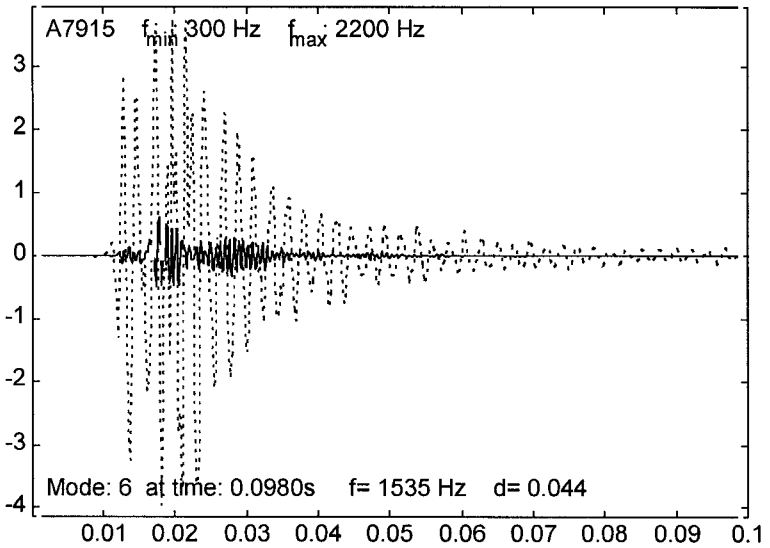

Figure A.4 (e) The system response dominated by mode six.

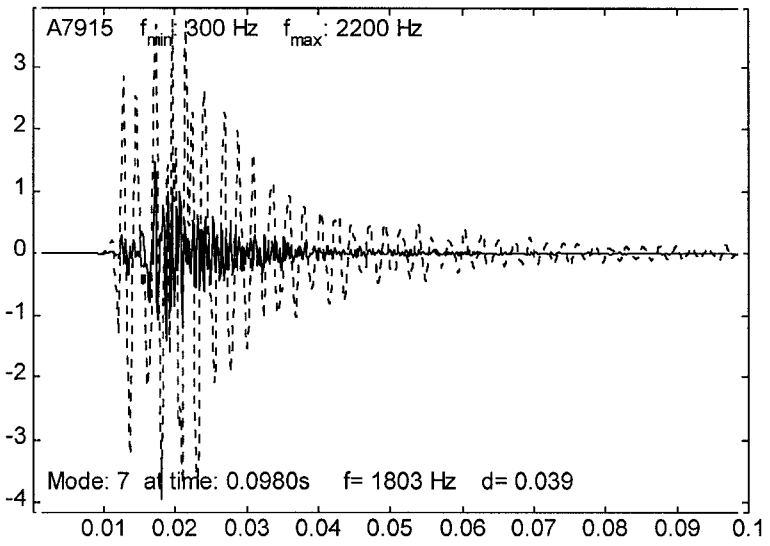

Figure A.4 (f) The system response dominated by mode seven.

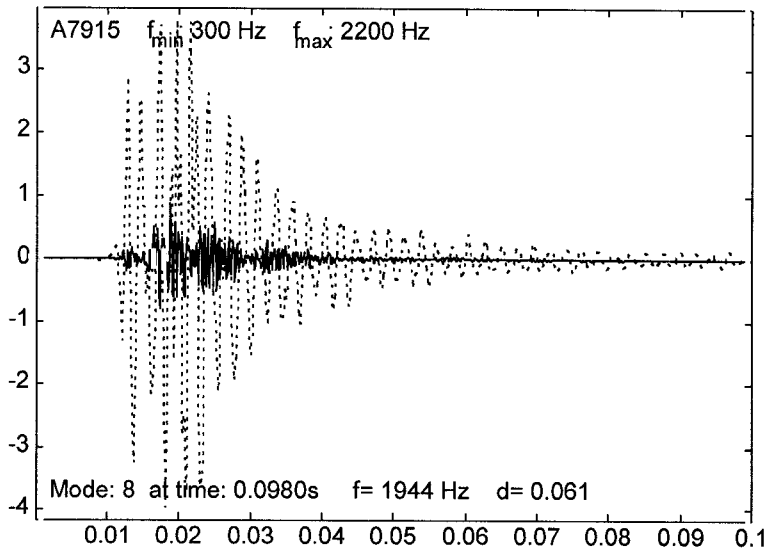

Figure A.4 (g) The system response dominated by mode eight.

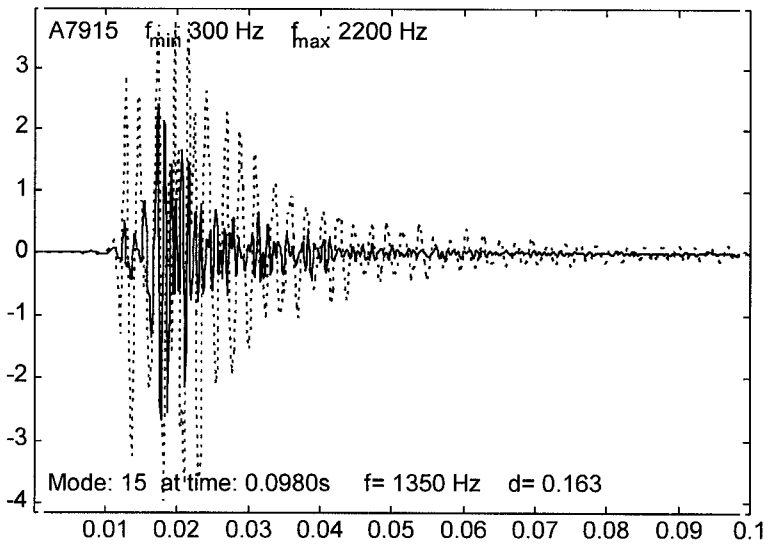

Figure A.4 (h) The system response dominated by mode fifteen.

Figure A.5 shows the sum of 15 modal responses calculated at the time of 0,0980 s; the match with the real ground motion is very good. As expected (see Figure A.3) a transfer function calculated at the end of seismogram is not suitable for modelling of the P wave pulse.

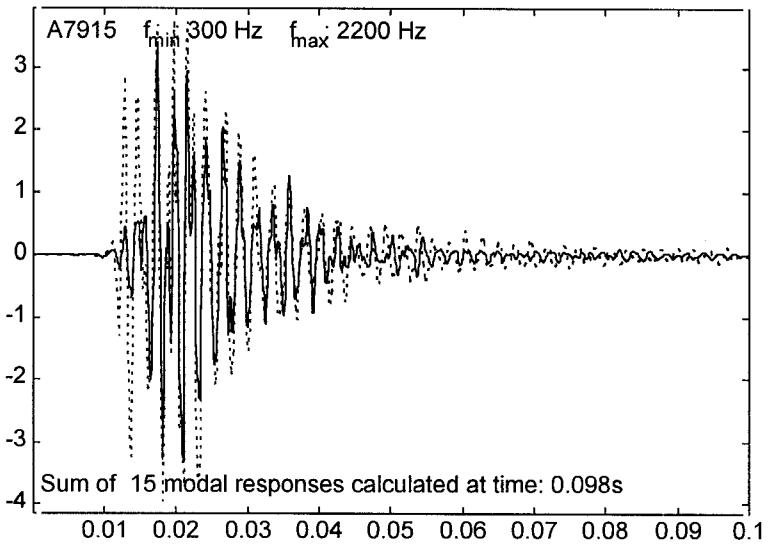

Figure A.5 Sum of fifteen modal responses calculated at time of 0,0980 s.

Figure A.6 shows spectra of real output and that calculated. The spectral match of two signals is obvious. The match can be used as an independent verification of the inversion method. The third curve is the transfer function in frequency domain.

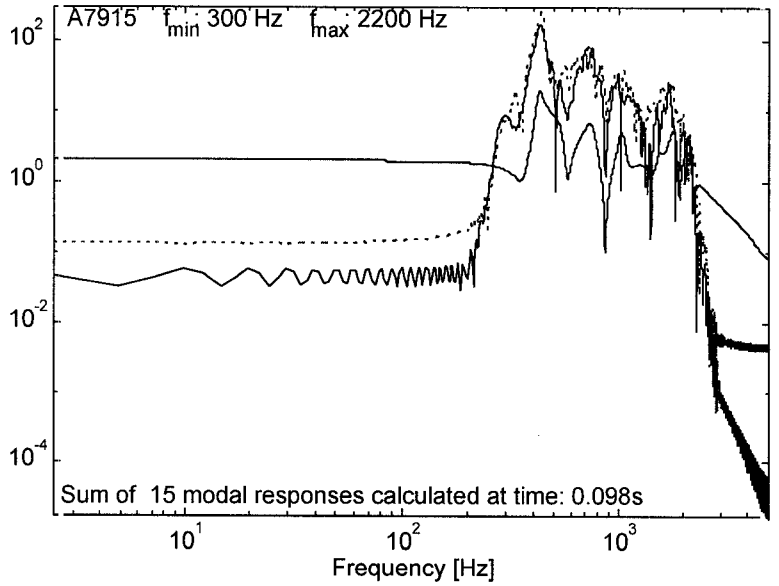

Figure A.6 The spectrum of the seismograms from Figure A.5 and their transfer function.

There are also several other modes with significant amplitudes. Those modal frequencies change from model to model of transfer function. This can be caused by either, the inversion process not being perfect, or by the different response of site effect.

The same calculation of transfer function was repeated for 5 pairs of seismograms. Two examples of simulation of waveform are shown throughout Figure A.7 to A.12. It is encouraging that the main features of the transfer function are similar in all examples.

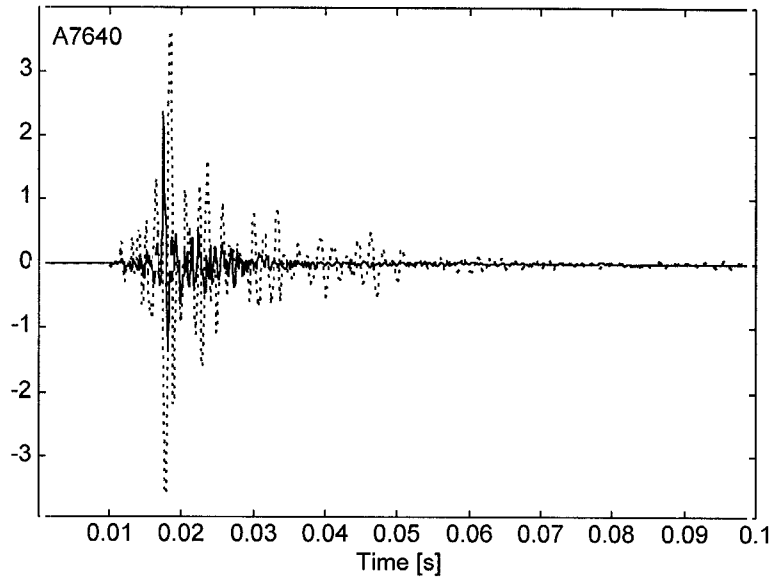

Figure A.7 An example of real seismograms (event A7640), recorded in solid rock - solid line, and in a footwall drive - dashed line.

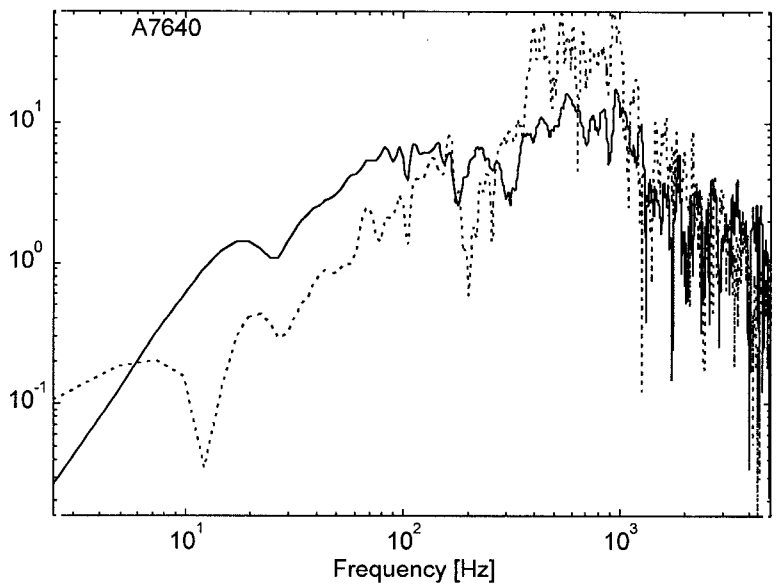

Figure A.8 Velocity spectrum of the seismograms from Figure A.7.

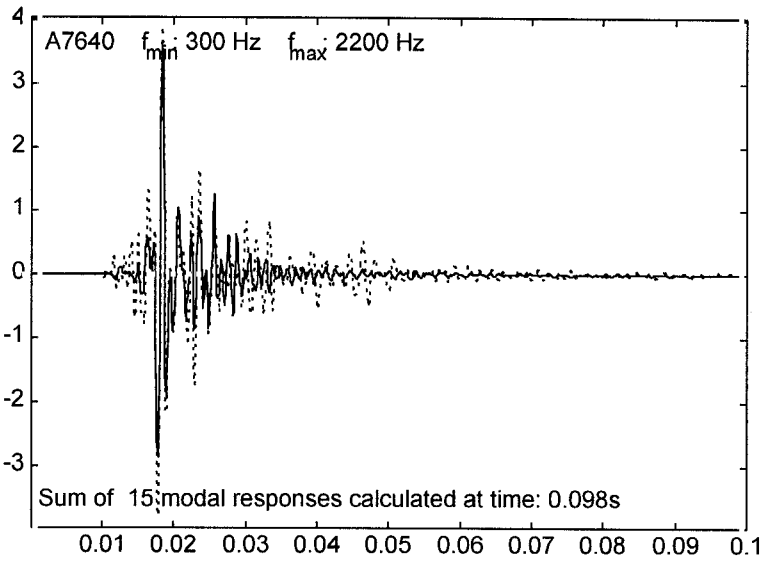

Figure A.9 Sum of 15 modal responses calculated at time 0,098 s

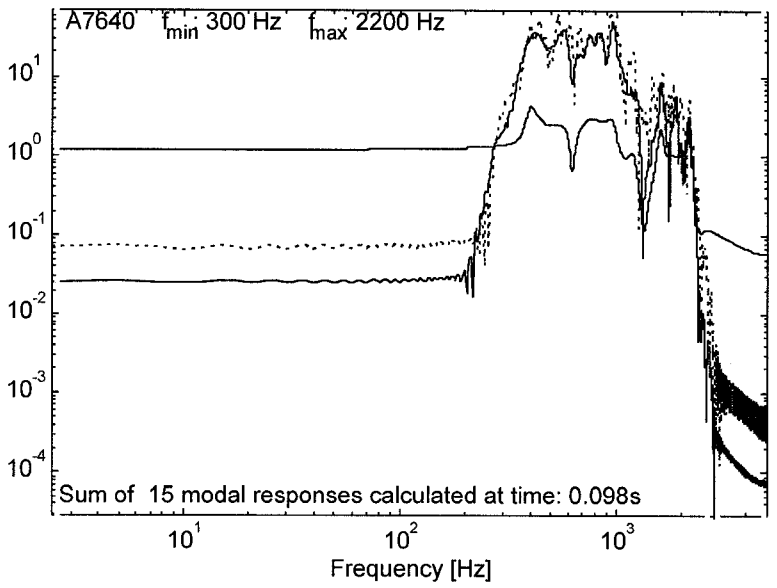

Figure A.10 The spectrum of the seismograms from Figure A.9 and their transfer function.

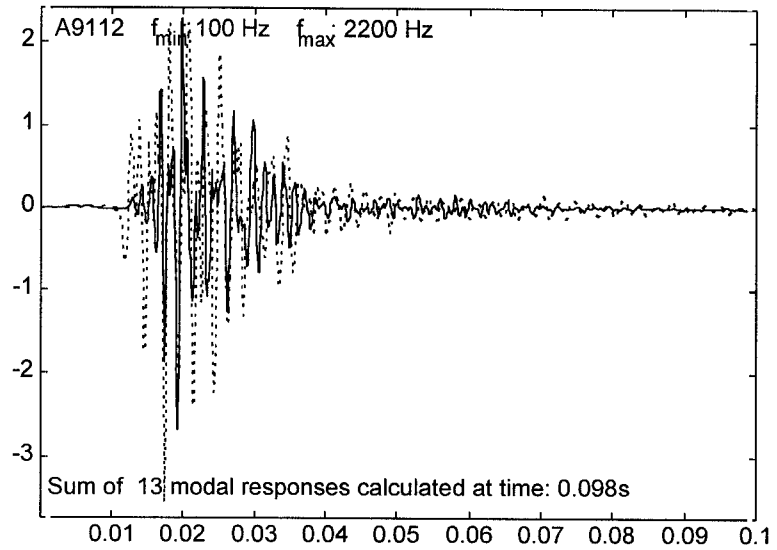

Figure A.11 Sum of thirteen modal responses calculated at time 0,098 s.

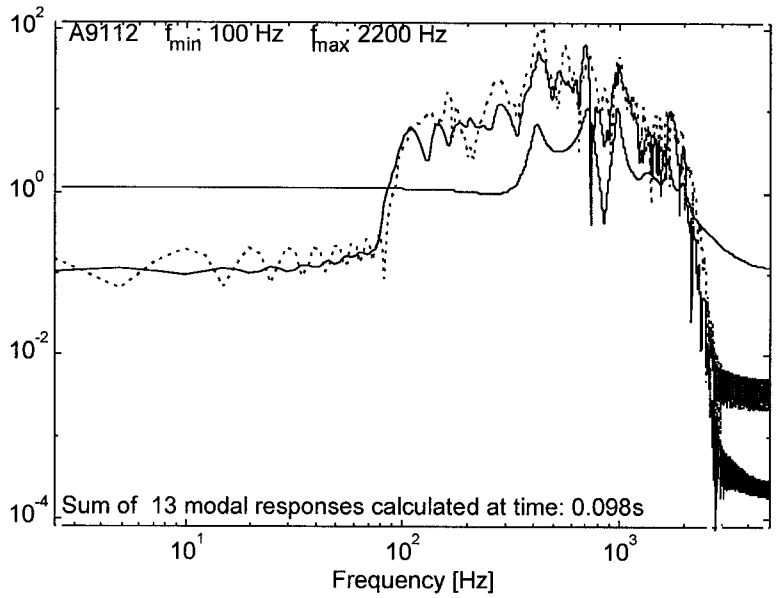

Figure A.12 The spectrum of the seismograms from Figure A.11 and their transfer function.

Table A.1 shows modal frequencies and damping ratios obtained at the end of seismogram for all five pairs of seismograms. The first row of Table A.1 shows a number of seismic events and a frequency range for which calculation was performed.

Table A.1

Modal frequencies and damping ratios obtained at the end of seismogram for all five pairs of seismograms.

Modal Frequencies and Damping Ratios				
No: A7915 300-2200 Hz	No: A7640 300-2200 Hz	No: A8114 300-2200 Hz	No: A8328 300-1500 Hz	No: A9112 100-2200 Hz
426 Hz 0,032	399 Hz 0,048	425 Hz 0,014	380 Hz 0,056	413 Hz 0,051
			456 Hz 0,312	425 Hz 0,611
532 Hz 0,082	611 Hz 0,077			
746 Hz 0,064	764 Hz 0,200	741 Hz 0,189	731 Hz 0,074	718 Hz 0,035
1038 Hz 0,029	971 Hz 0,047	837 Hz 0,125	1006 Hz 0,044	985 Hz 0,021
1350 Hz 0,163		1303 Hz 0,319		1371 Hz 0,091
1532 Hz 0.044				
1803 Hz 0,039			1711 Hz 0,022	1683 Hz 0,025

An examination of Table A.1 shows that the modal frequencies of 400+/-20Hz and 740+/-20Hz are present in all models of the transfer function. The modal frequency located between 837 and 1038 Hz is also present in all models of the transfer function.

There are also several other modes with significant amplitudes. Those modal frequencies change from model to model of transfer function. This can be caused by either, the inversion process not being perfect, or by the different response of site effect.

4.4 Experiment 2 (Vaal Reefs No.5 Shaft)

Two geophones were installed in hangingwall of stope; one close to support and another 1,1 m away.

The inspection of seismograms and their spectra shows strong similarity of the two seismograms and spectra (see Figure A.13 and Figure A.14). Only after processing of data was it possible to quantify the difference between them (see Figure A.15 to Figure A.45).

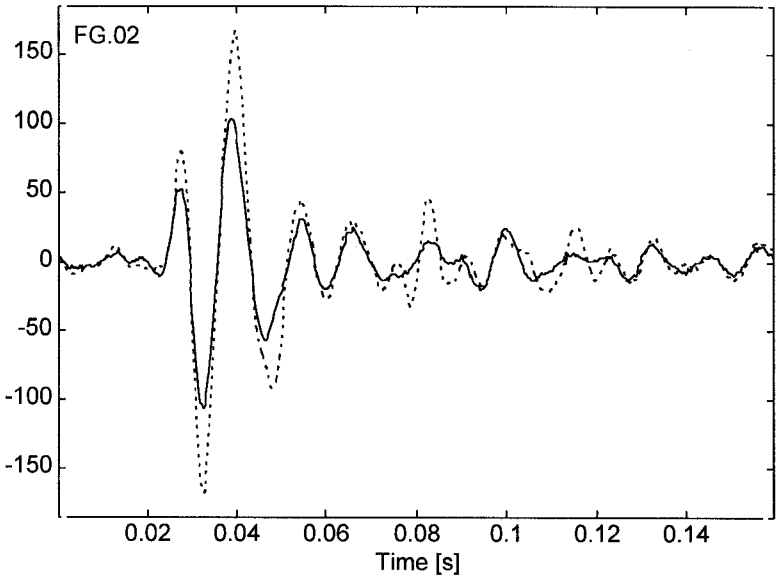

Figure A.13 An example of real seismograms (event FG02), recorded in solid rock - solid line, and in a fractured rock - dashed line.

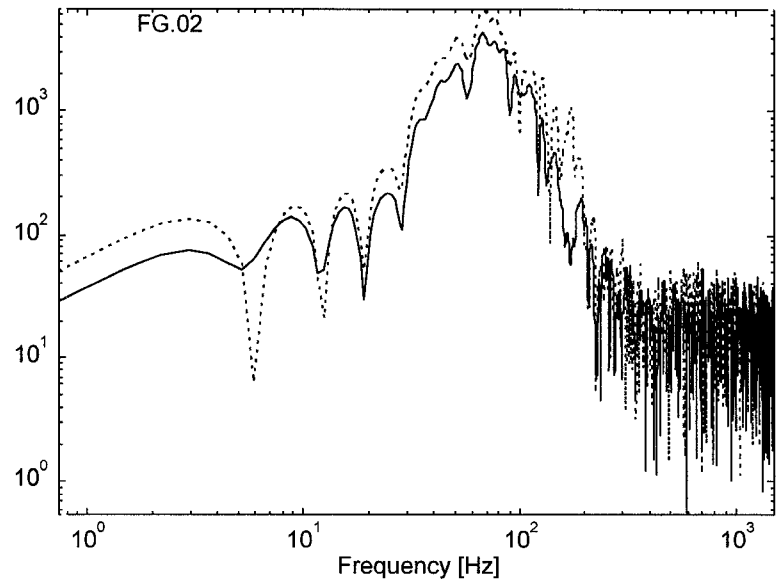

Figure A.14 Velocity spectrum of the seismograms from Figure A.13.

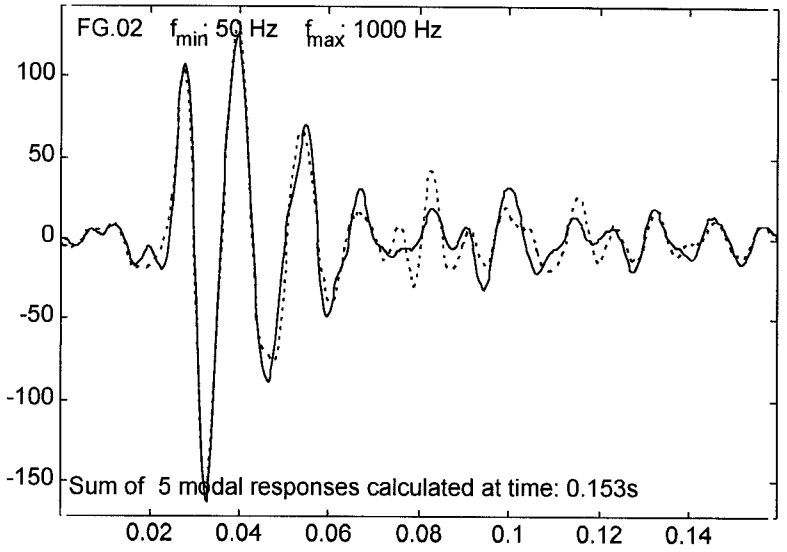

Figure A.15 Sum of five modal responses calculated at time 0.153 s.

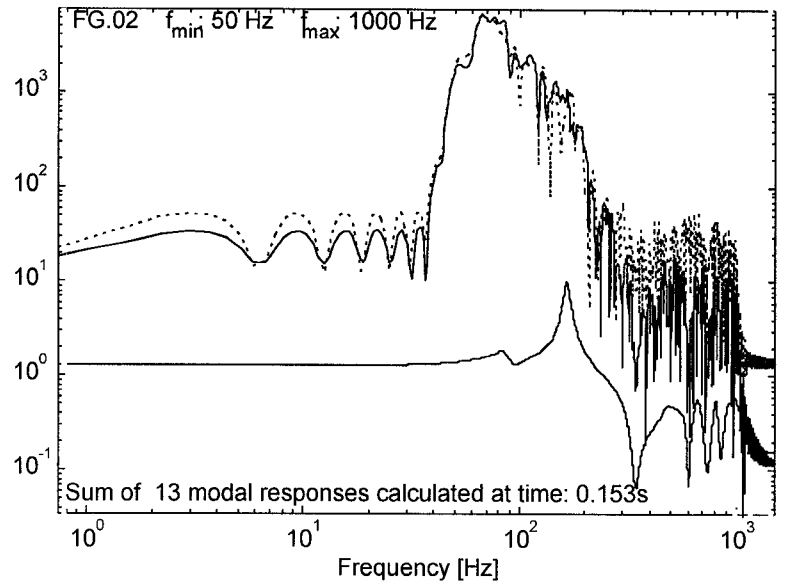

Figure A.16 The spectrum of the seismograms from Figure A.15 and their transfer function.

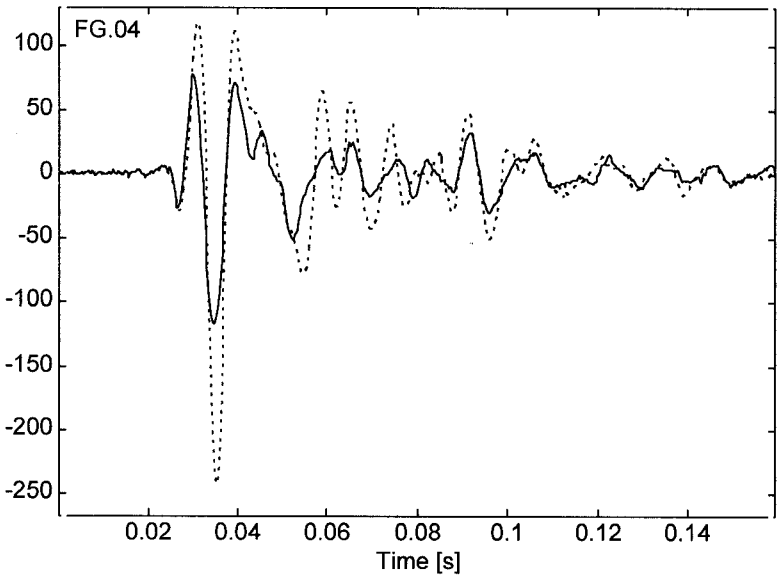

Figure A.17 An example of real seismograms (event FG04), recorded in solid rock - solid line, and in a fractured rock - dashed line.

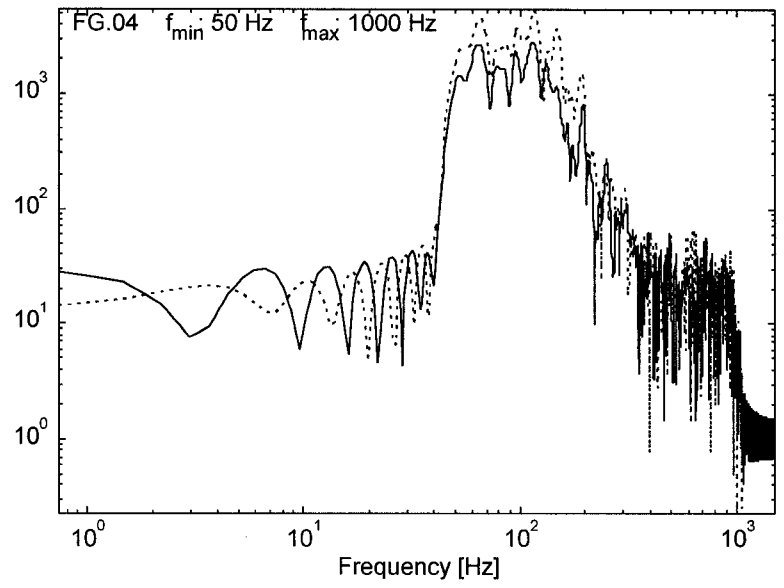

Figure A.18 Velocity spectrum of the seismograms from Figure A.17.

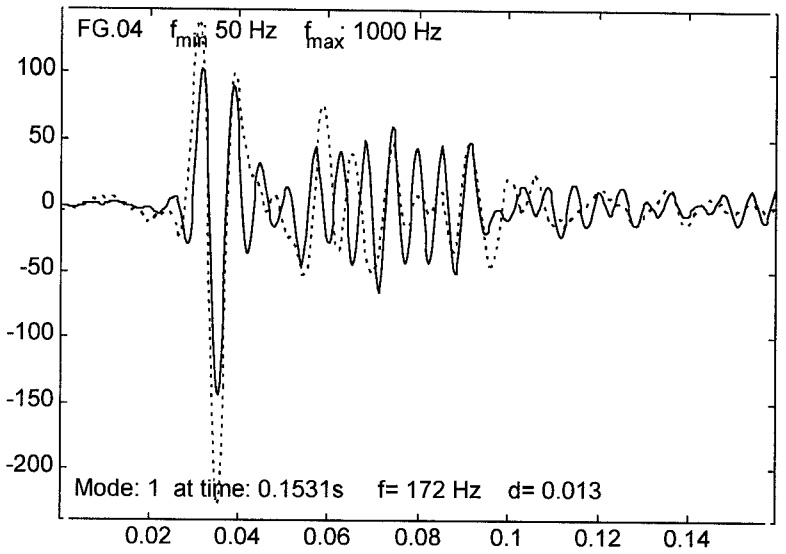

Figure A.19 (a) The system response dominated by mode one.

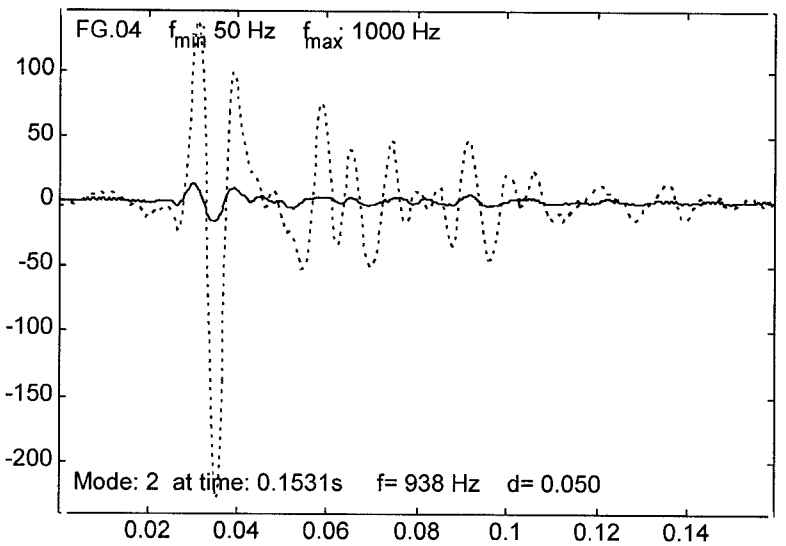

Figure A.19 (b) The system response dominated by mode two.

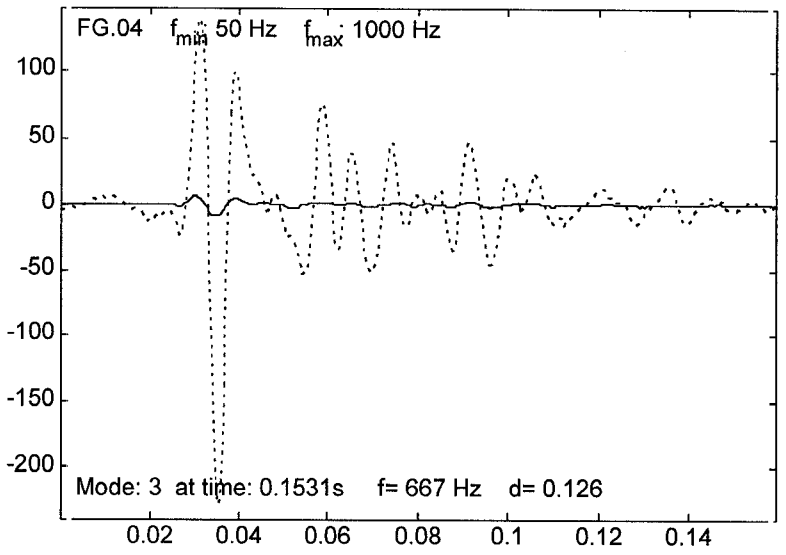

Figure A.19 (c) The system response dominated by mode three.

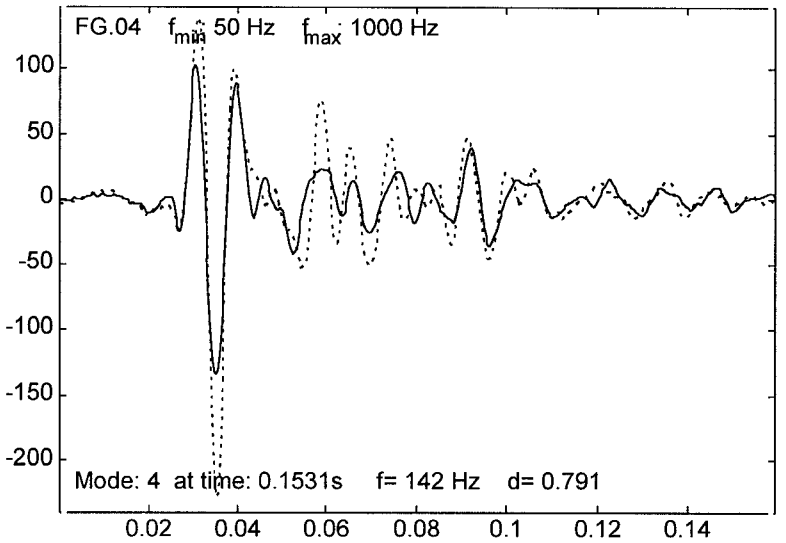

Figure A. 19 (d) The system response dominated by mode four.

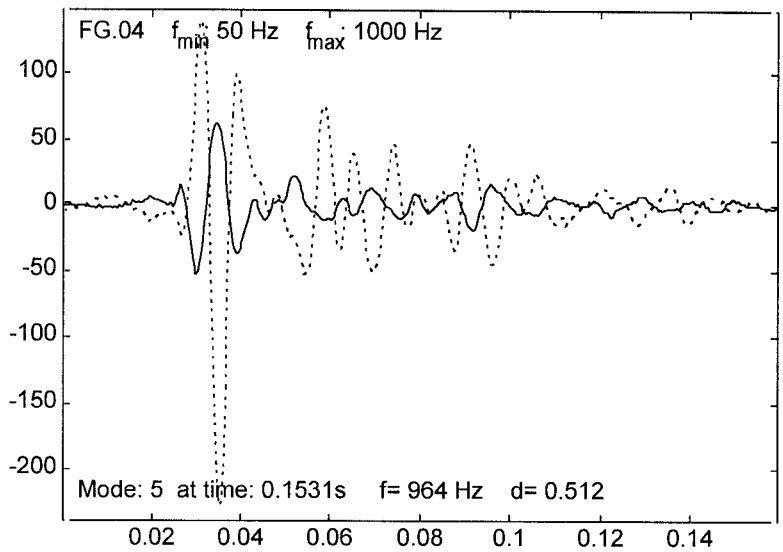

Figure A.19 (e) The system response dominated by mode five.

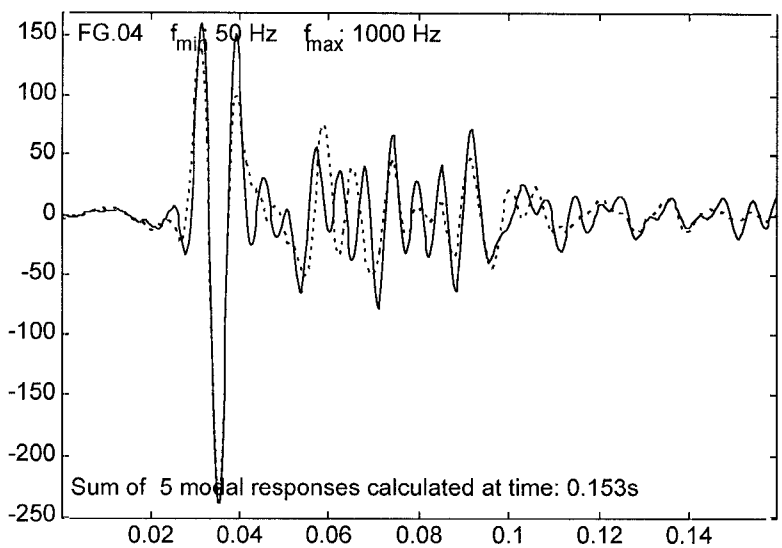

Figure A.20 Sum of five modal responses calculated at time 0,153 s.

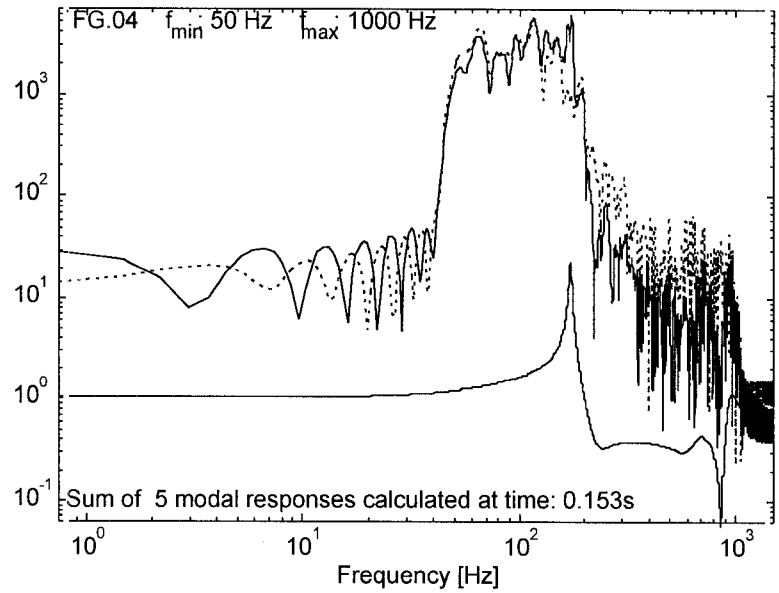

Figure A.21 The spectrum of the seismograms from Figure A.20 and their transfer function.

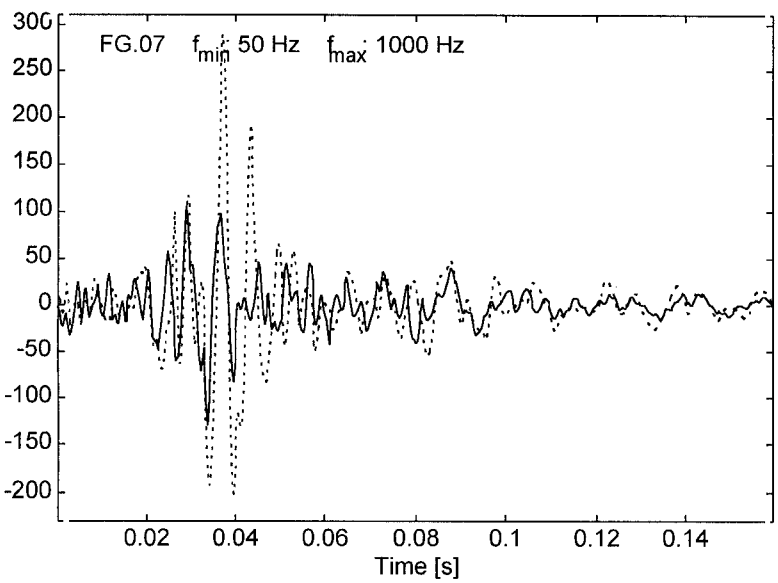

Figure A.22 An example of real seismograms (event FG07), recorded in solid rock - solid line, and in a fractured rock - dashed line.

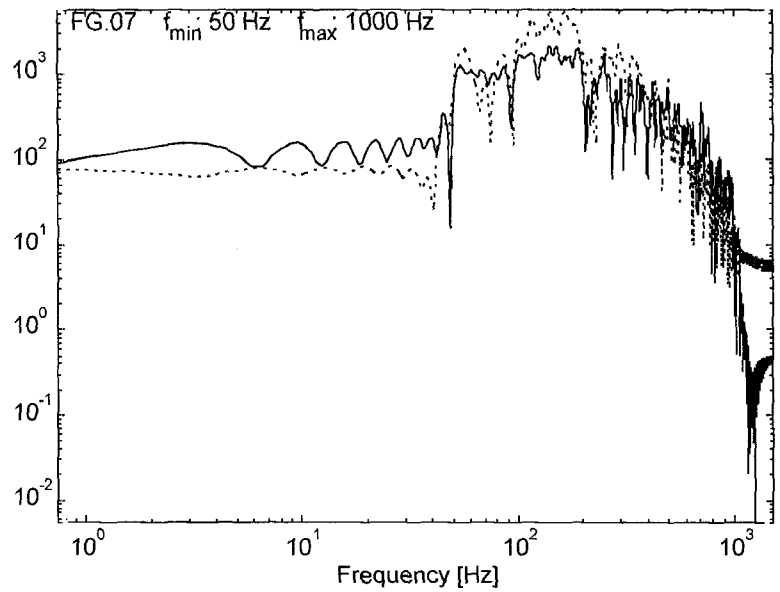

Figure A.23 Velocity spectrum of the seismograms from Figure A.22.

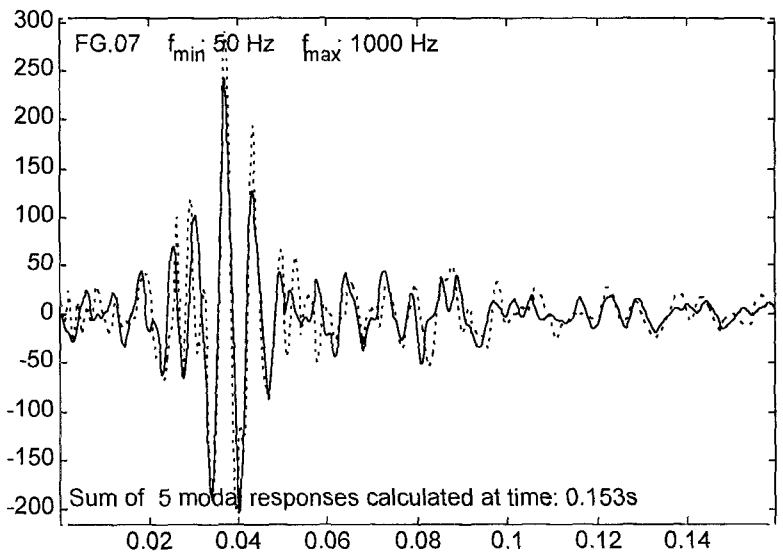

Figure A.24 Sum of five modal responses calculated at time 0.153 s.

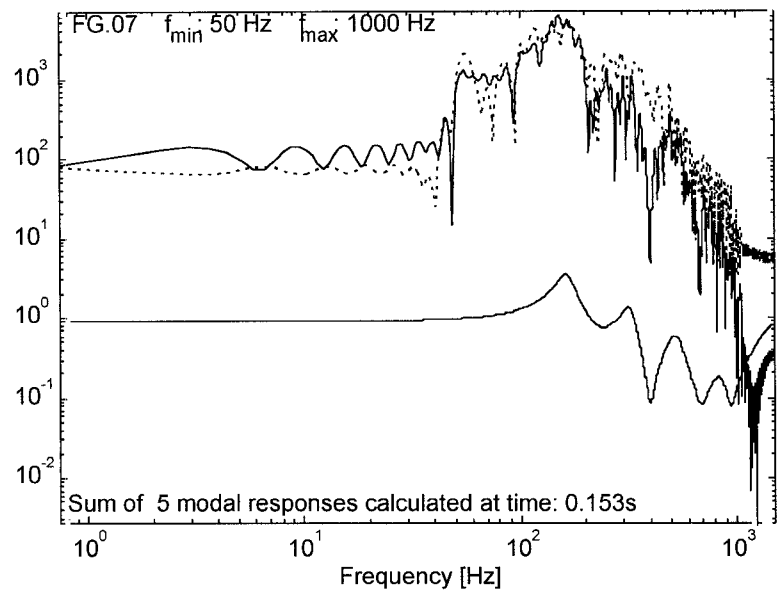

Figure A.25 The spectrum of the seismograms from Figure A.24 and their transfer function.

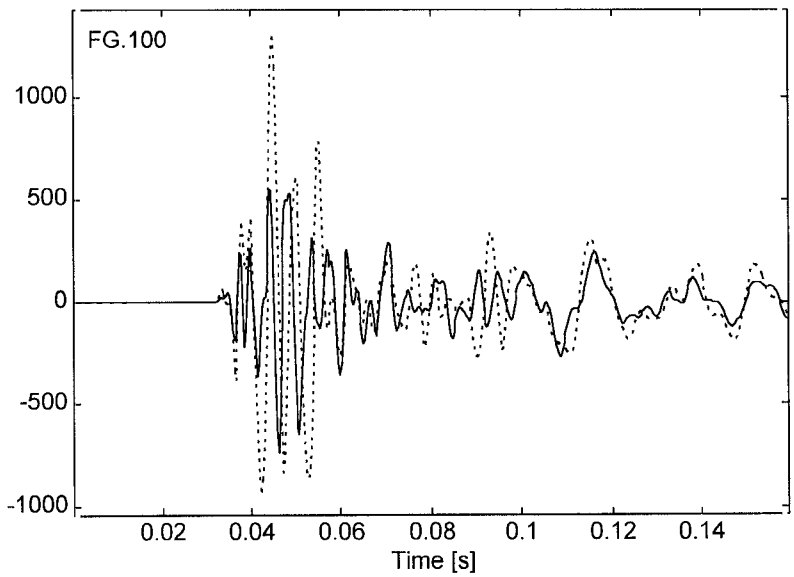

Figure A.26 An example of real seismograms (event FG100), recorded in solid rock - solid line, and in a fractured rock - dashed line.

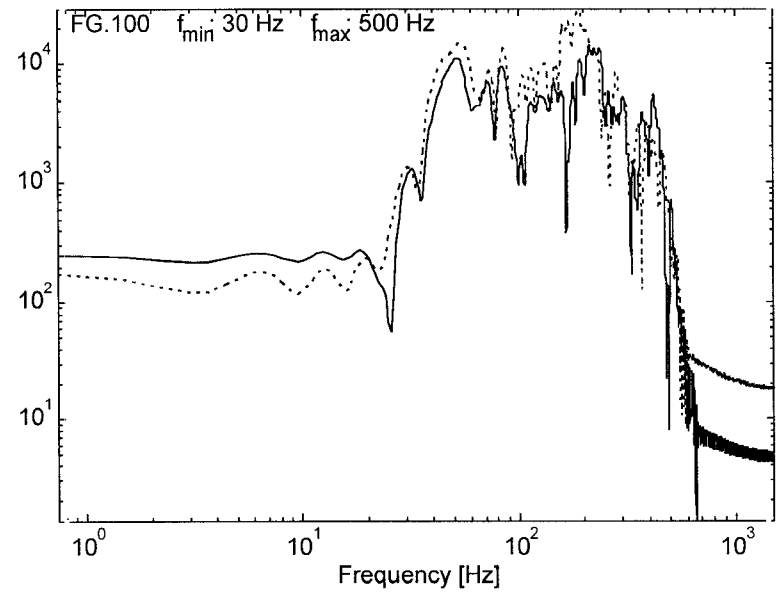

Figure A.27 Velocity spectrum of the seismograms from Figure A.26.

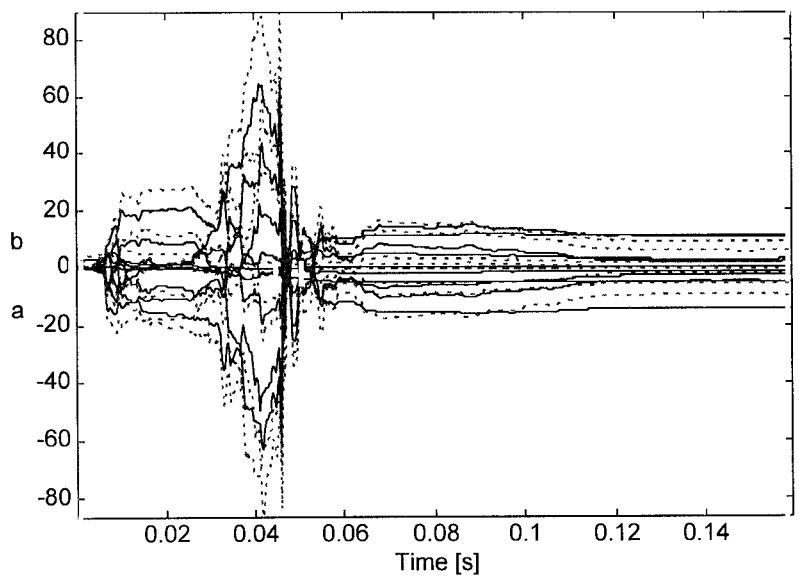

Figure A.28 The coefficients of the polynomials A (q) and B (q) versus time.

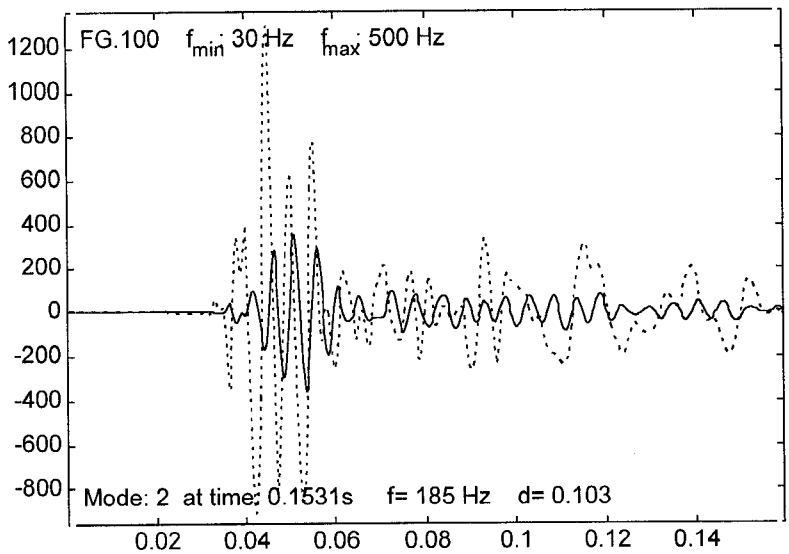

Figure A.29 (a) The system response dominated by mode two.

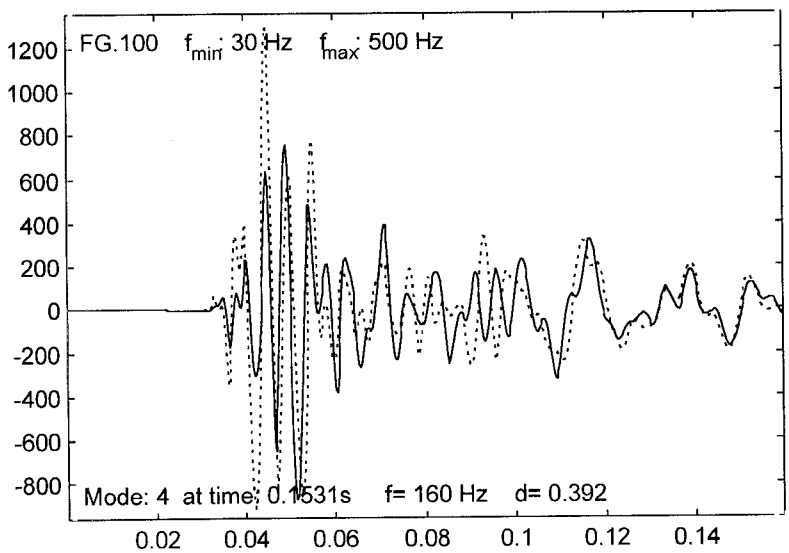

Figure A.29 (b) The system response dominated by mode four.

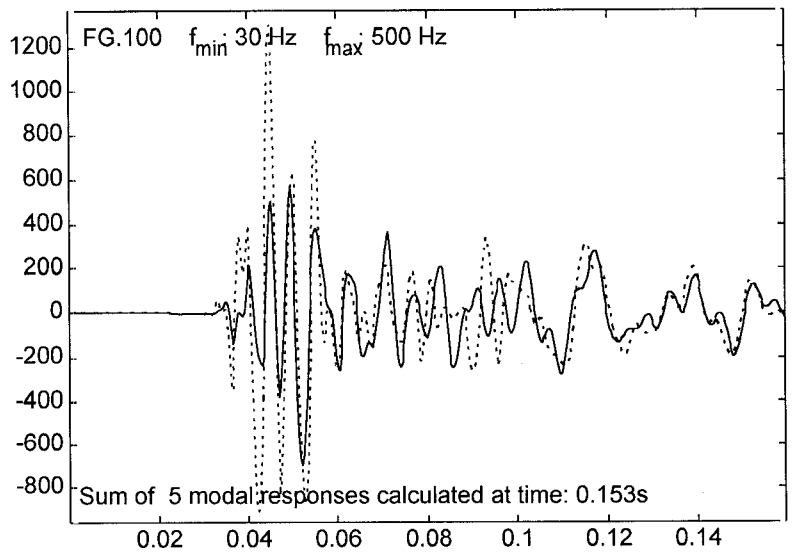

Figure A.30 Sum of five modal responses calculated at time 0.153 s.

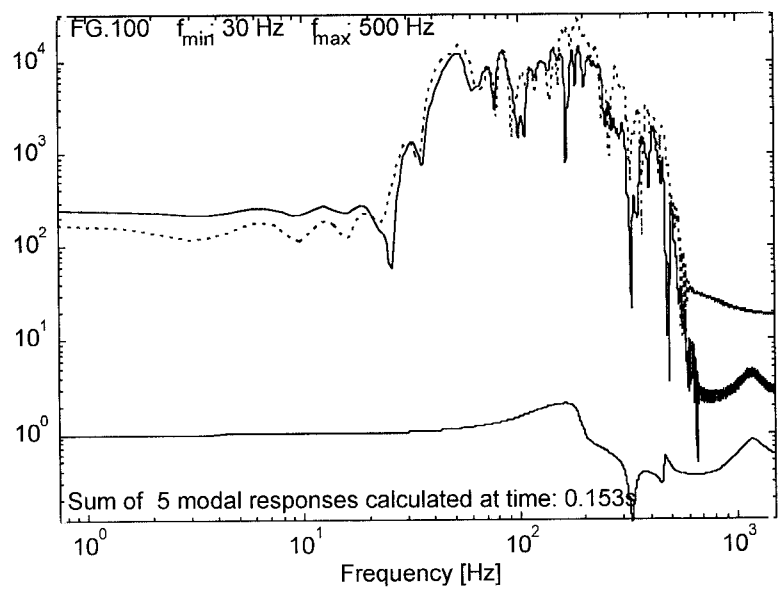

Figure A.31 The spectrum of the seismograms from Figure A.30 and their transfer function.

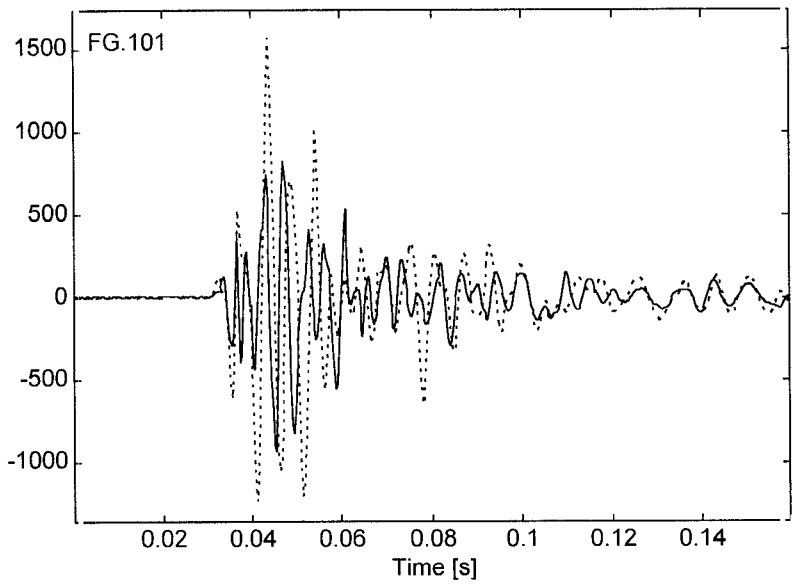

Figure A.32 An example of real seismograms (event FG101), recorded in solid rock - solid line, and in a fractured rock - dashed line.

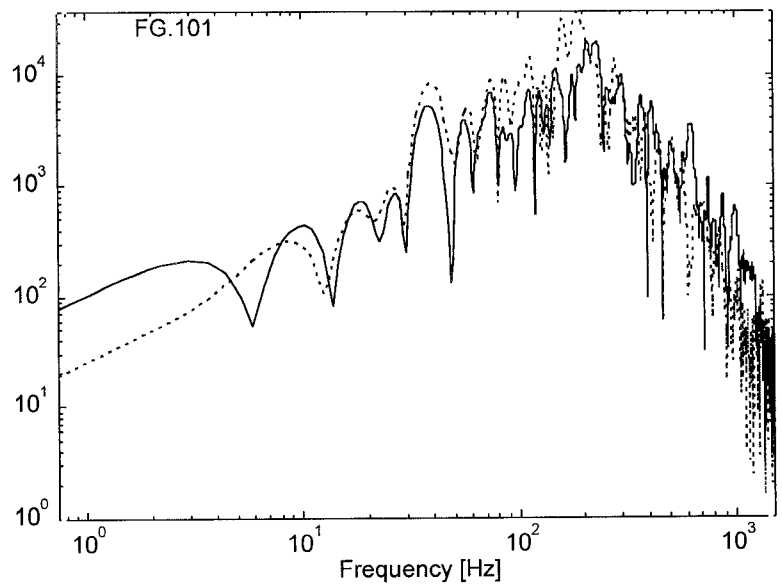

Figure A.33 Velocity spectrum of the seismograms from Figure A.32.

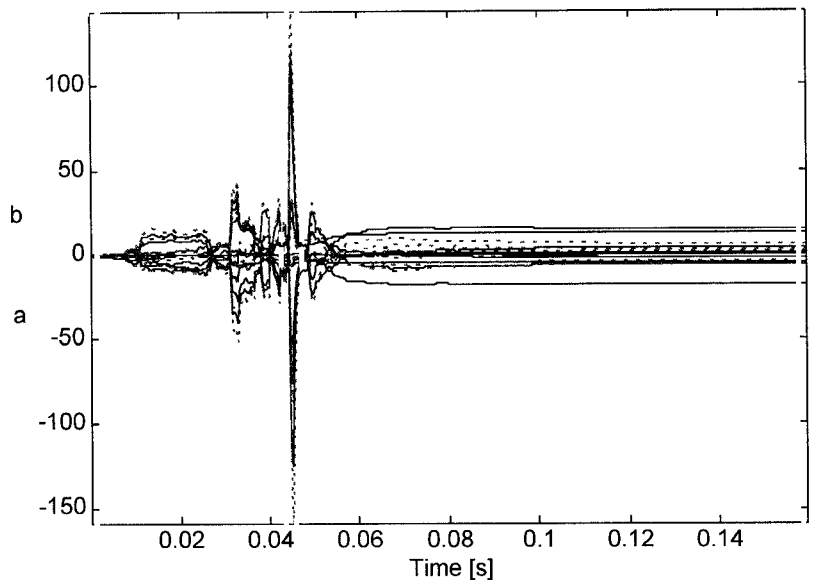

Figure A.34 The coefficients of the polynomials A (q) and B (q) versus time.

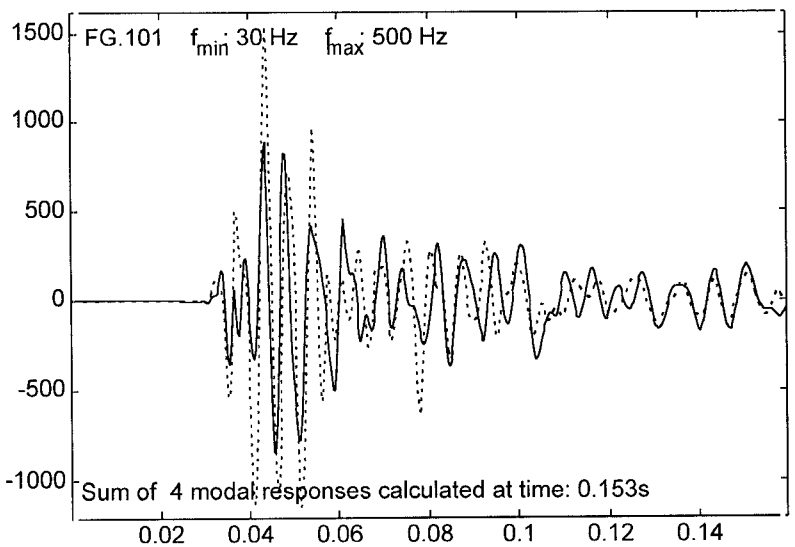

Figure A.35 The sum of four modal responses calculated at time 0,153 s.

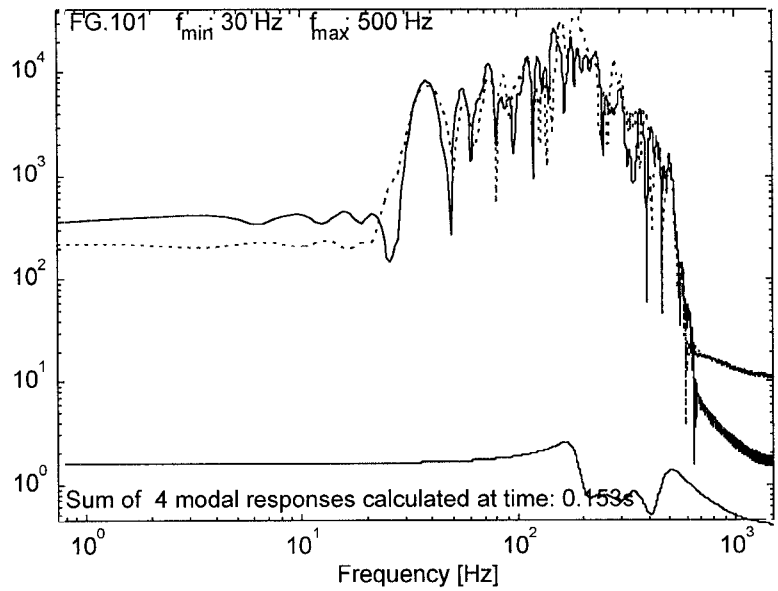

Figure A.36 The spectrum of the seismograms from Figure A.35 and their transfer function.

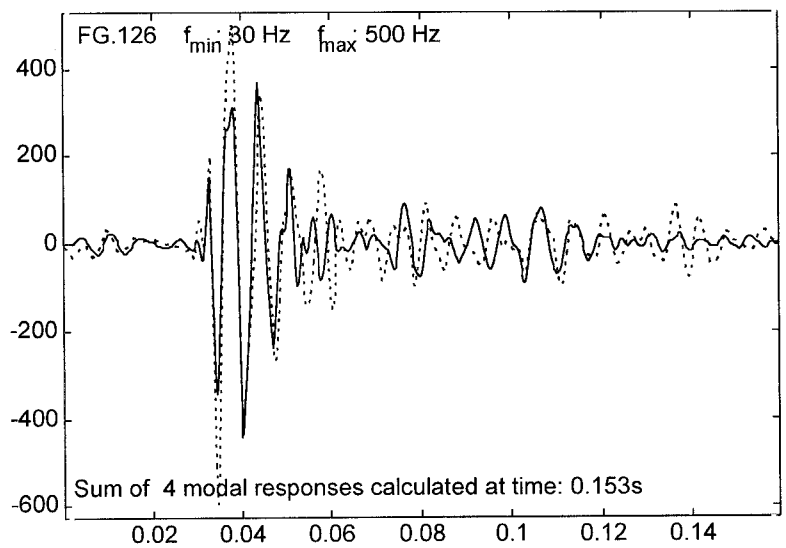

Figure A.37 The sum of four modal responses calculated at time 0,153 s.

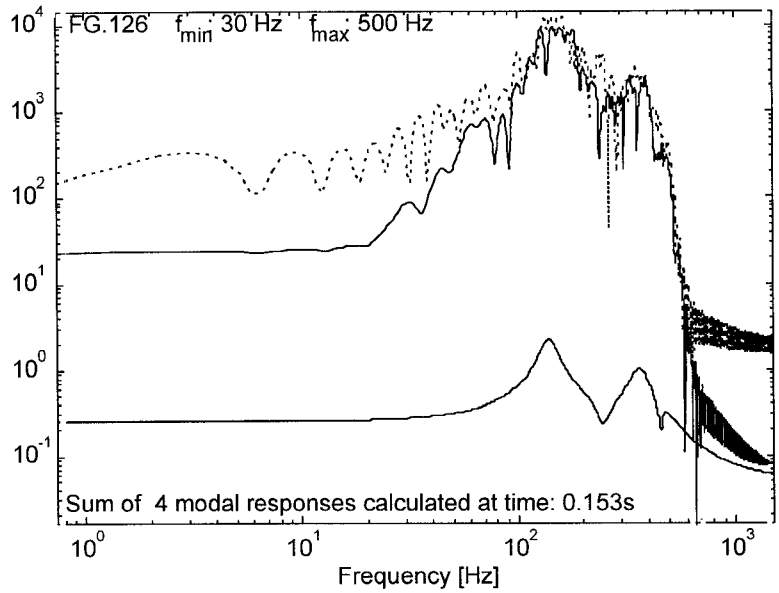

Figure A.38 The spectrum of the seismograms from Figure A.37 and their transfer function.

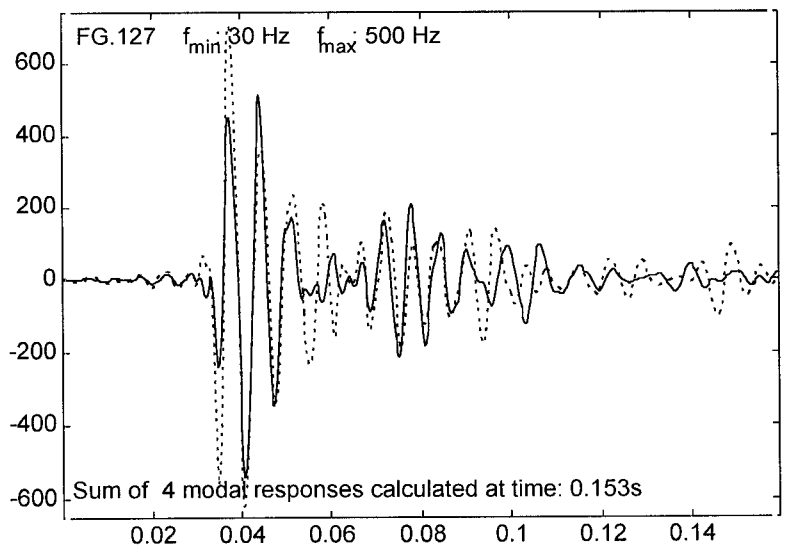

Figure A.39 The sum of four modal responses calculated at time 0,153 s.

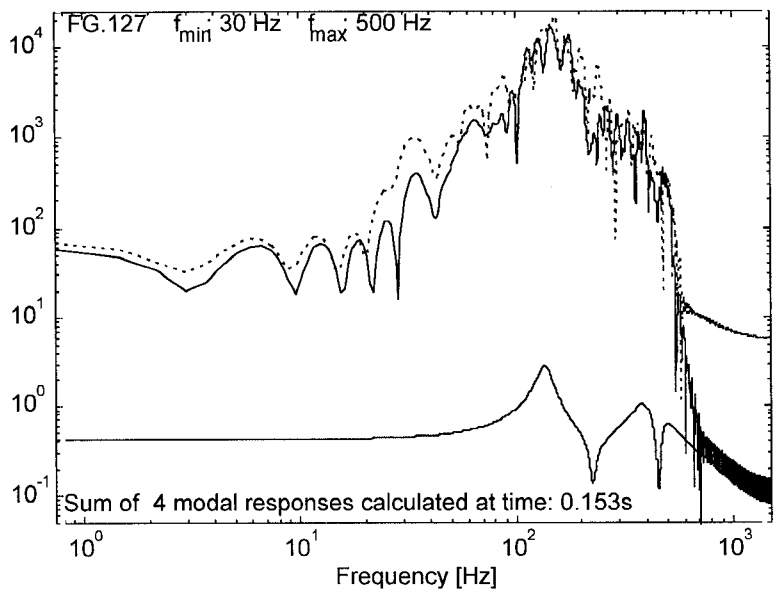

Figure A.40 The spectrum of the seismograms from Figure A.39 and their transfer function.

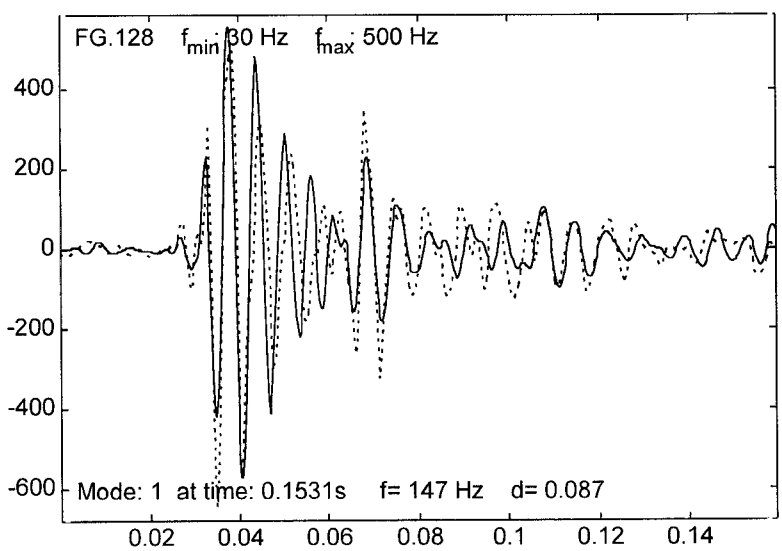

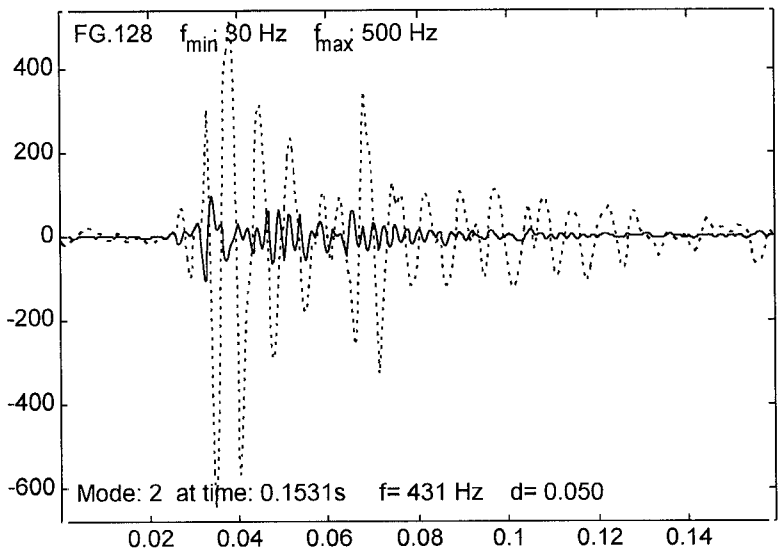

Figure A.41 (b) The system response dominated by mode two.

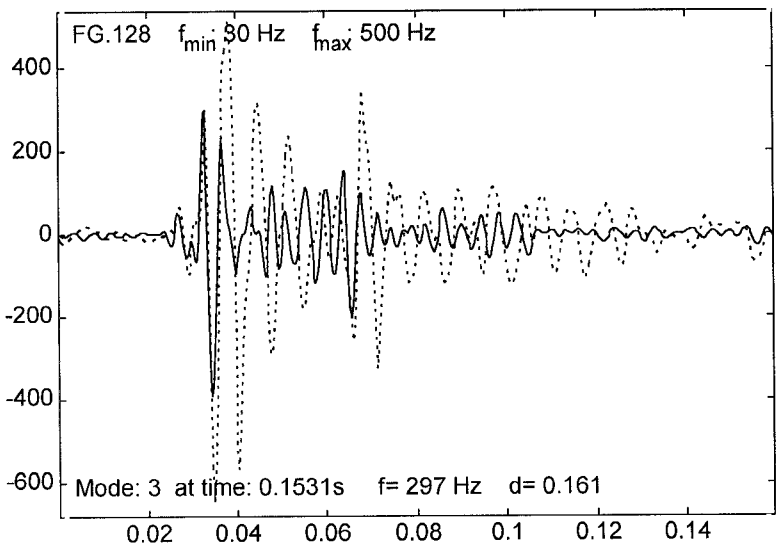

Figure A.41 (c) The system response dominated by mode three.

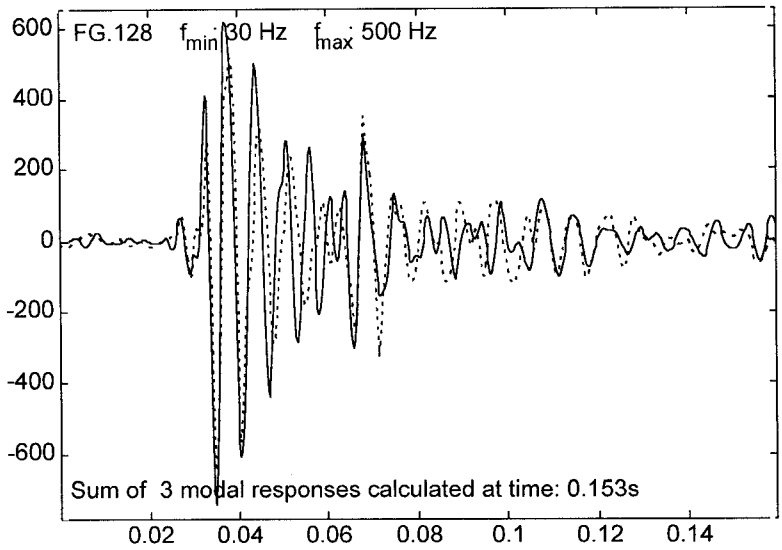

Figure A.42 The sum of three modal responses calculated at time 0,153 s.

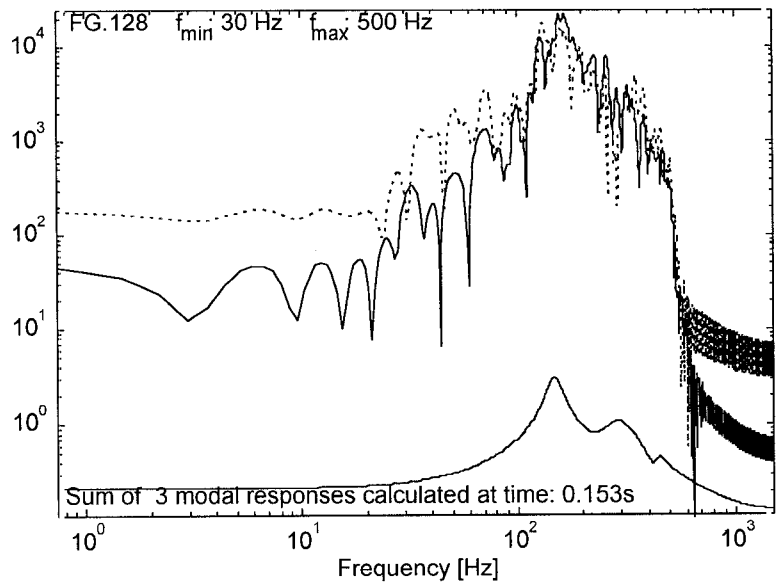

Figure A.43 The spectrum of the seismograms from Figure A.32 and their transfer function.

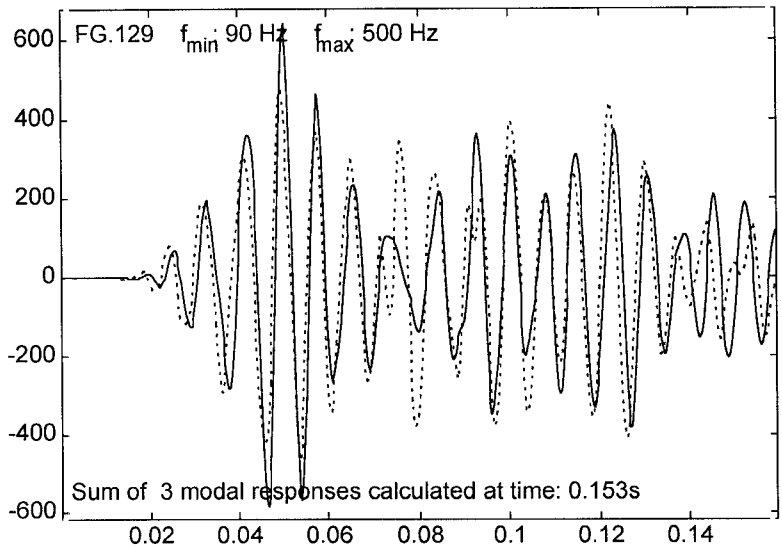

Figure A.44 The sum of three modal responses calculated at time 0,153 s.

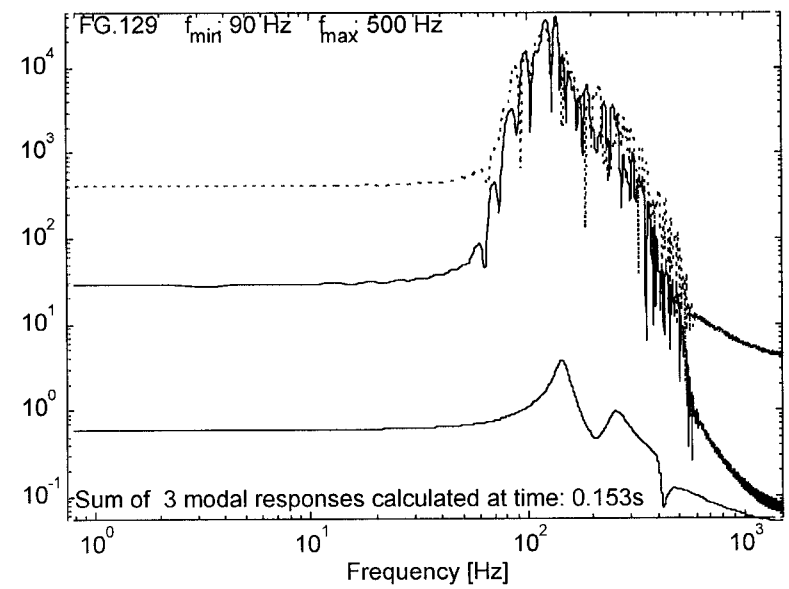

Figure A.45 The spectrum of the seismograms from Figure A.44 and their transfer function.

The transfer function was well modelled in several cases, as the modal response matches the real response of the system (see seismograms: FG02 (Figure A.15), FG04 (Figure A.20), FG07 (Figure A.24), FG128 (Figure A.42) and FG129 (Figure A.44)). In several cases there was a problem with modelling of initial pulse using the transfer function obtained at the end of ground motion (see seismograms: FG126 (Figure A.37) and FG127 (Figure A.39)), as before, the non-linear effect can be an explanation.

Some examples are more difficult. The inversion process can only reproduce the main feature of real ground motion waveform (see seismogram FG100 (Figure A.30) and FG101 (Figure A.35)).

The transfer functions in all examples are very similar (see Figure A.16, A.21, A.25, A.31, A.36, A.38, A.40, A.43 and A.45). The dominant frequency is around 150 +/-20 Hz, the second peak in transfer functions is between 200-300Hz (see Table A.2 and Table A.3).

Table A.2 shows data recorded in May 1997 and Table A.3 shows data collected in June 1997. There is an evident decrease of the first and second modal frequencies in Table A.3 compared to Table A.2. This observation is extremely important and can be used as a tool to monitor the changes in site conditions. The number of seismic events processed in Table A.2 and A.3 is too small to make a convincing statement, however, it can be used as an indication of a trend. In future research, the same type of seismic source should be used to study the changes in site effect.

Table A.2

The data recorded in May 1997.

May 1997; Modal Frequencies [Hz] and Damping Ratios							
No:FG02 50- 1000Hz	FG03 30- 1000Hz	FG04 50- 1000Hz	FG05 50- 1000Hz	FG06 50- 1000Hz	FG07 50- 1000Hz	FG08 50- 1000Hz	FG09 50- 1000Hz
	59 0,072						
103 0,229		142 0,791				130 0,183	
176 0,115		172 0,013	152 0,066	155 0,055	163 0,098		153 0,126
			289 0,242				
			358 0,140	317 0,304	321 0,076		355 0,154
583 0,056	477 0,399		592 0,082	536 0,324	519 0,097	480 0,150	507 0,120
794 0,034	722 0,114	964 0,512			858 0,111	844 0,192	875 0,044

Table A.3

The data recorded in June 1997.

June 1997; Modal Frequencies [Hz] and Damping Ratios						
No:FG100 30-500Hz	FG101 30-500Hz	FG102 30-500Hz	FG126 30-500Hz	FG127 30-500Hz	FG128 30-500Hz	FG129 90-500Hz
160 0,392			138 0,089	136 0,081	147 0,087	145 0,070
185 0,103	181 0,116	172 0,040				
	257 0,482	281 0,072	241 0,148	223 0,082	297 0,161	253 0,011
			365 0,101	393 0,127		
				468 0,072	431 0,050	404 0,051

4.5 Experiment 3 (Vaal Reefs No.5 Shaft)

Two geophones were used in this experiment: one was installed on the footwall and the second in the hangingwall (The hangingwall geophone is the geophone from Experiment 2). Table A.4 shows modal frequencies for five pairs of seismograms.

Table A.4

Modal frequencies for five pairs of seismograms.

Modal frequencies: [Hz]				
FG02	FG03	FG04	FG05	FG100
	48			
80				
		111		
155	153	132	154	154
		165	189	264
			305	
			363	381

The common feature is the presence of modal frequency around 150 Hz. Figures A.46 throughout A.63 shows some results of calculations of transfer function.

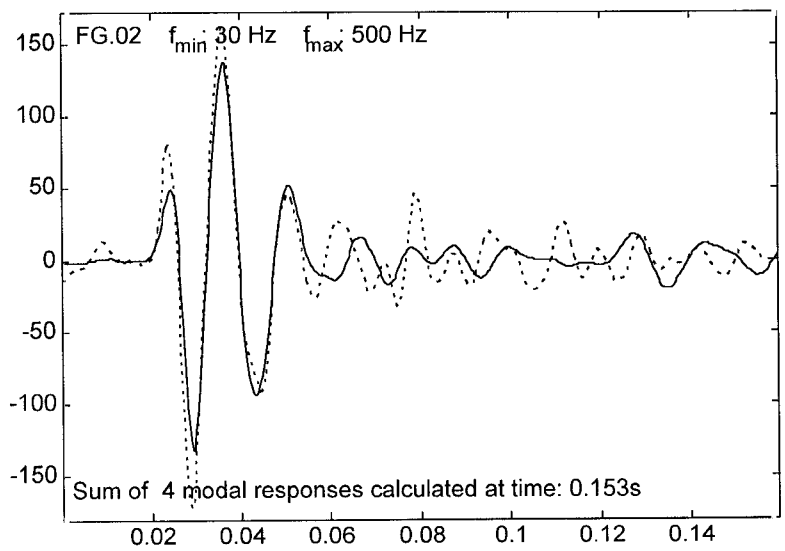

Figure A.46 The sum of four modal responses calculated at time 0,153 s.

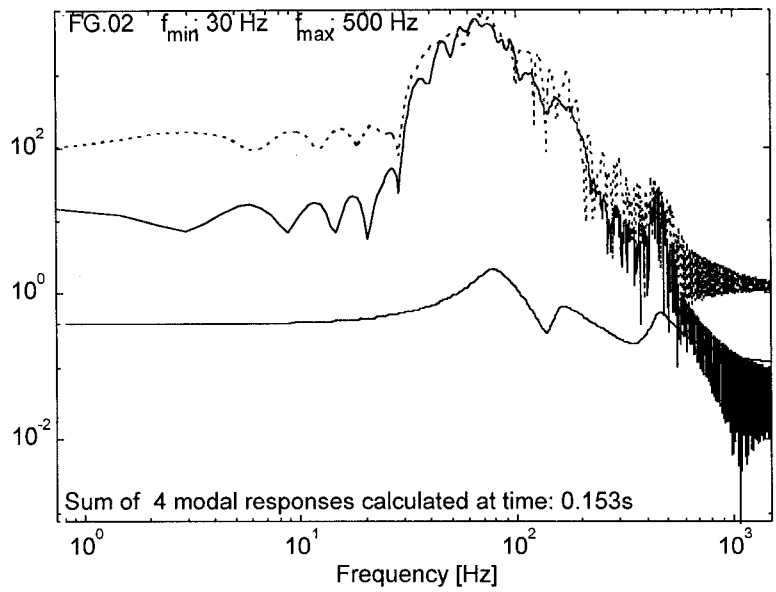

Figure A.47 The spectrum of the seismograms from Figure A.46 and their transfer function.

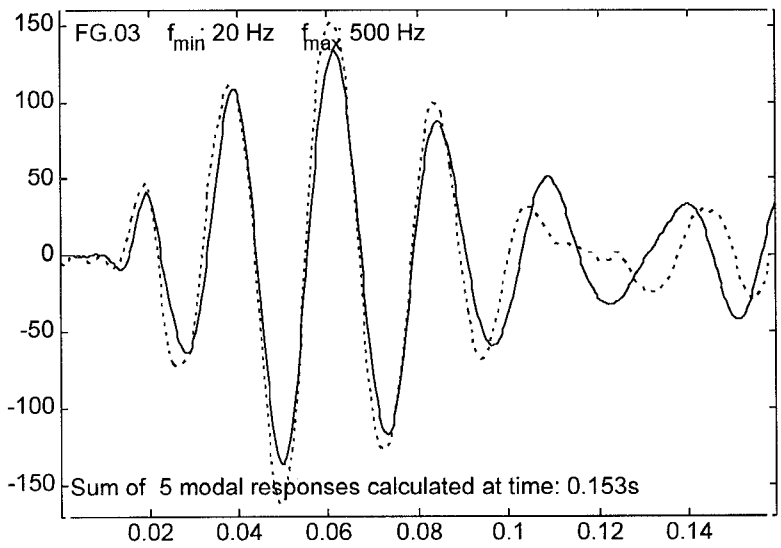

Figure A.48 Sum of five modal responses calculated at time 0,153 s.

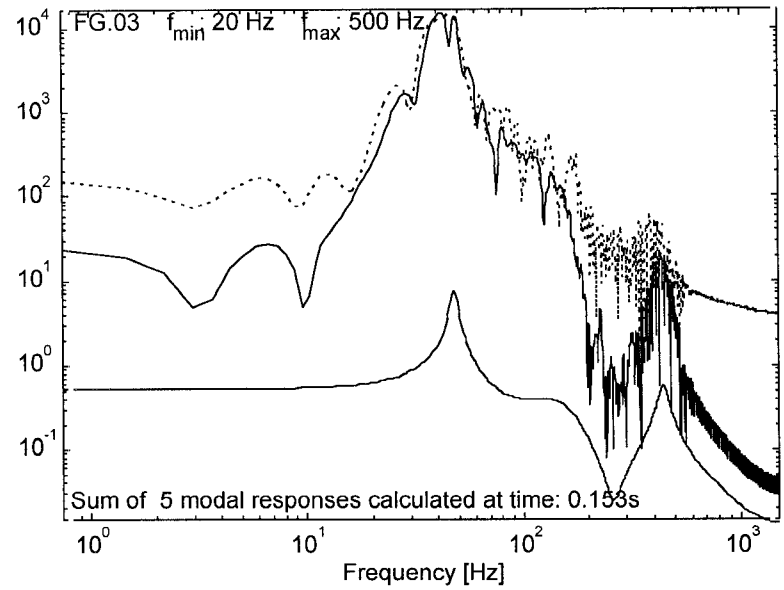

Figure A.49 The spectrum of the seismograms from Figure A.48 and their transfer function.

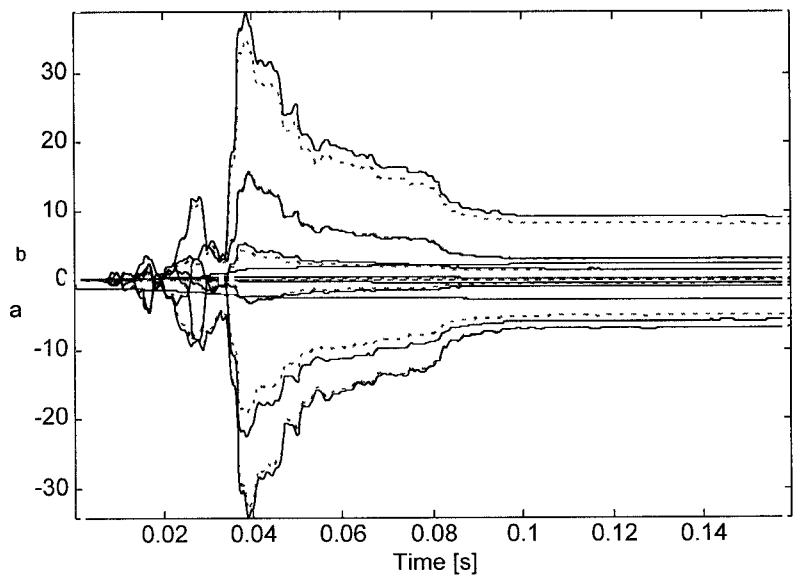

Figure A.50 The coefficients of the polynomials A (q) and B (q) versus time.

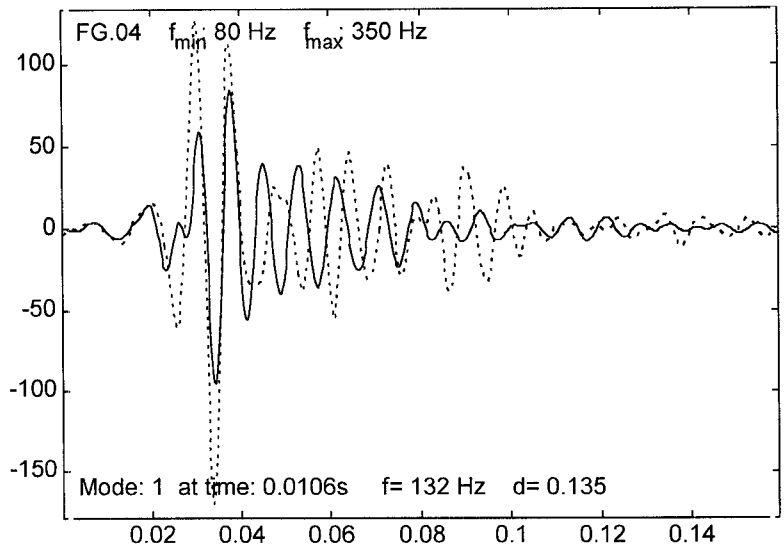

Figure A.51 (a) The system response dominated by mode one.

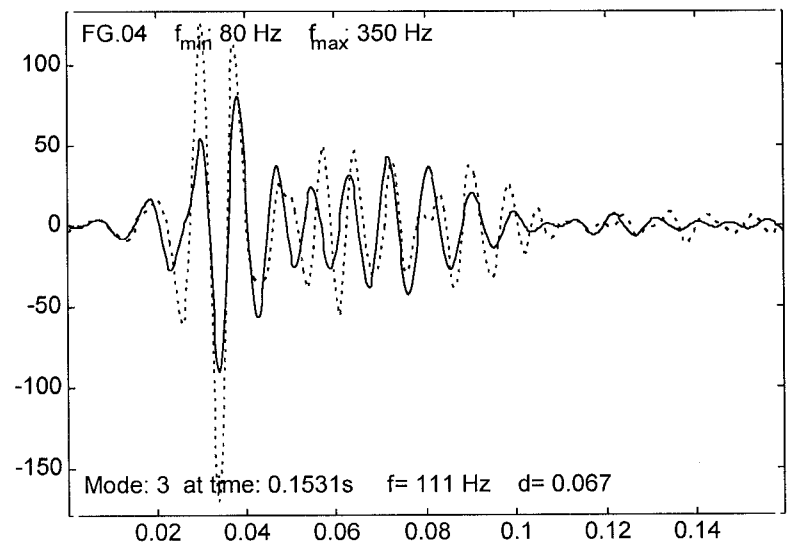

Figure A.51 (b) The system response dominated by mode three.

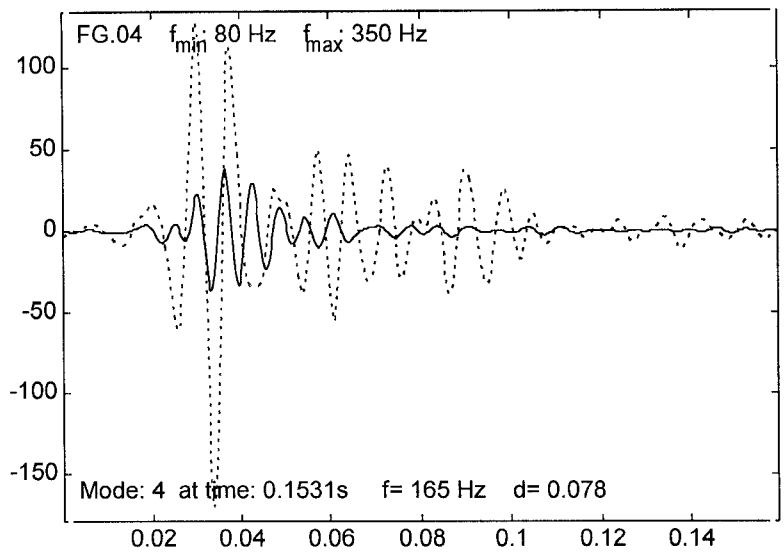

Figure A.51 (c) The system response dominated by mode four.

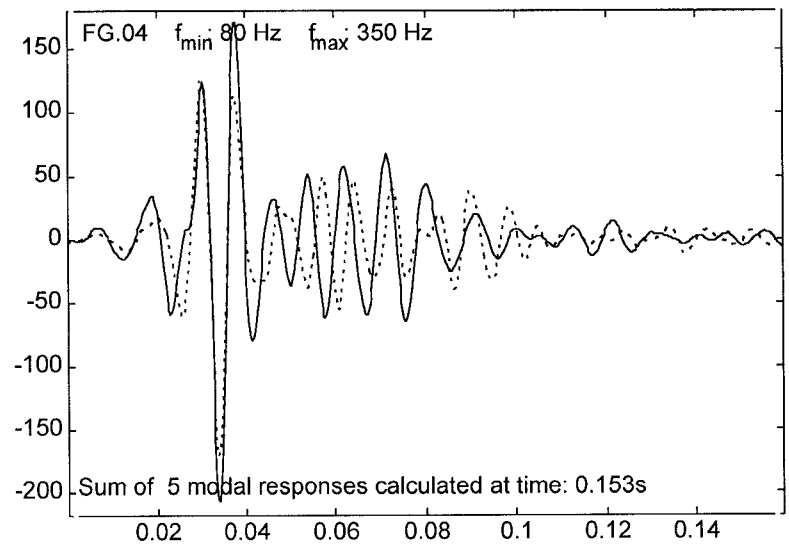

Figure A.52 Sum of five modal responses calculated at time 0,153 s.

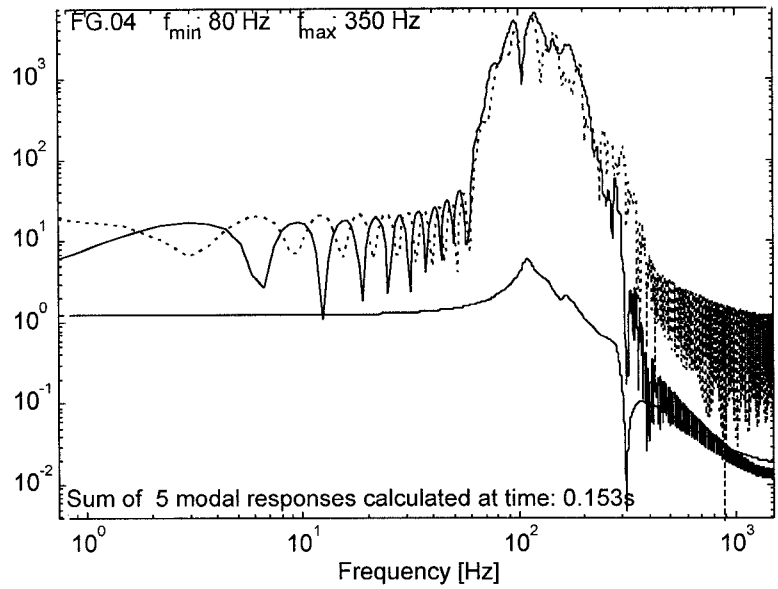

Figure A.53 The spectrum of the seismograms from Figure A.52 and their transfer function.

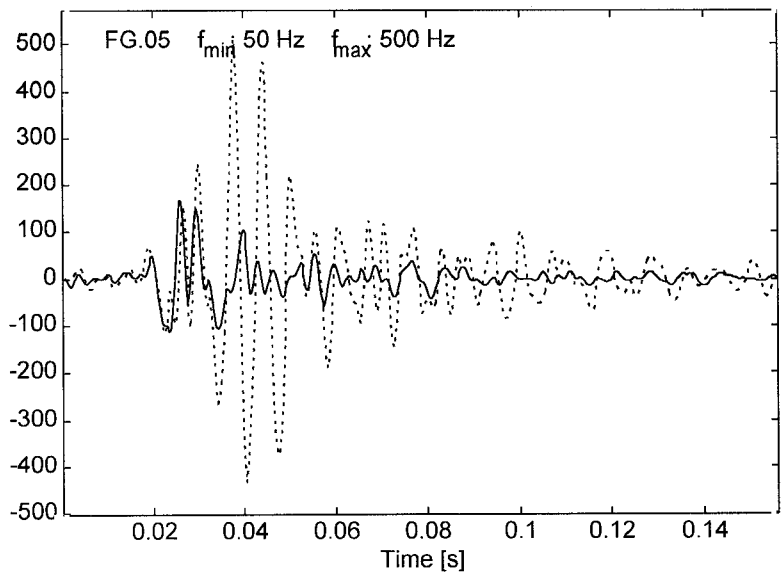

Figure A.54 An example of real seismograms (event FG05), recorded in solid rock - solid line, and in a fractured rock - dashed line.

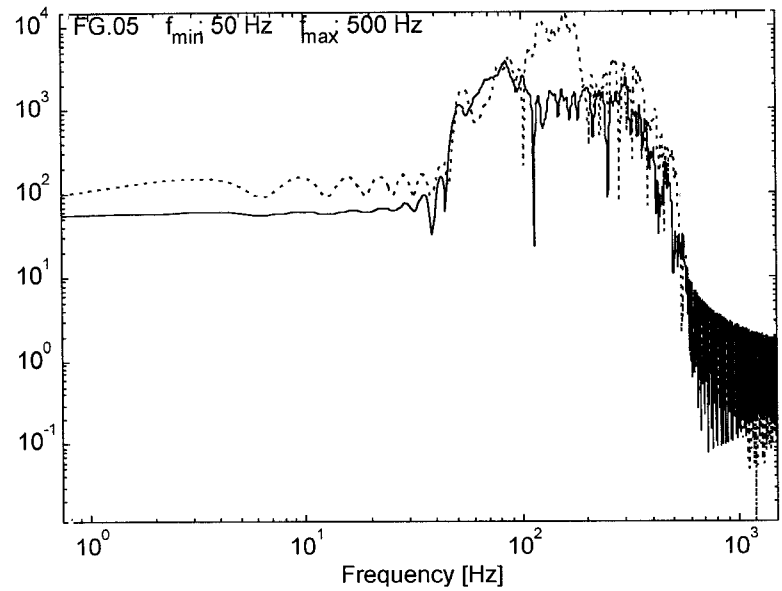

Figure A.55 Velocity spectrum of the seismograms from Figure A.54.

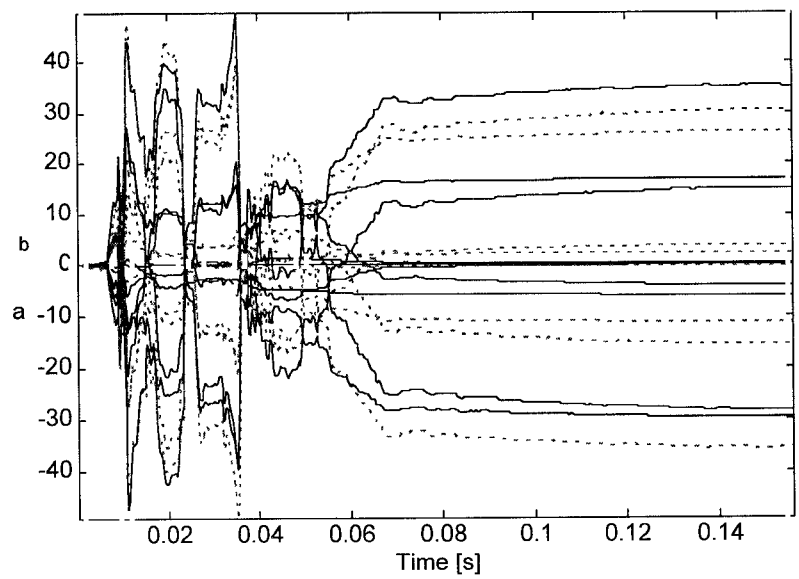

Figure A.56 The coefficients of the polynomials A (q) and B (q) versus time.

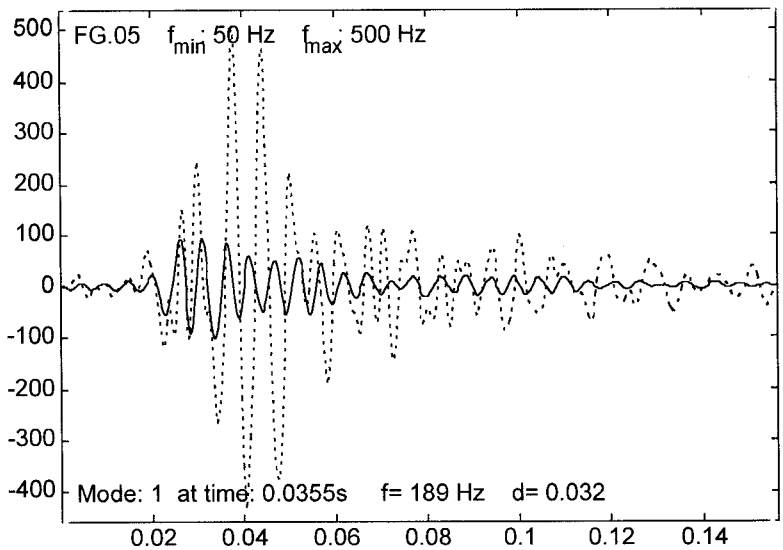

Figure A.57 (a) The system response dominated by mode one.

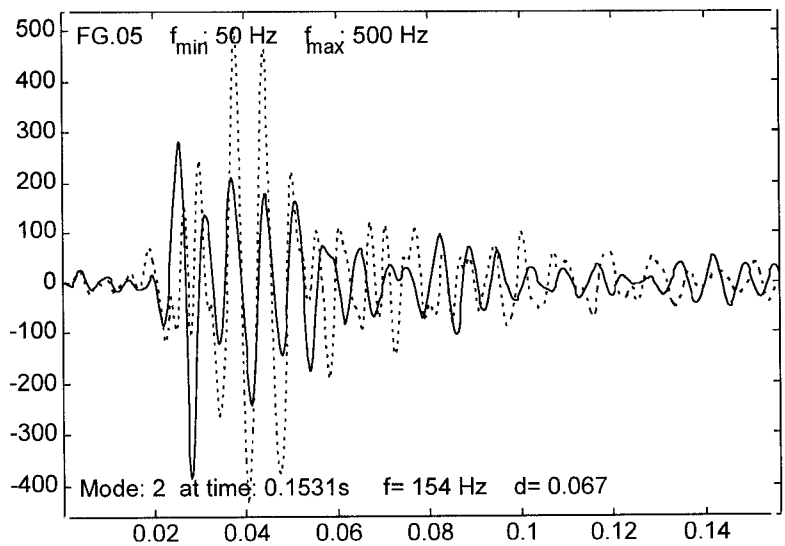

Figure A.57 (b) The system response dominated by mode two.

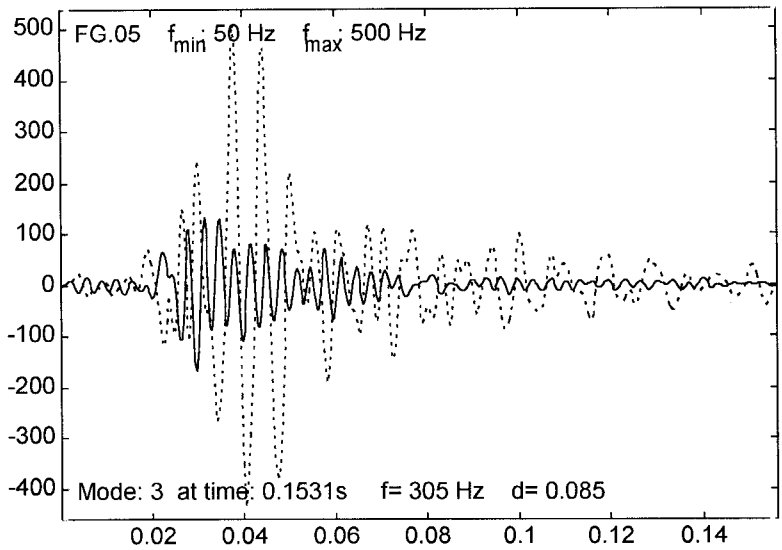

Figure A.57 (c) The system response dominated by mode three.

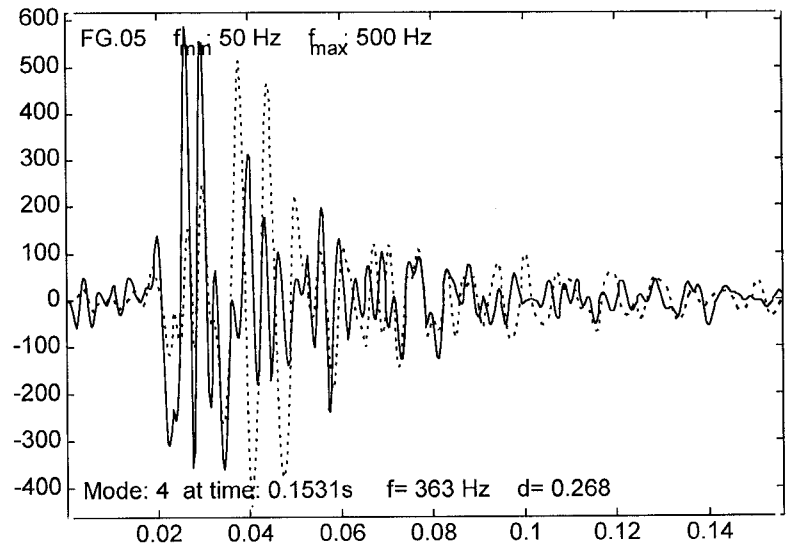

Figure A.57 (d) The system response dominated by mode four.

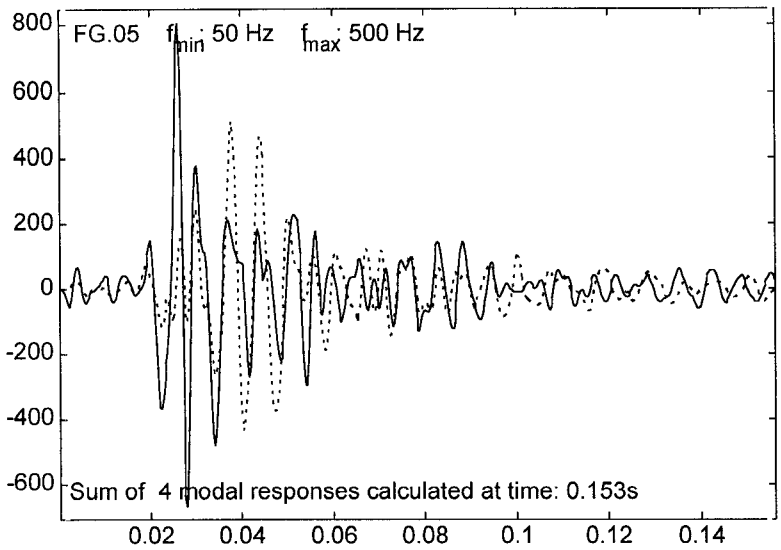

Figure A.58 Sum of four modal responses calculated at time 0,153 s.

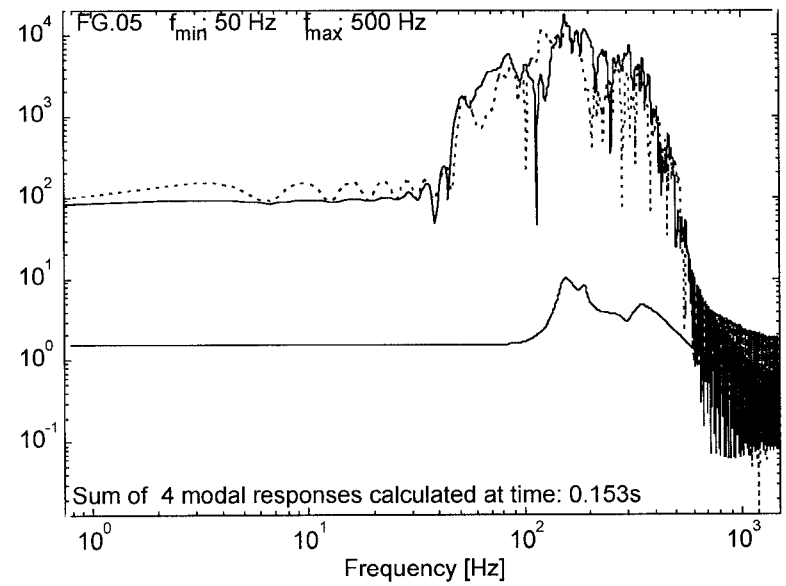

Figure A.59 The spectrum of the seismograms from Figure A.58 and their transfer function.

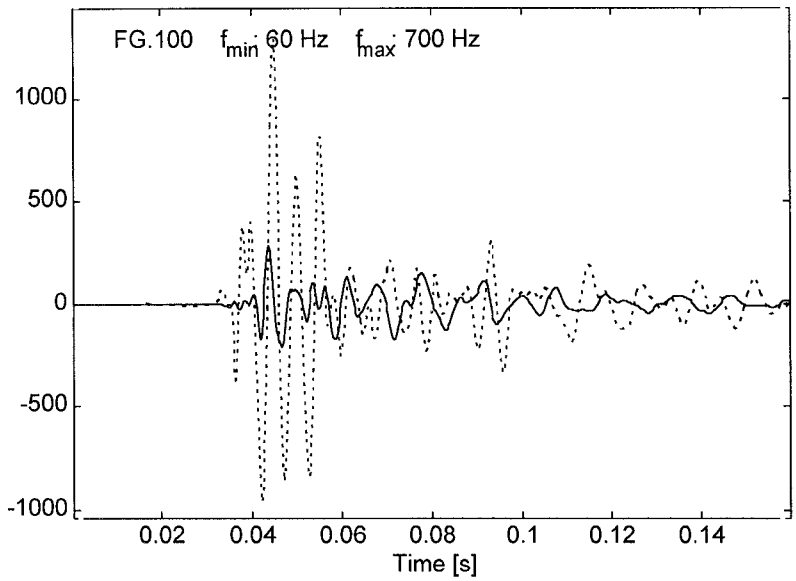

Figure A.60 An example of real seismograms (event FG100), recorded in solid rock - solid line, and in a fractured rock - dashed line.

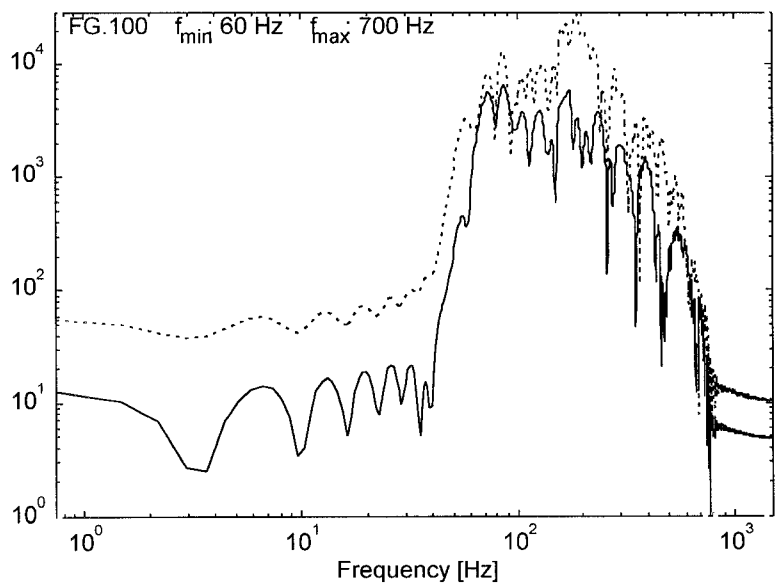

Figure A.61 Velocity spectrum of the seismograms from Figure A.60.

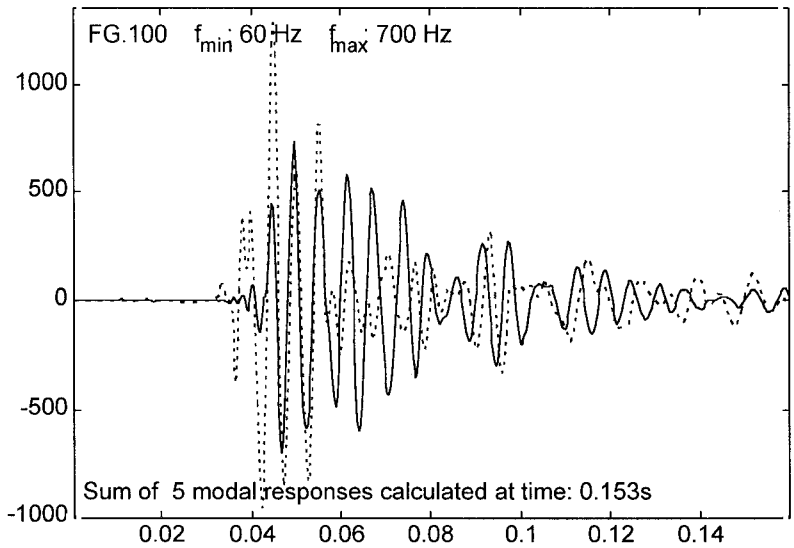

Figure A.62 Sum of five modal responses calculated at time 0,153 s.

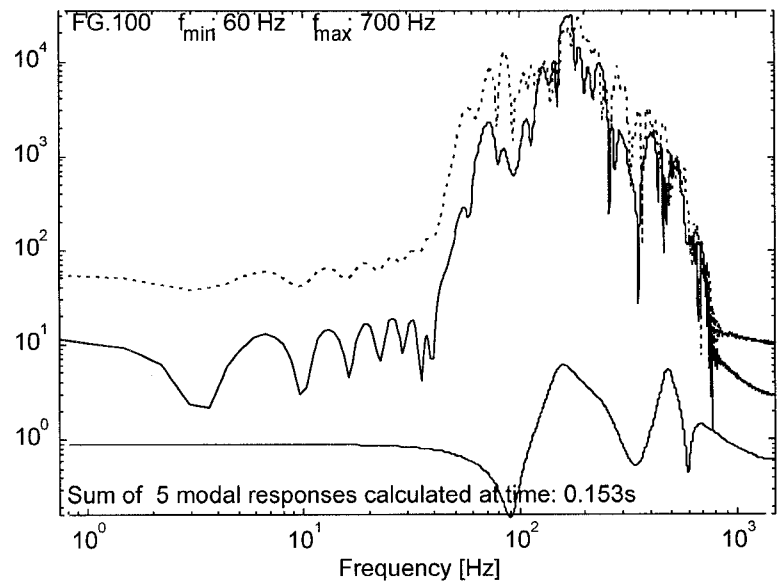

Figure A.63 The spectrum of the seismograms from Figure A.62 and their transfer function.

The calculated and real response match perfectly (see Figure A.52, A.58 and A.62). It is only in a few cases that the calculated response overlaps with real ground motion (see Figure A.48). The dominant peak in transfer function relates to the lowest modal frequency (see Table A.4) The position of this peak changes significantly from model to model of transfer function. At this stage of understanding, transfer function in Experiment 3 cannot be modelled using series of damped oscillators.

5 CONCLUSIONS

Experiment 1

The models of transfer function are reliable, as all models are similar.

The first pulse of the seismogram has a different transfer function from the rest of record. This could be an indication that the initial behaviour of the site is non-linear.

Experiment 2

The influence of support on vibration in the hangingwall is measurable. The algorithm presented in this report estimated different vibrations in the different sites in the hangingwall. The obtained model of transfer function is reasonable.

There is strong indication that properties of the sites change with time (weeks).

Experiment 3

The difference between ground motion in the footwall and ground motion in the hangingwall cannot be properly modelled with modal transfer function.

APPENDIX B

Rockburst case studies

1 Leeudoorn, 10/1/94, M_L=2,6 and M_L=1,9

1.1 Introduction

At 12h15 on 10 January 1994 a rockburst occurred at Leeudoorn Gold Mine, damaging the 24-74 stope at a depth of about 1840 m below surface and fatally injuring 11 people. Two seismic events with local magnitudes M_L = 2,6 and 1,9 occurred within a 30 s interval at this time. A team was formed to investigate the rock engineering aspects of the incident at the request of Gold Fields of South Africa and Mr D Bakker of the Department of Minerals and Energy (DME). The mandate of the team was to conduct a thorough scientific investigation into the cause of the rockburst, with the objective of preventing future occurrences.

1.2 Mining environment

The Ventersdorp Contact Reef (VCR) in the area of the 24-74 stope is underlain by quartzites of the Turffontein Subgroup and overlain by lava of the Alberton Porphyry Formation (known as hard lava). This is currently the most common association of hangingwall and footwall rocks in VCR mining. The strata that unconformably underlies the VCR at Leeudoorn Gold Mine dips towards the south-east (Figures B.1 (a) and B.1 (b)). A shear plane is developed at the contact between the quartzite and the underlying Booysens Shale Formation. The shear plane is situated about 80 m beneath the accident site. Whether or not this interface represents a seismically active zone needs to be assessed through more accurate analysis of the foci of seismic events.

Faults and dykes are prominent over the Leeudoorn lease area. However, no major faults or dykes are recorded in close proximity to the rockburst site.

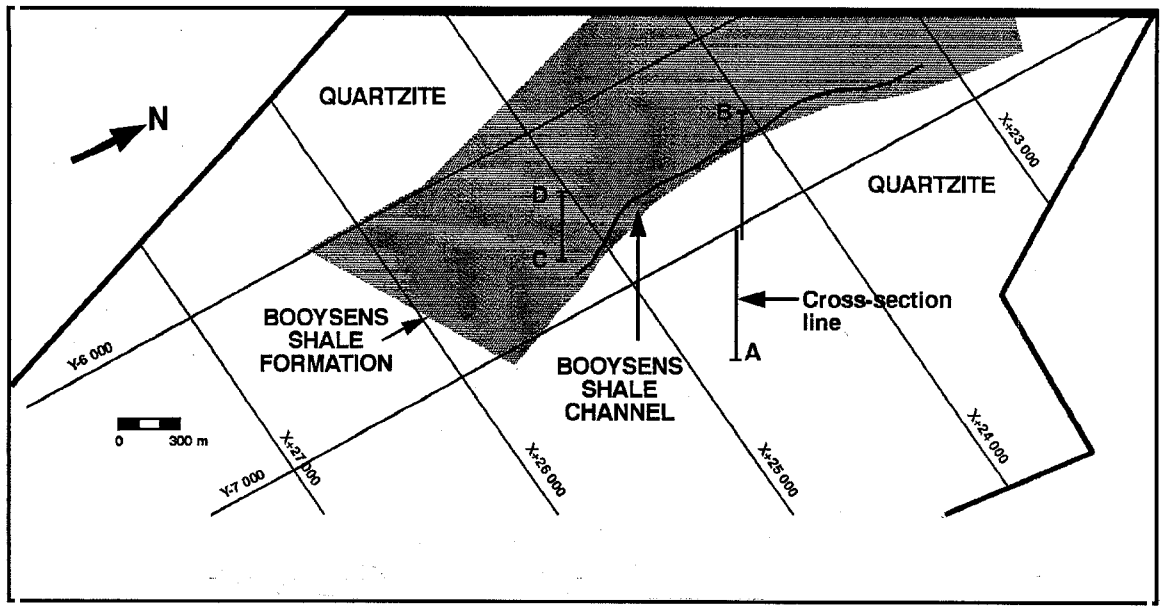

Figure B.1(a) Map of Leeudoorn Gold Mine showing the sub-outcrop of the Booysens Shale Formations and the locations of the cross-sections used to construct the composite cross-section shown in Figure B.1 (b).

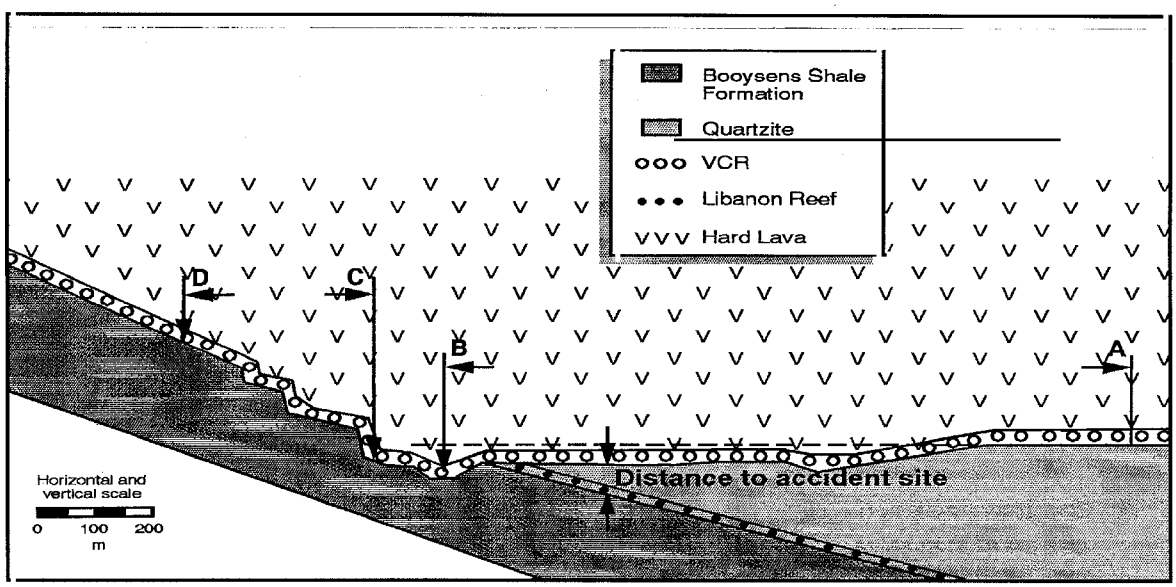

Figure B.1 (b) Composite geological cross-section of Leeudoorn Gold Mine. The VCR stope in which the accident occurred is situated about 80 m above the quartzite/shale contact.

1.3 Observations at the rockburst site

The site of the rockburst was visited by the team and mine management on 14 January 1994, a day after the inspection by officials of the DME. The accident site was undisturbed after the rockburst, apart from the necessary rescue work. Figure B.2 is a location plan showing the site of the rockburst and Figure B.3 is a stope plan of the affected panels.

As the lower strike gully was traversed (A-B-D in Figure B.3), it became apparent, from damage to the packs that, convergence because of the rockburst increased. At A the stope closure was 0,2 m, while at B the convergence had increased to 0,5-0,8 m, mainly by footwall punching.

The strike gully dipped steeply upwards from B to D indicating that the reef rolled steeply upward along this section. C marks the approximate site of six of the eleven fatalities. At C it was possible to examine a mat pack consisting of 13 layers of 100 mm rise timber. As this pack was installed close to the face just prior to the rockburst, it would have been subjected to very little stope closure prior to the rockburst. By counting the rises and measuring the total pack height it was apparent that 150 mm of closure had occurred in this area during the rockburst. Inspection of the area around C indicated that the stope face had been ejected into the stope. The thickness of hangingwall that had fallen was estimated to be 0,5-0,8 m. The rock was very fragmented, the average size being 100 mm. Based on observations at the site it is believed that the face ejected first, followed by the fragmentation and collapse of the hangingwall. This could correspond to the two seismic events. This assertion is supported by the report of a witness that one of the deceased was able to run from position C to position D before being fatally injured by the fall of hanging.

Four of the eleven fatalities occurred in the panel between positions H and I (see Figure B.3). A mine pole that had punched through its timber headboard indicated stope closure of 150 mm. Falls of hanging were noted in the face area between H and I. No face ejection occurred, and damage was by falls of hanging only. Once again, the very fragmented nature of the hangingwall was noted. It was clear from the underground observations that stope closure increased towards position B as shown in Figure B.3.

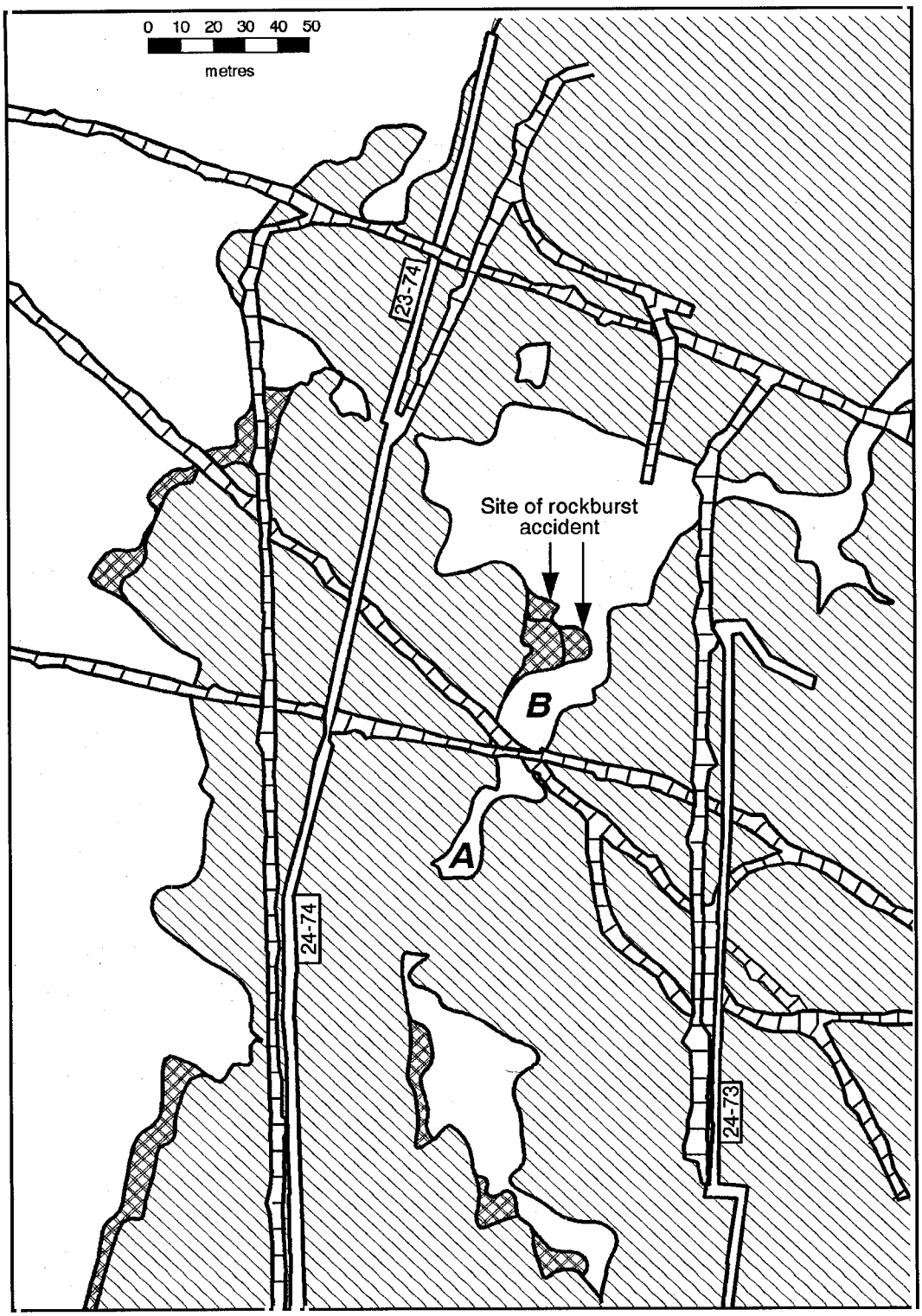

Figure B.2 Map showing the site of the rockburst on 10 January 1994 damaging the 24-74 stope, Leeudoorn Gold Mine. Mined out areas are indicated by diagonal lines. Areas of active mining are cross-hatched.

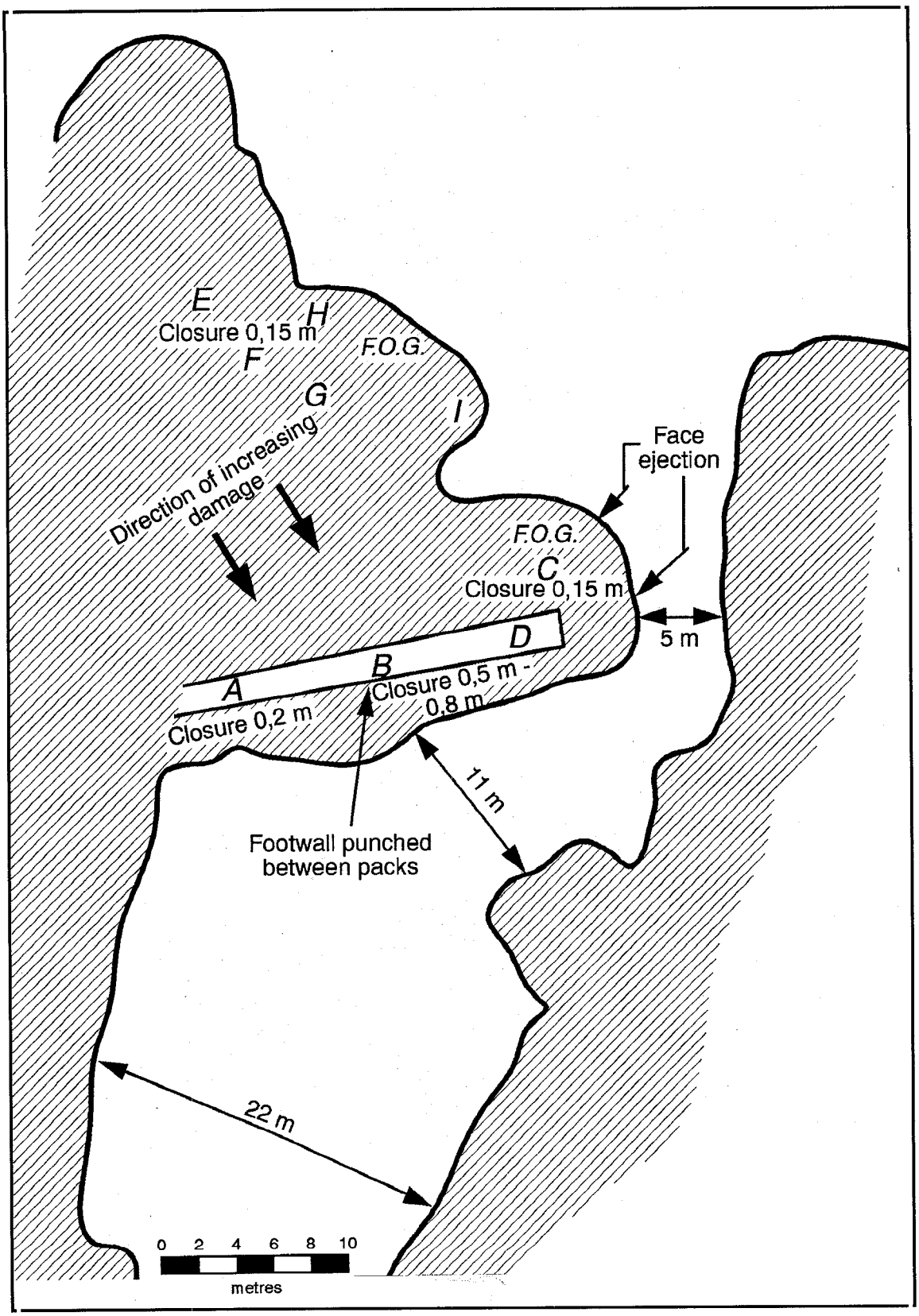

Figure B.3 Plan of the panels damaged by the rockburst, indicating rockburst damage and estimates of co-seismic closure.

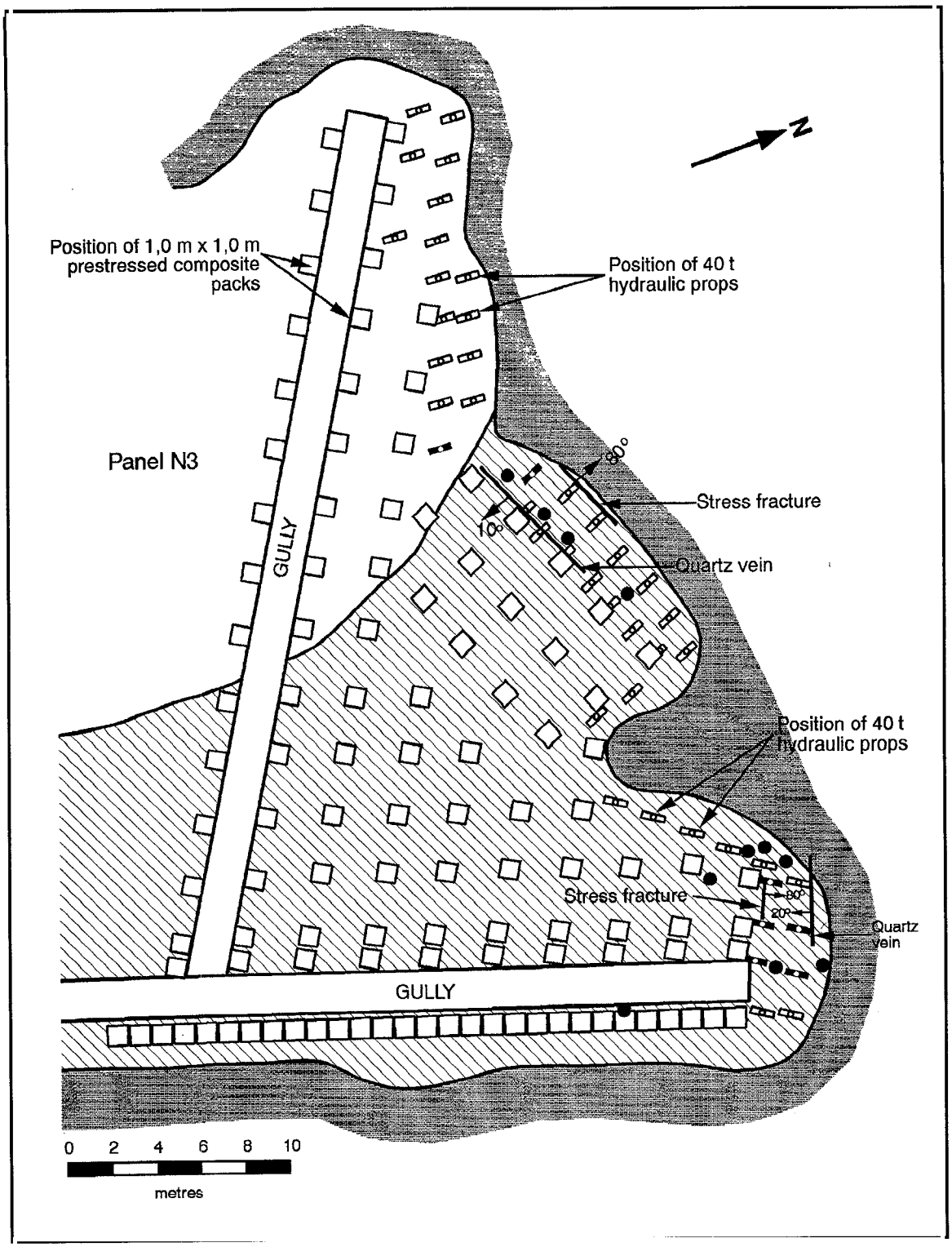

Figure B.4 Plan showing stope support. Solid circles indicate the positions of the fatalities.

1.4 Assessment of support performance

The support system consisted of composite packs and 400 kN telescopic hydraulic props, with 300 mm long headboards, installed in the face area (see Figure B.4). Although many of the hydraulic props were removed during the rescue effort, it was clear from an examination of the remaining props that the props had not been effective in preventing falls of ground owing to the fragmentation of the hangingwall. Hangingwall fallout had also occurred between the composite packs for the same reason, although this was less common further back from the face where the packs had effectively contained the damage. Fresh timber was exposed on most of the packs, providing further evidence of stope closure.

These observations indicate that the support was rendered ineffective by co-seismic fragmentation of the highly fractured and jointed VCR hangingwall. The use of 800 mm load spreaders on the hydraulic props might have reduced the damage, though probably would not have prevented all injuries. This type of fragmentation of the hangingwall is particularly difficult to support, and is most commonly encountered where the hangingwall is comprised of hard lava.

1.5 Assessment of layout

It appears that the strike gully was being developed for a holing with the worked out stope, about 5 m ahead. Stoping of the panels immediately up-dip was taking place simultaneously. The additional stress transfer resulting from the increased area of mining may have contributed to the occurrence of the face burst in the wide advanced heading north of position C (see Figure B.3).

During routine layout design, the Leeudoorn rock engineering department estimate the average pillar stress and potential ERR values by means of global mine simulations using the MSCALC program. In the vicinity of the 24-27 stope the MSCALC results indicated low to moderate pillar stresses (not exceeding 200 MPa on the remnant marked B in Figure B.2) and ERR values of about 12,8 MJ/m^2. However, the MSCALC modelling was carried out using a 10 m grid size, while the width of the remnant varied from 5 to 22 m.

Consequently the pillar geometry was only very crudely represented: some areas of the pillar were modelled as being larger than they in fact were; and narrow areas of the pillar were modelled as solid when, in fact, they would have been incapable of carrying load. The MSCALC modelling showed the pillar size to be about 1200 m^2. However, if the narrow pillar areas are assumed not to carry load, and the remaining portions of the pillar are modelled accurately, the load-bearing area of the remnant is, in fact, only 600 m^2.

MINSIM-D modelling undertaken by Mining Technology subsequent to the rockburst, using finer grid sizes, showed the development of peak stresses of 400 to 500 MPa in parts of the pillar. Clearly, this situation is far less favourable than that predicted by the large grid MSCALC modelling. The MINSIM-D modelling incorporates a coarse mining window that is used to calculate the global field stress acting on an area, but also allows the incorporation of a fine grid window to analyse stresses in more detail in areas of interest. The lack of this facility in MSCALC caused the Leeudoorn rock engineers to model the pillar using inaccurate dimensions. This, in conjunction with modelling the narrow pillar areas as solid and load-bearing, led to the under-estimation of the potential peak stress and the average pillar stress and may have been partially responsible for the failure to identify the potential risk involved with mining this area.

1.6 Rockburst mechanism

The seismic events of M_L = 2,6 and 1,9 occurring at 12h15 on 10 January 1994 were located by the seismic network on Kloof Gold Mine to be some 600 m away from the site of the rockburst damage. As this network is located about 5 km to the north-east of Leeudoorn Gold Mine, the locations may be less accurate than the cited deviations of 99 m (for the M_L = 2,6 event) and 139 m (for the M_L = 1,9 event) suggest. On the basis of the rockburst damage, the source of the M_L = 2,6 event is interpreted to be within remnant B shown in Figure B.2. The only other seismic events located within the boundaries of Leeudoorn Mine on 10 January 1994 and recorded by the Kloof seismic network occurred at 17h26 and 18h33 with M_L of 1,1 and 1,4, respectively.

As a result of limited seismic data, the actual mechanism of the rockburst is uncertain, but there are a number of observations that strongly suggest a particular sequence of events.

A rockburst occurred several months earlier in the same remnant, 50 m to the south of the current fatality site. The site of this rockburst is labelled A in Figure B.2. Failure of this part of the pillar would have increased the load on the remaining 600 m^2 area of the remnant (area B in Figure B.2).

With respect to the rockburst of 10 January 1994, observations of increasing convergence (up to a maximum of 0,8 m) and damage towards the south strike gully parallel to the pillar abutment (down-dip of A-B-D in Figure B.3) are consistent with foundation failure of portion B of the remnant. This remnant is large enough to account for a seismic event with M_L=2,6.

The foundation failure probably loaded the 5 m wide portion of the remnant to the point of failure, producing the face burst in the wide advanced heading simultaneously with the M_L=2,6 event.

Failure of this remnant and foundation failure along the pillar abutment down-dip from the gully A-B-D in Figure B.3 would have resulted in an increase in horizontal stress in the lava hangingwall that would have contributed to the co-seismic fracture and fragmentation of the hangingwall, resulting in the observed large scale falls of ground.

The M_L=1,9 event, which occurred 30 s after the M_L=2,6 event, involved 10 times less energy release. The mechanism and location of this event are unclear, although it probably caused further falls of ground.

The analysis of the sequence of the events would have been facilitated by the availability of accurate seismic locations provided by a local seismic network. Seismic monitoring by a local seismic network could have assisted in identifying areas of increased seismic hazard, and would also have contributed to understanding the cause of previous rockbursts in this area.

1.7 Conclusions

It is believed that the hazard posed by the remnant (pillar B in Figure B.2) was not recognised.

The stress redistribution produced by up-dip stoping, carried out simultaneously with the development of the strike gully and wide advanced heading, may have contributed to the face burst.

The support installed in the stope was not effective in preventing falls of ground owing to the fragmentation of the hangingwall.

1.8 Recommendations

Procedures used to estimate average and peak pillar stress and ERR values should be reviewed.

Defined remnant areas should be modelled in detail, using an appropriate mesh size.

The seismic history should be considered when assigning strength to blocks of ground.

Narrow pillars should not be modelled as solid, but rather as failed pillars incapable of carrying significant load.

Both average and peak pillar stresses should be considered, with an appreciation of their interaction. The mining sequence should be carefully planned to avoid hazardous stress transfers.

A local seismic network (yielding locations with an accuracy better than 40 m) would facilitate the identification of hazardous areas, and aid in the back analysis of rockbursts.

The fitting of larger headboards to hydraulic props should be more effective in containing falls of ground in areas where the hangingwall is prone to fragmentation.

2 Deelkraal, 4/5/94, M_L=2,1

2.1 Introduction

On 4 May 1994 a rockburst occurred at Deelkraal Gold Mine, damaging the 21-3E VCR stope and fatally injuring four workers in the 1W up-dip working place, 2294 m below surface (Figure B.5). The seismic network recorded a single seismic event at 09h49 with a local magnitude M_L = 2,1. At the request of Mr D. Bakker of the Department of Minerals and Energy, a team was mobilized to investigate the rock engineering aspects of the rockburst. The aim of the investigation was to determine the causes of the rockburst in order to prevent future occurrences. The site was visited on 9 May and 20 May 1994. The site was undisturbed apart from the rescue activities.

2.2 Mining environment

At Deelkraal Gold Mine the Ventersdorp Contact Reef (VCR) is underlain by quartzites and conglomerates of the Mondeor Conglomerate Formation. Hard lava of the Alberton Porphyry Formation overlies the VCR. The angle of unconformity between the VCR and the underlying, sub-cropping rocks is 4° on average. Shear planes parallel to the bedding have been documented within the footwall strata *e.g.* at the top of the Mondeor Conglomerate Formation. The joint orientation is variable, with north/south and NNE/SSW being the dominant strike directions. The joints dip steeply towards the east or west. The dominant joint orientations coincide with the most prominent fault and dyke direction. The Holly dyke, which is within 40 m of the rockburst site, has a NNE/SSW orientation (Figure B.5). This direction is parallel to sub-parallel to the mining on the western side of the panels. Faults and dykes running in a NW/SE direction are less common. Throws along these faults may vary from a few metres to tens of metres.

Faulting along and sub-parallel to the VCR plane also occurs, referred to as bedding parallel faulting. These fault planes commonly undulate, crossing the boundary of different strata, and are frequently observed along the VCR/hard lava contact. Bad hangingwall conditions are encountered in these areas.

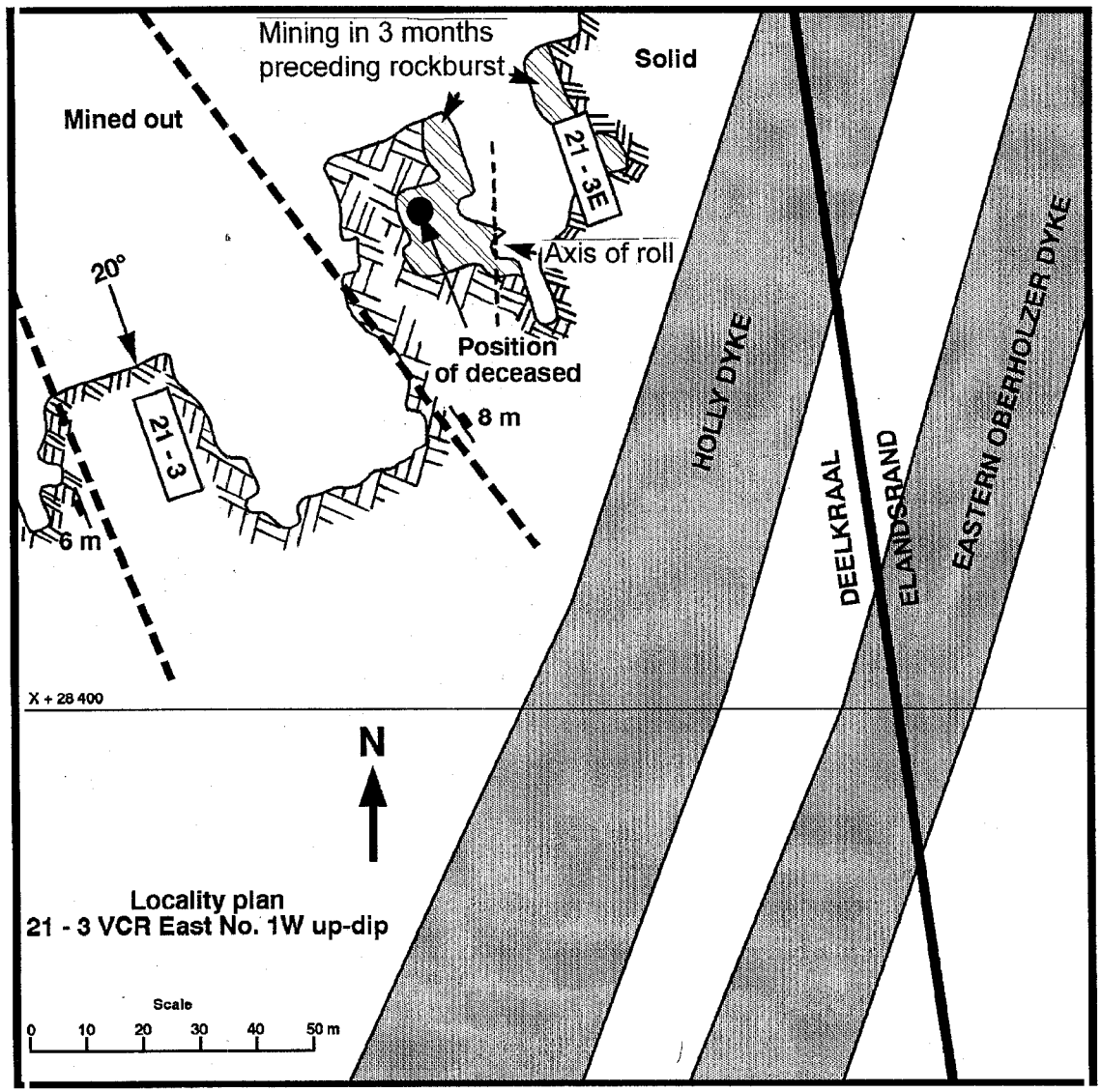

Figure B.5 Map of a portion of Deelkraal Gold Mine showing the site of the rockburst of 4 May 1994 and major geological features. Stoping in the 3 months preceding the accident is indicated by diagonal hatching. The 1W up-dip working place where the fatalities occurred is 2294 m below the surface.

2.3 Observations at the rockburst site

Figure B.5 is a location plan showing the site of the rockburst. Figure B.6 is a plan showing the type of support installed at the time of the rockburst and the extent of the fall of ground. A cross-section through the rockburst site parallel to strike is shown in Figure B.7. The principal observations are described with reference to Figure B.8.

Fresh timber was exposed in a gully pack at point A, indicating that dynamic loading had occurred. The convergence was estimated to be 50-100 mm.

A normal fault with an 8 m downthrow towards the east-north-east forms the western boundary of the remnant. The fault strikes in the dip direction of the reef. Inspection of the fault plane, where it had been exposed by mining, showed no evidence of recent movement.

The area around the upper strike gully was inspected. Some of the down-dip siding packs had been pushed into the gully between C and E by broken rock ejected from the exposed down-dip face.

Fresh splits in the timber indicated that dynamic loading on packs had occurred between C, D and E. The dynamic convergence was estimated to be 100-150 mm.

The breast face had stopped along the line F-G as the reef rolled down towards the west by about 2 m. This roll may correspond to the edge of an ancient river channel. Up-dip mining had then been commenced to extract this block of ground. Trenching was required to establish the up-dip face. The brow to the west of the roll collapsed during the rockburst (Figures B.7 and B.9).

A line of end grain packs had been installed in front of the breast face (from F to G, Figure B.8). At the top of the breast panel (position F) a small amount of intact reef could be seen in the stope face. The hangingwall lava was exposed over the remainder of the face. Between F and G rock had been ejected into the void between the original face position and the first dip line of packs, typical of a face burst (Figure B.10). It was clear that no hangingwall had fallen. Fresh splitting on packs in this area indicated dynamic convergence of 100-150 mm.

Between F and G the bulked rock had pushed the packs away from their previous positions. Timber material was smeared on the hangingwall.

The mining induced extension fracturing exhibits features typical of VCR areas where quartzite/conglomerate comprises the footwall and hard lava comprises the hangingwall. Flat fracturing occurs within the hangingwall lavas, while steep fractures are encountered in the quartzite footwall.

A large amount of rock was shaken from the roof at position I, burying a winch, fortunately not being operated at the time of the rockburst.

The strata associated with the VCR at the rockburst site are structurally disturbed by a roll in the reef and an undulating, bedding parallel fault. To the east of the roll, the fault plane is located close to the VCR/lava contact. To the west of the roll the fault plane is found within the hangingwall lava about 2 m above the VCR/lava contact. This phenomenon has been observed at VCR rolls at other mines, where the bedding parallel fault does not follow the VCR/lava contact when straddling rolls. Towards the west of the roll the undulating fault plane marks the top of the fall of ground area (Figures B.7 and B.9).

Calcite is a secondary mineral found along the bedding parallel fault, as well as along associated minor fault surfaces. Minor faults and randomly oriented joints, filled with calcite, are most prominent in the vicinity of the roll and appear to decrease in abundance with increasing distance away from the roll. The presence of the calcite-coated joints weakens the hangingwall.

The hangingwall above the up-dip stope (H) had been shattered into small fragments. The support that had been installed (1,1 m x 1,1 m timber packs and hydraulic props at the face) had been ineffective in supporting the hangingwall. No support had been installed to provide horizontal confinement to the brow.

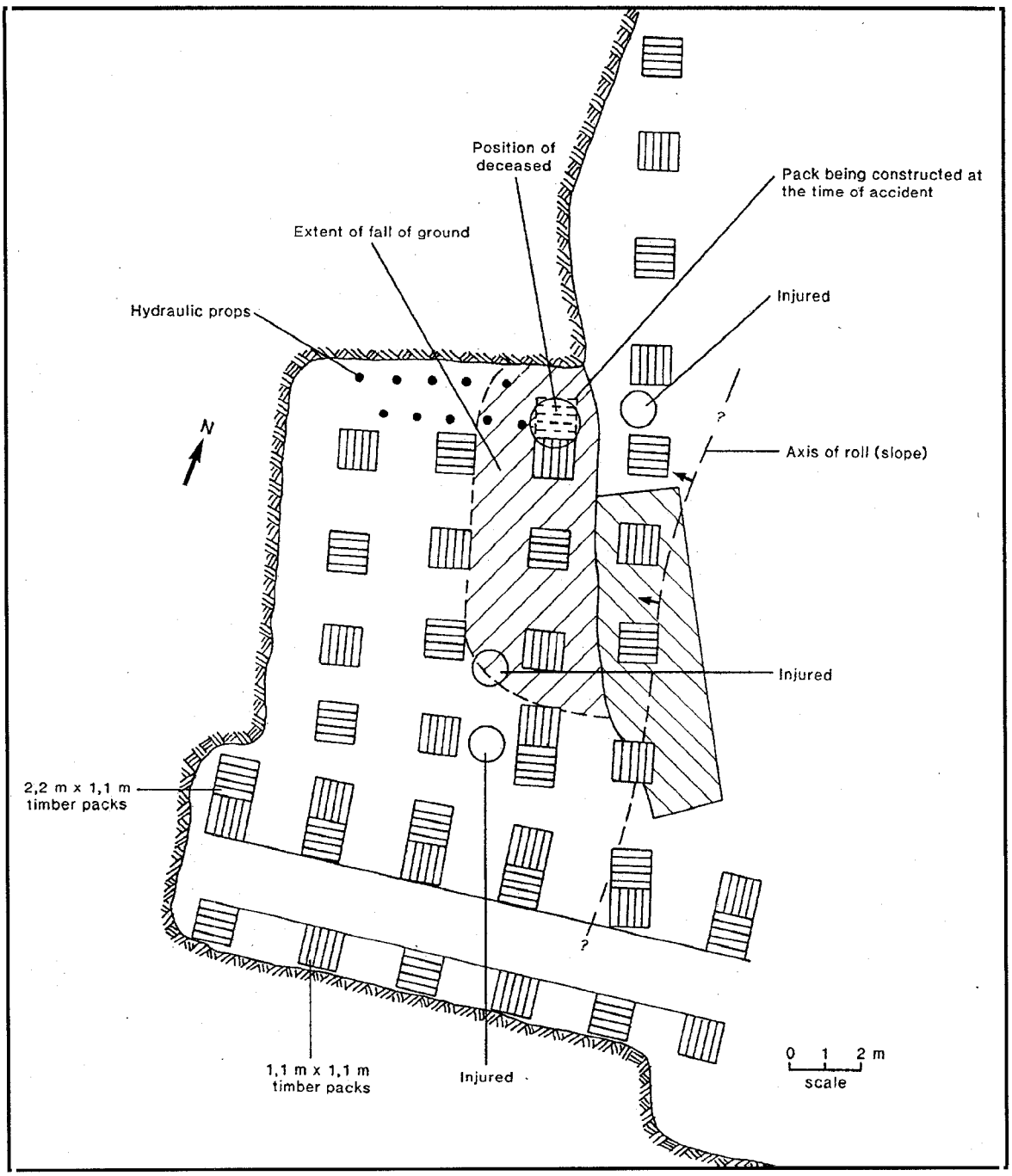

Figure B.6 Plan showing the support installed in the 21-3E VCR 1W Up-dip working place at the time of the rockburst, and the extent of the fall of ground.

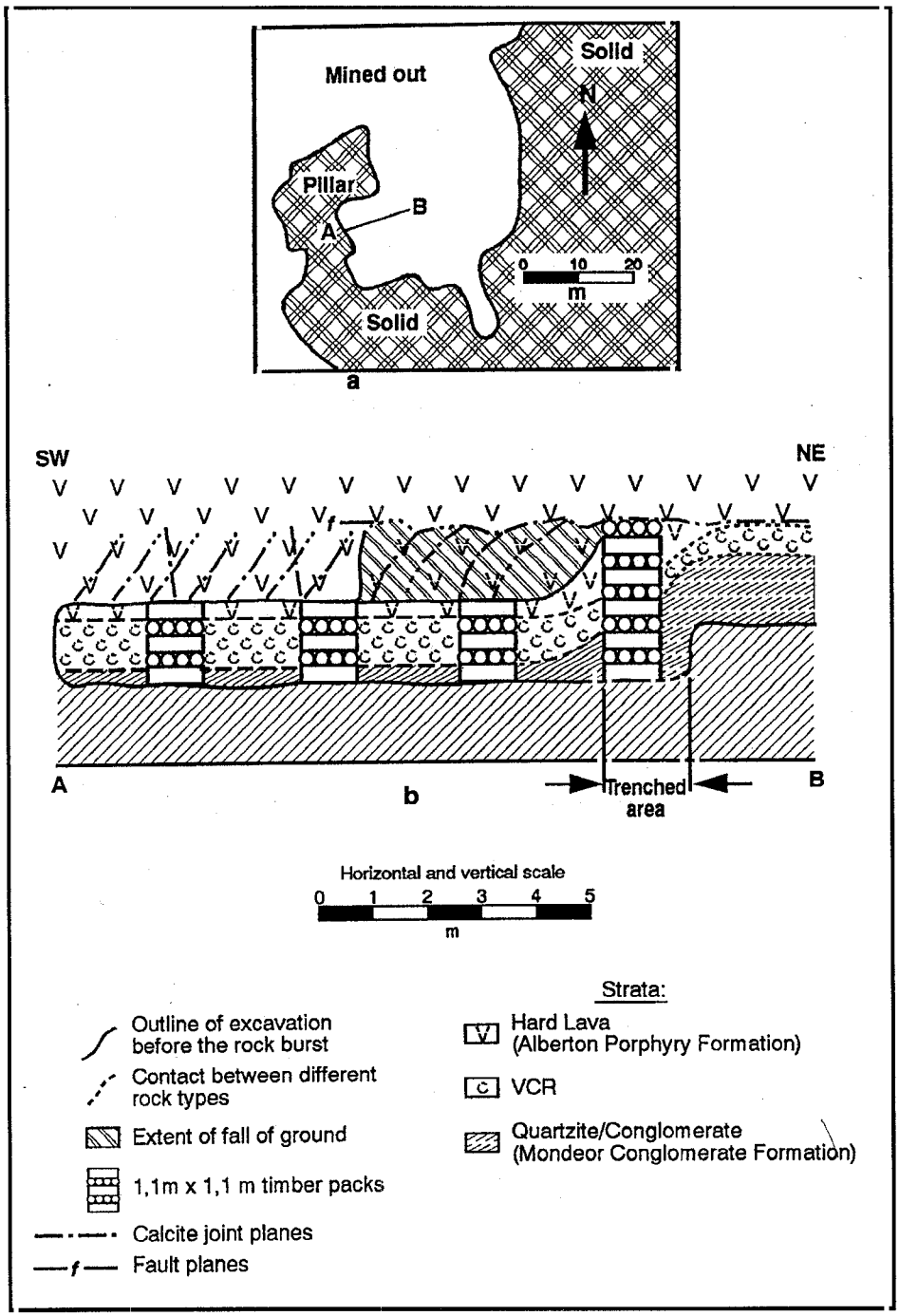

Figure B.7 Cross-section through the 21-3E VCR 1W Up-dip working place.

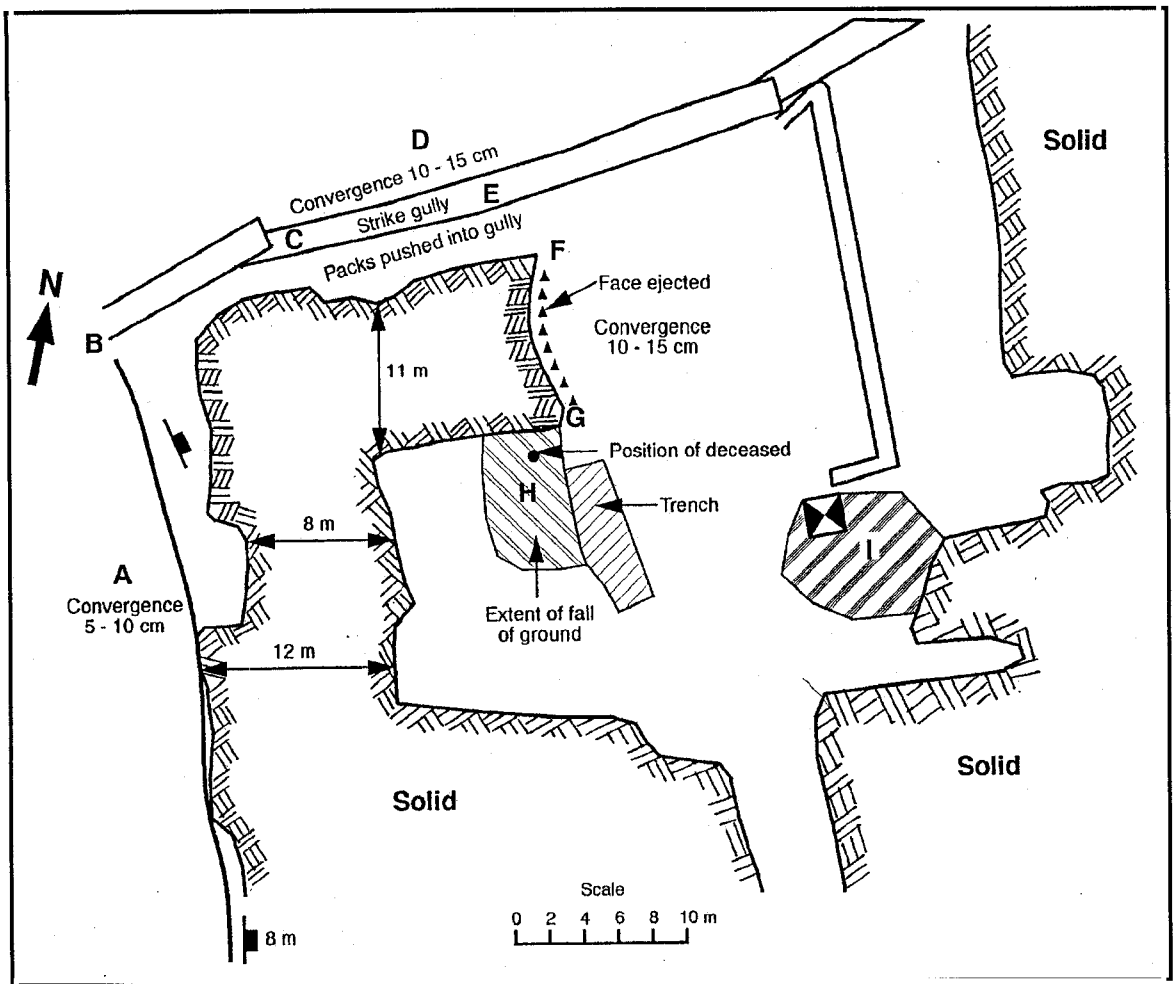

Figure B.8 Plan of the 21-3E VCR stope showing the positions of observations made during the inspection of the rockburst site.

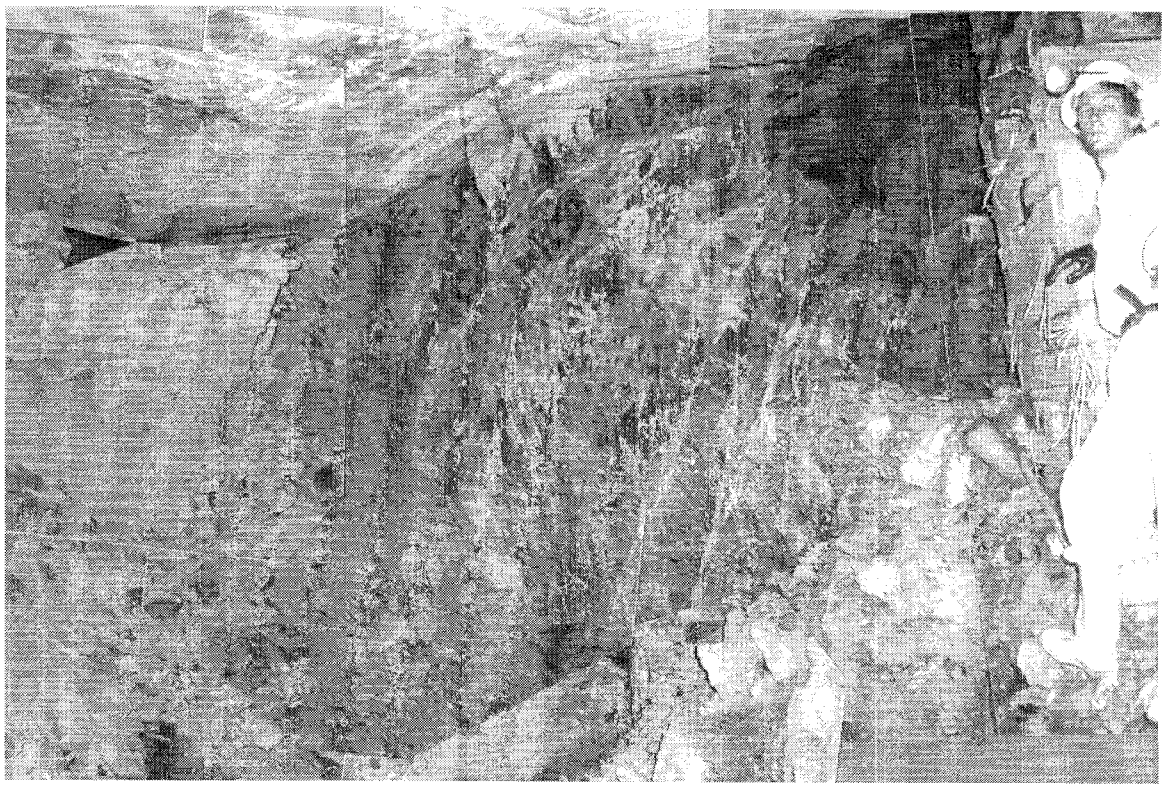

Figure B.9 Photo-mosaic showing the up-dip face where the fatalities occurred, viewed from position H (Figure B.8) and looking up-dip. The timber packs on the right are situated to the east of the roll. The corresponding section is shown in Figure B.7. The hangingwall fragmented during the rockburst. Most of the fallen rock was sub-sequently removed. Note the numerous fractures and joints in the face, and the smooth surface marking the parting above the collapsed brow.

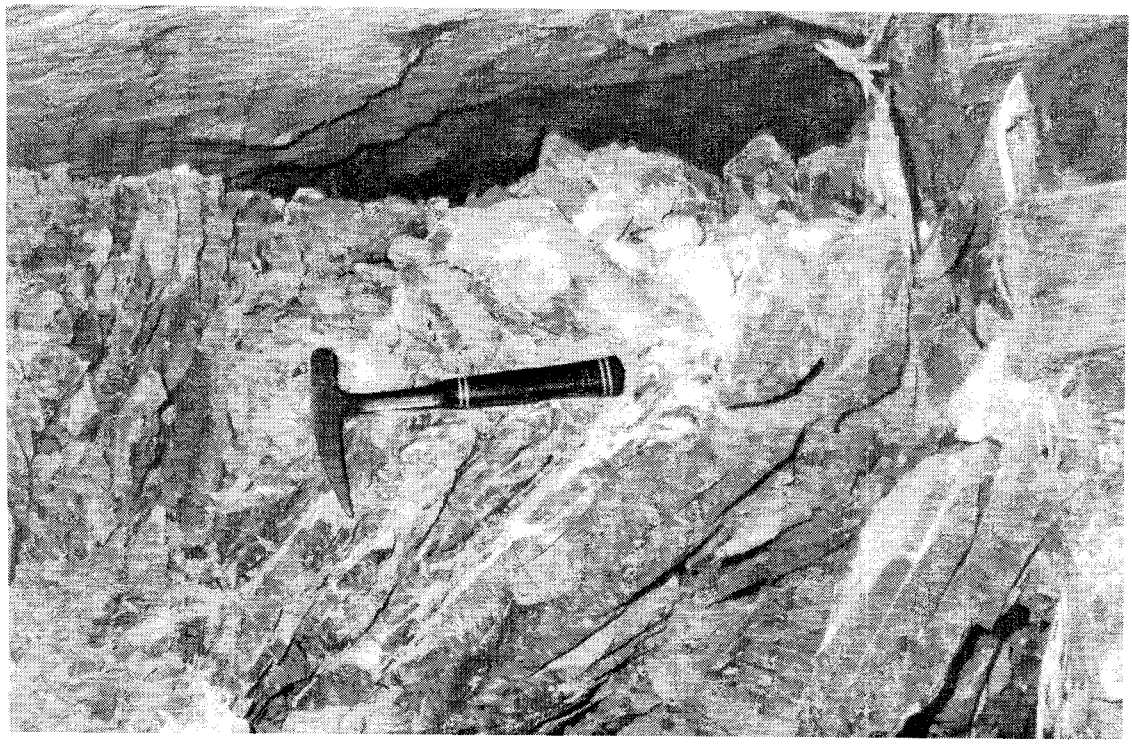

Figure B.10 Rock ejected from the footwall and face between F and G (see Figure B.8) into the space between the original face position and the first dip line of packs. The photograph is taken looking up-dip with the face to the left. Note the intact hangingwall.

2.4 Assessment of support performance

The support system in the 21-3E VCR 1W Up-dip working place consisted of 1,1 m x 1,1 m timber packs, and hydraulic props with headboards at the face (see Figure B.6). Although many of the hydraulic props were removed during the rescue effort, it was clear from examination of the remaining props that they had been ineffective in preventing falls of ground owing to the fragmentation of the hangingwall.

The pack support underneath the brow at H was well installed, but clearly not adequate to hold the brow up. No horizontal confinement was provided, without which the brow was prone to disintegrate when subjected to violent shaking. The shepherds, crooks installed

in the vicinity of the crosscut-reef intersection (position I) were also ineffective in preventing shake out of the fractured hangingwall.

2.5 Assessment of layout

Numerical modelling was conducted to determine whether or not a high seismic hazard was indicated. The main results of MINSIM-D modelling are summarized below.

The energy release rate (ERR) on the advancing faces were low (<20 MJ/m^2) on account of the limited mining span, giving no indication of face bursting.

The principal stresses on the Holly dyke were low (85-95 MPa), and the changes in the stress owing to mining were small (less than 2 MPa). No slip on the dyke was indicated.

Stresses on the faces being mined were in the range of 150-250 MPa at the start of mining (1/94), increasing to 200-350 MPa at the time of the rockburst (5/94). The stresses in the core of the remnant were interpreted to be in the range 250-275 MPa. Considering a value of 180 MPa to be the minimum UCS value of the host rock, the APS: UCS ratio would have been less than 1,6. This is safely below the limit of 2,5 given in the Industry Guide to Methods of Amelioration of Rockfalls and Rockburst (COMRO, 1988, p. 87) for a pillar with a width:height ratio > 10. However, the stresses normal to the reef plane reach values exceeding 500 MPa on the perimeter of the remnant. These values are derived from elastic analysis, which does not take into consideration the fracturing of the faces of the remnant. In reality these areas would be crushed and the load transferred to the interior of the remnant. This may reduce the effective width of the pillar from 9-13 m to, say, 5-9 m. This would almost double the effective stress in the core of the remnant to 500-550 MPa, a point where failure is possible.

2.6 Seismic history

Seismic monitoring results were available over the mining lease area of Deelkraal Gold Mine covering the period from the beginning of 1984 to the time of the rockburst in May 1994 (Figure B.11). Fairly detailed seismic coverage only commenced in 1987, and continuous cover exists only from the start of 1989. The seismic network in its present state comprises some sixteen geophone sites. The reported magnitudes of some 14 larger events were compared with results published by the Council for Geoscience in Pretoria from the national seismic network. Although the scatter in the differences was appreciable (±0,53), the average difference is insignificant (-0,07), and the Deelkraal magnitudes were accepted at face value.

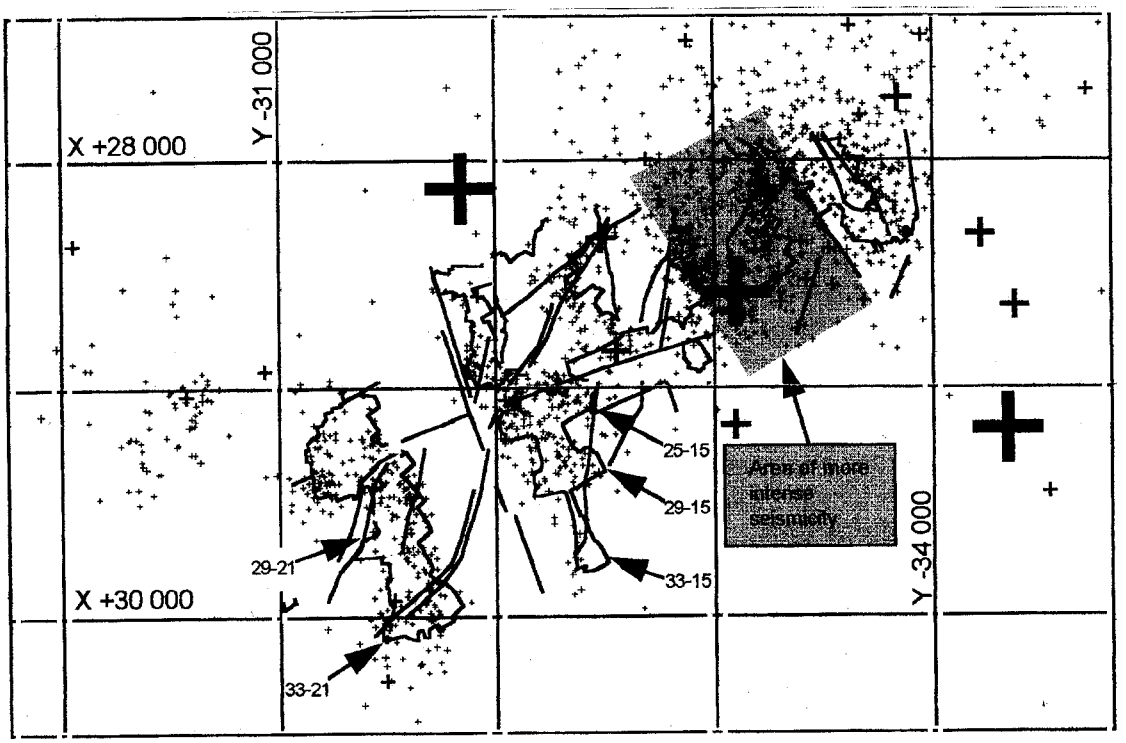

Figure B.11 Spatial distribution of all seismic events with $M_L \geq 1$ recorded at Deelkraal Gold Mine during the period 1984 to 1994. The size of the symbols is proportional to magnitude, the largest event in the area displayed having M_L=3,9.

The frequency-magnitude distribution for the entire area covered by the network was used to calculate a b-value of 0,72. The mine-wide b-value has not changed significantly during recent years, with only a slight steepening of the slope in the first half of 1994, thus indicating a fall-off in larger events. The variations in b-value were also investigated for different areas. The area of more intense seismicity shown in Figure B.11 has a slightly lower b-value of 0,67, indicating a slightly higher propensity for larger magnitude events. A count of events with $M_L \geq 2,5$ has shown that approximately 70 per cent of such events occurred in this area, which constitutes only about 20 per cent of the mining area.

The location of seismic events with respect to face positions at the time was also investigated (Figures B.12 (a) and B.12 (b)). Location error varies from as little as 30 m, to more than 100 m, which seldom allows for unambiguous identification of causative structures. The prospect of positively identifying geological seismic hazards is therefore not good. In the area of 29-21 and 33-21 longwalls the majority of events tend to cluster at the stope face with some events ahead of the face, while in the area of 25-15, 29-15 and 33-15 longwalls there appears a tendency for the seismic events to locate in the immediate back area of the stopes.

2.7 Rockburst mechanism

The focus of the rockburst was close to the eastern boundary of the mine and outside the mine seismic network, resulting in poor location accuracy. Consequently it was not possible to determine from the seismograms alone whether the focus of the rockburst was associated with slip along the Holly Dyke or failure of the peninsular remnant. Calculations were made to determine whether it was feasible for the failure of the remnant to release sufficient energy to produce a magnitude M_L=2,1 event. The greatest uncertainty in making this calculation is the estimate of the volume of convergence. However, it was possible to get a fairly reliable estimate from observations of the damage to packs surrounding the remnant. It was also necessary to estimate the area of the pillar which could have stored the elastic energy released by the rockburst, by excluding the fractured perimeter of the peninsular remnant.

The following parameters were used in the calculation:

Area of "elastic" pillar	300 m^2
Convergence	100 mm
ΔV_C (volume of convergence)	30 m^3
G (rigidity modulus of quartzite)	4 x 10^4 MPa

The seismic moment is estimated using the equation from McGarr and Wiebols (*Int. J. Rock Mech. Min. Sci & Geomech. Abstr., v. 14, pp. 139-145, 1977*).

$$M_O = G\Delta V_C = 1{,}2 \times 10^{12} \text{ Nm} \qquad \text{(B.1)}$$

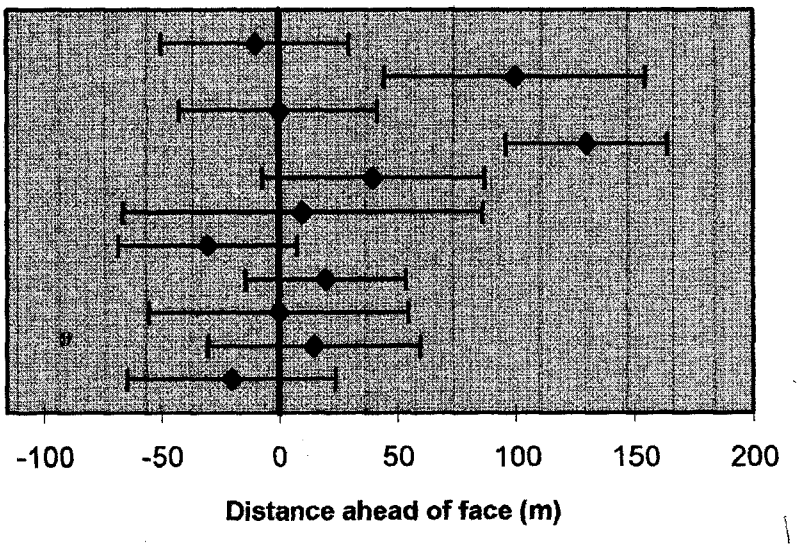

Figure B.12 (a) Location of events with M≥2 in relation to face positions in the areas of 29-21 and 33-21 longwalls. The horizontal error bars indicate location error. Negative distances indicate the back area.

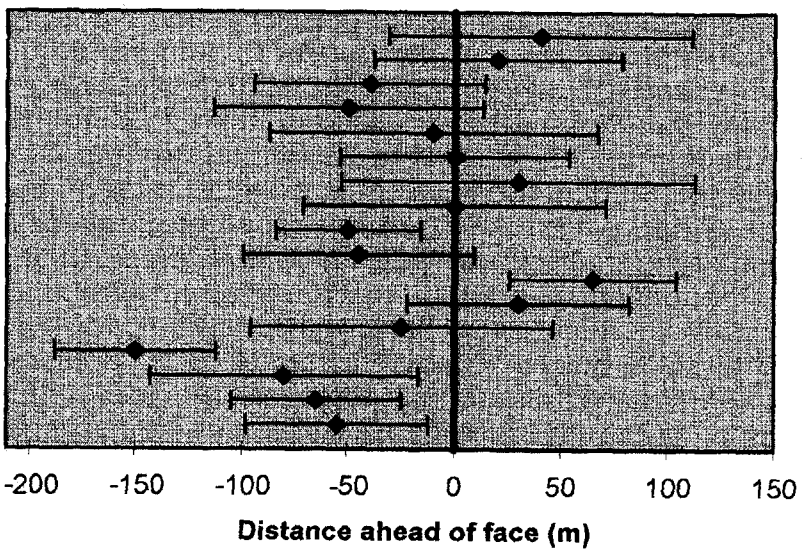

Figure B.12 (b) Location of events with $M_L \geq 2$ in relation to face positions in the areas of 25-15, 29-15 and 33-15 longwalls. Location error is indicated by the horizontal error bars. Negative distances indicate the back area.

The magnitude of the event can then be estimated using the Hanks-Kanamori (1979) moment magnitude relationship:

$$\log_{10} M_0 = 1{,}5\, M_L + 9{,}1 \qquad \text{(B.2)}$$

thus:

$$M_L = (12{,}08 - 9{,}1)/1{,}5 = 2{,}0 \qquad \text{(B.3)}$$

To give some indication of the sensitivity of this calculation to the assumptions made above, the calculation was repeated assuming a volume of convergence of only 15 m^3. A magnitude M_L=1,8 is obtained. Thus it is possible that the M_L=2,1 event was caused by pillar failure.

On the basis of the above calculations and the distribution of damage it was concluded that failure of the peninsular remnant was the source mechanism of the rockburst, rather than slip along the Holly dyke. Several other factors have been identified which may have given the peninsular remnant a predisposition to fail violently and caused the hangingwall to fragment when subjected to violent shaking.

The stoping layout resulted in an L-shaped peninsular remnant. At the time of the rockburst the width of the remnant ranged from 8-12 m (see Figure B.8). If the strength of one limb of the remnant was exceeded, it is likely that the entire remnant would have failed simultaneously. In contrast, a stoping layout giving rise to a triangular-shaped remnant would tend to fail at the apices of the triangle, with the core remaining intact.

Width:height ratio is a design criterion used to predict pillar performance. If the ratio becomes small, the pillar is in danger of crushing. With a pillar width of 8-12 m and an average stoping height in the area of 1,6 m, the nominal width:height ratio was about 6 at the time of the rockburst. Trenching carried out in order to establish the up-dip face to the west of the 2 m roll increased the unconfined height of the south-eastern sector of the remnant. A similar effect may have been produced by the up-dip strike gully. Fissile or weak partings, such as the bedding parallel fault, may also increase the effective "height" of a pillar (COMRO, 1988, p. 87). Thus the effective width:height ratio may have been considerably smaller than the nominal value of 6.

The rock type exposed by stoping around the peninsular remnant is mostly the hangingwall lava. Referring to Figure B.8, the hangingwall lava is exposed from A to B owing to the fault with an 8 m downthrow to the east; the lava is exposed between B and F as the down-dip siding of the strike gully does not follow the 26° dip of the reef; while from F to G the lava is exposed because stoping overshoots the 2 m roll. Recent measurements at Mining Technology indicate that the lava hangingwall and VCR have similar values of Young's modulus (about 80 GPa). However, the UCS of the hard Alberton lava (>250 MPa) is substantially greater than that of the VCR conglomerate (>180 MPa), and consequently can store more elastic energy. Should the remnant fail, it would do so more violently than if it were comprised of conglomerate.

The numerous calcite-coated joint planes found in the hangingwall in the vicinity of the roll indicates that the rock comprising the brow was weak and prone to fragmentation during violent shaking.

2.8 Conclusions

The magnitude M_L=2,1 rockburst which occurred at 9h49 on 5 May 1994 is considered to be owing to the failure of the peninsular remnant, and not slip on the Holly dyke or on the 8 m fault.

The peninsular remnant was particularly vulnerable to rockbursting owing to:
it's L-shaped geometry;
a high effective unconfined pillar height owing to trenching and bedding parallel faulting; and a weak hangingwall owing to faults and joints in the vicinity of the roll in the reef.

There has been no significant change in the general level of seismicity since the establishment of the mine seismic network in 1989. The majority of events are located close to the mining face, though some events have occurred in back areas. Larger events ($M_L \geq 2,5$) are not evenly distributed over the mining area, but are concentrated in an area towards the east of the mine.

Elastic modelling does not indicate any significant transfer of stress onto the Holly dyke or indicate immediate failure of the remnant. However, if the reduction in the effective width of the remnant owing to fracturing of the face is taken into account, the effective stress in the core of the remnant is increased to 500-550 MPa. Failure is possible at these stress levels.

The stope support system (packs and hydraulic props) was ineffective in preventing falls of ground owing to the fragmentation of the hangingwall. The lack of support, providing horizontal confinement to the brow probably increased its susceptibility to fragmentation. Shepherds, crooks were ineffective in preventing shake out of the hangingwall in the vicinity of the crosscut-reef intersection.

2.9 Recommendations

Avoid the formation of peninsular remnants. If possible, carry out underhand mining from the raise.

If trenching is carried out, install support that will provide lateral confinement to the brow. Avoid the formation of rectangular or L-shaped remnants. Rather form a triangular remnant and mine in a direction such that the apex to be mined last is closest to the nearest large solid area.

Special care should be taken to support the hangingwall when mining in the vicinity of rolls, especially when associated with faulting, as the frequency of weak calcite-coated joints appears to increase in these areas.

Support should be installed to provide horizontal clamping to the brow that is formed when a roll is encountered.

The equipping of hydraulic props with larger headboards should be more effective in containing falls of ground in areas where the hangingwall is fragmented.

The interpretation of calculations of stress and ERR must be done with extreme care. Elastic modelling techniques (such as MSCALC and MINSIM) do not take the fracturing of the face into account, and produce unrealistically high values of stress at the edges of pillars and abutments. In reality these areas fracture and crush, are shifting the load away from the face. The core of the pillar is subjected to greater stress than is indicated by the numerical model, and can become critical when the pillar dimensions are small. Another important factor is the size of the window used for numerical modelling. The number of elements was fixed in the version of MSCALC used at the time. While the resolution was improved through the use of small elements, the size of the window was also reduced and loads produced by excavations outside the window were ignored.

A local seismic network (yielding locations with an accuracy better than 20 m) would facilitate in the identification of hazardous areas, and in the back analysis of rockbursts.

3 Western Deep Levels (West), 3/11/94, M_L=2,5

3.1 Introduction

On 3 November 1994 a rockburst occurred at Western Deep Levels (West) Mine, damaging the 113-36 Carbon Leader stope about 3000 m below surface, and fatally injuring six workers in the W3 panel (Figure B.13). The seismic network recorded a double seismic event at 07h19, the larger event having a local magnitude M_L=2,5. A team from CSIR Mining Technology was mobilized to investigate the rock engineering aspects of the rockburst at the request of Mr D. Bakker of the Department of Minerals and Energy. The aim of the investigation was to determine the causes of the rockburst in order to prevent future occurrences. The site was visited on 8 and 16 November 1994, and again on 4 January 1995.

3.2 Mining environment

Stratigraphy

The Carbon Leader reef (CLR) lies close to the base of the Central Rand Group. The orebody itself is 30-50 cm in thickness in the W3 panel, with a discontinuous carbon seam developed at its base, typical of a channel/overbank transition. The stratigraphy of the CLR zone is shown in Figure B.14. The hangingwall of the CLR is a package comprised of, from bottom to top, a siliceous quartzite horizon (about 1,20 m in thickness, horizontally bedded with bedding intervals of about 1 cm), the Rice Pebble Marker (a matrix-supported small pebble conglomerate, exceeding 20 cm in thickness), and the Green Bar (a horizon predominantly comprised of shale). The footwall of the CLR is a massive, competent quartzite. In the 113-36 stope the CLR dips to the south at approximately 20°.

Intrusions

The Acid dyke intersects the W3 panel of the 113-36 longwall. It is 5-15 m in thickness, has a NE-SW strike, and dips to the west at 70°. The CLR is downthrown by about 15 m to the west of the dyke. The Tarentaal dyke is sub-parallel to the Acid dyke (see Figure B.13), and dips to the east at 71°. The exposure of the Acid dyke in the W3 panel was examined during the site visits. The dyke rock is strongly fragmented in appearance, resembling the soft Westonaria Formation lava overlying the VCR. The Acid dyke contains several prominent quartz veins up to 10 cm in thickness. Euhedral pyrite is associated with the veins. Petrographic examination of thin sections yielded the (approximate) mineralogies for the dykes listed in Table B.1. The high proportion of secondary minerals indicates that both dykes are strongly altered. However, the style of alteration is distinct for the dykes, mainly expressed by the high percentage of calcite in the Tarentaal dyke.

A single whole rock geochemical analysis of the Acid dyke (performed by Anglo American Research Laboratories) obtained a SiO_2 content of 55 per cent indicating an intermediate to mafic, rather than acid, composition. The SiO_2 content of the Tarentaal dyke was only 48 per cent. However, in both cases the total of the major elements is less than 90 per cent, indicating that these values should be treated with caution. Consequently, only the trace elements are considered in comparing the geochemistry of the dykes.

Relative to the Acid dyke, the Tarentaal dyke is significantly enriched in base metals (Ni, Cu and Zn), Ba and Zr, and depleted in Sr. The three-fold enrichment of Zr, which is an immobile and incompatible element, strongly suggests that the Acid and Tarentaal dykes are distinct intrusions, and not merely a bifurcation of a single intrusion. The apparent merging of the dykes in the vicinity of the shaft pillar is probably owing to both dykes invading the same pre-existing joint or fracture.

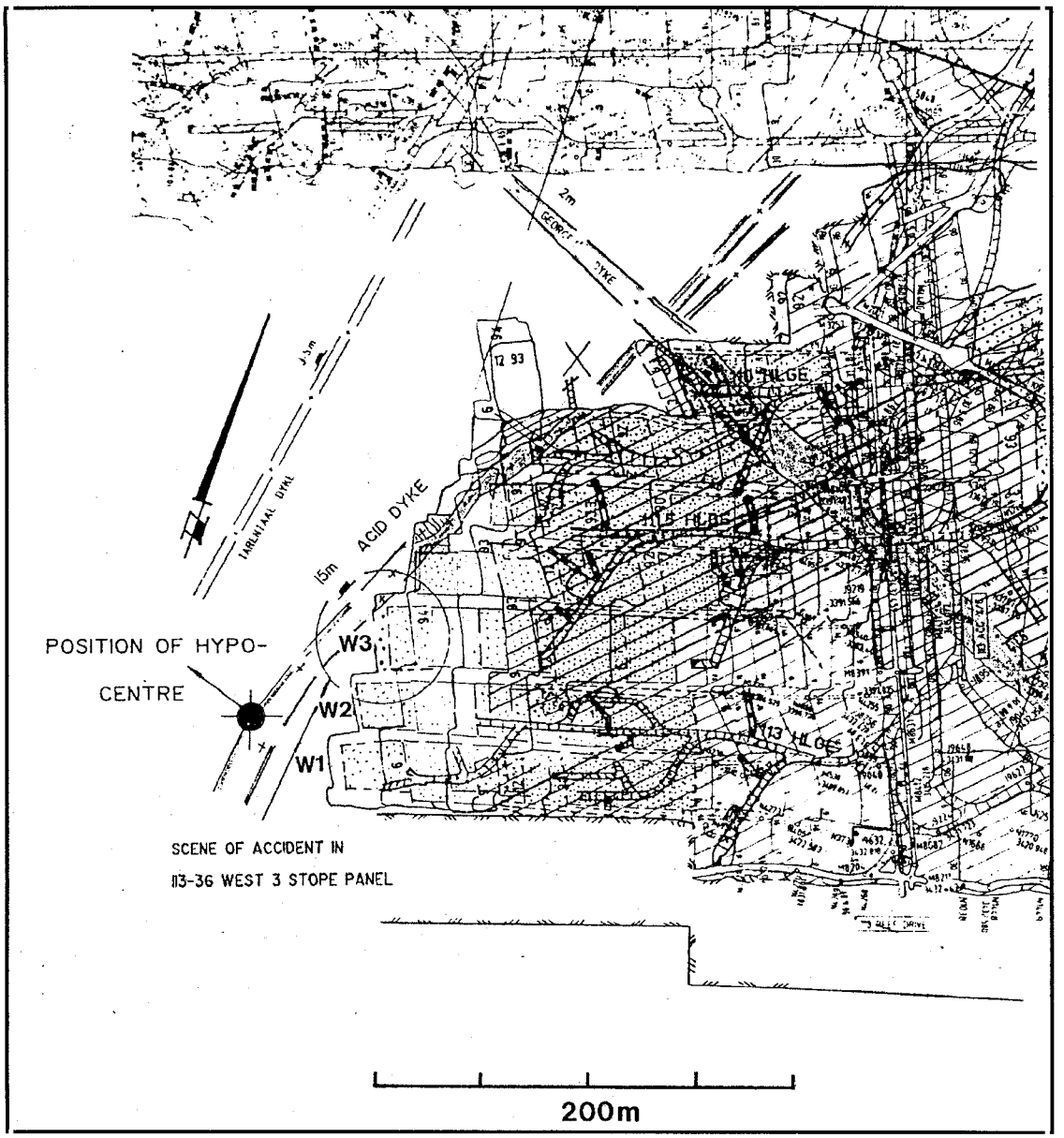

Figure B.13 Plan showing the location of the rockburst at Western Deep Levels (Ltd.) West Mine on 3 November 1994 damaging the 113-36 West 3 Carbon Leader panel.

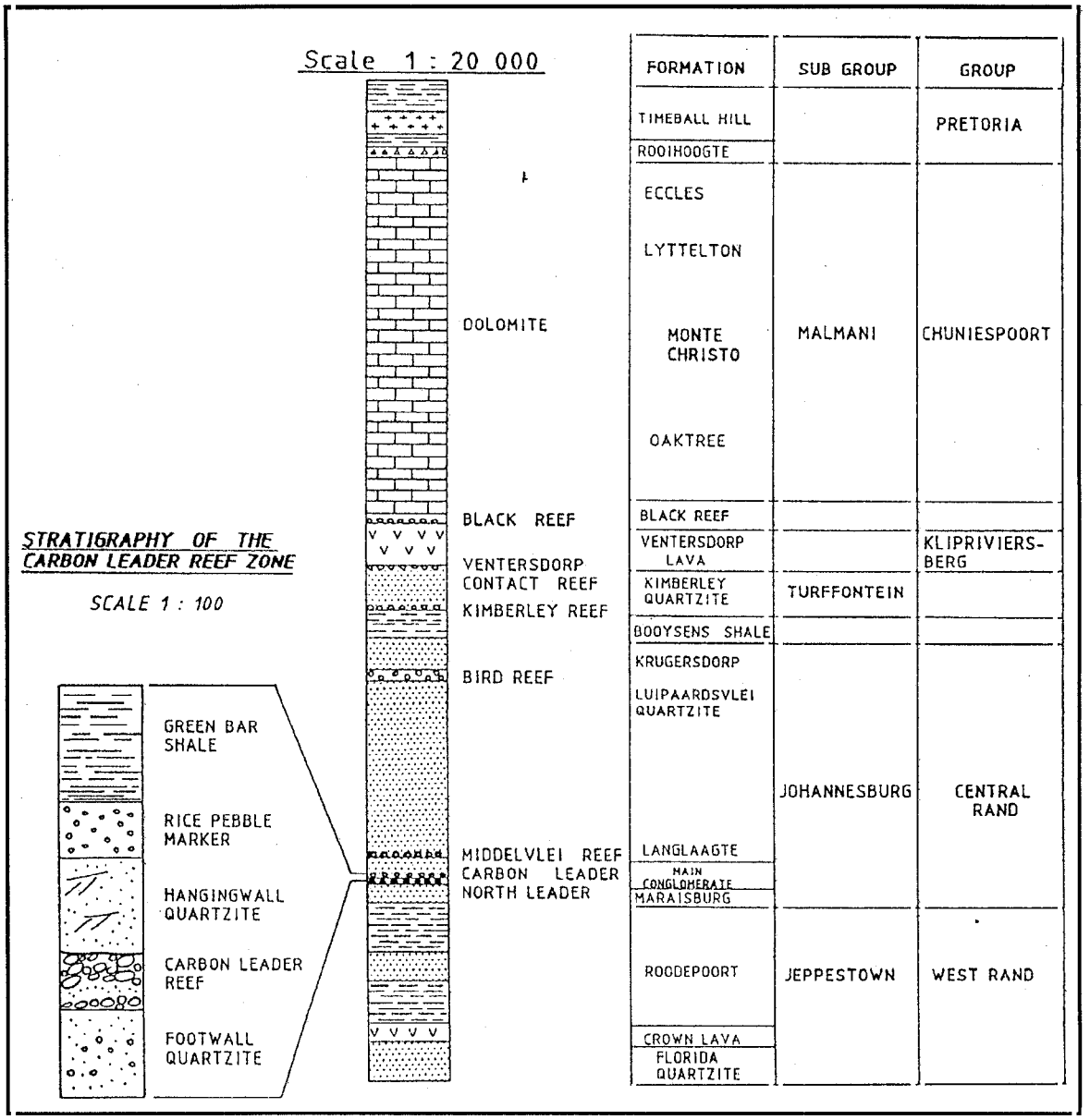

Figure B.14 Stratigraphy of the Carbon Leader reef (CLR) zone. The CLR forms part of the Main Conglomerate Formation close to the base of the Central Rand Group.

Table B.1

Dyke mineralogy determined by thin section petrography

	Tarentaal Dyke	Acid Dyke
Calcite	45%	
Chlorite	35%	55% (pseudomorph after plagioclase?)
Amphibole	3%	20% (pseudomorph after clinopyroxene?)
Quartz	3%	5%
Opaques	8%	15%
Accessories	6%	5%

UCS of strata

Core from a borehole which intersected both the Acid and Tarentaal dykes in the vicinity of the W3 panel was supplied by the mine. The borehole (GBH2414) was drilled from the 113 level footwall drive perpendicular to the strike of the dykes. The borehole was sub-parallel to the strata: the inclination of the borehole was 20° up, while the apparent dip of the strata in the vertical plane through the borehole was 13°. Point load tests were carried out at roughly 20 cm intervals. The results are summarized in Table B.2.

Table B.2

Uniaxial compressive strength determined by point load tests

Formation	Distance along borehole (m)	Av. UCS (MPa)	Range (MPa)	Std dev.	No. of samples
Quartzite above Green Bar	127,8-135,2	249	118-310	67	20
Green Bar	118,4-120,7	295	190-321	38	10
Rice Pebble marker	114,6-118,4	253	85-364	72	10
Hangingwall Quartzite	102,8-114,6	287	149-321	37	33
Carbon Leader Reef zone	97,7-102,8	287	117-349	45	8
Tarentaal dyke	120,7-127,8	284	128-342	45	28
Acid dyke	82,7-97,7	276	128-450	86	49

The Acid and Tarentaal dykes and country rock have similar uniaxial compressive strengths. However, the range of values obtained for some formations is large. The core was carefully examined, and it was concluded that the variation can largely be ascribed to geological features. Several low-strength zones are found within the formations: the Rice Pebble Marker contains a weak mineralized zone, failure within the dykes sometimes occurred along calcite-coated joints, and the contact between the Acid dyke and Carbon Leader Reef (where pseudotachylite is intruded) also failed at a low load. The composition of the Green Bar varies from shale to fine-grained quartzite. The facies intersected by the borehole appears to be quartzitic, accounting for its high strength.

3.3 Observations at the rockburst site

The 113-36 Carbon Leader stope is a longwall being mined on breast in a westerly direction (see Figure B.13). The most severe rockburst damage was found in the W3 panel. The W1 and W2 panels, located down-dip and closer to the focus of the M_L=2,5 seismic event, were virtually undamaged. Events with M_L>2 are a daily occurrence on West Mine, and most cause little or no damage. The key question to be answered in this instance is the cause of the intense damage in the W3 panel. Observations are described with reference to Figures B.15 and B.16.

Rockburst damage

A fall of ground was noted in the upper part of the W2 panel where it is intersected by the heading of the strike gully. The fall of ground in the W3 panel extended from the down-dip strike gully to the intersection with the Acid dyke, a distance of about 20 m (Figure B.15). The distance from the face to backfill was about 3 m, and about 1 m of the hangingwall above this area had collapsed. The fall of ground was bounded on the up-dip side by a weak joint, filled by a quartz vein locally containing pyrite; to the west by face-parallel fractures; and to the south-east by face-parallel and longwall-parallel fractures (see Figure B.16). Part of the hangingwall had remained standing in the W3 panel and formed a brow, in which partings of 1 cm or more had formed along bedding planes. No finely crushed rock was observed in these partings, but rather coarse quartzite aggregates a

few millimetres in diameter, interpreted to indicate tensional failure. It appeared that about 0,5 m of material had ejected from the stope face of the W3 panel. The rock forming the face was crushed and had a granular texture, indicating that the face had experienced compression during the rockburst. This contrasted sharply with the fractured (but uncrushed) face in the W2 panel. This was interpreted to indicate that the rock between the face of the W3 panel and the dyke had failed, possibly triggered by slip on the dyke. The face of the W3 panel was inspected again on 4 January 1995 after it had advanced by several metres. In contrast to the earlier observation, no unusual crushing of the face was evident.

Mining-induced fractures

Numerous mining-induced fractures were observed in the 113-36 stope. While no detailed survey was made of fracture orientations, several sets were observed (Figure B.16): a NNW-striking set essentially parallel to the stope face, perhaps refracted by the lag between the W2 and W3 panels; a NNE-striking set parallel to the overall orientation of the longwall and the Acid dyke; and a set parallel to NW-trending quartz-filled joints.

The mining induced extension fractures exhibit a turning point of inflection at the level of the Carbon Leader reef, as is typical for reefs with sedimentary bedded foot- and hangingwalls. These fractures intersect the ore body perpendicularly. The orientation of the fractures was measured in the arches between gully packs formed by falls of ground. It was noted that the dip flattened to 40° immediately below the Green Bar, some 1,5 m above the stope. The number of extension fractures increased close to NW/SE trending joints. This feature was prominent in the W3 panel and in the uppermost portion of the W2 panel. Both these areas were characterized by falls of ground during the event. About 40 fractures per metre occur within 1 m of the NW/SE trending joints, while further away this decreases to only some 20 fractures per metre. Extension fracturing within the quartzite underlying the Carbon Leader reef is less frequent than in the hangingwall, averaging about 15 fractures per metre. No evidence of significant co-seismic movement could be detected on the extension fractures. A quartz vein noted in the upper end of the W2 panel was displaced by extension fractures. This movement probably represents the aseismic closure of the stope and is unrelated to the rockburst.

Shear fractures are formed at intervals of about 1 m. Movement also occurred along the quartz-filled joints that run sub-parallel to the extension fractures and are most pronounced within the hangingwall. These joints are encountered in the hangingwall of the areas where falls of ground occurred. Other planes recording movement are the shear plane that runs close to the contact between the Acid dyke and the abutting rocks of the CLR zone, and several shear fractures.

The contact between the Acid dyke and country rock was inspected in the W3 panel on 16 November 1994. It was irregular, with a planar shear zone positioned along a fault rock (pseudotachylite), which had intruded the dyke close to the contact. The contact was inspected again on 4 January 1995, after the face had advanced by several metres. The contact was straight with pseudotachylite present along the interface. The shear plane was absent, implying that the shear along the dyke/host rock contact was restricted to the vicinity of the face at the time of the rockburst.

The hangingwall was intensely fractured along the strike gully. Falls of ground were observed between the packs on both sides of the strike gully, forming arches which extended about 1 m into the hangingwall. In some instances the Green Bar shale was exposed. The gully sidewalls were severely fractured in places. The resultant spalling had undermined the foundations of several packs.

Joints and bedding-parallel partings

Extension gashes, or joints, are common at the rockburst site. These planes are usually occupied by secondary quartz. The most prominent joint directions trend NNE/SSW (roughly parallel to the Acid dyke) and NW/SE, and generally dip steeply towards the west. Joints trending E/W and NE/SW are less common. A bedding-parallel quartz vein (or joint) about 2 cm in thickness is developed at the Rice Pebble Marker/Green Bar contact, with slickensides (trending NE/SW) being prominent at the base of this zone.

Several bedding-parallel partings were examined in the arches formed by the fallout between the gully packs. Pulverized host rock material was found along these surfaces, indicating that recent movement had occurred along these planes. The partings where noticeable movement had occurred are the contacts between the Green Bar Shale and

the Rice Pebble Marker, the Rice Pebble Marker and the siliceous quartzite, and along some bedding planes within the siliceous quartzite. No movement was observed on the carbon seam at the base of the Carbon Leader reef.

Co-seismic closure

Dynamic closure of the W3 panel was estimated to have had a maximum value of 100 mm. This estimate was made by observing the distance that a prop had punched into the stope hangingwall, as well as the deformation of various mine poles. The normal stope closure that had occurred prior to the rockburst was taken into account in making the estimate.

Support

The support system in the W3 panel consisted of backfill placed within 3,5 m of the face and 40 ton (1 m/s) hydraulic props without headboards, packs in the area of the dyke intersection, and pipe sticks to support the backfill bags (see Figure B.15). Apparently the installation of a second line of props had just commenced at the time of the rockburst. Part of the hangingwall had remained standing in the W3 panel and formed a brow. A single Camlock prop and two poles were installed beneath the brow during the rescue effort. The placement of uncemented backfill in the area was good. It was noted that a space of about 1 m was left between the backfill in the W3 panel and the timber packs lining the strike gully for the storage of pipes and equipment. The backfill bag at the top of the W2 panel was tightly filled but did not completely fill the void as the bag was too small and the hangingwall irregular.

Freshly split timber was observed in several gully packs, indicating damage during the rockburst. The timbers of several packs, particularly on the up-dip side of the gully, had been ejected into the gully. The foundation of the gully packs had been severely eroded in places.

3.4 Assessment of support performance

Twenty-eight 40 ton props were recovered from the W3 panel by Western Deep Levels staff and tested at Mining Technology. The props were exposed to both slow and rapid yield (1 m/s) tests. The results are summarized below.

Seven props were non-functional and could not be tested. Problems included water leaking through the main seal or rockburst valve, jamming of the hydraulic ram, and dirt in the filler valve. It is not known whether these props were damaged during the rockburst. Three props exhibited setting problems and could not be tested at slow yield, and were only subjected to the rapid yield test. All twenty-one props subjected to the 1 m/s rapid yield test survived without catastrophic failure. However, there was a considerable range in the force characteristics of the props. Not a single prop met the force characteristics specified for 40-ton props, although most would have been able to absorb some energy. Two props were re-tested about a month after the initial tests, and gave results, which differed considerably from the initial test. Consequently it is difficult to infer the performance of the props during the rockburst from the laboratory tests.

Props which were marked as having punched into the hangingwall did not show an unusual force characteristic. It was not possible to determine whether or not these props had been fully closed prior to the rockburst.

3.5 Assessment of the layout

When interpreting the results of numerical modelling, it must be understood that the values obtained from elastic modelling are not the actual values expected to exist within the rock mass, but are useful for evaluating different mining options. For example, face stresses greater than 400 MPa would probably not exist as the rock would have already failed and transferred the stress deeper into the confined rock mass. However, highly stressed areas indicate a potential for violent failure.

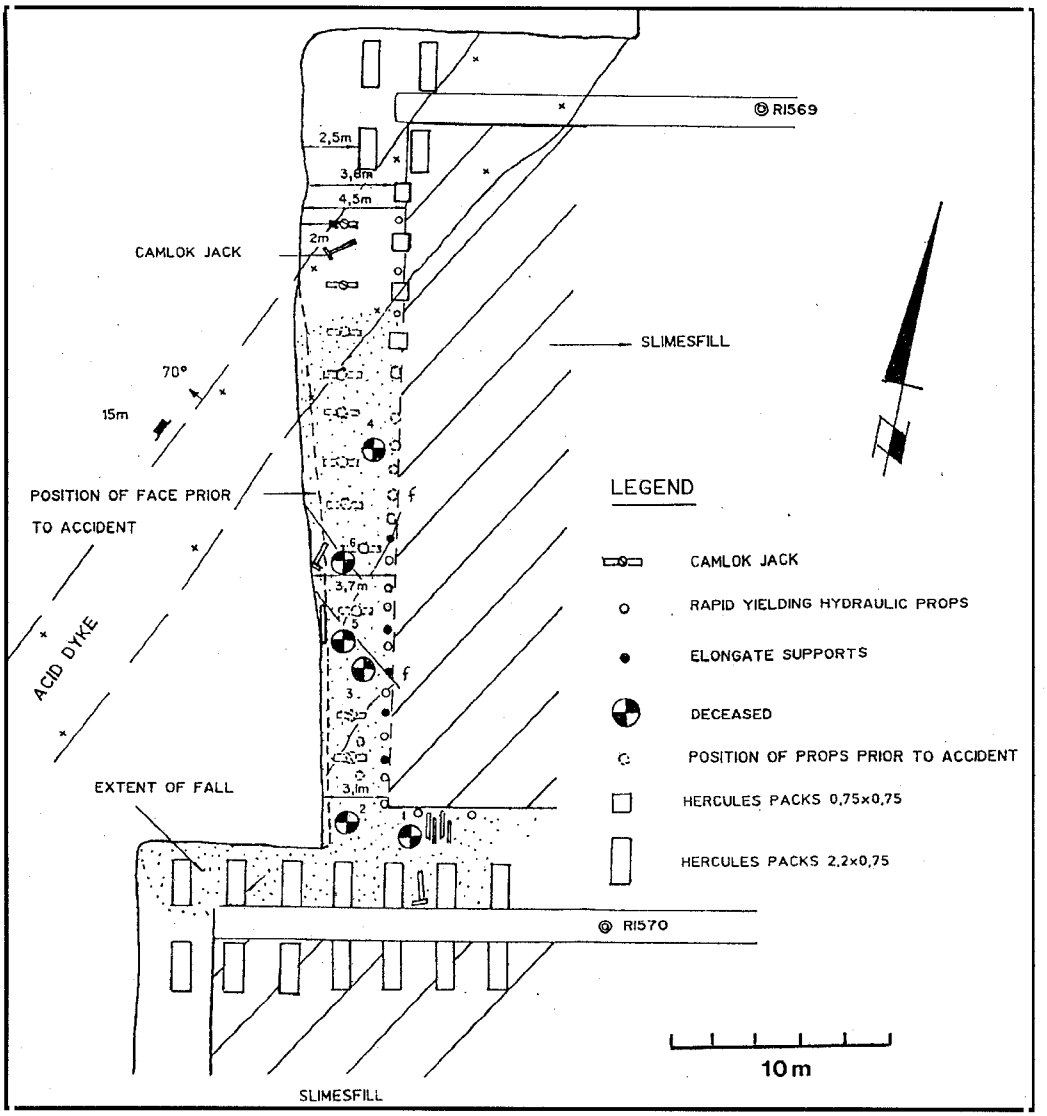

Figure B.15 Plan showing the support in the 113-36 West 3 Carbon Leader panel and the extent of the fall of ground during the rockburst of 3 November 1994.

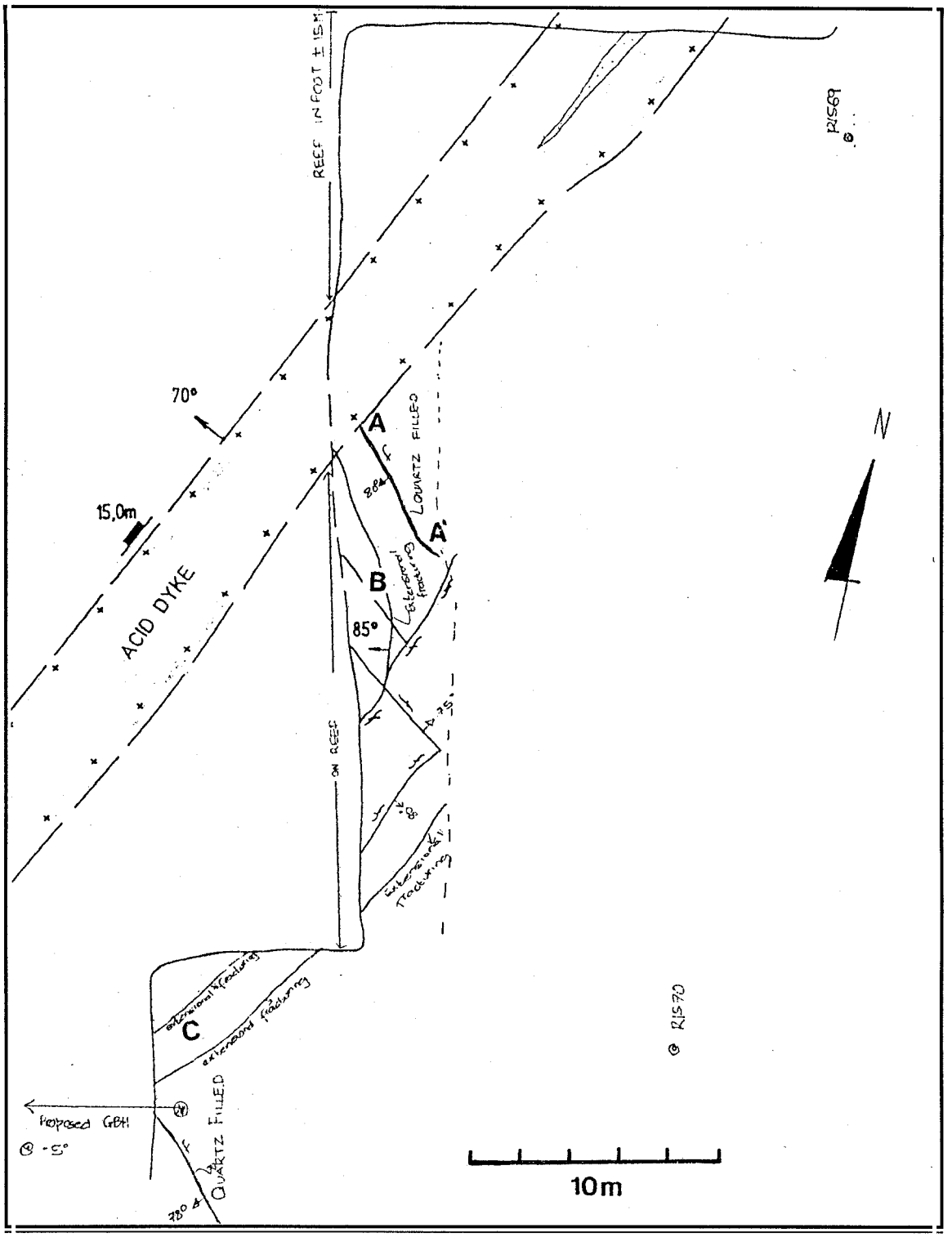

Figure B.16 Plan showing major fractures and joints in the 113-36 West 3 Carbon Leader panel (mapped by S. Reddy, Senior Geologist, Western Deep Levels (Ltd) West Mine).

A back analysis of the 113-36 longwall was carried out using MINSIM. The face positions at the time of the M_L=2,5 event were used in order to establish the energy release rate (ERR) associated with the working faces, excess shear stress (ESS) on the plane of the Acid dyke, and the major principal stress (SIG1). The results are summarized below.

At the time of the rockburst, the ERR was in the range 30-40 MJ/m^2 along most of the working faces, and approached 50 MJ/m^2 in the corners of the leads and lags. The acceptable upper limit of ERR for the CLR at Western Deep Levels Mine is considered to be 40 MJ/m^2 (Dr N. Gay, Mining Technology, personal communication).

High stresses (SIG1>500 MPa) were found up-dip of the strike gullies.

Very large ESS lobes (TAU1>10 MPa over 12000 m^2) were present on the plane of the Acid dyke.

A back analysis was also conducted of a rockburst which took place along the Acid dyke on 25 September 1993, resulting in six fatalities. In this instance, part of the shaft pillar was being mined. The results are summarized below.

At the time of the rockburst, the ERR was generally < 30 MJ/m^2 with a few localized areas in the range 40-50 MJ/m^2.

Extremely high stresses (SIG1>500 MPa) occurred along the faces.
ESS lobes were large (TAU1>10 MPa over 5000 m^2).

Strategies for mining through the Tarentaal dyke were evaluated using MINSIM-D modelling. The ERR, ESS and SIG1 values for each of the basic layouts were compared with those operating at the time of the rockburst on the Acid dyke. The Tarentaal dyke strikes N-S and dips to the east at 70°. The reef is downthrown to the west of the dyke by about 3 m. The results are summarized below.

Layout 1: Mining to continue with existing configuration, resulting in a face-parallel to the Tarentaal dyke (longwall orientation N-S).
ERR 20-40 MJ/m^2, which is within acceptable limits
High values of stress (SIG1>500 MPa) up-dip of strike gullies.

Relatively large ESS lobes on dyke plane (TAU1>10 MPa over 3000 m^2).

Layout 2: Right hand overhand (longwall orientation N30°E)
ERR generally < 30 MJ/m^2.
Very high values of stress (SIG1>500 MPa) up-dip of strike gullies owing to the large leads.
Relatively large ESS lobes (TAU1>10 MPa over 2000 m^2), similar in area to those obtained for Layout 1.

Layout 3: Left hand overhand (longwall orientation N30°W).
ERR generally < 20 MJ/m^2.
Stress more evenly distributed along face and the occurrence of localized high stress zone is minimized.
ESS lobes far smaller than Layout 1 and 2 (TAU1>10 MPa over 850 m^2).

The left hand overhand layout appears the most favourable of the options considered. After consultation with mine personnel the layout was modified slightly to facilitate mining operations.

3.6 Seismic history

The seismicity for the period 1 January - 3 November 1994 is shown in Figures B.16 and B.17. Two events with M_L>2 occurred close to the current position of the 113-36 W3 panel during this interval. A M_L =2,6 event occurred 60 m in the hangingwall on 4 January 1994, and a M_L =2,3 event occurred 60 m in the footwall on 14 April 1994. This would imply that the W3 panel was being mined close to a volume of rock where failure had previously occurred, which could account for some of the shear fractures observed in the W3 panel.

A M_L =3,2 event occurred on 9 February 1994 with its focus close to the Tarentaal dyke.

3.7 Rockburst mechanism

Source mechanism

An Integrated Seismic System (ISS) was installed on West Mine. The seismologist managing the ISS was A. G. Butler, who provided the information below.

The event occurring at 07h19 on 3 November 1994 was recorded by 12 remote stations ranging in distance from 440-3300 m from the damaged W3 panel. The focus of the M_L=2,5 seismic event was close to the western boundary of the mine and outside the mine seismic network, resulting in an uncertainty of +/- 40 m in the location (2,3 per cent of the average station distance). Nevertheless it is clear that the focus of the event was close to the Acid dyke, about 50-100 m down dip of the W3 panel, and close to the reef plane (see Figures B.14, B.16 and B.17 (*a, b*)).

The seismic source parameters were determined for the M_L=2,5 event by the ISS and are given in Table B.3. A slip-type source mechanism was determined by the ISS for the M_L=2,5 event. This contrasted with the crush-type mechanisms of most events occurring on the Acid dyke. The M_L=2,5 event was preceded (by a few milliseconds) by a much smaller event with a similar location.

Damage mechanism

The following factors are considered to have predisposed the W3 panel to severe damage, while panels closer to the focus of the event were unscathed:

The angle between the Acid Dyke and longwall is about 17°, which is considered unfavourable as faults and dykes are often accompanied by adjacent sympathetic features which can lead to friable ground conditions. An oblique angle of approach (>30°) is recommended to avoid exposing large contiguous areas of potentially weak or unstable ground (COMRO, 1988).

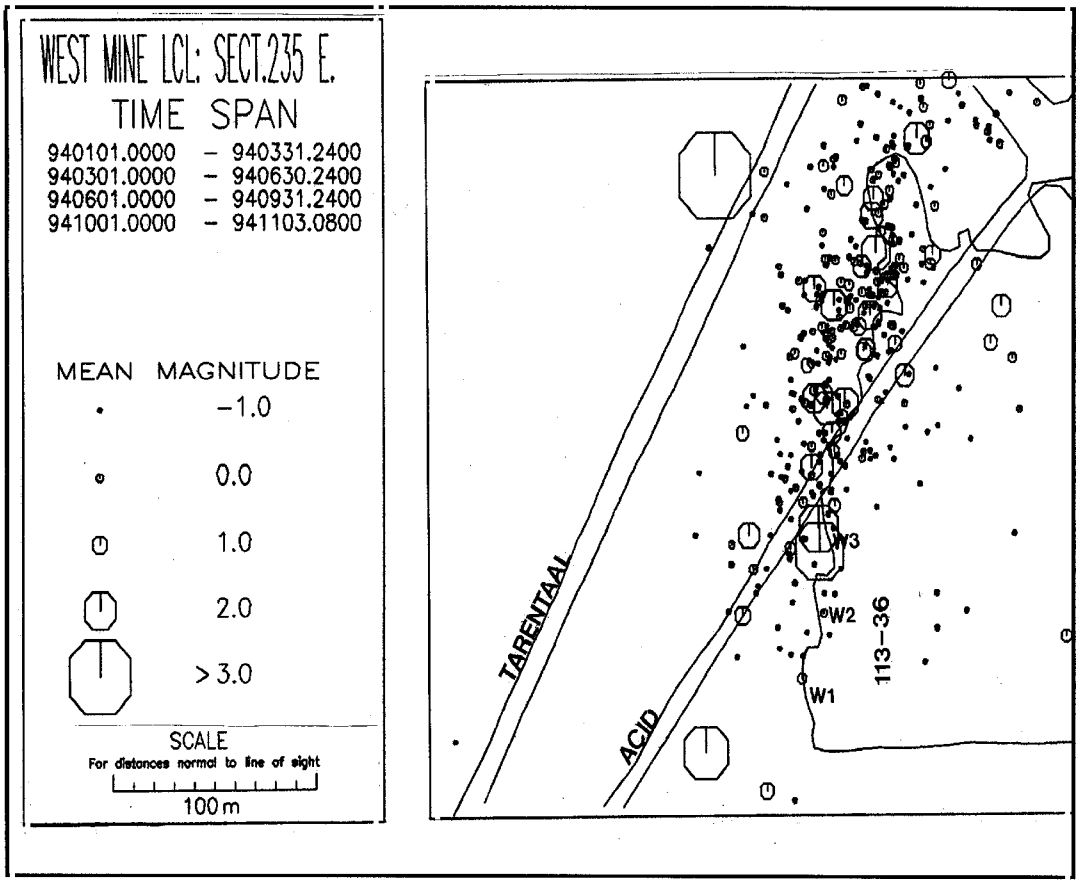

Figure B.17(a) Plan and section showing seismicity for the period 1/1/94 to 3/11/94 in the vicinity of the 113-36 Carbon Leader longwall. Face positions as at June 1994. Data provided by A. G. Butler (Senior Seismologist, Western Deep Levels (Ltd) West Mine). Note the M_L=2,3 and M_L=2,6 events close to the position of the W3 panel, and the M_L=3,2 event close to the Tarentaal dyke; (a) plan; (b) section.

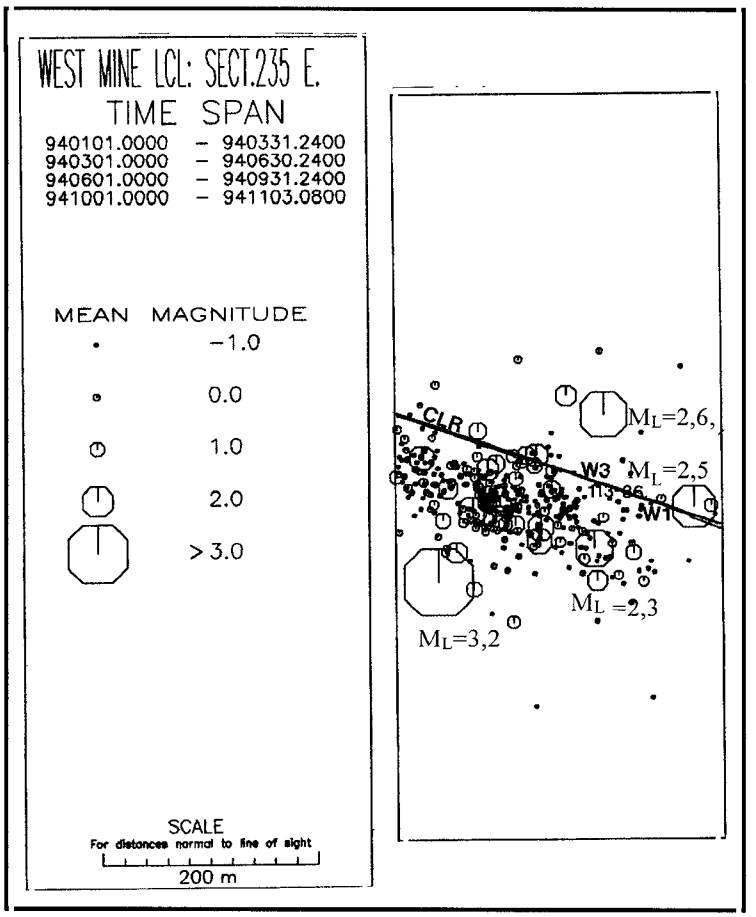

Figure B.17(b) Section from Figure B.17 (a) showing seismicity in the vicinity of the 113-36 Carbon Leader longwall.

The crushing of the face of the W3 panel to a granular texture is interpreted to indicate failure of the triangular quartzite wedge between the panel face and the dyke. The failure was probably initiated by the stress redistribution following the M_L=2,5 event. The fact that no face crushing had occurred in the W2 panel strongly indicates that geometrical considerations are important factors leading to the failure of the rock mass between the panel face and the dyke. The seismic event associated with the failure of the face/dyke wedge would probably have had a magnitude in the range M_L=0 to M_L=1, and the seismic signal would have been obscured by the M_L=2,5 event.

The hangingwall of the W3 panel was weakened by several sets of joints and fractures. The hangingwall of the W3 panel fragmented and collapsed owing to the dilation of the failed quartzite wedge and the effects of seismic shaking.

Table B.3

Source Parameters

Time:	7h 19m 1,95s on 3 November 1994		
Location:	29374 m S, -39454 m W, 3421 m down		
Local Magnitude	2,5		
EVENT SIZE			
Brune source radius	64 m	**Apparent volume**	0,35 x 10^6 m^3
MOMENT		**ENERGY**	
Seismic moment:	4,66 x 10^{12} Nm	**Radiated Energy**	1040 MJ
P Moment	3,45 x 10^{12} Nm	**P Energy**	12,9 MJ
S Moment	5,82 x 10^{12} Nm	**S Energy**	1010 MJ
Moment Magnitude	2,4	**Energy Magnitude**	2,8
S Moment/P Moment	1,7	**S Energy/P Energy**	78,7
		Energy Index	0,5 (rel. to CLR)
			1,2 (rel. to VCR & CLR)
STRESS		**CORNER FREQUENCY**	
Apparent Stress	6,70 MPa	**Corner Frequency**	31,8
Static Stress Drop	14,9 MPa	**P Corner Frequency**	35,2 Hz
Dynamic Stress Drop	14,7 MPa	**S Corner Frequency**	28,2 Hz

3.8 Conclusions

The seismic history of mining near the Acid dyke shows that it is rockburst prone.

The M_L=3,2 event recorded on the Tarentaal dyke indicates that this dyke is probably also rockburst prone and should be approached with extreme caution.

The quartzite wedge between the Acid dyke and face of the W3 failed, probably in reponse to the M_L=2,5 slip event occurring on the Acid dyke. The size and geometry of the wedge is thought to have been critical.

Several sets of joints, partings and mining-induced extension and shear fractures occur in the W3 panel.

Previous seismic events along the Acid dyke may have caused the rock mass in the W3 panel to be exceptionally fractured prior to the rockburst.

The small angle between the longwall and the Acid dyke is thought to be an important factor contributing to the rockburst damage in the W3 panel, as faults and dykes are often accompanied by adjacent sympathetic features which can lead to friable ground conditions.

The hangingwall of the W3 panel fragmented and collapsed owing to the dilation of the failed quartzite wedge and seismic shaking.

The single row of props and poles situated against the backfill did not give adequate support to the 1 m thick hangingwall slab. The presence of a row of rockburst resistant hydraulic props with load spreading headboards between the face and backfill would probably have limited the damage.

The uncemented backfill was generally well placed. However, the gap between the backfill and gully packs contributed to the fallout between the packs.

3.9 Recommendations

The mine should develop a layout strategy to mine in the proximity of geological discontinuities such as dykes and faults. Back analyses of past rockbursts using ESS and ERR should provide empirical design criteria. For example, the use of a bracket pillar to clamp the structures should be considered.

The angle between the longwall and the dyke should also be carefully considered. Experience shows that an angle greater than 30° along the entire longwall is desirable.

Preconditioning of the dyke should be considered.

Two rows of hydraulic props with load-spreading headboards should be used between the backfill and the face to give a better areal coverage in the face area. An unsupported span of 3 m between face and backfill should be avoided.

It should be ensured that the backfill bags are large enough to tightly fill the stope.

Backfill should be extended to the gully packs. This would increase the filling by about 5 per cent and reduce the potential for falls of ground between the gully packs.

The following mining strategy was recommended based on the results of the back analysis and MINSIM modelling:

- Mining on the W1, W2 and W3 panels of the 113-36 longwall should be discontinued to create a bracket/stabilizing pillar around the Acid and Tarentaal dykes.
- The left hand overhand layout modified by mine personnel should be adopted. This layout gives an optimal angle between the longwall and the dyke.
- Leads and lags should not exceed 5 m to prevent the creation of highly stressed pieces of ground.

4 Buffelsfontein, 4/7/95, M_L=3,4

4.1 Introduction

On 4 July 1995 a M_L=3,4 seismic event caused significant damage to tunnel excavations within the immediate vicinity of the Orangia shaft pillar at Buffelsfontein Gold Mine and fatally injured one worker. A visit was conducted on 4 December 1995 to assess the rockburst damage to these tunnel excavations and the performance of the support systems. The damaged areas had been abandoned since the rockburst, and mine personnel reported that there had been no significant change in the state of these areas in the intervening months. Observations concentrated on tunnels on 24 level, at a depth of approximately 2221 m below surface, as shown in Figure B.18.

4.2 Mining environment

Extraction of the reef in the shaft pillar is complex owing to the presence of large normal faults, dykes and thrust faults parallel to the bedding plane. This results in complex extraction sequences and associated complex stress histories and seismicity on tunnel excavations in close proximity to the reef plane. During the initial phases of the extraction of the Orangia shaft pillar, a series of seismic events with magnitudes M_L>2,0 occurred over a two year period, culminating in this event. Much of the seismicity was associated with the Station dyke, which comprises a large proportion of the shaft pillar. Consequently many of the tunnel excavations in the immediate shaft area were developed within the dyke.

Typical tunnel support systems utilised in this area comprised of 3 m x 16 mm shepherds crook smooth bar on a 1,0 m x 1,0 m pattern with mesh (100 mm weld) and lacing (10 mm).

The sections of the 24 level tunnels that were inspected were sited either in the Station dyke, which has an epidiorite composition, or in the MB5, a quartzite formation which lies in the footwall of the reef horizon.

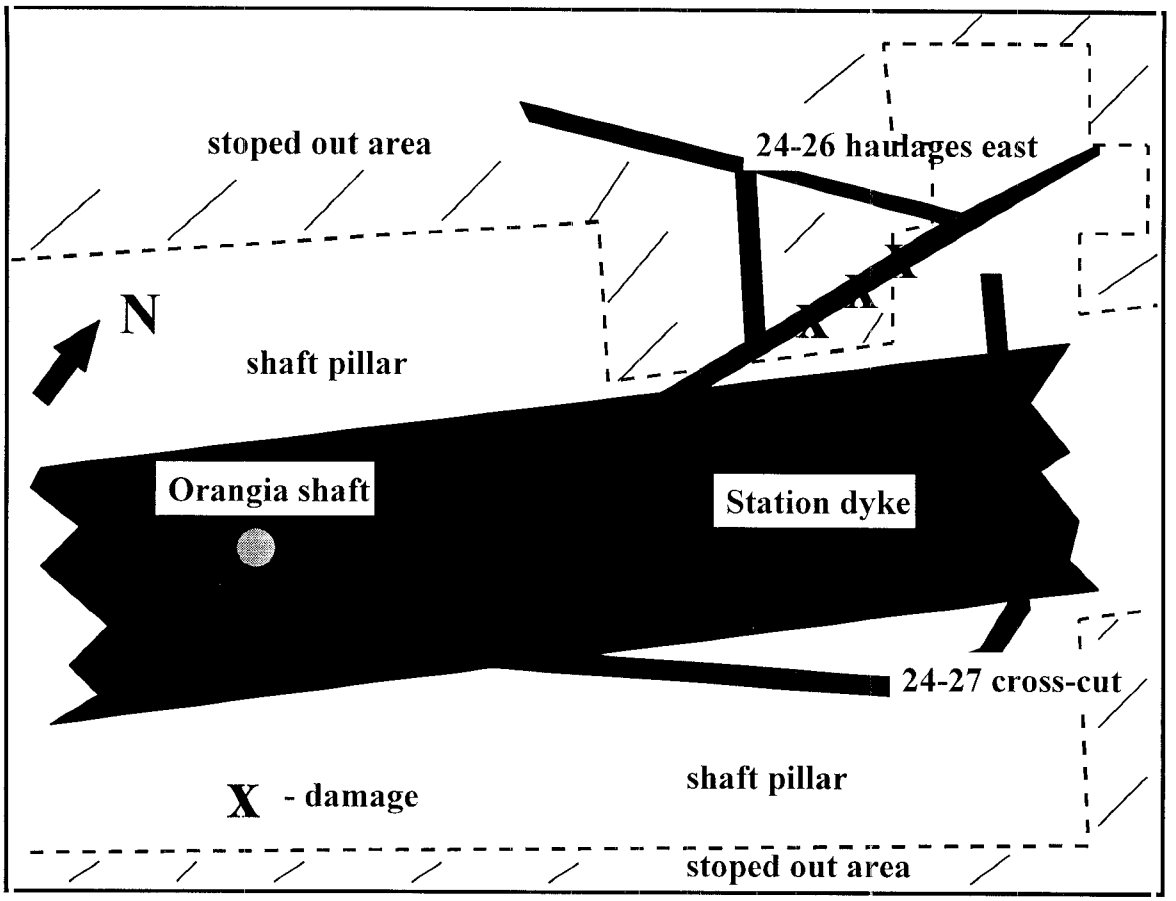

Figure B.18 Schematic plan of 24 level tunnels, Orangia Shaft, Buffelsfontein Gold Mine, damaged by the M_L=3,4 rockburst on 4 July 1995.

4.3 Observations at the rockburst site

Orangia Shaft, 24 level station area

Tunnels in the immediate shaft area were characterised by highly fractured side- and hangingwalls, and a large amount of deformation, indicating a history of high quasi-static or dynamic stress. A significant amount of footwall heave, 1,0-1,5 m, was also observed in this area. Footwall heave could either have been a result of direct failure and bulking of the footwall strata, or owing to large sidewall deformations causing buckling and shear of the fractured footwall rock mass and track ballast.

24-26 haulages east

Detailed observations of damage were made within the main 24-26 haulages east, close to the boundary of the shaft pillar and in close proximity to current shaft pillar stoping operations. The tunnels were developed with typical square profiles with minimum design dimensions of 3,0 m x 3,0 m. Damage to these excavations, sited in MB5 footwall quartzite close to the western contact of the Station Dyke, was extensive over a distance of approximately 60 m. Observations of tunnel damage in this area indicated large overall sidewall deformations, particularly on the east side of the excavation (Figure B.19).

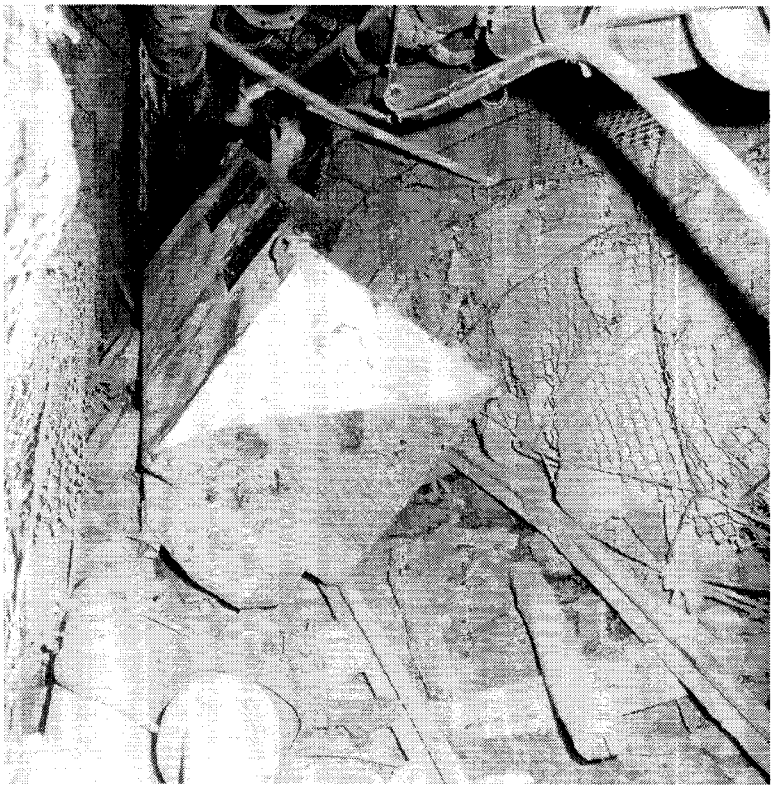

Figure B.19 View north along 24-26 haulages east showing severe damage and deformation of the eastern sidewall of the tunnel. Note displacement of tracks (bottom right) and material rail car.

Immediately to the north of this damage site, deformation of the tunnel had resulted in its complete closure. At this point direct observations of the performance of the rock bolt reinforcement could be made. Within the highly fractured and bedded rock mass, significant shear deformation of the smooth bar rock bolts was observed (Figure B.20), as well as tensile failure (Figure B.21).

Figure B.20 Shear deformation of smooth bar rock bolt in upper east sidewall of 24-26 haulages east.

Figure B.21 Tensile failure of a smooth bar rock bolt in the immediate hangingwall of the 24-26 haulage east.

Further observations of damage to the 24-26 haulages east were conducted from the north side of the fall of ground. In this area significant damage was associated with the hangingwall of the excavation. Total collapse had occurred, and it was possible to gain access above the fall of ground (Figures B.22 and B.23). Although specific failures of rock bolts were not observed here, the density of the remaining hangingwall rock bolt support was low (Figure B.22), and thus the hangingwall profile may essentially be considered to be self supporting in this area and the remaining rock bolt units may be considered to be anchored within the stable rock mass. The estimated height of collapse, which corresponded approximately to the depth of the hangingwall instability, was about 1,5 m to 2,0 m.

24-27 cross-cut

This excavation traverses the Station dyke within the shaft pillar area and was developed for the purposes of accessing reef for stoping of the shaft pillar. Rockburst damage within this excavation was primarily the general large deformation of the sidewalls of the excavation (Figure B.24).

The deformation of the sidewall again indicated the increased deformation associated with the lower portion of the sidewall. In this area the extent of deformation resulted in some damage to the mesh and lacing fabric support where differential deformation within the sidewall profile had occurred. The integrity of the support system and profile of general displacement of the sidewall rock mass maintained the stability of the excavation with regard to safety. Areas of failure of the fabric support may be indicative of localised differences in the interaction of the support system with the rock mass, resulting in different deformation response, and thus differential deformation with resultant increased strain within the fabric.

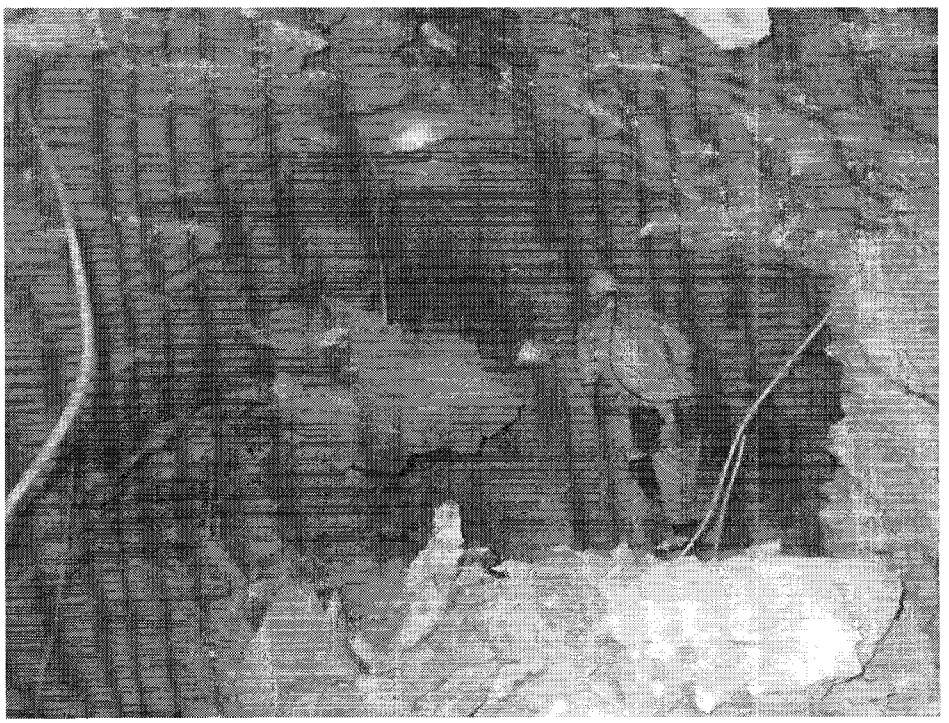

Figure B.22 View south along 24-26 haulages east showing collapse of hangingwall over an estimated height of 1,5 m to 2,0 m.

Figure B.23 View south along 24-26 haulage east at end of area of hangingwall collapse showing the highly fractured nature of the immediate hangingwall rock mass, and remaining rock bolt reinforcement.

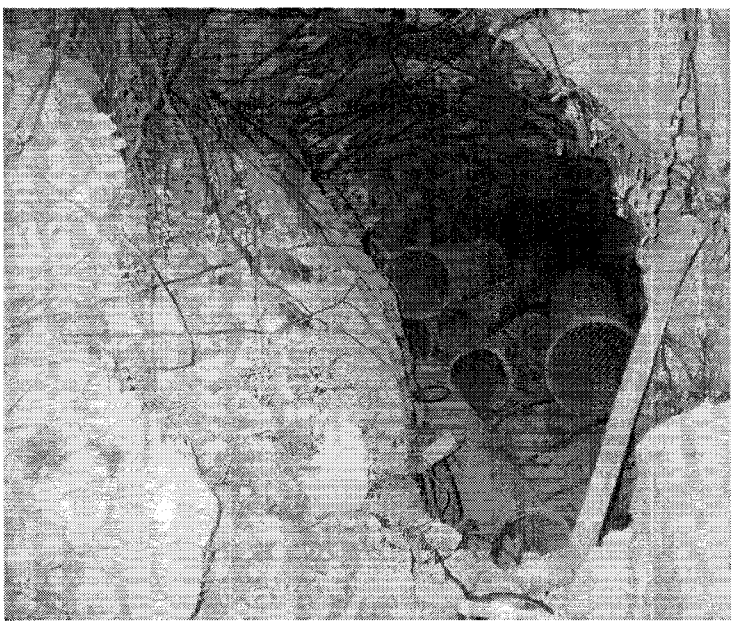

Figure B.24 View north-west along 24-27 cross-cut showing large deformation of the south-west sidewall of the tunnel.

4.4 Assessment of support performance

Interpretation of tunnel sidewall profiles

The large, generally uniform deformation of the sidewall of the 24-26 haulages east and 24-27 cross-cut may indicate either: the loss of anchorage of the rock bolt reinforcement, owing to snapping or debonding of the bolts, or the depth of instability of the rock mass around the tunnels is in excess of the rock bolt length.

This uniform deformation profile is in contrast to that exhibited by a stiff support system anchored in stable ground, which generally shows greater differential deformation and bulking over the sidewall profile (Figure B.25). With regard to safety, a more uniform deformation of the sidewall rock mass structure is preferable, as the general integrity of the support system and peripheral rock mass is more likely to be maintained.

It was noted the deformation was greatest in the lower part of the sidewall. This may be owing to the presence of dominant sub-horizontal bedding planes and the lack of lower sidewall support. The presence of hangingwall support, together with the general upward inclination of the upper sidewall support, creates a more competent reinforced rock mass structure and thus constrains the upper part of the sidewall more effectively.

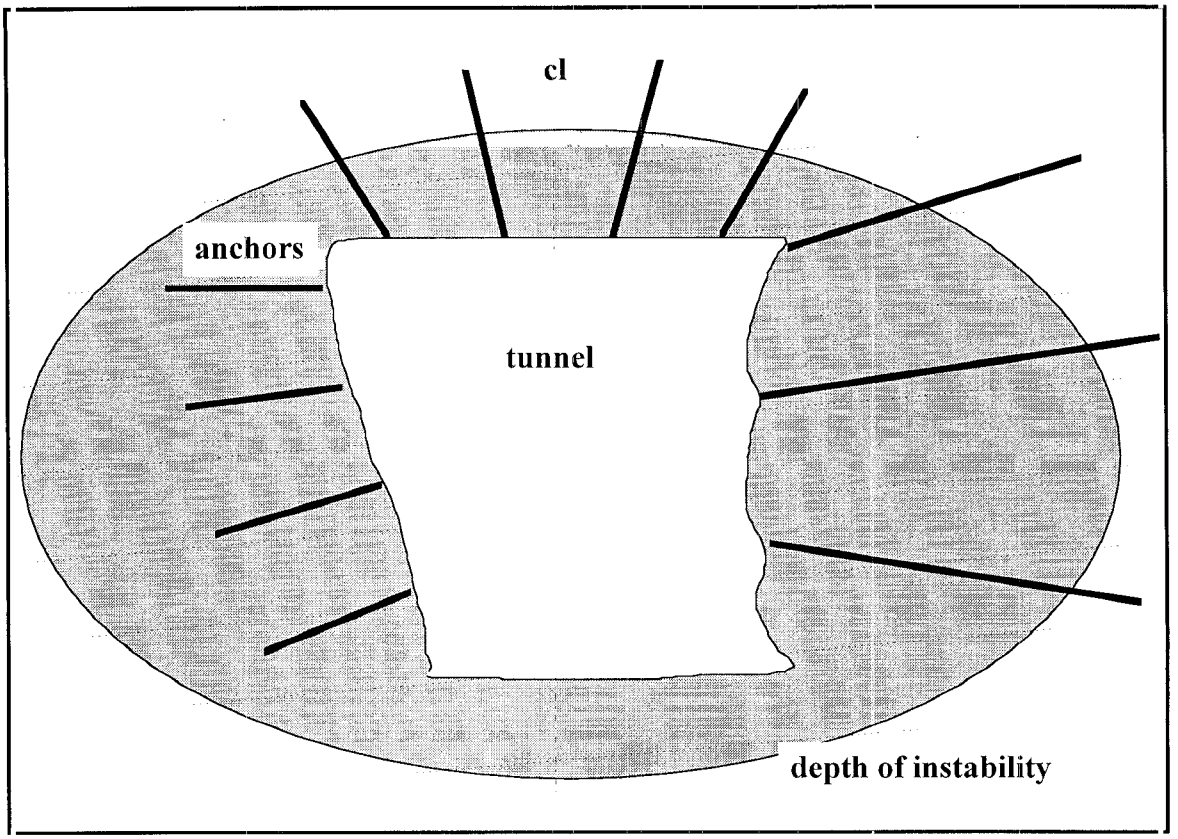

Figure B.25 Diagram showing conceptual mechanisms of excavation deformation as a function of support interaction with the rock mass. Within the South African gold mining environment the vertical virgin stress level is approximately twice that of the horizontal, and induced stresses are generally sub-vertical, the depth of failure within the sidewalls of the excavations is substantially greater than in the hangingwall or footwall. The tendons on the left hand side of the tunnel are anchored within the zone of instability, hence the entire sidewall is displaced inwards owing to bulking of the unstable rock mass. A similar effect will be observed if the tendons snap or debond. In contrast, the tendons on the right hand side of the tunnel remain anchored in solid rock, hence the sidewall bulks between the tendons.

Breaks in support

The presence of a ventilation wall within the 24-26 haulages formed a discontinuity within the mesh and lacing fabric support system, resulting in localised damage. This is attributed to the decreased containment and thus increased degree of freedom of the rock mass at this point under the dynamic loading conditions.

Rock bolt / rock mass interaction

The rock bolts were able to accommodate relatively large shear deformations owing to the highly discontinuous nature of the rock mass. This allowed numerous incremental shear dislocations along the rock bolt length, each within the shear capacity, and debonding of the rock bolt system; and result in reduced interaction between the rock bolt and the general rock mass. Based on the general observations of the exposed rock bolt reinforcement in the area, shear deformation within the rock mass was more prevalent in the hangingwall of the excavation.

Where the rock mass was more massive, direct interaction between the rock bolt and the rock mass may have resulted in failure of the rock bolt unit, particularly under dynamic loading conditions. Figure B.21 indicates that although significant debonding along the length of the rock bolt had occurred, anchorage of the rock bolt within the stable rock mass was sufficient to cause tensile failure.

4.5 Rockburst mechanism

Stress history

This section of the 24-26 haulages east which had sustained severe damage had been subjected to a more complex quasi-static stress history compared to other areas within the shaft pillar, as a result of the history of stoping activities approximately 65 m above the tunnel elevation.

These activities would certainly have resulted in a higher sub-vertical field stress, causing an increased tangential stress level in the peripheral rock mass of the excavation, with an associated increase in rock mass damage. This localised deterioration of the rock mass owing to the quasi-static stress environment resulted in the excavation being more prone to rockburst damage.

Damage mechanism

The general mechanism of hangingwall stabilisation by the support system is considered to be primarily that of rock mass containment by anchorage outside of the limit of instability. The failure of the support system in the 24-26 haulage east area appears to be owing to the failure of the mesh and lace fabric support and a general unravelling of the rock mass from the rock bolt reinforcement (Figure B.22 and B.23). The highly fractured nature of the rock mass appears to have resulted in poor interaction of the rock bolt reinforcement in the immediate hangingwall, leading to increased direct loading of the mesh and lacing fabric support system. The relatively stiff nature of the smooth bar support under conditions of end anchorage will result in differential deformation of the rock mass between the rock bolt and the mesh and lace, where stiffness relatively low, that will result in a further weakening of the inherent rock mass strength and lower rock bolt interaction. Under dynamic loading conditions it is considered that the kinetic energy associated with this unstable rock mass volume was in excess of the capacity of the mesh and lacing fabric support panels, between the points of anchorage to the relatively stiff rock bolt containment.

4.6 Conclusions

Mechanisms of tunnel excavation stability and the performance of the support systems associated with the quasi-static stresses and history of seismic events within the Orangia shaft pillar may be summarised as follows:

Large deformations were associated with the sidewalls of tunnels. The deformation profile was generally uniform, indicating bulk movement of the sidewall and support system. The depth of instability is considered to be generally in excess of the length of rock bolt reinforcement.

The lack of lower sidewall and footwall constraint results in a potential weakness within the support system / rock mass structure and resultant increased deformation of the lower sidewall and footwall heave.

Shear deformation may be associated with the hangingwall rock mass of tunnels although the highly discontinuous nature of this rock mass generally does not result in shear failure of the rock bolt reinforcement.

The depth of instability within the hangingwall of the tunnel excavations (3,0 m x 3,0 m) is estimated at 1,5 m to 2,0 m. Thus hangingwall stabilisation is based on anchorage of the rock bolt reinforcement and containment of the potentially unstable rock mass by mesh and lace fabric support systems of sufficient capacity.

4.7 Recommendations

Use rock bolts with high shear capacity in the hangingwall of the excavations.

Increase the capacity of fabric (mesh and lace) and attachments to rock bolts (with sufficient yield) where rock mass stabilisation is a function of "containment".

Design tunnel support on the basis of the depth of the zone of rock mass instability and a mechanistic evaluation of support/reinforcement interaction.

5 ERPM, 24/7/95, M_L<0,5 and 15/8/95, M_L=0,9

5.1 Introduction

On 24 July 1995 a rockfall occurred at East Rand Proprietary Mine (ERPM), damaging the secondary incline of the Hercules shaft between 32- and 33-level, about 1500 m below surface (Figure B.26). The rockfall, which fatally injured four workers, took place at 01h45. No seismic event was recorded by the seismic network at this time, although the subsequent investigation led to the conclusions that the rockfall was associated with a small seismic event. Mr P. Mitchell (Rock Mechanics Manager, ERPM) requested that a team from CSIR Mining Technology investigate the rock engineering aspects of the incident.

The aim of the investigation was to determine the cause of the rockfall in order to prevent future occurrences. The site was visited on 26 July 1995. A draft report (dated 7 August 1995) containing an analysis of the rockfall was submitted to ERPM on 8 August 1995.

Following the rockfall, the task of installing support in the shaft between 32- and 33-levels was contracted to Shaft Sinkers. A CSIR ground motion monitor (blackbox) was installed on 8 August 1995 near the site of the rockfall. A second rockfall occurred on 15 August 1995 at 22h09, causing injuries to workers installing support in the incline shaft. A seismic event of local magnitude M_L=0,9 was detected by the mine seismic network at this time. The event was also recorded by the ground motion monitor. The site was visited on 18 August 1995 by CSIR staff.

5.2 Mining environment

The upper part of the Hercules secondary incline shaft is about 10 m wide and 3 m high, and dips to the south at 45°. At the 32- to 33-level the incline shaft is situated about 3 m below the composite Main Reef and Main Reef Leader. The rockfall site is about 150 m from the Hercules vertical shaft. Mining within 100 m of the rockfall site last took place

more than 70 years ago. The stoping height of the composite reef is believed to be less than 2 m.

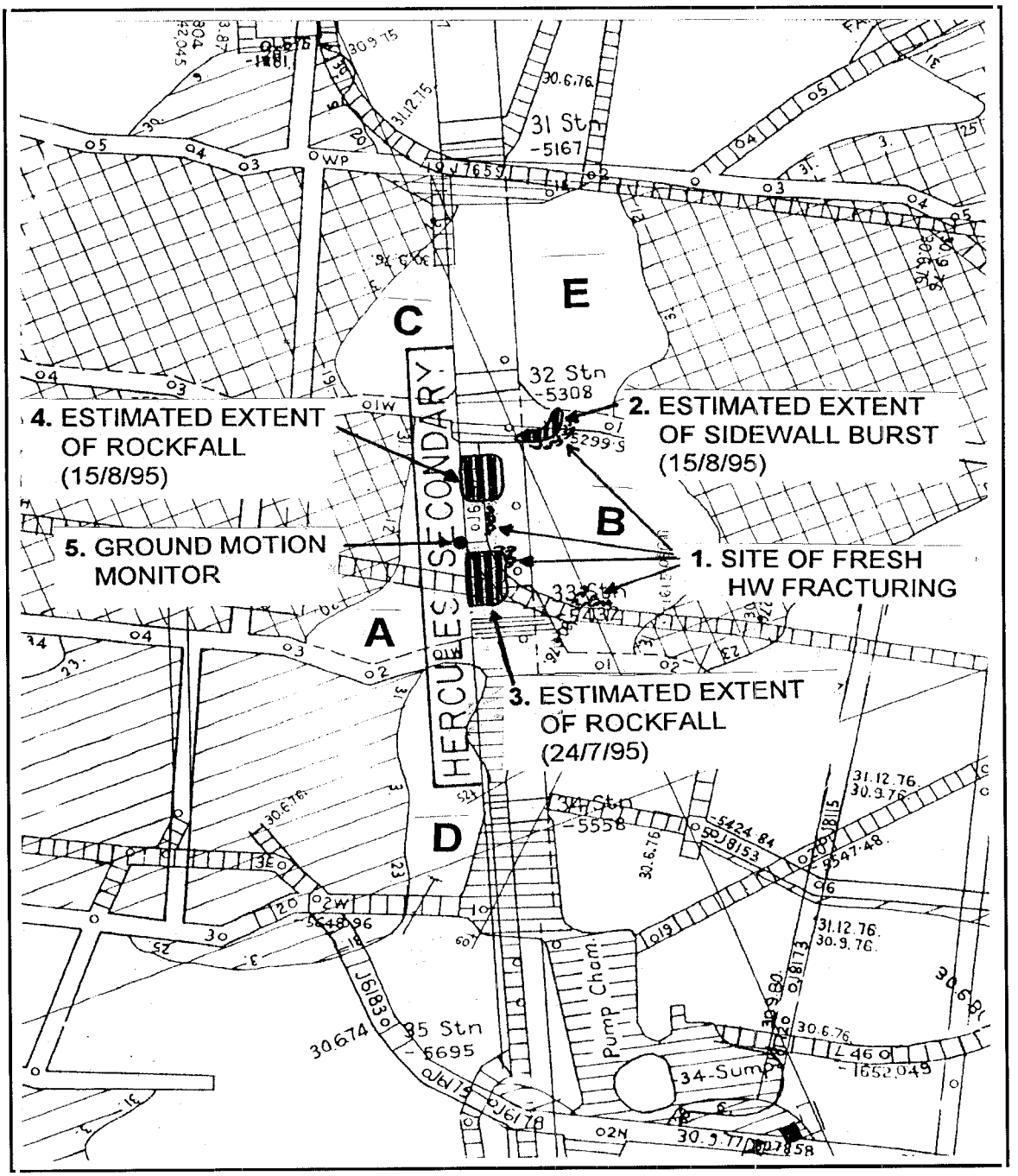

Figure B.26 Plan showing the location of the rockfalls at ERPM on 24 July and 15 August 1995 damaging the Hercules secondary incline shaft between 32- and 33-level.

A 20 m wide dyke lies roughly parallel and 80 m to the west of the incline shaft. Stoping to the west of the dyke last took place in the 1970's. The distance between this stoping and the rockfall site is 120 m at the nearest point. Following several rockbursts, it was decided that no further stoping should be carried out within 300 m of the Hercules vertical shaft. Further stoping commenced in 1995 on 38 level, about 200 m from the accident site.

The secondary incline shaft was being rehabilitated at the time of the rockfall on 24 July 1995. The rock mechanics department had previously noticed that a deterioration in the condition of a section of the incline shaft. Cracks had been noted in the concrete lining on the west side of the shaft, and several falls of ground had occurred. The following remedial measures were implemented: barring down of loose rock, Installation of new timber sets, and Installation of 9 m cable anchors.

Following the rockfall of 24 July 1995, the task of installing support in the shaft between 32- and 33-levels was contracted to Shaft Sinkers. The following remedial measures were then implemented: barring down of loose rock, Installation of shepherd's crooks, cable lacing and wire mesh, Installation of new steel sets (RSJ girders at 1 m spacing, sets tied together), and Installation of 6 m cable anchors.

The seismic event on 15 August 1995 caused damage both to the incline shaft and the 32-level station.

5.3 Observations at the rockburst site

Rockburst damage

The first rockfall took place at 01h45 on 24 July 1995. A small rockfall had occurred earlier, causing a minor injury to a worker. It is believed that the rehabilitation team had just returned to the working place and were preparing to install a cable anchor into a previously drilled hole when the event occurred. The rockfall took place midway between the 32- and 33-level stations. Owing to dangerous conditions in the incline shaft it was difficult to determine accurately the dimensions of the fall of ground. It appeared that about 0,5 m of the hangingwall had collapsed over the entire 5 m width of the conveyance

section of the incline shaft. A steeply dipping fracture marked the up-dip limit of the the fall of ground. The hangingwall was blocky and irregular, with fresh fracture surfaces present. Separation had not taken place along a bedding plane.

The support installed in the inclined shaft consisted of steel and timber sets. Apparently the bulging of the western wall of the incline shaft had caused the legs of the sets to be kicked out at the time of the rockfall. The concrete siding on the west side of the inclined shaft was broken in several places. Apparently fractures had developed over a period of several weeks prior to the rockfall. Squeezing of the steel girders across the shaft hangingwall was also noted. It was reported that this had also taken place over a number of weeks.

The second rockburst took place at 22h10 on 15 August 1995, some 3 weeks after the rockfall described above. Injuries were sustained by some of the workers installing support in the incline shaft. The site of this fall was just below the 32-level station, with some damage also occurring in the 32-level station area. The damage appeared very similar to the fall of 24 July 1995, in that large volumes of freshly broken rock fall into the incline immediately below the point where the new support had been installed. The area around the toilets in the 32-level reef drive (**2** in Figure B.26, inspected on 26 July) had burst into the excavation. The hangingwall of the shaft above 32-level exhibited damage in the form of fresh cracks and small areas of freshly exposed rock. Some squeezing of the sets was also apparent. Some damage to the hangingwall of the 32-level station was noted. A cracked concrete wall in the 32-level station area provided proof that convergence had occurred.

Mining-induced fractures

The 32-level cross-cut and hangingwall drive were inspected following the rockfall of 24 July 1995, and several freshly exposed fracture surfaces were noted. As these tunnels were not in regular use, it is not known whether these fractures formed prior to the rockfall or at the time of the fall. The dimensions of the freshly exposed surfaces ranged from 10 cm x 10 cm to 1 m x 1m. Slabs 1-2 cm thick had spalled from the sidewall. The surfaces were glassy, with sharp angular grains still adhering to the surface. These surfaces bore no trace of rusty staining, which was otherwise ubiquitous.

The 32-level cross-cut, which lies immediately above the rockfall site, was inspected. The drive is about 15-20 m above the rockfall site. Several freshly exposed fracture surfaces were noted on the upper sidewall on the eastern side of the cross-cut. The 32-level hangingwall drive to the east of the cross-cut was inspected. Freshly exposed fracture surfaces were observed on the upper sidewall on the northern side of the drive within 10 m of the cross-cut/drive junction. The 32-level hangingwall drive was inspected to the west of the cross-cut as far as the dyke. No freshly exposed surfaces were observed over this 80 m section. There was no evidence of recent movement along the contact between the dyke and country rock. Freshly exposed fracture surfaces were also observed near toilets in a reef drive to the east of the 32-level station.

Following the rockburst on 15 August 1995, the 32-level hangingwall drive to the east of the cross-cut was inspected again (see 1 in Figure B.26). Further freshly exposed stress fracture surfaces were observed on the upper sidewall on the northern side of the drive within 10 m of the cross-cut/drive junction, indicating a further increase in stress on Pillar B.

5.4 Seismic history

During the 6 years preceding the rockfall, 108 events (with M_L>0,5) had been recorded in the 1 km x 1 km area centred on the Hercules shaft. No events were recorded in the 5 months prior to the rockfall, the most recent event being a M_L=0,9 event on 26 February 1995.

5.5 Rockburst mechanism

A Portable Seismic System (PSS) is installed on ERPM. No seismic events were recorded in the vicinity of the Hercules shaft at the time of the rockfall. However, the Hercules shaft area is remote from the seismic network. The nearest geophone station is about 1 km from the rockfall site. An inspection of the seismic history indicated that only events occurring in the vicinity of the Hercules shaft with M_L>0,5 would be recorded. It

was reported that audible microseismic activity was noted prior to the rockfall, and on visits to the site after the rockfall. It was reported that the banksman heard a seismic event at the time of the rockfall.

The following rockburst mechanism is proposed (see Figure B.27).

The pillar to the west of the incline shaft was 8-10 m wide between 32- and 33-level (pillar marked **A** in Figure B.26). This pillar had gradually lost its capacity to bear load in the months preceding the major rockfall, probably owing to the evolution of stress fractures around the incline shaft and stope, exacerbated by any barring away of the hangingwall in the incline shaft adjacent to the pillar. This would tend to weaken the pillar by increasing the height to width ratio.

The fracturing within the pillar caused dilation, which buckled the strata over the incline shaft downwards. This buckling caused the hangingwall to become unstable, and minor rockfalls to occur.

The position of fractures observed in the 32-level cross-cut and drive are consistent with increased load being placed on the 22-30 m wide pillar to the east of the incline shaft (**B** in Figure B.26) as pillar **A** failed or partially failed, and stress was transferred across the incline.

The rockfall was triggered by the failure or partial failure of pillar **A**. This probably gave rise to a small seismic event (with M_L<0,5) which produced some shaking. Dilation of the pillar caused damage to the concrete sidewall of the incline shaft, caused the sets to collapse by pushing out their legs, and initiated new fractures in the hangingwall. The fall of ground followed.

A ground motion monitor was installed in the 32-level cross-cut on 8 August 1995 (see 5 in Figure B.26). A total of 19 seismic events were recorded in the interval 8-31 August 1995, including a large event at the time of the rockburst on 15 August 1995. A seismic event with M_L=0,9 was recorded on the mine seismic network at the time of the rockburst on 15 August 1995. The accelerograms clearly showed that the seismic sources were located within a distance of 15 m to 50 m from the monitor, strongly suggesting that the pillars were the source of the seismicity (most probably pillar **A** in Figure B.26).

The disposition of the rockfall and the seismicity recorded by the ground motion monitor indicate continuation of the failure of the narrow pillar to the west of the incline shaft (pillar **A** in Figure B.26).

5.6 Conclusions

The first rockfall (on 24 July 1995) was triggered by the failure of the narrow pillar to the west of the shaft (pillar **A** in Figure B.26).

The barring of unstable rock from the hangingwall of the incline shaft adjacent to the pillar during resupporting had the effect of increasing the height to width ratio of the pillar. This would have had the result of weakening the previously stable pillar. As pillar **A** progressively failed, the load was transferred to adjacent pillars (such as pillar **B** in Figure B.26). Evidence for the increase in stress is provided by fresh stress induced fractures observed in the hangingwall drive (see **1** in Figure B.26).

The progressive failure of pillar **A** resulted in the horizontal dilation of both the hangingwall and in the footwall of adjacent strata, causing the hangingwall beam of the incline shaft to buckle and ultimately to collapse. It is possible that the collapse was triggered by a small seismic event with magnitude M_L<0,5. A similar phenomenon had previously been noted by M.K.C.Roberts (CSIR Mining Technology) in bord and pillar workings, where underdesigned pillars progressively failed and dilated, causing the hangingwall to deflect and collapse into the bord.

The second rockfall (on 15 August 1995) and the seismicity recorded by the ground motion monitor indicate continuation of the failure of the narrow pillar to the west of the incline shaft (pillar **A** in Figure B.26). The sidewall burst of pillar **B** east of the incline (at **2** in Figure B.26) is further evidence that stress was being transferred to the pillars to the east of the incline shaft.

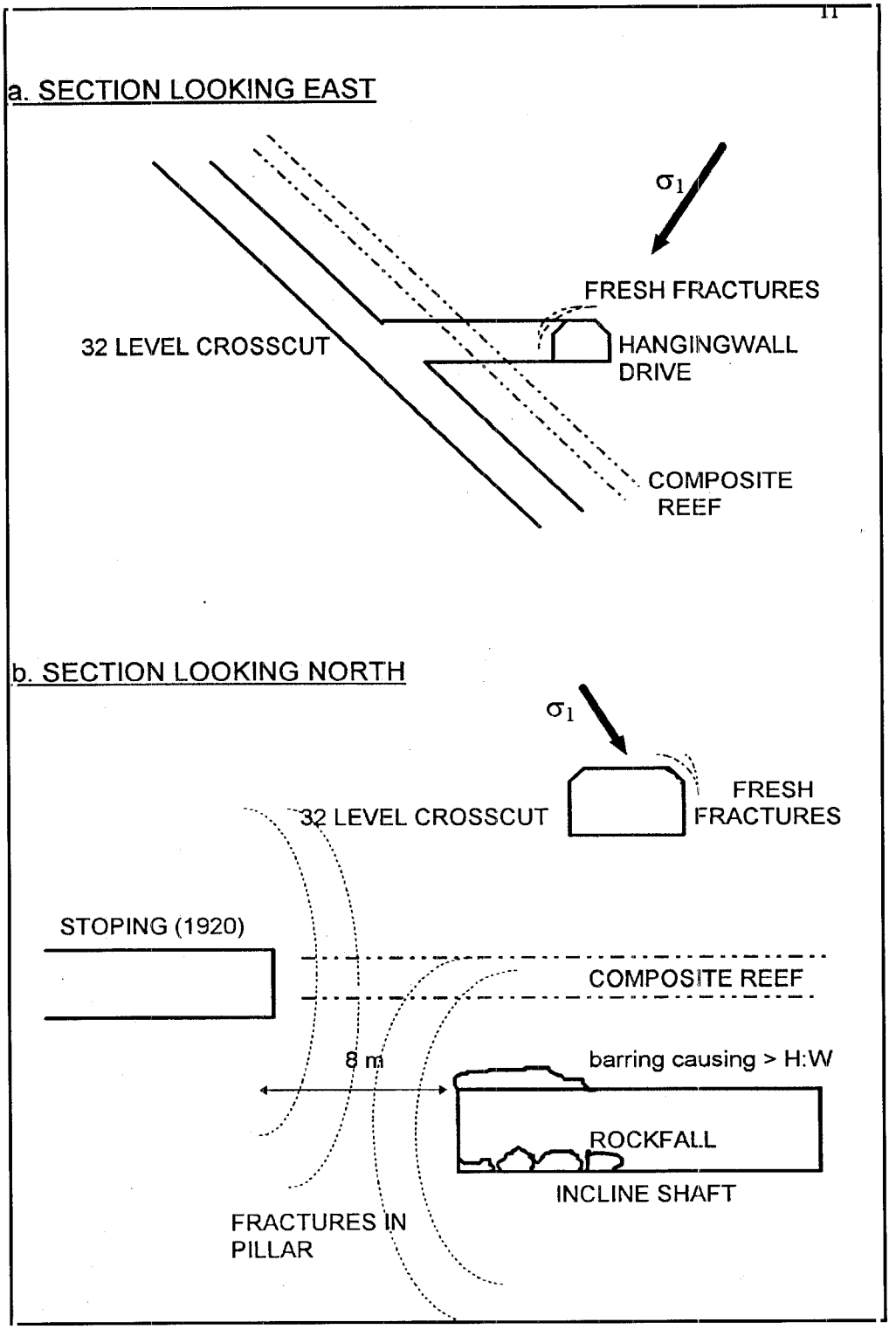

Figure B.27 Diagram showing the interpreted mechanism of the rockbursts on 24 July and 15 August 1995 damaging the Hercules secondary incline shaft between 32- and 33-level.

5.7 Recommendations

Similar narrow pillars were identified elsewhere in the incline shaft. As the transfer of stress from one pillar to another is a time dependent process, seismicity could occur in the future, particularly if further rehabilitation work is carried out. The following precautions were recommended:

Identify situations where the pillar abutting the incline shaft is narrow *e.g.* between 33- and 34-level of Hercules secondary incline shaft, marked **D** in Figure B.26. Extensometers may be used to establish whether dilation of the pillar is taking place.

Microseismicity in the vicinity of the narrow pillars should be monitored. The CSIR ground motion monitor may prove useful for this purpose. It can detect events with M_L>-1,5 which occur within 50 m of the monitor.

Inspect excavations close to the incline shaft for any fresh fractures, which may indicate a change in the state of stress.

Inspect the shaft hangingwall for instability. Ground penetrating radar may prove useful in identifying parting planes.

Avoid increasing the unconfined height of the shaft pillar through barring down the hangingwall.

Investigate using grouts and resins to consolidate the fractured hangingwall.
Ensure adequate temporary support is in place when cable anchors are installed *e.g.* mine poles.

The stability of sets in a steeply dipping excavation can be improved through the use of ties.

6 East Driefontein, 14/9/95, M_L=3,6

6.1 Introduction

On 14 September 1995 a rockburst occurred at East Driefontein Mine, causing extensive damage to haulages east of No. 4 Shaft between 31- and 36 levels, about 2500 m below surface (Figure B.28). The rockburst, which caused no injuries, took place at 16h04 in the afternoon after the day shift had left the mine. A seismic event with magnitude M_L=3,6 was recorded by the seismic network based at West Driefontein Mine. A new Integrated Seismic Systems International (ISSI) seismic network was being installed at East Driefontein Mine, and was not operating at the time of the rockburst.

Mr H Lombard (Chief Consulting Engineer, GFSA) requested that a team from CSIR Mining Technology investigate the rock engineering aspects of the incident. The aim of the investigation was to determine the cause of the rockburst in order to prevent future occurrences. The team visited the site on 21 September and 3 November 1995.

6.2 Mining environment

The seismic event affected excavations from 31 to 36 Levels over a wide area east of No. 4 Shaft. The damage was confined mainly to cross-cuts and drives that provide access to the K- and L longwalls situated to the south-east of No. 4 Shaft. This area has a history of large seismic events, many of which have caused damage to the access development, with stoping being less severely affected. This strongly suggests that the seismic events are related to geological structures remote from the stopes. Candidates include the Bank Fault, the Skelm Fault (which is exposed in the northern part of the K longwall), eastwards downthrow faulting both east and west of the L longwall, and the many other structures associated with the folding and thrusting in the area (Vermaakt et al., 1989). All recorded seismic events with M_L>2,0 for the period September 1993 to September 1995, together with the most prominent geological structures, are plotted in Figure B.28.

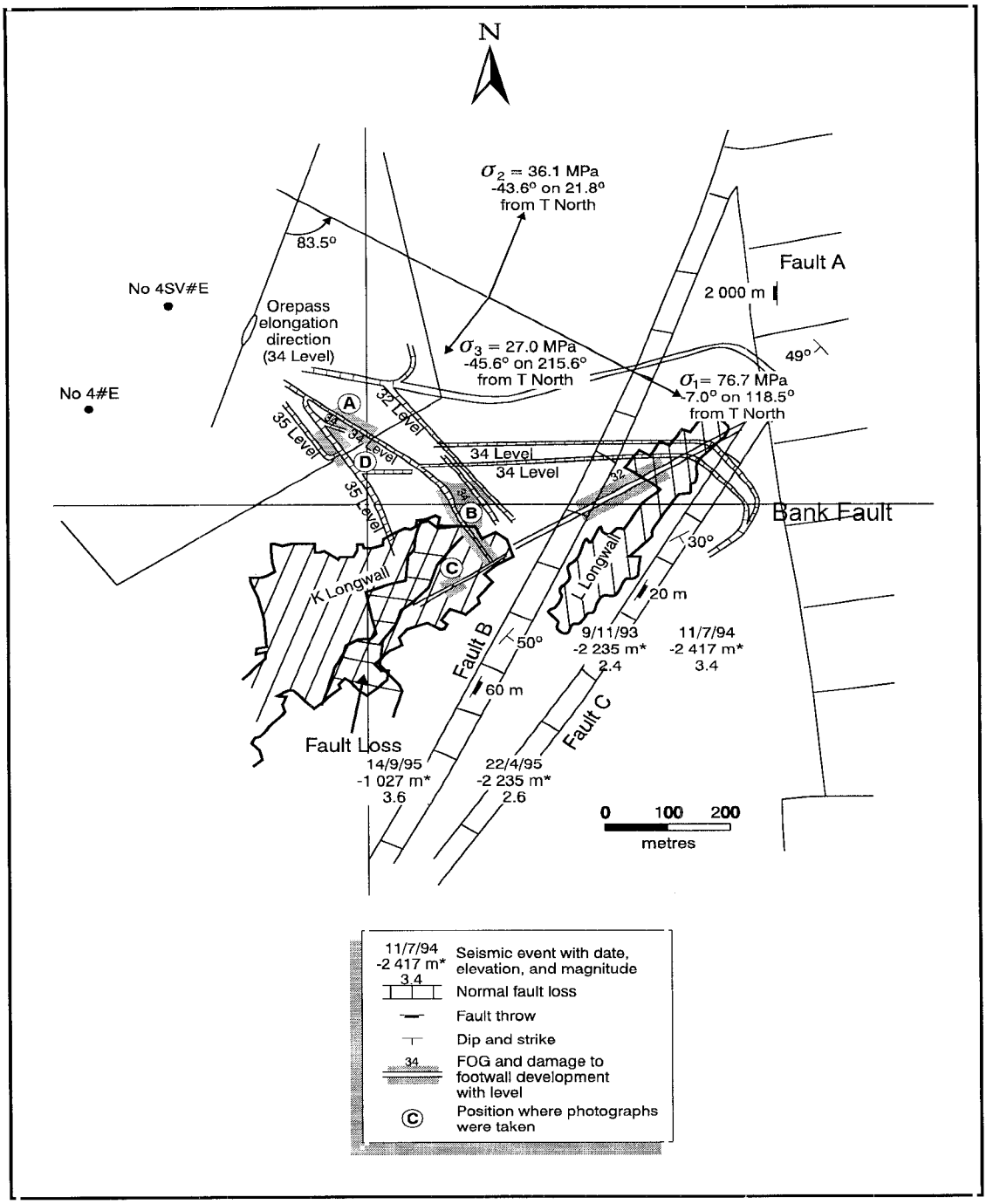

Figure B.28 Plan showing damage to tunnels serving No. 4 Shaft, East Driefontein Gold Mine, by a M_L=3.6 seismic event on 14 September 1995. The locations of all seismic events with M_L>2 which occurred in the preceding two year period are shown. Falls of ground (FOG) and damaged sections of tunnels are indicated by shading.

Geology

The area is underlain by the Ventersdorp Contact Reef (VCR) which is enclosed by lavas belonging to the Klipriviersberg Group in the hangingwall and shales, shaly quartzites and quartzites belonging to the Jeppestown Subgroup in the footwall. Further to the east, downthrow faulting has resulted in the preservation of the Carbon Leader Reef which is enclosed by quartzites belonging to the Main Conglomerate Formation. The Bank Fault on the eastern boundary of the mine dips in a westerly direction at an average 45°-50°, and is described by Vermaakt et al., (1989) as a listric (concave up) normal fault with an average downthrow to the west of 2000 m.

The Witwatersrand and Ventersdorp age rocks are folded into an open, southwards plunging syncline which is considered to be a local drag feature associated with the Bank Fault (Coward, 1987). The VCR has cut down to the Main Conglomerate Formation in the area, thus eliminating the Middelvlei and Carbon Leader Reefs over a wide area. Eastwards downthrow faulting has preserved the Carbon Leader Reef in some areas in the extreme east, for example the L Longwall. The history of faulting, folding and thrusting in the area has left its imprint not only on the structure, but also on the *in situ* stress state in the area, which is described below.

Local *in situ* stress state

Observations of tunnel fracturing by mine personnel indicated that the usual assumption of the stress state at depth did not appear to be valid in the No. 4 Shaft area, especially towards the east. The vertical component of stress is normally assumed to be proportional to depth, given by the following formula:

$$\sigma_{vertical} = \rho g h \qquad \text{(B.4)}$$

where ρ is the rock density, g the acceleration owing to gravity and h the depth below surface. The stress tensor at any point below surface is then assumed to consist of a vertical component of stress as defined above and two horizontal components, each equal in value, and half the magnitude of the vertical component.

The above assumption of the stress state was investigated on 42 level RAW south of No. 4 Shaft in early 1995 by drilling three horizontal boreholes into the RAW sidewall and taking strain relief measurements from which the *in situ* stress tensor could be calculated (Vlietstra and Smith, 1995). The results in Table B.4 below are based on the strain relief measurements given in the report, with minimised errors. To do this, three measurements out of the ten taken were rejected because they suggested tensile stresses. While such stress states are possible in blocky rock masses, they are not generally representative of the stress state at depth and were thus omitted from this analysis. It was found that the maximum compressive stress (σ_1) is almost horizontal, and orientated north-west to south-east.

Table B.4

Results of in situ Stress Measurements

Stress Component	Stress[1] (MPa)	Bearing[2]	Inclination[3]
σ_1 major principal stress	76.7±7.0	118.5°	-7.0°
σ_2 minor principal stress	36.1±3.4	21.8°	-43.6°
σ_3 minor principal stress	27.0±3.2	215.6°	-45.6°

[1]Compressive stresses are positive.

[2]Measured from true north.

[3]Negative downwards from the horizontal

The above principal stress tensor has been re-expressed in the mine co-ordinate system for use in MINSIM simulations of stresses and displacements induced by mining. The result is given in matrix form below, with all stresses expressed in MPa.

$$\begin{bmatrix} \sigma_{xx} & \sigma_{xy} & \sigma_{xz} \\ \sigma_{yx} & \sigma_{yy} & \sigma_{yz} \\ \sigma_{zx} & \sigma_{zy} & \sigma_{zz} \end{bmatrix} = \begin{bmatrix} -42.2 & 18.9 & 7.0 \\ 18.9 & -65.5 & 1.4 \\ 7.0 & 1.4 & -32.1 \end{bmatrix} \text{ MPa} \qquad \text{(B.5)}$$

The above stress tensor (expressed in terms of the engineering sign convention) was used in the MINSIM-W model described in Section 6.5 below in an attempt to identify the structure or structures responsible for seismicity in the area.

Mining induced fractures

The tunnels inspected were all driven in shaly quartzites and shales belonging to the Jeppestown Subgroup, which have a strongly developed cleavage parallel to bedding. The high horizontal and relatively low vertical stress would suggest a lack of stress induced fracturing in the sidewalls of the tunnels, and hangingwall failure predominantly associated with stress induced fracturing and weak bedding planes. However, this distribution of fracturing was not generally observed during the underground visit. This is owing to the fact that most of the tunnels inspected are orientated sub-parallel to σ_1. Consequently, these footwall drives are influenced primarily by the σ_2 and σ_3 stress components (which act within the plane of the excavation cross-section), and account for the stress induced fracturing observed in the upper sidewalls of the footwall drive excavations. The potential for damage is greatest when the orientation of the stress induced fractures is parallel to the bedding. Where the excavation deviates significantly from the σ_1 direction, the influence of this component becomes more pronounced, and stress induced fractures are formed in the hanging- and footwall.

The ore pass in the 34 level tip cross-cut was also examined and was observed to have a markedly elliptical cross-section, with the long axis of the ellipse orientated on a bearing of 21° from true north. This suggests a major horizontal stress direction on a bearing of 111°, which is in excellent agreement with the bearing of 118,5° for the major compressive stress component measured in the 42 Level RAW south of No.4 Shaft (see section 6.2 above). The scaled ore pass therefore provides good supporting evidence for the measured *in situ* stress tensor. The relationship between the measured stress and

the ore pass scaling are illustrated in plan in Figure B.28. The effects of the stress tensor on mining are discussed further in the section on modelling.

6.3 Observations at the rockburst site

Distribution of rockburst damage

The damage on 34 and 35 Levels was generally associated with the north-eastern sidewall and the hangingwall of the excavation where the excavations were orientated in a south-easterly direction, i.e. parallel to the local strike. A key factor controlling the distribution of the damage was the type of support in place at the time of the rockburst. Some sections were supported by grouted ripple bars, mesh, lacing and shotcrete, and suffered little damage. Other sections, where mesh and lacing had not yet been installed, sustained severe damage.

In the 34K Deep Footwall Drive East the pattern of damage to the north-eastern sidewall and hangingwall persisted, except at the first tramming loop east of the shaft where the southern sidewall was severely damaged for a short distance where the loop approached the main development (Figure B.29). The bullnose at the junction between the drive and tramming loop was also severely damaged. A section of the 34K Footwall Drive East was completely blocked by the bulking of the sidewall (Figure B.30). Footwall heave from a north-easterly direction was also evident in the 34K Deep Footwall Drive in almost all places where damage was noted.

In the 34K Cross-cut South, damage was confined to a 20-30 m long section where bad rock conditions had been encountered in the past. In this area both sidewalls were damaged, and footwall heave appeared to be more prominent on the north-western sidewall of the cross-cut.

The damage on 35 level was generally less severe than on 34 level. The damage was characterised by the collapse of the north-eastern sidewalls and falls of the hangingwall.

Influence of geology

Damage associated with the shaly quartzites and shales resulted from the rock mass being friable, with the mode of failure of the support system predominantly rock mass unraveling between the support units.

Heave of the footwall of the tunnels was generally from the up-dip/north-eastern side of the excavation within the strike orientated tunnels, and it is considered that this may be due in part to the anisotropic nature of the quartzite rock mass exhibiting inherent weakness parallel to the bedding. Footwall heave observed in the dip orientated tunnel was fairly uniform over the footwall of the excavation, perhaps owing to the excavation orientation relative to the direction of anisotropy.

Damage was therefore generally associated with the up-dip side of excavation. This could be owing to the more inherently unstable orientation of the bedding relative to the sidewall of the excavation, and that the up-dip sidewall of the excavation is significantly higher owing to the geology and excavation technique, resulting in a more unstable structural configuration.

Alternatively, the damage distribution could be owing to the seismic source of the rockburst being located somewhere north-east of the damaged haulages. This would explain the damage being confined almost exclusively to the up-dip side of the haulages, as well as the heave from this direction.

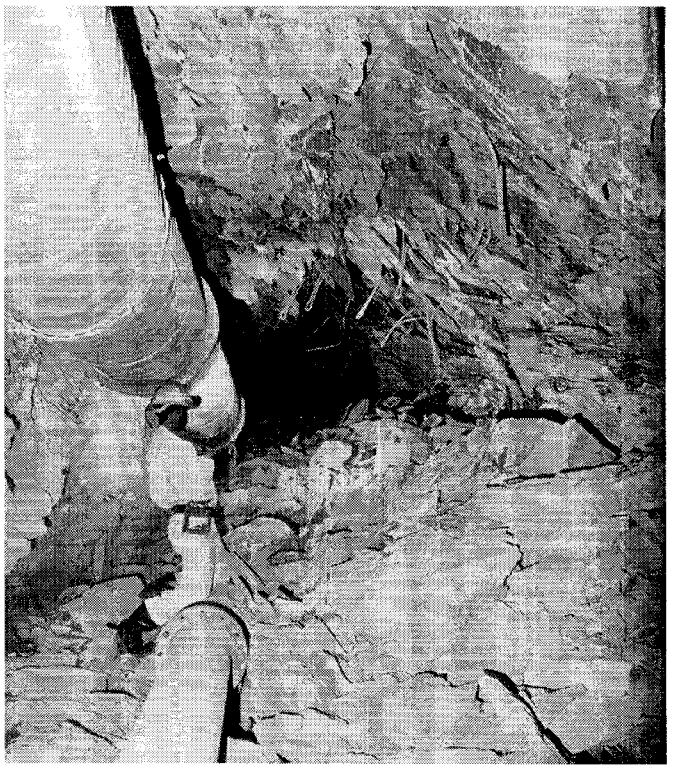

Figure B.29 Damage to 34K footwall drive at Site A showing falls of ground between grouted shepherd's crook rebars. Mesh and lacing had not yet been installed in this section of the tunnel. In this area the south-western (right hand) side of the drive was most severely damaged. The view is taken looking to the south-east, away from the shaft.

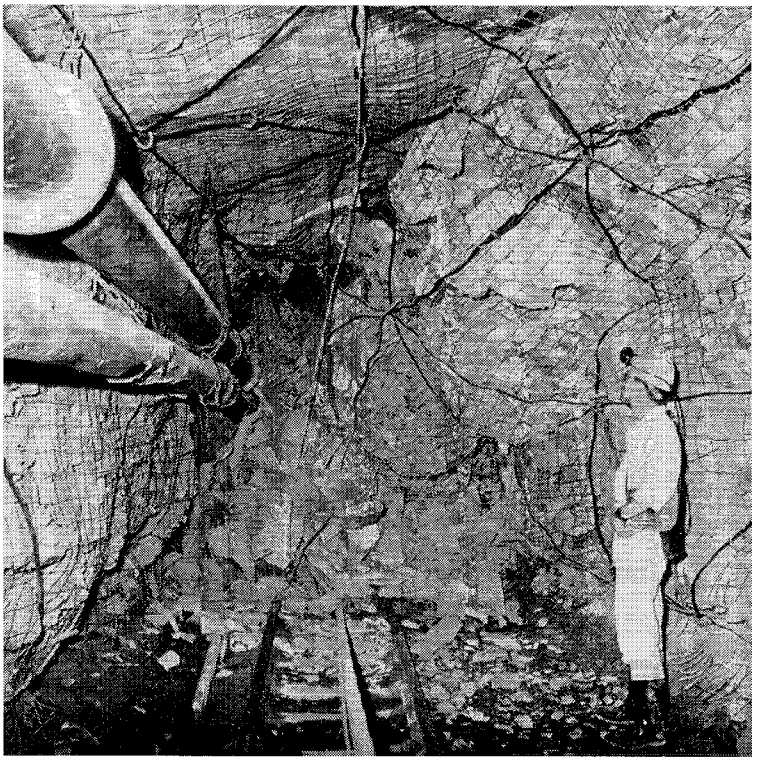

Figure B.30 Damage to 34K footwall drive at Site B showing complete closure of the tunnel.

6.4 Assessment of support performance

The influence of support on the distribution of damage was clearly evident. In areas where grouted ripple bars were the only means of support, damage was very severe. In areas where wire mesh and lacing was installed, sidewall and hangingwall damage was evident to varying degrees. In some places serious bulking of the north-eastern sidewall and hangingwall made bleeding and resupport of the haulages necessary for re-opening. In areas where shotcrete had been applied, for example at the 34K Deep Footwall Drive and 34K Cross-cut South intersection, there was no damage at all (Figure B.31).

Failure of the support system was owing to either direct tensile or shear failure of the shepherd crook rebar rock bolts. The most of the failure was fresh and was probably associated with the seismic event, however one example of an old failure (rusted failure surface) was exposed by the collapse of the rock mass. Direct shear failure of the bolts was predominantly associated with hangingwall of the excavation at the position of clearly

defined bedding planes, where clean guillotining of the bolts had occurred in the down dip direction (Figure B.32). Within the sidewall of the excavation, tensile failure of the bolts was generally observed. The majority of the bolts, however, indicated some degree of plastic bending prior to failure, which suggests some component of shear movement.

The most extensive failure of the tunnel excavations occurred in areas that had not been meshed and laced. This is considered to be a function of the low integrity of the rebar support alone under rockburst conditions, where the failure of a single support unit would result in damage to the excavation. Within the meshed and laced tunnel sections, the higher integrity of the support system meant that even if individual support units within the system failed, the remaining support units could still prevent collapse. Both shear and tensile modes of failure of the rebar support occurred within the meshed and laced areas of the tunnels, but the system integrity was largely maintained. However, should the excavations be subjected to further seismic loading, total failure of the system may occur.

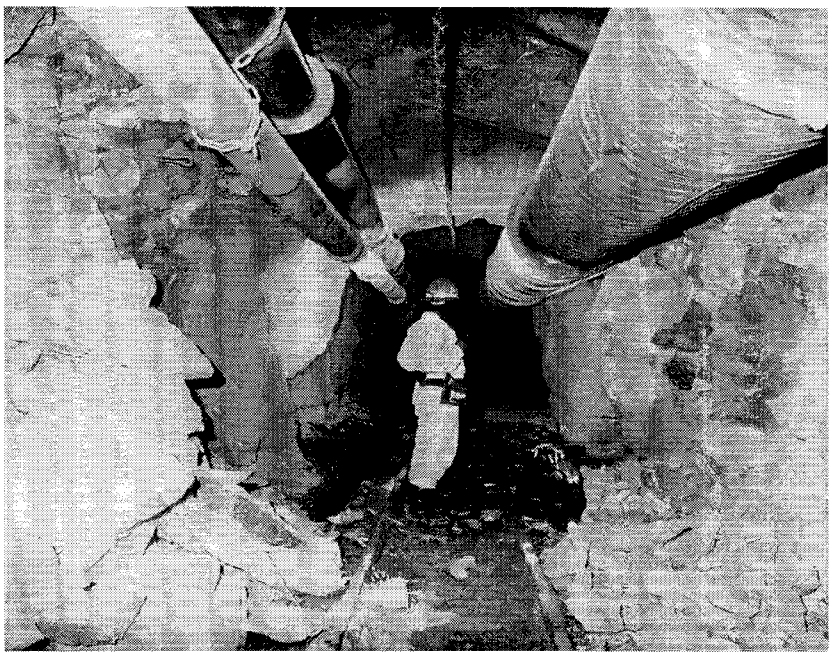

Figure B.31 A haulage on 34 level showing the effect of the support system on damage. The section of the tunnel in the foreground was supported only by grouted rebars, and significant damage was sustained. The support system in the section of the tunnel beyond the miner consisted of grouted rebars, mesh, lacing and shotcrete. Damage was negligible.

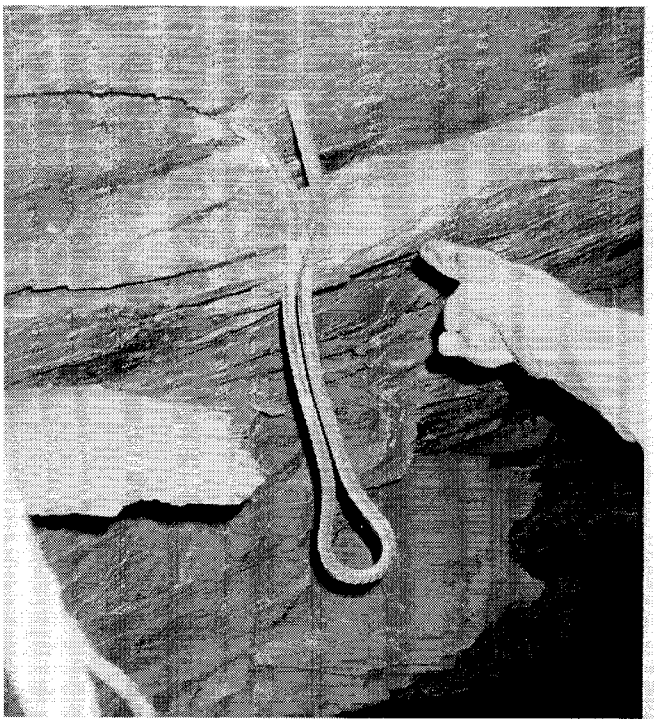

Figure B.32 Kinked shepherd's crook rebar observed in the hangingwall of the 34K footwall drive between Sites B and C. Some bars had been sheared by the movement along bedding planes.

6.5 Assessment of layout

The MINSIM-W suite of program was used to analyse the stresses and displacements induced by mining in an attempt to find out why such a relatively insignificant amount of mining should cause such a strong seismic response in the area. The elastic constants of the rock mass were assumed to be 70 GPa and 0,2 for Young's Modulus and Poisson's Ratio respectively, but the *in situ* stress state was taken to be that given in Table B.4 above. A second control model was run in which the standard *in situ* stress state was assumed. The purpose of this was to compare the Excess Shear Stress (ESS) on selected geological structures given the two initial stress states.

The mining in the model included only excavations on the limbs of the syncline in order to avoid intersection of mined elements (which MINSIM is unable to compute), which would occur if the mining along the fold axis were included. Because the structure responsible for the seismicity could not be identified from the available seismic data, three candidates were chosen for ESS calculations in the model; the Bank Fault, and two offshoots that lie east and west of the Carbon Leader Reef stoping above 32 level in the 32L longwall. The analysis of the ESS on these three faults serve purely as an indication of whether or not the measured *in situ* stress state on the eastern side of the mine could destabilise structures. The benchmark sheet representing the Bank Fault was assigned a dip of 45° to the west (current estimate of average Bank Fault dip is 49°), while the East and West Fault benchmark sheets were assigned dips of 30° and 50° respectively to the east. The results of the analysis are listed in Table B.5. The West Fault benchmark sheet appears unaffected by the different *in situ* stress states, while the Bank and East Faults are less stable when compared with the normal stress state.

Table B.5

Summary of ESS Results (MPa) for Three Benchmark Sheets

	Bank Fault	Fault B (West Fault)	Fault C (East Fault)
Dip	45°W	50°E	30°E
Normal Stress State (k-ratio = 0,5)	-12,1	-12,5	-22,5
Measured In Situ Stress State (k-ratio ≈ 2)	-4,5	-12,6	-14,9
Difference between Normal and Measured	+7,6	-0,1	+7,6

The above results come from a static elastic model, and as such should not be interpreted as seismicity predictors. What the model *does* indicate is that there is probably a higher potential for seismicity in some structures (e.g. certain faults and dykes) because of a combination of their orientation and the local stress state. More underground stress measurements, seismic data and numerical modelling are necessary for a clearer identification of features responsible for seismicity in the area.

6.6 Rockburst mechanism

Source mechanism

The seismic event with magnitude M_L=3,6 took place at 16h04 on 14 September 1995. The event was located to the south-east of the K longwall by the regional seismic system based at West Driefontein. The location of the event and earlier events with M_L>2,0 on the local magnitude scale are shown in Figure B.28. The error of location of seismic events in this area is typically up to 100 m. The spacing of the geological structures in the area are 100 m or less, thus it is not possible to say with certainty whether any particular geological feature was involved in the event or not. The location is not in agreement with damage patterns observed underground, which suggest that the seismic energy may have come from a northerly direction.

Calculation of ejection velocity

The minimum peak particle velocity in the 34K Deep Footwall Drive was estimated from a large block, attached to a failed ripple bar support, that had been ejected from the hangingwall. The approach is similar to that described in the *Industry Guide to Methods of Amelioration of Rockfalls and Rockbursts* (COMRO, 1988, p. 101, Figure F1(c)). The bar protruding from the block exhibited necking for a distance of about 10 mm. It is assumed that similar necking occurred on the section of the bar still grouted in the roof. It is estimated that the bar was extended by about 10 mm before failure.

Kinetic + Potential energy of block $\geq$ Elastic energy absorbed by bar up to failure:

$$E_k + E_p \geq E_f \qquad \text{(B.6)}$$

where:

m = mass of block = 800 kg

h = extension of bar at failure = 0,01 m

g = gravitational acceleration = 10 m/s^2

Tensile strength of tendon = 15 tons = 150 kN

$$E_f = \int_0^h \mathrm{F}\,\mathrm{dx} \approx \frac{1}{2}(150000)(0.01) \approx 750\,\mathrm{J} \qquad \text{(B.7)}$$

where: E_f is area under force – displacement curve

$$E_k + E_p \geq 750\,\mathrm{J}$$

$$\tfrac{1}{2}mv^2 + mgh \geq 750\,\mathrm{J} \qquad \text{(B.8)}$$

$$(\tfrac{1}{2})(800)v^2 + (800)(10)(0.01) \geq 750\,\mathrm{J}$$

$$\therefore v \geq 1.3\,\mathrm{m/s}$$

The *Industry Guide* (COMRO, 1988, p. 79) provides a set of graphs relating event magnitude, distance from source and peak particle velocity. From the graph and the recorded event magnitude it was estimated that the seismic event could have taken place as far as one kilometre away if peak particle velocities at excavation boundaries are magnified by a factor of ten. A remote location of the seismic event is supported by the lack of damage in the stopes. It is thus suggested that the seismic event took place on a geological structure somewhere in the region within a kilometre of the observed damage. The most likely position is somewhere to the north or the north-east of the 34K longwall, a location further west or south is likely to have resulted in either shaft or stope damage respectively.

6.7 Conclusions

In summary, the following conclusions have been reached :

The seismic event was remote from the mining excavations because of the lack of damage to the stoping, and as such is most likely to be associated with one or more geological structures, either faults or dykes found in the area.

The anomalous stress state in the region is probably responsible for the instability of the geological features, but exactly which features are responsible will only be determined by a combination of detailed seismic monitoring, stress measurements, geological mapping, and modelling.

The damage in the access development was controlled by the friability of the shaly rock mass, and the intensity of the support.

The partial failure of the mesh and lace support system was owing to the limited yield and shear resistance capacity of the grouted rebars.

6.8 Recommendations

The following recommendations were made:

Long term excavations, that are expected to be subjected to seismicity sometime in the future, should be supported by pre-stressed yielding units that can accommodate shear deformations (grouted rope anchors, or cone bolts) integrated with mesh and lacing. In areas where severe damage is expected, these support units should be supplemented with shotcrete.

In short term excavations, support tendons with limited yield capacity (e.g. smoothbar) that is cheaper than cone bolts or long rope anchors, should be installed. These rock bolts should still be integrated with wire mesh and lacing.

The newly installed Integrated Seismic System (ISS) must be brought into operation as soon as possible to identify the structure(s) responsible for the seismicity. Ensure that there are enough geophones to make accurate seismic locations possible.

Undertake a further three *in situ* stress measurements in the eastern half of the mine with the purpose of determining the area over which the anomalous stress state is found (one measurement should be undertaken at depth in No. 5 Shaft, the other two to the north-east and south-east of No. 4 Shaft).

Compile a geological structure plan of the eastern half of the mining lease from the surface *Vibroseis* survey as soon as possible.

Combine the structural, seismic and *in situ* stress data to identify and locate seismically active structures, and then devise a plan for mining the eastern half of the mine lease where the anomalous stress state is known to exist.

7 Western Deep Levels (South), 18/9/95, M_L=2,2

7.1 Introduction

At 08h17 on 18 September 1995, a seismic event with a local magnitude M_L=2,2 caused damage to the W4 panel and heading of the 84-61 West longwall at Western Deep Levels South Mine, about 2200 m below surface. Three people were injured, one fatally. CSIR Mining Technology had a special interest in this area as mine management had requested the Rockburst Control team to assist production personnel in implementing a preconditioning programme to reduce the incidence of face bursts in the W4 panel. Mr M. L. Treloar (Section Head, Rock Mechanics Department) requested that a team from CSIR Mining Technology investigate the incident in order to determine the cause of the rockburst and to assess what effect preconditioning had on the rockburst damage. The rockburst site was visited on 20 September 1995.

7.2 Mining environment

Geology

The rockburst site (see Figures B.33 and B.34) lies approximately 2200 m below surface. Mining was taking place on the Ventersdorp Contact Reef (VCR), the sole ore resource exploited by Western Deep Levels (Ltd.) South Mine. In this area, the reef consists of two conglomerate bands separated by a green quartzite. The quartzite is typically between

0,5 m and 1,0 m thick. The reef is underlain by quartzites belonging to the Kimberley Formation of the Central Rand Group, and overlain by hard andesitic lavas of the Alberton Formation of the Ventersdorp Supergroup.

The VCR was deposited on an undulating terraced topography composed of level terraces at differing elevations, separated by slopes of varying steepness. These slopes are termed reef rolls, and often pose serious mining problems both from a practical extraction and rockburst point of view. The W4 panel and heading were on a level terrace at the time of the rockburst, but the existence of reef rolls in the area is indicated by changes in roadway directions (Figure B.33). The lava hangingwall has a blocky structure owing to the interaction of face-parallel joints (with nearly vertical dips) and curved lava flow surfaces (approximately parallel to the footwall strata).

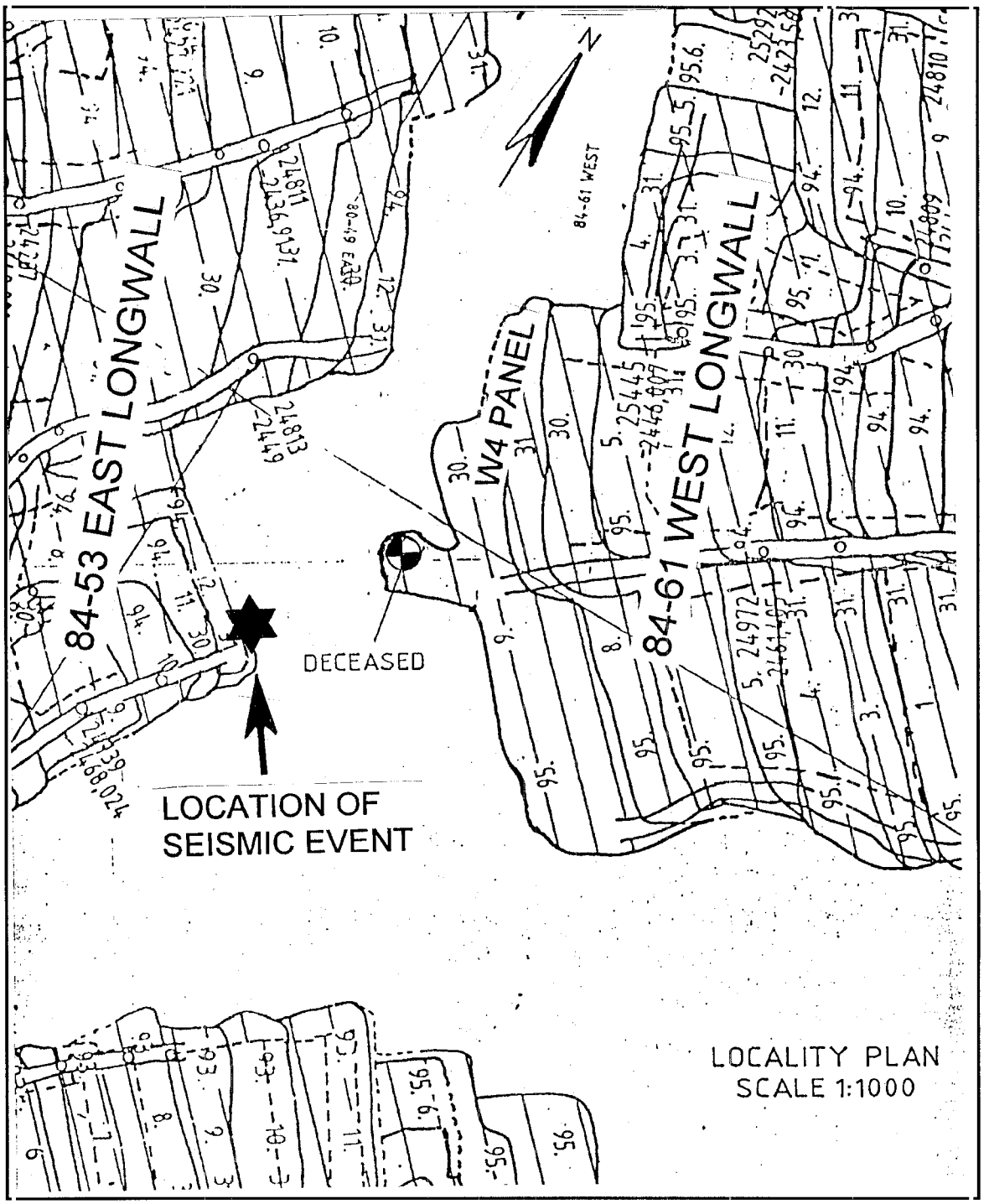

Figure B.33 Plan showing the location of the rockburst at Western Deep Levels South Mine on 18 September 1995 damaging the 84-61 West 4 VCR panel.

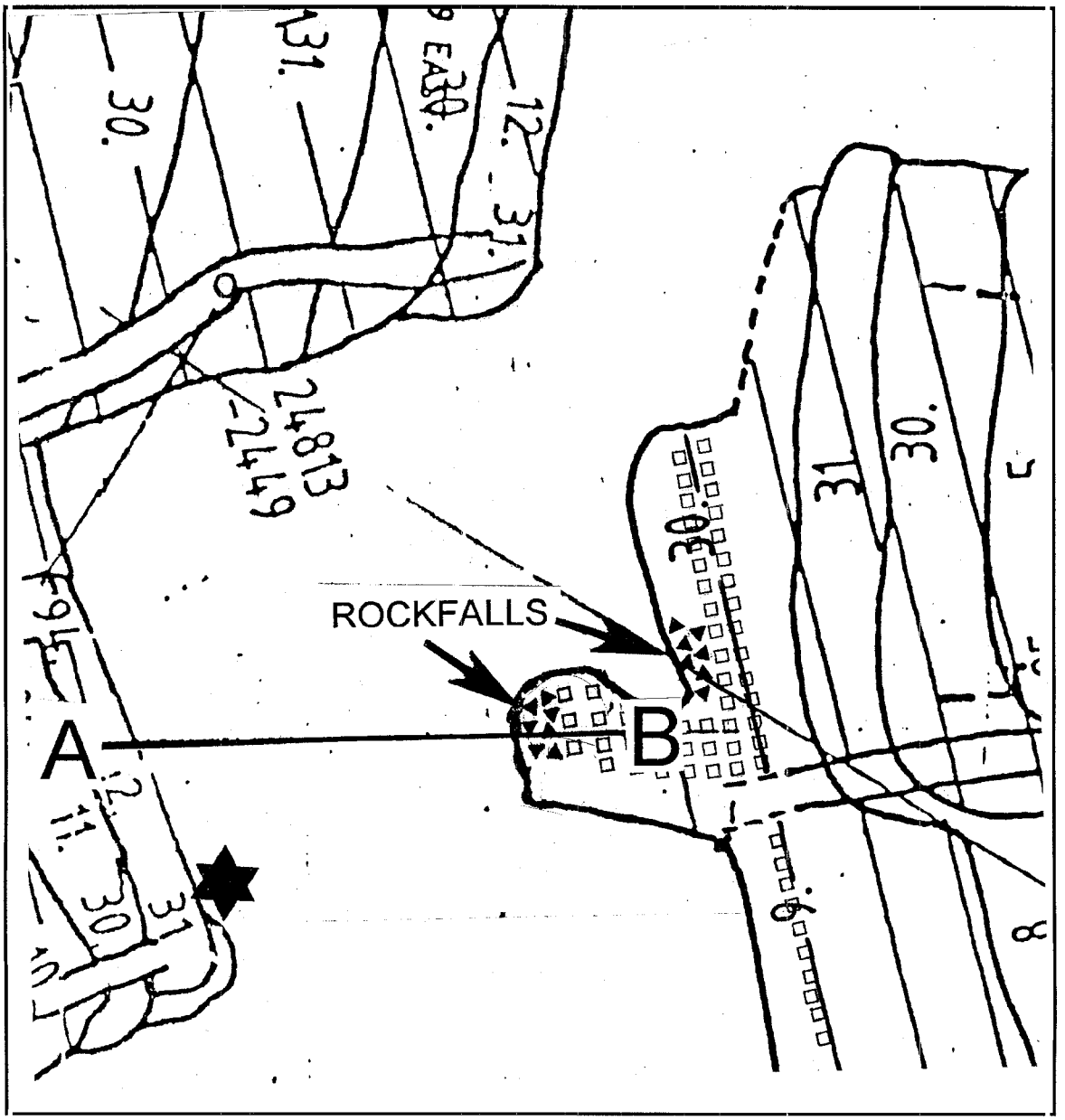

Figure B.34 Plan showing the extent of the damage to the 84-61 West 4 VCR panel caused by the rockburst of 18 September 1995. Open squares show the approximate position of packs. AB is the section line along which Figure B.36 is drawn. Scale 1:500

Mining Strategy

Rockburst damage occurred in the 84-61 W4 panel and heading, which had approached to within 30 m (on strike) of the 84-53 East longwall (Figure B.34). Mining on the 84-53 East longwall was stopped in January 1995 so as to minimize the rockburst hazard. The planned mining strategy was to advance the W4 heading and roadway until it holed with the 84-53 longwall, and then to establish up-dip panels to remove the remaining ground between the two longwalls. All mining on the 84-61 West longwall up-dip of the W4 panel was stopped in June 1995 in order to execute this extraction strategy.

Support

The support systems implemented by the mine for the 84-61 longwall are described below:

Face area: two rows of rapid yielding hydraulic props with headboards.

Back area: 1,1 m x 1,1 m solid timber mat packs spaced 1,5 m apart (skin to skin) both on dip and strike, and pre-stressed with the HL&H Packsetter system.

Roadway hangingwall: fully grouted 2,2 m long ripple bars set in rows of four, spaced 1,5 m apart on strike. Some 15 m back from the current heading position the ripple bar support was replaced by Swellex Rockbolts (installed in a similar pattern) for a distance of approximately 10 m.

Roadway shoulders: 2,2 m x 1,1 m solid timber mat packs set 1,5 m apart on strike.

Regional support: a combination of strike stabilising pillars and bracket pillars left on seismically active geological structures.

Preconditioning

As a result of the encouraging results obtained at the Mining Technology experimental preconditioning site (87-49 West longwall), mine management requested the Mining Technology Rockburst Control team to assist in implementing a preconditioning programme in the 84-61 West longwall in order to reduce the incidence of face bursts associated with the West 4 panel.

The West 4 panel was first visited by the preconditioning team in July 1995. The hangingwall conditions in the upper (northern) half of the panel were very good. A low angle fault cut up through the reef horizon and intersected the contact between the apple-green quartzite middling and the top band of the VCR, creating a smooth parting. The upper (poorly mineralised) reef band was left in the hangingwall. This resulted in a smooth hangingwall contact. In this area no major falls of ground were noted. Hangingwall problems were noted in the lower half of the panel. Collapses as high as 3 m above the original stope were observed. To support the roof in these areas, solid timber packs up to 4 m in height had been built and placed as close together as 0,8 m. Repeated attempts to undercut and regain hangingwall control were evident in the panel.

The preconditioning programme was initiated about a week after the visit. The working place was visited by the preconditioning team on 9 September 1995, eleven days prior to the rockburst. It was observed that the production personnel had stopped advancing the entire panel, and were developing a 10 m wide heading at the bottom of the panel in order to establish an up-dip face. No preconditioning holes were observed on the face. The production personnel indicated that the holes had not been drilled the previous day as preconditioning was not implemented with every production blast. However, the hangingwall conditions were observed to be satisfactory. Both the temporary and permanent support in the heading met mine standards, although the south side of the heading was unsupported.

7.3 Observations at the rockburst site

The site was visited by the Mining Technology team on 20 September, two days after the rockburst. It was undisturbed apart from the rescue operations.

Geology

No major geological structure was detected in the immediate vicinity of the rockburst site. Face-parallel joints with dips close to 90° were found in the area, which, in combination with curved flow surfaces more or less parallel to the footwall strata, resulted in a blocky lava hangingwall. Many of the steeply dipping joints showed sulphide mineralisation, indicating that the joints were pre-existing geological features and not induced by mining. Slickenslides were noted on several flow surfaces in the hangingwall and steeply dipping joints.

Rockburst damage

Damage to the 84-61 W4 panel was localized in two places (see Figure B.34): the wide heading of the 84-61 roadway, the victims were involved in early shift examination here at the time of the rockburst, and the part of the W4 panel immediately up-dip of the wide heading.

The damage was confined to face areas where the distance from the face to support exceeded 2 m. Collapse had occurred to a height of 1,0 to 3,0 m above the original stope hangingwall. Little or no fallout occurred between the packs. In general, the fallout consisted of lava, and was bounded by joint surfaces. The hangingwall fragments graded from pebble sized fragments at the base of the falls, to large intact blocks at the top. In the wide heading, it appeared that the face was about 3,5 to 4,5 m ahead of the last row of packs. It appears that hydraulic props were not installed at the time of the rockburst. Fresh splitting of timbers was observed in several packs installed in the stope. It was inferred that the convergence associated with the rockburst was about 100 mm. In one instance, a pack exhibiting recent splitting, interpreted to indicate 100 mm of co-seismic convergence, was in the fourth row from the face (a distance of about 8 m).

Roadway Damage

The 84-61 W4 roadway was damaged by a previous rockburst for a distance of approximately 30 m on strike, beginning some 50 m back and ending 20 m from the heading face. In this area, roadway hangingwall fallout occurred to a height of 1,8 m, without damaging the installed ripple bar support, which was left hanging from the roof. Exposure of the rockbolts indicated good grouting of the support units over their entire length. Within the heading, the roadway remained largely intact, both in the area where Swellex bolts had been installed, and at the heading face, where grouted ripple bars had again replaced the Swellex support. It appears, therefore, that the rockfalls in the roadway were not controlled by the type of support installed or its quality, but rather by other factors such as jointing. Crushing of the reef was noted on the south side of the heading, probably as a result of stope convergence induced by the rockburst. There was no evidence of significant face ejection. No roadway shoulder had been developed here.

7.4 Assessment of support

Face area

The falls of ground in the face area appeared to be related to areas where the unsupported span exceeded 2 m. It appears that hydraulic props were not in place in the 84-61 W4 panel, and that the distance from the first line of packs to the face was between 3,5 m and 4 m at the time of the seismic event. It is imperative that the face area is supported at all times, and that workers do not venture into unsupported areas.

Roadway

The falls of ground in the roadway appeared to be owing to disintegration of the jointed rock mass between tendons, rather than shear or tensile failure of the tendons themselves. This highlights the need for good areal coverage in areas where the rock mass quality is poor.

7.5 Assessment of layout

The APS between the 84-61 West longwall and the 84-53 East longwall was calculated using MINSIM-W, and a value of 230 MPa was obtained. If the fractured zone around the perimeter of the pillar is simulated by a weak zone extending 1 m into the rock mass, the APS increases to 270 MPa. Considering a value of 180 MPa to be the minimum UCS value of the host rock, the APS: UCS ratio is less than 1,5. This is safely below the limit of 2,5 given in the Industry Guide to Methods of Amelioration of Rockfalls and Rockburst (COMRO, 1988, p. 87) for a pillar with a width/height ratio > 10.

7.6 Rockburst mechanism

Source mechanism

The seismic event took place at 08h17 on 18 September 1995, and was recorded by the ISS network installed on the mine. The seismic data was provided by Mr F. Naude (Senior Seismologist, Western Deep Levels (Ltd) South Mine). The source parameters are listed in Table B.6, and the location of the event is shown in Figure B.35. The location obtained by the ISS network indicates that the point at which rupture commenced lies a few metres above the reef plane near the southern end of the 84-53 East longwall.

Using the empirical relationship

$$\log L_{max} = 1 + M_{max}/2 \qquad \text{(B.9)}$$

the maximum linear extent of the rupture giving rise to a M_L=2,2 event is about 125 m.

Analysis of the moment tensors of the event determined by the ISS indicated predominantly shear type movement, with little volumetric change. One of the nodal planes obtained in the best double couple solution for the full tensor had a strike of 135°, and a dip (to the south-west) of 76°. As the strike of this nodal plane was similar to the strike of the lowermost panel of the 84-53 East longwall, it was considered more likely to

be the slip plane. The polarity of first motions indicates the slip to be normal *i.e.* downward movement of the hangingwall above the 84-53 East longwall (see Figure B.36).

Table B.6

Source parameters of the seismic event, which damaged the 84-61 West longwall.

Date:	18/09/95
Time:	08:17
Magnitude:	2,2
Location:	close to the reef plane, about 10 m in the hangingwall (x = 28634, y = -42225, z = -2453)
Moment:	$3,2 \times 10^{12}$ Nm
Energy:	$5,0 \times 10^{7}$ J
Apparent stress	0,47 MPa
Energy Index	0,6
Radius of apparent volume:	90,4 m

The source mechanism of the rockburst was slip along a steeply dipping surface aligned parallel to the lowermost panel of the 84-53 East longwall. The slip surface could be either a new rupture or a pre-existing joint. The confirming evidence that the seismic source was not in the immediate proximity of the W4 panel lies in the fact that the 3-4 m high packs were able to prevent falls of ground almost entirely, while sustaining little damage. This is an indication that ground motions in the stope itself were not violent enough to cause more extensive damage.

Foreshocks

In the 50 days preceding the rockburst there had been 11 events with M>1 in the ground between the longwalls (see Figure B.35).

Damage mechanism

The main factor controlling damage in the wide heading of the 84-61 roadway is believed to be the lack of support in the face area. The span between the face and first line of packs was too great to remain self-supporting during the shaking caused by the seismic event.

Damage in the lower part of the W4 panel immediately up-dip of the wide heading appears to be associated with the difficult hangingwall conditions, and appears to be a repetition of earlier falls of ground evident further back from the face.

The possibility that preconditioning influenced the style of fracturing in the hangingwall was considered. Careful studies in the 87-49 West longwall, where similar geological conditions exist, indicate that preconditioning reduces fracturing and produces a hangingwall with a less blocky character. Hangingwall fragmentation thus appears to be a function of mining-induced fracturing, rather than preconditioning or rockburst-induced crushing.

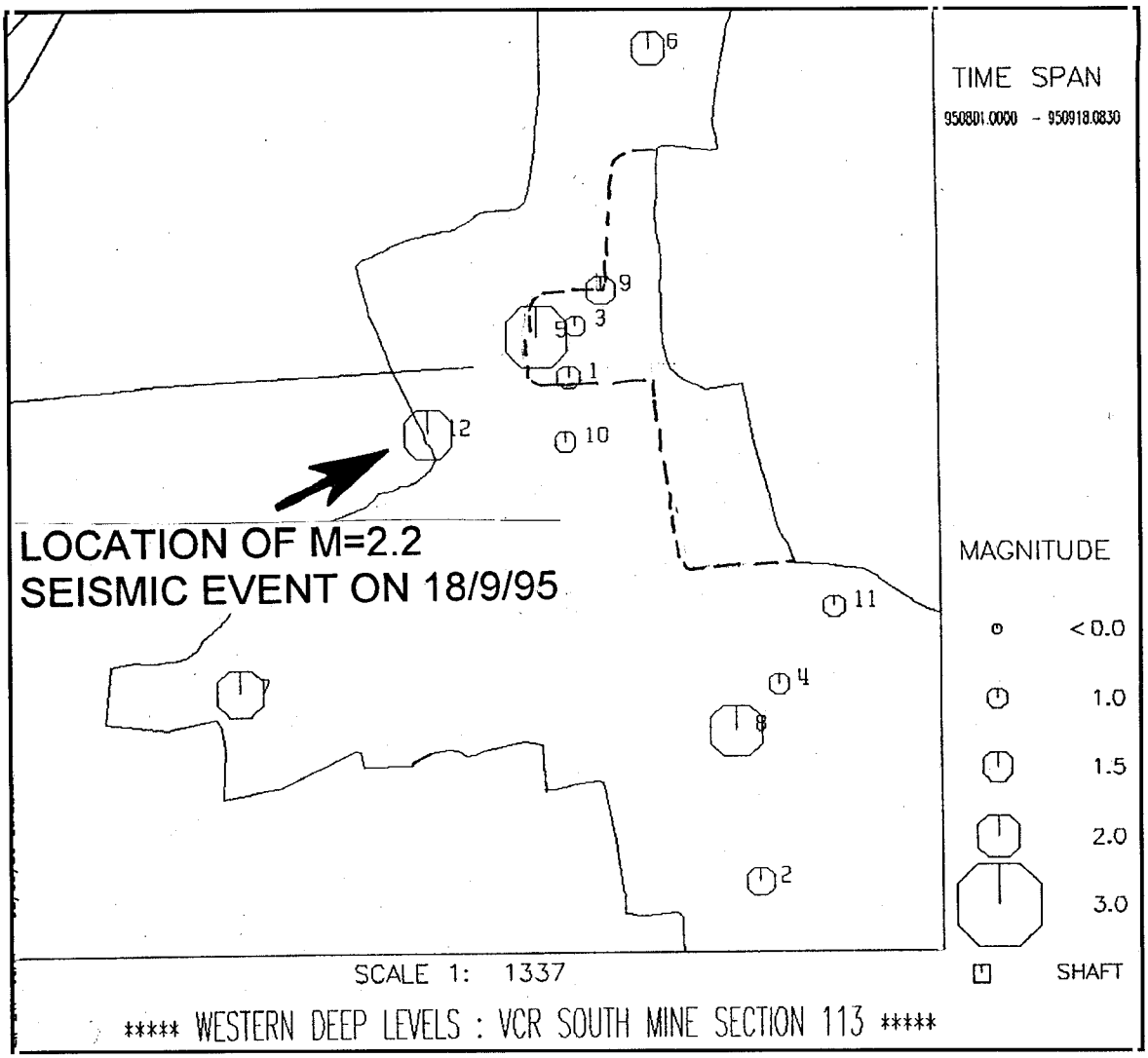

Figure B.35 Plan showing the seismicity (events with M>1) in the vicinity of the 84-61 West longwall for the period 1 August - 18 September 1995. The approximate face position on 18 September is indicated by a dashed line. Data provided by F. Naude (Senior Seismologist, Western Deep Levels (Ltd) South Mine).

The rockburst damage in the wide heading of the 84-61 roadway was owing to the wide unsupported span (3,5-4,5 m) between the face and first row of packs. The shaking produced by the seismic event caused the hangingwall to collapse. Crushing of the face was only noted on the south side of the wide heading with no evidence of actual ejection of the face.

The rockbust damage in the West 4 panel up-dip of the heading was mainly owing to the fall of ground on pre-existing joints, caused by shaking associated with the seismic event. This is consistent with hangingwall control problems encountered previously, and can probably be attributed to the approximately 4 m unsupported span between the face and the first row of support.

The falls of ground occurred on pre-existing joints. There is no evidence that preconditioning exacerbated the damage.

Damage in the face area may have been reduced if 2 rows of rapid yielding hydraulic props had been present.

7.8 Recommendations

The mining of the remnant between longwall faces is inherently hazardous and must be carefully managed. It is recommended that the approaching longwall faces be stopped at least 50 m apart so that the heading (used to establish up-dip panels) can be developed in a low stress environment. Modelling should be used to verify that the average stress in the remnant does not exceed 250-350 MPa after the development of the heading. It is important to take the fractured zone around the perimeter of the remnant into account in this calculation.

Face area support should be in place 24 hours a day, and not removed under any circumstance.

Methods of maintaining the integrity of the roadway hangingwall during seismic events must be investigated.

8 Blyvooruitzicht, 30/1/96, M_L=2,2

8.1 Introduction

A rockburst occurred at Blyvooruitzicht Gold Mine on 30 January 1996, causing extensive damage to the strike gully serving panels mining the 17-24W stabilizing pillar, about 1900 m below surface (Figure B.37). The rockburst, which fatally injured five workers, took place at 08h52 while stope workers were manually transporting timber along the gully. A seismic event with a local magnitude M_L=2,2 was recorded by the mine-wide seismic network. It was followed (within a second) by a M_L=2,3 event. Mr D Bakker (Acting Government Mining Engineer, DME) requested that a team from CSIR Mining Technology investigate the cause of the rockburst. The investigation was fully supported by Mr I. Vidulich (General Manager, Blyvooruitzicht Gold Mine). The team members visited the site on 1 February 1996.

8.2 Mining environment

The 17-24W stope (Figure B.37) was the site of a preconditioning project being conducted by the Mining Technology Division of the CSIR (Mining Technology) under the auspices of SIMRAC *(Project GAP030 Rockburst Control)*. Detailed observations of seismicity, convergence and fracturing have been carried out continuously since 1990.

Geology

The ore body mined in the 17-24W stope is the Carbon Leader Reef, which dips to the south at 18°. In this area the footwall is a slightly argillaceous quartzite, and the hangingwall is a cleaner arkosic quartzite. Approximately 2 m above the top reef contact lies a shale horizon known as the Green Bar. The Green Bar is several metres thick, and is comprised of dark green finely laminated metamorphosed shales. The upper and lower contacts are typically highly sheared and contain a variety of fault generated minerals including vein quartz, pseudotachylite and clay gouge.

There are no known major faults or dykes within the immediate vicinity of the pillar, however one of the dominant fracture sets in the pillar lies parallel to the regional trend (that is NNE to SSW) of the faults and dykes on Blyvooruitzicht Gold Mine. These prominent, steeply dipping shears were initially formed by large scale tectonism and regional faulting.

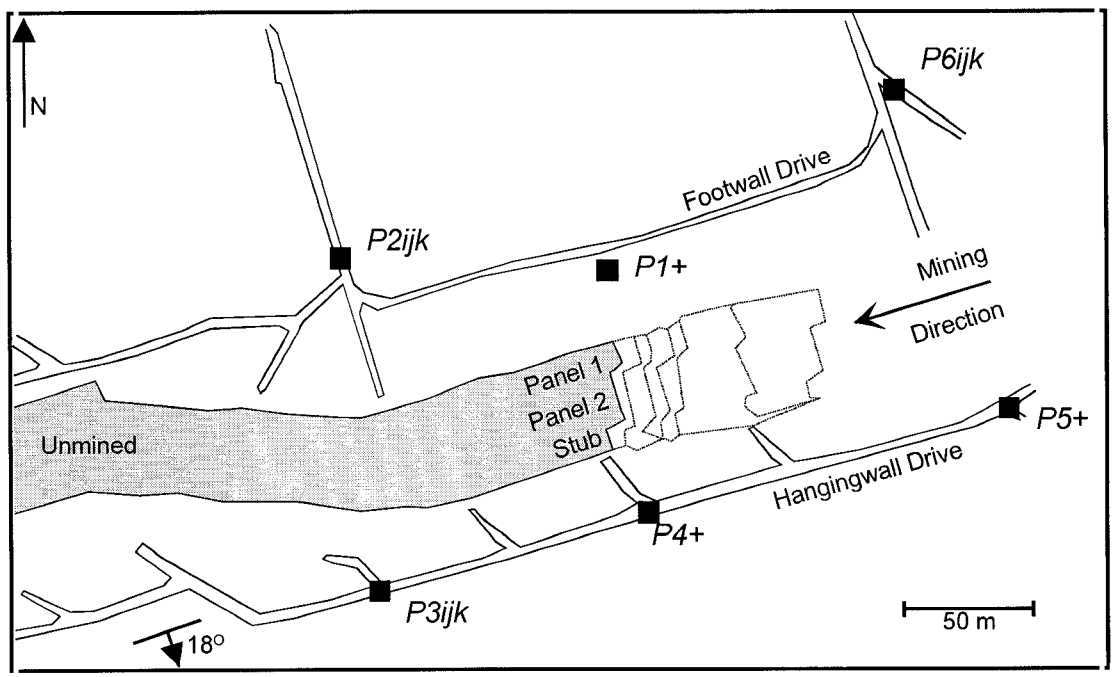

Figure B.37 Plan of the 17-24W stope, Blyvooruitzicht Gold Mine, showing the layout of the panels being mined at the time of the M_L=2,2 rockburst on 30 January 1996. The position of the research seismic network, monitoring the preconditioning experiment at the site, is also shown (black squares indicate the geophone positions: triaxial sites are labelled e.g. P2ijk; uniaxial sites are labelled e.g. P1+). Face position as at 31 December 1995.

Mining induced fractures

Six major sets of fractures (Groups I to VI in Figure B.38 (b)) have been identified on the basis of their dip and strike orientations (Lightfoot et al., 1996). Group III (steeply dipping shear zones) are thought to be the oldest as they are aligned with the regional strike of dykes and faults across the mine, which suggests that their initial development was owing to large-scale faulting. Associated with Group III are the low-angle faults of Group VI, which formed as second-order shears during the shearing of the Group III fractures. Group I and Group II fractures (pillar-parallel faults and joints with a steep to intermediate dip) are thought to have developed after Group III, as a result of mining of the surrounding ground. The shallower dipping Group II fractures later dilated as the pillar slowly failed at the edges. Group IV fractures, which lie parallel to the panel faces, formed in response to stress changes caused by the approaching mining. Group V fractures are thought to be the result of the failure in tension of the stope hangingwall in the broken rock mass immediately ahead of the stope face.

Preconditioning

Mechanism

The mechanism of preconditioning is discussed in detail by Lightfoot et al., (1994). The rock mass ahead of a stope face is subjected to extremely high abutment stresses, which result in the complex network of fractures observed underground (Figure B.39). Movement along the fracture planes results in the deformation of the rock mass, which is revealed by the convergence of the hangingwall and footwall in the stope. Inhibition of this movement might be induced by 'locking up' of blocks against one another, resulting in the accumulation of strain energy ahead of the stope face. As the face approaches this lock-up, confinement is significantly reduced, allowing movement to occur. If sufficient energy is available in the rock mass, its sudden release can take the form of a face burst, ejecting large quantities of rock into the working area.

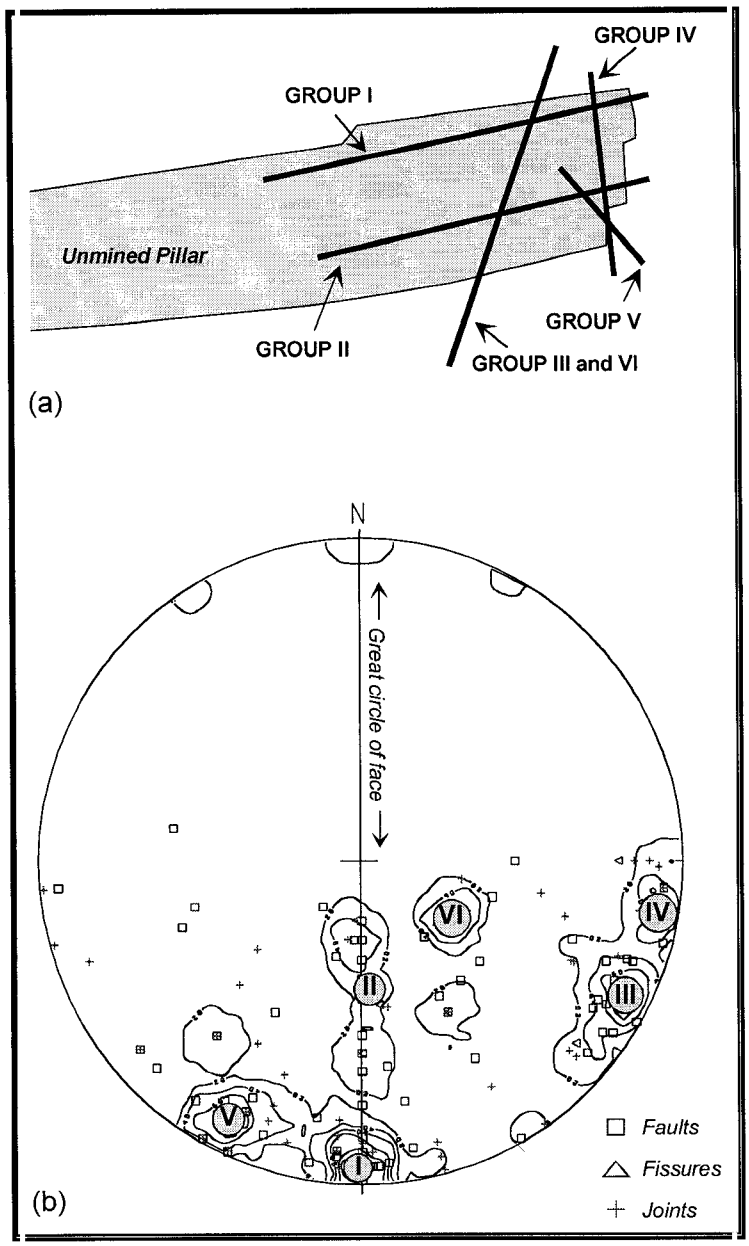

Figure B.38 (a, b) Orientations of the six major fracture sets (Groups I to VI) identified at the 17-24W site. (a) Plan showing the orientations with respect to the pillar geometry. (b) Contoured Schmidt Net (lower hemisphere projection) of poles to all mapped fractures.

Preconditioning is intended to prevent the accumulation of strain energy ahead of the working face or, at least, control its release. The gas and shock generated by a blast within the rock mass mobilizes the blocks by shearing through any asperities responsible

for a lock-up. Strain energy release is facilitated by the sliding of blocks past one another, thus reducing the risk of a face burst during the production shift. The stress redistribution away from the working face by a well-executed preconditioning blast provides a low stress zone ahead of the stope face which is able to absorb energy from more distant events. In this way, it is possible to minimise the extent and severity of damage that may occur from more distant events, while controlling the size and timing of seismic events near the face.

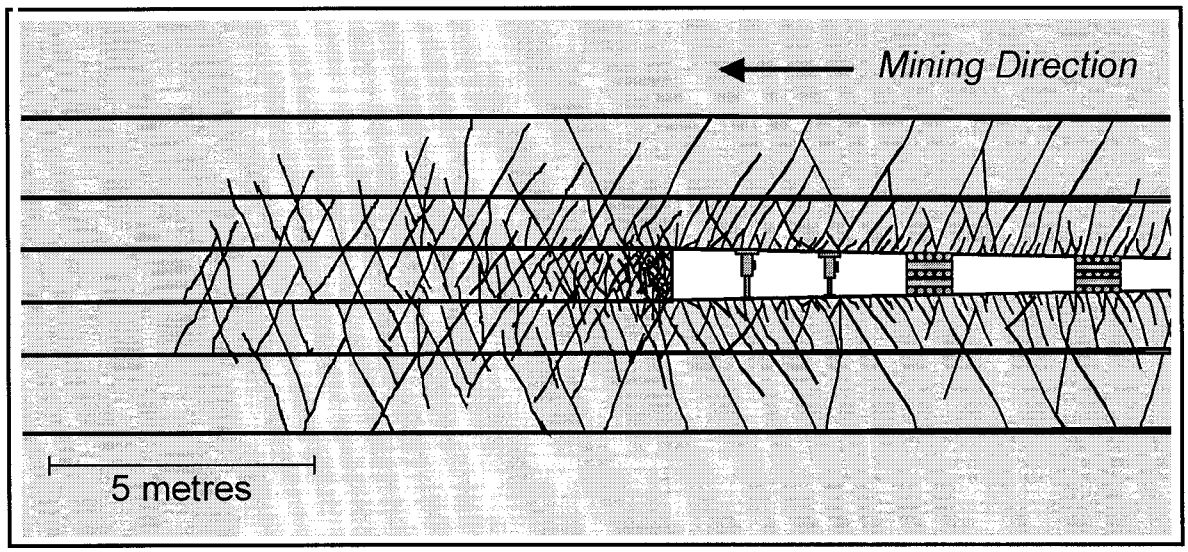

Figure B.39 Schematic vertical section through a deep-level stope illustrating the fractured nature of the rock mass surrounding the opening.

Because the mechanical properties of the rock mass are not affected by a preconditioning blast, there is reason to believe that energy could accumulate at the face once again. Stress redistribution resulting from seismicity and time-dependent deformation of the rock mass could result in the reloading of the face area, if too much time is allowed to pass before mining the preconditioned zone.

Preconditioning of the 17-24 W stabilizing pillar

Face-parallel preconditioning requires that the stope be laid out to accommodate the drilling of the preconditioning holes. As these holes need to be drilled parallel to the face (and angled slightly above horizontal to facilitate cleaning), an overhand mining configuration is preferable (Figure B.40). Individual panels should not exceed the length that can be drilled in one shift; in the case of 17-24W, the maximum face length is 20 m.

The lead between panels is kept to a minimum (less than 7 m) to prevent the development of adversely oriented fractures while still accommodating the drilling of the preconditioning holes. The position of a preconditioning hole is considered to be the limit of the preconditioned zone and no mining should take place beyond that point. Once a panel has mined to limit, another preconditioning blast is required and the cycle continues (Figure B.40).

A great deal of experimentation was required to define the area ahead of the stope face in which the preconditioning blast would provide adequate results. For an 89 mm diameter hole, the best results (for the conditions encountered in the project stope) were obtained when the hole was positioned between 3,5 m and 5,5 m ahead of the face. Limited experimentation has also been conducted with 76 mm drill bits, for which the maximum effective distance has been found to be about 4 m ahead of the face.

Figure B.41 illustrates the effects of positioning the preconditioning hole at various distances ahead of the stope face. Blasting too close to the face will result in a minimal preconditioning effect and can cause severe damage to the face area. Beyond the optimum zone exists an area in which a blast could redistribute stress back towards the stope face, resulting in stress conditions that could lead to a face burst. Seismic evidence has shown that this reloading of the face can occur (Kullmann et al., 1994). At some point, the confining stress becomes so large that the blast has virtually no effect on the rock mass beyond some small distance from the blast hole. This condition is not necessarily restricted to intact rock.

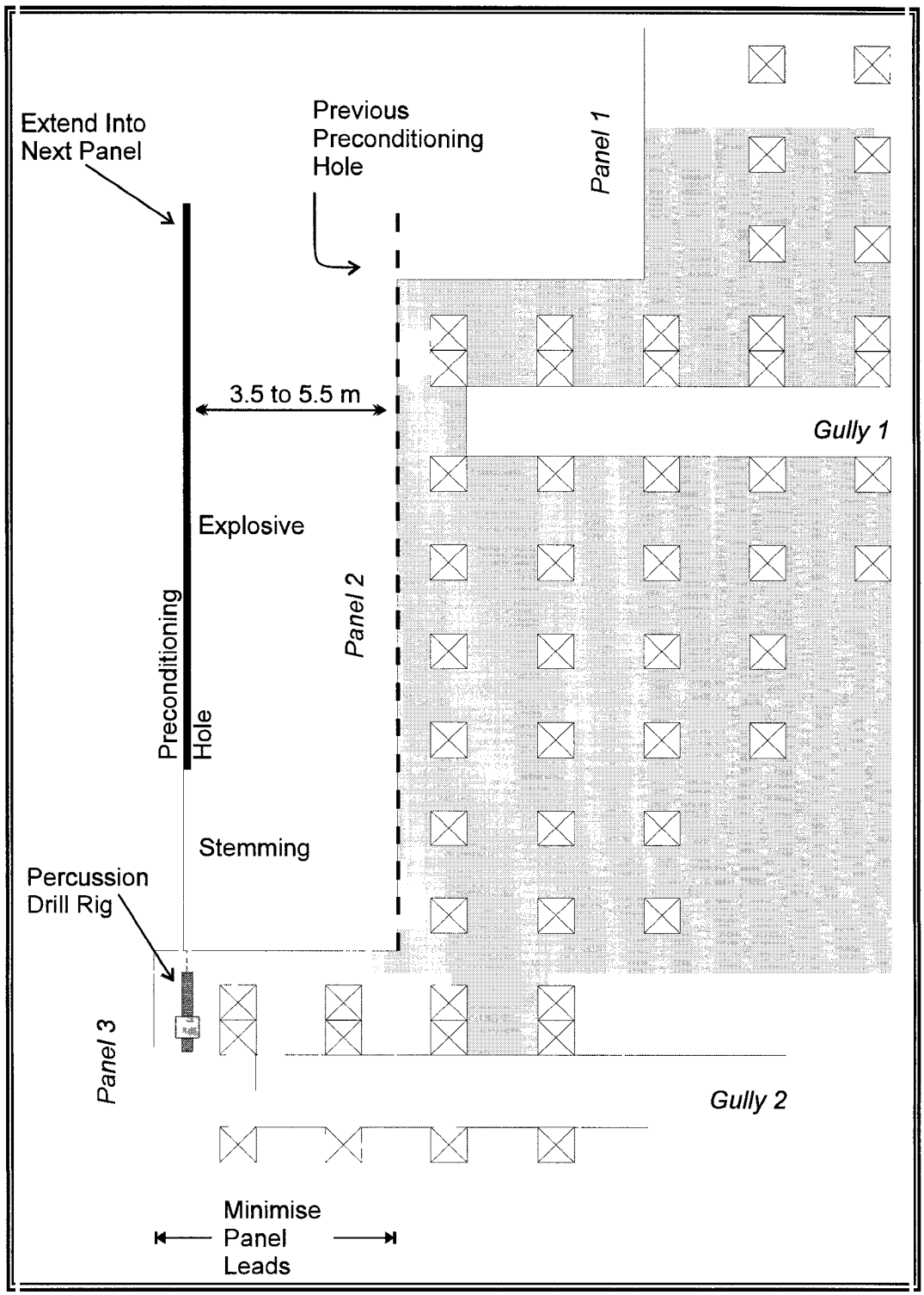

Figure B.40 Preconditioning layout in an overhand mining sequence. Panel 2 has been mined to limit and the next hole is drilled up to 5,5 m from the current face.

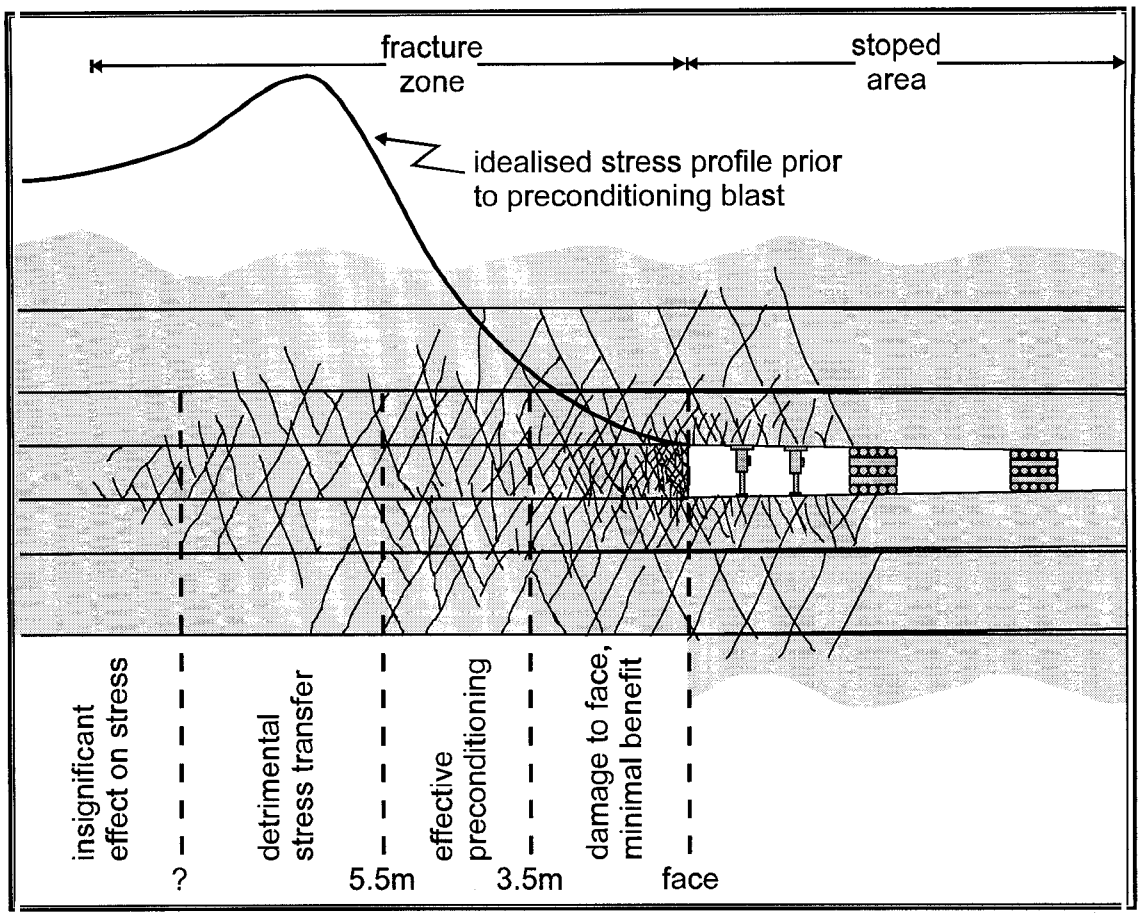

Figure B.41 Conceptual diagram showing the effects of positioning an 89 mm diameter preconditioning hole within the fractured rock mass ahead of the stope face.

Effect of Preconditioning on Seismicity

The seismic expression of preconditioning includes the blast event itself, an increase in the seismicity rate induced by the blast, and the frequent occurrence of larger seismic events triggered by the blast (Lightfoot et al., 1996; Kullmann et al., 1996). The magnitude of the seismic event recorded from a preconditioning blast is typically in the order of M_L=1,0 for 100 kg of an emulsion explosive. Significantly larger recorded blast events (considered in proportion to the amount of explosive used) have indicated the release of additional stored strain energy, beyond that accounted for by the interaction of the blast with the surrounding rock mass. Smaller blast events have been recorded from inadequate preconditioning blasts.

Effective preconditioning blasts have been found to induce stress transfer away from the preconditioned area (as shown by the spatial migration of subsequent seismicity towards unpreconditioned ground), and to facilitate the release of stored strain energy from the rock mass ahead of the preconditioned face (as shown by relatively larger blast events and/or by the triggering of separate larger seismic events). In addition, effective preconditioning blasts have been found to have an indirect positive effect on the rock mass in adjacent areas, through the mechanism of stress transfer into those areas. This often loads those highly stressed areas to failure, which results in the triggering of larger seismic events within hours of a preconditioning blast.

Also important is the observation that the direction of the spatial migration of subsequent seismicity, particularly in the case of panel 1 preconditioning blasts, is parallel to the orientation of the Group III fractures discussed above. These fractures have been identified as those which are mobilized by preconditioning.

8.3 Observations at the rockburst site

The layout of the panels mining the 17-24 W stabilizing pillar is shown in Figure B.37. Falls of ground have previously taken place in the lower strike gully. A sketch of the fracture set which controlled these falls is shown in Figure B.42.

Panel 1

The support installed in panel 1 consisted of timber packs. The distance from the face to the first row ranged from 1,6-2,0 m. Minor falls of ground from the hangingwall and face were noted between the face and first row of packs. There was no evidence of crushing of the face, or of any violent ejection of rock. The packs and mine poles were carefully inspected for signs of fresh splitting, which would indicate co-seismic convergence. The closure experienced by the first row of packs was estimated to be 50-60 mm, while the convergence experienced by the third row was estimated to be about 20 mm.

Measurements at five closure-ride stations on 30 January 1996 (made in the hour preceding the rockburst) and on 1 February 1996 indicated that closure ranging from 38 mm to 70 mm had taken place during this two day period. The normal rate of closure in panel 1 (in the absence of production blasts) is 3 mm/day.

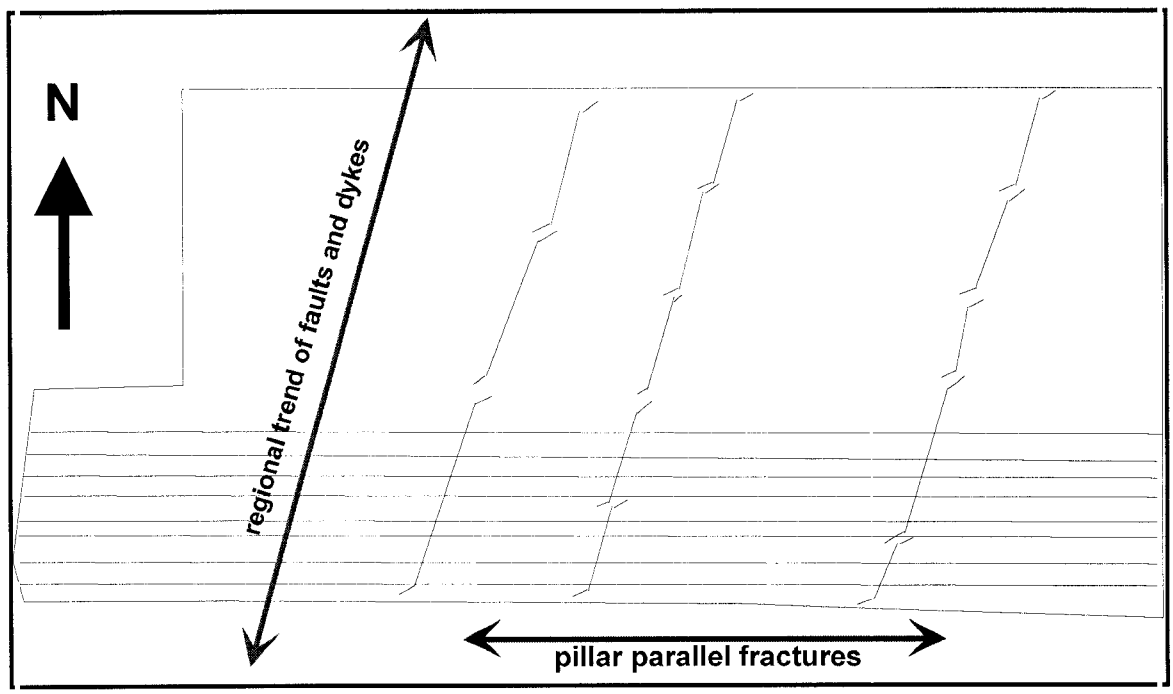

Figure B.42 Sketch plan of the lower portion of the pillar showing the orientation and position of the two major fracture sets that have controlled size of the falls of ground. Note that the lower gulley is positioned within the zone of intense pillar-parallel fractures.

Panel 2

The support installed in panel 2 consisted of timber packs, with the first line approximately 2 m from the face. The lower half of panel 2 had been blasted on the 27 January 1996, and the face area had not been cleaned prior to the rockburst and thus was inaccessible. Owing to a misfire, the upper half of panel 2 had not been blasted. The uppermost 5 m of the face of panel 2 was closely inspected. Some slabbing of the face was noted. There was no evidence of crushing of the face or of the violent ejection of rock.

The falls of ground between the face and first row of packs were more substantial in panel 2 than that observed in panel 1. Slabs ranging in thickness from 10 cm to 30 cm had fallen from the hangingwall between the face and the first row of packs over a distance of about 5 m.

Scattered falls of ground behind the front row of packs resulted in the loss of the top two closure-ride stations, with the bottom one being inaccessible at the time of writing this report. The back areas of panel 2 were inspected on 6 February. All packs exhibited significant convergence. A buckled mine pole located next to the central closure ride station (in the second row of packs) indicated convergence of about 140 mm during the time period 29 January 1996 to 6 February 1996. The rockburst on 30 January occurred before the Mining Technology observer had taken closure-ride measurements in panel 2. The normal rate of closure in panel 1 (in the absence of production blasts) is 4 mm/day.

Stub and panel 2 strike gully

Three substantial falls of ground had occurred in this area, one at the stub face and two along the strike gully (see Figure B.43). The fallout comprised both the hangingwall quartzite and Green Bar, which have a combined thickness of about 3 m. The support in the face area and along the gully consisted of timber packs. Two packs were under construction within 2 m of the face at the time of the rockburst. No hydraulic props were installed in the face area. Much rubble was removed from the face area during the rescue effort. Consequently, no observation was made of crushing or ejection of the face. It appeared that several of the gully packs had toppled over.

The principal set of fractures that governed the extent of the fall of ground were steep dipping (at approximately 85°) pillar-parallel joints (Group II in Figure B.38 (b)). These are thought to have developed during the mining out of the surrounding ground during the early 1980's. The subsequent concentration of stress on the pillar resulted in the evolution of intense fracturing along the lower edge of the pillar.

The combination of intense pillar-parallel fracturing and the finely laminated nature of the hangingwall has resulted in a highly fragmented blocky rock mass in the immediate hangingwall. Even to a depth of several metres into the hangingwall, the rock mass above

the gully consists of small (centimetre size) fragments. Fracture evidence suggests that dip-slip movement occurred on the Green Bar (either during the seismic event itself or triggered by the seismic event). As a result of this slip, the Green Bar was thrust downwards as it encountered the highly fractured bottom edge of the pillar (Figure B.44 (a, b)).

The underthrusting occurred immediately over the gully, as this was the first weak portion of the rock mass beneath the Green Bar that the dip-slip movement encountered. This downward thrusting into the highly fragmented rock mass at the base of the pillar caused the unstable hangingwall to fallout, and the weak Green Bar to collapse shortly afterwards (see Figure B.44 (b)). The areal extent of the damage was controlled by the limited extent of two sets of steeply dipping fractures - the most important being the pillar edge parallel fractures. The second controlling fracture set is that which lies parallel to the regional trend of faults and dykes, that is, it lies at about 70° to pillar-parallel fractures. Fine white powdery gouge on these vein quartz faults indicates that these planes were reactivated during the rockburst.

Observations suggest that the damage closest to the face of the stub could have been caused by slip on the Green Bar. This slip resulted in the underthrusting of the up-dip portion beneath the down-dip portion. This underthrusting occurred at the weak point in the rock mass, generated by extensive pillar-parallel fracturing. The underthrust slice punched through the weakened rock mass immediately above the lower gulley, causing it to fallout. This, in turn, left the fractured Green Bar exposed and as a result this also fell out.

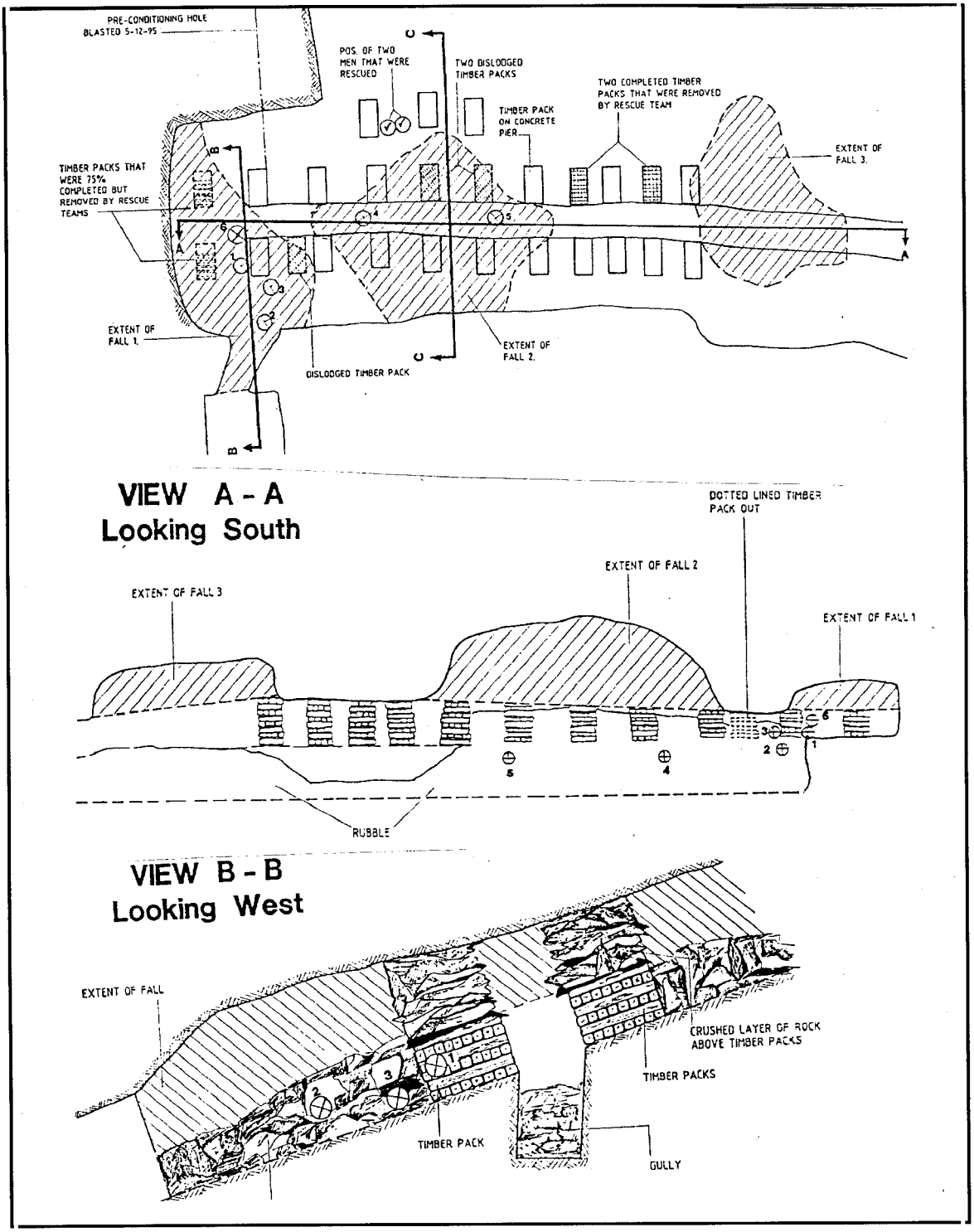

Figure B.43 Plan and sections showing the damage caused by the rockburst on 30 January 1996 to the panel 2 strike gully in the 17-24W stabilizing pillar, Blyvooruitzicht Gold Mine: Prepared by L. Schultz and H. Redelinghuys, Blyvooruitzicht Gold Mine.

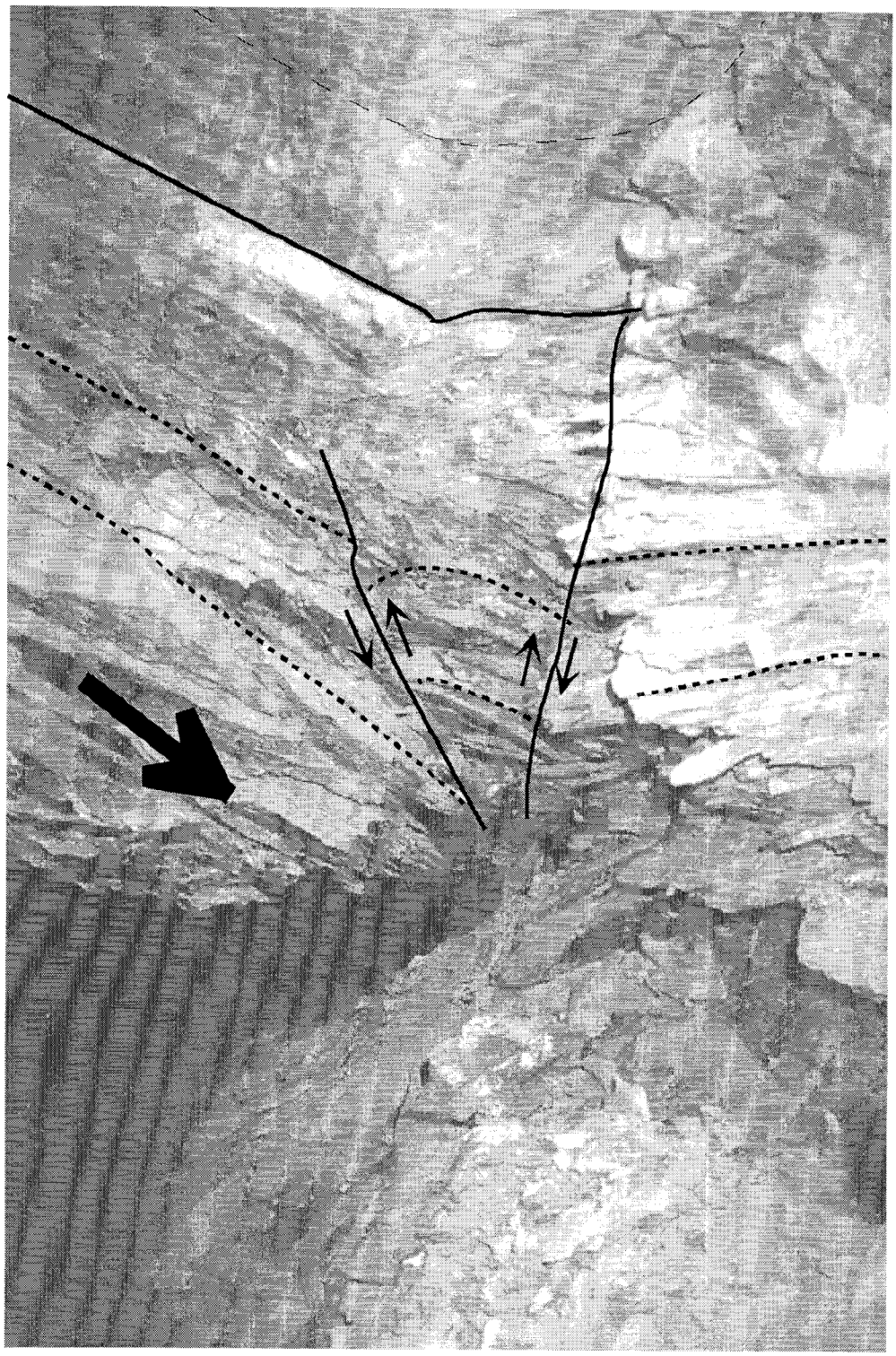

Figure B.44 (a) Photograph showing a rockburst damage to a Carbon Leader Reef gully.

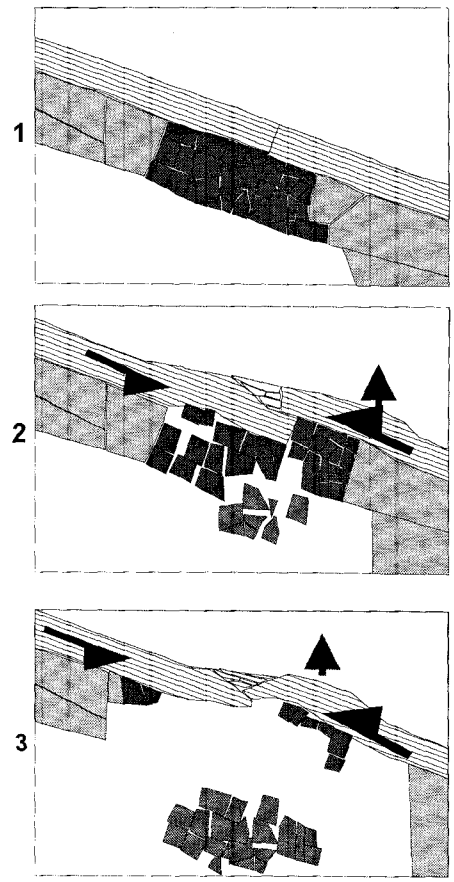

Figure B.44 (b) Sketch diagram showing the possible mechanism of rockburst damage to a Carbon Leader Reef gully. Prior to damage, note the region of intense pillar-parallel fractures (dark shading); slip on the Green Bar (direction is shown by arrows) causes buckling and underthrusting of the Green Bar. The underthrusting causes fallout of the hangingwall quartzite below the Green Bar. Continued thrusting and buckling causes extensive falls of both hangingwall quartzite and Green Bar.

8.4 Assessment of support performance

Stope panels

The support in the panels consisted of 1,1 m x 1,1 m solid timber packs. The spacing between packs was less than 1,5 m skin-to-skin. Close scrutiny of the timber packs and some mine poles showed fresh timber exposed on some of the support units as a result of dynamic loading during the seismic event. The maximum amount of dynamic closure was approximately 140 mm, leading to buckling of some mine poles.

No hydraulic props were installed in the face area of panels or stub. Although the damage was not severe in panel 1 and the upper half of panel 2, it is believed that the presence of hydraulic props would have reduced the shake out. The face area of the advance strike gully (the stub) sustained severe damage as a result of the collapse of the hangingwall. This damage may have been limited if props were present.

Stope Gully

The gully was supported by solid timber packs, generally spaced closer than 1,5 m skin-to-skin. The stoping height is about 1 m. However, the gully packs were considerably taller in places because of past instabilities such as falls of ground, and damage by scrapers to the pack or its foundation. No hydraulic props were present in the face of the stub. Occasional split sets were noted in the hangingwall of the gully.

Clearly the support had failed to retain the hangingwall of the stope gully during the rockburst. Owing to the fragmented nature of the hangingwall, it is thought that tendons would have been ineffective, unless combined with strapping or mesh and lace. Furthermore, owing to the existence of parting planes at the base and top of the Green Bar, any tendons would have had to be at least 8 m in length to be effective. Evidence of shear movement in the Green Bar suggests that tendons would have been subjected to shear movement during the rockburst.

It appeared that several of the gully packs had also toppled during the rockburst. This could have been caused either by lateral movement, or be a consequence of hangingwall fragmentation and severe shaking.

8.5 Assessment of layout

MINSIM modelling (which assumes perfect elasticity) yielded average pillar stresses of 425 MPa. This result is far in excess of the actual average pillar stress, estimated by Handley et al., (1996) to be about 160 MPa, and by Adams et al., (1992) to be 150 MPa. Relatively low average pillar stresses do not rule out local areas of high stress, a condition that probably existed in the pillar at the seismic event location. No model, whether it is elastic or inelastic, can be used to predict such situations in the pillars ahead of the face.

8.6 Seismic history

The seismicity associated with mining the 17-24W pillar has been monitored continuously since 1990. Since the change to breast mining in September 1992, 51 events with $M_L \geq 1$ and 15 events with $M_L \geq 2$ have been recorded from the 17-24W pillar. Several of the larger events caused falls of ground in the strike gullies. There is no evidence to suggest that the seismicity associated with this rockburst was in any way remarkable when compared with the occurrence of the other larger seismic events at the site.

These larger events were spaced fairly evenly through the time period since September 1992. While most of the events occurred during or shortly after blasting time, three did occur at on-shift times. Of the 40 days on which large events $M_L \geq 1$ took place, 11 days had pairs of such events. The events in four of these pairs were separated by more than one hour, but all of these incidents involved triggering by preconditioning or production blasting. None of the on-shift events were followed by a second large event within 24 hours.

8.7 Rockburst mechanism

Source mechanism

The rockburst took place at 08h52 on 30 January 1996. Two seismic events occurred within 1 s, and were recorded by both the research (B17) seismic network surrounding the pillar and the mine-wide (BGM) seismic network, as well as by the Western Deep Levels South Mine (WDLS) seismic system. The seismograms recorded by the B17 network were saturated owing to the intense shaking close to the source. Consequently, the seismograms recorded by the BGM network were used in the determination of the source parameters. The local magnitude of the first event was M_L=2,2, as determined from the BGM network (the WDLS network assigned the event a local magnitude of M_L=2,3, confirmed by the national seismic network administered by the SA Council for Geoscience). The B17 network seismograms enabled the focus of the event to be located with an error of less than 5 m. The focus was located about 20 m ahead of panel 2 and 15 m in the hangingwall of the reef (see Figure B.45). The large amount of S-wave energy suggests that the event had a slip mechanism. The stress drop was moderate (a static stress drop of about 5 MPa). The Brune source radius was 60 m.

The M_L=2,3 event (local magnitude determined from BGM network), was located about 100 m to the north of the stabilizing pillar and in the footwall of the reef (see Figure B.45). The waveforms recorded from this second event were superimposed on the tail of the first event, so the location was not determined with the same degree of confidence as that for the first event. It is thought likely that the observed damage resulted from the combined effects of both of these large seismic events.

Three possible rupture surfaces were considered for the first event:

A steeply dipping surface parallel to the axis of the pillar, favoured by pre-existing fracturing fracturing (Group II in Figure B.38 (b)).

A steeply dipping surface roughly parallel to the mining faces. As the pillar is only 40 m wide and the Brune source diameter 120 m, the rupture surface would have extended beyond the pillar. Alternatively slip occurred on multiple sub-parallel fracture surfaces.

A shallowly dipping surface parallel to bedding. Observations indicate that the Green Bar has a low strength and cohesion, which would suggest that the seismic event should have had a relatively low stress drop.

Thirty aftershocks (with magnitudes in the range $-2,3 \leq M_L \leq 0,1$, the $M_L=0,1$ event occurring within a minute of the main shock) were recorded by the B17 network in the 24 hours following the main event, some causing small falls of ground which resulted in minor injuries to members of the rescue team. The locations of these events were used in an attempt to define the rupture surface. These events clustered around the location of the main shock within the pillar area, with some indications of planarity sub-parallel to the dip of the strata.

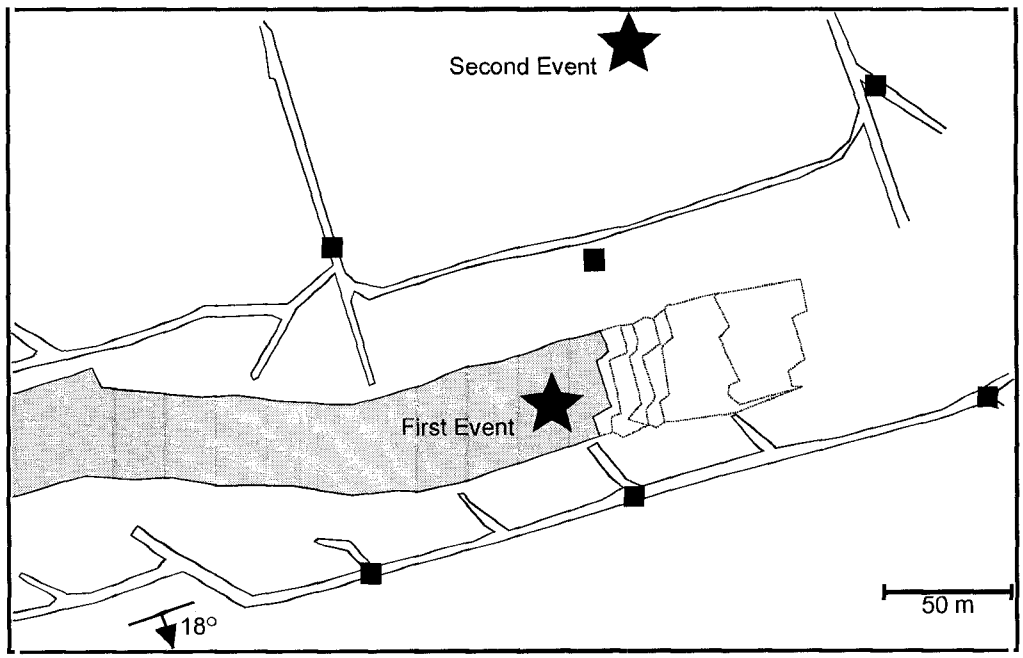

Figure B.45 Plan showing the locations, as determined from the research seismic network records, of the $M_L=2,2$ and $M_L=2,3$ seismic events which occurred on 30 January 1996 damaging the 17-24W stope, Blyvooruitzicht Gold Mine.

Damage mechanism

It is believed that the rockburst damage was owing to the disintegration of the highly fractured and inadequately supported hangingwall when subjected to seismic shaking. Damage is directly related to the duration of shaking. Thus the effect of the shaking was exacerbated by the second M_L=2,3 event occurring immediately after the M_L=2,2 event.

Strong ground motion measurements

Two CSIR Ground Motion Monitors (each with three separate accelerometers) were installed in panel 1 at the time of the rockburst. The accelerometers are mounted in aluminium containers which were stuck to the rock surface using Pratley Putty. Several of the slabs to which the sensors were attached were dislodged by the main event. Others slabs were dislodged several hours later by aftershocks. These slabs were typically brick sized.

The sensors of one Ground Motion Monitor were attached to the face, hanging- and footwall about 5 m above the toe of panel 1. This was about 40 m from the focus of the M_L=2,2 event. This event produced shaking with a duration of about 80 ms, with peak acceleration a_{max} = 420 m/s^2 and peak velocity v_{max} = 470 mm/s. A further four aftershocks were recorded in the 10 minutes after the main event. The two larger events (M_L=0,1 and M_L=-0,5) were also recorded by the microseismic network. Both these events produced a_{max} = 110 m/s^2. The sensors then became detached from the skin of the excavation. The monitor also recorded a M_L=-1,0 event on the evening prior to the rockburst (19h33 on 29 January 1996), with a_{max} = 32 m/s^2.

The sensors of the other Ground Motion Monitor were attached to the face at distances of 1, 4 and 8 m from the toe of panel 1. These all became detached at the time of the M_L=2,2 event. No useful information was obtained from this monitor.

8.8 Seismic hazard

The rockburst had no recorded precursory seismicity. The last event prior to the rockburst was recorded over eight hours before the occurrence of the main shock. The sensitivity threshold for seismic events located within the network is M_L=-2,0.

Hazard assessment

The seismicity recorded in this area has been used to devise a technique for estimating the seismic hazard. Ten parameters are monitored during the evaluation of seismic hazard by means of this technique (Lightfoot et al., 1996). These parameters are determined from consideration of frequency-magnitude statistics, spatial clustering of seismicity, and various source parameters such as stress drops. Previous large events have been used to define critical values of the parameters. When these critical values are exceeded, the probability of occurrence of a large event is considered to be increased.

The technique was used to evaluate the level of seismic hazard on a daily basis prior to the stope team entering the working place. Review of the seismicity indicated that the level seismic hazard when assessed for the day of the rockburst was similar to that which prevailed in the preceding weeks. Even in hindsight, no increase in hazard was detected.

Preconditioning and seismic hazard

As noted in Section 8.2, the preconditioning blast causes an increase in the seismic event rate. The locations of these events indicate a transfer of stress away from the face and towards unpreconditioned areas. Large events ($M_L \geq 1$) have been regularly triggered by preconditioning blasts.

Preconditioning may be the reason for the relatively minor damage to panel 1 and panel 2. However, as the most recent preconditioning blast was detonated on 5 December 1995 (some 8 weeks prior to the rockburst), and the effect of preconditioning is believed to diminish with time, this claim is made with some caution.

Drilling of a preconditioning borehole was owing to commence following a final production blast in the stub. The long time interval between preconditioning blasts was owing to slow face advances during the holiday period around Christmas and New Year.

8.9 Conclusions

Two seismic events with M_L>2 occurred at 8h52 on 30 January 1996, causing extensive damage to the 17-24W strike gully at Blyvooruitzicht Gold Mine. The first event had a magnitude M_L=2,2. The focus of the event was located within the stabilizing pillar about 20 m ahead of the face. The static stress drop was moderate (5 MPa), with a Brune source radius of 60 m. The ratio of S- to P-wave energy indicates a shear rather than crush source mechanism. The M_L=2,2 event was followed, within a minute, by a M_L=2,3 event located about 100 m to the north of the stabilizing pillar.

Events of this magnitude within the stabilizing pillar are not unusual. Fifteen events with M_L>2 have been recorded since September 1992.

Although the average pillar stress is estimated to be low (about 150 MPa) and much lower than predicted by an elastic model (MINSIM-W estimation was 425 MPa), there are probably volumes of rock in the pillar that are highly stressed, and such volumes are believed to be responsible for the seismic events. The stress within the pillar has been relieved by a combination of footwall punching and complete stope closure right up to its flanks.

Some 30 aftershocks occurred within 24 hours of the event. The epicentres of aftershocks are often used to define the rupture surface. These aftershocks form a cluster within the stabilizing pillar around the focus of the first (M_L=2,2) event, roughly in the reef plane. It is not possible to unequivocally distinguish between a rupture surface orientated sub-parallel to bedding; or several steeply-dipping and spaced rupture surfaces.

Damage to panel 1 and the upper half of panel 2 was relatively minor. Access was not gained to the lower half of panel 2. The damage was largely confined to the 2 m wide area between the face and the first row of packs. Damage consisted a scattered falls of ground and slabbing from the face. There was no evidence of crushing or ejection of the face. Co-seismic closure was estimated from the splitting of packs and mine poles, as well as measurements at closure-ride stations. It ranged from about 40 mm at the top of panel 1 to 140 mm in the centre of panel 2. Observations from the panel 2 strike gully indicated that substantial closure had occurred at the toe of panel 2.

Damage was severe in the heading of the panel 2 advance strike gully owing to the collapse of the hangingwall. No observations could be made regarding the state of the face (e.g. degree of crushing), as material was removed during the rescue effort.

Another two substantial collapses occurred in the strike gully. The thickness of the fall of ground was about 3 m, including the hangingwall quartzite and the Green Bar.

The support installed in the panel 2 strike gully was clearly unable to cater for the fractured nature of the hangingwall. It consisted of timber packs and occasional split set anchors. This gully had been excavated along the lower edge of the stabilizing pillar where a prominent set of mining induced fractures orientated parallel to the edge of the pillar is present. This gives rise to poor hangingwall conditions. Several substantial falls of ground had previously occurred in this gully, fortunately without causing injury to workers.

No hydraulic props were present in the face area of the panels or the strike gully. It is believed that they would have reduced the damage in the face area.

Several gully packs had toppled during the rockburst.

Preconditioning may be the reason for the relatively minor damage to panel 1 and panel 2. However, as the most recent preconditioning blast was detonated on 5 December 1995 (some 8 weeks prior to the rockburst), and the effect of preconditioning is believed to diminish with time, this claim is made with some caution.

8.10 Recommendations

Rockburst resistant support such as rapid yielding hydraulic props with headboards must be installed in the face area, including the advance strike gully.
The strike gully is hazardous owing to the poor ground conditions which exist along the lower edge of the stabilizing pillar. Either the gully must be moved to less fractured ground, or the support must be greatly improved.

Preconditioning should be continued to reduce the possibility of face bursting.

The intervals between preconditioning blasts should be based on both the time elapsed, and the face advance.

9 Western Deep Levels (South), 15/2/96, M_L=1,8

9.1 Introduction

On 15 February 1996, a rockburst occurred at Western Deep Levels South Mine, causing damage to the West 2 (W2) panel of the 87-49 stope, about 2500 m below surface (Figure B.46). The rockburst, which caused five injuries, took place at 07h56. A seismic event with magnitude M_L=1,8 was recorded by the mine's seismic network at that time. A preconditioning experiment was being conducted in this stope by a team from CSIR Mining Technology. Consequently the rockburst was of great interest and relevance, and a detailed investigation into the incident was conducted. The team visited the site on 16 February 1996.

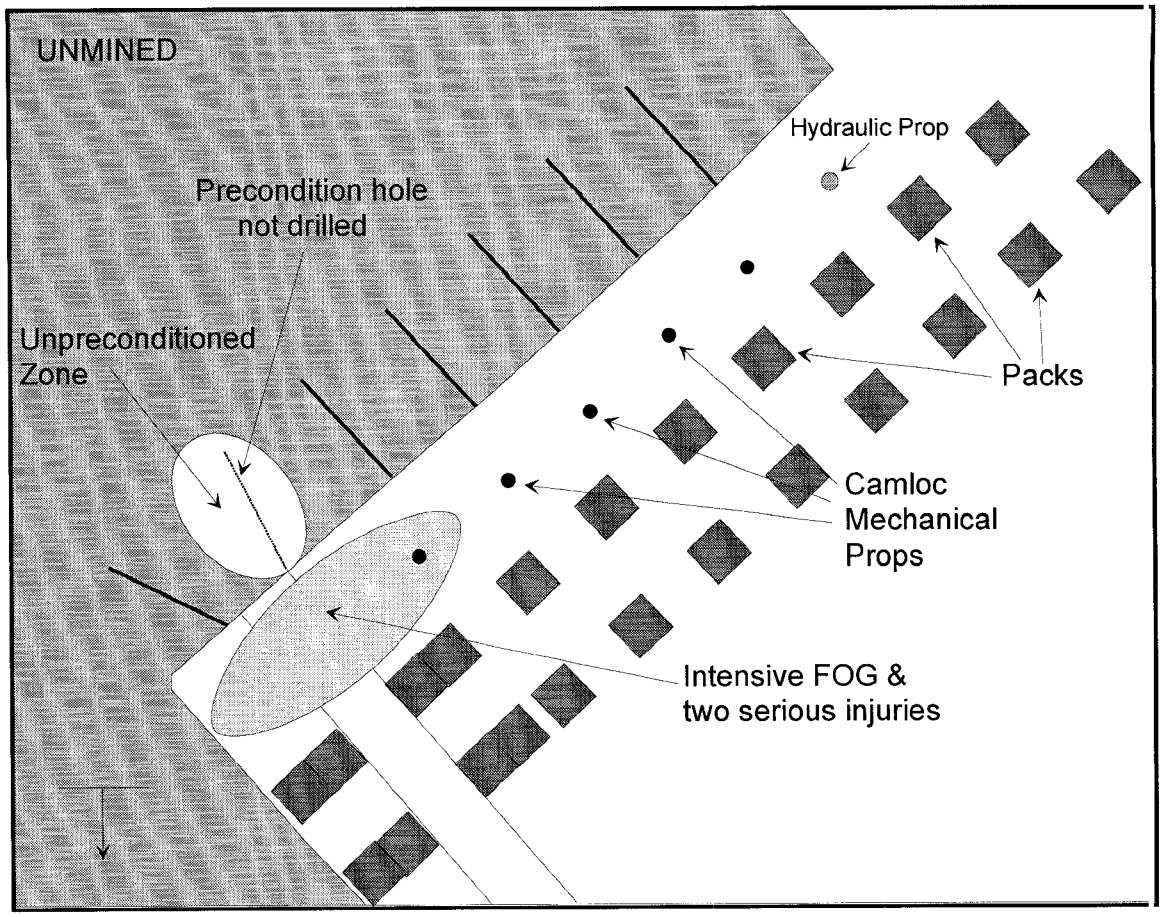

Figure B.46 Schematic plan of West 2 (Diagonal) panel (Not to scale).

9.2 Mining environment

The 87-49 stope is located at the south-west corner of Western Deep Levels South Mine. The mining of this stope on the Ventersdorp Contact Reef (VCR) began in the middle of 1992. The dominant joint set was oriented in the dip direction which caused serious instability problems in the face area and it was decided, on the recommendation of the rock mechanics department, to change from the breast mining to an up-dip mining layout at the end of 1992. Although the instability problems and the levels of damaging seismicity were reduced by changing the mining direction, face bursts were still being experienced. Thus, Mining Technology's Preconditioning Team was asked at the end of 1993 to start a preconditioning project in this stope. The actual preconditioning began on 23 May 1995 on a single up-dip panel. During the course of 1995, preconditioning was

started on other panels. The effect of preconditioning resulted in a significant improvement in hangingwall conditions and an increase in face advance per blast.

In August 1995 the mining direction was again changed, from up-dip to "diagonal" mining, which is a compromise between breast and up-dip mining. The rockburst resulting from the M_L=1,8 seismic event on 15 February 1996 caused five injuries and damage to the W2 diagonal panel (Figure B.46). The preconditioning of this panel was started on 20 October 1995, although it was found during regular visits to the panel that the preconditioning guidelines were often disregarded.

9.3 Observations at the rockburst site

Rockburst damage

Members of Mining Technology's Preconditioning Team visited the site (W2 panel) on 16 February 1996. The section shift-boss accompanied the team during the visit. The face area was supported by one row of Camlok (mechanical) props. The distance between the face and the first row of packs was 3,0–3,5 m. The Camlok props were in place at the time of the rockburst. All the props had remained standing and supported the hangingwall to some extent, although one of the props had been bent owing to closure which had accompanied the event. Falls of ground were observed throughout the panel. Blocks had been ejected from the hangingwall in the area between the face and the first row of packs. The damage was most severe in the heading of the diagonal gully area, where no support was present and two serious injuries occurred (Figure B.46). In this area, blocks up to 1m in thickness had fallen. Over the remainder of the panel, the falls were confined to the area between the face and the mechanical props. The thickness of the ejected blocks was generally less than 30 cm. The other three workers were also injured in the face area, but away from the gully.

The face was intensively fractured and crushed in some parts of the panel. No face bursting was observed, but some (maximum 20–30 cm deep) reef scaled down and spread to about 1 m from the face. The face was blasted the day prior to the rockburst and the sockets of both preconditioning and production holes were visible at the face. It was observed that one of the preconditioning holes had not been drilled on the day before the rockburst. This hole should have been drilled from the gully and angled in an up-dip direction (Figure B.46). Since the hole was not drilled, the distance between the two neighbouring preconditioning holes was almost 6 m, which could have caused an undesired stress transfer onto that part of the panel where the most damage occurred.

Another important and unusual observation was that the average length of the sockets of production holes was measured as 40-50 cm. In addition, no sockets could be found from the preconditioning holes that should have been drilled two days before the rockburst. The section shift-boss explained that the last few production rounds were drilled with 1,8 m long drill steels and because of the production pressure, he had decided to drill longer production holes to achieve a higher advance rate per blast. He also said that the preconditioning holes were drilled with 2,4 m drill steels (maximum hole length 2,2 m), although 3,2 m drill steels were in the underground store. The recommended preconditioning set-up requires 3 m long preconditioning holes to be drilled and blasted together with normal 1 m production holes. This ensures a 2 m preconditioned zone ahead of the face with every production blast. Assuming an average of 1,4 m face advance per blast, only a 0,8 m zone ahead of the face was preconditioned with the degraded technique. It can thus be concluded that the panel was not being preconditioned effectively.

Convergence-Ride Measurements

Daily measurements had been taken at a number of convergence-ride stations. The convergence and ride calculated for stations in W2 and W3 panels are shown graphically in Figures B.47 (a, b) and B.48 (a, b), respectively. These four stations were located about 20 m behind the faces on the day of the rockburst. Another two stations were installed about 10 m closer to the W2 face a few days prior to the rockburst. These measurements are included in Figure B.47 (a, b).

The last measurement shown on each graph in Figures B. 47 (a, b) and B.48 (a, b) was on 16 February 1996, the day after the rockburst.

For some time prior to the rockburst, a steady convergence rate of 2,0 to 2,4 mm/day was noted for the stations 20 m from the face. The rockburst itself did not result in any significant increase in convergence. Even for the stations closer to the face (which indicated 8-9 mm convergence after the event), the convergence rate did not vary significantly from the older stations when they were first installed. The times of noticeable increase in convergence rate in Figures B.47 (a, b) and B.48 (a, b) are all correlated with the occurrence of large (M_L>1) seismic events in the vicinity of the 87-49 longwall. The buckling of a Camlok prop at the face (installed just prior to the event) implies that significant convergence did take place at the face, but the lack of notable convergence in the back areas of the panels indicates the localised nature of this event, even though it had a relatively large magnitude.

Fracture mapping

It is important to note that the diagonal mining faces lie sub-parallel to the large mining induced shear zones. These shears develop tens of metres ahead of the face, parallel to the overall shape of the longwall. When the panel mines through them, the combined effect of the face-parallel fractures and the large shears causes periodic falls of ground. These falls are large, extending 0,5 m up into the hangingwall and often the entire length of the panel between rows of packs. Such falls are not prevalent in the up-dip panels, as the face shape is not parallel to the overall shape of the longwall, so that the two sets of fractures do not combine to form a weak plane from which falls of ground can occur. In addition, the orientation of the pack lines in up-dip panels is not parallel to the large shears.

Investigation of the damage following the rockburst on 15 February 1996 revealed that no new fractures had developed in the area. Most of the damage occurred owing to fallout on face-parallel fractures (both steeply dipping mining induced fractures and shallowly dipping extensional cracks). The apparent reduction in the number of face-parallel fractures can be partially explained by the fact that the seismic event caused the slabs formed by these fractures to be shaken out.

These thin slabs of reef were clearly evident within the first 1,0 m from the face. Very few slabs of reef were seen further back, and none were found wedged into the packs (as one might expect if the face had ejected).

However, even when this shakeout is taken into account, the depth of face-parallel fracturing was less than is normally observed. This reduction in the zone of fractured rock was owing to relatively long production holes being drilled with short length preconditioning holes. Thus, the zone of influence of the preconditioning blast ahead of the face was severely reduced.

9.4 Rockburst mechanism

Source mechanism

The Portable Seismic System (PSS) monitoring the seismicity from the WDLS 87-49W stope recorded a seismic event of magnitude M_L=1,9 (seismic moment 10^{12} Nm; seismic energy release 10^7 J) at 07h56 on 15 February 1996. This event was clearly the cause of the rockburst, as it was located within 10 m of the face of W2 panel (with an estimated location error of 15 m). Given that the source radius was estimated (from the Brune model of a seismic source) to be 55 m, a large part of W2 panel was within the region of influence of the source of the event. The location of the event is shown in plan in Figure B.49. The mine-wide ISS network also recorded the seismic event, assigning it a magnitude of M_L=1,8. The location of the event as given by the ISS was within 40 m (in plan) of that given by the PSS, and approximately on the reef plane. No foreshock activity was recorded from the vicinity of the rockburst event.

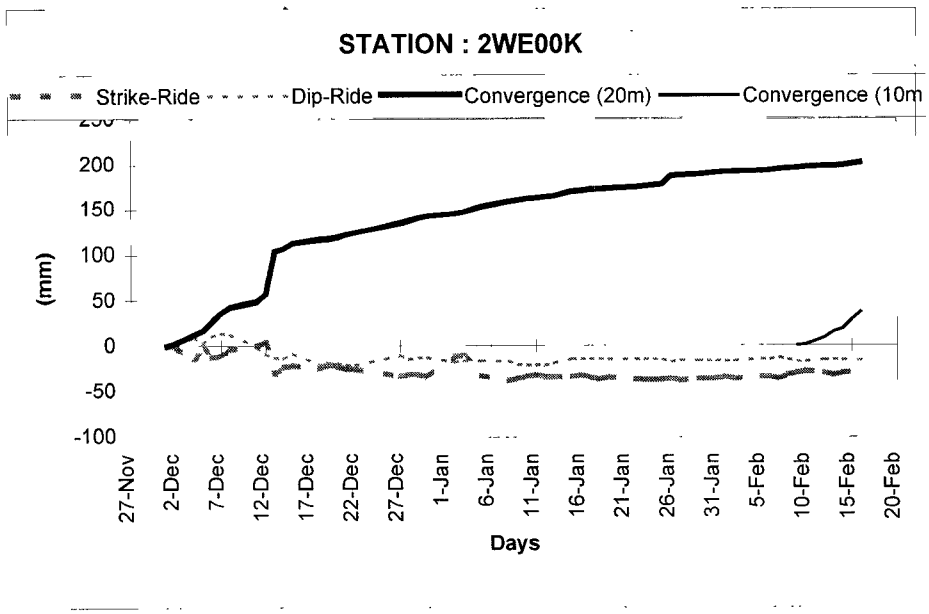

Figure B.47 (a) Convergence-ride measurements at West 2 (Diagonal) panel; at station 2WE00K.

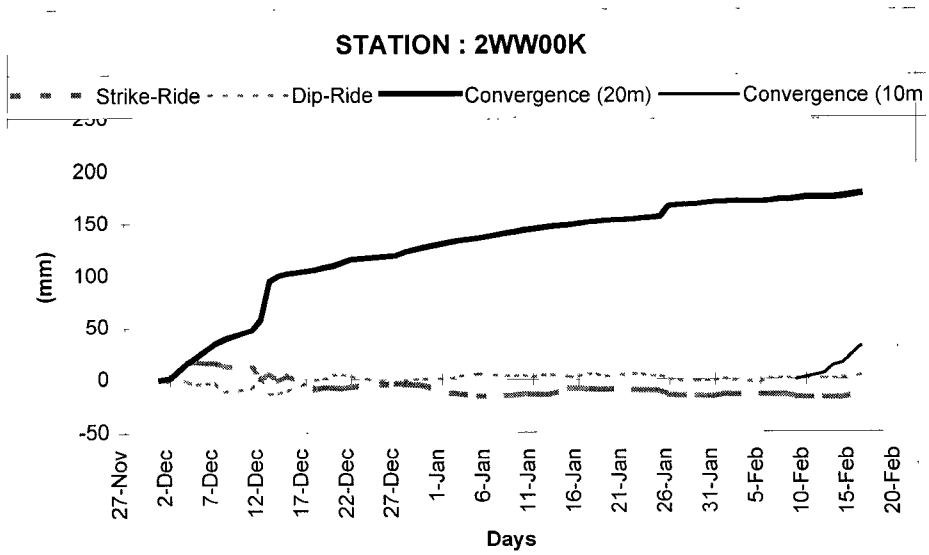

Figure B.47 (b) Convergence-ride measurements at West 2 (Diagonal) panel; at station 2WW00K

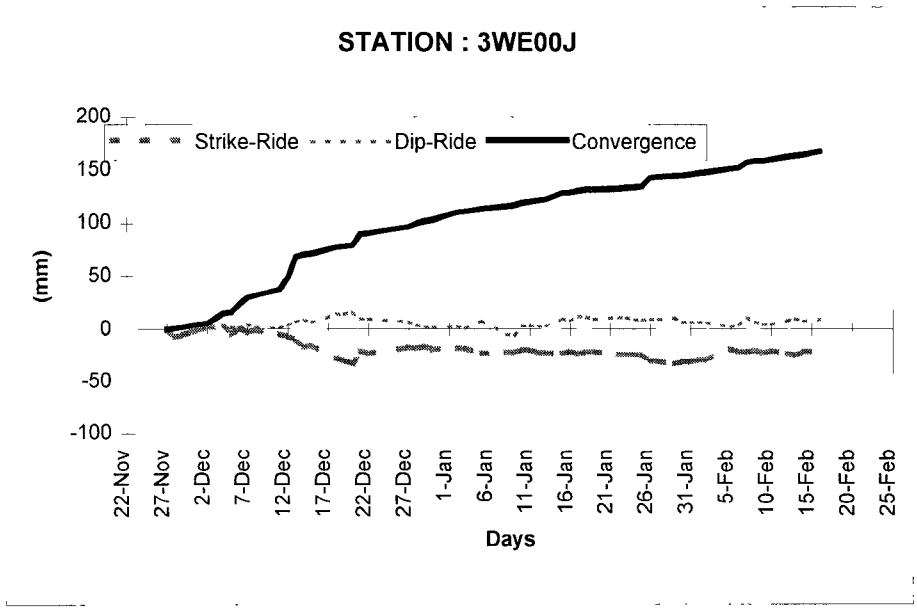

Figure B.48 (a) Convergence-ride measurements at West 3 (Diagonal) panel at station 3WE00J.

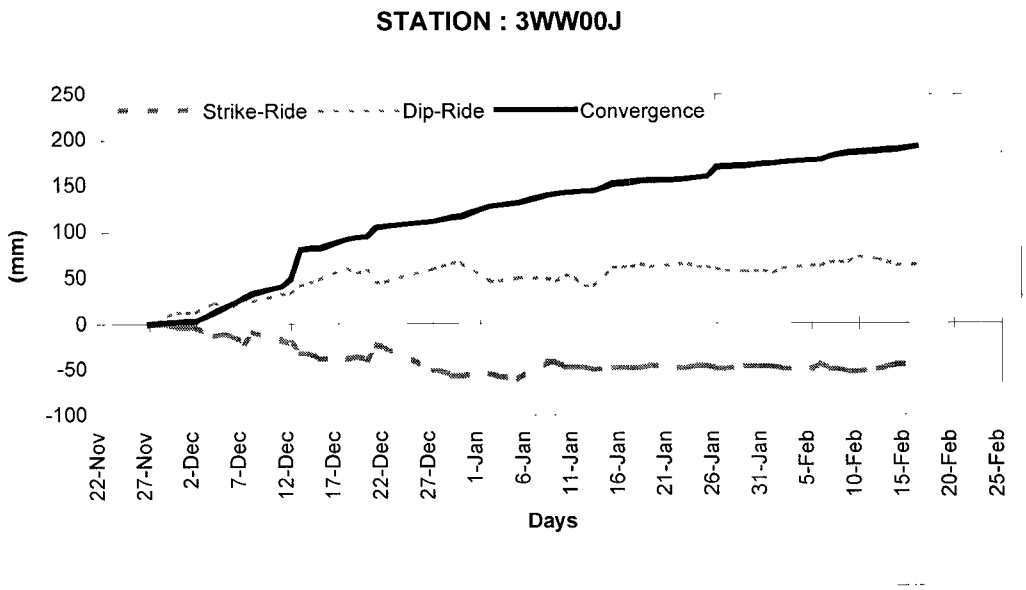

Figure B.48 (b) Convergence-ride measurements at West 3 (Diagonal) panel at station 3WW00J.

The consistency between the seismic data recorded by the PSS and ISS networks is demonstrated by the fact that the locations determined for 13 seismic events recorded by both the PSS and the ISS in 24 hours before and after the rockburst were in agreement to within 51±28 m in plan (76±40 m in three dimensions). The magnitudes assigned to these events agreed to within 0,07±0,17 magnitude units. The source parameters (such as seismic moment and seismic energy release) determined for the seismicity recorded from the vicinity of the 87-49 stope by the two networks also show similar trends.

Some six other seismic events of magnitude M_L>1.0 were recorded by the PSS in 24 hours before and after the rockburst event; two of these other events located on the 87-49W stope faces. Most of the seismicity recorded from the 87-49 stope by the PSS during this period was associated with development blasting and production blasting activity in W5 and W6 panels. Only two other seismic events were recorded from the W2 panel in the 24 hours before and after the rockburst: a M_L=0,0 event at 13h40 on 14 February, and a M_L=–0,7 event at 17h06 on 15 February.

Seismic events of magnitude M_L<–1,0 are not reliably recorded by the PSS network. The rockburst event did not have a specific trigger, but it does appear to have been the time-dependent response of the rock mass to the stress changes induced by the mining. The other two large events mentioned appear to have been triggered by blasting activity. At 13h49 on 15 February, a M_L=1,4 seismic event occurred at the bottom of W6 panel and, at 13h52, a M_L=1,1 seismic event occurred just ahead of the face of W1 panel. Both of these events took place during or shortly after the face blast on W6 panel.

In the three months before the rockburst on 15 February, some 33 seismic events of magnitude M_L>1,0 were recorded from the vicinity of the 87-49W stope faces by the PSS. The majority of these events were located close to the stope faces (within 40 m of the faces). Fortunately, most the events took place during or shortly after blasting time (only six events took place separately from the blast-induced seismicity). The large events tended to cluster in the vicinity of the faces of panels W5 (seven events), W6 (nine events) and W2 (seven events). One interesting feature of the clustering is that, while the large events tended to locate ahead of the faces in the case of panels W5 and W6, the events located exclusively in the vicinity of the siding or (as in the case of the rockburst event) in the vicinity of the angle between the siding and the face in the case of W2 panel.

This was brought about, no doubt, by the long lead-lag situation which had developed behind W2 panel.

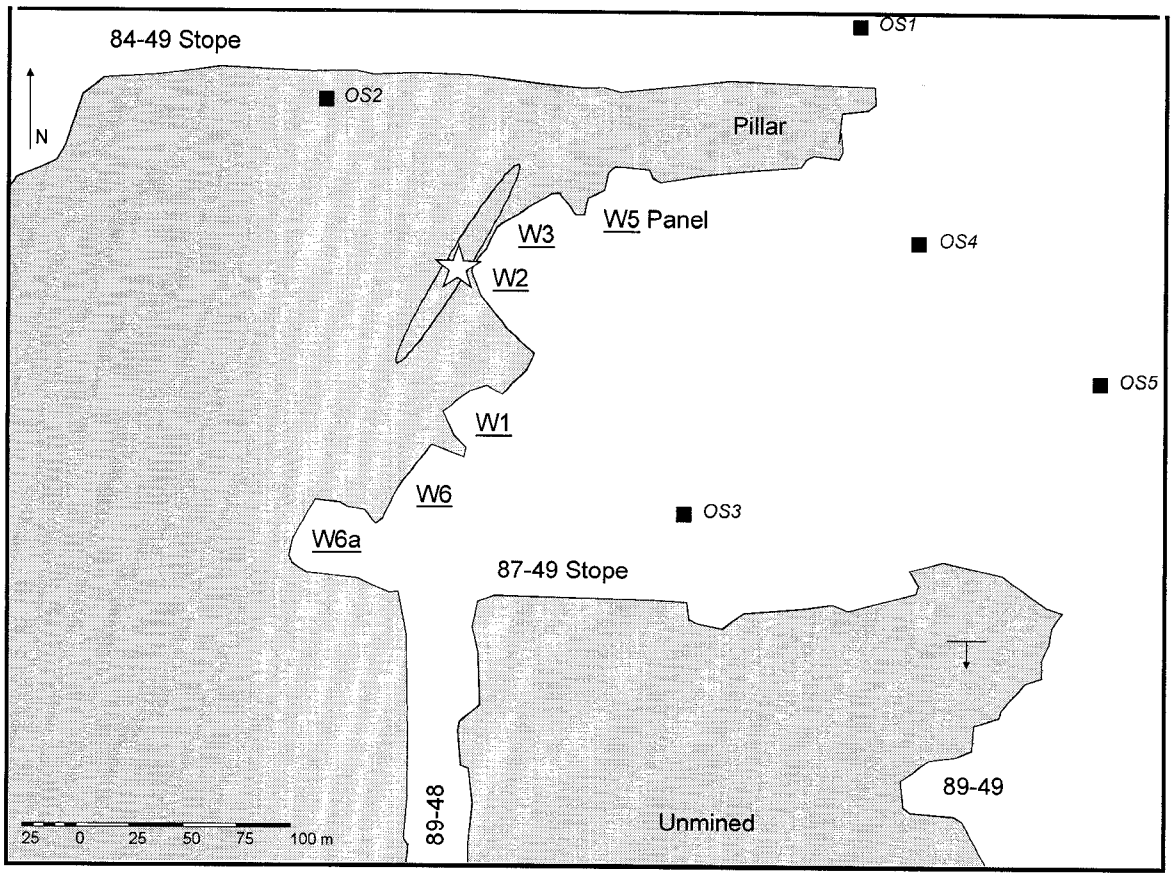

Figure B.49 Plan of WDLS 87-49 stope, showing the location of the rockburst seismic event (star) as determined from the PSS recording. The ellipse around the star indicates the possible source region as given by the Brune model of the seismic source, assuming slip on a steeply dipping plane oriented parallel to the large seismically induced shear zones observed underground. The positions of the PSS recording sites are shown by the labelled squares.

While the general seismicity rate recorded from the 87-49W stope remained fairly constant during the three-month period, the occurrence of the large seismic events was strongly clustered in time, as well as in space. The 33 events took place on just 25 different days; six of the days had more than one large event; on five occasions, consecutive days had at least one large event each.

While the maximum number of days between large events was 15, successive events were separated by less than three days, on average. The temporal clustering is further illustrated by the fact that 38 per cent of the events occurred within a day of a previous event, 60 per cent, within two days, and fully 80 per cent of the events occurred within five days of a previous event. That is, the large events tended to occur in clusters in time, with longer periods of time separating individual clusters.

Spatially, the large events within the temporal clusters tended to distribute themselves across the whole longwall, so that individual panels suffered large events less frequently than did the longwall considered in its entirety. Events occurred on panels W5 and W6 every 11 days on average; on W2, the average recurrence rate was 15 days. The other panels had lower recurrence rates of M_L>1,0 events. The previous M_L>1,0 seismic event on W2 panel occurred 21 days prior to the rockburst.

9.5 Conclusions

Since preconditioning was started in the 87-49 stope west panels, significant improvements have been observed in the hangingwall conditions and the face advance rate. The face bursting has completely stopped where preconditioning has been implemented correctly. The damage caused by rockbursts has rather been due to shake-down. The effects, in terms of improving the safety of the working area, have been evident. However, since changing the mining direction from up-dip to diagonal, similarly encouraging results have been minimal.

Seismicity at the project site was monitored by both the mine's ISS and Mining Technology's PSS network. Magnitude M_L>1 seismic events occur frequently in this stope. These events were generally located in the abutment, tens of metres away from

working areas of the up-dip panels. For this reason, the mining panels which were being preconditioned were not being significantly damaged by the large events. In contrast, the large event on 15 February 1996 was located a few metres ahead of the W2 diagonal panel and resulted in damage to the panel and injury to five workers in the face area of the panel.

The diagonal faces lie parallel to the large seismically induced shear zones which develop tens of metres ahead of the face, parallel to the overall shape of the longwall. This configuration should be avoided if the periodic falls of ground resulting from the combined effect of the face-parallel fractures and the large shears are to be prevented. Such falls are not prevalent in the up-dip panels, as the face shape is not parallel to the overall shape of the longwall. Thus the two sets of fractures do not combine to form a weak plane from which falls of ground can occur. The majority of the damage occurred owing to falls of ground associated with these face-parallel fractures in the diagonal panel.

Drilling long production holes with short preconditioning holes caused an apparent reduction in the depth of face-parallel fracturing. Thus, it is likely that the zone of influence of the preconditioning blast ahead of the face was significantly reduced. Although it appears that preconditioning did prevent a face burst from occurring, properly applied preconditioning might have reduced the damage even further. Although the effects of different preconditioning hole lengths had not been studied at the time of this investigation, 3 m long preconditioning holes (with a maximum production hole length of 1 m) had shown satisfactory results on up-dip panels. Even 2,4 m preconditioning holes had been reasonably effective, provided that 1 m production holes were drilled. However, since the production holes were 1,8 m long and the preconditioning holes 2,4 m long, the face was effectively preconditioned to a depth of less than 1 m, assuming a face advance of 1,4 m. It is also interesting that, although the damage was distributed along the entire panel length, the damage was concentrated in the area where one preconditioning hole had not been drilled (this was, of course, also the part of the panel closest to the source of the event, and at the head of the diagonal gully where support was reduced.

The removal of all face area support prior to a production blast is not advocated. The resulting span from pack to face of 3,5 m after a blast can result in a significant hangingwall instability leading to extensive falls of ground during a seismic event or even

a production blast. This must have contributed significantly to the extent of the damage following this seismic event.

9.6 Recommendations

Special attention should be given to the support standards in rockburst prone areas. Only one row of Camlok mechanical props was installed in the face area of W2 panel. It is believed that, had 3 m/s (blast on) hydraulic props with proper headboards supported the face area, the damage would have been much reduced.

An up-dip mining direction should again be utilised and the overall longwall orientation should be maintained in a NE-SW direction. This will ensure that the up-dip panels obliquely approach the large seismically induced shear zones which develop ahead of the faces.

Production personnel should adhere to the preconditioning guidelines with respect to hole length and spacing.

10 East Driefontein # 1, 5/6/96, M_L=2,7

10.1 Introduction

The 34-19 Carbon Leader stope, East Driefontein Gold Mine, was recognised by mine personnel as an area with an unusually high level of seismic activity. Mr. G Hepburn (Manager, East Driefontein Gold Mine) requested that a team from CSIR Mining Technology investigate the support and mining of the 34-19 Carbon Leader stope. A visit was made on the 17 May 1996, and a report identifying areas of high seismic hazard and providing recommendations was forwarded to the mine on 30 May 1996.

A rockburst occurred at East Driefontein Gold Mine on 5 June 1996, causing widespread damage to the 34-19 Carbon Leader stope, about 2300 m below surface (Figure B.50). The rockburst, which caused 22 injuries, took place at 10h57. A seismic event with a local magnitude M_L=2,7 was recorded by the mine-wide seismic network.

Following this rockburst, Mr N. Pole (Production Manager) requested that the CSIR team investigate the factors contributing to the rockburst, and recommend measures that would reduce the likelihood of similar damaging events. A site visit was made on 6 June 1996. It was gratifying to note that many of the areas identified as hazardous on the visit of 17 May 1996 did, in fact, sustain damage during the rockburst on 5 June 1996.

10.2 Mining environment

The plan of the 34-19 Carbon Leader stope and environs shows that several structures are present, notably the Aardvark fault immediately up-dip of the 32 level reef horizon, the Shaft fault to the west of the current stoping, and the Jean's fault further down dip (Figure B.50). In addition, there appears to be significant minor sympathetic faulting throughout the area, associated with these major features.

In this area the Rice Pebble Marker (which forms the hangingwall of the Carbon Leader Reef) is difficult to distinguish from the Carbon Leader Reef. As a result this horizon has often been mined. The Green Bar shale horizon lies above the Rice Pebble Marker, and the parting between these two horizons is particularly prone to separation. The majority of hangingwall collapses were observed to occur up to the Green Bar horizon, with a height of 0,75 m to 1,5 m.

10.3 Observations at the rockburst site

As a general observation, it was noted that mining-induced fractures were unusually well-developed, considering the relatively small span of the stope. Two prominent fracture sets were present: a steeply dipping face-parallel set, and a set which dipped towards the face at approximately 40°.

32-level stope entrance

Falls of ground were noted at the entrance to the stope on 32-level.

2W & 3W panels

Rocprops were present in the upper part of the panel, and no significant falls of ground were noted in this area. Sufficient convergence had occurred to cause splitting of the outer steel cylinder of a Rocprop (Figure B.51). Rockfalls had occurred in the lower part of the panel, where Rocprops had not been installed at the time of the event.

4E panel

No significant falls of ground were noted in this panel. Support consisted of backfill, a row of Rocprops (spaced at 1,5 m on dip) about 2 m ahead of the backfill, and a row of Camlock props about 2 m ahead of the Rocprops. The face to backfill distance was about 6,5 m.

5E panel

No significant falls of ground were noted in this panel. The face to backfill distance was about 3,3 m.

5W panel

No significant falls of ground were noted in this panel. Support consisted of Hercules packs (1,2 m x 1,2 m, spaced at 1,8 m skin-to-skin on dip and strike). The face to pack distance was about 2 m.

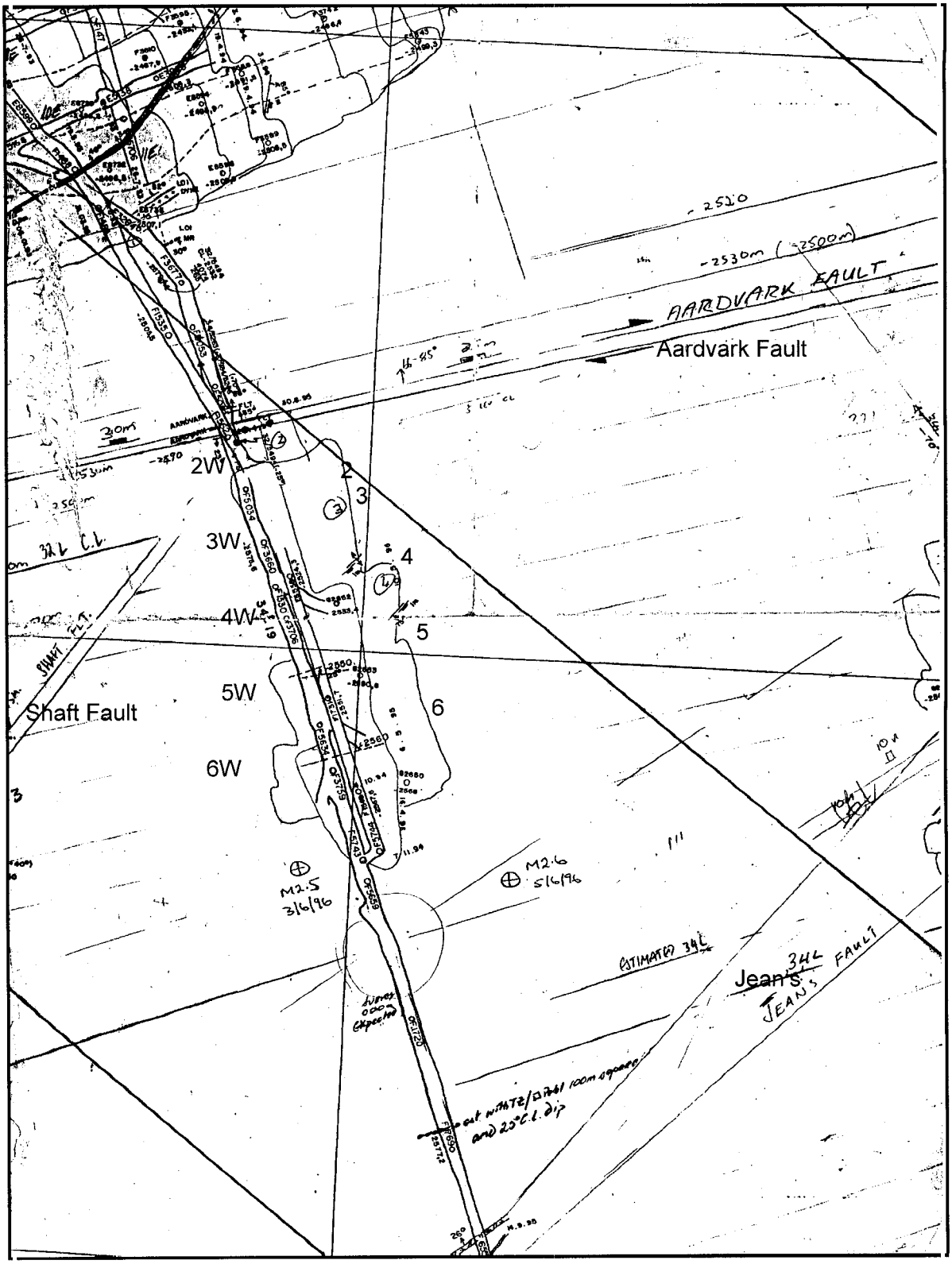

Figure B.50 Plan showing the 34-19 Carbon Leader stope, No. 1 Shaft, East Driefontein Gold Mine, damaged by a M_L=2,7 rockburst on 5 June 1996.

6W panel

No significant falls of ground were noted in the face area of this panel. The face to pack distance was about 4 m. The production holes had been charged before the rockburst. No support was present in the face area at the time of the visit. It was reported that Camlock props had been in place during drilling and charging, and had been subsequently removed. Falls of ground were noted between packs near the bottom of the 6W panel. Up to 1 m of hangingwall had fallen out.

6W-6E strike gully

Several falls of ground were noted between packs on the up-dip side of the strike gully. The thickness of the falls was about 1 m.

6E panel

A fall of ground was observed at the bottom of the panel. It was reported that drilling was in progress at the time of the rockburst and that the machine operators had been injured. The thickness of the fall was 0,5-1,0 m. The fall extended for about 2 m from the face and 4 m along dip. Two bent Camlock props provided evidence that co-seismic closure was approximately 150 mm. The face had been buckled by the convergence.

Dip gully to 34-level stope entrance

A gully pack had been pushed into the gully by a bulging backfill bag.

34-level Cross-cut

Damage was quite severe in the vicinity of the reef-cross-cut intersection. The eastern sidewall of the cross-cut had been ejected into the haulage, pushing in the vertical supports of the RSJ sets. Several of the horizontal girders of the RSJ sets were twisted through 90°. A materials car had been tilted.

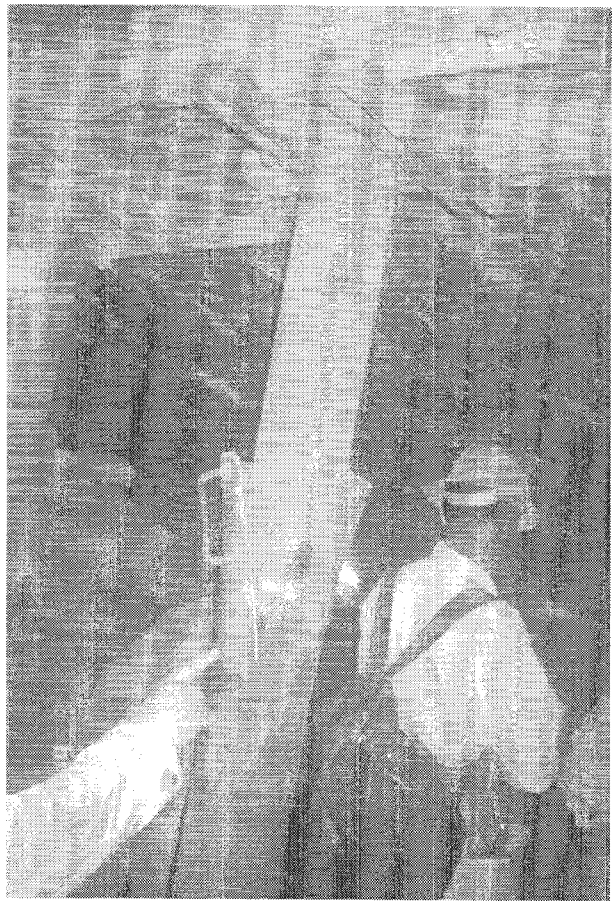

Figure B.51 A rocprop observed in the 2W panel of the 34-19 Carbon Leader stope showing a barrel that had split as a result of closure.

10.4 Assessment of support performance

Face area

Rocprops generally appeared to have performed well in supporting the hangingwall. However, the headboards were frequently severely distorted (Figure B.52), resulting in a point load being exerted on the hangingwall by the head of the prop. Consequently these head boards were not performing a load-spreading function, which is essential in highly fractured ground. In areas where face advance is slow, convergence rapid, or subject to repeated rockbursts, the headboard may disintegrate while still in a position where its contribution to areal support is desired.

The recommendation that RYHP's not be used in the stope was based essentially on the reported fallout rate that has been experienced. It is important however, that the real cause of the poor performance of the props be determined. Factors which could contribute to the high fall-out rate are:

Loadspreaders not being used. In the highly fractured ground the relatively small diameter of the end of the prop or extensions could punch a few millimetres and thus drop load. A similar effect is obtained from setting on a poorly cleaned footwall.

Pump pressures incorrect, this could be caused by low air or water supply to the pump or dirty filters. Not causing the pump to stall properly when setting a prop. Extensions not seated properly. Valves faulty.

Figure B.52 A Rocprop showing a headboard that had failed so that the prop was exerting a point load on the hangingwall.

Back area

Falls of the highly fractured hangingwall were noted between packs in the back areas. These areas should be barricaded off to prevent access. Owing to the fallout of hangingwall, the backfill bags were sometimes not high enough to provide effective support.

Gullies

Falls of highly fractured hangingwall were noted between packs near the gullies, and could equally easily have occurred in gullies.

Cross-cuts

The steel sets at the 34-level reef intersection sustained severe damage owing to bulking of the foot- and sidewall of the cross-cut.

10.5 Assessment of layout

Some of the panels had linear dimensions exceeding 50 m (combined 2E & 3E, combined 5E & 6E). In order to limit the dimensions of any seismic rupture (and hence magnitude of the event) that may occur along a face-parallel shear zone, it is desirable to limit panel lengths by introducing leads or lags.

10.6 Seismic history

The M_L=2,7 seismic event which occurred at 10h57 on 5 June 1996 caused widespread damage to the 34-19 Carbon Leader stope at East Driefontein Gold Mine. Events of this magnitude are not unusual in the environs of the 34-19 Carbon Leader stope. Seven events with $M_L \geq 2$ were recorded between 1 May 1996 and 5 June 1996. Although the ERR would be expected to be low as the maximum span is only about 50 m, an abnormally high level of seismicity has been encountered, and the intensity of mining-induced fracturing is exceptionally high. These factors indicate abnormally high virgin stresses in this area.

Two damaging events occurred in the environs of the 34-19 CL stope on 3 June 1996. A M_L=2,6 seismic event occurred at 16h06 with its hypocentre located close to the 5W panel, with an energy index of 0,7 and an apparent volume of 2,1 x 10^6 m^3, yielding a source radius of about 80 m. A M_L=1,0 event located on the Aardvark fault occurred at 15h57. This event had an energy index of only 0,3.

10.7 Rockburst mechanism

Source mechanism

The hypocentre of the M=2,7 event on 5 June was about 30 m from the bottom of the 6E panel, and close to the reef plane. The source parameters are listed in Table B.7.

Table B.7

Source parameters of the seismic event which damaged the 34-19 Carbon Leader stope

Date:	5 June 1996
Time:	10h57
Local Magnitude:	2,7
Location:	close to the reef plane,
	(x = 20458, y = -8253, z = -2568)
Moment:	3,98 x 10^{12} Nm
Energy:	5,01 x 10^{8} J
Apparent stress	4,16 MPa
Energy Index	2,9
Apparent volume	0,4 x 10^{6} m^{3}
Radius of apparent volume:	45 m

Damage mechanism

Damage in the stope largely consisted a scattered falls of ground in the face area where the face to support distance exceeded 3 m, and falls of ground between packs in the back areas. There was no evidence of crushing or ejection of the face. Co-seismic closure was estimated from the bending of Camlock props to be about 150 mm at the bottom of panel 6E. The Rocprops generally performed well in supporting the hangingwall, although the distortion of their headboards is cause for concern as their ability to provide areal support in a subsequent rockburst is probably diminished.

Substantial damage occurred in the 34-level cross-cut near the reef intersection owing to bulking of the eastern sidewall and footwall, causing the sets to topple.

10.8 Conclusions

The 34-19 Carbon Leader stope has experienced an unusually high level of seismicity, and exhibits an abnormally high density of mining induced fracturing, given the amount of mining in the area. This indicates unusually high levels of tectonic stresses and extra precautions must be taken when mining in this area.

The hangingwall quartzite is prone to failure owing to the high density of fracturing and the low cohesion parting between the quartzite and the Green Bar Shale.

The Rocprops generally provided good face area support, although the design of the headboard could be improved.

10.9 Recommendations

Rockburst resistant support such as rapid yielding hydraulic props or Rocprops must be installed in the face area. Owing to the highly fractured nature of the hangingwall, good areal coverage is essential and headboards should be used. This is especially critical in the highly stressed regions at the top and bottom of the panels. Mechanical props (such as Camlocks) and mine poles have little value in rockburst conditions and should not be used.

Attention should be given to improving the Rocprop headboards as they are prone to distortion and failure.

The reason for the reported high fall-out rate of hydraulic props should be established.

In the prevailing difficult geological circumstances (thick reef, thin quartzite middling in the Green Bar, resulting in a high intensity of stress fracturing) it is imperative that careful blasting be practised and a conservative blast design implemented. Consideration should be given to the following:

Burdens and the charge per hole, particularly in the top row, should be reduced.
Marking off and alignment of holes should be as accurate as possible and drill holes should not end up above the top reef contact.

To establish an undercut, shorter holes should be considered, the upper row of which should be drilled 500 mm below the top reef contact until backfill has been placed under the undercut brow.

A reduction in stoping width will improve the effectiveness of both the face area support and the backfill.

In areas where fallout of the hangingwall has occurred, larger backfill bags should be used.

Back areas which are supported by packs should be barricaded to prevent casual access, as these area are prone to shake out.

Tunnels must be adequately supported, especially when traversing faults and approaching the reef intersection. Support with a yield capability superior to ripple bars should be used, together with mesh and lacing. In long term or highly vulnerable excavations, fully yielding support systems should be installed.

The stress change of the 32-19 CL cross-cut owing to the proposed undermining requires careful assessment of the stress change and suitability of support.

Attention should be given to longer term planning to ensure that known structures are approached optimally. For example, breasting onto the Shaft fault to the west of the 34-19 stope must be avoided. Mining should initially concentrate on the west side, as mining to the east would generate extra span that could compound the adverse conditions expected in the vicinity of the Shaft fault. This suggestion is, however, in conflict with the

mining planned up-dip of the Aardvark fault, and the relative advantages and risks must be weighed up carefully.

The use of shorter panels is recommended to limit the magnitude of ruptures on face-parallel shears, and the extent of damage.

The concentration of people in seismically hazardous areas should be avoided. The location of the 32-level stope top entrance infrastructure (timber and material bay) is immediately adjacent to the Aardvark fault, and should be relocated to a more suitable position. Similarly the location of the refuge bay and waiting place on 34-level should be reconsidered.

Mining in the vicinity of major faults may result in increased fault instability. The design of bracket pillars parallel to the major faults should be considered.
The number of accessways to the face should be increased as this will aid rescue and rehabilitation following a rockburst.

The seismicity data should be carefully analysed to identify which parameters are most useful as indicators of increased rockburst hazard.

11 Western Deep Levels (East), 18/11/96, M_L=3,0

11.1 Introduction

A rockburst occurred at Western Deep Levels East Mine on 18 November 1996, causing severe damage to the strike gullies serving the 115 W1 and 115 W2 Carbon Leader panels, about 3300 m below surface (Figure B.53). A seismic event with a local magnitude M_L=3,0 was recorded at 9h10 by the mine-wide seismic network. A worker installing sets in the lower (115 W1) gully was fatally injured. A further 15 workers were trapped in the face area of the 115 W1 panel. They were extricated by 18h00 on the same day by rescuers digging through the collapsed ground in the upper (115 W2) gully. One of the trapped workers suffered lacerations caused by falling rock, while all the

others were unscathed. Falls of ground were also reported in the face area of the 116 W3 panel.

Following the rockburst on 18 November 1996, a request was received from Mr M. O'Hare (Production Manager, East Mine) that a team from CSIR Mining Technology investigate the factors contributing to the rockburst, and recommend measures to reduce the likelihood of similar damaging events. Specific objectives included: assessment of the performance of Madoda elongates, assessment of the integrated elongate-backfill support system, and assessment of the gully support.

Several planned visits were postponed owing to difficulties in creating access to the site. The visit eventually took place on 19 December 1996, a month after the rockburst. The 115 W1 gully had not been opened, so the 115 W2 gully provided the only access to the face area. Ventilation was poor and conditions in the face area were extremely hot.

11.2 Mining environment

Several geological structures are present in the environs of the 115 W1 Carbon Leader panel, notably the Serpent Dyke and the Serpent Dyke Offshoot, and minor sympathetic faulting associated with these features (Figure B.53). The Serpent Dyke is about 10 m thick and dips to the south-east at approximately 70°. It was exposed in the upper half of the W1 panel, while the W2 panel had already mined through it. Quartz veins were noted close to the dyke/country rock contact. In this area the Rice Pebble quartzite, which forms the hangingwall of the Carbon Leader Reef, is about 1,8 m thick. The Green Bar shale horizon lies above the Rice Pebble quartzite. The parting at the base of the Green Bar is particularly prone to separation.

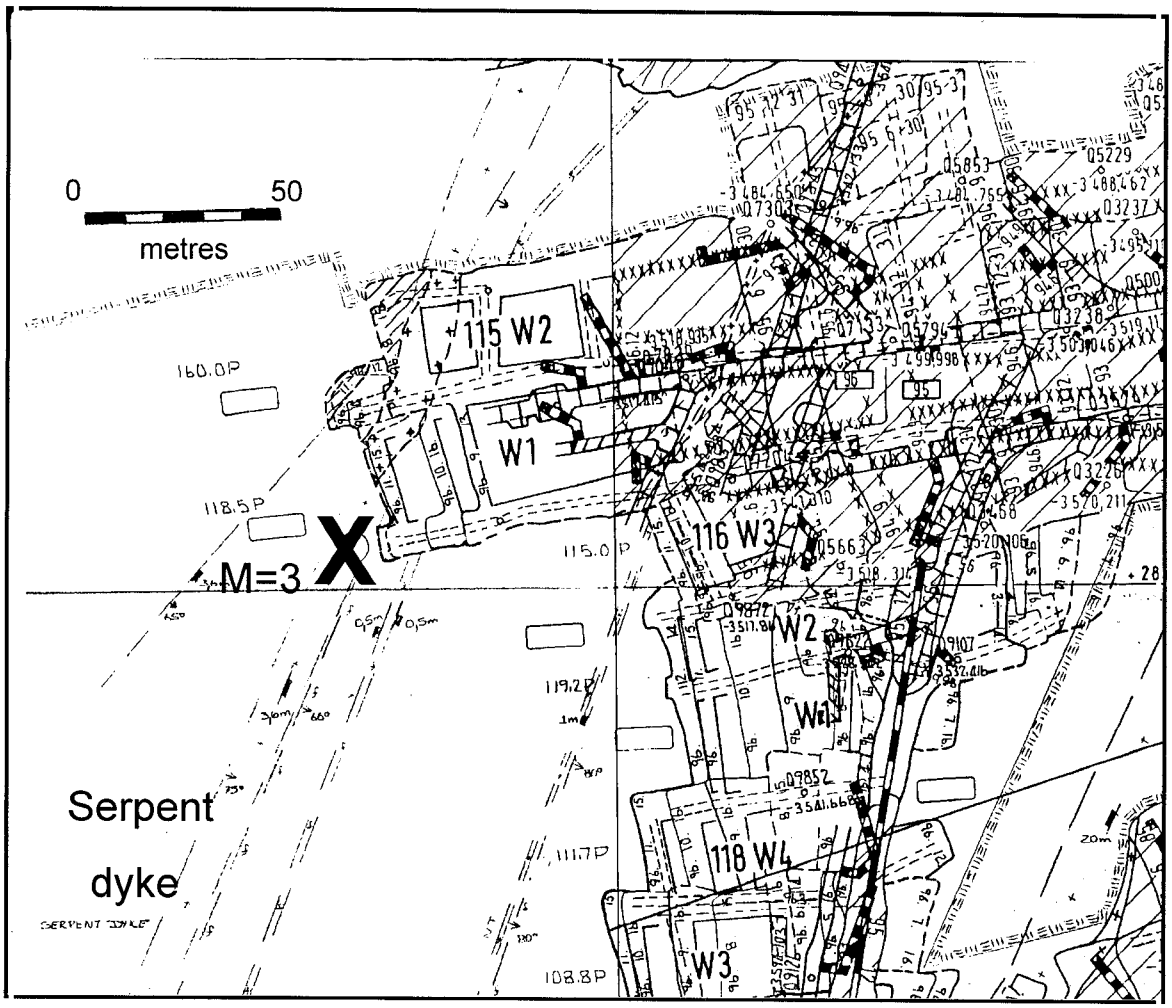

Figure B.53 Plan showing the stoping layout and epicentre of the M_L=3,0 seismic event which occurred on 18 November 1996 damaging the 115 W1 lower strike gully, Western Deep Levels East Mine. Areas which sustained rockburst damage are shaded.

11.3 Observations at the rockburst site

115 W2 panel

At the time of the rockburst, up-dip mining was being carried out to re-establish this panel following the negotiation of the Serpent Dyke. The pattern of mining-induced fracturing appeared normal, consisting of face-parallel fractures with a range of dips. No evidence of rockburst damage was observed in this panel.

115 W2 gully

It was reported that only minor damage had been sustained in the 115 W2 gully. Flat lying fractures were noted in the hangingwall. Poor ground conditions were noted in the face area of the gully. Poor ground conditions had previously been encountered in the vicinity of the Serpent Dyke intersection. Sets had been installed and Aerocem used to fill the void above the sets. No visible damage to the sets had occurred during the rockburst. The use of concrete piers as foundations for the gully packs was noted, indicating previous failure of the gully sidewall.

115 W1 panel

Stope workers were drilling the face at the time of the rockburst. Only minor falls of ground, consisting of book-sized slabs ,occurred at the time of the rockburst. Bending of a Camlock prop and the splitting of Madoda props suggested closure of up to 20-30 cm in certain places. Closure generally increased towards the bottom of the panel, which is closer to the focus of the event. Damage to the backfill bags also increased to the bottom of the panel, though this may be owing to tighter filling and hence better contact with the hangingwall. Slip surfaces co-planar with the dyke were noted. No recent powder was evident on these surfaces.

115 W1 gully

The rockburst damage in the 115 W1 gully was briefly inspected by the team. The 115 W1 panel was leading the 116 W3 panel by some 60 m. It was reported that hangingwall collapses extended for much of this distance, with the exception of about 10 m near the face. The fallout generally extended to the base of the Green Bar horizon (about 1,8 m), and in some instances included the Green Bar itself, creating caverns up to 6 m high. Ground conditions in the face area of the gully were reasonable.

116 W3 panel

The damage sustained in the face area of 116 W3 panel was not inspected by the team.

11.4 Assessment of support performance

Face area

The support installed in the 115 W2 up-dip panel consisted of Madoda elongates, with Hercules packs lining the dip gully. The support in the 115 W1 breast panel consisted of backfill (classified tailings), installed to a distance of about 4 m from the face, with a row of props between the face and backfill. The Madoda props were in the process of being installed at the time of the rockburst, and so were only present in the upper half of the panel, with Camlock props present in the lower half of the panel as temporary support.

The seismic event with magnitude M_L=3,0 with its focus only 60-90 m from the W1 face would be expected to cause severe shaking and closure in the nearby panels, with a peak ground velocity exceeding 1 m/s. As there was only minor damage to the 115 W1 and W2 panels, the stope support system consisting of Madoda elongates integrated with backfill generally appeared to have performed well. However, about 30 per cent of the Madoda props in the 115 W1 panel had failed, usually by tilting of the headboard and cap.

As a result the steel collar cut into the timber, causing buckling and fracture of the prop (Figure B.54). The Camlock props had also buckled as a result of the co-seismic stope closure. The backfill was generally well placed, with a small gap between the top of the backfill bag and the hangingwall at the top of the panel.

In the 115 W2 up-dip panel it was noted that elongates had been installed vertically, rather than normal to the strata.

Gullies

It was reported that the support in the 115 W1 (lower) strike gully had been changed about a month prior to the rockburst, to a system which integrated Mododa props and two block Hercules packs (2,2 m x 0,75 m on up-dip siding; 1,1 m x 0,75 m on down-dip siding, 1,8 m skin-to-skin). This system was installed in the most advanced section of the 115 W1 gully, which only sustained minor damage during the rockburst. Split sets would normally form part of the gully support system, but none had been installed in this section at the time of the rockburst. The support system used in the part of the gully that sustained severe damage included stiffer (4 block) Hercules packs. It would thus appear that the new gully support system performed considerably better. It is possible that the softer support reduced the amount of sidewall failure and hangingwall fracturing, thereby improving the effectiveness of support and hence improving stability.

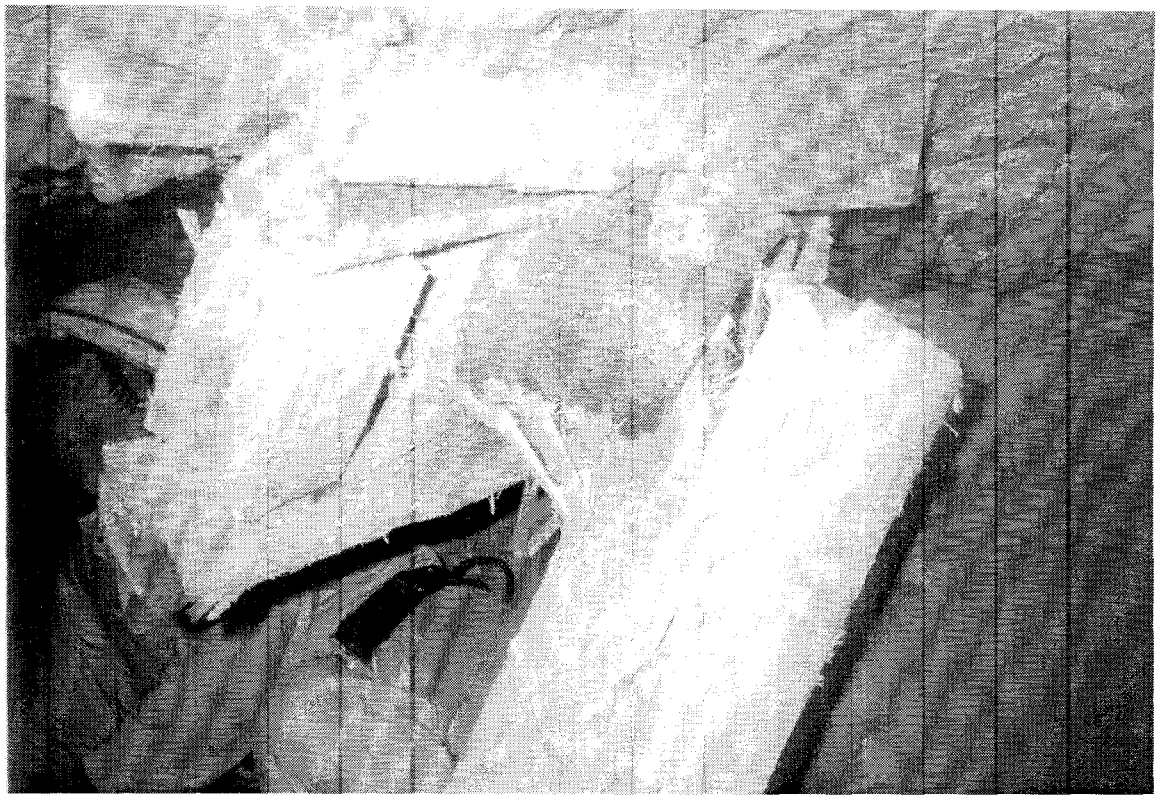

Figure B.54 Tilting of the headboard and cap of a Madoda prop.

11.5 Assessment of layout

The strategy adopted to negotiate the Serpent Dyke involved advancing one panel at a time through the structure. The shape of the longwall face was being changed in order to ensure that the Serpent Dyke was approached at the most favourable angle possible in the circumstances. At the time of the rockburst the 116 W3 panel lagged the 115 W1 panel by about 60 m. Consequently the ERR was high ahead of the 116 W3 face. It was reported that a value of 68 MJ/m^2 had been calculated.

11.6 Seismic history

Seismic events with M_L>2 are not uncommon on East Mine, which typically experiences 15 events with M_L>2 per month, an event with M_L>3 every 1-2 months, and an event with M_L>4 every 1-1½ years (D. Amadzic, pers. comm).

11.7 Rockburst mechanism

Source mechanism

The hypocentre of the M_L=3,0 event on 18 November located on the Serpent Dyke and about 60 m in the footwall beneath the toe of the 115 W1 panel (see Figure B.53 for location). The event had a slip mechanism. According to the Brune model, a seismic event with M_L=3 would be expected to have a source radius between 100 m (for an average stress drop of about 15 MPa) to 300 m (for an average stress drop of 1 MPa).

Damage mechanism

Little rockburst damage was observed on this visit. The main objective was to inspect the performance of the face area support under rockburst conditions, and the support had performed well. The collapse blocking the entrance to the 115 W1 panel had been already cleared, and damage to the lower W1 strike gully was not inspected owing to poor ventilation.

11.8 Conclusions

The M_L=3,0 rockburst which caused damage to the strike gullies serving the 115 W1 and W2 Carbon Leader panels was owing to slip on the Serpent Dyke induced by the nearby mining.

The face area suffered little damage. The support system, consisting of Madoda prestressed yielding elongates integrated with backfill, performed well.

The design of the headboard and cap of the Madoda prop appears to make the cap prone to tilting.

11.9 Recommendations

Rockburst resistant support such as rapid yielding hydraulic props (RHYPs) or Madoda props must be installed in the face area as soon as possible. Owing to the highly fractured nature of the hangingwall, good areal coverage is essential and headboards should be used. This is especially critical in the highly stressed regions at the top and bottom of the panels. Mechanical props (such as Camlocks) and mine poles have little value in rockburst conditions. They do, however, make for good rockfall support, and should be used to support the hangingwall before yielding support is installed.

Attention should be given to improving the Madoda headboards as they are prone to distortion and failure. Failure may be owing to some extent to their limited yield capability. Consideration can be given to improving the yield capability by combining the Madoda pre-stressing device and the Cone prop.

Mine management indicated an eagerness to cease using RYHPs owing to the problems and unreliability experienced in using the devices. We believe that it is important that the real cause of the poor performance of the props be determined as RYHPs are most likely to be effective supports and certainly the most cost effective.

Gullies must be adequately supported, especially when traversing faults and dykes. Split sets must be installed in the hangingwall. The idea of using softer support on gully edges (e.g. two-block Hercules packs, or bringing backfill down to the gully edge with gaps left for storage) is encouraged. The integration of elongates with packs on gullies appears to show improved performance when compared to current standards. The idea of using elongates with special headboards to allow lagging across gullies also looks promising.

Gullies should be scraped clean daily to reduce the risk of choking and blockage owing to FOGs. Gully sidings must be mined strictly on dip so that the Green Bar contact is kept a maximum distance above the stope. The final cleaning of the siding can take place from the following down-dip panel where applicable.

Gullies providing access to panels with long leads are subjected to high stresses back from the face. A more closely spaced rockbolt pattern should be considered for such gullies with some form of areal coverage.

Panels lagging by large amounts are subjected to high ERR's and should be supported particularly well with a strictly enforced "no blast if support not up to standard" regulation. Attention should be given to longer term planning to ensure that known structures are approached optimally. For example, breasting onto the Dougie fault to the west of the Serpent Fault must be avoided. Mining in the vicinity of major faults may result in increased fault instability. The design of bracket pillars parallel to the major faults should be considered. The planned implementation in this area of the Sequential Grid Mining Method should improve matters in this regard.

An adequate number of access ways to the face should be created and kept open to aid rescue and rehabilitation following a rockburst.

The seismicity data should be carefully analysed to identify which parameters are most useful as indicators of increased rockburst hazard.

12 Vaal Reefs # 5, 10/2/97, M_L=4,0

12.1 Introduction

A rockburst occurred at Vaal Reefs Gold Mine on 10 February 1997, causing severe damage to haulages and cross-cuts in the vicinity of the No 5 Shaft, about 1900 m below surface (Figure B.55). A seismic event with a local magnitude M_L=4,0 was recorded at 18h08 by the mine-wide seismic network (the magnitude determined by the national seismic network was M_L=4,4, G. Graham, Council for Geoscience, pers. comm.). The focus of the event was near the intersection of the No 5 Shaft Fault and the Clemcor Dyke, about 1,2 km north of the No. 5 Shaft. Damage was sustained over 2 levels (60-50 and 62) and an area of about 1200 m x 600 m. The damage to the haulages caused severe disruptions to production. Fortunately there were no workers in the area which sustained damage at the time of the seismic event.

Mine management requested that a team from CSIR Division of Mining Technology investigate the factors contributing to the rockburst, and recommend measures that would reduce the likelihood of similar damaging events. The team visited the site on 21 February 1997. Issues of specific interest were:
Performance of tunnel support
Performance of gully support
Predictability of large seismic events.

12.2 Mining environment

Geology

The geological structure of the Klerksdorp gold field is more complicated than that found in other Witwatersrand basin goldfields (Gay et al., 1984). In particular, this sector of the basin is cut by a series of major normal faults, which trend north-east and displace the strata by 600-1500 m. The faults form two sets that dip NE and SE respectively, resulting in graben-horst structures on a variety of scales.

Other faults, which strike north and east, also occur, as do bedding plane faults, which appear to be the youngest structures in the region. In addition, the strata are cut by dykes and sills of different ages and compositions. The widths of these intrusives range from 1-40 m and many of them extend for 10 km or more. The effect of these structures, particularly the faults, is to subdivide the mining area into relatively small areas of reef separated by areas of barren ground.

In the area of No 5 Shaft the Vaal Reef is less than 1 m in thickness. The footwall and hangingwall strata in the vicinity of the Vaal Reef comprise a series of argillaceous to siliceous quartzites. The reef hangingwall is an argillaceous quartzite (the MB4, with UCS=189 MPa, E=70 GPa), while the reef footwall is a siliceous quartzite (the MB5, with UCS=268 MPa, E=81 GPa) (Gay et al., 1984).

The focus of the M_L=4,0 seismic event was near the intersection of the No. 5 Shaft Fault and the Clemcor Dyke (see Figure B.55). The No. 5 Shaft Fault strikes approximately NNE, with a downthrow to the east of about 250 m. The dip of the fault plane is approximately 45° to the east. The fault loss is about 200 m wide with a dyke intruded along the fault plane. The fault trace is sinuous and exhibits several splays. The Clemcor Dyke strikes approximately SE, and is about 25 m wide. The Makrap dyke is orientated parallel to the No. 5 Shaft Fault and some 500 m to the west. It is 10-20 m in thickness.

Minimal stoping was taking place in the area of influence of the rockburst, as the reef was largely mined out. An exception was the remnant of reef (the 5/60-50 stopes) lying within the triangle formed by the Makrap and Clemcor Dykes and the No. 5 Shaft Fault (Split 2). The gullies within this stope were inspected.

Layout and Regional Support

Owing to ubiquitous faults with substantial throws, Vaal Reefs Gold Mine makes use of a scattered mining system. Fault losses limit the mining spans and contribute to regional stability. Backfill is also used. In most cases the reef is mined right up to the fault plane and no bracket pillars are left adjacent to the faults. The fault losses are quite broad owing to the intermediate dip of the No. 5 Shaft Fault and other faults in the area, and probably contribute to the clamping of the fault.

Main haulages have been developed in the fault loss associated with the No. 5 Shaft Fault. This was a design decision at the early planning stage.

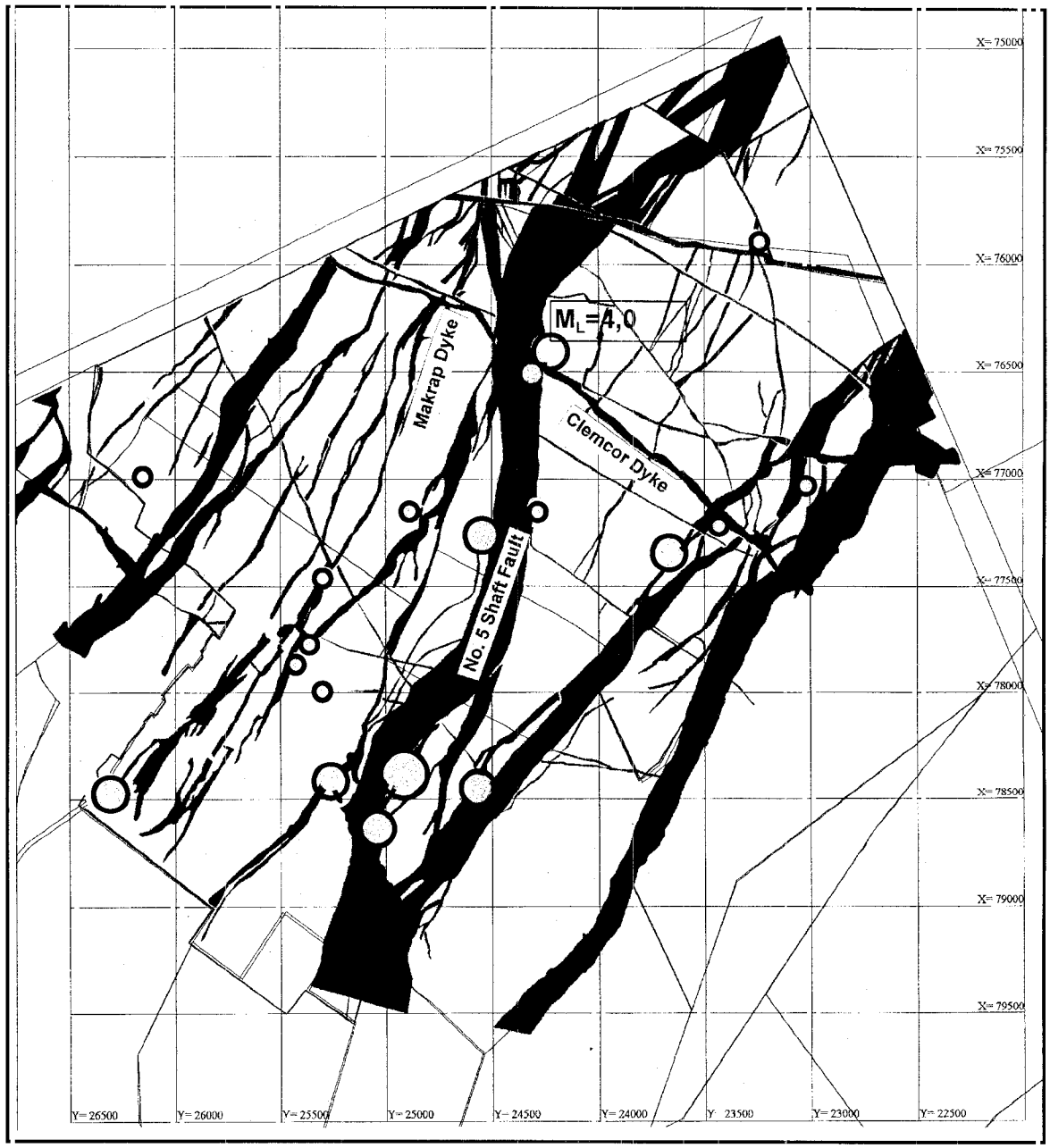

Figure B.55 Plan showing the epicentre of the M_L=4,0 seismic event which occurred on 10 February 1996, damaging the haulages on 50-50 and 62 levels, No. 5 Shaft, Vaal Reefs Gold Mine. Major geological structures and the location of 19 other events with $M_L \geq 3,9$ occurring since 1972 are also shown.

Tunnel and cross-cut support

The main haulages on 60-50 and 62 level were developed within the fault losses associated with the No. 5 Shaft Fault and other faults. Tunnel support in the No. 5 Shaft Fault area was installed in 3 phases:

Primary support installed during development consisted of 2,4 m Gewibar rockbolts. Secondary support consisted of a 1 m diamond pattern of 2,2 m grouted wire rope loops, mesh and lacing i.e. 5 loops/ring, rings spaced at 0,5 m. Tertiary support was only installed in critical areas, and consisted of 6 m or 4,5 m tendons.

Gully support

The entrance to the 5/60 50 53 stope was supported by Apollo timber packs. The strike gullies in the stope were supported by Durapaks.

Stope support

The back area of the 5/60 50 53 stope is supported with prestressed Durapaks. It was reported that the face area had sustained little damage and consequently was not inspected.

12.3 Observations at the rockburst site

Level 60-50

The in situ investigation commenced at the 60-50 level (see Figure B.56). There was little damage to the 5/60-50 main haulage. Most damage was found in cross-cuts passing from solid to over-stoped ground, especially in the vicinity of the dyke which was intruded close to the fault surface.

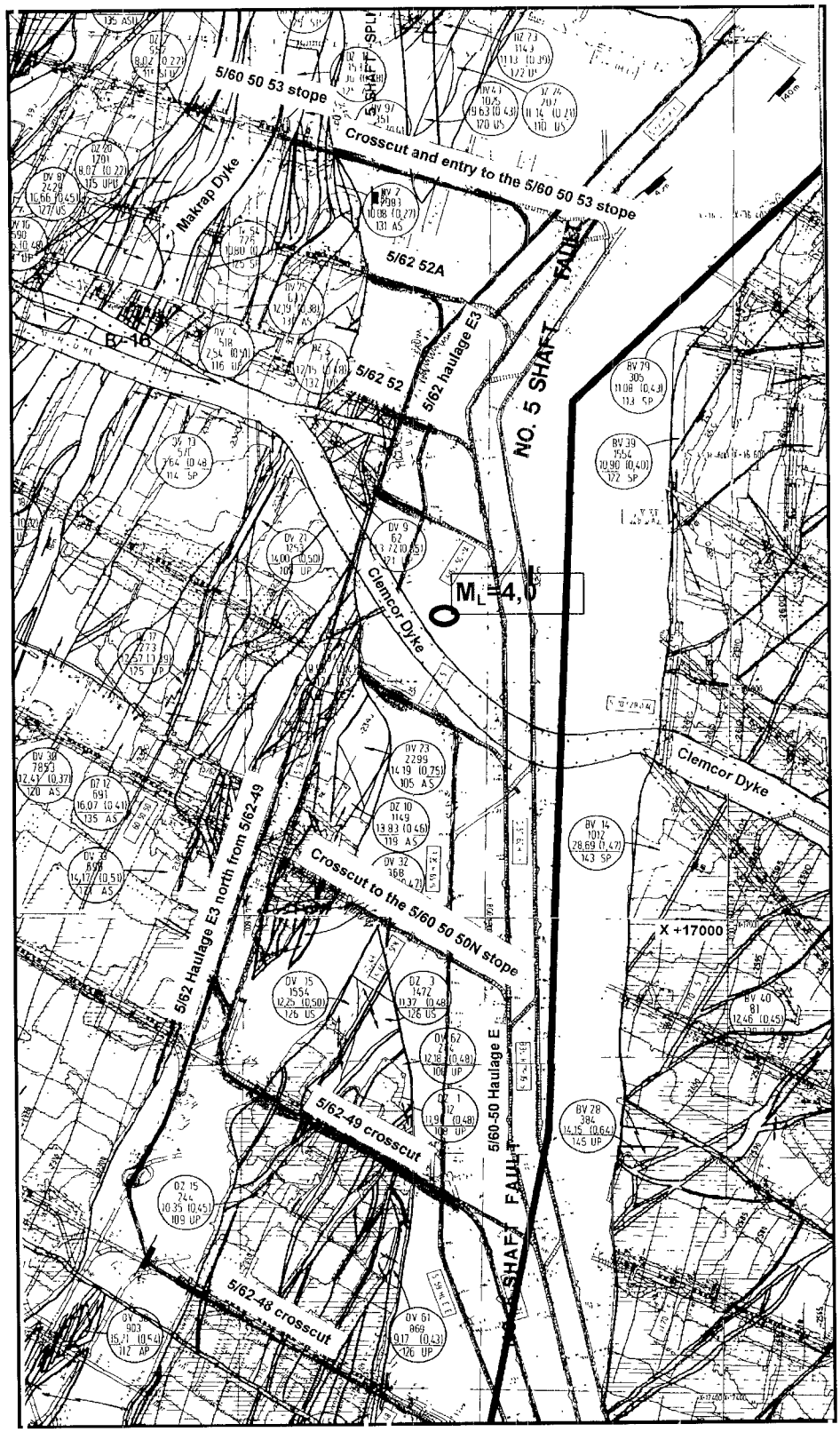

Figure B.56 Plan showing tunnels damaged by the M_L=4,0 seismic event which occurred on 10 February 1996, No. 5 Shaft, Vaal Reefs Gold Mine.

Cross-cut to the 5/60 50 50N stope

Both the hanging- and sidewalls of the cross-cut had experienced bulking. In places the support system had failed owing to the breaking of the lacing made of destranded hoist rope. The cross-cut was completely blocked owing to collapse of the hangingwall owing to the failure of grouted wire rope loops - either the cable had snapped or the loop been pulled out of the holes. The collapse occurred about 20 m to the west of the fault plane.

It was possible to inspect the support elements behind the outermost skin of failed rock in an area near the stope entrance. The following modes of failure of the tunnel support were observed:

An end-anchored Gewibar which had pulled out of its hole.
A wire rope loop still grouted in the rock, but where the cable lacing threaded through the loop it had snapped and been pulled through.

A grouted cable which had snapped. It was noted that this cable had suffered corrosion, as had the lacing. Corrosion may well have weakened elements of the support system.

Cross-cut and entry to the 5/60 50 53 stope

The centre gully was blocked by collapse of the hangingwall. Ahead of the collapsed section, rubble was lying in the gully. As the centre gully had been vamped shortly before the rockburst (pers. comm., B. Rautenbach, mine overseer), it was clear that the rubble lying in the floor centre gully had been ejected from the side- and footwall during the rockburst.

Stope 5/60 50 53

The 50 53 stope was entered by traversing an escape route through the back area. The Durapaks had been installed about a year prior to the event. They had experienced some crushing and down-dip ride, and appeared to be working well. The hangingwall was in good condition.

The strike gully contained a considerable amount of loose rubble produced by footwall blasting. The area around the centre gully tip was inspected. Tall timber packs had experienced lateral displacement.

62 Level

5/62-49 cross-cut

On 62 level the most severe damage was sustained by this northern haulage, which was closer to the source of the seismic event. The damage was similar to that observed on 60-50 level: bulking of side- and hangingwall, failure of areal support owing to breaking of destranded hoist rope lacing, and collapse of hangingwall leading to the total closure of the tunnel. Damage commenced close to the fault contact, which also defined the limit of the above mining abutment. Significant closure of the sidewalls, hangingwall and footwall had occurred at this point. The integrity of the mesh and lacing support had generally been maintained. However, significant bagging had occurred and large overall deformations may be indicative of the loss of the reinforcement tendon anchorage in this area. To the west of this point, the mesh and lacing areal support had failed on the north sidewall, but the grouted wire rope reinforcement had generally maintained its anchorage, although a few units were observed to have failed.

The cross-cut from this point to the down-dip stope abutment is generally over-stoped. Damage was still observed to the north sidewall, hangingwall and footwall, but of lower severity compared to the damage close to the mining abutments. Unravelling of the rock mass between reinforcement resulted in severe bagging of the mesh and lacing fabric support in parts of the tunnel. Evidence of the severity of the dynamic ground motion experienced by the tunnel was given by the movement of a pipe, originally stacked against the sidewall, to a position below the rails and sleepers of the haulage.

Complete closure of the tunnel had occurred close to the western stoping abutment. To the east of this mining abutment, closure appears to be owing to the failure of the mesh and lacing fabric support and unravelling of the rock mass, while the reinforcement units remained intact and anchored in stable ground.

To the west of the mining abutment, viewed from the opposite side of the fall of ground, the mesh and lacing fabric support remained intact, but failure of the reinforcement units resulted in collapse of the hangingwall rock mass. The mechanism of failure of the reinforcement (tendons) was either owing to failure (tension or shear) of the unit owing to dynamic loading, or failure of the anchorage and suspension of the hangingwall beam.

5/62-48 cross-cut

The 5/62-48 cross-cut sustained relatively minor damage in comparison to the 5/62-49 cross-cut, approximately 100 m to the north. Hangingwall collapse had occurred close to the western down-dip mining abutment, owing to failure of the mesh and lacing fabric support and unravelling of the rock mass between end anchored rock bolts.

5/62 Haulage E3, north from 5/62-49 cross-cut

Much of this section of the haulage had suffered deformation of the hangingwall and footwall, although the support system prevented collapse of the hangingwall strata. Rehabilitation work on the hangingwall consisted of removal of the bagged mesh and lacing fabric support. Observation of the stability of the rock mass subsequent to the removal of the mesh and lacing indicated an unstable zone of approximately 1,5 m. The unstable rock mass in the hangingwall of the tunnel consisted of some relatively large blocks, but in general the block size was estimated to be approximately 0,2 m.

In discussions with the rehabilitation crew, the comment was made that the hangingwall of the tunnel had unravelled rapidly when the central strand of the lacing system was cut. This may be indicative of the sensitivity of the rock mass to the loss of a component of the fabric support system, and the level of interaction with the rock bolt reinforcement, on the stability of the excavation.

5/62 haulage E3 between 5/62 52 and 5/62 52A cross-cuts

This section of the haulage lies to the north of the Clemcor Dyke. At this site catastrophic failure of the eastern sidewall and hangingwall of the haulage, closest to the event source, had occurred. Failure of the sidewall of the tunnel was principally a result of the failure of the mesh and lacing fabric support and subsequent unravelling of the rock mass. In the hangingwall of the excavation, the failure of the support system was owing to the violent guillotining, or tensile snapping of the reinforcement units under hangingwall shear, and subsequent collapse of the hangingwall rock mass. More violent failure seemed to be associated with the stiff, fully grouted Gewi bar support system than the wire loop reinforcement. The reason for the severity of the damage in this section of the haulage is not clear, and may be a function of previous seismic history, proximity of the intersection of the 5 Shaft Fault (Split 2), complex seismic wave interaction, or local variation in rock mass strength (potentially owing to rock mass disruption owing to faulting), or the quality of installation of the support.

12.4 Assessment of support performance

Tunnel and cross-cut support

It should be noted that tunnels in this area have been exposed to repeated seismic loading. Since 1985 there have been 23 seismic events with $M_L \geq 2,5$ in this area. Of 2,1 km of tunnel on 62 level, mostly in the loss of the No. 5 Shaft Fault, only 100 m were severely damaged by the event on 10 February 1997. In these sections, the support was clearly unable to control and contain the already fractured rock during the violent shaking caused by the $M_L=4,0$ event. The unravelling of mesh and lacing during the rockburst and rehabilitation is of concern. Many tendons appear to have failed during the event.

The support system interaction with the rock mass is generally based on anchorage into stable ground. Where major stoping abutments exist the depth and intensity of rock mass fracturing may increase the extent of the zone of instability beyond the length of the anchors. The large closures associated with the haulages at stoping abutments may be indicative of low levels of rock mass reinforcement and thus weak structural competency.

Under these conditions, the basis of support design should be the formation of a competent rock mass structure (beam, arch or shell). To provide sufficient structural strength to the rock mass it is important to ensure sufficient interaction between the reinforcement units, and not only to rely on the fabric support. Thus support unit spacing should be reduced. The ability to maintain rock mass confinement and have yield capability are also important considerations.

The areas where it was observed that the reinforcement anchorage was stable, generally suffered from a failure of the mesh and lacing fabric support. Under dynamic loading conditions, analysis of the energy associated with a highly fractured unstable rock mass indicates that there is a loss of interaction between the reinforcement and the rock mass and thus a surcharge loading of the fabric which may result in failure. Under these conditions of severe bagging of the fabric, total loss of reinforcement interaction may result and unravelling of the rock mass may occur, to leave the tendons protruding from the stable ground subsequent to the event.

The orientation of the excavations where damage was sustained also seemed to influence the mode of support system failure. In the cross-cuts, the haulages were unstable close to mining abutments and in overstoped ground. Under these conditions the adverse stress history, both high vertical stress increase and potential subsequent stress reduction, have resulted in increased instability of the general rock mass in the periphery of the excavation. Dynamic wave interaction with the stoping horizon and the haulage excavations may also be more complex in these vicinities. The general mode of failure of the support system under these conditions is bulking of the rock mass in the sidewall (and close to abutments, also the hangingwall), causing axial loading of the support system.

In haulages orientated sub-parallel to the general strike of the reef horizon and country rock stratigraphy, damage to the hangingwall of the haulage was more pronounced. Bulking of the hangingwall and footwall was observed at 5/62 E3 haulage at 5/62-49 north, and this was considered to be owing to shearing on bedding planes orientated sub-parallel to the haulage. At 5/62-52, complete failure of the hangingwall was observed owing to shearing and guillotining of the hangingwall reinforcement. Under shear loading conditions cable tendons and/or cables with high yield capability have been shown to have greater shear capacity under static and dynamic loading conditions. The principle

support design consideration under these conditions is thus to maintain the integrity of the fairly competent hangingwall by use of reinforcement with shear capacity. The use of fabric support to maintain hangingwall integrity between the reinforcement units is dependent on the degree of discontinuity.

Sidewall failure at 5/62-52 was again primarily a function of the loading and failure of the fabric support under dynamic loading with stable reinforcement anchorage.

Gully Support

The Durapaks performed well and did not appear to induce additional or unnecessary damage to the gully sidewall and still provided good hangingwall support. The Apollo packs did not perform as well. Some damage to the gully sidewall was noted. Some gully packs were excessively tall, and had suffered lateral displacement during the rockburst.

Stope Support

The Durapaks in the stope back area appeared to be performing very well. They had maintained their integrity for over a year, and were still providing effective support to the hangingwall.

12.5 Assessment of layout

Back analysis of the seismic event with M_L=4,0 in the area of Vaal Reefs No 5 Shaft was carried out. The stresses arising from tabular excavations, as well as slip movements on discontinuity planes, can be modelled by numerical methods. The possible hazard on a given discontinuity plane can be interpreted by means of excess shear stress (Dede and Handley, 1997). A representative section across the No. 5 Shaft Fault was modelled using DIGS (the 2-D boundary element Discontinuity Interaction and Growth Simulation program, Napier, 1990). The elastic constants used were a Young's Modulus of 78 GPa and a Poisson's ratio of 0,21.

The discontinuity was modelled using a simple crack with an internal friction angle of 30° and zero cohesion. Mining occurs to the fault. The plane strain model provided a slip profile, which is constant in the out of plane direction. Figure B.58 shows the slip profile on the fault. The area of integration was then assumed to be a Brune type circle, the diameter of which was the dip length undergoing slip. The seismic moment (M_0) was calculated based on a relationship given by Hanks and Kanamori (1979):

$$M_0 = G\,A\,D \ \text{(Nm)} = G\,V \quad \text{(Nm)} \qquad \text{(B.10)}$$

where

A= area of slip = area of circle (m^2),

$D = \int_a^b R\,dx$ = average slip (m), a,b = start / end of slip pitch,

$V = \frac{\pi}{4}(b-a)^2 D$ = volume of slip (m^3).

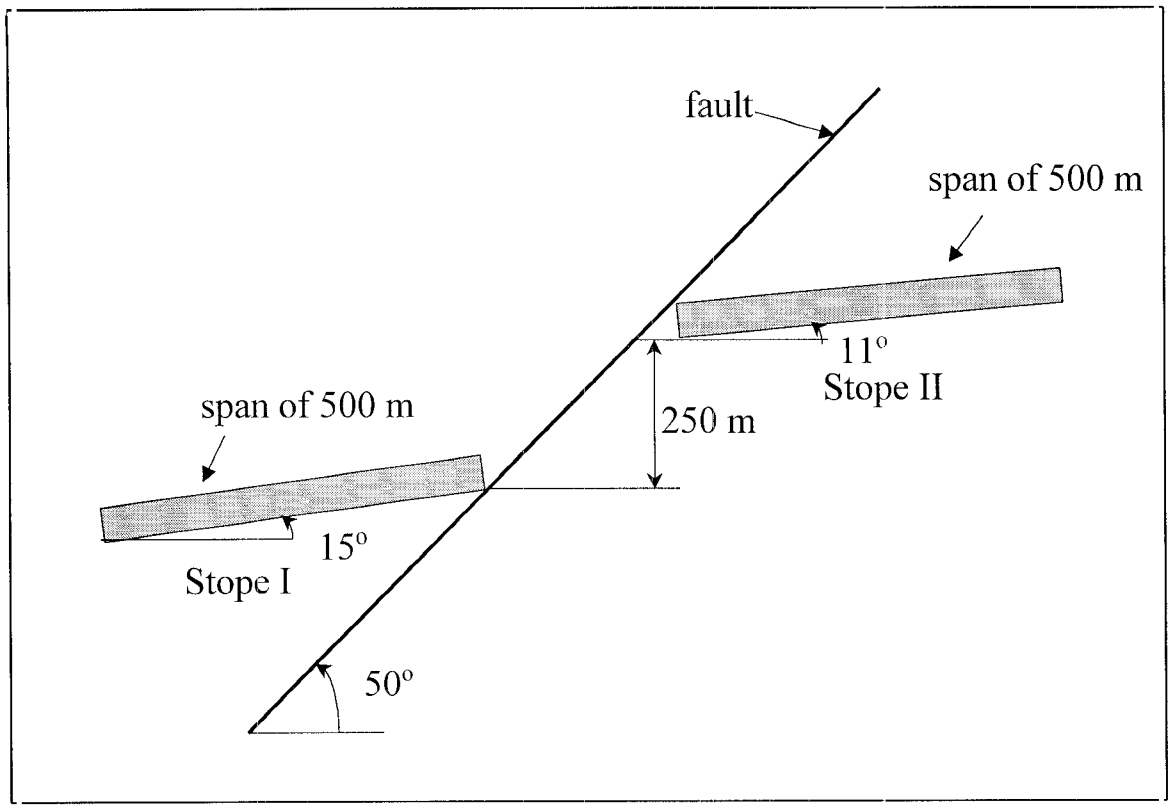

Figure B.57 Cross-section of seismic event area where mining is approaching the fault from both sides

The distribution of slip provided by the plane strain model was numerically integrated over the (dip) length of the discontinuity undergoing slip, and the average slip was calculated by dividing the integrated slip value by the dip length undergoing slip. The area of the circle was calculated and multiplied by the average slip. This can be thought of as the *volume* of slip. The seismic moment based on the above procedure was found to be 1,59 x 10^{15} Nm.

The maximum potential magnitude (M) was then obtained from the empirical relation derived by Hanks and Kanamori, (1979):

$$M = \frac{2}{3} [\log (M_o) - 9.1] \qquad \text{(B.11)}$$

$$M = 4.08$$

This theoretically calculated value of the maximum magnitude is in reasonable agreement in the observed value of the moment magnitude of 3,8.

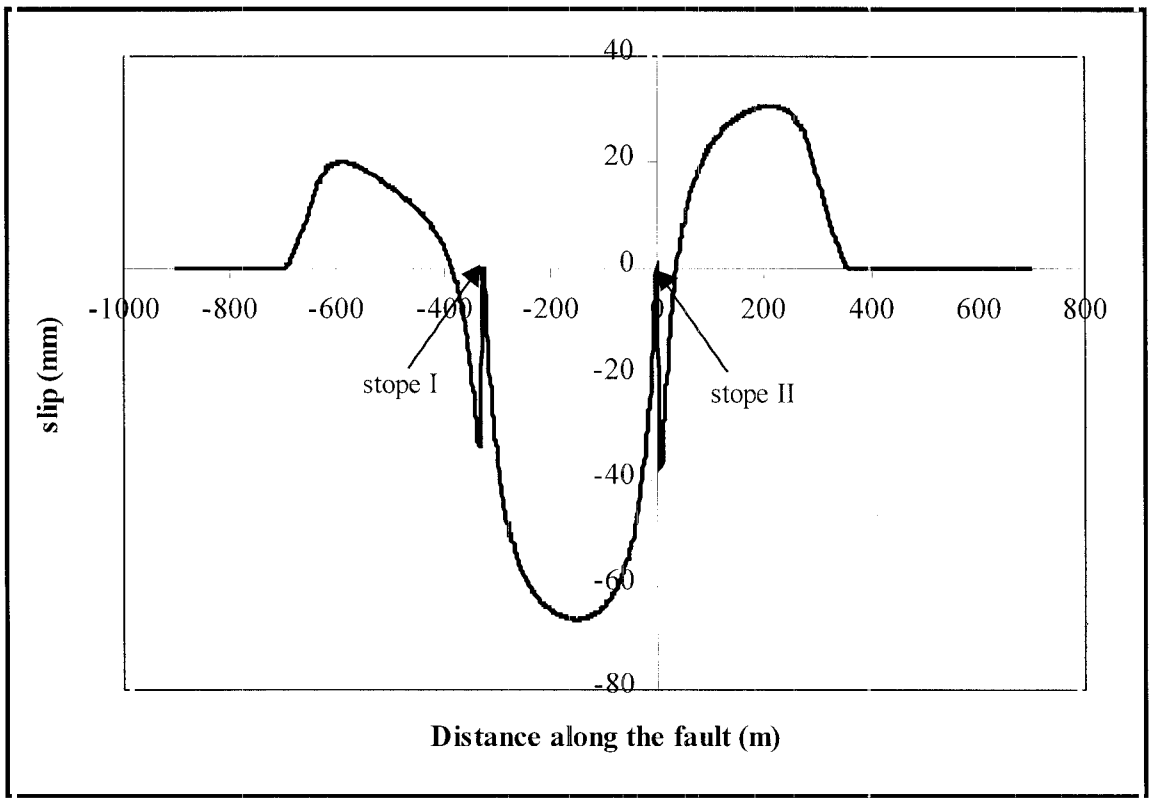

Figure B.58 Slip profile on the fault

12.6 Seismic history, prediction, forecasting and warning

Seismic history

The No. 5 Shaft Fault area has a history of large seismic events. In the period from 1 January 1979 to 11 February 1997 a total of 20 events with $M_L \geq 3,9$ have been recorded in the general area (see Figure 12.1). Sixteen of these events took place in the five years period 1983 to 1988 when extensive stoping was being carried out in the area. Only four

large events have occurred since the start of 1989. Minimal stoping was been carried out in this area since 1989 as the reef had largely been mined out.

Earthquake forecasting and prediction

There is a fundamental dilemma inherent in earthquake forecasting which demands that a rigorous statistical approach be adopted. Suppose that seismological measurements indicate that an earthquake of a certain magnitude will occur during a certain period of time. Presumably the area is seismically active (or the study would not have been initiated in the first place), so a certain probability exists that an earthquake will occur during the predicted period. Thus the occurrence of an earthquake cannot be taken as decisive proof that the methods used to make the prediction are correct, and that they will succeed on future occasions. Of course, if a firm prediction is made and nothing happens, that must be taken as proof that the method is invalid (Bolt, 1988, p. 159-160). The IASPEI Sub-commission on Earthquake Prediction (Wyss, 1991) has provided guidelines to evaluate proposed earthquake precursors stipulating that an earthquake prediction should specify the following parameters with errors less than or equal to those indicated:

- location ±½ rupture length,
- size ±½ rupture length (or magnitude ±0,5),
- time ±20% recurrence time, and
- probability (in most cases the ratio of successes to the sum of successes and false alarms).

Forecasting and prediction at Vaal Reefs

Remarkable claims have been made regarding the success of seismic prediction at Vaal Reefs. For example, Glazer (1997) concludes *"The results of practical application of the instability concept in the test area was a success. Today the success rate of predicting events in this area is as high as 80%".* Ebrahim Trollope and Glazer (1997) write *"Interpretation software became available at the end of 1994 and during 1995 the forecasting concepts were tested and proved to be 60% successful. During 1996 this was increased to 90%".*

Glazer (1997) found that the energy index provides the most reliable detailed information, while the apparent volume had more of a regional application. Ebrahim Trollope and Glazer (1997) note that the parameters more direectlyy related to energy and moment (energy index and apparent volume) proved to be the most successful for stability analysis.

It is important to appreciate what Ebrahim Trollope and Glazer (1997) and Glazer (1997) mean by the terms "warning", "prediction" and forecasting", as these vary from the conventional earthquake seismology usage described above. Glazer (1997) notes that *"A seismic warning is strictly limited to indicating an area, that in future might experience a seismic event. Its strength (magnitude) or time is unknown. In other words seismic warnings are limited to space predictions, and as such are still in a developing stage"*. Glazer (1997) lists 77 cases for the 17 month duration of the experiment. The minimum magnitude considered appears to be 1,7, which presumably is the threshold for "potentially damaging" events. In 62 cases an event followed the warning (between 1 and 41 days later), in 5 cases a false warning was given, and in 10 cases an event occurred without a warning being issued. In the 56a polygon, where *".. the success rate of the concept is very high, and all 13 events were predicted"* , the time between warning and event varied from 1 to 14 days, with an average of 6,5 days. The average time interval between seismic events in the 56a polygon was 13 days.

Other difficulties noted by Glazer (1997) relate to the method of defining the areas of interest, the polygons themselves. Furthermore, the underground conditions undergo constant changes, yielding changes in the energy index "baseline". Other uncertainties include the reliability of the source parameters, area, time span and type of curve used to calculate the energy index.

Ebrahim Trollope and Glazer (1997) discuss results from the No. 5 Shaft north area. Between January 1996 and 6 June 1997, warnings were issued prior to 76 out of a total of 87 events with M_L>2,0 which occurred in the forecast area. In 63 cases the time between the warning and the subsequent event was less than 7 days. While these results appear very promising, Ebrahim Trollope and Glazer (1997) note that *"within the 5 shaft pillar network three large damaging events occurred and none of them were forecast nor could an instability be identified in a back analysis. In addition between 10-15 February 1997, nineteen large very damaging events occurred in the 5 shaft north area along all of*

the major structures and none of them were forecast either". The M_L=4,0 event investigated here was one of these large damaging events that was not predicted. Neither were any precursory changes in parameters detected, even in hindsight, when the location of the event was known and an appropriate polygon could be selected (Ebrahim Trollope, Vaal Reefs, pers. comm.)

Another important point noted by Ebrahim Trollope and Glazer (1997) is that the stopping of production in an area recognised as unstable does not lead to the aseismic dissipation of the strain energy. Rather, the event is delayed to the time when production resumes, resulting in an increased hazard for rockfalls owing to a deterioration in the ground conditions.

Assessment of prediction/forecasting at Vaal Reefs

Very high success rates for seismic prediction at Vaal Reefs have been claimed. However, the criteria used to calculate the "success" of a prediction are far less stringent than used in earthquake seismology, as neither the time nor the magnitude of the forthcoming event are predicted. The statistical techniques used at Vaal Reefs to quantify the success of prediction should be carefully assessed so as to ensure that an unrealistic expectations are not created, particularly as the warning system failed to predict several large and very damaging events, and no instability was detected, even in hindsight.

Glazer (1997) notes that Vaal Reefs has adopted a policy that the success rate should be measured in preventive actions taken rather than the success of prediction itself, and mentions several actions taken by the mine, including additional safety pillars, changes in mining sequences and directions, and a review of the mining strategy for the whole area.

To the extent that seismic warning system has raised the level of awareness of seismic hazard, and motivating the implementation of remedial actions, credit should be given. However, several failures of the warning system to predict large damaging events should caution the seismologists against raising unrealistic expectations amongst management and workers.

12.7 Rockburst mechanism

Source mechanism

The focus of the M_L=4,0 event on 10 February 1997 located on the intersection of the No. 5 Shaft Fault and the Clemcor Dyke. The following source parameters were derived by the Integrated Seismic System (Table B.8).

Table B.8

Source parameters

Time: 18 h 8 m 9,31 s on 10 February 1997			
Location: 76265 m S, 24356 m W, 2419 m down			
Local Magnitude 4,0			
EVENT SIZE			
Brune source radius m		**Apparent volume**	x 10^6 m^3
MOMENT		**ENERGY**	
Seismic moment:	6,97 x 10^{14} Nm	**Radiated Energy**	3,01 x 10^{14} J
P Moment	5,56 x 10^{14} Nm	**P Energy**	2,04 x 10^9 J
S Moment	8,38 x 10^{14} Nm	**S Energy**	2,80 x 10^{10} J
Moment Magnitude	3,8	**Energy Magnitude**	4,4
S Moment/P Moment	1,51	**S Energy/P Energy**	13,7
STRESS		**CORNER FREQUENCY**	
Apparent Stress	1,29 MPa	**Corner Frequency**	4,3 Hz
Static Stress Drop	7,04 MPa	**P Corner Frequency**	5,1 Hz
Dynamic Stress Drop	4,27 MPa	**S Corner Frequency**	3,5 Hz

Fore- and aftershocks

No foreshocks were recorded. Fifteen aftershocks with local magnitudes M_L>1,4 were recorded in the 24 hours after the M_L=4,4 event. The largest aftershock had a magnitude of M_L=2,7. The aftershock locations coincided with the Clemcor Dyke.

12.8 Conclusions

Rockburst damage was found in haulages developed in the fault loss associated with the No. 5 Shaft Fault, and in cross-cuts developed from these haulages, especially where the cross-cuts intersected the fault plane and passed from solid to overstoped ground. Damage was found over a linear distance of 1200 m parallel to the No. 5 Shaft Fault. The M_L=4,0 event which occurred at 18h08 on 10 February 1997 was inititated at the intersection of the No. 5 Shaft Fault and the Clemcor Dyke. Based on the distribution of damage, slip on the No. 5 Shaft Fault is thought to be the most likely source mechanism. Aftershock activity was confined to the Clemcor Dyke, and was probably a response to the stress redistribution caused by the M_L=4,0 event.

Even in hindsight, no change in seismic parameters, (e.g. Energy Index, Apparent Volume) which could have indicated an increase in the seismic hazard, was detected.

The area around the No. 5 Shaft Fault has a history of large ($M_L \geq 3,9$) seismic events. The siting of excavations within the loss associated with major faults was a design decision made at the start of mining. In retrospect, it would appear that the siting of tunnels and cross-cuts in those areas where extensive stoping was planned should have been avoided.

The tunnel and cross-cut support was clearly unable to control and contain the already fractured rock over sections of the tunnels and cross-cuts which bulked further during the violent shaking caused by the M_L=4,0 event. Many tendons appear to have failed during the event. The unravelling of mesh and lacing during the rockburst and rehabilitation is of concern.

The Durapaks in the gullies performed well and did not appear to induce additional or unnecessary damage to the gully sidewall and still provided good hangingwall support. The Apollo packs did not perform as well. Some damage to the gully sidewall was noted. Some Apollo packs were excessively tall, and had suffered lateral displacement during the rockburst.

The Durapaks in the stope back area appeared to be performing very well.

12.9 Recommendations

The siting of tunnels and cross-cuts in the fault loss of major faults should be avoided, especially where extensive stoping is planned to take place.

The design of reinforcement spacing, and mesh and lace fabric support capacity should be based on analysis of reinforcement interaction with the rock mass, the desired mode of anchorage, and the anticipated influence of dynamic loading.

The length of the reinforcement (tendons) should be based on anchorage beyond the zone of unstable ground. At this site it was observed that in the hangingwall the extent of unstable ground was approximately 1,5 m and in the sidewall it was estimated at approximately 2 m. The extent of unstable ground increased at the mining abutments, or adjacent to geological features. Either the length of the tendons should be increased in these areas, or the spacing between tendons should be decreased to increase the interaction between reinforcements and form a stable arch.

The capacity of the reinforcement unit should be based on tributary area analysis of the support system as isolated block loading may occur, and fabric anchorage must be accommodated by the reinforcement system.

Hangingwall support design in strike haulages must give particular consideration to shear capacity of the reinforcement units.

All reinforcement units, under dynamic loading conditions, should have sufficient yield capacity in the anticipated design environment.

Lacing must be well clamped at regular intervals to prevent unravelling over large sections after failure at a single point.

Yielding tendons should be used in gullies. The use of Durapaks as support for gullies and stopes should be continued.

13 Leeudoorn, 10/4/97, M_L=1,7 and 16/4/97, M_L=2,3

13.1 Introduction

A seismic event of local magnitude M_L=1,7 occurred at Leeudoorn Gold Mine on the evening of 10 April 1997. This event was located close to the 35/78 VCR north mining face, at a depth of approximately 2630 m below surface (Figures B.59 and B.60). It was associated with the collapse of the immediate face area, fatally injuring a worker who was busy rigging the scraper ropes in order to clean the face area. It was reported that, prior to this event, only limited seismic activity had been recorded in this area. A seismic event with local magnitude M_L=2,3 then occurred on the night of 16 April 1997 in advance of the 35 / 78 VCR south mining faces (Figures B.59 and B.60). Damage was sustained by the bottom strike gully of the stope, but fortunately no injuries were sustained. A team from CSIR Mining Technology was invited by Mr. R. Jaggard and Mr. O. Meier to investigate the apparent increase in seismic activity and associated rockburst damage. An underground visit was conducted on 21 April 1997.

13.2 Mining environment

Geology

The rockbursts affected the 35/78 Ventersdorp Contact Reef (VCR) stope. No major geological structures were known to exist in the immediate vicinity of the seismic event locations. In this area the VCR dips at approximately 24° to the south-east, with a stoping width of approximately 1,4 m, and a hard lava hangingwall and a quartzite footwall. The VCR lies unconformably on the quartzite footwall. The VCR was structurally disturbed in the vicinity of the rockburst damage associated with the M_L=1,7 event. Multiple small thrust faults (or nappes) had been mapped and indicated in the original raise line by the geology department. The reef at this locality had also rolled (approximately 1 m) into the footwall of the stope. Stoping operations included trenching at the stope face to expose the reef horizon.

The Kloof reef, which is also mined in this area, sub-crops with the VCR on the south-western side of the stope, and dips at approximately 40° to the east. The Kloof reef has a stoping width of approximately 1,5 m with conformable quartzite hanging- and footwall. The footwall of the Kloof reef was indicated to be highly bedded, with shear movement associated with the bedding planes.

Mining Layout

Stoping on the VCR horizon was conventional breast mining with approximately 30 m panels with small leads, creating an overall overhand face configuration. The extent of mining, on a regional basis, in this area was very limited (see Figure B.59). The large lead of the panel immediately down dip of the M_L=1,7 event increased the stress concentration on the lagging face position. This, however, did not seem to contribute to an instability of this lower portion of the panel on which the hangingwall collapse occurred. Overall the general stope face configuration on the VCR, is considered to comply to standard rock engineering practice.

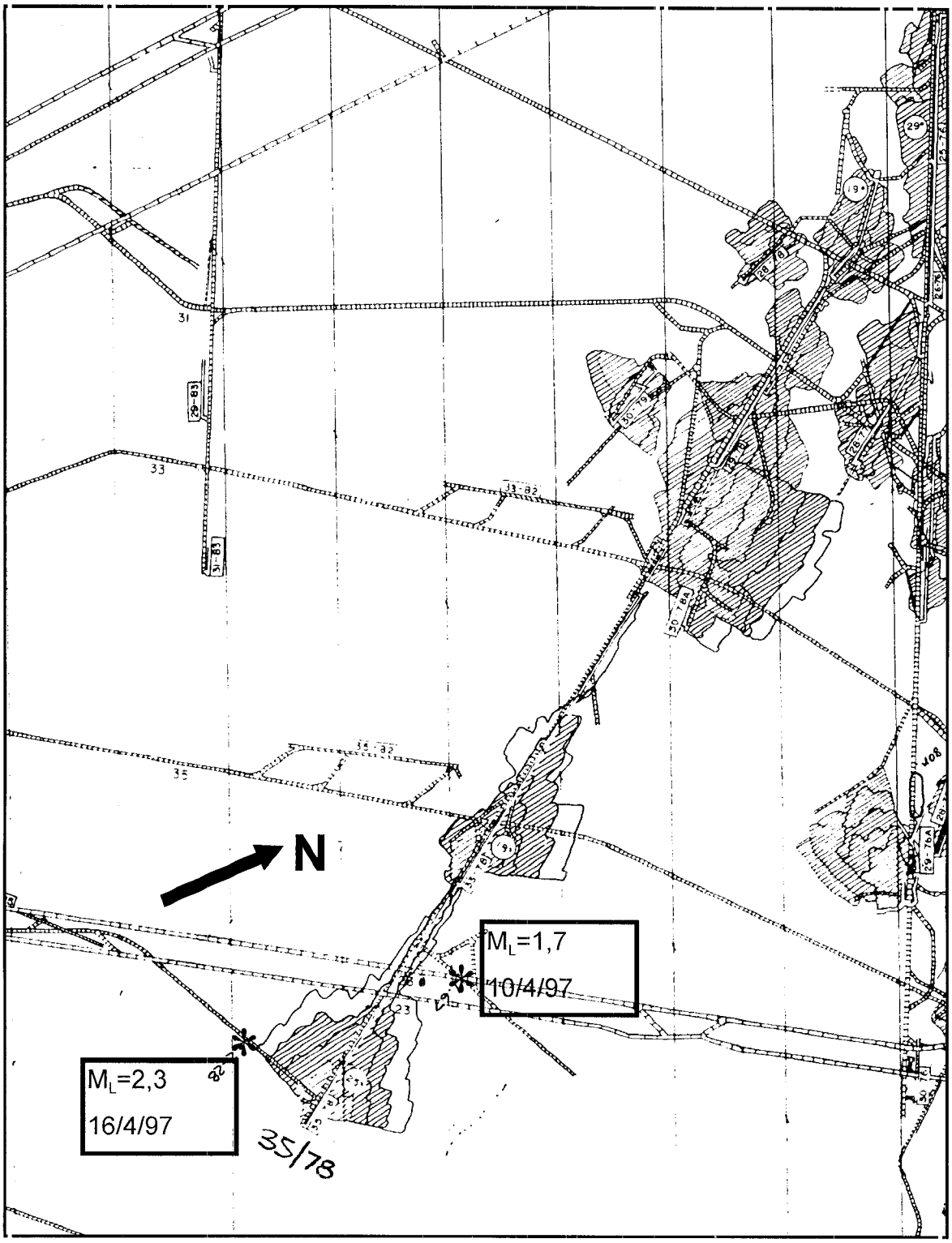

Figure B.59 Regional mining plan showing the stoping layout in the vicinity of the 35 Level 78 Line, Leeudoorn Division of Kloof Gold Mine, which experienced damage owing to a M_L=1,7 seismic event on 10 April 1997 and a M_L=2,3 seismic event on 16 April 1997.

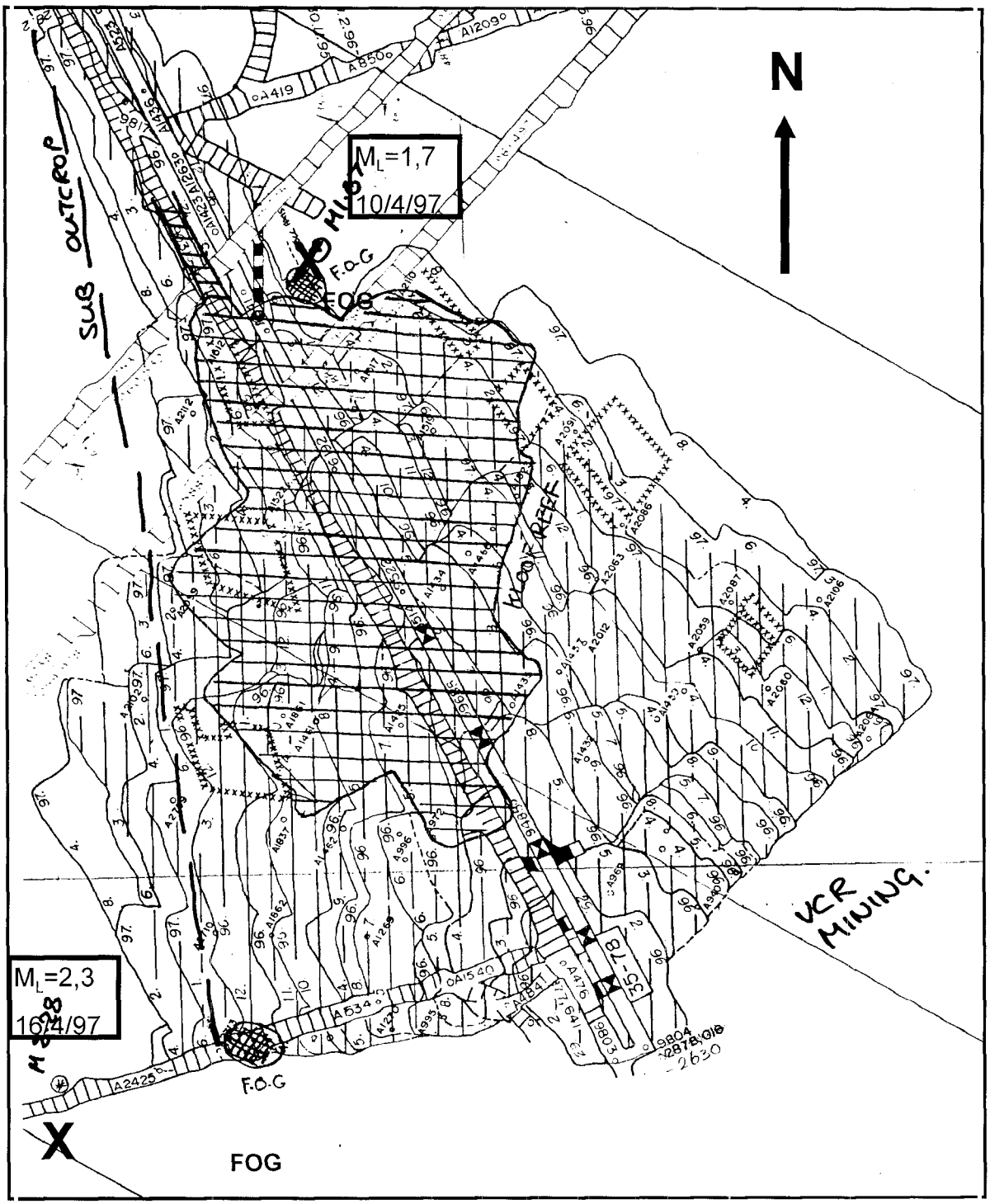

Figure B.60 Local mining plan showing the locations of the M_L=1,7 seismic event on 10 April 1997 and a M_L=2,3 seismic event on 16 April 1997 and the distribution of damage in the 35/78 VCR stope, Leeudoorn Division of Kloof Gold Mine. The stoped out area of the VCR and the sub-cropping Kloof reef are shown by vertical and horizontal hatching, respectively.

The negotiation of the roll in the reef at the site of the M_L=1,7 event had necessitated trenching at the mining face in order to expose the reef horizon at the lower elevation. This would have resulted in the exposure of the hangingwall lava at the face position and a higher than normal unconfined face dimension.

The Kloof reef stope lies below the VCR, and sub-crops within the VCR stope approximately 10-20 m back from the position occupied by the south-western face of the longwall at the time of the rockburst (Figure B.59). A crown pillar was originally planned for the mining of the Kloof reef to prevent holing of the two stopes. However, a holing was made on the upper portion of the sub-crop. The extent of mining north on the Kloof reef horizon was indicated to coincide approximately with the plan position of the VCR faces, in the vicinity of the upper (north-eastern) portion of the VCR stope, as indicated in Figure B.60. Significant stope closure was reported from the Kloof reef horizon.

Support

Permanent stope support, on both VCR and Kloof reefs, consisted of 1,1 m, 9 pointer configuration composite packs. Backfilling had commenced on the south side of the VCR stope recently. Standard face support consisted of two rows of rapid yielding hydraulic props (RYHP's).

13.3 Observations at the rockburst site

Rockburst damage owing to the M_L=1,7 event on the 10 April was very localised but fairly severe in nature. Hangingwall collapse in the stope face area had occurred over an area of approximately 10 m x 5 m, to an estimated height of 3-4 m. Observation of the collapsed rock mass indicated the highly fractured and discontinuous nature of the hangingwall in this vicinity. Damage to support in the stope back area was very limited, and confined to the immediate vicinity of the collapse. Dynamic closure damage was observed to the timber headboard of a stick immediately adjacent to the fall.

Rockburst damage associated with the M_L=2,3 event on 16 April was limited to the bottom strike gully on the south side of the stope in the vicinity of the Kloof reef sub-crop, approximately 20 m back from the stope face. Damage consisted of the loss of the down dip gully sidewall, collapse of the pack support in this area, and thus subsequent collapse of the gully hangingwall. The hangingwall condition in this area is generally poorer than the typical stope hangingwall condition owing to the proximity of the stope down dip abutment. The presence of fractures, dipping shallowly towards the north, in the footwall of the VCR in this vicinity also contributed to the instability of the south-west side of the gully sidewall. No rockburst damage was observed in the vicinity of the stope face, which lay closer to the plotted position of the seismic event.

13.4 Rockburst mechanism

The source mechanisms of the seismic events are fairly speculative, particularly as there was little history of seismicity. The location accuracy is considered to be within 10 m. The source parameters did not indicate abnormal stress drop levels. No major geological structures were known to exist in the near vicinity of the events on the VCR horizon.

M_L=1,7 event

It is believed that the seismic event of 10 April of magnitude M_L=1,7 was associated with a face shear / crush type event. The mechanism of the face burst type event may be owing to the exposure of the relatively hard Ventersdorp lava at the face as a result of the roll in the reef horizon. This harder rock type will enable the storage of greater strain energy within the rock mass. The higher mining face, again owing to the trenching operations to expose the reef horizon, will create a less confined, more unstable face condition (Figure B.61). This, in conjunction with the brittle, post peak failure characteristic of the lava rock type, may lead to violent failure of the face rock mass and associated disintegration of the hangingwall in the immediate vicinity. This failure mechanism has been documented by the rockburst task force, associated with a violent pillar failure at Deelkraal gold mine (see Case History 2), and is considered to be the most likely source mechanism in this instance.

An alternative seismic mechanism may be related to the location of the Kloof reef undermining relative to the VCR horizon. The position of the Kloof reef north face is almost directly below that of the VCR, with an approximate middling of 35 m. This may cause a more adverse orientation of the maximum principle stress relative to the unconformable VCR footwall stratigraphy, with resultant potential shear failure (Figure B.62). This mechanism is discussed in more detail below, with regard to the M_L=2,3 event.

The rockburst damage at this location is considered to be a function of both the seismic event and the local rock mass characteristics. The highly disturbed nature of the stope hangingwall in this area is considered to be owing to small scale thrust faulting of the VCR in a zone striking sub-parallel to the VCR strike in this vicinity, in addition to the disruption of the hangingwall integrity owing to the presence of the VCR roll. This complex geotechnical environment is considered to lead to a highly friable hangingwall rock mass condition, which would be abnormal to anticipated hangingwall conditions and prone to collapse under dynamic loading.

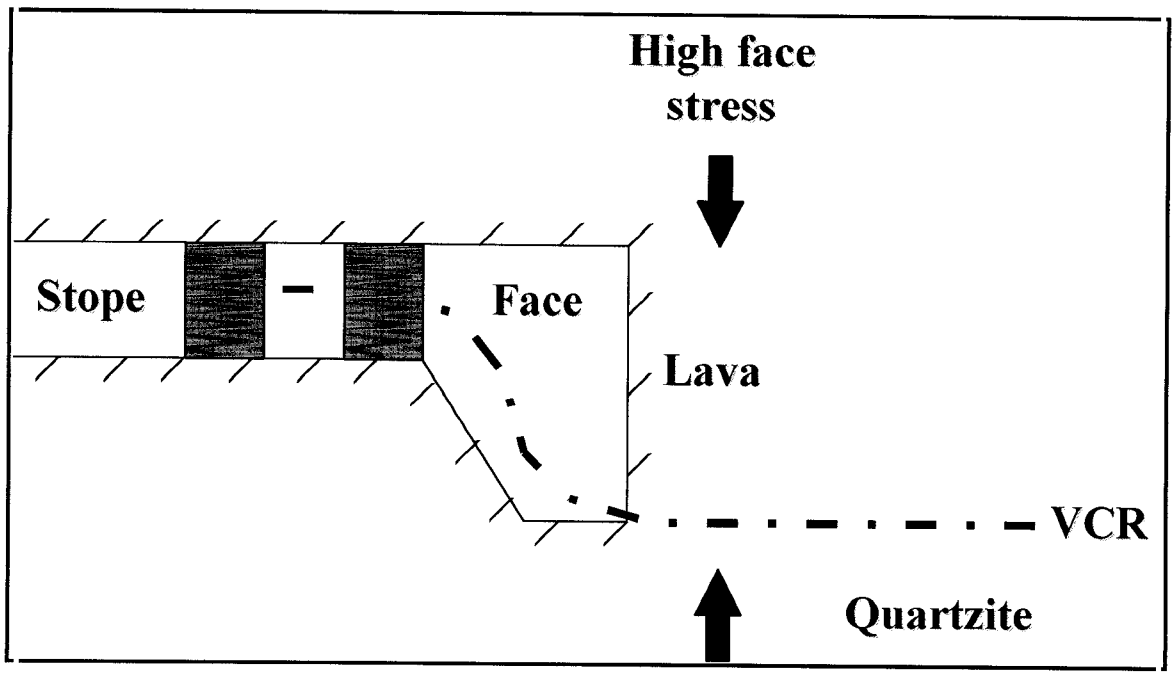

Figure B.61 Possible source mechanism of face burst owing to lava in face, and high face dimension

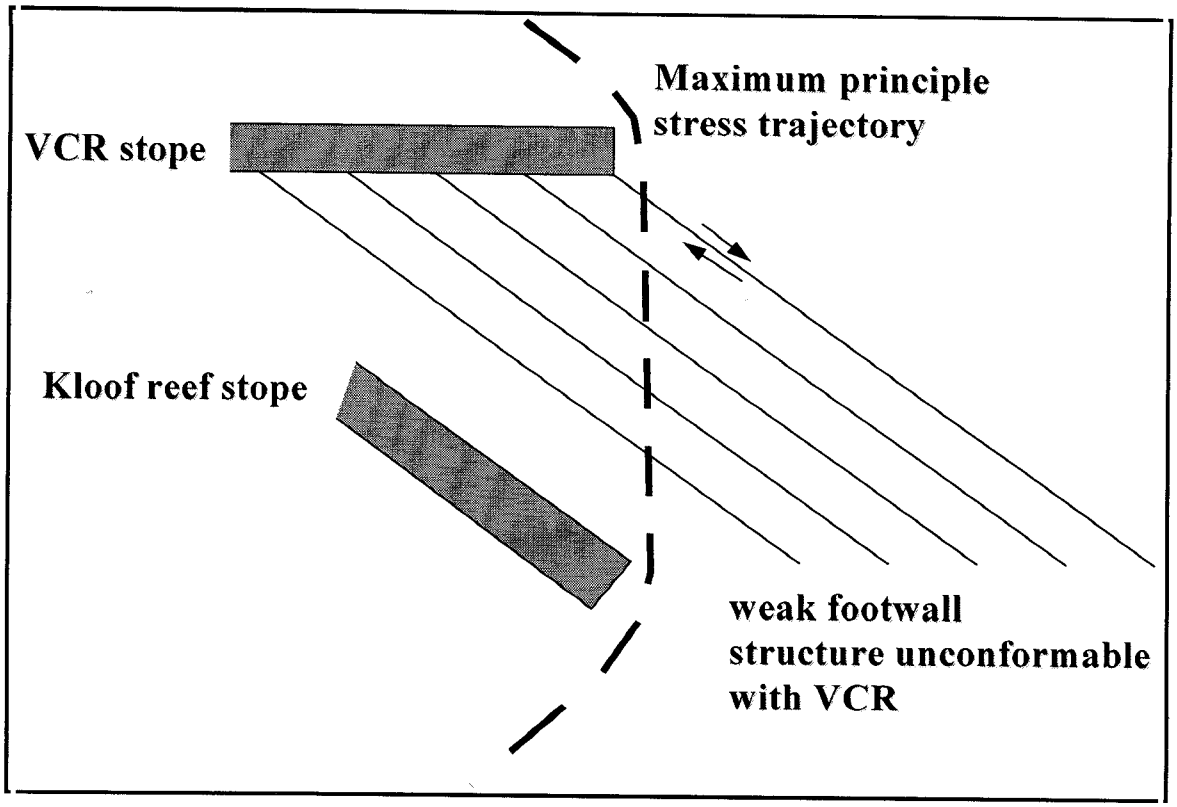

Figure B.62 Possible seismic mechanism owing to relative position of Kloof reef under-mining.

M_L=2,3 event

A M_L=2,3 seismic event occurring in advance of the stope face would generally be associated with a weak geological structure such as a fault or dyke. No such structure was known to exist on the VCR horizon. It is postulated that the event was related to the presence and orientation of the weak bedding planes associated with the unconformable footwall stratigraphy. The trajectory of the maximum principle stress, refracted by the mined out VCR stope, was adversely orientated relative to the footwall stratigraphy. As a result, violent shear movement occurred on weak planes within the footwall rock mass once the stess reached a critical level (Figure B.63).

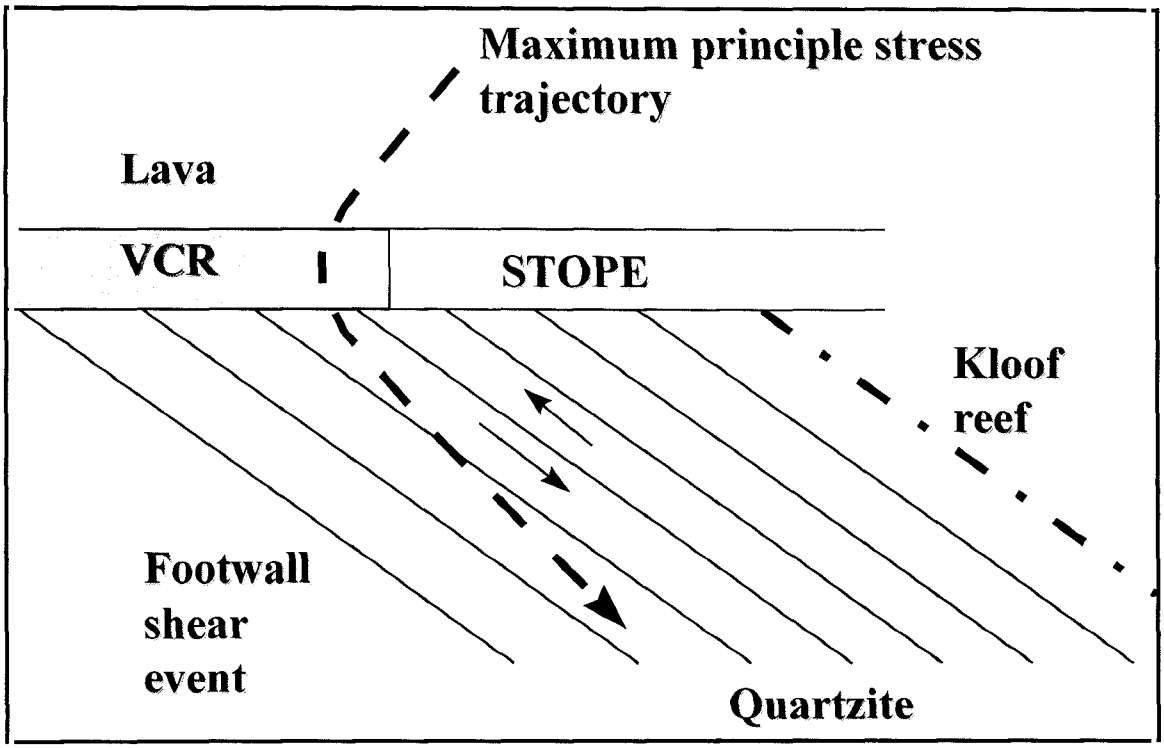

Figure B.63 Proposed mechanism of footwall shear owing to unconformable footwall stratigraphy (north-south section, up dip view)

No hangingwall damage was associated with the stope face area in the bottom stope panels immediately adjacent to the event. However, the observed damage was associated with the stope east siding in the vicinity of the Kloof reef sub-crop. The damage was associated with the loss of the gully east side, the loss of the east siding packs and the subsequent collapse of the hangingwall in the immediate vicinity. The location and mechanism of this rockburst damage may be indicative of a footwall associated event interacting with weakness associated with the Kloof reef sub-crop. The generally poorer hangingwall conditions associated with a stope down dip siding, owing to low dipping and complex fracturing around the stope heading during mining in this vicinity, would result in hangingwall collapse owing to the loss of pack support.

13.5 Conclusions

Both areas of rockburst damage are associated with areas of abnormal geology, in the first instance, localised thrust faulting and a reef roll, in the second instance, the position of the Kloof reef sub-crop.

The negotiation of roll structures on the VCR generally results in the exposure of lava on the working face, increased face height, and poorer ground conditions, which may have an increased propensity for face bursting and subsequent rockburst damage to the hangingwall.

Steeply dipping, unconformable footwall stratigraphy, with associated weak parting planes, may be susceptible to shear-type seismic events when the mining face is sub-parallel to the strike of the footwall stratigraphy, and the strata dip beneath the stope. Thus, in the 35/78 VCR stope where the footwall strata dip towards the east, the faces mining towards the west may be more susceptible to seismicity than the faces mining towards the east.

13.6 Recommendations

Areas of abnormal geology (e.g. localised thrust faulting, reef rolls, sub-crop of Kloof reef) should be recognised as geotechnical anomalies. Special support strategies, such as increased support density or additional support measures, should be implemented to cater for anticipated weaker ground conditions. Yielding support units (hydraulic props etc) of sufficient capacity and suitable spacing should be utilised in areas of seismic potential.

Multi-reef mining layouts should consider the relative positions, and resultant stress fields, of the stope faces relative to the geotechnical structure of the hanging- or footwall rock types; in order to limit the potential for shear, and associated seismicity, on geotechnical structures within the rock mass.

In this case the north mining faces of the Kloof reef should lag the VCR face position by an amount equal to the middling distance until reef separation is such that interaction of the face stresses (orientation and magnitude) is no longer problematic.

14 Western Deep Levels (East), 17/4/97, M_L=2,7

14.1 Introduction

A rockburst occurred in Section 336, Western Deep Levels East Mine at 22h32 on 17 April 1997, damaging the 106/E1 gully alongside a stabilising pillar (Figure B.64). The seismic event measured M_L=2,7 on the local magnitude scale and resulted in a number of injuries to workers. Three workers were fatally injured. Mine management requested that a team from CSIR Mining Technology investigate the incident to determine the cause of the seismic event and resultant rockburst damage. The team visited the site on 22 April 1997.

14.2 Mining environment

Section 336 consists of two mini-longwalls separated by a strike stabilising pillar. They are the 101/102E and 104/106E longwalls. The 107.5/109 mini-longwall, down-dip of the section, had been allowed to mine far ahead of Section 336, and was separated from Section 336 by another stabilising pillar (Figure B.64). The situation had arisen as the result of a fire in the 104/106E longwall in 1987, resulting in the closure of the longwall for five years. Mining of the 107.5/109 longwall continued, resulting in a peninsular of highly stressed ground. Much of the seismic problem currently experienced in this area can probably be attributed to this.

The two mini-longwalls (101/102E and 104/106E) making up Section 336 are shown in Figure B.64. A fault zone known as the Break Fault is shown traversing both mini-longwalls (Figure B.65). This fault zone made for difficult mining in the upper reaches of

the section. Subsequent speeding up of mining in the lower reaches of the section resulted in both longwalls breasting on to the fault at the same time. It is likely that a magnitude M_L=4,0 seismic event, which occurred on 5 May 1996, was initiated as a result. Since then, strict face control measures have resulted in the successful negotiation of the Break Fault in both mini-longwalls, with the exception of the 106E1 panel. It was in the strike gully, leading to the bottom of this panel, that the damage associated with the rockburst of 17 April 1997 occurred (see Figure B.65).

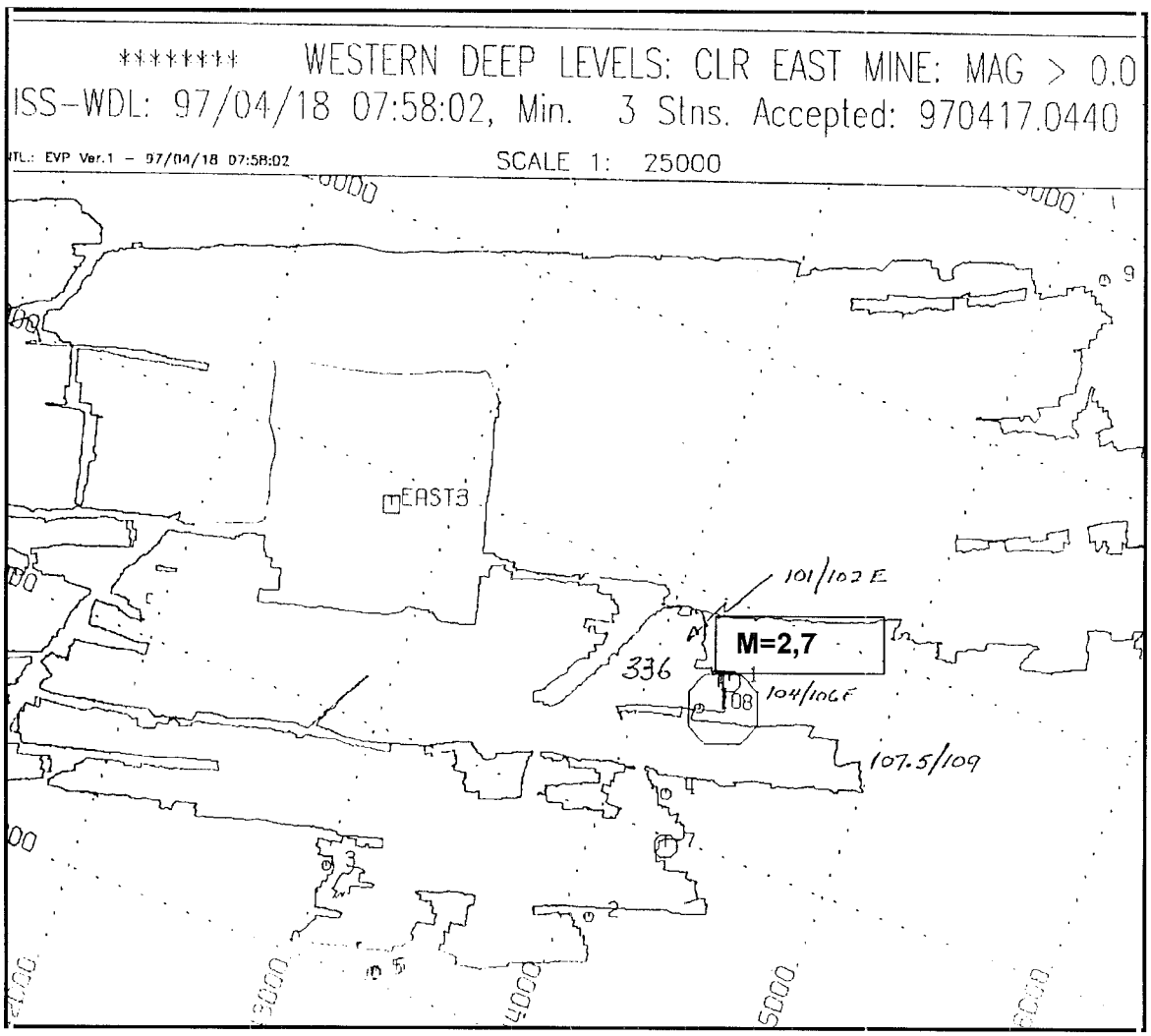

Figure B.64 Plan showing the location of the M_L=2,7 seismic event which occurred at 22:32 on 17 April 1997, Section 336 Western Deep Levels East Mine.

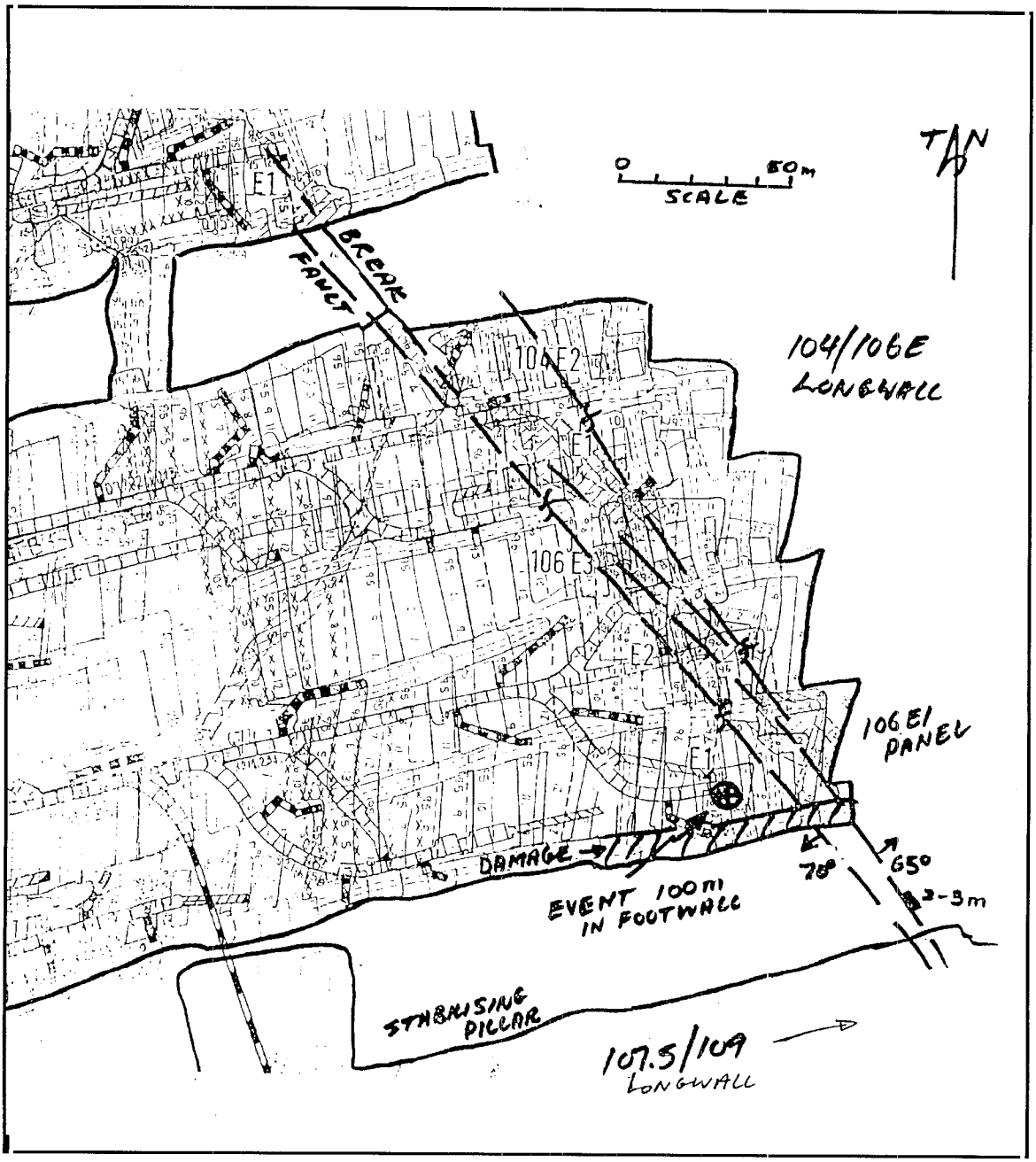

Figure B.65 Plan showing the location of the M_L=2,7 seismic event which caused damage to the 106/E1 gully along a stabilising pillar, Section 336 Western Deep Levels East Mine.

14.3 Rockburst mechanism

Source mechanism

The location indicates that the event initiated 100 m in the footwall of the Carbon Leader reef, beneath the intersection of the Break Fault and the pillar. Moment tensor analysis shows that slip could either have taken place along the Break Fault or along the pillar edge. The consensus of opinion was that the event probably occurred as a result of pillar foundation failure along a shear plane parallel to the pillar, terminating on the weak plane of the Break Fault. This mechanism is suppported by the following evidence:

- Damage is largely restricted to the gully parallel to the pillar edge.
- A small aftershock was recorded on the pillar (Figure B.65).
- There is no evidence of violent damage in the footwall haulages in the vicinity of the Break Fault itself.
- MINSIM modelling by Western Deep Levels East Mine Rock Engineering Department suggests no significant increase of ESS on the Break Fault during the previous month.
- The moment tensor solution requires a low angle of dip if the slip had been along the Break Fault.

Damage mechanism

The observed damage suggests violent dilation of the rock in the vicinity of the pillar edge resulting in compression, bulk movement and buckling of the hangingwall beam just up-dip of the pillar (Figure B.66). The latter caused rockfalls in the gully for a distance of approximately 60 m back from the current face position (Figure B.65). The Green Bar was exposed, and in places the hangingwall had fallen out beyond the Green Bar into quartzite. The Green Bar appeared to be only 0,5 m thick at these sites. Localised gully packs were severely damaged by the hangingwall movement and by closure brought about by the dilation along the pillar edge.

14.4 Assessment of support performance

The gully hangingwall was pinned using 2,3 m grouted re-bar which proved to be totally ineffective. The highly fractured and laminated hangingwall rock fell away from around the support when subjected to compression as a result of dilation of the rock in the vicinity of the pillar.

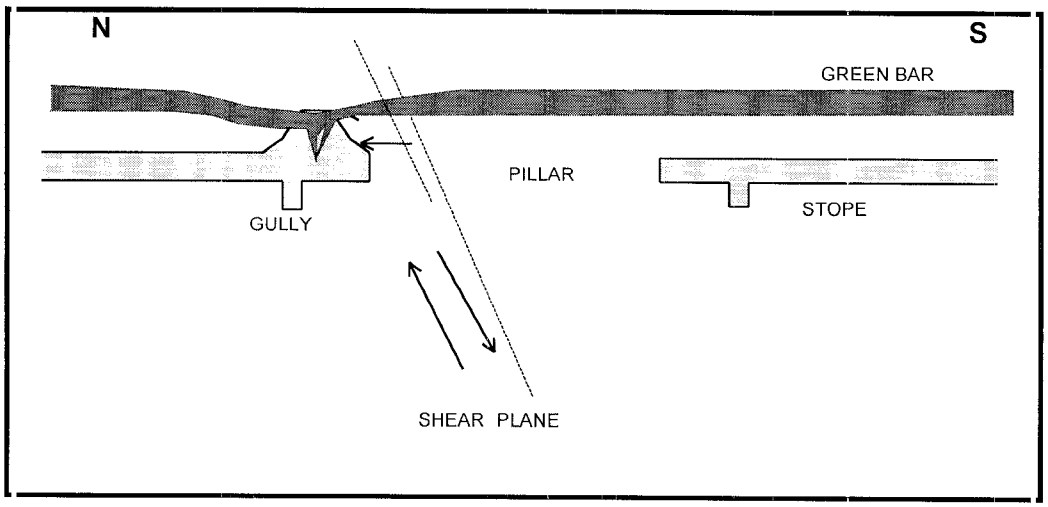

Figure B.66 Section of a stope and stabilising pillar that failed. Horizontal dilation of the rock in the vicinity of the shear plane cause buckling and collapse of hangingwall above the gully.

14.5 Conclusions

Evidence suggests that foundation failure of a highly stressed pillar was the cause of the seismic event.

Resultant dilation of rock into the excavation along the pillar edge caused failure and buckling of the Green Bar and 1 m quartzite beam below the Green Bar.

14.6 Recommendations

1. The load on the pillar could be reduced through a higher volume of backfill and improved placement techniques, thereby reducing the likelihood of further foundation failures.
2. Consideration should be given to improving the support of the gully along pillars and abutments to alleviate damage should similar events occur. Some suggestions are:-
    - Use foam cement in the south siding alongside and behind the packs to absorb the impact of the dilating rock and to maintain the integrity of the hangingwall rocks.
    - Precondition the pillar edges by drilling and blasting from the heading. This will create a buffer zone and ensure that the shear zone, resulting from foundation failure, is that much more distant from the pillar edge.
    - Use Split Sets or cables for gully hangingwall pinning. This type of support is more capable of accommodating shear along weak planes parallel to the hangingwall. The tendons should be angled at right angles to the dominant fracturing.
    - Try blasting a slot in the hangingwall behind the south-side packs to reduce the likelihood of buckling because of violent dilation of rock from the pillar edge. Use foam cement to maintain the integrity of the hangingwall in this area.
    - Get backfill closer to the gully edge, and prevent backfill from dilating into gully by using mesh between packs (as per experiments on Western Deep Levels West mine).

15 West Driefontein # 6, 23/5/97, M_L=2,7

15.1 Introduction

A rockburst occurred at No. 6 Shaft, West Driefontein Gold Mine at 12h58 on 23 May 1997, causing damage to the 3W panel and 3W strike gully of the 36-35 C/L West mini-longwall, about 2300 m below surface. Several workers were injured, one seriously. Two

seismic events, both with local magnitudes of M_L=2,7, occurred within a second, and were recorded by the mine-wide seismic network. The foci of the events were close to the Skelm Dyke, in the block of unmined ground immediately south of the 36-35 mini-longwall (see Figure B.67).

Mine management requested that a team from CSIR Mining Technology investigate the factors contributing to the rockburst, and recommend measures that will reduce the likelihood of similar damaging events. The performance of gully support was of specific interest. The team visited the site on 30 May 1997.

15.2 Mining environment

Geology

The Carbon Leader Reef (CLR) is a narrow conglomerate band, seldom exceeding 10 cm in thickness. In the environs of the 36-35 C/L West mini-longwall, the CLR dips to the south at 23°. The CLR is immediately overlain by a competent siliceous quartzite, typically 1,4 to 4 m in thickness in the Carletonville area. This is, in turn, overlain by the Green Bar, a 1 to 2,5 m thick argillaceous shale unit. CLR gullies appear to be particularly prone to rockburst damage owing to the geotechnical properties of the hangingwall strata. Owing to the poor cohesion between the hangingwall quartzite and the Green Bar shale, the quartzite beam is susceptible to fracture and collapse.

There are several significant geological structures in the environs of the 35-36 C/L West mini-longwall (see Figure B.67). The mini-longwall lies within a trapezoid, approximately 200 m x 200 m in area, bounded by the Jean's Fault Zone to the north-west, the Skelm Dyke to the east, Deon's Dyke to the south, and the Spotted Dick Horst Zone to the west. Several smaller structures are also present, for example a fault with a 2 m downthrow to the west was being negotiated by the (lagging) 1W panel at the time of the rockburst. The (leading) 2W and 3W panels had already mined through this fault.

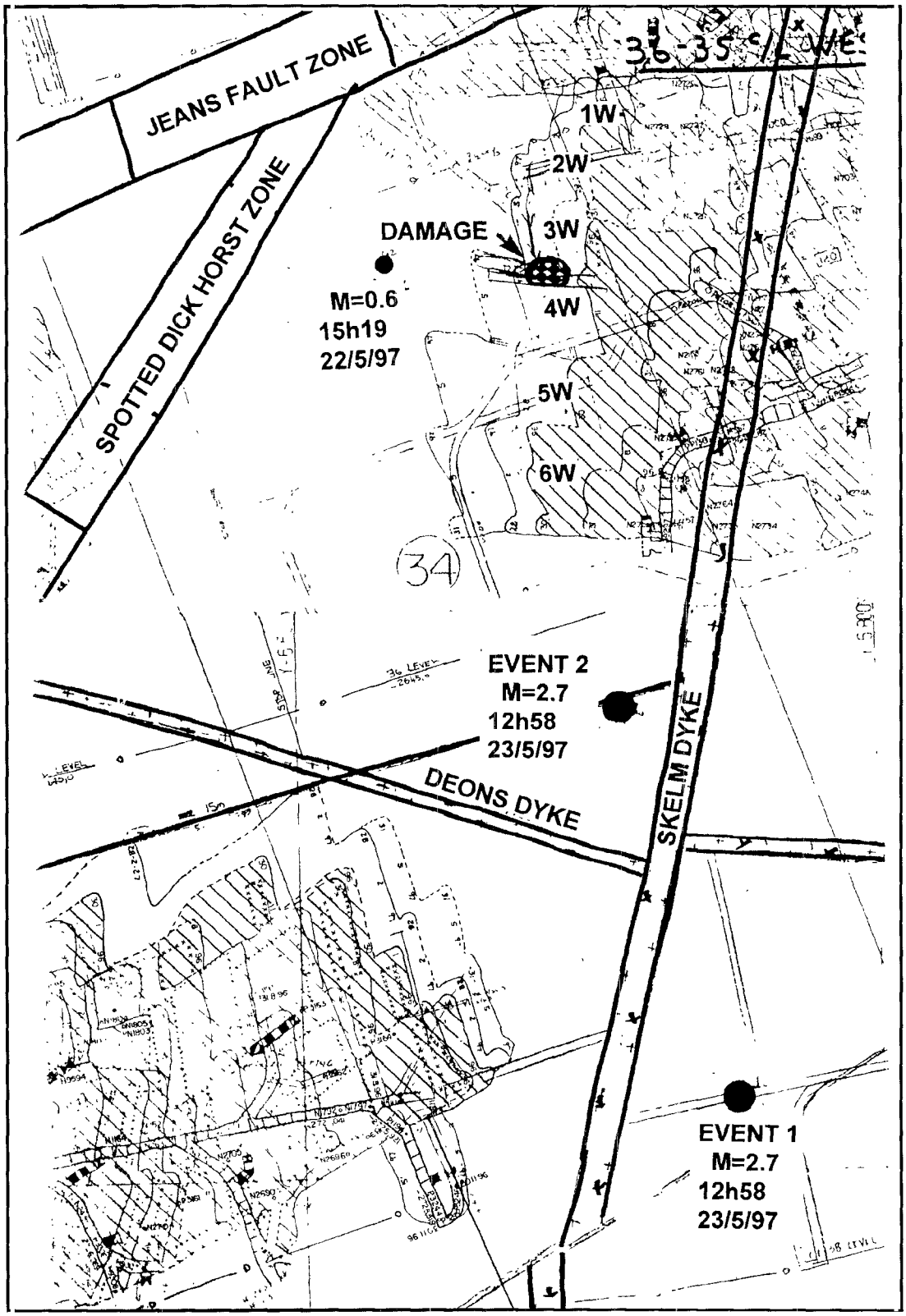

Figure B.67 Plan showing the stoping layout and epicentre of the M_L=2,7 seismic events which occurred on 23 May 1997 damaging the 36-35 C/L West mini-longwall, West Driefontein Gold Mine.

Regional Layout and Support

The 36-35 C/L West stope was being mined as a mini-longwall with an overhand configuration and a dip span of 160 m. No stabilizing pillar was left between this mini-longwall and the up-dip mini-longwall. It was mine practice to leave bracket pillars adjacent to faults and dykes in some instances. The 36-35 C/L West stope was approaching the Spotted Dick Horst Zone (SDHZ). At the time of the rockburst the faces were between 60 m and 120 m away from the SDHZ. The angle between the overall mini-longwall orientation and SDHZ is about 20°.

Backfill was installed in stopes for regional support. The specific gravity of the classified tailings is nominally 1,7 - 1,8. The standard practice at No. 6 Shaft was to fill the panel as far as the second pack above the gully, leaving space for storage or the transportation of material by mono-winch (see Figure B.68). This is in contrast to the practice at No. 5 Shaft, where the backfill extends right to the gully packs (A. W. Stillwell, pers. comm.). The percentage fill at No. 6 Shaft was reported to be about 67 per cent, although the filling of the upper panels of the 36-35 C/L mini-longwall was reported to be considerably less owing to operational problems. The lower panels were reported to be well filled.

Stope and Gully Layout and Support

The support standard for West Driefontein GM No. 6 Shaft is shown in Figure B.68. Rapid yield hydraulic props (RYHPs) were used in the face area. The panel support design was considered to be of a high standard, except that loadspreaders were not specified for the RYHPs.

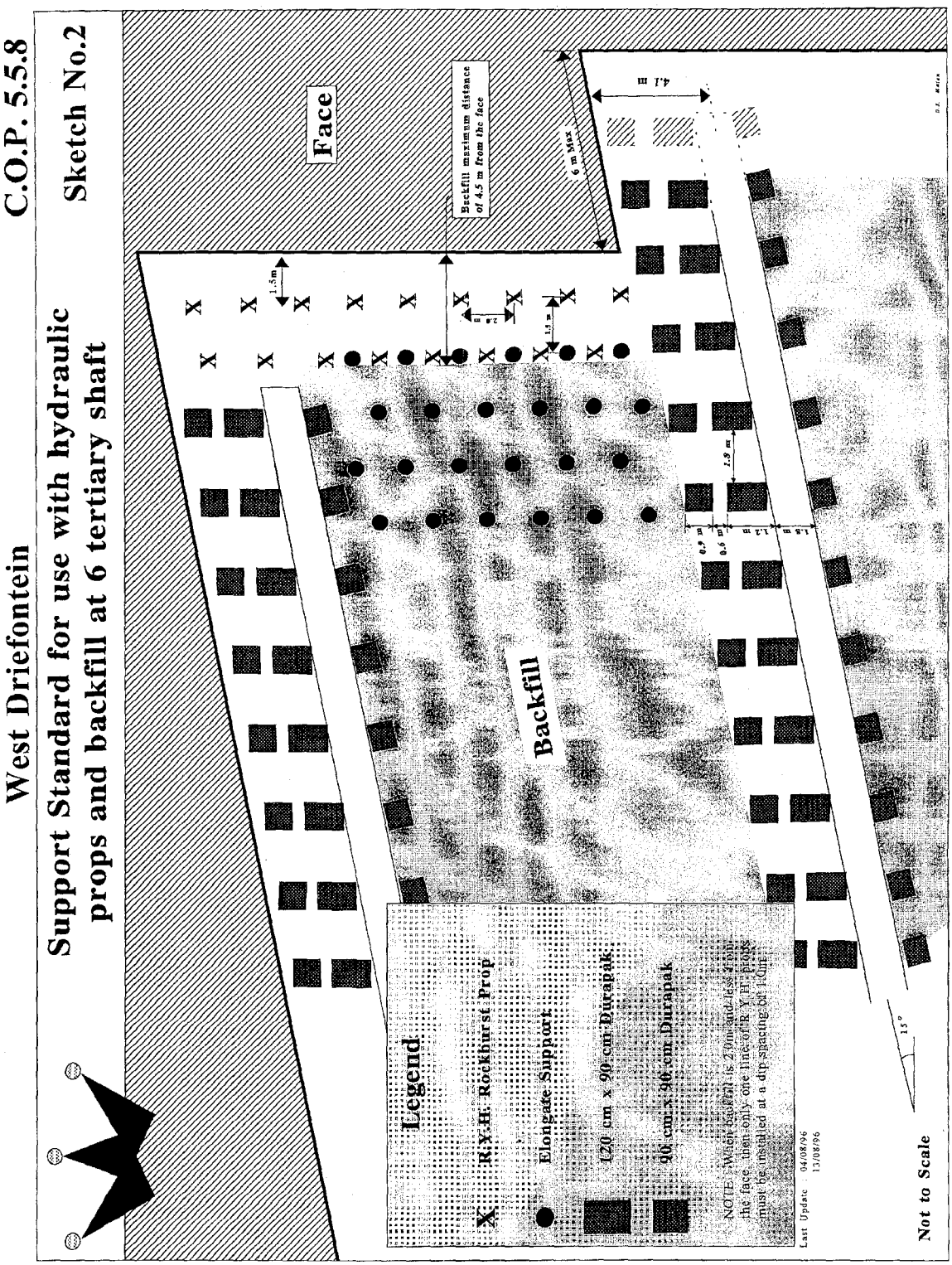

Figure B.68 Stope and gully support standard for West Driefontein No. 6 Shaft.

Gullies were lined with 1,2 m x 0,9 m Durapaks, with a yield load of 1400 kN. The gullies were oriented at 15° up-dip of strike. The lack of tendons to reinforce the hangingwall in the gully was a point of concern. Furthermore, experience gained from this investigation indicates that benefit might be gained by bringing the backfill closer to the gully.

15.3 Observations at the rockburst site

1W Strike Gully

The stope was entered from a cross-cut near the bottom of the 1W panel. The footwall of the 1W strike gully was being excavated in order to negotiate a fault with a 2 m down-throw to the west. The gully sidewall had been damaged by the scraper, undermining the foundation of some of the gully packs.

2W and 3W Dip Gullies

The team traversed dip gullies in the 2W and 3W panels to reach the 3W strike gully, where the major fall of ground occurred. The face area of the 2W and 3W panels was not inspected. Progress through the travellingway was arduous as considerable closure had taken place, and the footwall and hangingwall were irregular. The dip gullies were lined by Durapaks. It was of interest to note that one of these packs had failed in shear. However, there was no evidence to indicate that this was related to dynamic closure, and there was no rockburst damage in the area. It was noted that the dip towards the face of the face-parallel mining-induced fractures was relatively flat for a Carbon Leader stope.

3W Strike Gully

Backfilling of the 3W panel had been sporadic owing to breaks in the backfill supply caused by falls of ground. Packs were installed in these areas. It was reported that the pack support system was designed so that its load/deformation characteristics were similar to that of backfill.

The hangingwall of the 3W strike gully was intact where backfill was present in the adjacent stope. The major fall of ground in the 3W strike gully occurred at the foot of a section of the panel where no backfill had been placed because of operational problems. This area had been used as a dip travelling way, and was supported by 0,9 m x 0,9 m Durapaks. The fall of ground extended for 8,5 m along the gully, forming a semi-circle on the up-dip side with a radius of 5 m, that coincided almost exactly with the change from backfill to pack support in the 3W panel. The fall of ground included the hangingwall quartzite and the Green Bar, and ranged in thickness from 2 m above the gully to the west, to 1,4 m above the gully to the east (Figure B.69) The damage was probably exacerbated by the unusual thinness of the quartzite between the reef and the Green Bar. By the time of the visit, all the fallen rock had already been removed, together with the collapsed gully packs. No evidence of significant recent co-seismic closure (e.g. compression of packs) was detected in the immediate vicinity of the fall of ground, except for the pack at the eastern extremity of the fall of ground.

The section of the gully passing through the Skelm Dyke had suffered serious falls in the past, and was supported using void filling material (aerated cement). No recent rockburst damage was noted in this area.

15.4 Assessment of support performance

The support system in a section of the 3W strike gully had failed. Backfill, packs and rockbolts are generally used together as a system for the support of gullies.

Backfill: It was immediately apparent that the section of the gully which had suffered severe damage was the section where the adjacent stope was not backfilled. The span over which violent motion of the hangingwall took place was probably much greater in this section of the gully. Normally backfill would clamp the hangingwall, forming a shorter beam. Every effort should be made to place backfill, if possible right up to the gully packs.

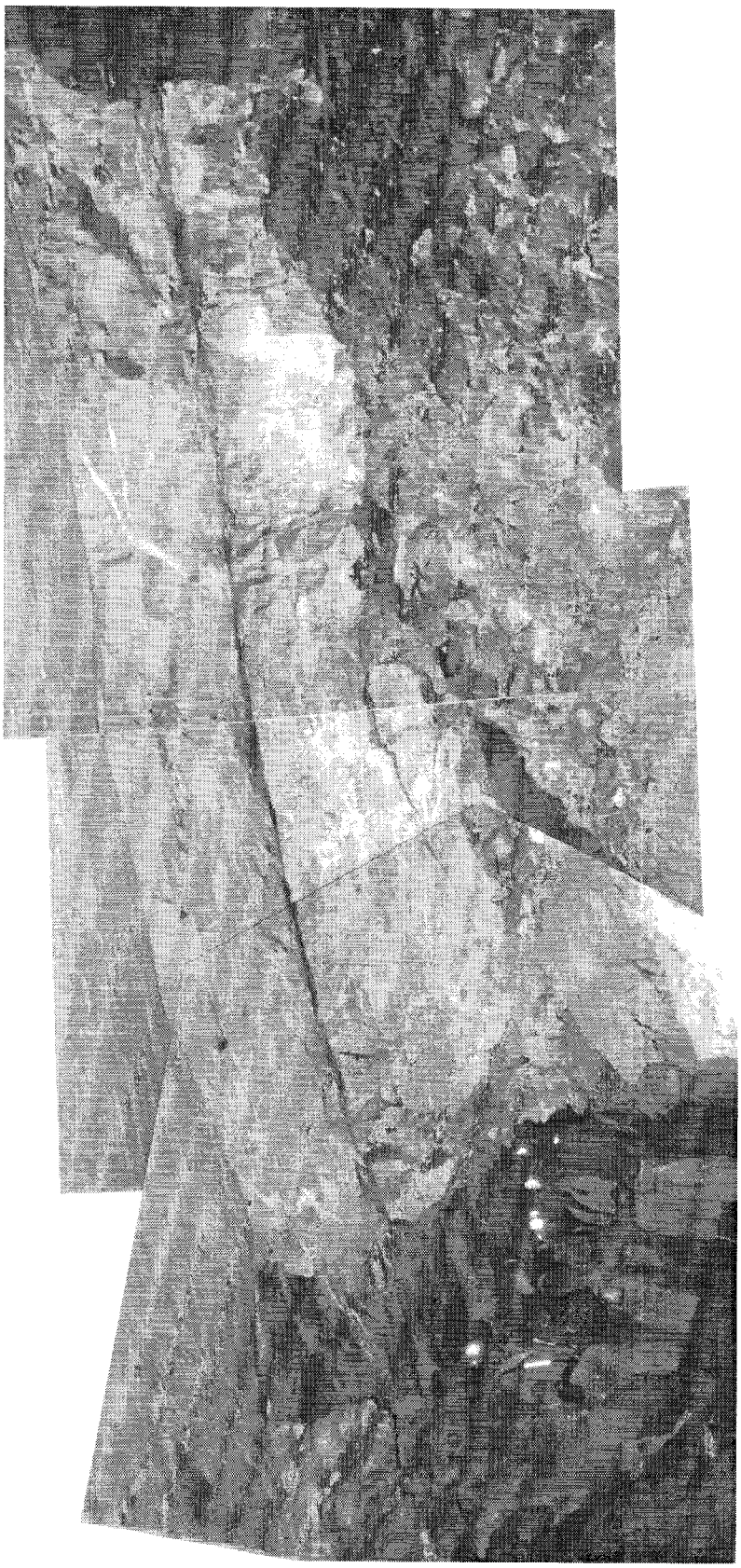

Figure B.69 View towards the west of the fall of ground in the 3W strike gully, 36-35 C/L west mini-longwall, West Driefontein No. 6 shaft.

15.5 Rockburst mechanism

Source mechanism

Seismic information was provided by J. Malan (mine seismologist).

Two seismic events, both with local magnitudes M_L=2,7, were recorded at 12h58 by the mine-wide seismic network. The second event occurred within 1 s of the first event. The foci of the events were about 200 m apart, with both foci close to the Skelm Dyke in the block of unmined ground immediately south of the 36-35 mini-longwall (see Figure B.67). The source parameters are listed in Table B.9 The Skelm Dyke was reported to be the most seismically active structure in the area, and slip on the dyke considered to be the most likely source mechanism.

Table B.9

Source parameters

	Event 1	Event 2
Time	12:58:08, 23 May 1997	12:58:08, 23 May 1997
Location	21173 m S, -6754 m W 2315 m down	21034 m S, -6712 m W 2348 m down
Seismic Moment	7,13E+12 Nm	9,54E+12 Nm
Radiated Energy	2,3E+8 J	1,22E+8 J
Apparent Stress	0,86E+06 Pa	0,39E+06 Pa
Local Magnitude	2,7	2,7
Energy Index	not calculated	1,5
Radius	not calculated	133 m
S Energy/P Energy	9,2	3,9

Damage mechanism

The shaking produced by a seismic event several hundred metres away was exacerbated by the absence of backfll, leading to the disintegration of a friable hangingwall.

Fore- and aftershocks

In the 24 hours preceding the damaging events, only one event with magnitude $M_L \geq 0,5$ was recorded in the vicinity of the 36-35 C/L West mini-longwall. It was a M_L=0,6 event with its epicentre about 30 m ahead of the 4W panel (see Figure B.67), which occurred at 15:19 on 22 May 1997. No damage was reported. As the focus of this event was over 200 m from the M_L =2,7 events on 23 May 1997, and not associated with the Skelm Dyke, it is not regarded as a precursor of the rockburst events.

In the 12 hours following the damaging events, no events with magnitude $M_L \geq 0,5$ were recorded in the vicinity of the 36-35 C/L West mini-longwall.

15.6 Conclusions

The source mechanism of the two M_L=2,7 events was probably slip on the Skelm Dyke induced by the mining of the 36-35 C/L West mini-longwall. The stress redistribution owing to the first event almost certainly acted as a trigger for the second event. Events of this magnitude (and greater) should be expected to occur in future, as mining in this area is already extensive, and many dykes and faults are known to exist, some of which (such as the Skelm Dyke) are known to be seismogenic.

No damage was reported in the lower panels (4W, 5W, and 6W) which were closest to the foci of the seismic events. It was also reported that the percentage backfill in these lower panels is high. It is deemed significant that the section of the 3W strike gully that sustained severe damage was the section where backfill was absent. It is believed that the lack of backfill severely compromised the ability of the support system to withstand seismically induced shaking.

The damage mechanism appeared to be shakedown of the gully hangingwall after the failure of the hangingwall beam. There was no evidence of dynamic stope convergence. The section of the 3W gully supported by void filling was undamaged.

15.7 Recommendations

The integrity of the gully hangingwall is governed by the entire stope support system, and thus the entire system should be reassessed. Seismic events of a similar or greater magnitude are possible, and the support should be able to withstand shaking. In particular:

The absence of backfill was a critical factor contributing to the gully damage in this particular rockburst. Gaps in backfill placement must be avoided. If extreme circumstances make it impossible for backfill to be placed, the spacing and force/deformation characteristics of the packs must be chosen carefully to ensure stability.

Backfill should be placed right up to the gully packs in order to increase the percentage fill and maximize its contribution to the support of the gully hangingwall. Apparently this is being done successfully on other shafts at Driefontein Gold Mine.

The use of rockbolts to support the gully hangingwall should be considered. The problem of the disintegration of the rock around the bolts giving rise to dangerous protruding units should be addressed through the use of suitable base plates. It appears that the hangingwall quartzite and Green Bar may be less than 2 m thick in some areas, therefore it may be realistic to anchor the rockbolts in the quartzite layer above the Green Bar. An alternative approach is to install a system, which provides areal coverage, e. g. mesh, and lacing.

The thickness of quartzite in the hangingwall below the Green Bar should be maximized by keeping the reef contact as close to the hangingwall as is possible without compromising gold recovery. Sampling should be conducted to determine this distance.

The construction of the Durapaks should be reviewed, as a yield force of 1400 kN may be transferring too great a load to the gully siding and causing damage. A yield force of 1000 kN may be more appropriate.

The approach of the stope to the Spotted Dick Horst Zone must be carefully managed to avoid a long face that is sub-parallel to the structure, or the mining of highly stressed remnants in the final stage.

It would appear from the mine plan that some gullies are orientated as much as 30° up-dip of strike (e.g. panel 4W). The refraction of stresses around the acute angle formed at the top of these leading panels could cause fracturing unfavourable to the integrity of the hangingwall of the panel above. It was recommended that gully orientations should not be more than 15° up-dip.

16 East Driefontein # 4, 25/9/97, M_L=4,4

16.1 Introduction

A seismic event with local magnitude M_L=4,4 occurred at 2h06 on 25 September 1997 in the vicinity of No. 4 Sub-vertical Shaft, East Driefontein Gold Mine, fatally injuring one worker on 42 level. The M_L=4,4 event was followed by aftershocks at 2h10 (M_L=2,0) and 2h12 (M_L=3,2). These events caused widespread damage to the shaft area and haulages accessing the major production areas (Figure B.70). The locations of these events were based on information from adjacent mines, because of loss of data at the East Driefontein seismic network. This has resulted in a relatively low confidence in the locations of the seismic events. Mine management requested that a team from CSIR: Mining Technology investigate the factors contributing to the rockburst, and recommend measures that will reduce the likelihood of similar damaging events. The team members visited the site on 29 September 1997 and 31 October 1997.

16.2 Mining environment

The No.4 shaft area of East Driefontein has a history of large seismic events associated with relatively little mining activity in the general area. The CSIR team had investigated another large rockburst two years prior to this event (see Case History 6).

Damage was inspected on 35, 38, 40 and 42 levels. These excavation range in depth from approximately 2400 m to 2800 m below surface. The majority of observed damage was associated with excavations sited within quartzitic rock in the footwall of the Venterdorp Contact Reef. The shaft area is in close proximity to the Bank fault, which represents a major sub-vertical regional discontinuity, and the Master bedding plane fault (MBF). The MBF is a major sub-horizontal plane, which intersects the No.4 Sub-vertical Shaft on 40 level, and haulages on 42 level approximately 200 m south-west of the shaft axis (Figure B.71). The M_L=4,4 seismic event is thought to be associated with these structures. It had previously been thought that the Bank fault was a listric fault which flattened out at depth and became the MBPF. However, reflection seismic surveys over the southern portion of East Driefontein indicated that the Bank fault continues with a steep dip to great depth (P. Jenkins, pers. comm.).

16.3 Observations at the rockburst site

35 Level

Damage on 35 level was inspected approximately two months after the main event, after completion of rehabilitation work in the main haulage west. Rockburst damage consisted primarily of the failure of the south sidewall of the tunnel to a depth of approximately 1,5 m. The failure of the support system was due to the bulking of the sidewall, and the failure of the mesh and lacing fabric support, with the subsequent unravelling of the rock mass from around the rock bolt reinforcement. At a breakaway position adjacent to peg D3492 in the 35 level footwall drive, observations were made of rock bolt failure under shear deformation, failure of mesh and lacing, and significant closure of the cross-cut excavation. The rock mass in the immediate periphery of the excavation was highly

fractured, contributing to the significant bulking of the sidewall mesh and lacing systems, and reducing direct interaction with the rock bolt reinforcement.

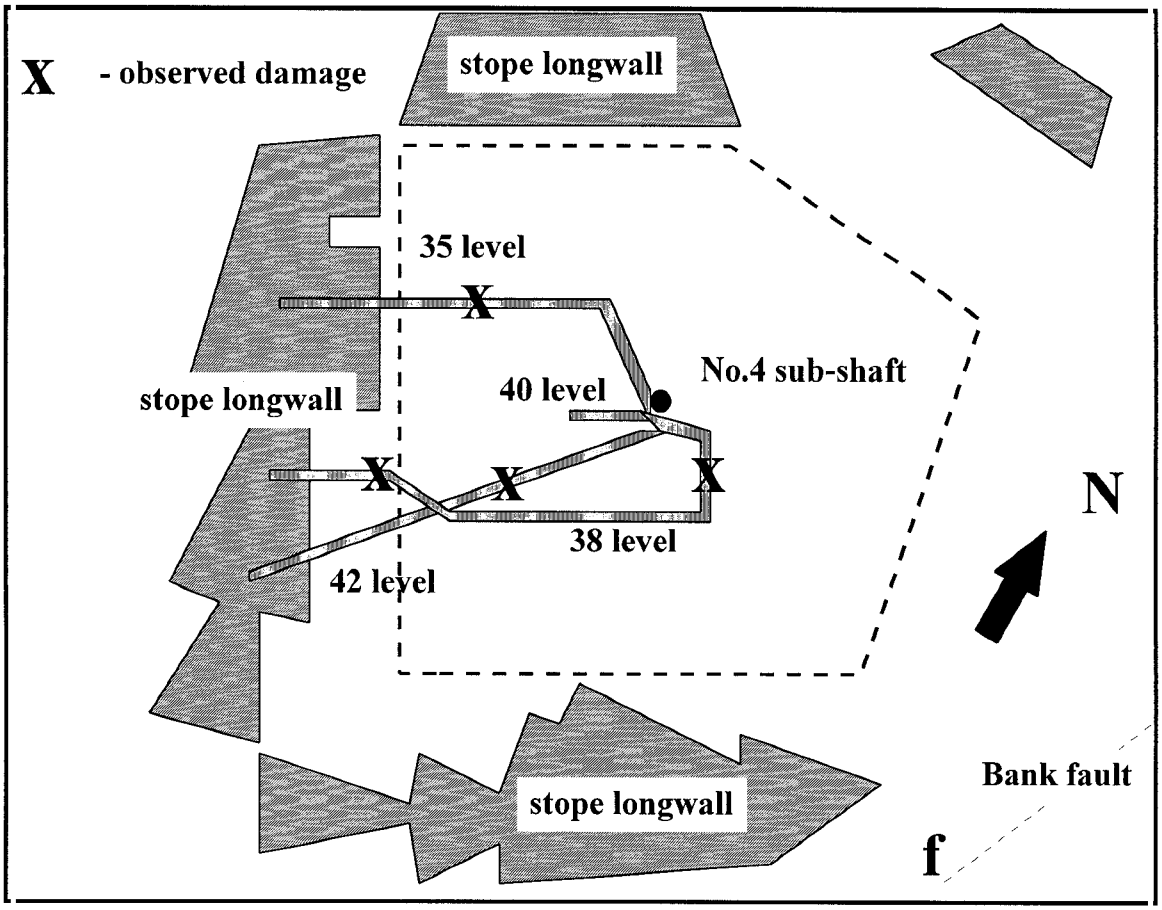

Figure B.70 Schematic plan of tunnel and stoping layout, East Driefontein No. 4 Sub-vertical Shaft, and the distribution of damage caused by the M_L=4,4 event on 25 September 1997 and inspected during the investigation.

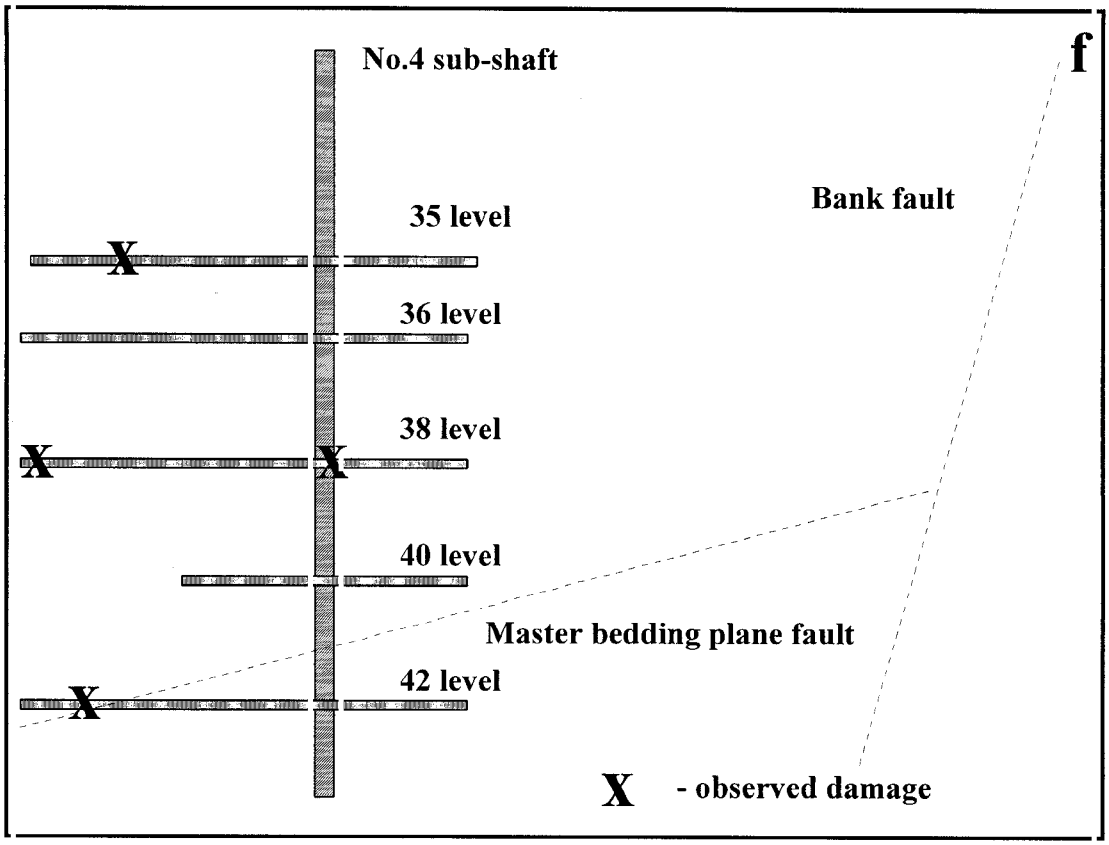

Figure B.71 Schematic section of shaft layout and major fault planes with distribution of damage.

38 Level

38 level pump station

Heave of the footwall concrete work was noted in the inclined access travellingway (orientated approximately north). Failure of shotcrete on the hangingwall and upper sidewalls, and heave of the footwall concrete work was noted in the adjacent electrical sub-station excavation (orientated approximately north-east). Only very minor damage was noted to the pump chamber excavation, consisting of the scaling of small areas of shotcrete, even though the rock mass condition in the immediate sidewall of the pump chamber was highly fractured (Figure B.72). It was reported that pipe columns and pumps within the chamber had been displaced by up to 55 mm along the axis of the pump chamber. Increased damage to the sidewalls of the dam excavations, orientated

perpendicular to the main pump chamber, was noted, as well as some damage to the dam walls. This disruption to the rock mass owing to dynamic loading was reported to have resulted in further quasi-static deformation subsequent to the event.

Figure B.72 View of south sidewall of 38 level pump chamber showing distribution of fracturing within the sidewall rock mass at the junction of the pump chamber and dam access excavations.

38/37 X/C SOUTH (Shaft tip cross-cut)

Damage within the shaft tip cross-cut, orientated approximately north, was primarily associated with the hangingwall and footwall. Hangingwall failures were of the order of 1,5 m to 2,0 m in height and consisted of failures of rock bolt reinforcement units and mesh and lacing fabric support components of the support system. Large blocks, with a long axis up to 1 m, had fallen from the hangingwall. Much of this excavation is sited within a dyke. The more competent rock mass structure is considered to have resulted in the increased failure of the rock bolt reinforcement, compared to observations of hangingwall damage at other sites. A characteristic of the rock mass in this area was the relatively high inflow of water. Failure of the rock bolt reinforcement was associated with a high degree of corrosion. The position of failure generally corresponded to a well defined plane within the rock mass on which significant outflow of water could be observed.

Damage was noted at several points in this tunnel. The largest fall of ground extended for about 6 m from the brow of cubby, excavated for the raise boring of an ore pass. This section of tunnel had been supported by Split Sets, shepherds crook rebars, mesh, lacing and shotcrete. It was noted that the Split Sets exhibited corrosion. Several modes of failure were noted:

- shear failure of a shepherds crook rebar,
- a shepherds crook rebar that had been pulled out of its hole,
- cable lacing broken,
- mesh torn open,
- Split Sets that had shed the rock slabs above by yielding of the square washers.

38/37 FW DRIVE WEST

The section of tunnel bearing south-west was undamaged. The section of the tunnel bearing north-west had experienced damage, but rehabilitation was virtually complete at the time of the visit. A protruding Split Set indicated that the zone of instability had extended to about 1 m in the hangingwall. The new hangingwall profile exhibited a sharp notch running parallel to the tunnel axis, giving it a "pagoda" profile.

38 AIRWAY WEST

The area of damage to this excavation is close to the edge of the shaft pillar area in the vicinity of a longwall mining abutment. Significant quasi-static damage had been experienced by this excavation prior to the M_L=4,4 seismic event and rehabilitation work to this effect was in progress. Damage occurred over a distance of approximately 50 m, and comprised of general sidewall deformation and collapse of hangingwall at the breakaway to the 38-37 CONNECTING X/C NORTH.

Damage to the sidewall of the excavation comprised significant bulging of the rock mass, confined by mesh and lacing, between the points of rock bolt reinforcement anchorage (Figure B.73). This was particularly evident in the lower portion of the sidewall, and on the north (up dip) side of the excavation. In areas of higher rock bolt reinforcement and lacing density, improved control of sidewall deformations were obtained (Figure B.74). This is considered to be a function of the increased overall stiffness of the system and thus increased compatibility of loading between the rock bolt reinforcement and the mesh and lace fabric. However, the lower confinement of the rock mass between the rock bolt reinforcement may still be evident with associated localised bulking of the rock mass at this point and potential failure of the mesh fabric.

Observations of damage at the 38-37 CONNECTING X/C NORTH breakaway location indicated a collapse of approximately 1,0 m to 1,5 m of hangingwall over the breakaway excavation. The rock mass in this area was again highly fractured in nature, but the dominant mode of failure was that of the rock bolt reinforcement, with subsequent collapse of the mesh and lacing fabric support system. Failure of the rock bolts was primarily localised corrosion of both the Split Sets and shepherds crook rebars, usually associated with a major discontinuity within the rock mass structure, and subsequent tensile failure at this point. Other modes of failure of the rebars were noted, such as straightening and snapping of shepherds crook loops

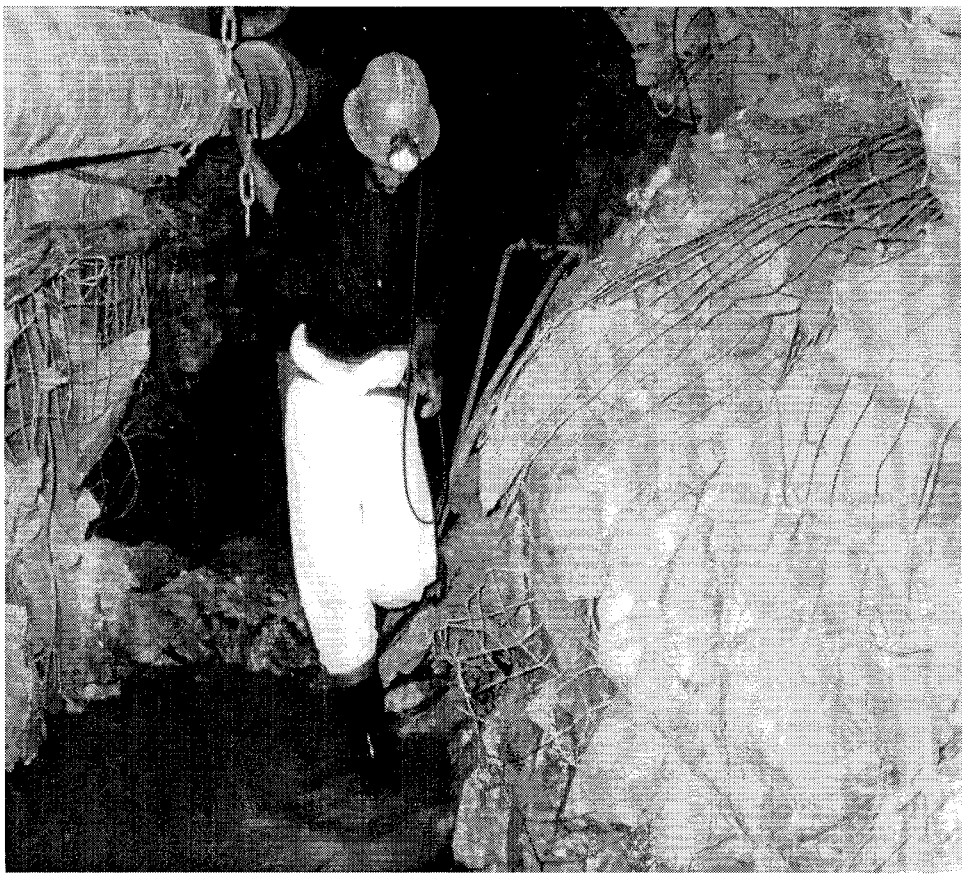

Figure B.73 View west along 38 level deep footwall drive showing large scale bulking of the rock mass, particularly of the lower north sidewall.

Figure B.74 View east along 38 level deep footwall drive of south sidewall showing more uniform containment and deformation of the sidewall rock mass with isolated areas of mesh failure.

40 Level

Observations of damage on 40 level included the collapse of the shaft cross-cut hangingwall at the location of a breakaway. Previous ground control problems had been associated with this area as indicated by the use of steel support sets in this area in addition to mesh and lacing. The MBF zone intersects 40 level at this point (see Figure B.71), dipping with the bedding at 23°. Pseudotachylite lenses were observed within the MBF zone.

Damage of a "shake down" nature was also associated with the access tunnel to the 40 to 42 level travelling way. The depth of stress-induced fracturing owing to the main 3,5 m x 3,5 m tunnel, as observed within the 38-40 travelling way, was estimated to be approximately 2,5 m, of which approximately 1,0 m had collapsed around the rock bolt reinforcement because of the seismic event.

40 to 42 level travelling way

Very limited damage was observed in the 40 to 42 level travelling way. A fault, believed to be a splay of the Bank Fault (see Figure B.71) intersects the travelling way The fault zone is characterised by thick gouge, with a vitreous green quartzite footwall. Mesh, lacing, and tendons were severely corroded in the vicinity of the fault zone.

42 Level

The damage inspected on 42 level was in close proximity to the intersection of the MBF. Although direct movement on this feature was not observed, the zone is associated with generally poorer ground conditions because of the disturbed nature of the rock mass.

42-37 TIP X/C SOUTH

A large collapse had occurred at the intersection of the 42-37 TIP X/C SOUTH and a workshop area, and one worker was fatally injured. Support in this area had been up graded to include the use of long cables and shotcrete, in addition to the standard mesh and lacing on rock bolts. Rehabilitation work had commenced in this area at the time of the visit and thus direct observation of the damage was not possible; although the failure was indicated to be associated with in-filled joints within the hangingwall to a height of approximately 2,0 m, and approximately 1,0 m of sidewall and footwall heave. This breakaway excavation is within 10 m of a second breakaway excavation (42-37 CONNECTING X/C WEST), and the interaction of these excavations with associated

higher induced stress levels, in addition to the general poor ground conditions, may have contributed to the area being more prone to rockburst damage.

Immediately to the south-west of this collapse, direct observations of damage to the support system could be made (Figure B.75). This damage consisted of a combination of mechanisms of bulk sidewall deformation, with failure or loss of anchorage of the rock bolts and cables, and containment of the unstable rock mass by mesh and lace anchored to stable rock bolts. The large scale deformations of the overall sidewall were generally associated with the lower portion of the excavation and perhaps in association with the observed footwall heave. The extent of differential deformation within the rock mass, particularly where rock bolt anchorage was maintained, resulted in significant damage to the mesh and lacing fabric support system. This again illustrates the low interaction between the rock bolt reinforcement and the rock mass in this highly fractured immediate skin of the excavation, and thus, the large loading of the fabric support.

Further observations in this area indicated mechanisms of failure of the rock bolt reinforcement and thus subsequent collapse of the mesh and lacing system (Figure B.76). In this area tensile failure of the rock bolts and cable anchors had occurred because of localised corrosion of these reinforcement units within the rock mass. The subsequent collapse of the rock mass was to a depth of approximately 1,5 m. The rock mass in this area appeared highly weathered in nature which is indicative of the occurrence of ground water and a highly corrosive environment.

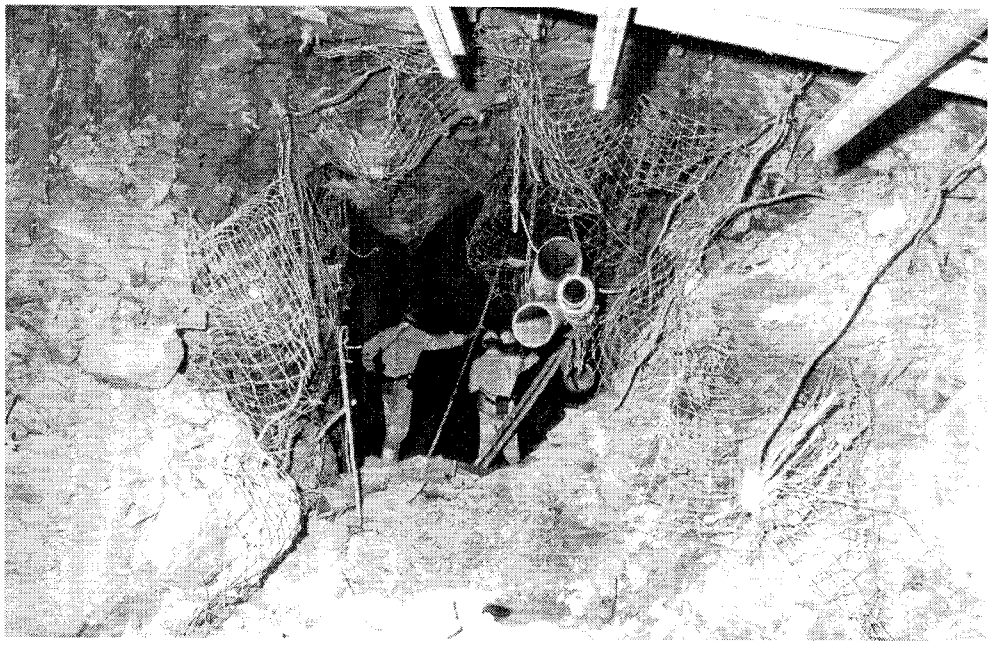

Figure B.75 View south-west along 42 level haulage showing highly fractured nature of the rock mass, footwall heave of approximately 1,5 m, bulk sidewall deformation (bottom right) and failure of mesh and lacing in upper portions of excavation.

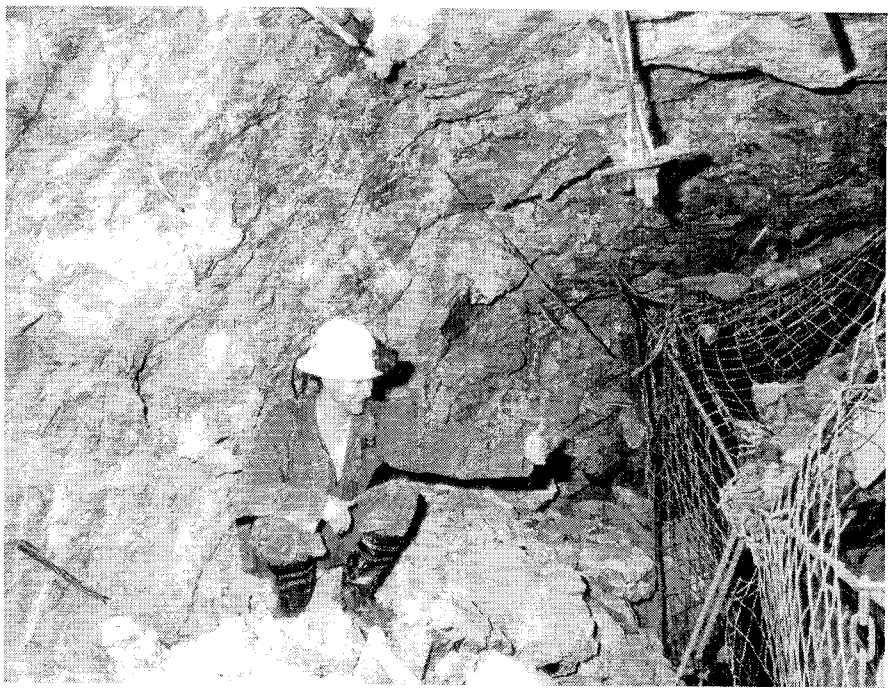

Figure B.76 View north east along 42 level haulage showing failure of rock bolt reinforcement (left) and thus loss of fabric anchorage (right) and collapse of approximately 1,5 m of fractured sidewall rock mass.

Stability of sections of the tunnel were maintained, but again characteristic bulking of the rock mass between the rock bolts and the lacing is evident with associated loading of the mesh panels (Figure B.77). This again clearly illustrates the limited extent of interaction of the rock bolt reinforcement within the immediate peripheral rock mass of the sidewall of the excavation in this environment.

In areas of the 42-37 TIP X/C SOUTH where shotcrete was applied, isolated failures were noted. The highly corrosive nature of this environment had resulted in the severing of cable anchors at the shotcrete / rock mass boundary because of corrosion.

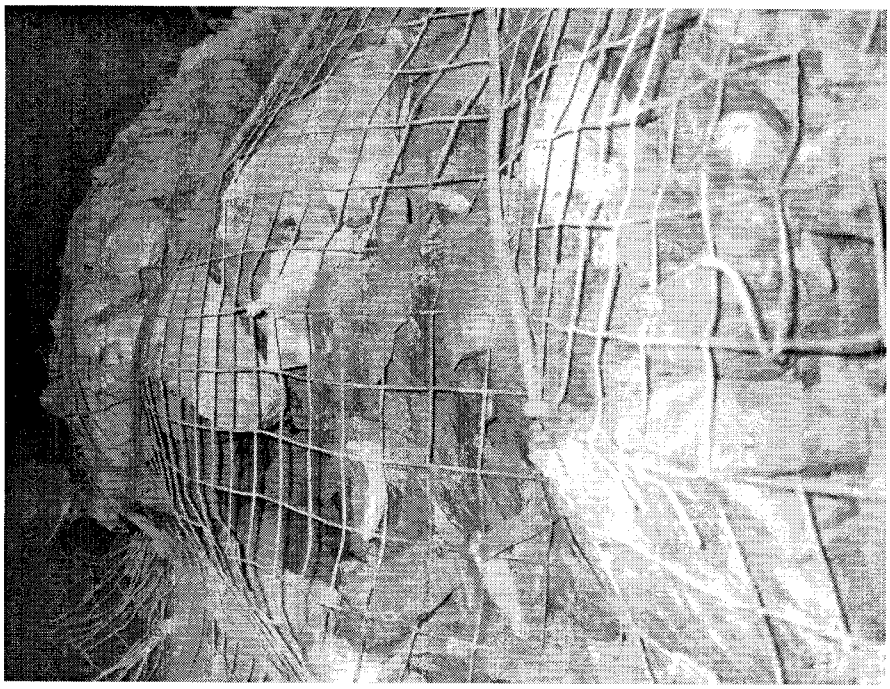

Figure B.77 Bulking of fractured sidewall rock mass between rock bolt reinforcement and lacing within 42 level haulage.

16.4 Assessment of support performance

Damage in the 38-37 AIRWAY WEST is consistent with a highly fractured rock mass with relatively stiff rock bolt reinforcement which is anchored at depth to a more competent rock mass structure. The highly fractured nature of the immediate sidewall rock mass is considered to result in very limited direct interaction between rock bolts and the rock mass, thus causing excessive direct loading of the mesh and lacing fabric support. The large scale bulking of the rock mass in the lower portion of the sidewall is considered to be owing to the lower support system resistance in this area, particularly of the fabric support.

The highly corrosive nature of the environment in 42-37 TIP X/C S had resulted in the severing of cable anchors at the shotcrete / rock mass boundary because of the concentration of corrosion at this interface. The tunnel excavation would act as a free surface within the rock mass towards which groundwater would naturally drain. The

implementation of the shotcrete represented an impermeable skin on the upper boundary of the excavation along which potential groundwater would gather and drain to the base of the excavation either along this interface or within the immediate fractured rock mass. Under these conditions the concentration of groundwater flow is considered to have resulted in very localised corrosion of the steel reinforcement within the rock mass to the extent that the dynamic energy associated with the shotcrete skin was sufficient to cause failure of these units.

The most important factor affecting the performance of support noted in this investigation was corrosion, which was particularly severe in the vicinity of major geological structures. Other points of consideration are:

1. The importance of excavation orientation in relation to the degree and location of damage within the excavation.
2. The reduced interaction between the rock bolt reinforcement and the rock mass in the immediate skin of the excavation.
3. As a consequence of (2) above, the importance of the consideration of the demand on, and capacity of, the fabric support system under these conditions.
4. The weakness of the lower portion of the sidewall of the excavation, reduced rock mass / support system interaction and thus this area being more prone to rockburst damage.

16.5 Rockburst mechanism

Source mechanism

As the East Driefontein seismic network lost the recordings of the event, the locations and source parameters of the M_L=4,4 event and aftershocks were obtained from networks on adjacent mines. There were considerable discrepancies between the locations obtained by these networks. The locations considered to be best are shown on Figure 1a, together with a tabulation of the source parameters. The locations were not sufficiently accurate to identify the structure on which the slip occurred. The findings of an earlier rockburst investigation (see Case History 6), together with new observations, were used to deduce the most likely source mechanism. The key factors are:

- The East Driefontein No. 4 Shaft area has a history of large seismic events with relatively little mining, suggesting that structures in the area are close to instability.
- Stress measurements and observations of tunnel profiles in the No. 4 Shaft area indicate that the horizontal stress exceeds the vertical stress (i.e. k-ratio > 1). This is unusual for the Far West Rand gold field. However, in the tunnels visited during this investigation there was no clear evidence of a high k-ratio.
- Several major faults, such as the Bank fault and Master Bedding Plane Fault, are present, together with numerous smaller faults.
- The surface of a fault, interpreted to be a splay of the Bank fault, was characterized by thick layer of water-saturated gouge, suggesting a low cohesion.
- The Master Bedding Plane Fault has been implicated in previous events, such as an event on 26 June 1978, which caused damage to an excavation at a depth of 2500 m below surface near the No. 1 Sub-vertical Shaft, fatally injuring 17 workers.
- The source diameter of the M_L=4,4 event was probably greater than 500 m, suggesting slip on a geological structure.

Damage mechanism

Damage was caused by the failure of the tunnel support systems when subjected to strong seismic shaking. The sections which sustained damage were generally those areas where:

- the ground conditions were poor,
- the support system was compromised by corrosion, or the excavation was disrupted by features such as breakaways, cubbys, ore passes and tips.

The two senior members of the team (W. D. Ortlepp and A. J. Jager), who have decades of mine experience, commented that the degree and extent of corrosion of support elements was very unusual. A particular issue is the role played by shotcrete in localising corrosion of cable anchors and rebars at the rock/shotcrete interface, and concealing this weakness from sight.

In considering strategies to contain rockburst damage owing to future large events, the following factors should be considered:

- It was reported that only minor damage was sustained in stopes.
- The tunnels have been exposed to repeated seismic loading over the course of the past few years.
- The sum of the sections of tunnels which sustained damage (on 35, 38, 40 and 42 levels) amounts to a few hundred metres, while several kilometres of tunnel were undamaged.

Thus we concluded that there is a good prospect of improving support so that the hazard associated with future large events is not excessive.

16.6 Conclusions

Source mechanism:

- The reason for the occurrence of large events following relatively little mining is a complex problem, and cannot be solved by a superficial analysis of limited data.
- The M_L=4,4 event on 25 September 1997 was probably due to slip on the Bank fault, or an associated structure.
- The two aftershocks, which occurred within 6 minutes of the main event, were due to stress redistribution.
- Similar large events are likely to occur again in the future. Without a better understanding of the nature of this unusual seismicity and its' relationship to mining, it is not poossible to make regional support and mining layout recommendations to reduce this hazard.

Damage mechanism:

- The most severe damage appears to have occurred in areas with relatively poor ground conditions and increased spans, often exacerbated by the corrosion of support elements.
- The damage is due to the failure of the support system when subjected to strong seismic shaking.
- The degree of corrosion of support elements observed near fault zones was extreme.
- Many different failure mechanisms were noted:
  - bulking of the side- and hangingwall,
  - shearing and tensile failure of rebars,
  - rebars pulled out of holes,
  - corrosion of rebars, Split Sets, mesh and lacing, and cable anchors
  - poor quality joins of lacing.

16.7 Recommendations

Establish the integrity of tunnel support

It is important that tunnels be carefully inspected by means of a systematic programme of pull tests and short rock bolt overcoring drill holes to identify areas where the integrity of the support system has been compromised, are thus prone to rockburst damage,and require rehabilitation. Indications of vulnerablity include:

- presence of corrosive ground water,
- poor adhesion of shotcrete to rock surfaces,
- damage due to previous seismic loading,
- areas where the rock mass is highly fractured.

Map the unstable zone

The depth of the unstable zone surrounding tunnels may vary according to factors such as rock type, tunnel orientation, stress field etc. The length and spacing of tendons is dependent on the depth of the unstable zone and the method of support/rock mass interaction invoked. The depth of the unstable zone should be carefully analysed, and used in the design of tunnel support systems. The depth of the unstable zone may be estimated by:

- petroscope inspection of drill holes,
- extensometer instrumentation,
- observations of rockburst damage and subsequent rehabilitation, and
- case studies of tunnel collapse.

Review the design of rock reinforcement tendon support

In areas where poor ground conditions exist it is apparent that, under dynamic loading, the interaction between reinforcement tendons is insufficient with the result that the fabric support is overloaded and fails, leading to complete ineffectiveness of the support system as a whole. At present the tendons are not subjected to the full load of their tributary area, and thus few fail in tension. However, once a more dense and interactive system of tendons and a stiffer fabric/shotcrete is implemented, the tributary forces will apply, with the consequence that yielding tendons will be necessary.

Review the use of shotcrete

The use of shotcrete should be reviewed, beginning with the rationale for using it, the design procedure and the application methodology. It is recommended that shotcrete be applied prior to meshing and lacing. Shotcrete should not be applied after mesh and lacing have been installed, as the presence of these elements limits adhesion and causes the thickness of the application to be uneven, and may even cause line weaknesses in the shotcrete.

Prevent corrosion of tendons

In areas that are prone to corrosion, it is recommended that tendons are installed after shotcreting, so that they will be protected from corrosion by the grout. The use of corrosion resistant materials should also be investigated.

Use injection resin

The use of injection resin grouting (e.g. Wimeco) should be considered in areas where rock mass condition is particularly poor.

Review seismic data

The seismic data must be carefully reviewed to identify the seismogenic structures and the seismic source parameters (especially the direction of shearing through moment tensor inversion), and to establish the relationship between mining, the stress field in the area and seismicity. In reviewing the data, assessment should be made of the need for additional seismometers in the No. 4 Shaft area in order to provide better and more comprehensive data. This would lead to a better understanding of the serious and unusual seismic problem in the area. Consideration could also be given to the installation of a local seismic system to study the problem in more detail.

Determine the virgin stresses in the area

There is evidence to suggest that the virgin stresses, and particularly the k-ratio, is variable in this area. It is important to quantify this in order to devise appropriate mining strategies.

Seek specialist assistance

The recommendations above are broad in scope and of critical importance for the future exploitation of the orebody. It is desirable that the rock mechanics department seek support from external specialists in implementing the recommendations.